Characteristics of Environmental Data Layers for Use in Species Distribution Modelling in the Newfoundland and Labrador Region

J. Guijarro, L. Beazley, C. Lirette, Z. Wang, and E. Kenchington

Department of Fisheries & Oceans, Canada
Maritimes Region,
Ocean and Ecosystem Sciences Division,
Bedford Institute of Oceanography,
PO Box 1006, Dartmouth,
Nova Scotia B2Y 4A2
CANADA

2016

Canadian Technical Report of Fisheries and Aquatic Sciences 3187

Fisheries and Oceans Canada | Pêches et Océans Canada

Canada

Canadian Technical Report of Fisheries and Aquatic Sciences

Technical reports contain scientific and technical information that contributes to existing knowledge but which is not normally appropriate for primary literature. Technical reports are directed primarily toward a worldwide audience and have an international distribution. No restriction is placed on subject matter and the series reflects the broad interests and policies of Fisheries and Oceans Canada, namely, fisheries and aquatic sciences.

Technical reports may be cited as full publications. The correct citation appears above the abstract of each report. Each report is abstracted in the data base *Aquatic Sciences and Fisheries Abstracts*.

Technical reports are produced regionally but are numbered nationally. Requests for individual reports will be filled by the issuing establishment listed on the front cover and title page.

Numbers 1-456 in this series were issued as Technical Reports of the Fisheries Research Board of Canada. Numbers 457-714 were issued as Department of the Environment, Fisheries and Marine Service, Research and Development Directorate Technical Reports. Numbers 715-924 were issued as Department of Fisheries and Environment, Fisheries and Marine Service Technical Reports. The current series name was changed with report number 925.

Rapport technique canadien des sciences halieutiques et aquatiques

Les rapports techniques contiennent des renseignements scientifiques et techniques qui constituent une contribution aux connaissances actuelles, mais qui ne sont pas normalement appropriés pour la publication dans un journal scientifique. Les rapports techniques sont destinés essentiellement à un public international et ils sont distribués à cet échelon. II n'y a aucune restriction quant au sujet; de fait, la série reflète la vaste gamme des intérêts et des politiques de Pêches et Océans Canada, c'est-à-dire les sciences halieutiques et aquatiques.

Les rapports techniques peuvent être cités comme des publications à part entière. Le titre exact Fig. au-dessus du résumé de chaque rapport. Les rapports techniques sont résumés dans la base de données *Résumés des sciences aquatiques et halieutiques.*

Les rapports techniques sont produits à l'échelon régional, mais numérotés à l'échelon national. Les demandes de rapports seront satisfaites par l'établissement auteur dont le nom Fig. sur la couverture et la page du titre.

Les numéros 1 à 456 de cette série ont été publiés à titre de Rapports techniques de l'Office des recherches sur les pêcheries du Canada. Les numéros 457 à 714 sont parus à titre de Rapports techniques de la Direction générale de la recherche et du développement, Service des pêches et de la mer, ministère de l'Environnement. Les numéros 715 à 924 ont été publiés à titre de Rapports techniques du Service des pêches et de la mer, ministère des Pêches et de l'Environnement. Le nom actuel de la série a été établi lors de la parution du numéro 925.

Canadian Technical Report of
Fisheries and Aquatic Sciences 3187

2016

Characteristics of Environmental Data Layers for Use in Species Distribution Modelling in the Newfoundland and Labrador Region

by

J. Guijarro, L. Beazley, C. Lirette, Z. Wang, and E. Kenchington

Science Branch
Ocean and Ecosystem Sciences Division
Fisheries and Oceans Canada
1 Challenger Drive
Dartmouth, NS
B2Y 4A2

Cat. No. Fs97-6/3187E-PDF ISBN 978-0-660-06873-2 ISSN 1488-5379

Correct citation for this publication:

Guijarro, J., Beazley, L., Lirette, C., Wang, Z., and Kenchington, E. 2016. Characteristics of Environmental Data Layers for Use in Species Distribution Modelling in the Newfoundland and Labrador Region. Can. Tech. Rep. Fish. Aquat. Sci. 3187: viii + 325p.

TABLE OF CONTENTS

ABSTRACT

Guijarro, J., Beazley, L., Lirette, C., Wang, Z., and Kenchington, E. 2016. Characteristics of Environmental Data Layers for Use in Species Distribution Modelling in the Newfoundland and Labrador Region. Can. Tech. Rep. Fish. Aquat. Sci. 3187: viii + 325p.

Species distribution models require spatially linked response (e.g., species, habitat type) and environmental (predictor) point data. Often, only limited environmental data types can be collected at the time of sampling, and it may be desirable to capture information both from different data sources and/or longer term data series in order to predict the distribution of a response variable. In order to link response and predictor variables that are not sampled at the same location or time, geospatial interpolation techniques are applied. Here, we provide a review of 104 environmental variables from each of 8 water column properties: Temperature, Salinity, Current Speed, Maximum Seasonal Mixed Layer Depth, Bottom Shear, Sea Surface Chlorophyll *a*, Primary Production and Dissolved Inorganic Nutrients for the 'Newfoundland and Labrador Region' (a combined spatial extent of DFO's Placentia Bay-Grand Bank and Newfoundland and Labrador Shelves Large Ocean Management Areas). All of these variables have potential biological relevance to benthic invertebrate species. Original data sources were the Global Ocean Reanalyses and Simulations (GLORYS), the Sea-viewing Wide Field-of-view Sensor (SeaWIFS), and the World Ocean Database 2013 (WOD13). For each variable, the original data characteristics and diagnostics produced from spatial interpolation using ordinary kriging are detailed. Standard error and prediction maps are shown for each variable. Based on these diagnostics, a subset of these variables was subsequently used in species distribution models of corals, sponges, crinoids, ascidians and bryozoans in the Newfoundland and Labrador Region.

RÉSUMÉ

Guijarro., J., Beazley, L., Lirette, C., Wang, Z., et Kenchington, E. 2016. Characteristics of Environmental Data Layers for Use in Species Distribution Modelling in the Newfoundland and Labrador Region. Rapp. Tech. Can. Sci. Halieut. Aquat. 3187: viii + 325p.

Les modèles de répartition des espèces exigent des données ponctuelles de variables explicatives spatiales (p. ex., espèces, types d'habitat) et de variables prédictives environnementales. Souvent, seuls quelques types de données environnementales peuvent être recueillis au moment de l'échantillonnage, et il peut être souhaitable de saisir des renseignements de diverses sources de données et/ou de séries de données à plus long terme dans le but de prévoir la répartition d'une valeur explicative. Afin d'établir un lien entre une variable explicative et une variable prédictive qui n'ont pas été échantillonnées au même emplacement ou au même moment, des techniques d'interpolation géospatiales sont utilisées. Dans ce document, nous proposons un examen de 104 variables environnementales de chacune des huit propriétés de la colonne de l'eau : la température, la salinité, la vitesse du courant, la profondeur maximale de la couche de mélange saisonnière, le cisaillement de fond, la chlorophylle *a* à la surface de la mer, la production primaire et les éléments nutritifs inorganiques dissous pour la « région de Terre-Neuve et du Labrador » (l'étendue spatiale combinée des zones étendues de gestion des océans (ZEGO du MPO) de la baie Placentia et les Grands Bancs et du plateau de Terre-Neuve et du Labrador). Toutes ces variables ont une pertinence biologique potentielle pour les espèces d'invertébrés benthiques. Les sources de données originales sont GLORYS (Global Ocean Reanalyses and Simulations), SeaWiFS (Sea-viewing Wide Field-of-view Sensor) et WOD13 (World Ocean Database 2013). Pour chaque variable, les caractéristiques des données d'origine et les diagnostics produits par interpolation spatiale à l'aide du krigeage ordinaire sont présentés en détail. Des cartes de prévision et d'erreur standard sont présentées pour chaque variable. En se fondant sur ces diagnostics, un sous-ensemble de ces variables a par la suite été utilisé dans les modèles de répartition des espèces de coraux, d'éponges, de crinoïdes, d'ascidies et de bryozoaires dans la région de Terre-Neuve et du Labrador.

INTRODUCTION

Species distribution modelling (SDM) is a tool that utilizes the relationship between a species and its environment to predict the species' distribution in unsampled areas. In Atlantic Canada and the eastern Arctic, species distribution models have been used to model the distribution of benthic invertebrates, specifically: corals and sponges (Beazley et al. 2016a, Beazley et al. 2016b, Guijarro et al. 2016a, Murillo et al. 2016), and crinoids, ascidians and bryozoans (Guijarro et al. 2016b). Data on the species (geo-referenced presence and absence data as well as biomass; response variables) were extracted from Fisheries and Oceans Canada (DFO) multispecies research vessel surveys. Environmental predictor variables were from direct measurements, modelled outputs, temporal averages, and derivations. Environmental variables are typically collected at different spatial and temporal resolutions, and are often spatially interpolated to provide continuous surfaces that can be used for predictive modelling at all spatial scales. While it would be possible to limit the SDMs to environmental predictor variables collected at the point source (e.g., depth, slope, temperature, salinity), such information is temporally limited and given the longevity of some of these sessile benthic species, may not be representative of their environmental niche.

Continuous interpolated surfaces produced at high resolution often show very detailed spatial variation, implying that the surfaces are very precise. However, spatial interpolation methods are affected by sample size, sampling design and data quality properties, and variation within the data has very large impacts on the performance of the spatial interpolators (Li and Heap, 2008). Beazley et al. (2016c) detailed the data characteristics and diagnostics produced from spatial interpolation of a suite of environmental data for the Gulf of St. Lawrence, which were subsequently used to predict the occurrence and biomass of sea pens, sponges, soft corals and stalked tunicates (Murillo et al. 2016) using random forest species distribution models (Breiman 2001). Here we provide a similar overview of variables used by Guijarro et al. (2016a,b) for species distribution models of corals, sponges, crinoids, ascidians and bryozoans in the Newfoundland and Labrador Region.

MATERIALS AND METHODS

Study Area

The 'Newfoundland and Labrador Region' used herein, is a combined spatial extent of DFO's Placentia Bay-Grand Bank and Newfoundland and Labrador Shelves Large Ocean Management Areas (LOMA). It was used as the spatial boundary for the construction of environmental variables in this report (see Figure 1). This area combines two of DFO's six administrative regions across Canada: the Newfoundland Region in the southern portion, and the Labrador Region to the north.

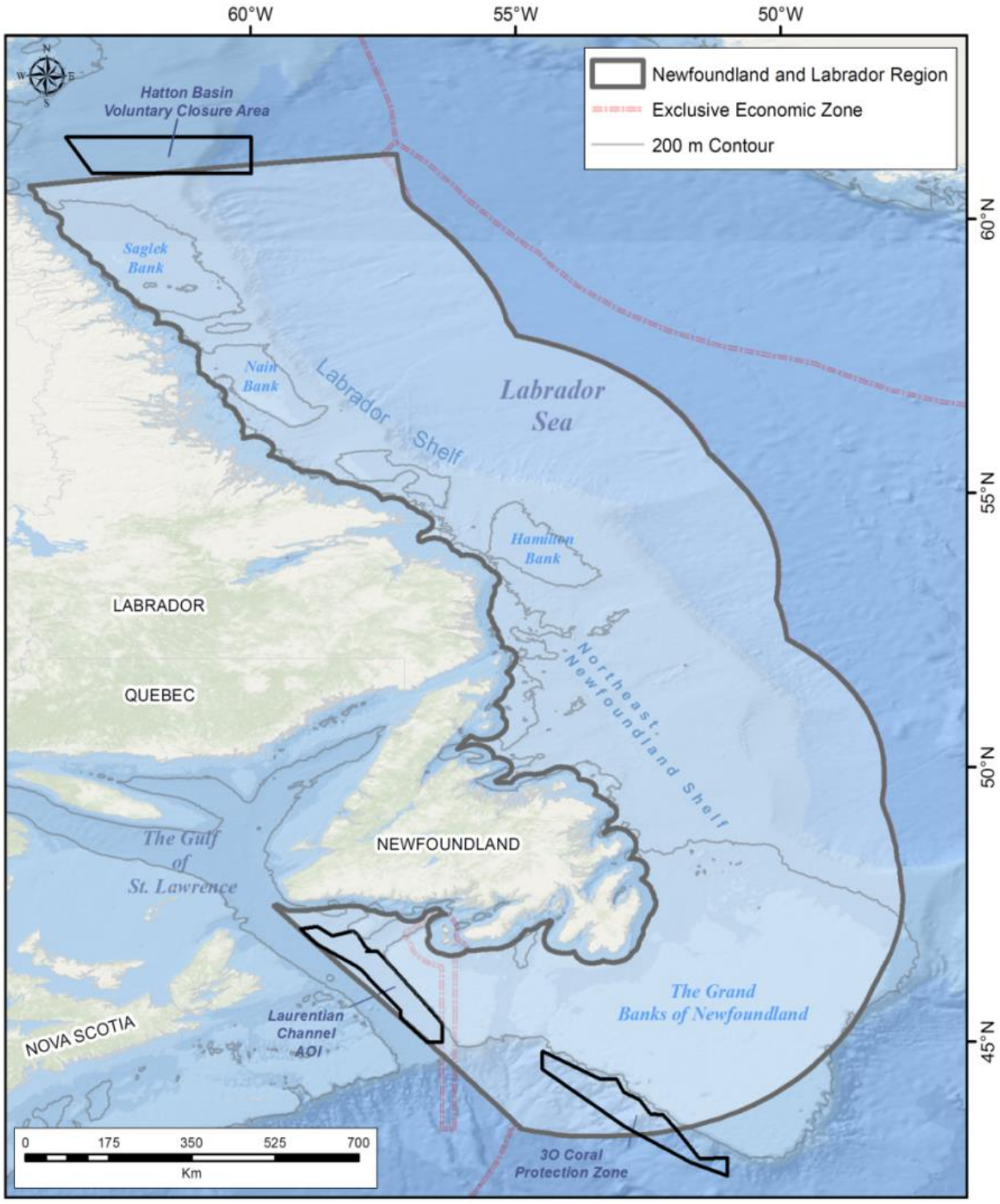

Figure 1. The 'Newfoundland and Labrador Region' (grey polygon) used for creating interpolated surfaces of environmental variables in the Newfoundland and Labrador Region. A 20 kilometres buffer was added around all land points.

Data Sources

Global Ocean Reanalyses and Simulations (GLORYS)

Data for surface and bottom temperature, salinity, current speed, bottom shear, and mixed layer depth were extracted from the Global Ocean Reanalyses and Simulations (GLORYS2V1; Figure 2). GLORYS2V1 is a numerical ocean general circulation model reanalysis product with ¼° horizontal resolution that aims to provide the mean and time-varying state of the oceanic states with a focus on capturing variation of meso-scale eddies (http://www.mercator-ocean.fr/eng/science/GLORYS). Details and caveats of this model can be found in Beazley et al. (2016c).

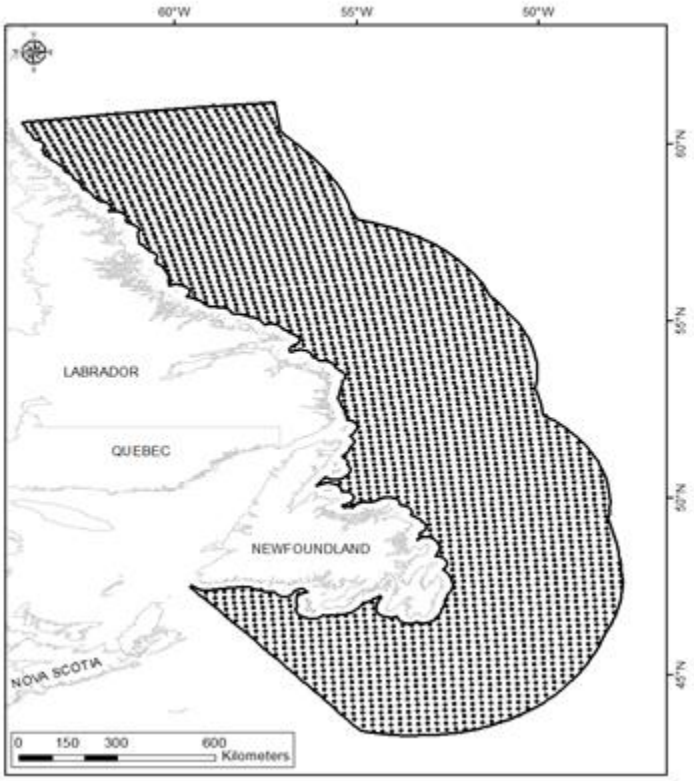

Figure 2. Distribution of point data extracted from the GLORYS2V1 model from 1993 to 2011 for the Newfoundland and Labrador Region. Point data have a native resolution of ¼°.

Sea Surface Chlorophyll *a*

Sea surface chlorophyll *a* data were derived from the Sea-viewing Wide Field-of-view Sensor (SeaWIFS) database. SeaWiFS data is primarily used to determine concentrations of chlorophyll in the oceanic water column. These values may be used to derive phytoplankton concentrations and oceanic primary productivity. The ocean optical data from SeaWiFS can also be used to determine light attenuation in the oceanic water column, which provides information on

suspended sediment concentrations and other parameters. Ocean color distribution can be used to investigate the forces influencing trophic productivity in the world's oceans.

Monthly SeaWIFS (Level 3 SMI) data from 2001 to 2010 were downloaded from NASA's OceanColor Group (http://oceandata.sci.gsfc.nasa.gov/) using Duke University's Marine Geospatial Ecology Tools (Roberts et al., 2010) in ArcGIS (ESRI, 2011). Composite images were displayed in raster format with a spatial resolution of 9 km. The native resolution of the point data for SeaWIFS chlorophyll *a* data are shown in Figure 3.

Annual and seasonal averages were computed for the SeaWIFS dataset. Seasons were delimited by the following 'day of year' ranges: days 91 – 181 (spring), 182 – 243 (summer), and 244 – 334 (fall). These seasonal delimitations capture the peak of the spring and fall phytoplankton blooms in most areas of Newfoundland and Labrador. Winter chlorophyll was considered inconsequential to the benthos and was not included in this report.

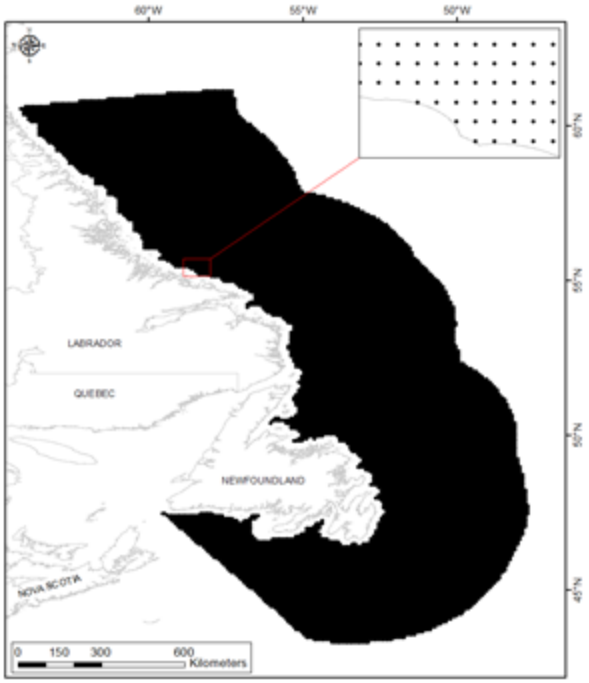

Figure 3. Distribution of sea surface chlorophyll *a* (SeaWIFS) point data (spring, summer, fall and annual) for the Newfoundland and Labrador Region. Point data have a native resolution of 9 km.

Primary Production

Primary production was calculated following the method of Platt et al. (2008) using software developed by the Remote Sensing Unit of the Bedford Institute of Oceanography (RSU-BIO) and the Department of Oceanography at Dalhousie University. The calculation of primary production requires input from multiple sources. Monthly mean surface chlorophyll *a* and photosynthetically active radiation (PAR) was obtained from NASA's SeaWiFS Level 3, 9-km global coverage (reprocessing R2010.0; Feldman and McClain, 2012). Sea surface temperature (SST) was obtained from NOAA PathFinder version 5.2 data and was reprocessed from its

native resolution of 4000 m^2 $pixel^{-1}$ to match the spatial and temporal resolution of chlorophyll data. Monthly images of total cloud fraction data used in the model were obtained in November 2014 from MYD08_M3, a monthly aggregation of MYD35, collection 51 (ftp://ladsweb.nascom.nasa.gov/allData/51/MYD08_M3/). The *in situ* parameters, such as photosynthetic performance, chlorophyll *a*, sea surface temperature, and water depth originate from ship-based observations made by DFO's Atlantic Zone Monitoring Program (AZMP; http://www.bio.gc.ca/science/monitoring-monitorage/azmp-pmza-en.php). Reliability of the resulting primary production data is therefore unknown for areas outside the AZMP region. The model described in Platt et al. (2008) results in pixel-by-pixel depth-integrated net primary production (mg C m^{-2} day^{-1}) calculated for the 15 day of each month from September 2006 to September 2010. Like the GLORYS2V1-derived variables, monthly values for primary production allowed for the calculation of both 'absolute' and 'average' minima, maxima, and range quantifications. However, for some months and years no data was available (see Table 1), therefore only spring (April – June), summer (July – August.), fall (September – November) and annual layers were created. For the creation of these variables, we ensured that each point location across the study extent had at least two months of data in each of the five years contributing to the quantifications. Summer and annual surfaces showed nearly full coverage across the Newfoundland and Labrador Region, whereas portions of the Saglek and Nain Banks are not covered in the spring as well as fall above the Labrador Shelf as these are locations with less than one month of data contributing across the 5-year data period (Figure 4).

Table 1. Contributing months* to each of the five years of data for the primary production dataset.

Season	Month	2006	2007	2008	2009	2010	Total number of years
	January	√	√		√	√	4
	February	√	√		√	√	4
	March	√	√		√	√	4
	April	√	√	√	√	√	5
Spring	May	√	√	√		√	4
	June	√	√	√	√	√	5
Summer	July	√	√		√	√	4
	August	√	√	√	√	√	5
	September	√	√	√		√	4
Fall	October	√	√	√		√	4
	November	√		√	√	√	4
	December			√	√	√	3

*The √ indicates that data exists for this month. Note that even though data exists for a particular month, each point location across the full Newfoundland and Labrador Region study extent may not have observation data.

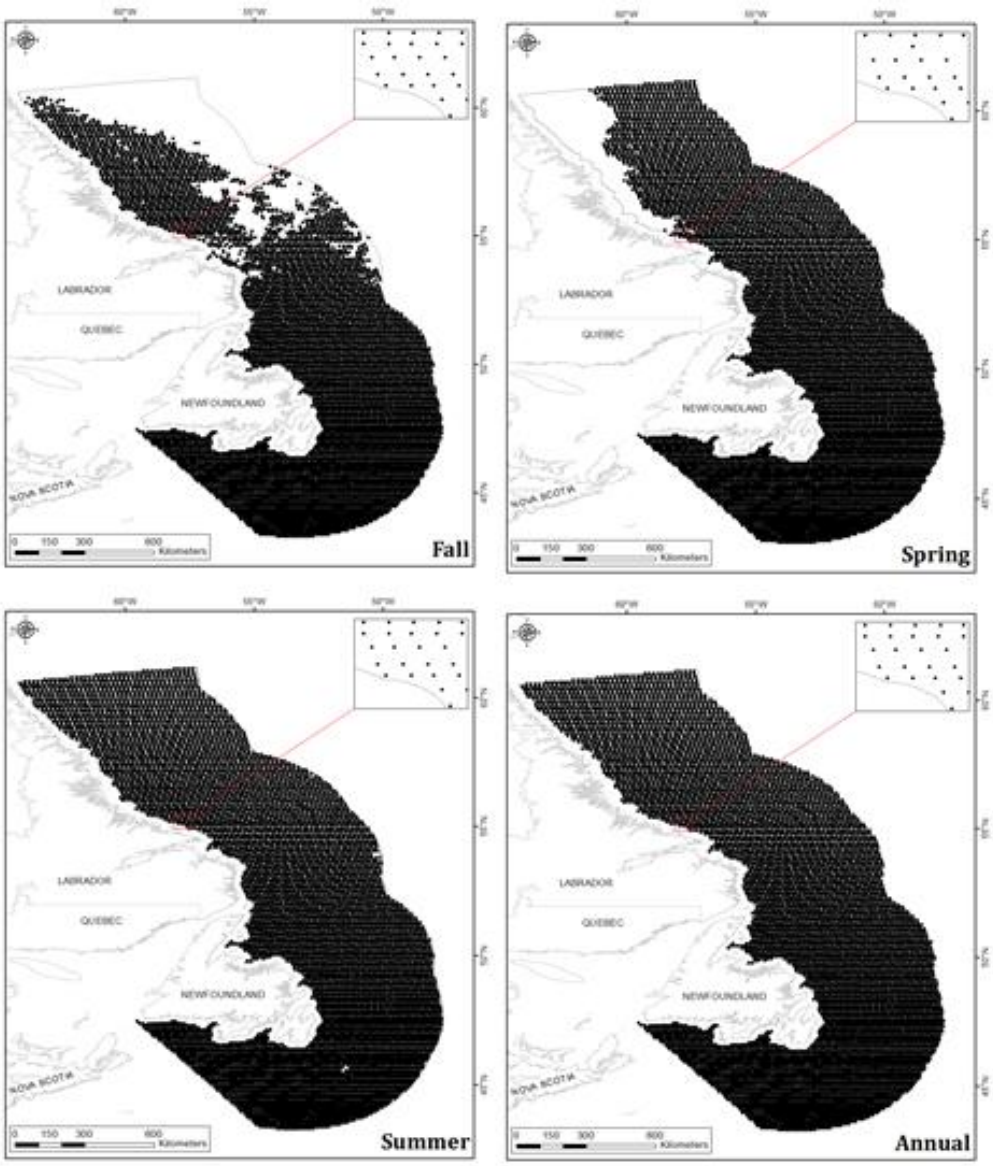

Figure 4. Distribution of fall, spring, summer, and annual primary production point data from 2006 to 2010 for the Newfoundland and Labrador Region. Point data have a native resolution of 9 km.

World Ocean Database 2013 (WOD13)

Dissolved oxygen and nutrients (phosphate and silicate) were extracted from the World Ocean Database 2013 (WOD13) (https://www.nodc.noaa.gov/OC5/WOD13/; Boyer et al., 2013) produced by the US National Oceanographic Data Center (NODC) Ocean Climate Laboratory (OCL). WOD13 houses ocean profile and plankton measurement data submitted by individual scientists and institutional, national, and regional data centres with the goal of providing a centralized source for large-scale oceanographic data and metadata that has been formatted in a similar way. Data in WOD13 are organized under four different operational definitions: profile, cast, station, and cruise. Each data value and profile in WOD13 are associated with their own

quality control flag. Data collected in a similar manner are further grouped together into 11 different datasets.

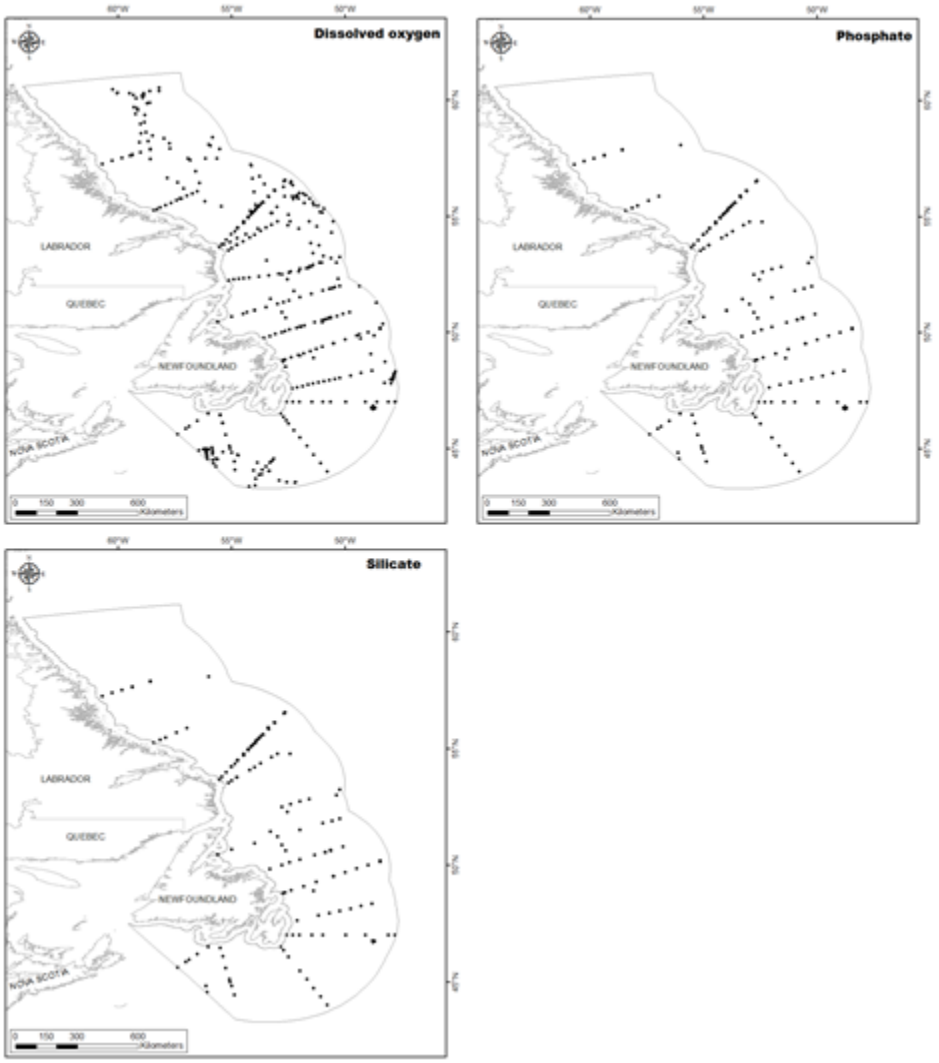

Figure 5. Distribution of dissolved oxygen, phosphate, and silicate point data from 2006 to 2011 extracted from WOD13 for the Newfoundland and Labrador Region. The spatial distribution of the data is not uniform across the study extent.

The data were queried from the WODselect retrieval system using user-specified search criteria under the following four categories: geographic coordinates, observation dates, dataset, and measured variables. Nutrient data were queried from the Ocean Station Data (OSD) dataset from the period of 2006 to 2011. The OSD dataset groups together bottle (Nansen and Niskin) and bucket data, plankton data, and low resolution CTD and expendable CTD (XCTD) data, and is the only dataset in WOD13 that contains nutrient data. Only data collected within the top 10 metres of water and with the highest quality control flag ('Accepted') were used. Data records for individual nutrients showed poor coverage over the Newfoundland and Labrador Region (see Figure 5). Nitrate data were also downloaded but were insufficient for spatial interpolation. In

the event where more than one value was measured at a single location, the data values were averaged.

Spatial Interpolation Methods

Data Exploration and Model Fitting (adapted from Beazley et al. 2016c)

Kriging is a family of geostatistical estimators used to interpolate spatial data. It is a generalized least-square regression technique that allows for spatial prediction in unsampled locations by accounting for the spatial dependence between observed data (Goovaerts 2000). Spatial dependence is captured by constructing an empirical semivariogram that shows the average semivariance between points by the distance between them. A semivariogram model is then fit to the points forming the empirical semivariogram, and predictions are generated for unmeasured locations based on a weighted average of neighbouring data and their spatial arrangement (Johnston et al. 2001).

Within the kriging family a number of different methods exist including but not limited to, ordinary kriging, universal kriging, and simple kriging. For this report, we chose ordinary kriging as the method of spatial interpolation as it assumes that the mean is unknown prior to modelling and approximately constant (stationary) only in the local neighbourhood of each estimation point and not over the entire data domain (Li and Heap 2008, Krivoruchko 2011). Thus ordinary kriging with a local search neighbourhood already accounts for trends in the data (Li and Heap 2008). When compared against the Inverse Distance Weighting (IDW) interpolation method, ordinary kriging produced better overall mean prediction and root-mean-square errors and smoother prediction surfaces for the same variables interpolated in the Gulf Region (see Beazley et al. 2016c).

Ordinary kriging as a geostatistical interpolator does not require the data to follow a normal distribution (Krivoruchko 2011). However, the generation of quantile and probability maps using ordinary kriging does require the data to meet this assumption (Krivoruchko 2011). Transformation of highly skewed data prior to ordinary kriging may result in improved estimates and prediction errors, particularly if the dataset is small and contains outliers (Kravchenko and Bullock, 1999). If a variable shows positive skewness, the confidence limits on the variogram are wider than normal resulting in higher variance (Robinson and Metternicht 2006, Yamamoto 2007). Thus, data are often transformed prior to spatial interpolation in order to improve the calculation of statistics and weighted averages (Yamamoto 2007). Transformation of the data results in estimates on a different scale than the original data, and so it is necessary to back-transform the kriging estimates to their original scale prior to creating the interpolation surface. However, for logarithmic transformation, back-transformation through exponentiation results in exaggerated interpolation-related errors, with extreme errors being the worst affected (Goovaerts 1997, Robinson and Metternicht 2006). In the Gulf Region, variables that had been back-transformed within the Geostatistical Analyst package had poorer prediction errors when compared to variables that were log-transformed outside the ArcMap forum (and thus, were not back-transformed in ArcMap) (Beazley et al. 2016c). Therefore, to avoid biased prediction errors, we chose not to transform our data prior to spatial interpolation.

Prior to interpolation we assessed the distributional properties of all variables by examining histograms and summary statistics generated in the 'Explore Data' option in ArcMap's Geostatistical Analyst package. These were reviewed to detect anomalous data points and to visually assess departures from a normal distribution (skewness, kurtosis) in advance of conducting geostatistics. Normal Q-Q plots were then constructed to compare the distribution of the data against a standard normal (Gaussian) distribution. The data values are ordered and cumulative distribution values are calculated as (i– 0.5)/n for the i^{th} ordered value out of n total values. If the data values are normally distributed they will form a perfect line at 45° to the origin. Data values that fell above and below the reference line were mapped to identify any spatial trend in the departure from normality.

Ordinary kriging models were created using all default settings in the Geostatistical Analyst wizard. Default settings are a stable semivariogram model type and a circular search neighbourhood with 4 sectors that capture a minimum of 2 and a maximum of 5 neighbours. The optimization function was set for each model, which determines the optimal partial sill, nugget, lag size, and number of lags based on the model range.

Caveat for Spatial Interpolation Using Ordinary Kriging

We noted that ordinary kriging of some GLORYS and chlorophyll *a* variables resulted in negative values in the prediction surfaces. This is in addition to some of the small negative values produced by the GLORYS model itself (Beazley et al., 2016c). In the Newfoundland and Labrador Region this phenomenon occurred in the following variables:

-Bottom Salinity Average Range
-Bottom Current Minimum
-Surface Current Minimum
-Surface Current Average Minimum
-Maximum Summer Mixed Layer Depth
-Bottom Shear Minimum
-Bottom Shear Average Minimum

This issue has been previously described by Deutsch (1996) and Ly et al. (2011), who found that negative weights were generated by ordinary kriging models when outlying data points occurred close to the location being estimated. Ly et al. (2011) suggested two methods for dealing with this issue: 1) apply an *a posteriori* correction as outlined in Deutsch (1996), or 2) to replace all negative interpolated values with zero. To determine the influence of these variables with negative values on a species distribution model, we ran several random forest models with these variables as-is (i.e. with the negative interpolated values), and models with the negative values changed to zero. We found very little difference in the resulting surfaces and accuracy measures between models run with the negative values and those negative values changed to zero. For example, a random forest model performed on a balanced large gorgonian presences and absences dataset (see Guijarro et al., 2016a) and in which Bottom Salinity Average Range was the top predictor, changing the negative values to zero and re-running the model resulted in a

similar prediction surface and AUC values compared to the original model (mean AUC = 0.807 in model with negative values changed to zero; mean AUC = 0.811 in original model). We conclude that these negative values have a negligible impact on species distribution modelling applications. The location of negative values in the prediction surface of each variable are shown in Appendix I.

Assessment of Model Performance (extracted from Beazley et al. 2016c)

Model performance was examined by performing cross-validation, a process where each data point is removed in turn from the model and predicted by the remaining data points. Geostatistical Analyst provides several graphical summaries of the cross validation results, including a scatterplot of the measured versus predicted values (called the Prediction plot), a scatterplot of the residuals of the measured values versus the predicted values (Error plot), a standardized error plot, which shows measured values subtracted from the predicted values and divided by the estimated kriging standard errors, and finally a Q-Q plot, which shows the quantiles of the difference between the predicted and measured values and the corresponding quantiles from a standard normal distribution to assess the normality of the error distributions. Of these, we show only the Prediction plot in the report, although all plots were visually assessed. In the Prediction plot, a horizontal relationship indicates that the model has no information content. With autocorrelation and a good geostatistical model, the relationship between the measured and predicted values should be 1:1.

Also provided by cross validation are five prediction error statistics used for performance evaluation (see Table 2). The overall mean error represents the difference between the measured and predicted values, and should be near zero if the prediction errors are unbiased (i.e., centred on the measured values). However, this value depends on the scale and units of the data, therefore it is better to assess the standardized prediction errors, which are given as prediction errors divided by their prediction standard errors. The mean (standardized mean) of these should also be near zero. If the average standard error is close to the root mean square prediction error, variability in the predictions has been correctly assessed. The root mean square standardized error should be close to one. If the average standard error is greater than the root mean square prediction error, or if the standardized root mean square prediction error is less than one, then the variability of predictions has been overestimated. If the average standard error is less than the root mean square prediction error or if the standardized root mean square prediction error is greater than one, then the variability of predictions has been underestimated. In summary, a good geostatistical model has an overall mean and standardized mean near zero, a small root mean square prediction error that is approximately equal to the average standard error, an average standard error approximately equal to the root mean square prediction error, and a standardized root mean square prediction error close to one (Johnston et al. 2001). These five prediction error statistics are provided for each variable and are assessed against the rules in Table 2 to provide an overall assessment of model performance.

Table 2. Prediction error statistics rules used to assess performance of ordinary kriging models.

Prediction error	Rule
Overall Mean Error	Close to 0
Root Mean Square Prediction Error	Close to 0 and approximately equal to the average standard error
Standardized Mean	Close to 0
Standardized Root Mean Square Prediction Error	Close to 1
Average Standard Error	Approximately equal to the root mean square prediction error

Finally, model performance was assessed through visual examination of a standard error map. A standard error map quantifies the uncertainty of the prediction and is calculated by taking the square root of the kriging variances. If the data comes from a normal distribution, the true value will be within ± 2 times the prediction standard errors about 95% of the time (Johnston et al. 2001). These maps were used to determine whether there was any spatial pattern in the error distribution.

During the assessment of model performance, we noted that data with a poor underlying distribution did not always result in poor cross validation statistics during the interpolation process. For instance, ordinary kriging on some variables displaying a bimodal distribution (e.g., Bottom Temperature Mean in Beazley et al. 2016c) produced a good fit between measured and predicted values and good to excellent cross validation statistics, suggesting the ordinary kriging is robust to non-normality. Similarly, a model displaying a good fit between measured and predicted values often showed poor cross validation statistics, particularly a higher-than-expected standardized root mean square error, indicating that variability in the predictions has been underestimated.

Report Layout

For each of the 104 environmental variables described in this report, we show the distributional properties of the raw data prior to spatial interpolation, the model semivariogram and Prediction plot, the five prediction error statistics for model assessment, and finally a map of the prediction standard error and interpolation prediction surfaces. We give an assessment of how well the ordinary kriging model interpolated the variable based on the five prediction error statistics, and comment on the spatial distribution of error (if any) in the final prediction surface.

RESULTS

Temperature

Both surface and bottom temperatures have biological relevance to benthic invertebrates. Temperature directly influences the rates of activities associated with feeding such as pumping, filtration and digestion, movement, and growth. Temperature can also influence larval duration and timing of metamorphosis (Vance 1973). Surface water temperature can influence primary and secondary production and hence benthic food supply. Temperature, along with salinity, can be used to indicate water mass structure.

Bottom Temperature Mean

This variable displayed a bimodal distribution prior to modeling (Table 3, Figure 6). At both of the tails and mid-range the actual data were greater than predicted by a normal distribution while the upper mid-range of the data was under-predicted (Figure 7). These areas of under- and over-prediction showed spatial bias over the region (Figure 7).

The semivariogram showed autocorrelation present in the data and the kriged model showed good fit between measured and predicted values (Figure 8). The model showed good cross-validation statistics (Table 4) indicating that the model was good at prediction. The error map showed a 'bullseye' pattern with error increasing with distance from data points (Figure 9). The kriged surface is presented in Figure 9.

Table 3. Distributional properties of Bottom Temperature Mean (°C).

Property	Value
Number of Observations	2975
Minimum	-0.702
Maximum	8.337
Mean	2.306
Median	2.508
Standard Deviation	1.408
Skewness	0.104
Kurtosis	3.878

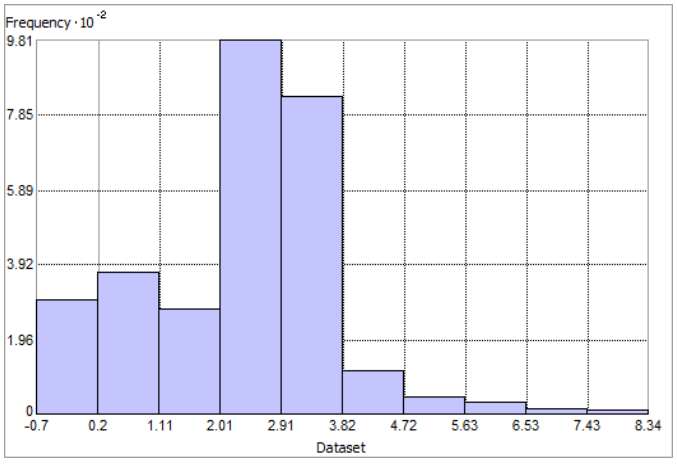

Figure 6. Distribution of Bottom Temperature Mean (°C). Histogram was illustrated using 10 bins. Y axis is shown at 10^{-2}.

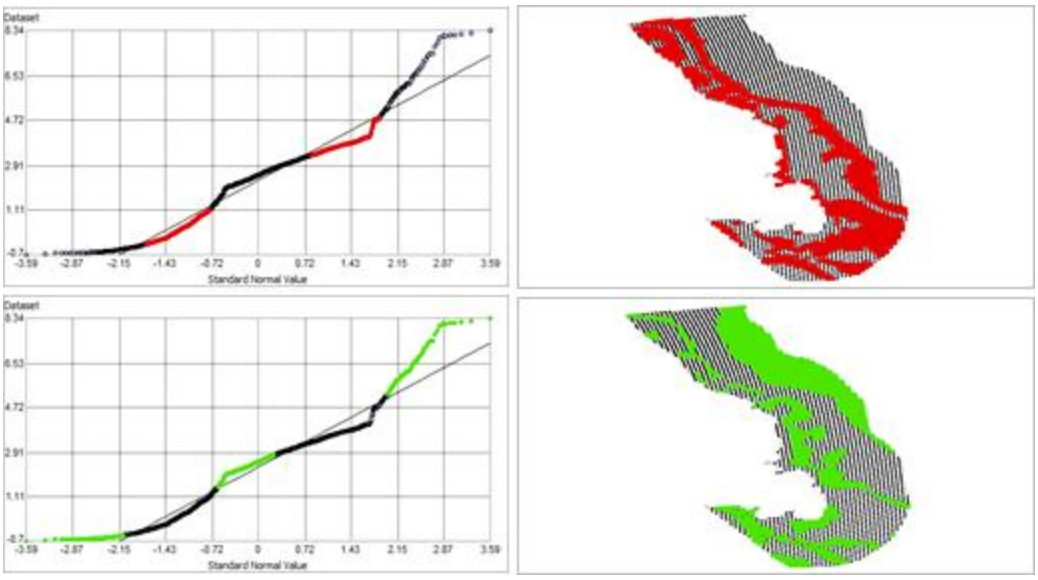

Figure 7. Normal Q-Q plot for data values of Bottom Temperature Mean (°C). Points falling under (top right panel) and over (bottom right panel) the reference line are mapped.

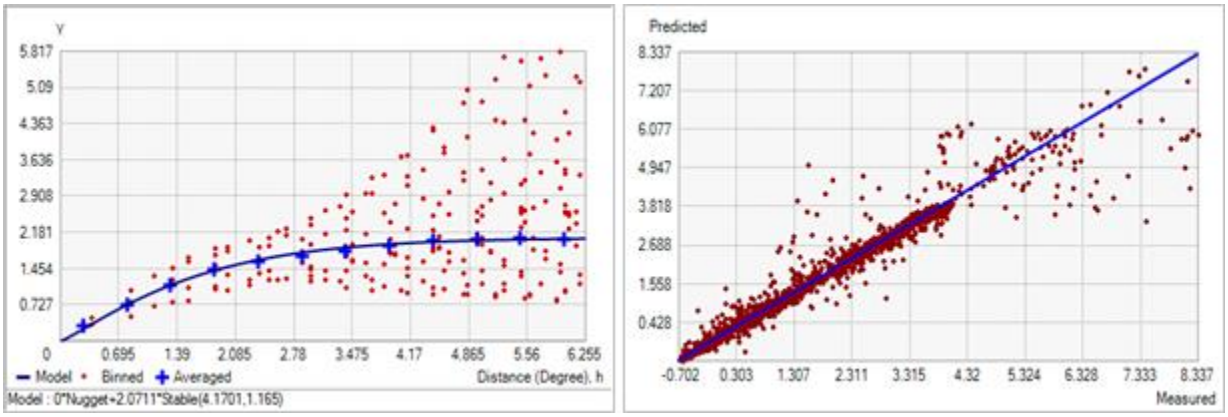

Figure 8. Left panel: Semivariogram of Bottom Temperature Mean (°C). Binned values are shown as red dots; average points are shown as blue crosses; the model fit to the averaged values is shown as a blue line. Lag size: 0.521 degrees; number of lags: 12; Parameter: 1.165; Range: 4.170 degrees; Partial Sill: 2.071. Right panel: Scatterplot of predicted values versus observed values for the model of Bottom Temperature Mean (°C).

Table 4. Results of cross-validation of the kriged model for Bottom Temperature Mean (°C).

Prediction error	**Value**
Number of Observations	2975
Overall Mean Error	5.638×10^{-4}
Root Mean Square Prediction Error	0.333
Standardized Mean	1.070×10^{-3}
Standardized Root Mean Square Prediction Error	0.958
Average Standard Error	0.337

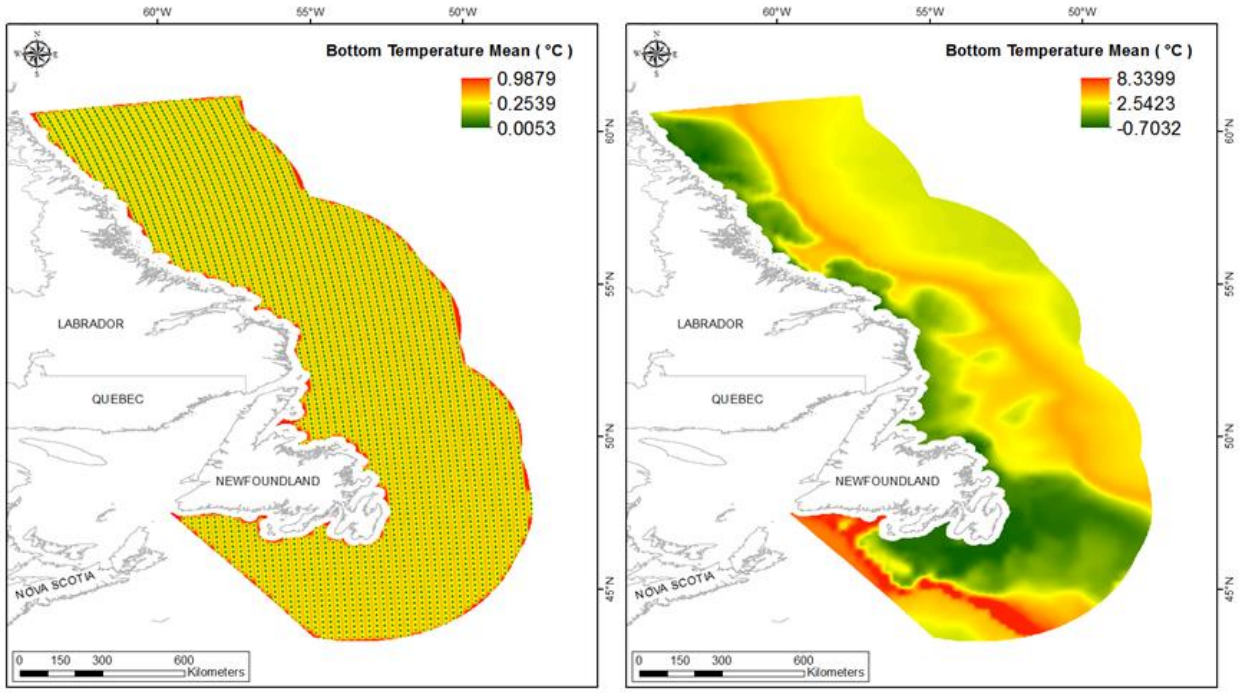

Figure 9. Left panel: Prediction standard error surface of Bottom Temperature Mean (˚C). Right panel: Interpolated prediction surface of Bottom Temperature Mean (˚C).

Bottom Temperature Minimum

This variable displayed a bimodal distribution prior to modeling (Table 5, Figure 10). The data were greater than predicted by a normal distribution at the smallest and mid-values and less than predicted at the highest and low mid-values (Figure 11). These areas of under- and over-prediction showed little spatial pattern over the region (Figure 11).

The semivariogram showed autocorrelation present in the data and the kriged model showed good fit between measured and predicted values (Figure 12). The model showed good cross-validation statistics (Table 6) indicating that the model was good at prediction despite the distribution of the underlying data. The error map showed a 'bullseye' pattern with error

increasing with distance from data points (Figure 13). The kriged surface is presented in Figure 13.

Table 5. Distributional properties of Bottom Temperature Minimum (°C).

Property	Value
Number of Observations	2975
Minimum	-2.419
Maximum	4.922
Mean	0.951
Median	1.698
Standard Deviation	1.592
Skewness	-0.406
Kurtosis	1.750

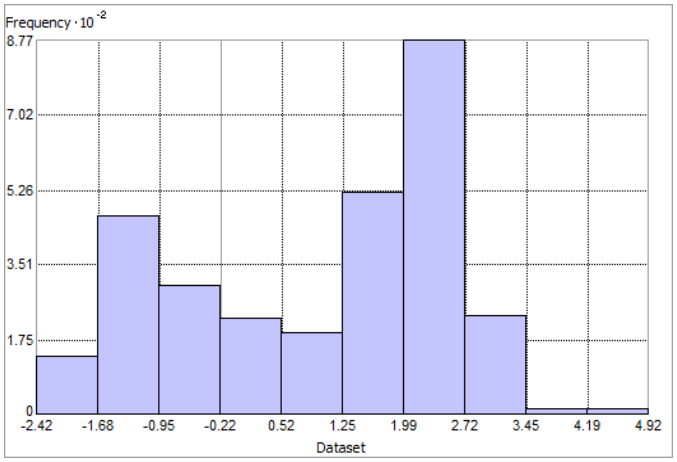

Figure 10. Distribution of Bottom Temperature Minimum (°C). Histogram was illustrated using 10 bins. Y axis is shown at 10^{-2}.

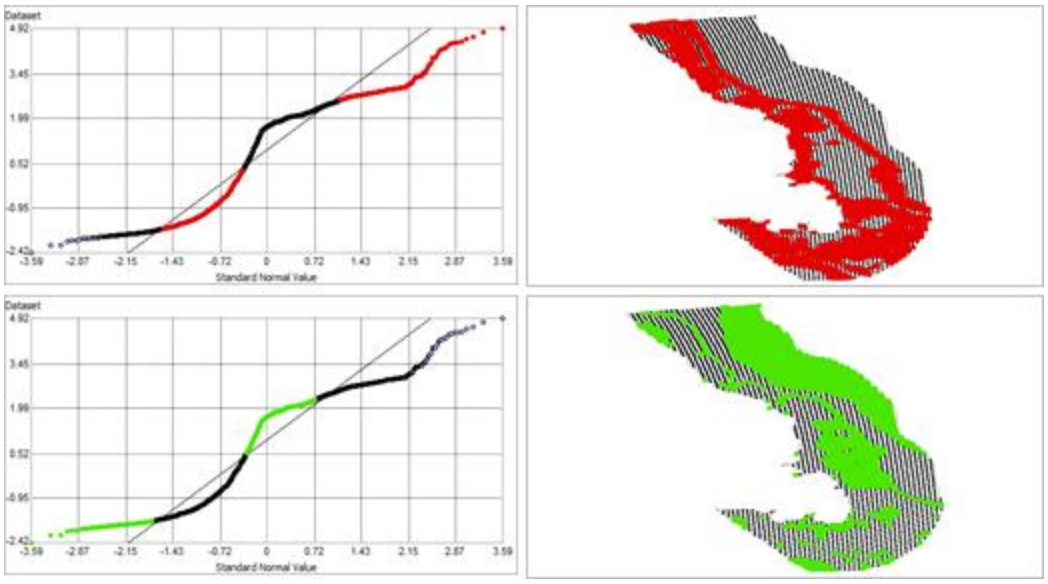

Figure 11. Normal Q-Q plot for data values of Bottom Temperature Minimum (°C). Points falling under (upper panel) and over (bottom panel) the reference line are mapped.

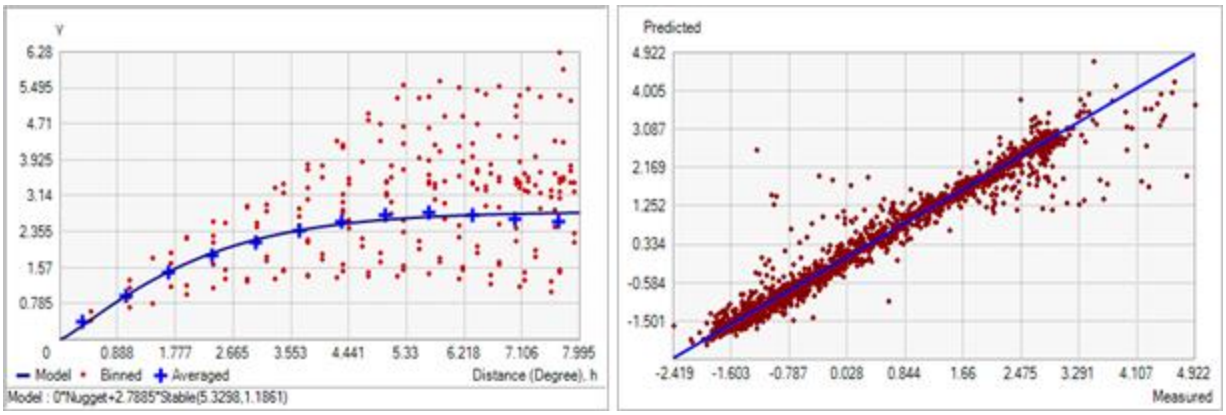

Figure 12. Left panel: Semivariogram of Bottom Temperature Minimum (°C). Binned values are shown as red dots; average points are shown as blue crosses; the model fit to the averaged values is shown as a blue line. Lag size: 0.666 degrees; number of lags: 12; Parameter: 1.186; Range: 5.330 degrees; Partial Sill: 2.788. Right panel: Scatterplot of predicted values versus observed values for the model of Bottom Temperature Minimum (°C).

Table 6**.** Results of cross-validation of the kriged model of Bottom Temperature Minimum (°C).

Prediction error	**Value**
Number of Observations	2975
Overall Mean Error	-3.856×10^{-5}
Root Mean Square Prediction Error	0.276
Standardized Mean	3.032×10^{-4}
Standardized Root Mean Square Prediction Error	0.834
Average Standard Error	0.323

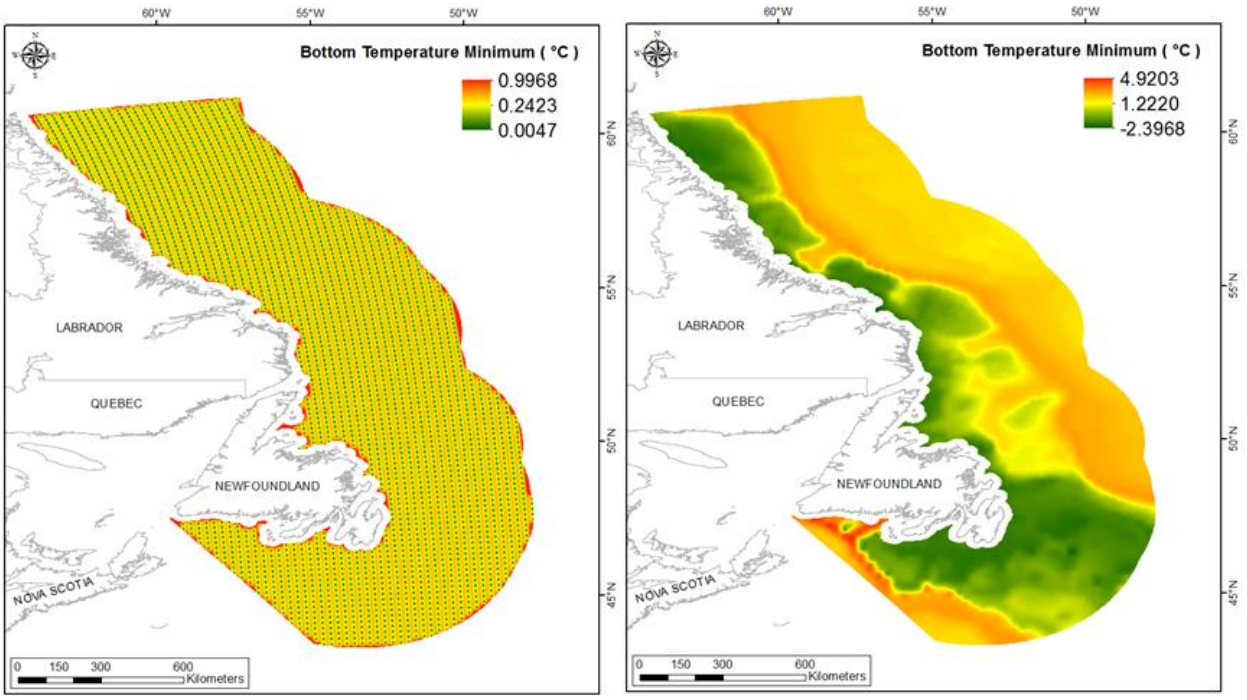

Figure 13. Left panel: Prediction standard error surface of Bottom Temperature Minimum (˚C). Right panel: Interpolated prediction surface of Bottom Temperature Minimum (˚C).

Bottom Temperature Maximum

This variable displayed a right-skewed distribution with kurtosis prior to modeling (Table 7, Figure 14). At both of the tails the actual data were greater than predicted by a normal distribution while the mid-range of the data was under-predicted (Figure 15). These data points were somewhat spatially cohesive with specific areas of over- and under-prediction (Figure 15).

The semivariogram showed autocorrelation present in the data and the kriged model showed a good fit between measured and predicted values (Figure 16). The model showed good cross-validation statistics (Table 8) indicating that it was good at prediction. The error map showed a 'bullseye' pattern with error increasing with distance from data points (Figure 17). The kriged surface is presented in Figure 17.

Table 7. Distributional properties of Bottom Temperature Maximum (°C).

Property	Value
Number of Observations	2975
Minimum	0.612
Maximum	13.154
Mean	3.779
Median	3.433
Standard Deviation	1.673
Skewness	2.109
Kurtosis	9.496

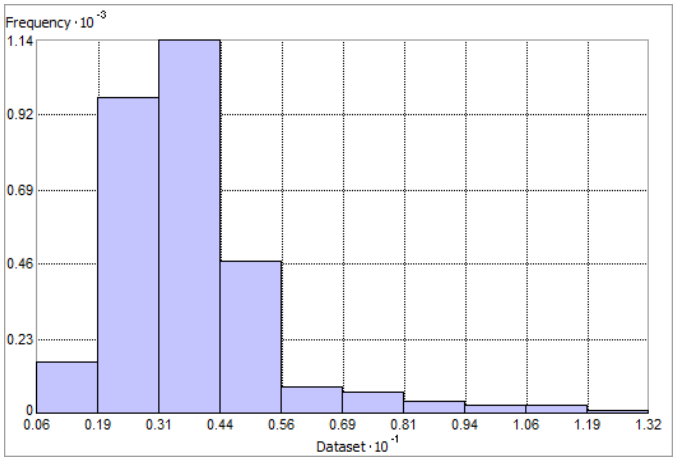

Figure 14. Distribution of Bottom Temperature Maximum (°C). Histogram was illustrated using 10 bins. X axis is shown at 10^{-1}; Y axis is shown at 10^{-3}.

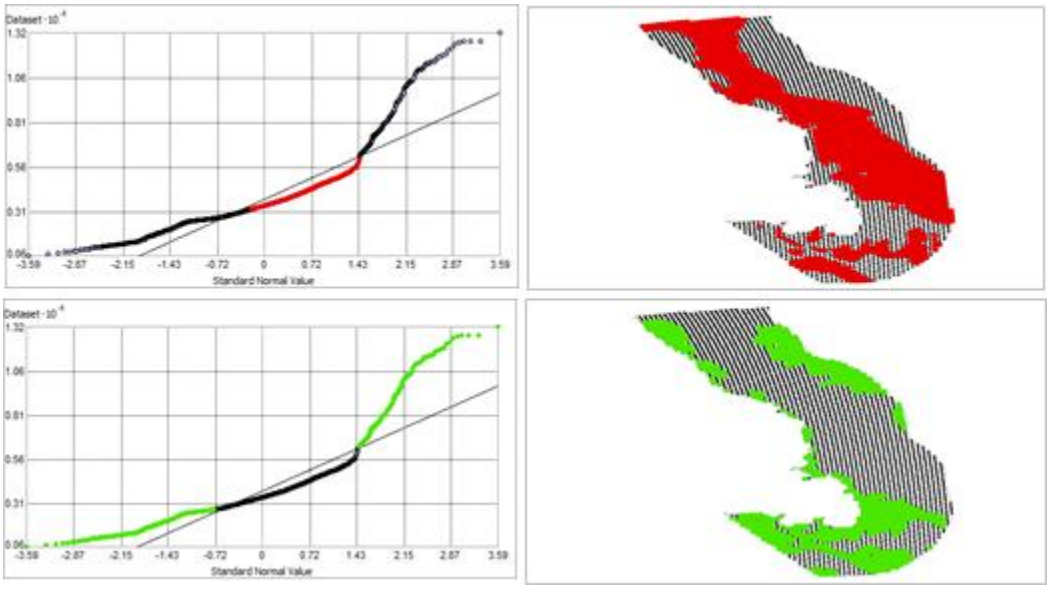

Figure 15. Normal Q-Q plot for data values of Bottom Temperature Maximum (°C). Points falling under (upper panel) and over (bottom panel) the reference line are mapped.

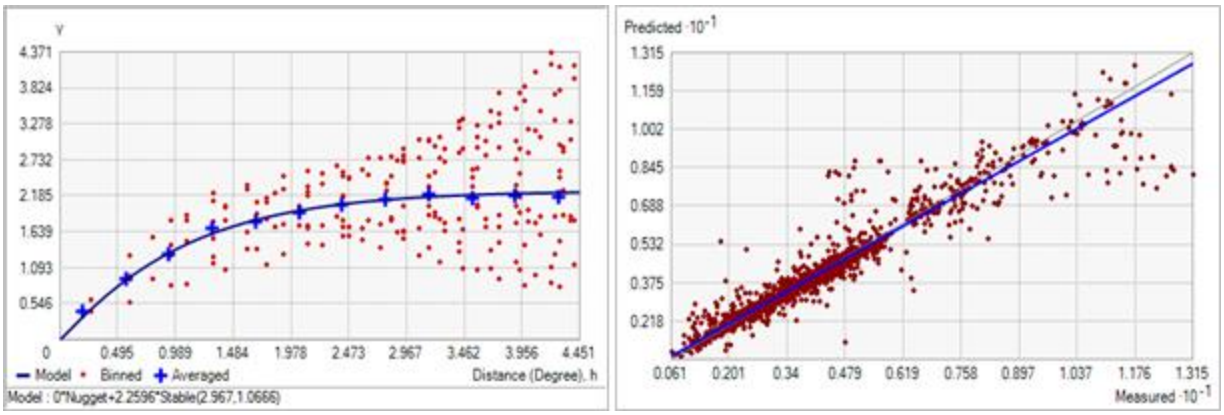

Figure 16. Left panel: Semivariogram of Bottom Temperature Maximum (°C). Binned values are shown as red dots; average points are shown as blue crosses; the model fit to the averaged values is shown as a blue line. Lag size: 0.371 degrees; number of lags: 12; Parameter: 1.067; Range: 2.967 degrees; Partial Sill: 2.260. Right panel: Scatterplot of predicted values versus observed values for the model of Bottom Temperature Maximum (°C).

Table 8. Results of cross-validation of the kriged model of Bottom Temperature Maximum (°C).

Prediction error	**Value**
Number of Observations	2975
Overall Mean Error	6.975×10^{-4}
Root Mean Square Prediction Error	0.482
Standardized Mean	8.945×10^{-4}
Standardized Root Mean Square Prediction Error	0.899
Average Standard Error	0.514

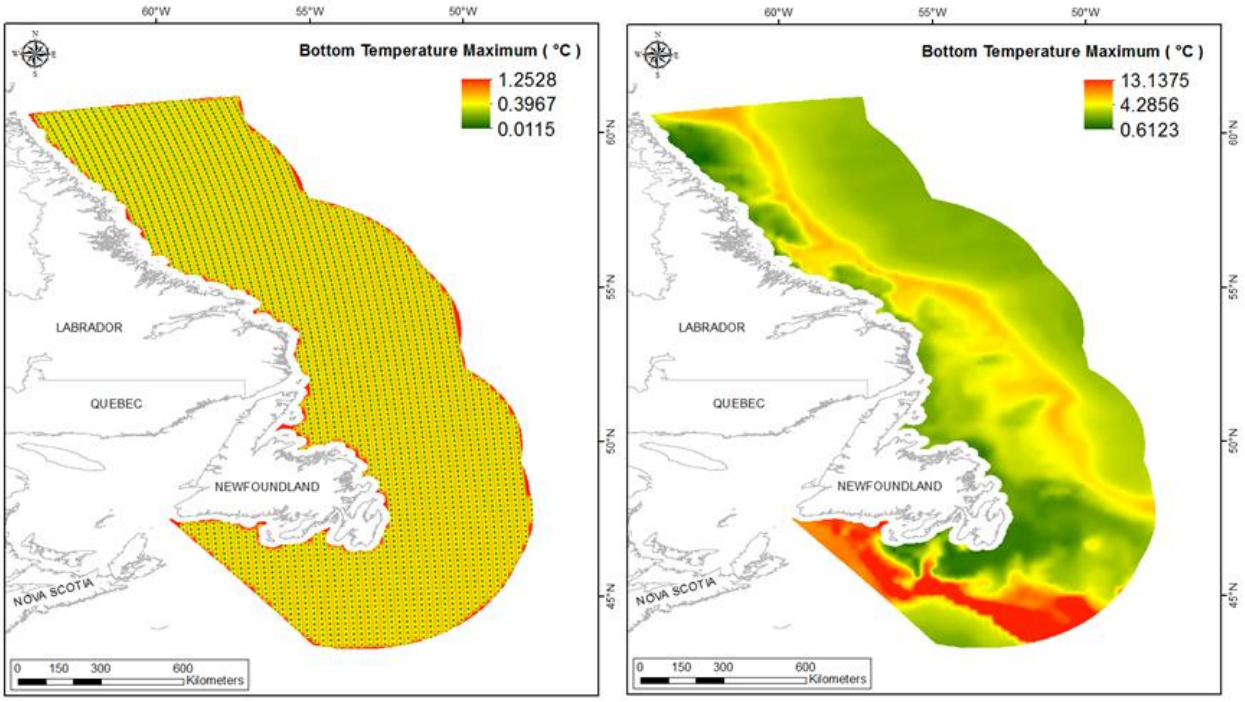

Figure 17. Left panel: Prediction standard error surface of Bottom Temperature Maximum (˚C). Right panel: Interpolated prediction surface of Bottom Temperature Maximum (˚C).

Bottom Temperature Range

This variable displayed a right-skewed distribution with kurtosis prior to modeling (Table 9, Figure 18). At both of the tails the actual data were greater than predicted by a normal distribution while there was an area of under-prediction at mid-range values (Figure 19). The areas of under- and over-prediction showed a spatial pattern over the spatial extent (Figure 19).

The semivariogram showed moderate autocorrelation present in the data and the kriged model showed good fit between measured and predicted values (Figure 20). The model showed fair cross-validation statistics (Table 10). The standardized root mean square was greater than 1 indicating that variability in the predictions has been underestimated. The error map showed low error and no strong spatial pattern over the spatial extent although error was highest along the edges of the study extent (Figure 21). The kriged surface is presented in Figure 21.

Table 9. Distributional properties of Bottom Temperature Range (°C).

Property	Value
Number of Observations	2975
Minimum	0.507
Maximum	12.463
Mean	2.828
Median	2.672
Standard Deviation	2.023
Skewness	1.464
Kurtosis	6.022

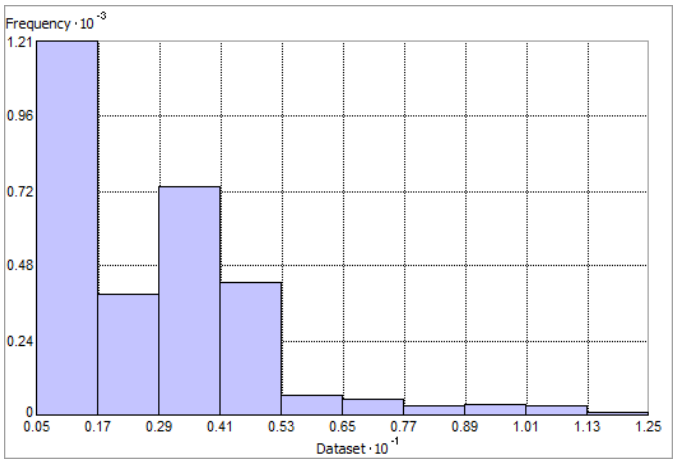

Figure 18. Distribution of Bottom Temperature Range (°C). Histogram was illustrated using 10 bins. X axis is shown at 10^{-1}; Y axis is shown at 10^{-3}.

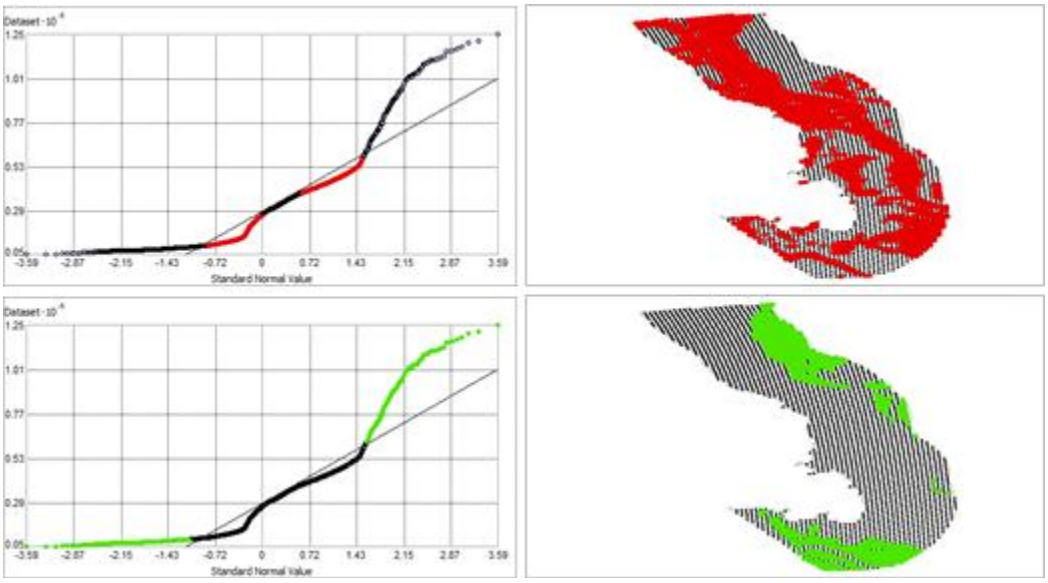

Figure 19. Normal Q-Q plot for data values of Bottom Temperature Range (°C). Points falling under (upper panel) and over (bottom panel) the reference line are mapped.

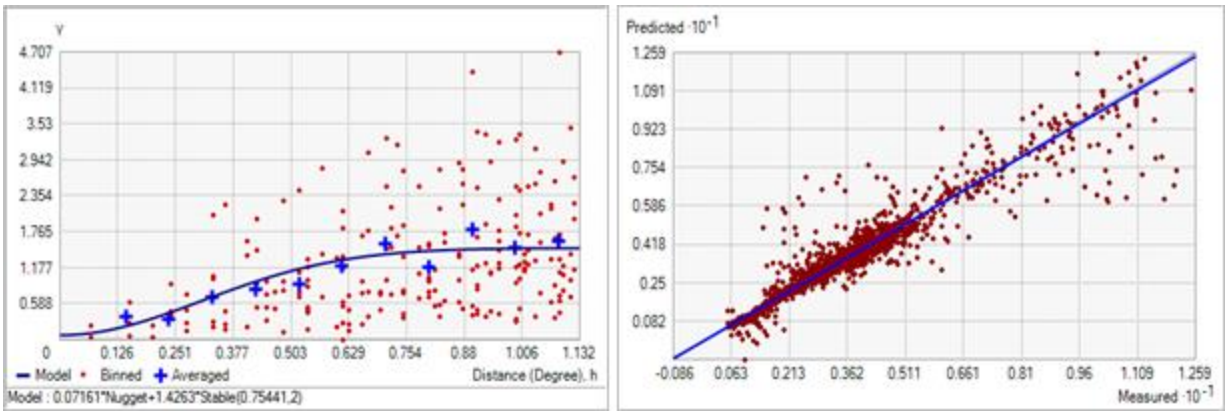

Figure 20. Left panel: Semivariogram of Bottom Temperature Range (°C). Binned values are shown as red dots; average points are shown as blue crosses; the model fit to the averaged values is shown as a blue line. Lag size: 0.094 degrees; number of lags: 12; Parameter: 2; Range: 0.754 degrees; Partial Sill: 1.426. Right panel: Scatterplot of predicted values versus observed values for the model of Bottom Temperature Range (°C).

Table 10. Results of cross-validation of the kriged model of Bottom Temperature Range (°C).

Prediction error	**Value**
Number of Observations	2975
Overall Mean Error	8.152×10^{-4}
Root Mean Square Prediction Error	0.526
Standardized Mean	1.971×10^{-3}
Standardized Root Mean Square Prediction Error	1.442
Average Standard Error	0.360

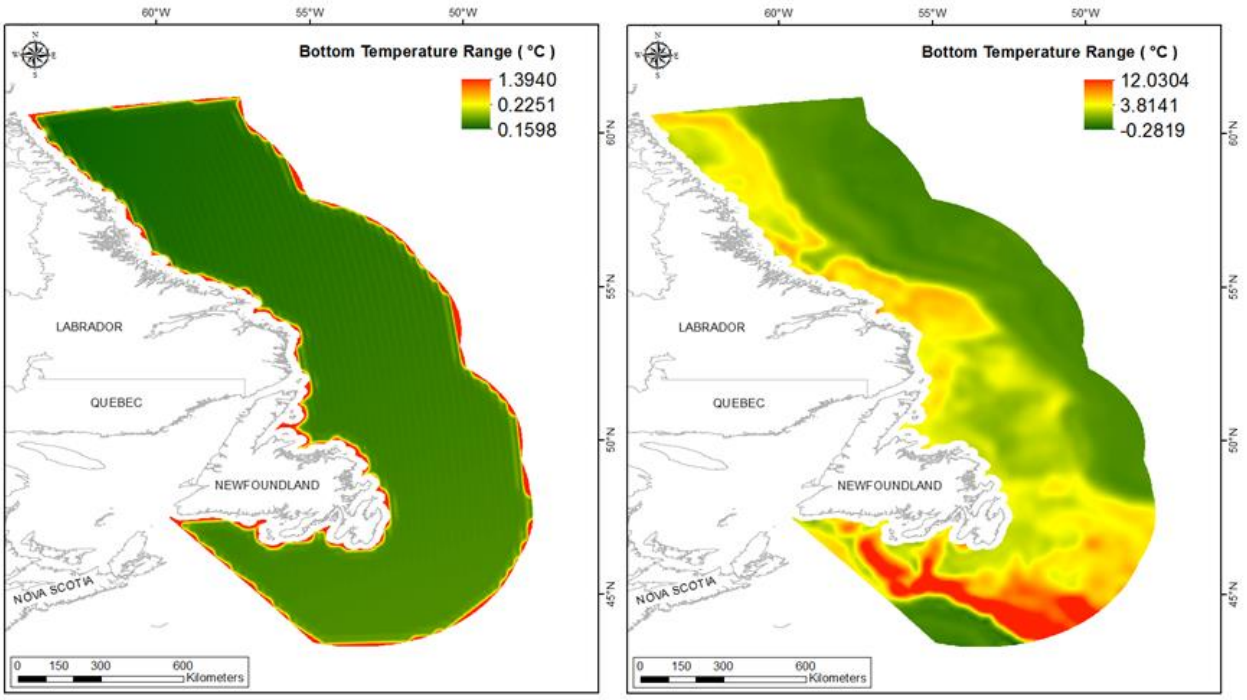

Figure 21. Left panel: Prediction standard error surface of Bottom Temperature Range (˚C). Right panel: Interpolated prediction surface of Bottom Temperature Range (˚C).

Bottom Temperature Average Minimum

This variable displayed a bimodal distribution prior to modeling (Table 11, Figure 22). The data were higher than predicted by a standard normal distribution in the lowest and mid-data range and lower than predicted at high and low values (Figure 23). These areas of under- and over-prediction showed no strong spatial pattern over the region (Figure 23).

The semivariogram showed autocorrelation present in the data and the kriged model showed good fit between measured and predicted values (Figure 24). The model showed good cross-validation statistics (Table 12) indicating that it was good at prediction. The error map showed a 'bullseye' pattern with error increasing with distance from data points (Figure 25). The kriged surface is presented in Figure 25.

Table 11. Distributional properties of Bottom Temperature Average Minimum (°C).

Property	Value
Number of Observations	2975
Minimum	-1.350
Maximum	6.333
Mean	1.769
Median	2.195
Standard Deviation	1.473
Skewness	-0.400
Kurtosis	2.320

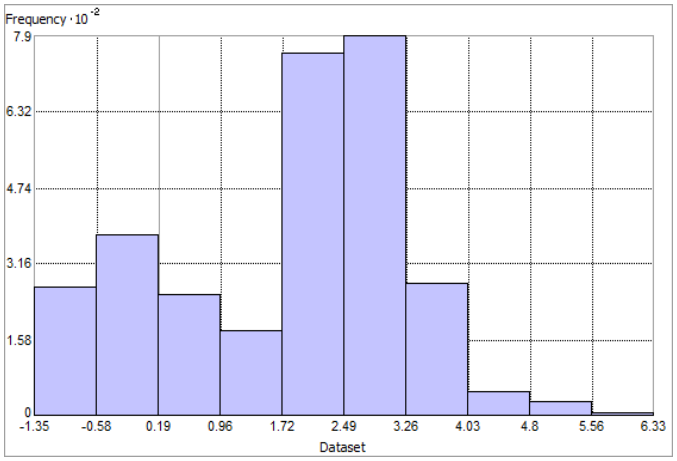

Figure 22. Distribution of Bottom Temperature Average Minimum (°C). Histogram was illustrated using 10 bins. Y axis is shown at 10^{-2}.

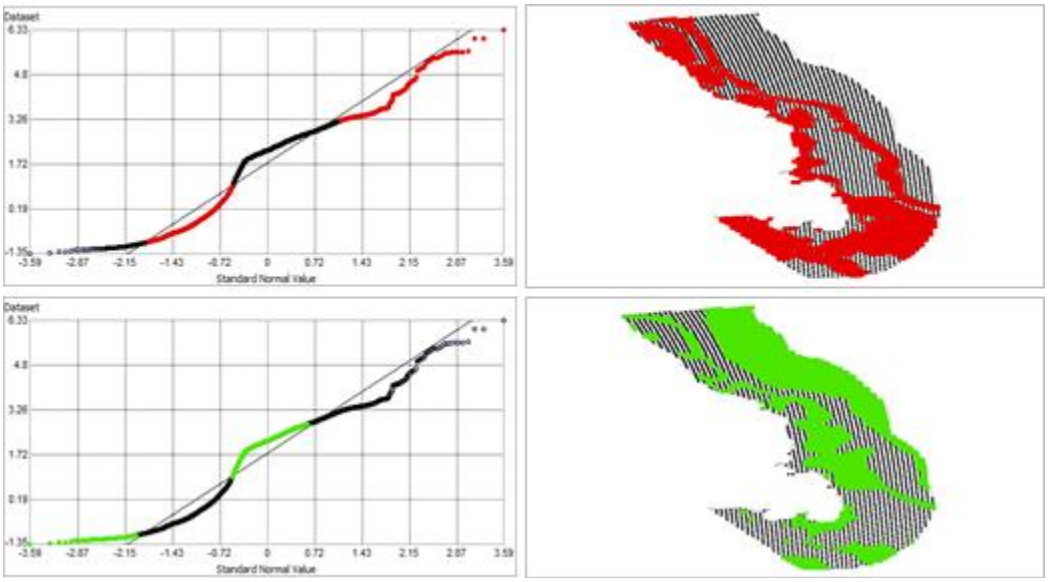

Figure 23. Normal Q-Q plot for data values of Bottom Temperature Average Minimum (°C). Points falling under (top right panel) and over (bottom right panel) the reference line are mapped.

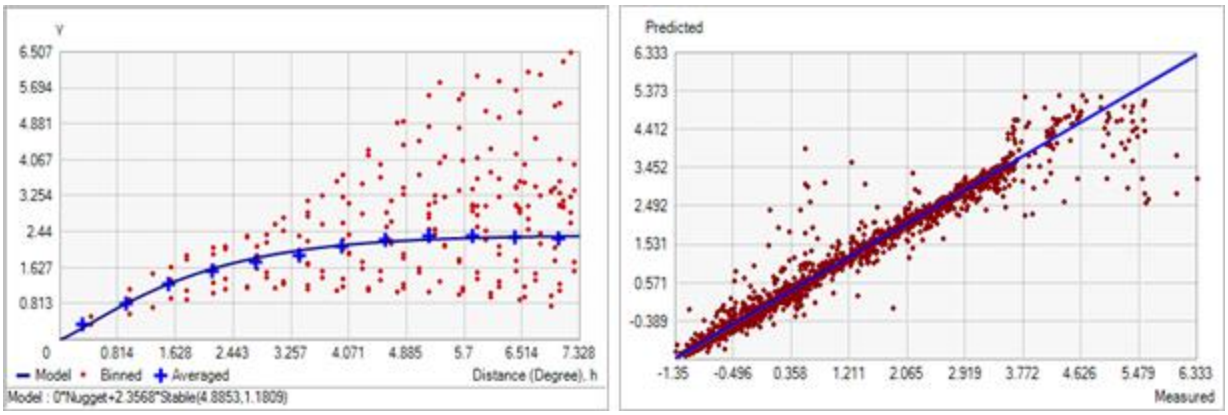

Figure 24. Left panel: Semivariogram of Bottom Temperature Average Minimum (°C). Binned values are shown as red dots; average points are shown as blue crosses; the model fit to the averaged values is shown as a blue line. Lag size: 0.611 degrees; number of lags: 12; Parameter: 1.181; Range: 4.885 degrees; Partial Sill: 2.357. Right panel: Scatterplot of predicted values versus observed values for the model of Bottom Temperature Average Minimum (°C).

Table 12. Results of cross-validation of the kriged model of Bottom Temperature Average Minimum (°C).

Prediction error	**Value**
Number of Observations	2975
Overall Mean Error	5.204×10^{-4}
Root Mean Square Prediction Error	0.286
Standardized Mean	1.069×10^{-3}
Standardized Root Mean Square Prediction Error	0.877
Average Standard Error	0.316

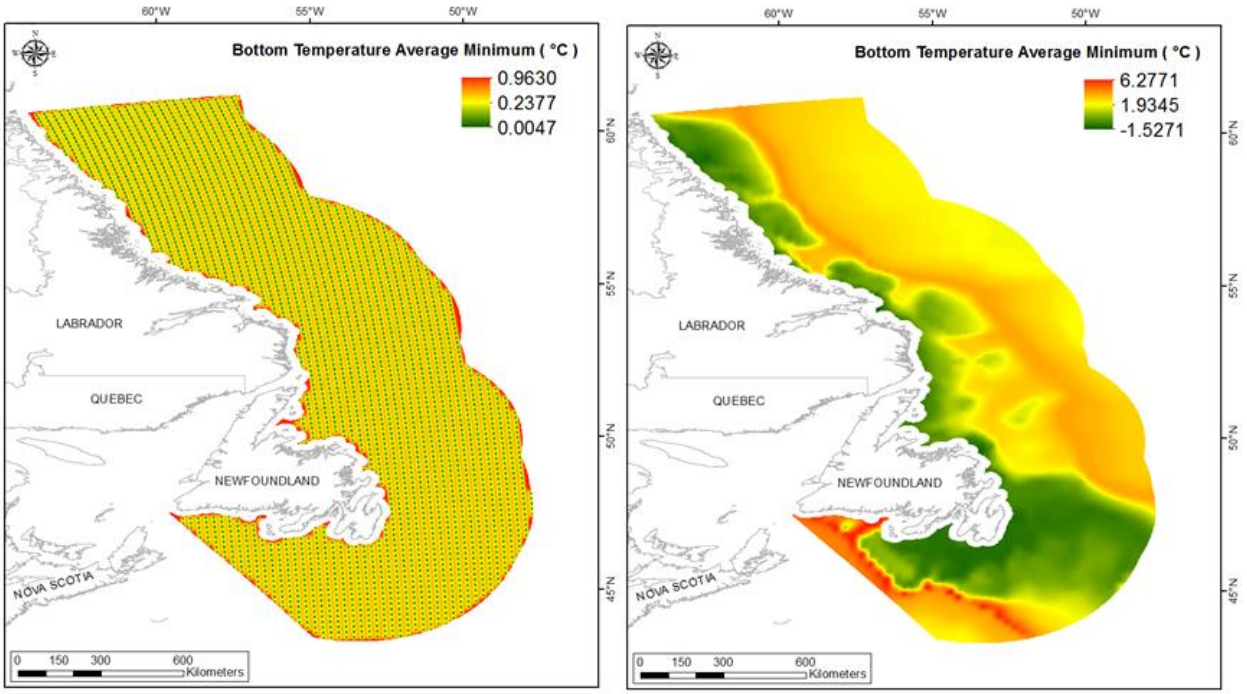

Figure 25. Left panel: Prediction standard error surface of Bottom Temperature Average Minimum (˚C). Right panel: Interpolated prediction surface of Bottom Temperature Average Minimum (˚C).

Bottom Temperature Average Maximum

This variable displayed a right-skewed distribution with kurtosis prior to modeling (Table 13, Figure 26). The data were higher than predicted by a standard normal distribution at the tails of the distribution and under-predicted through the upper-mid-range of the data (Figure 27). These data points were somewhat spatially cohesive with specific areas of over- and under-prediction (Figure 27).

The semivariogram showed autocorrelation present in the data and the kriged model showed good fit between measured and predicted values (Figure 28). The model showed good cross-validation statistics (Table 14) indicating that it was good at prediction. The error map showed a 'bullseye' pattern with error increasing with distance from data points (Figure 29). The kriged surface is presented in Figure 29.

Table 13. Distributional properties of Bottom Temperature Average Maximum (°C).

Property	Value
Number of Observations	2975
Minimum	-0.144
Maximum	10.558
Mean	2.879
Median	2.859
Standard Deviation	3.040
Skewness	2.341
Kurtosis	10.759

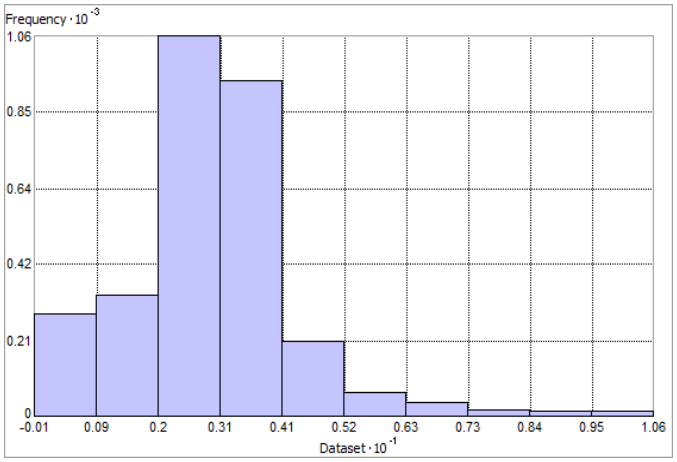

Figure 26. Distribution of Bottom Temperature Average Maximum (°C). Histogram was illustrated using 10 bins. X axis is shown at 10^{-1}. Y axis is shown at 10^{-3}.

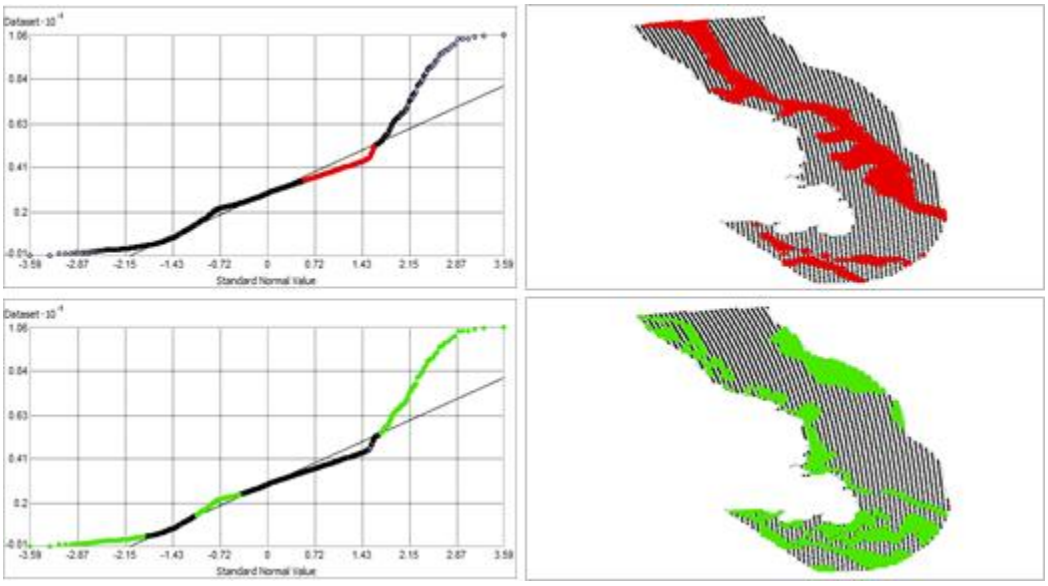

Figure 27. Normal Q-Q plot for data values of Bottom Temperature Average Maximum (°C). Points falling under (upper panel) and over (bottom panel) the reference line are mapped.

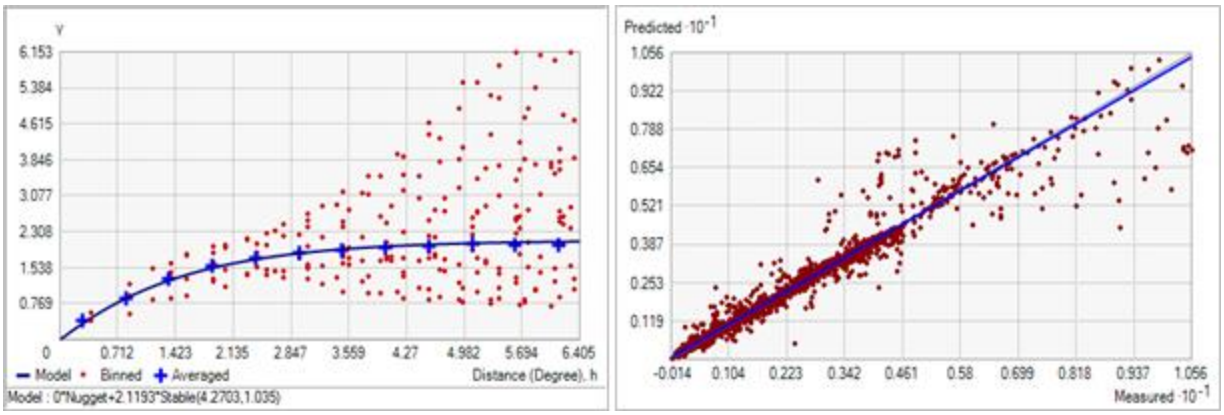

Figure 28. Left panel: Semivariogram of Bottom Temperature Average Maximum (°C). Binned values are shown as red dots; average points are shown as blue crosses; the model fit to the averaged values is shown as a blue line. Lag size: 0.534 degrees; number of lags: 12; Parameter: 1.034; Range: 4.270 degrees; Partial Sill: 2.119. Right panel: Scatterplot of predicted values versus observed values for the model of Bottom Temperature Average Maximum (°C).

Table 14. Results of cross-validation of the kriged model of Bottom Temperature Average Maximum (°C).

Prediction error	**Value**
Number of Observations	2975
Overall Mean Error	5.669×10^{-4}
Root Mean Square Prediction Error	0.387
Standardized Mean	8.436×10^{-4}
Standardized Root Mean Square Prediction Error	0.858
Average Standard Error	0.436

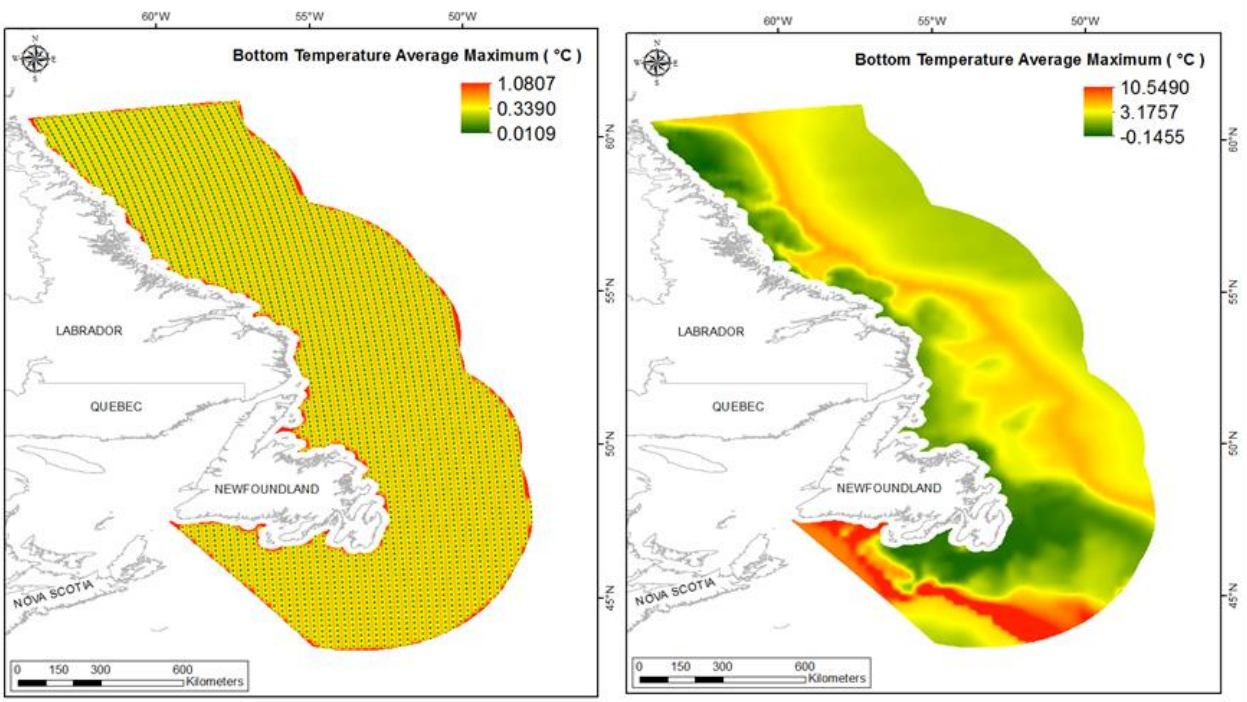

Figure 29. Left panel: Prediction standard error surface of Bottom Temperature Average Maximum (˚C). Right panel: Interpolated prediction surface of Bottom Temperature Average Maximum (˚C).

Bottom Temperature Average Range

This variable displayed a highly right-skewed distribution with kurtosis prior to modeling (Table 15, Figure 30). The data were higher than predicted by a standard normal distribution at the tails and lower than predicted through the mid-range of the data (Figure 31). The areas of under- and over-prediction showed a strong spatial pattern over the spatial extent (Figure 31).

The semivariogram showed moderate autocorrelation present in the data (Figure 32). The kriged model showed good fit between measured and predicted values. The model showed fair cross-validation statistics (Table 16). The standardized root mean square was greater than 1 indicating that variability in the predictions has been underestimated. The error map showed low error and no strong spatial pattern over the spatial extent although error was highest along the coast (Figure 33). The kriged surface is presented in Figure 33.

Table 15. Distributional properties of Bottom Temperature Average Range (°C).

Property	Value
Number of Observations	2975
Minimum	0.165
Maximum	5.820
Mean	1.110
Median	0.960
Standard Deviation	0.931
Skewness	1.972
Kurtosis	8.118

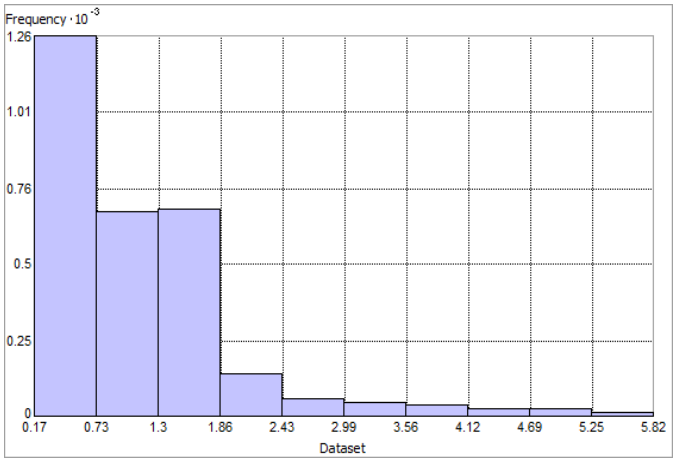

Figure 30. Distribution of Bottom Temperature Average Range (°C). Histogram was illustrated using 10 bins. Y axis is shown at 10^{-3}.

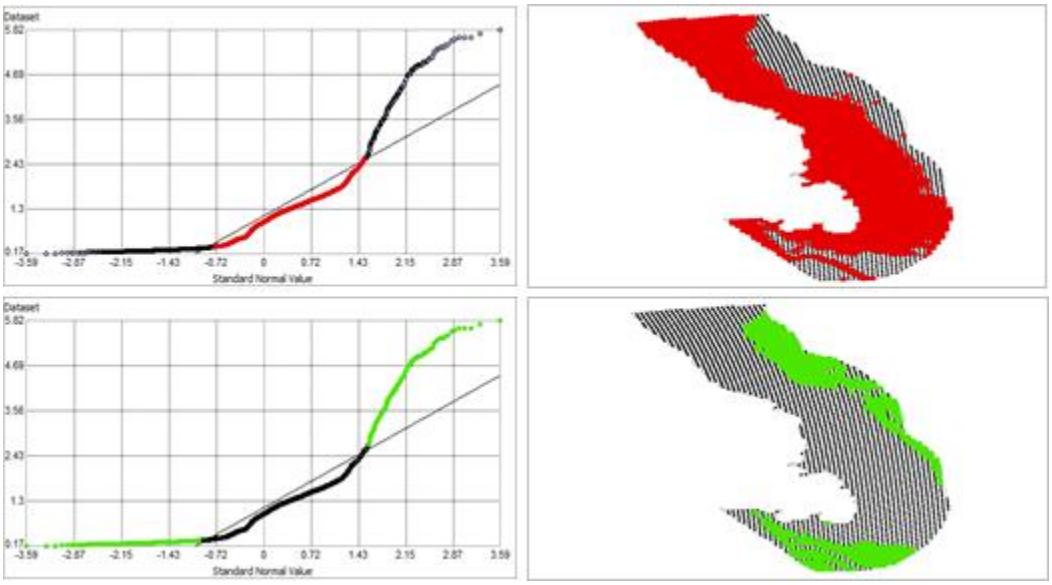

Figure 31. Normal Q-Q plot for data values of Bottom Temperature Average Range (°C). Points falling under (upper panel) and over (bottom panel) the reference line are mapped.

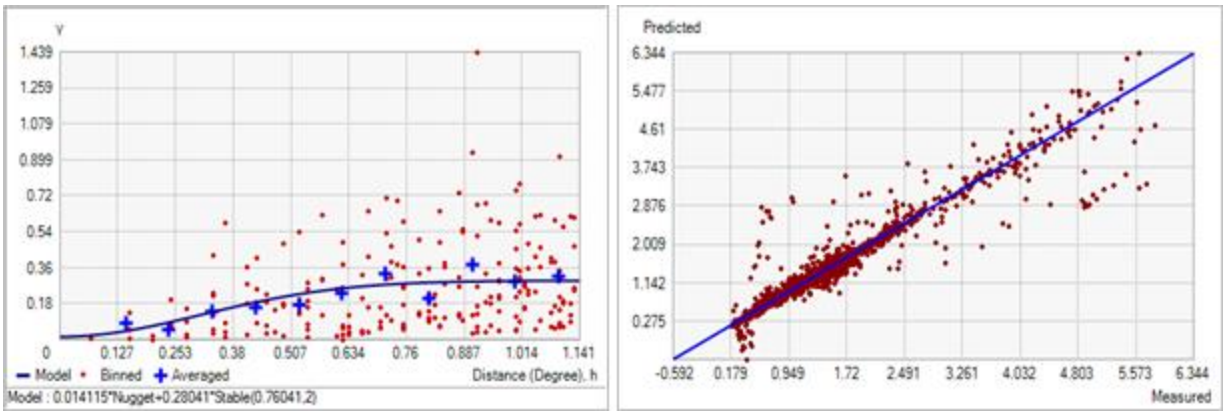

Figure 32. Left panel: Semivariogram of Bottom Temperature Average Range (°C). Binned values are shown as red dots; average points are shown as blue crosses; the model fit to the averaged values is shown as a blue line. Lag size: 0.095 degrees; number of lags: 12; Parameter: 2; Range: 0.760 degrees; Partial Sill: 0.280. Right panel: Scatterplot of predicted values versus observed values for the model of Bottom Temperature Average Range (°C).

Table 16. Results of cross-validation of the kriged model of Bottom Temperature Average Range (°C).

Prediction error	**Value**
Number of Observations	2975
Overall Mean Error	-1.461×10^{-4}
Root Mean Square Prediction Error	0.236
Standardized Mean	-3.691×10^{-6}
Standardized Root Mean Square Prediction Error	1.457
Average Standard Error	0.159

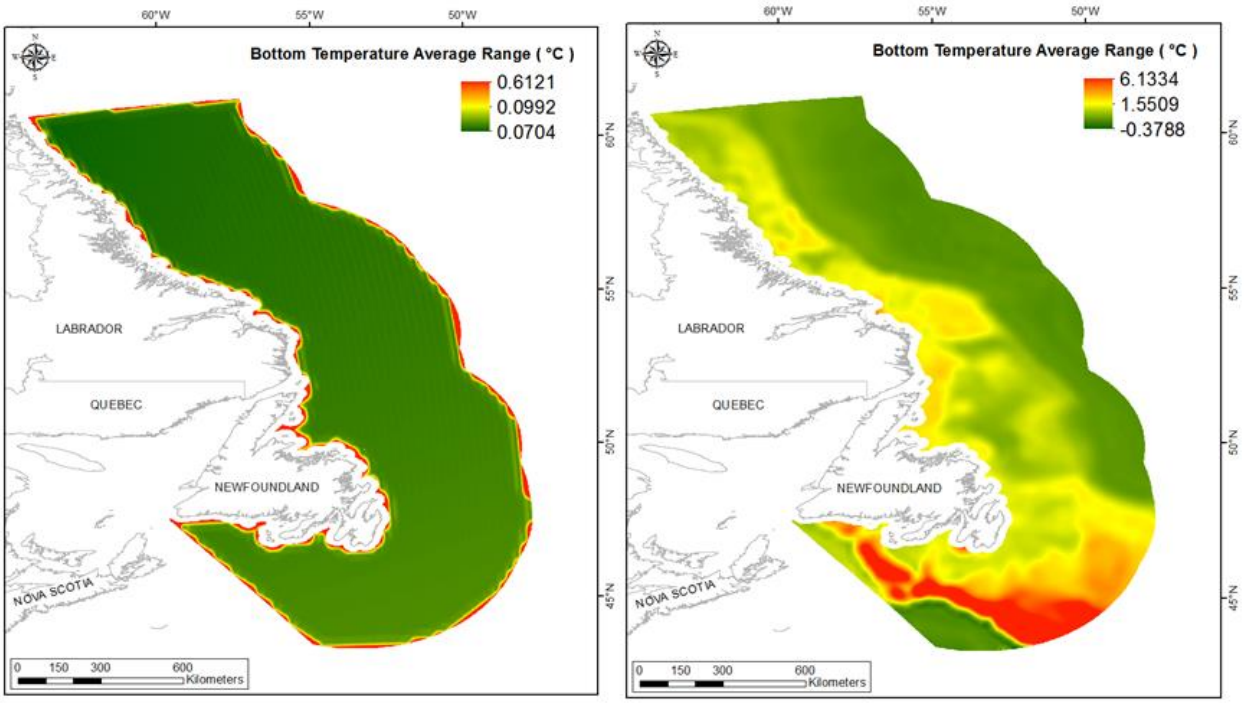

Figure 33. Left panel: Prediction standard error surface of Bottom Temperature Average Range (˚C). Right panel: Interpolated prediction surface of Bottom Temperature Average Range (˚C).

Surface Temperature Mean

This variable displayed a bell-shaped distribution prior to modeling (Table 17, Figure 34), with deviation from a standard normal distribution at the lowest and highest data values and slightly lower than predicted at mid values (Figure 35). The areas of under- and over-prediction showed a strong spatial pattern over the spatial extent (Figure 35).

The semivariogram showed weak autocorrelation present in the data and there was an excellent fit between the predicted and measured values (Figure 36). The kriged model showed poor cross-validation statistics (Table 18), the standardized root mean square was less than 1 indicating that variability in the predictions has been overestimated. The error map showed low error and no strong spatial pattern over the spatial extent although error was highest along the coast (Figure 37). The kriged surface is presented in Figure 37.

Table 17. Distributional properties of Surface Temperature Mean (°C).

Property	Value
Number of Observations	2975
Minimum	-0.188
Maximum	12.164
Mean	4.323
Median	4.309
Standard Deviation	2.273
Skewness	0.465
Kurtosis	3.373

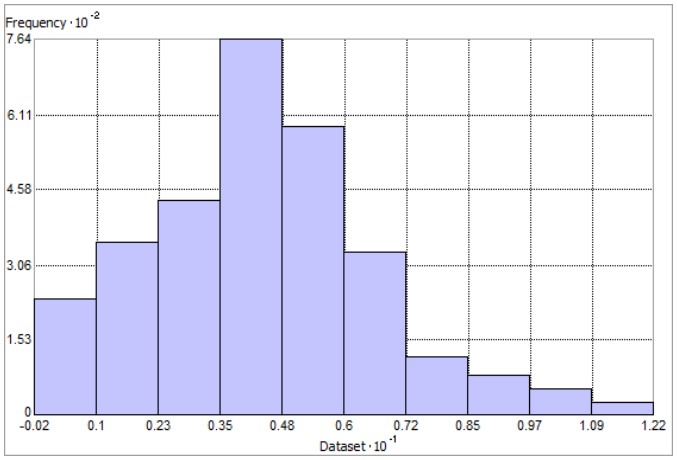

Figure 34. Distribution of Surface Temperature Mean (°C). Histogram was illustrated using 10 bins. X axis is shown at 10^{-1}. Y axis is shown at 10^{-2}.

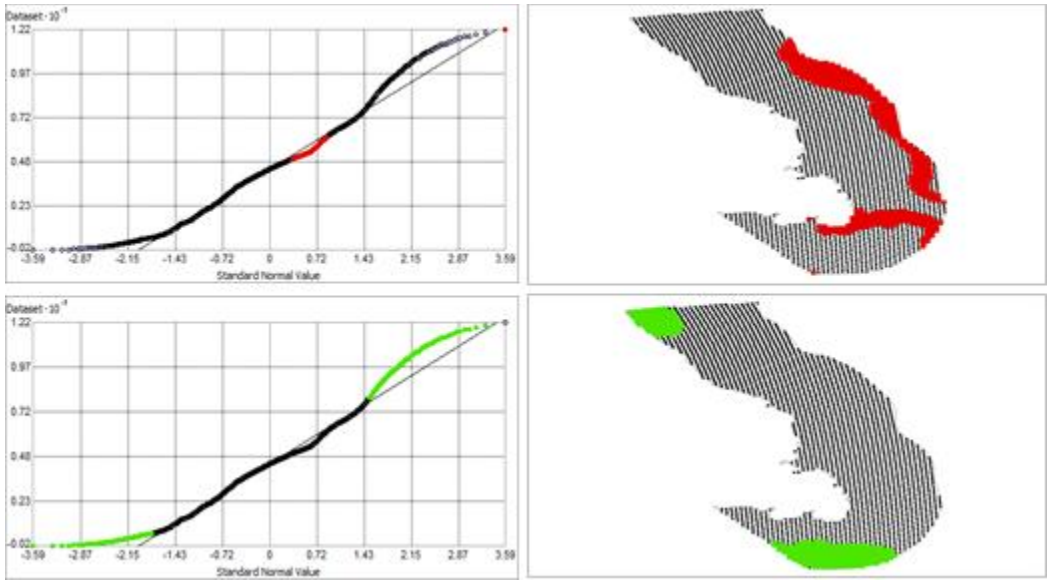

Figure 35. Normal Q-Q plot for data values of Surface Temperature Mean (°C). Points falling under (upper panel) and over (bottom panel) the reference line are mapped.

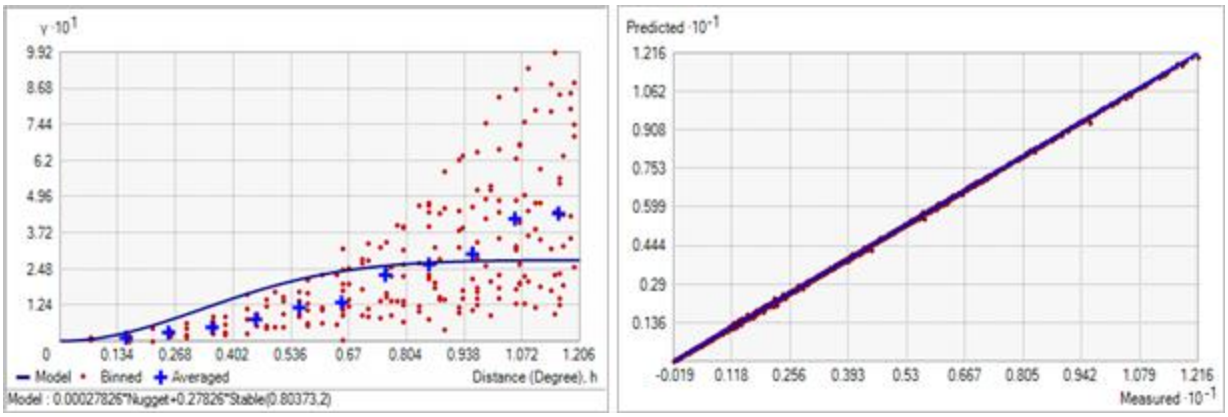

Figure 36. Left panel: Semivariogram of Surface Temperature Mean (°C). Binned values are shown as red dots; average points are shown as blue crosses; the model fit to the averaged values is shown as a blue line. Lag size: 0.100 degrees; number of lags: 12; Parameter: 2; Range: 0.804 degrees; Partial Sill: 0.278. Right panel: Scatterplot of predicted values versus observed values for the model of Surface Temperature Mean (°C).

Table 18. Results of cross-validation of the kriged model for Surface Temperature Mean (°C).

Prediction error	**Value**
Number of Observations	2975
Overall Mean Error	-8.631×10^{-4}
Root Mean Square Prediction Error	0.021
Standardized Mean	-5.463×10^{-3}
Standardized Root Mean Square Prediction Error	0.607
Average Standard Error	0.036

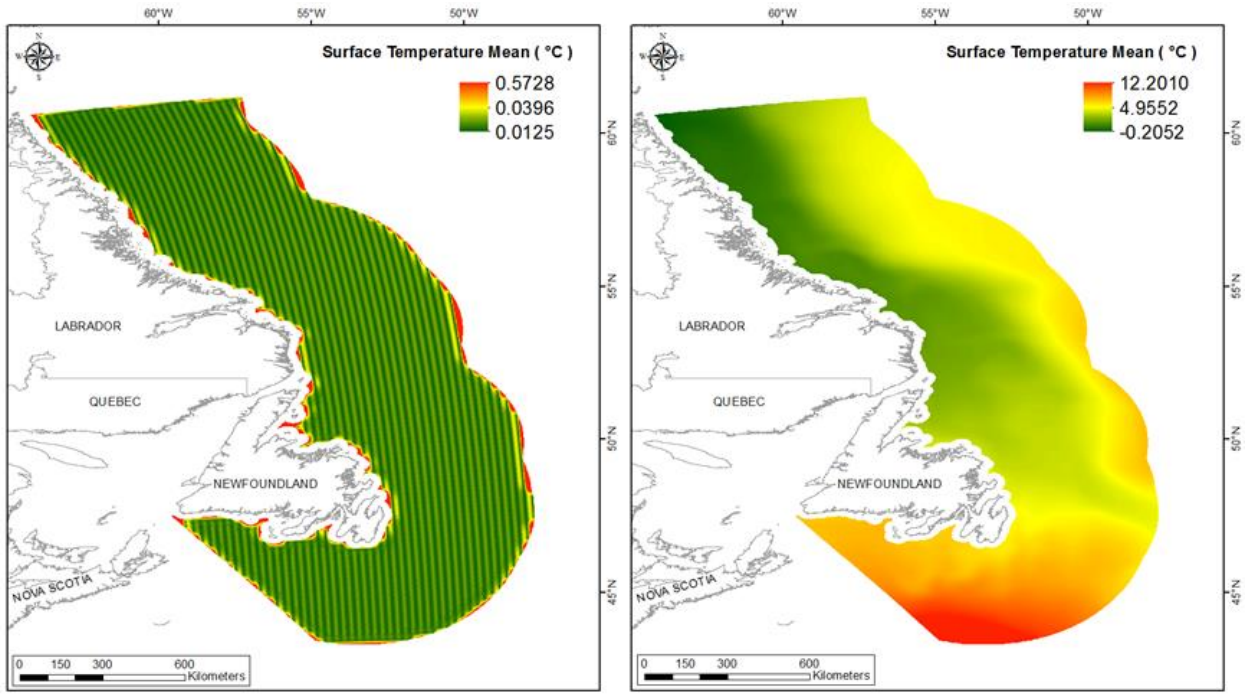

Figure 37. Left panel: Prediction standard error surface of Surface Temperature Mean (˚C). Right panel: Interpolated prediction surface of Surface Temperature Mean (˚C).

Surface Temperature Minimum

This variable displayed a right-skewed distribution with kurtosis prior to modeling (Table 19, Figure 38). The data were higher than predicted by a standard normal distribution at the tails and lower than predicted through the mid-range of the data (Figure 39). There was no strong spatial pattern to the under- and over-prediction (Figure 39).

The semivariogram showed moderate autocorrelation present in the data but an excellent fit between the predicted and measured values (Figure 40). The kriged model showed good cross-validation statistics (Table 20) indicating that it was good at prediction. The error map showed a 'bullseye' pattern with error increasing with distance from data points (Figure 41). The kriged surface is presented in Figure 41.

Table 19. Distributional properties of Surface Temperature Minimum (°C).

Property	Value
Number of Observations	2975
Minimum	-1.964
Maximum	2.954
Mean	-0.890
Median	-1.281
Standard Deviation	0.995
Skewness	1.331
Kurtosis	4.156

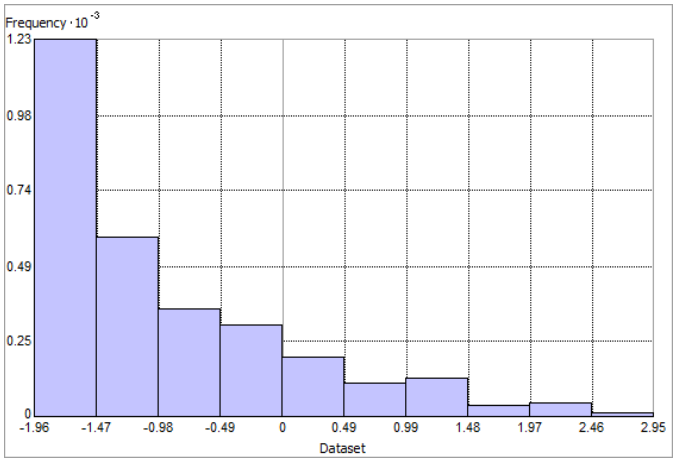

Figure 38. Distribution of Surface Temperature Minimum (°C). Histogram was illustrated using 10 bins. Y axis is shown at 10^{-3}.

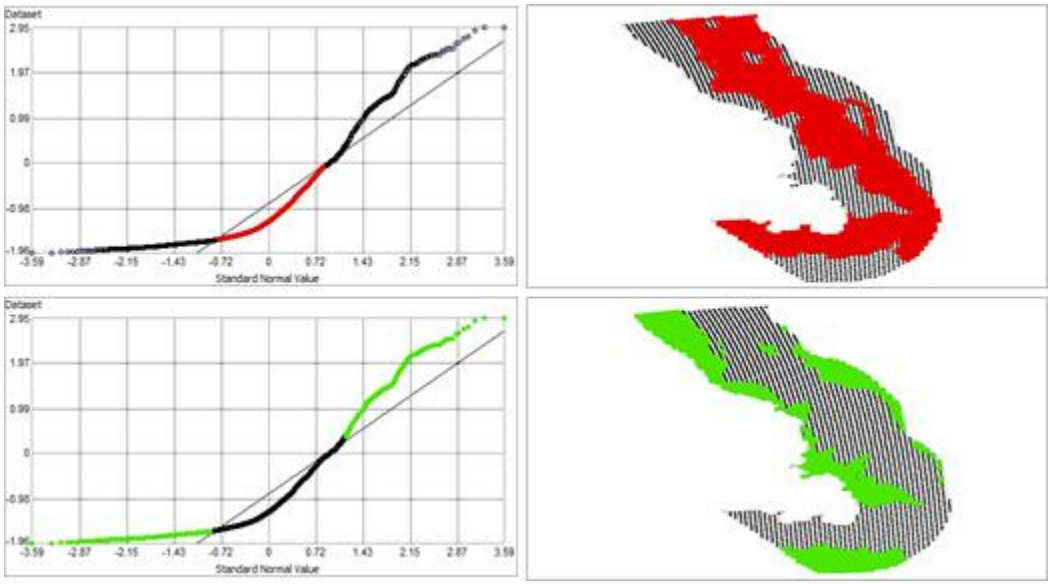

Figure 39. Normal Q-Q plot for data values of Surface Temperature Minimum (°C). Points falling under (upper panel) and over (bottom panel) the reference line are mapped.

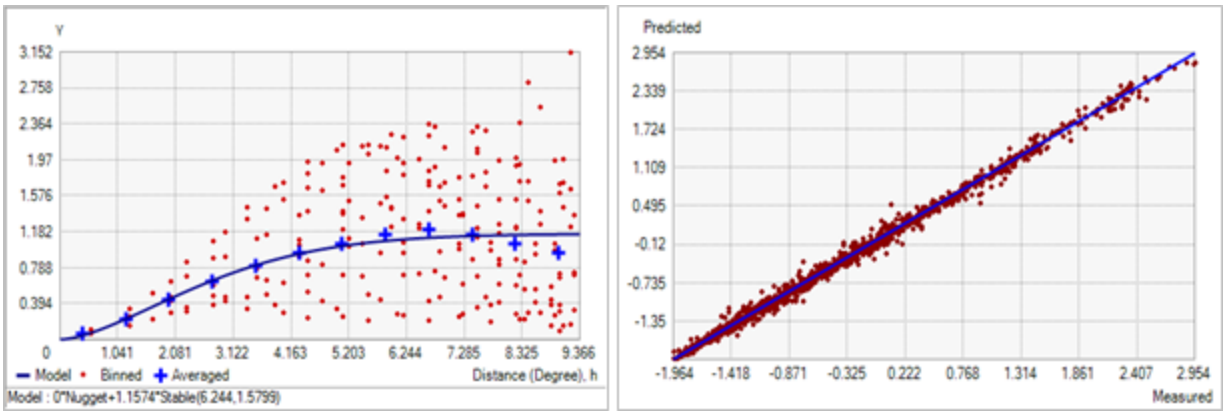

Figure 40. Left panel: Semivariogram of Surface Temperature Minimum (°C). Binned values are shown as red dots; average points are shown as blue crosses; the model fit to the averaged values is shown as a blue line. Lag size: 0.780 degrees; number of lags: 12; Parameter: 1.580; Range: 6.244 degrees; Partial Sill: 1.157. Right panel: Scatterplot of predicted values versus observed values for the model of Surface Temperature Minimum (°C).

Table 20. Results of cross-validation of the kriged model for Surface Temperature Minimum (°C).

Prediction error	**Value**
Number of Observations	2975
Overall Mean Error	-2.209×10^{-5}
Root Mean Square Prediction Error	0.051
Standardized Mean	5.433×10^{-5}
Standardized Root Mean Square Prediction Error	0.747
Average Standard Error	0.069

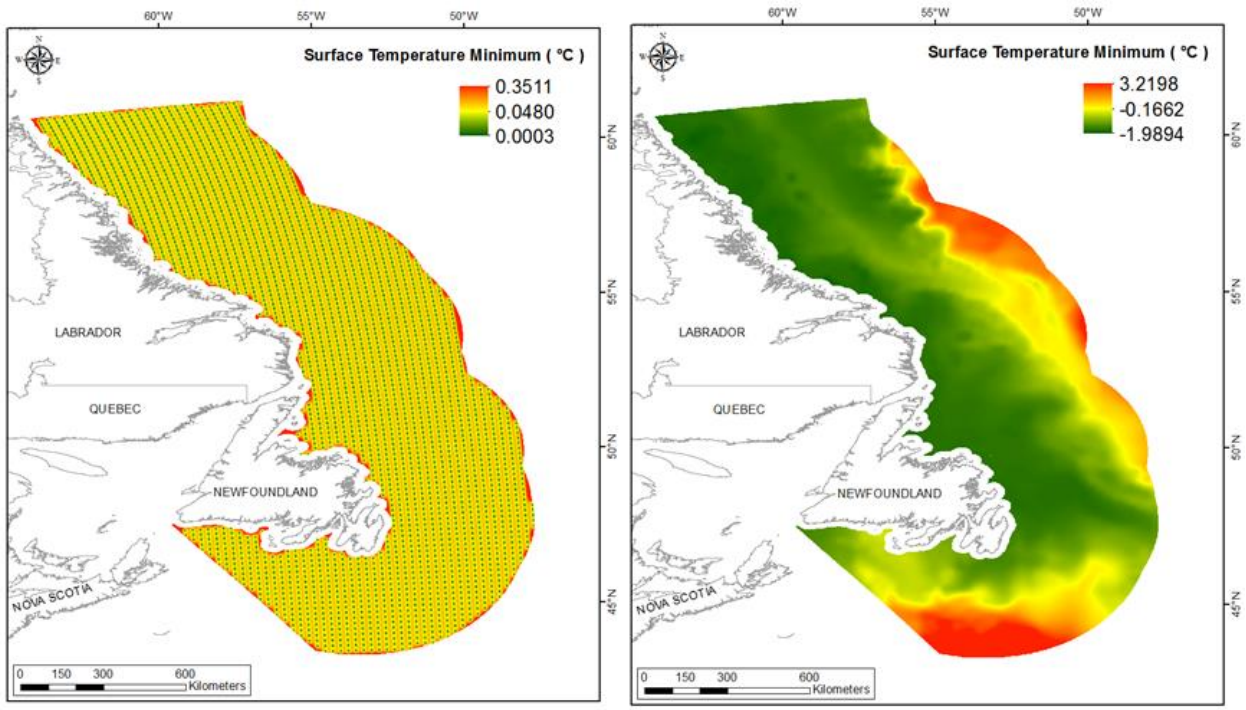

Figure 41. Left panel: Prediction standard error surface of Surface Temperature Minimum (˚C); Right panel: Interpolated prediction surface of Surface Temperature Minimum (˚C).

Surface Temperature Maximum

This variable displayed a near-normal distribution prior to modeling (Table 21, Figure 42). The data were higher than predicted by a standard normal distribution at the lower and upper-mid-range data and under-predicted through the -mid-range and highest values (Figure 43). There was a strong spatial pattern to the under- and over-prediction (Figure 43).

The semivariogram showed moderate autocorrelation present in the data and there was an excellent predictive fit (Figure 44). The kriged model showed fair cross-validation statistics (Table 22). The standardized root mean square was greater than 1 indicating that variability in the predictions has been underestimated. The error map showed low error and no strong spatial pattern over the spatial extent although error was highest along the coast (Figure 45). The kriged surface is presented in Figure 45.

Table 21. Distributional properties of Surface Temperature Maximum (°C).

Property	Value
Number of Observations	2975
Minimum	3.819
Maximum	22.546
Mean	12.436
Median	11.534
Standard Deviation	3.194
Skewness	0.257
Kurtosis	2.450

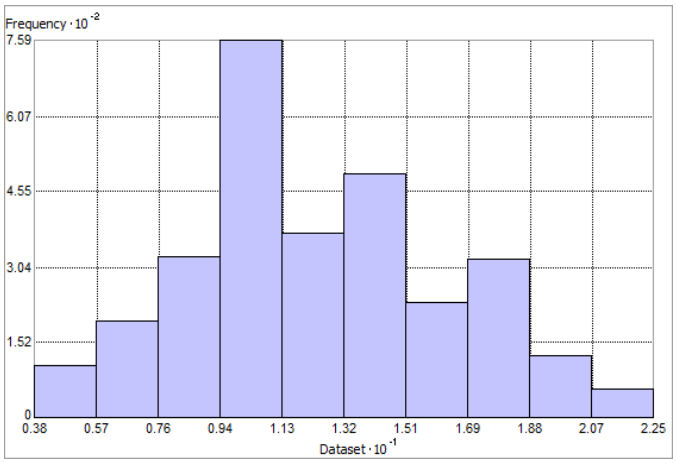

Figure 42. Distribution of Surface Temperature Maximum (°C). Histogram was illustrated using 10 bins. X axis is shown at 10^{-1}. Y axis is shown at 10^{-2}.

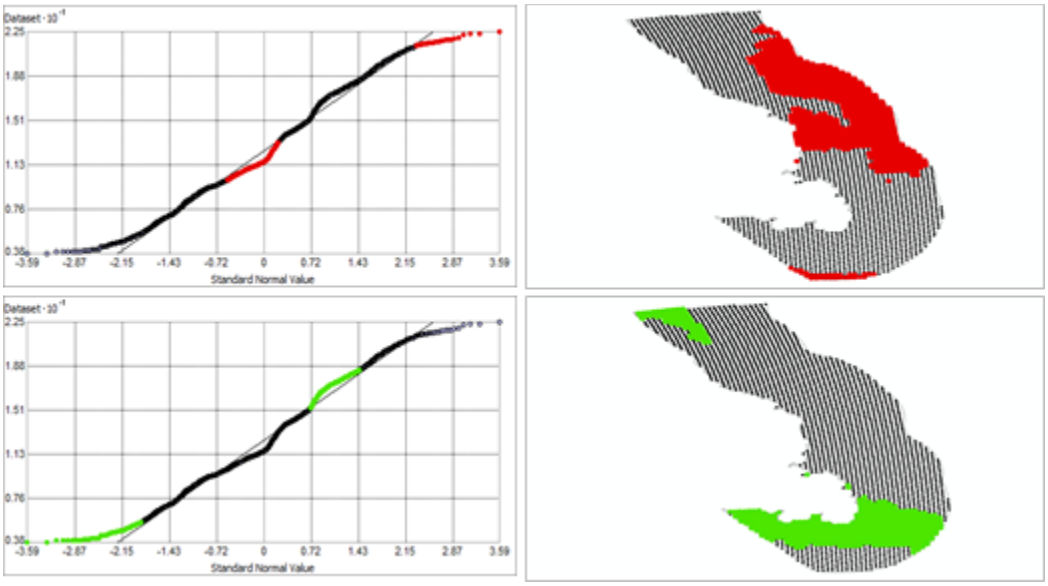

Figure 43. Normal Q-Q plot for data values of Surface Temperature Maximum (°C). Points falling under (upper panel) and over (bottom panel) the reference line are mapped.

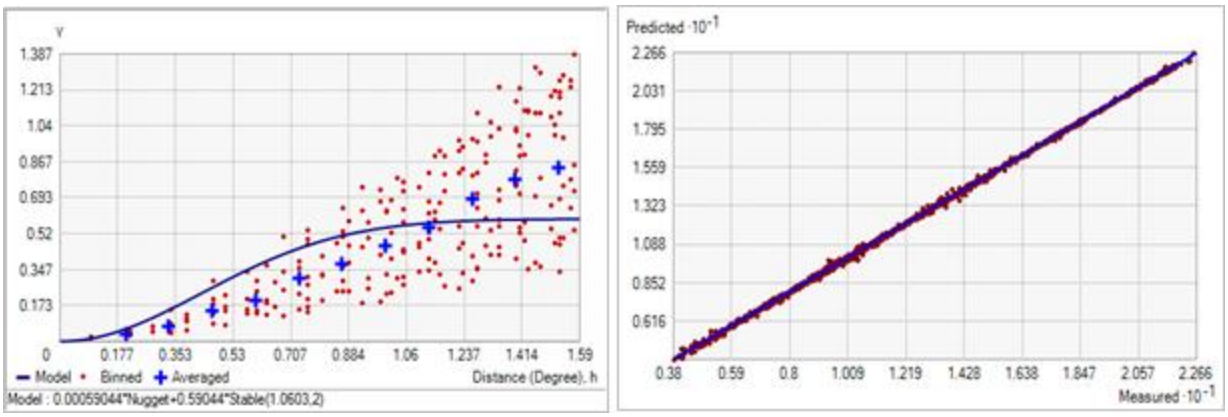

Figure 44. Left panel: Semivariogram of Surface Temperature Maximum (°C). Binned values are shown as red dots; average points are shown as blue crosses; the model fit to the averaged values is shown as a blue line. Lag size: 0.132 degrees; number of lags: 12; Parameter: 2; Range: 1.060 degrees; Partial Sill: 0.590. Right panel: Scatterplot of predicted values versus observed values for the model of Surface Temperature Maximum (°C).

Table 22. Results of cross-validation of the kriged model for Surface Temperature Maximum (°C).

Prediction error	**Value**
Number of Observations	2975
Overall Mean Error	-1.074×10^{-4}
Root Mean Square Prediction Error	0.069
Standardized Mean	-2.715×10^{-3}
Standardized Root Mean Square Prediction Error	1.904
Average Standard Error	0.040

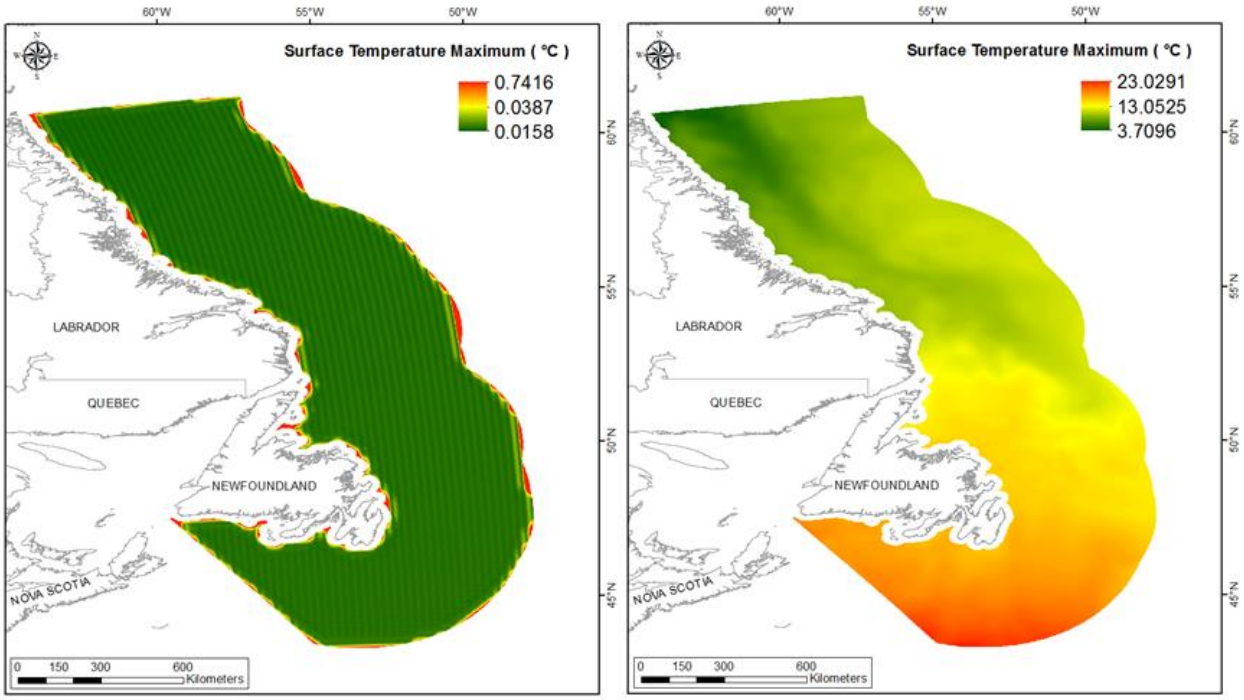

Figure 45. Left panel: Prediction standard error surface of Surface Temperature Maximum (˚C). Right panel: Interpolated prediction surface of Surface Temperature Maximum (˚C).

Surface Temperature Range

This variable displayed a bimodal distribution prior to modeling (Table 23, Figure 46). The data were greater than predicted by a normal distribution at the lower and upper-mid-range data and under-predicted through the -mid-range and the highest values of the data (Figure 47). These data points were spatially cohesive with specific areas of over- and under-prediction (Figure 47). However, the whole spatial extent was either over- or under-predicted.

The semivariogram showed weak autocorrelation present in the data and there was an excellent predictive fit (Figure 48). However, the model showed poor cross-validation statistics (Table 24). The standardized root mean square was less than 1 indicating that variability in the predictions has been overestimated. The error map showed a 'bullseye' pattern with error increasing with distance from data points (Figure 49). The kriged surface is presented in Figure 49.

Table 23. Distributional properties of Surface Temperature Range (°C).

Property	Value
Number of Observations	2975
Minimum	5.627
Maximum	20.443
Mean	13.325
Median	12.156
Standard Deviation	3.520
Skewness	0.117
Kurtosis	1.839

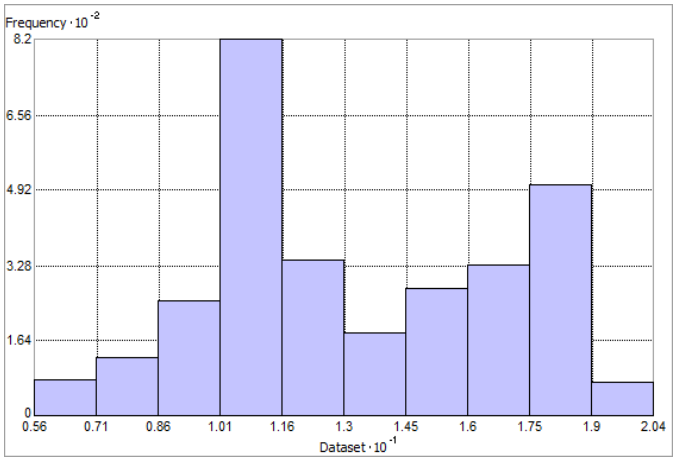

Figure 46. Distribution of Surface Temperature Range (°C). Histogram was illustrated using 10 bins. X axis is shown at 10^{-1}; Y axis is shown at 10^{-2}.

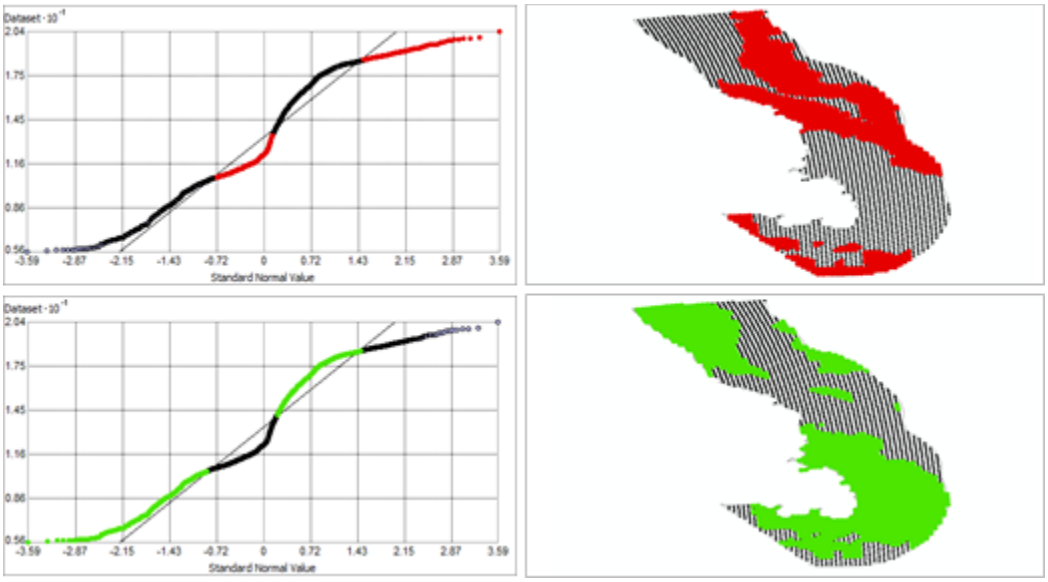

Figure 47. Normal Q-Q plot for data values of Surface Temperature Range (°C). Points falling under (upper panel) and over (bottom panel) the reference line are mapped.

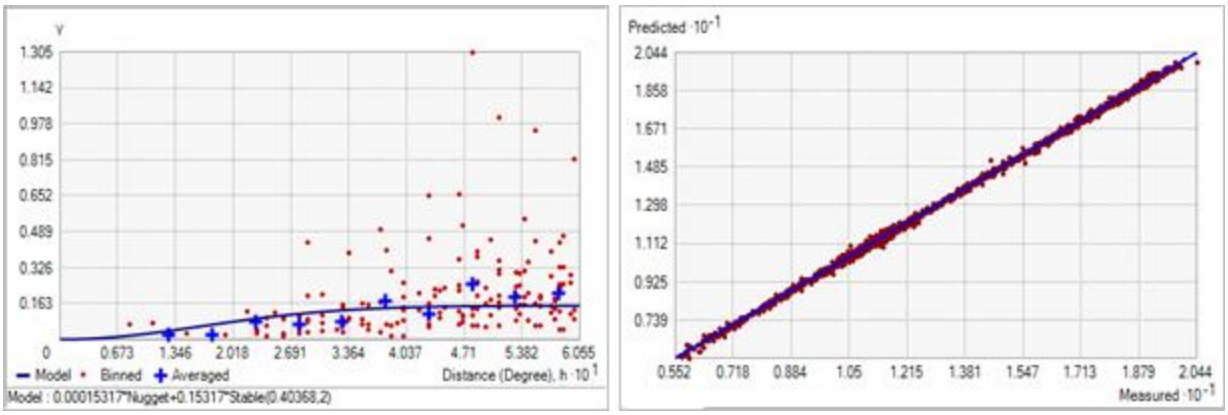

Figure 48. Left panel: Semivariogram of Surface Temperature Range (°C). Binned values are shown as red dots; average points are shown as blue crosses; the model fit to the averaged values is shown as a blue line. Lag size: 0.050 degrees; number of lags: 12; Parameter: 2; Range: 0.404 degrees; Partial Sill: 0.153. Right panel: Scatterplot of predicted values versus observed values for the model of Surface Temperature Range (°C).

Table 24. Results of cross-validation of the kriged model for Surface Temperature Range (°C).

Prediction error	**Value**
Number of Observations	2975
Overall Mean Error	2.818×10^{-4}
Root Mean Square Prediction Error	0.085
Standardized Mean	-1.85×10^{-3}
Standardized Root Mean Square Prediction Error	0.518
Average Standard Error	0.174

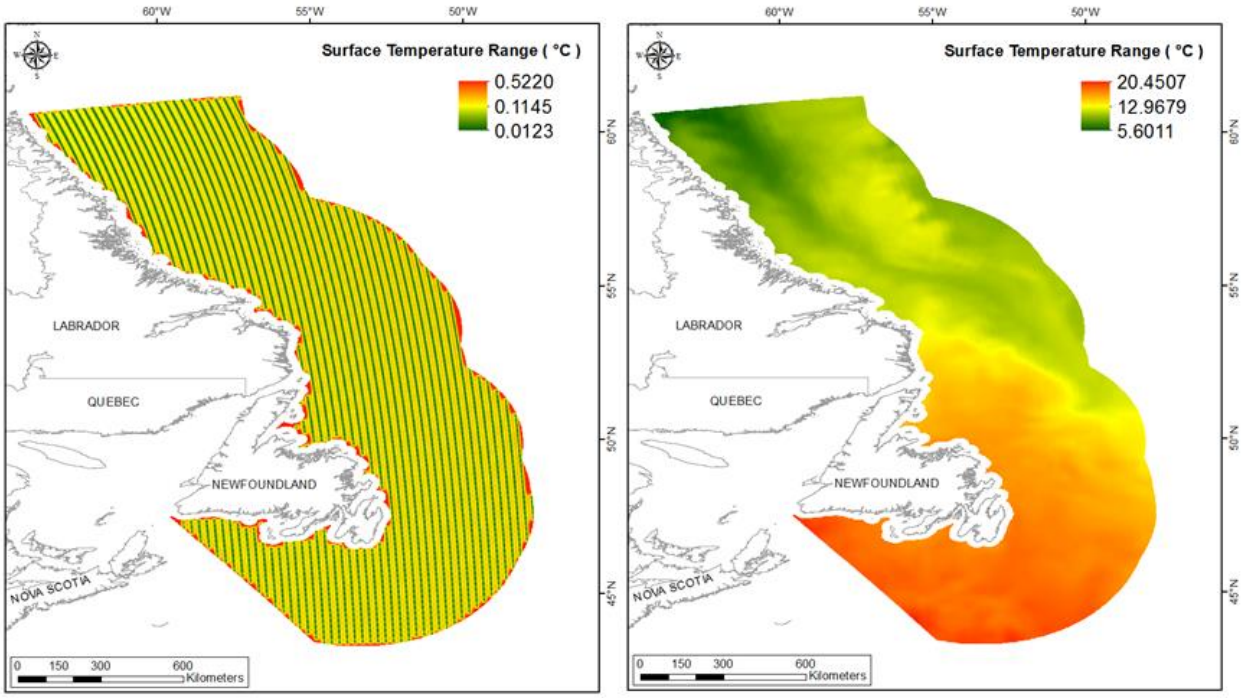

Figure 49. Left panel: Prediction standard error surface of Surface Temperature Range (˚C). Right panel: Interpolated prediction surface of Surface Temperature Range (˚C).

Surface Temperature Average Minimum

This variable displayed a right-skewed distribution prior to modelling (Table 25, Figure 50). The data were slightly higher than predicted by a normal distribution at upper mid-range and low values (Figure 127), with mid-range values and the highest value falling lower than the reference line (Figure 51). These data points were spatially cohesive with specific areas of over-and under-prediction (Figure 51).

The semivariogram showed autocorrelation present in the data and there was an excellent predictive fit (Figure 52). The model showed fair cross-validation statistics (Table 26). The standardized root mean square was greater than 1 indicating that variability in the predictions has been underestimated. The error map showed a 'bullseye' pattern with error increasing with distance from data points (Figure 53). The kriged surface is presented in Figure 53.

Table 25. Distributional properties of Surface Temperature Average Minimum (°C).

Property	Value
Number of Observations	2975
Minimum	-1.754
Maximum	5.412
Mean	0.434
Median	0.333
Standard Deviation	1.496
Skewness	0.384
Kurtosis	2.306

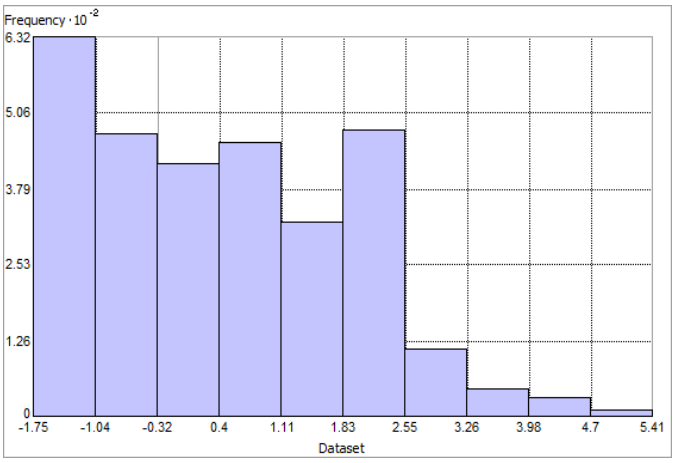

Figure 50. Distribution of Surface Temperature Average Minimum (°C). Histogram was illustrated using 10 bins. Y axis is shown at 10^{-2}.

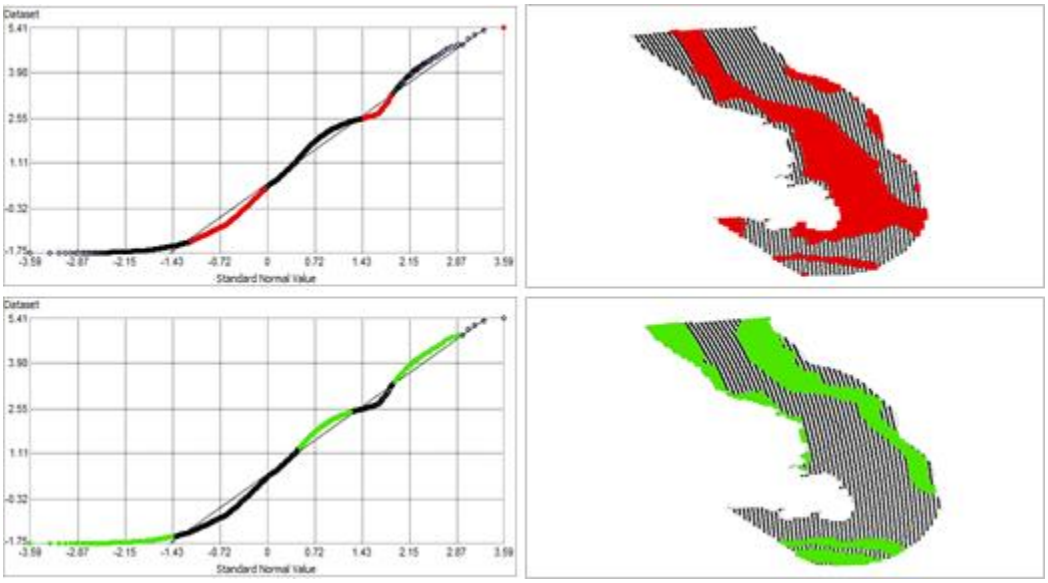

Figure 51. Normal Q-Q plot for data values of Surface Temperature Average Minimum (°C). Points falling under (upper panel) and over (bottom panel) the reference line are mapped.

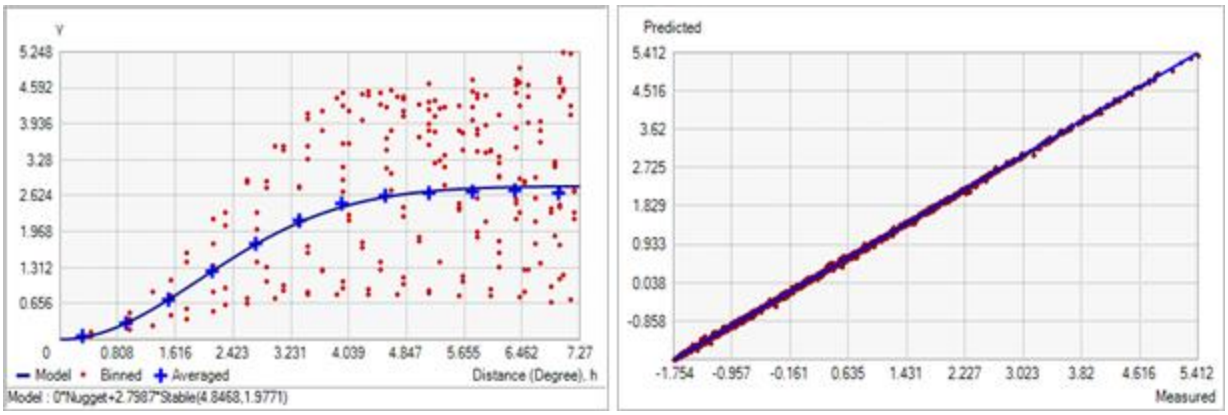

Figure 52. Left panel: Semivariogram of Surface Temperature Average Minimum (°C). Binned values are shown as red dots; average points are shown as blue crosses; the model fit to the averaged values is shown as a blue line. Lag size: 0.606 degrees; number of lags: 12; Parameter: 1.977; Range: 4.847 degrees; Partial Sill: 2.799. Right panel: Scatterplot of predicted values versus observed values for the model of Surface Temperature Average Minimum (°C).

Table 26. Results of cross-validation of the kriged model for Surface Temperature Average Minimum (°C).

Prediction error	**Value**
Number of Observations	2975
Overall Mean Error	-9.846×10^{-6}
Root Mean Square Prediction Error	0.022
Standardized Mean	3.360×10^{-4}
Standardized Root Mean Square Prediction Error	1.399
Average Standard Error	0.016

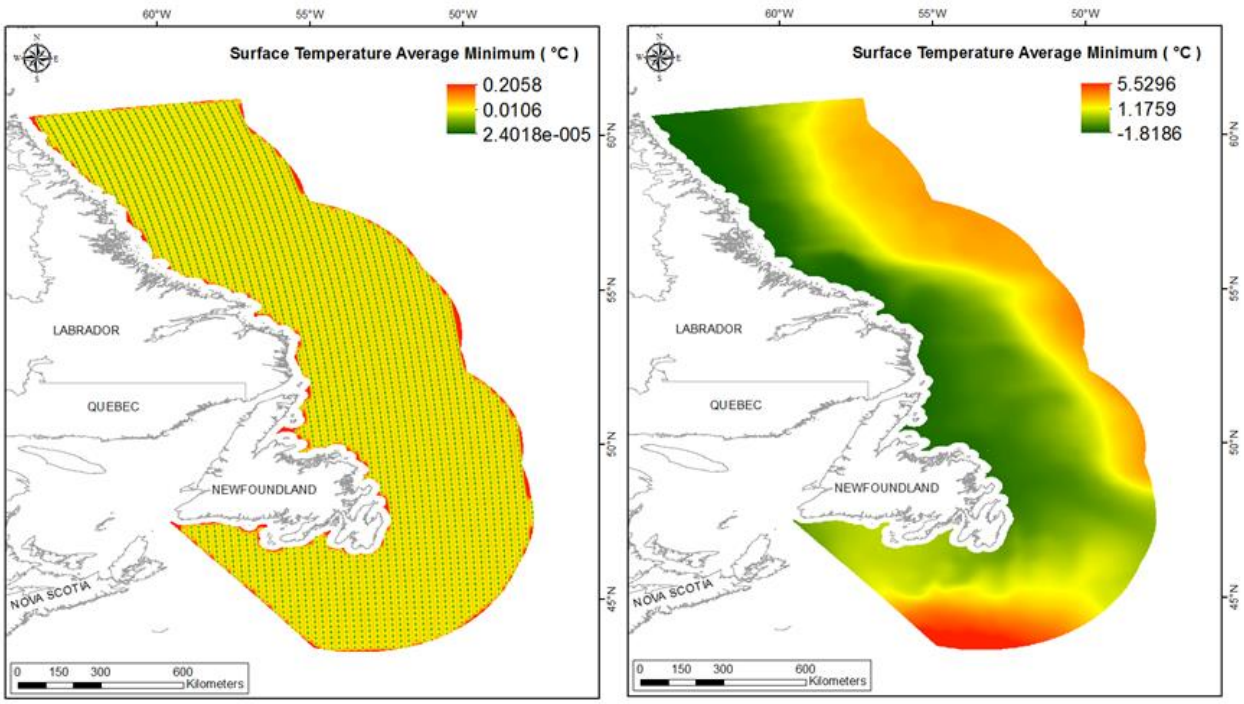

Figure 53. Left panel: Prediction standard error surface of Surface Temperature Average Minimum (˚C). Right panel: Interpolated prediction surface of Surface Temperature Average Minimum (˚C).

Surface Temperature Average Maximum

This variable displayed a slightly bimodal distribution prior to modeling (Table 27, Figure 54). The data were higher than predicted by standard normal distribution at the lower tail and upper-mid-range of the data and lower than predicted at the mid-range of the data and in the highest values (Figure 55). These data points were spatially cohesive with specific areas of over-and under-prediction, (Figure 55).

The semivariogram showed moderate autocorrelation present in the data but excellent predictive fit (Figure 56). The model showed good cross-validation statistics indicating that it was poor at prediction (Table 28). The error map showed low error and no strong spatial pattern over the spatial extent but was higher along the coast (Figure 57). The kriged surface is presented in Figure 57.

Table 27. Distributional properties of Surface Temperature Average Maximum (°C).

Property	Value
Number of Observations	2975
Minimum	2.854
Maximum	20.428
Mean	10.474
Median	9.605
Standard Deviation	3.50
Skewness	0.465
Kurtosis	2.455

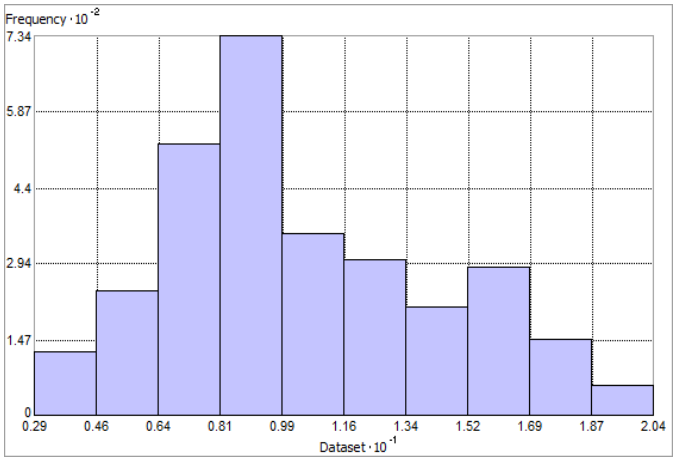

Figure 54. Distribution of Surface Temperature Average Maximum (°C). Histogram was illustrated using 10 bins. X axis is shown at 10^{-1}; Y axis is shown at 10^{-2}.

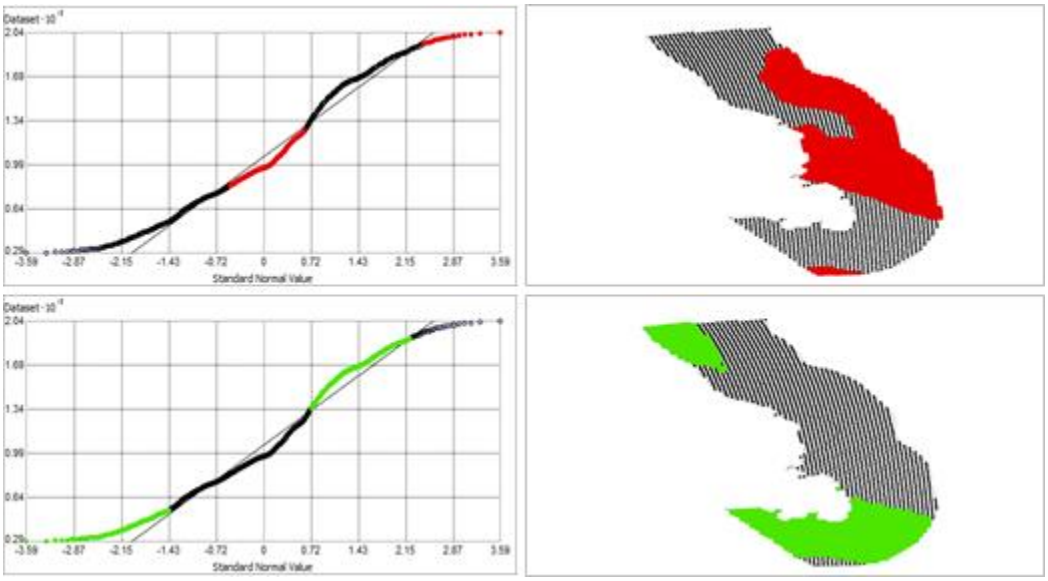

Figure 55. Normal Q-Q plot for data values of Surface Temperature Average Maximum (°C). Points falling under (upper panel) and over (bottom panel) the reference line are mapped.

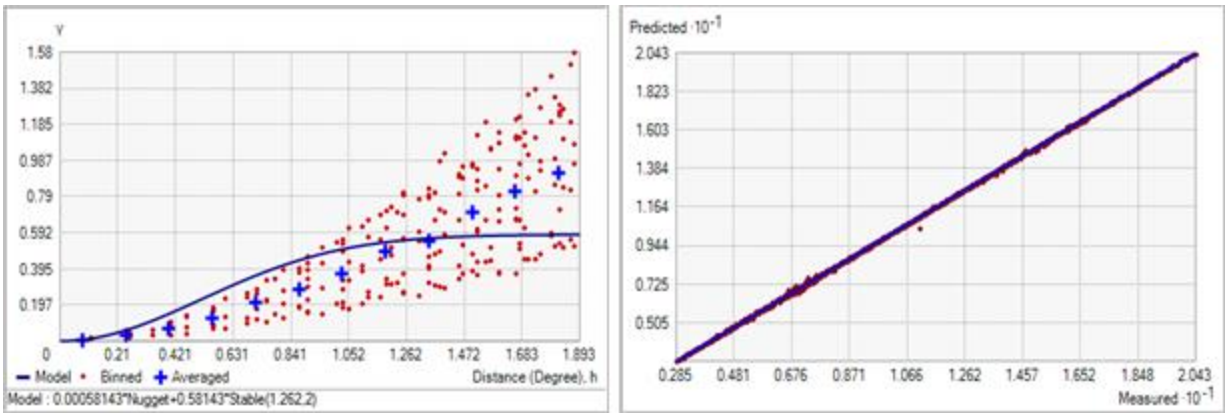

Figure 56. Left panel: Semivariogram of Surface Temperature Average Maximum (°C). Binned values are shown as red dots; average points are shown as blue crosses; the model fit to the averaged values is shown as a blue line. Lag size: 0.158 degrees; number of lags: 12; Parameter: 2; Range: 1.262 degrees; Partial Sill: 0.581. Right panel: Scatterplot of predicted values versus observed values for the model of Surface Temperature Average Maximum (°C).

Table 28. Results of cross-validation of the kriged model for Surface Temperature Average Maximum (°C).

Prediction error	**Value**
Number of Observations	2975
Overall Mean Error	-5.815×10^{-4}
Root Mean Square Prediction Error	0.033
Standardized Mean	-8.991×10^{-3}
Standardized Root Mean Square Prediction Error	0.862
Average Standard Error	0.034

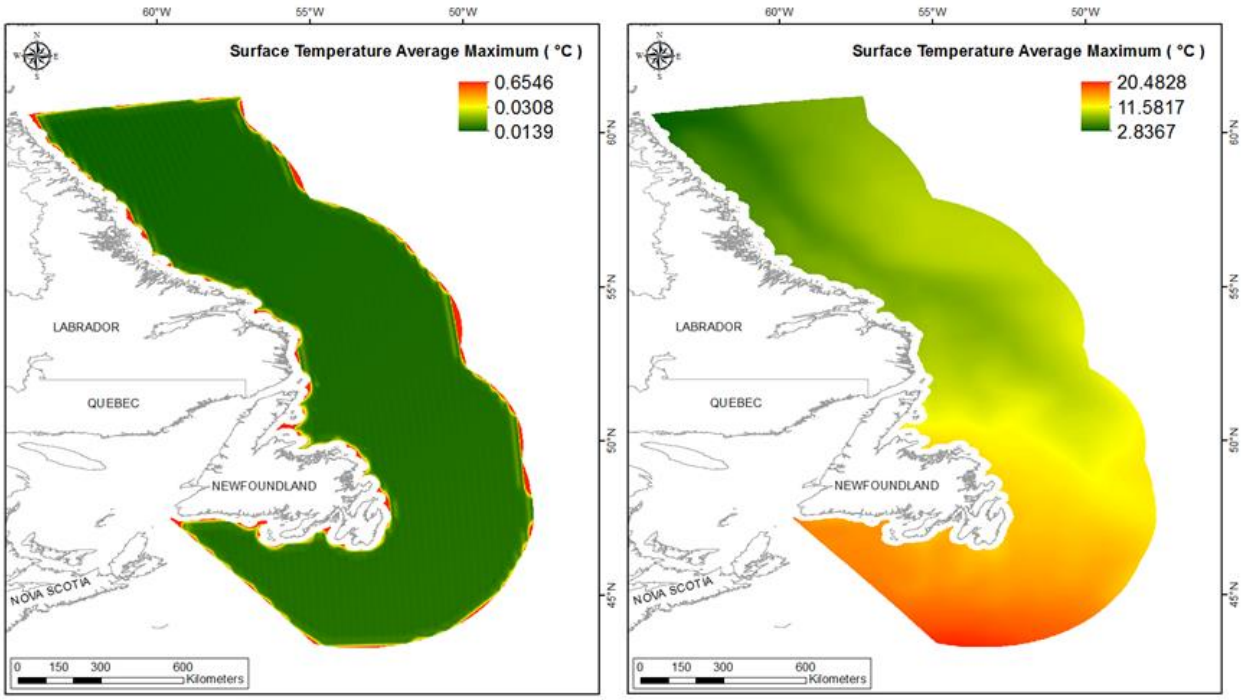

Figure 57. Left panel: Prediction standard error surface of Surface Temperature Average Maximum (˚C). Right panel: Interpolated prediction surface of Surface Temperature Average Maximum (˚C).

Surface Temperature Average Range

This variable displayed a bimodal distribution prior to modeling (Table 29, Figure 58). The data were greater than predicted by a normal distribution at the lowest and upper mid-range values and less than predicted at the mid-range and the highest values (Figure 59). These areas of under- and over-prediction showed strong spatial pattern over the region (Figure 59).

The semivariogram showed moderate autocorrelation present in the data and there was an excellent predictive fit (Figure 60). The kriged model showed good cross-validation statistics indicating that it was poor at prediction (Table 30). The error map showed low error and no strong spatial pattern over the spatial extent but was higher along the coast (Figure 61). The kriged surface is presented in Figure 61.

Table 29. Distributional properties of Surface Temperature Average Range (°C).

Property	Value
Number of Observations	2975
Minimum	4.572
Maximum	17.327
Mean	10.039
Median	8.925
Standard Deviation	3.516
Skewness	0.367
Kurtosis	1.647

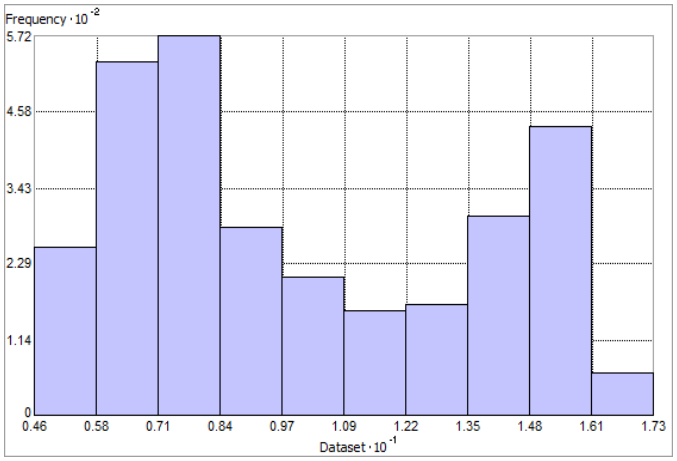

Figure 58. Distribution of Surface Temperature Average Range (°C). Histogram was illustrated using 10 bins. X axis is shown at 10^{-1}; Y axis is shown at 10^{-2}.

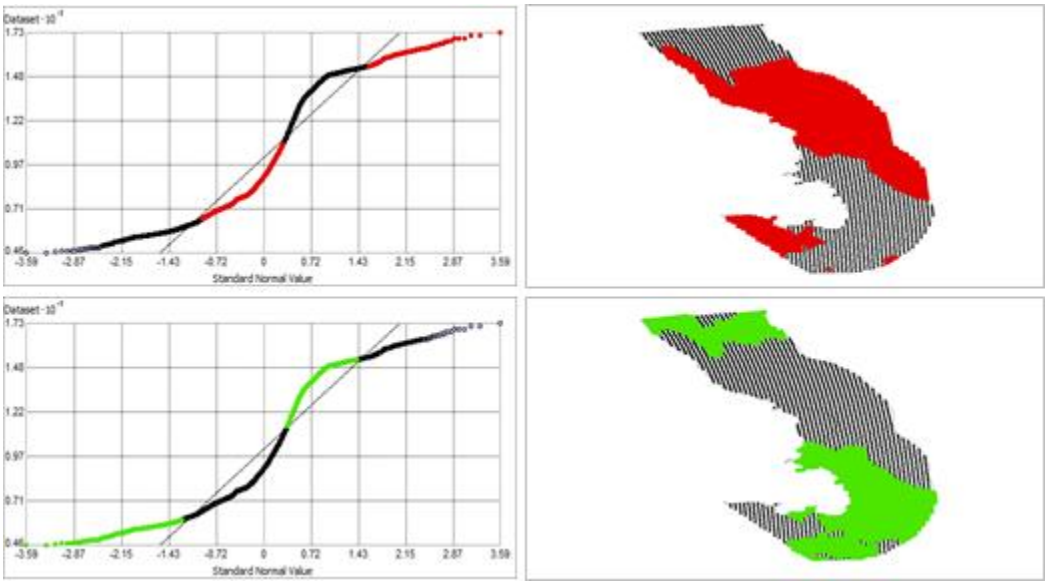

Figure 59. Normal Q-Q plot for data values of Surface Temperature Average Range (°C). Points falling under (upper panel) and over (bottom panel) the reference line are mapped.

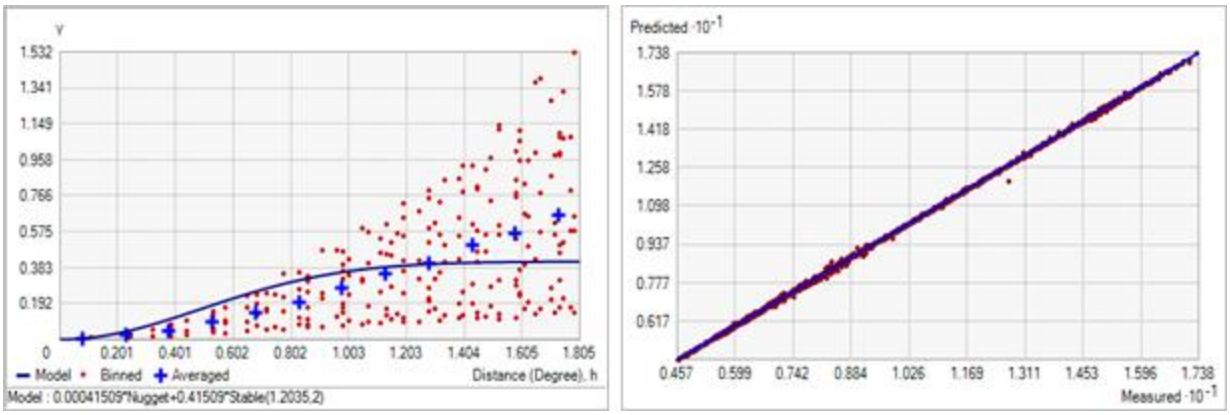

Figure 60. Left panel: Semivariogram of Surface Temperature Average Range (°C). Binned values are shown as red dots; average points are shown as blue crosses; the model fit to the averaged values is shown as a blue line. Lag size: 0.150 degrees; number of lags: 12; Parameter: 2; Range: 1.203 degrees; Partial Sill: 0.415. Right panel: Scatterplot of predicted values versus observed values for the model of Surface Temperature Average Range (°C).

Table 30. Results of cross-validation of the kriged model for Surface Temperature Average Range (°C).

Prediction error	**Value**
Number of Observations	2975
Overall Mean Error	3.308×10^{-4}
Root Mean Square Prediction Error	0.038
Standardized Mean	-3.436×10^{-3}
Standardized Root Mean Square Prediction Error	1.206
Average Standard Error	0.030

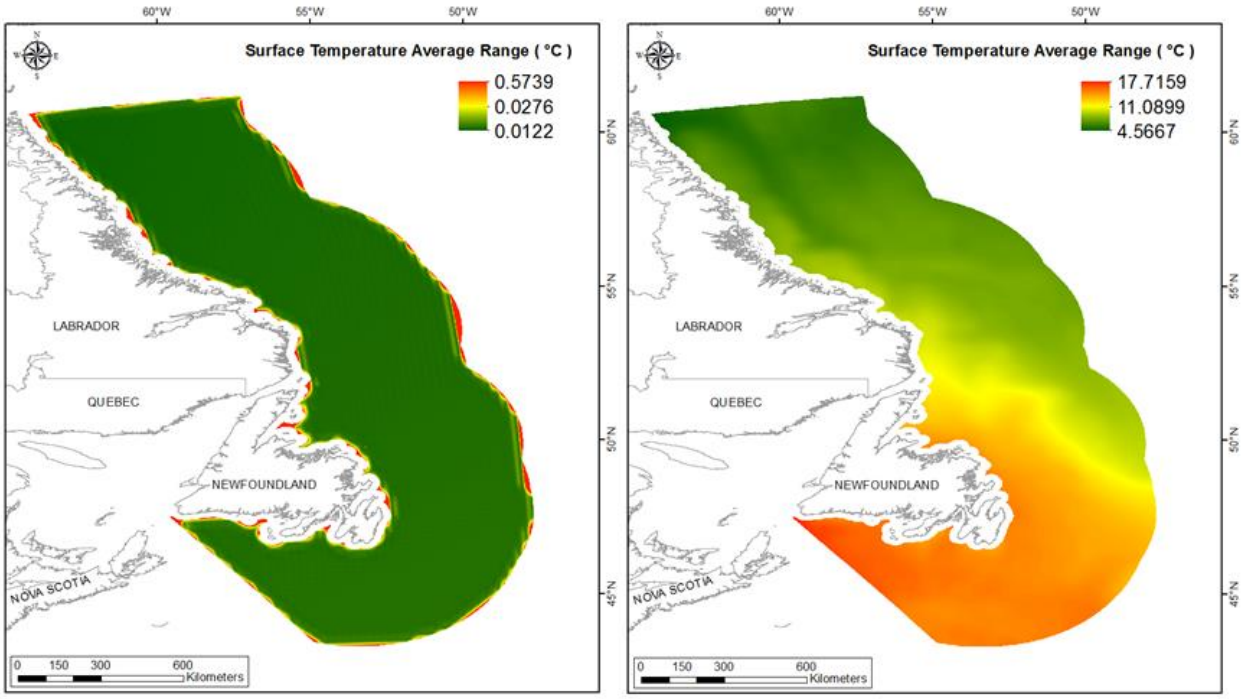

Figure 61. Left panel: Prediction standard error surface of Surface Temperature Average Range (˚C). Right panel: Interpolated prediction surface of Surface Temperature Average Range (˚C).

Salinity

Salinity influences osmoregulation (control of osmosis and diffusion) and is a very important determinant of species distribution. Salinity from the GLORYS model is Practical Salinity and is therefore unitless.

Bottom Salinity Mean

This variable displayed a left-skewed distribution prior to modeling (Table 31, Figure 62). The data were higher than predicted by a normal distribution at high and the lowest values, with mid-range and the highest values falling lower than the reference line (Figure 63). There was a spatial pattern to the under- and over-prediction (Figure 63).

The semivariogram showed weak autocorrelation present in the data. The model showed a good fit between measured and predicted values (Figure 64). The kriged model showed poor cross-validation statistics (Table 32). The error map showed a 'bullseye' pattern with error increasing with distance from data points (Figure 65). The kriged surface is presented in Figure 65.

Table 31. Distributional properties of Bottom Salinity Mean.

Property	Value
Number of Observations	2975
Minimum	32.359
Maximum	34.974
Mean	34.329
Median	34.728
Standard Deviation	0.700
Skewness	-0.904
Kurtosis	2.362

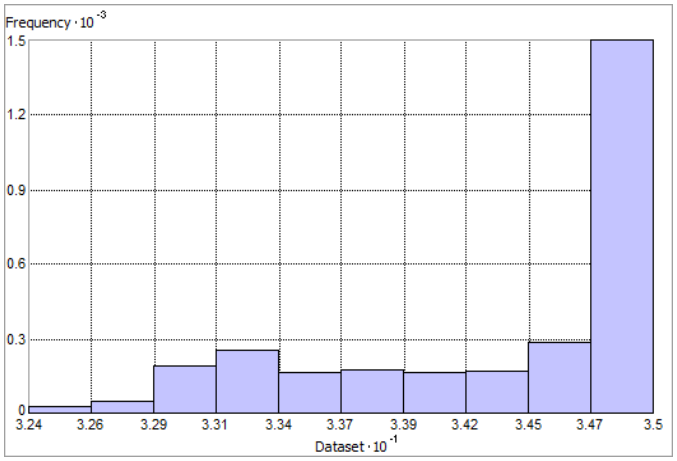

Figure 62. Distribution of Bottom Salinity Mean. Histogram was illustrated using 10 bins. X axis is shown at 10^{-1}; Y axis is shown at 10^{-3}.

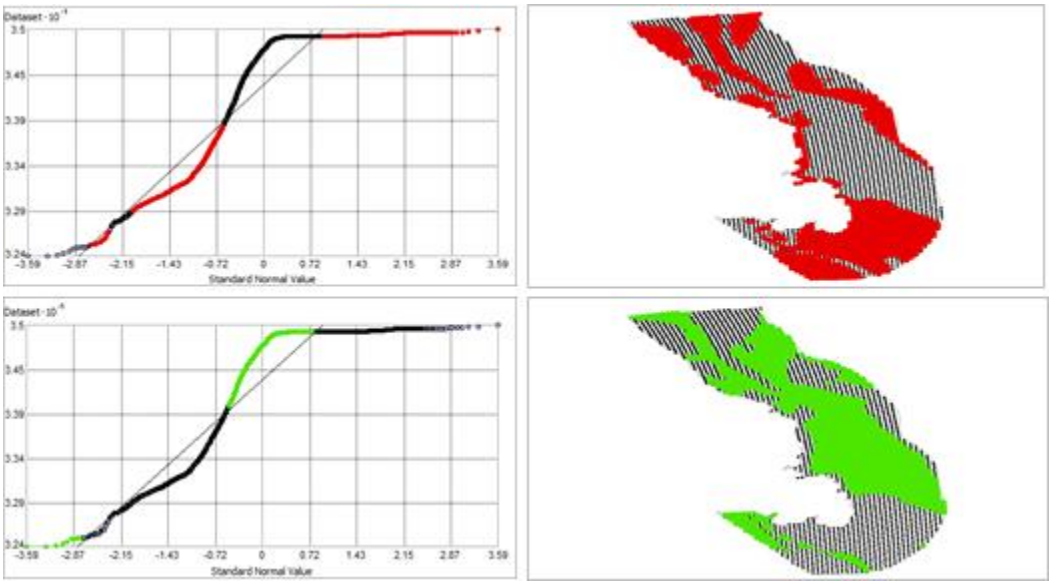

Figure 63. Normal Q-Q plot for data values of Bottom Salinity Mean. Points falling under (upper panel) and over (bottom panel) the reference line are mapped.

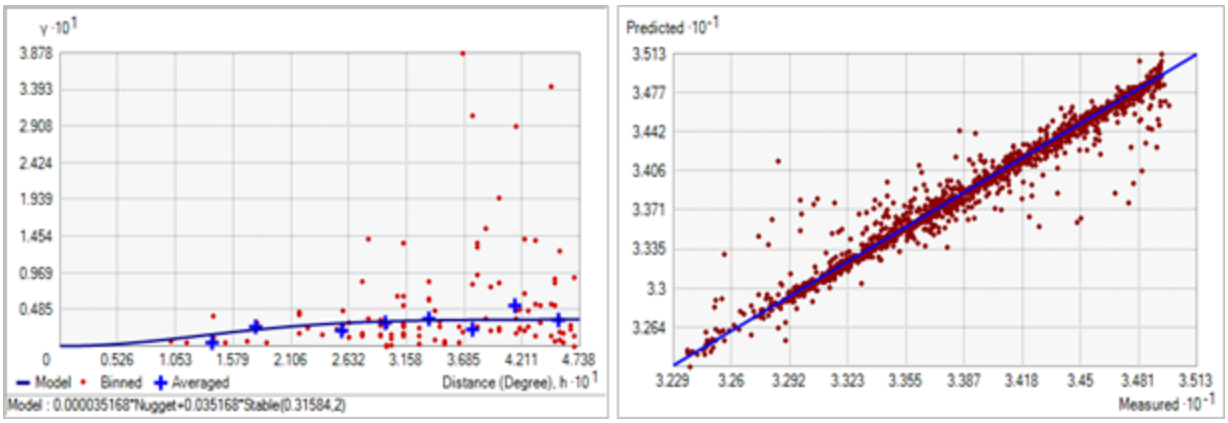

Figure 64. Left panel: Semivariogram of Bottom Salinity Mean. Binned values are shown as red dots; average points are shown as blue crosses; the model fit to the averaged values is shown as a blue line. Lag size: 0.039 degrees; number of lags: 12; Parameter: 2; Range: 0.316 degrees; Partial Sill: 0.035. Right panel: Scatterplot of predicted values versus observed values for the model of Bottom Salinity Mean.

Table 32. Results of cross-validation of the kriged model for Bottom Salinity Mean.

Prediction error	**Value**
Number of Observations	2975
Overall Mean Error	5.031×10^{-4}
Root Mean Square Prediction Error	0.093
Standardized Mean	1.614×10^{-3}
Standardized Root Mean Square Prediction Error	0.646
Average Standard Error	0.134

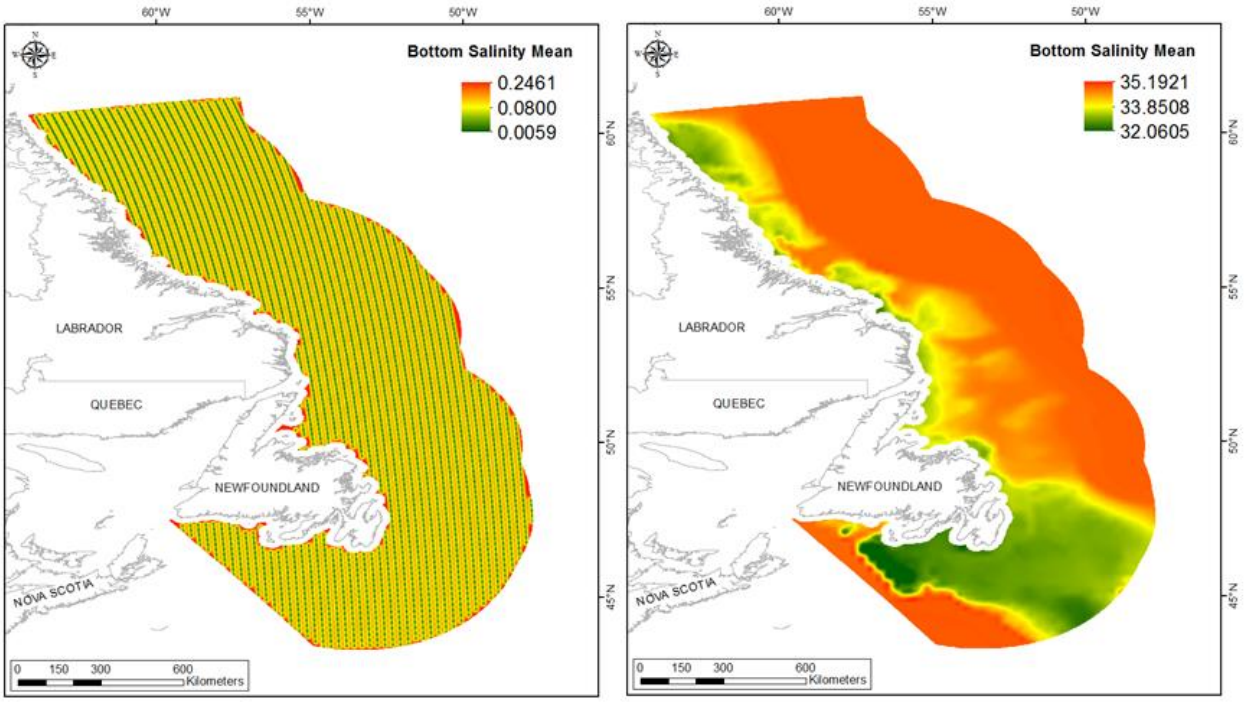

Figure 65. Left panel: Prediction standard error surface of Bottom Salinity Mean. Right panel: Interpolated prediction surface of Bottom Salinity Mean.

Bottom Salinity Minimum

This variable displayed a left-skewed distribution prior to modeling (Table 33, Figure 66). The data were lower than predicted by a normal distribution at mid-range and high values (Figure 67). Upper mid-range and the lowest values were higher than the reference line. These data points were spatially cohesive with specific areas of over-prediction found in the Northeast Newfoundland Shelf and areas of under prediction found in The Grand Banks of Newfoundland and along the coast (Figure 67). The entire spatial extent is either over- or under-predicted.

The semivariogram showed weak autocorrelation present in the data and there was a fair predictive fit (Figure 68). The kriged model showed fair cross-validation statistics (Table 34) indicating that it was fair at prediction. The standardized root mean square was greater than 1 indicating that variability in the predictions has been underestimated. The error map showed low error and no strong spatial pattern over the spatial extent but was higher along the coast (Figure 69). The kriged surface is presented in Figure 69.

Table 33. Distributional properties of Bottom Salinity Minimum.

Property	Value
Number of Observations	2975
Minimum	31.487
Maximum	34.888
Mean	34.056
Median	34.424
Standard Deviation	0.886
Skewness	-0.707
Kurtosis	2.089

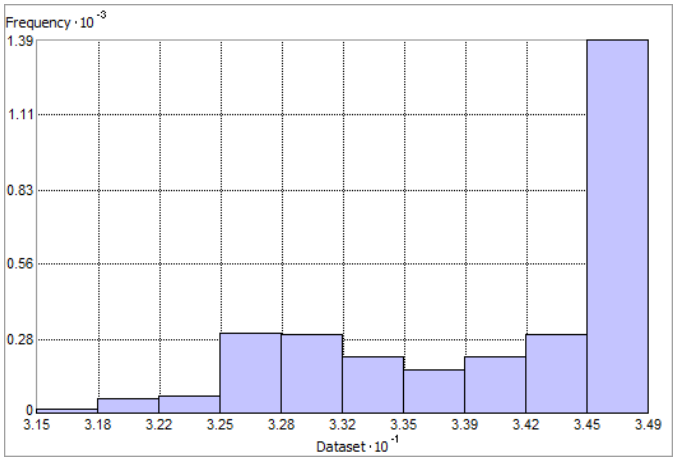

Figure 66. Distribution of Bottom Salinity Minimum. Histogram was illustrated using 10 bins. X axis is shown at 10^{-1}; Y axis is shown at 10^{-3}.

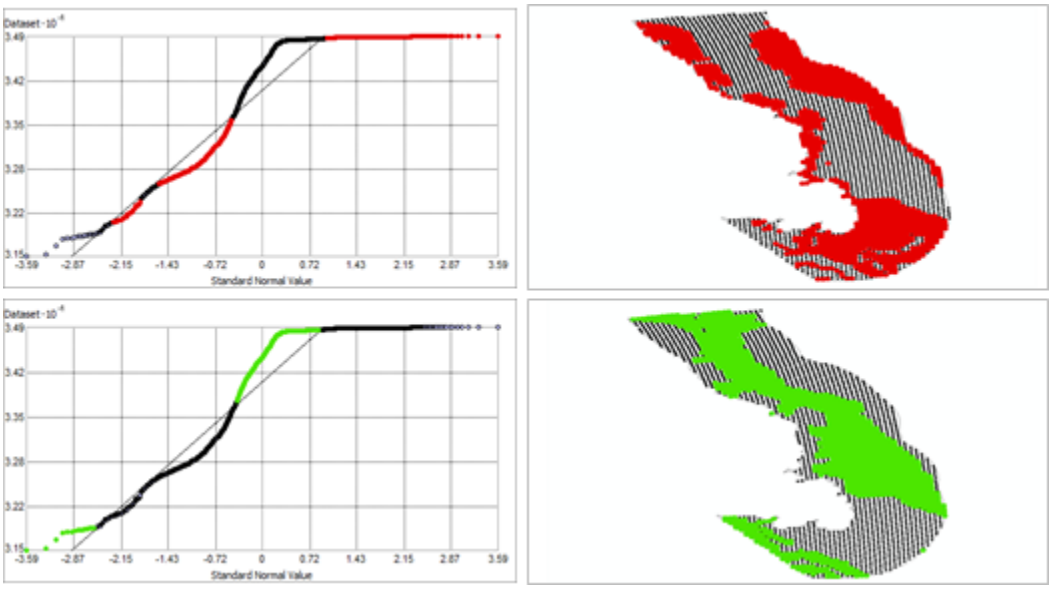

Figure 67. Normal Q-Q plot for data values of Bottom Salinity Minimum. Points falling under (upper panel) and over (bottom panel) the reference line are mapped.

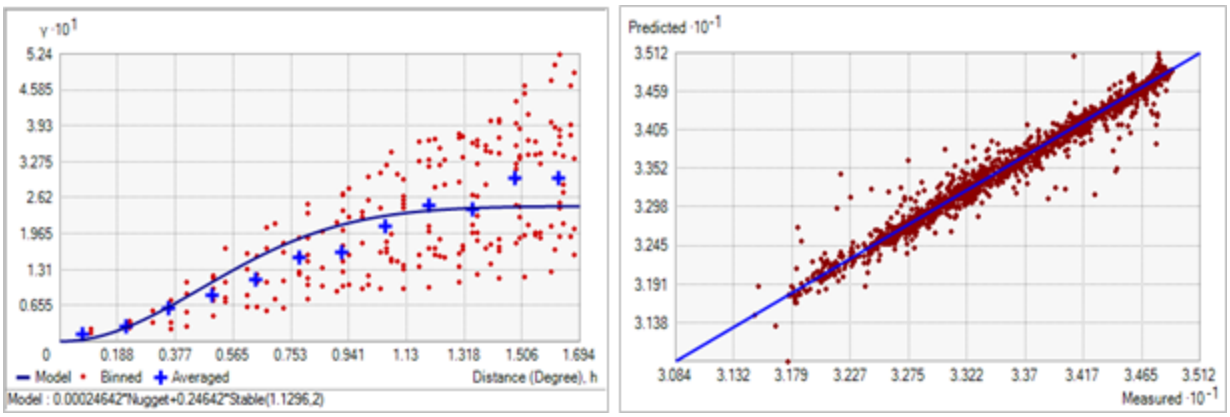

Figure 68. Left panel: Semivariogram of Bottom Salinity Minimum. Binned values are shown as red dots; average points are shown as blue crosses; the model fit to the averaged values is shown as a blue line. Lag size: 0.141 degrees; number of lags: 12; Parameter: 2; Range: 1.130 degrees; Partial Sill: 0.246. Right panel: Scatterplot of predicted values versus observed values for the model of Bottom Salinity Minimum.

Table 34. Results of cross-validation of the kriged model for Bottom Salinity Minimum.

Prediction error	**Value**
Number of Observations	2975
Overall Mean Error	-6.419×10^{-5}
Root Mean Square Prediction Error	0.110
Standardized Mean	1.255×10^{-3}
Standardized Root Mean Square Prediction Error	4.554
Average Standard Error	0.024

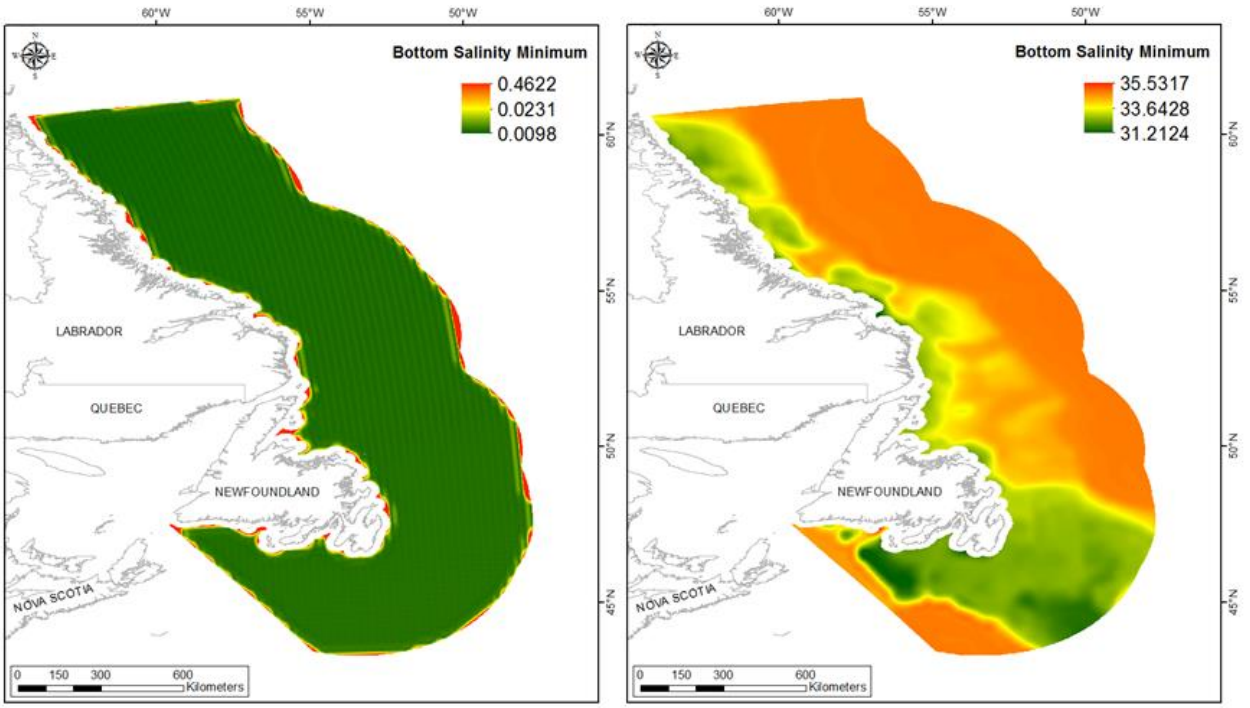

Figure 69. Left panel: Prediction standard error surface of Bottom Salinity Minimum. Right panel: Interpolated prediction surface of Bottom Salinity Minimum.

Bottom Salinity Maximum

This variable displayed a left-skewed distribution with kurtosis prior to modeling (Table 35, Figure 70). The data deviated strongly from a normal distribution at both the tails and mid-values. The areas of under- and over-prediction showed no strong spatial pattern over the spatial extent (Figure 71).

The semivariogram showed moderate autocorrelation present in the data and there was a good predictive fit (Figure 72). The kriged model showed fair cross-validation statistics (Table 36). The error map showed low error and no strong spatial pattern over the spatial extent but was higher along the coast (Figure 73). The kriged surface is presented in Figure 73.

Table 35. Distributional properties of Bottom Salinity Maximum.

Property	Value
Number of Observations	2975
Minimum	32.916
Maximum	35.744
Mean	34.615
Median	34.913
Standard Deviation	0.517
Skewness	-1.201
Kurtosis	3.344

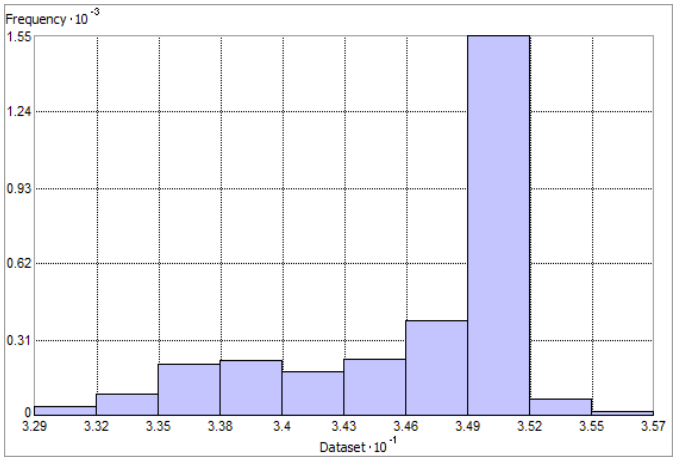

Figure 70. Distribution of Bottom Salinity Maximum. Histogram was illustrated using 10 bins. X axis is shown at 10^{-1}; Y axis is shown at 10^{-3}.

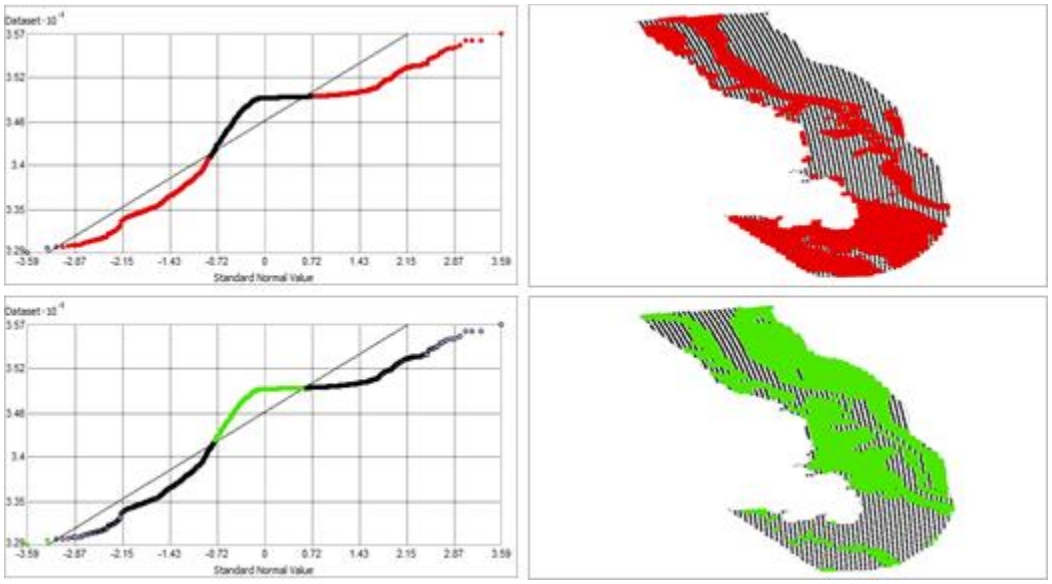

Figure 71. Normal Q-Q plot for data values of Bottom Salinity Maximum. Points falling under (upper panel) and over (bottom panel) the reference line are mapped.

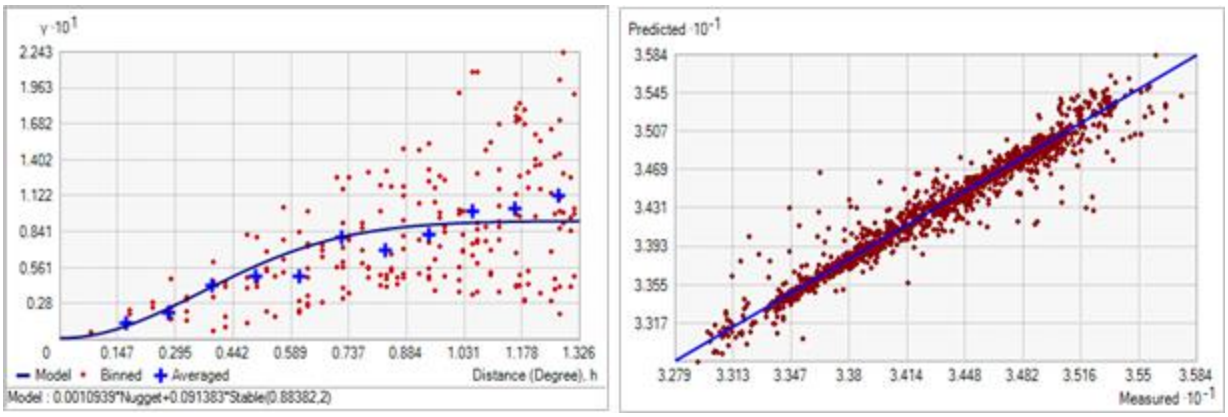

Figure 72. Left panel: Semivariogram of Bottom Salinity Maximum. Binned values are shown as red dots; average points are shown as blue crosses; the model fit to the averaged values is shown as a blue line. Lag size: 0.110 degrees; number of lags: 12; Parameter: 2; Range: 0.884 degrees; Partial Sill: 0.091. Right panel: Scatterplot of predicted values versus observed values for the model of Bottom Salinity Maximum.

Table 36. Results of cross-validation of the kriged model for Bottom Salinity Maximum.

Prediction error	**Value**
Number of Observations	2975
Overall Mean Error	2.572×10^{-4}
Root Mean Square Prediction Error	0.096
Standardized Mean	3.955×10^{-3}
Standardized Root Mean Square Prediction Error	2.046
Average Standard Error	0.046

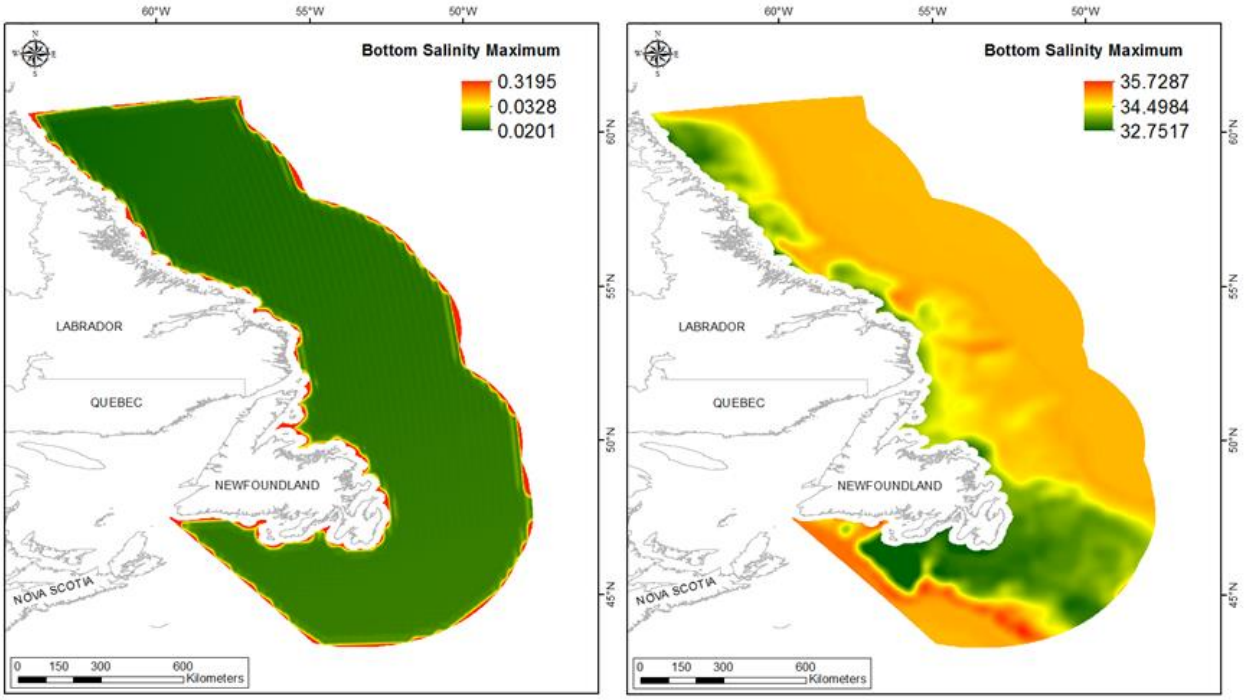

Figure 73. Left panel: Prediction standard error surface of Bottom Salinity Maximum. Right panel: Interpolated prediction surface of Bottom Salinity Maximum.

Bottom Salinity Range

This variable displayed a right-skewed distribution with kurtosis prior to modeling (Table 37, Figure 74). The data were lower than predicted by a normal distribution at low values and higher than predicted at high values (Figure 75). The data deviated strongly from a normal distribution at both tails (Figure 75). Values under and over the reference line showed a spatial pattern (Figure 92).

The semivariogram showed moderate autocorrelation present in the data and there was a good predictive fit (Figure 76). The kriged model showed fair cross-validation statistics (Table 38). The error map showed low error and no strong spatial pattern over the spatial extent but was higher along the coast (Figure 77). The kriged surface is presented in Figure 77.

Table 37. Distributional properties of Bottom Salinity Range.

Property	Value
Number of Observations	2975
Minimum	0.027
Maximum	2.653
Mean	0.559
Median	0.501
Standard Deviation	0.503
Skewness	0.959
Kurtosis	3.788

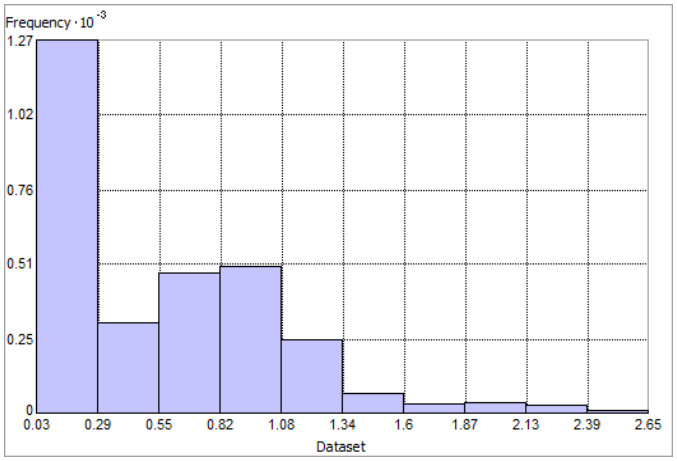

Figure 74. Distribution of Bottom Salinity Range. Histogram was illustrated using 10 bins. Y axis is shown at 10^{-3}.

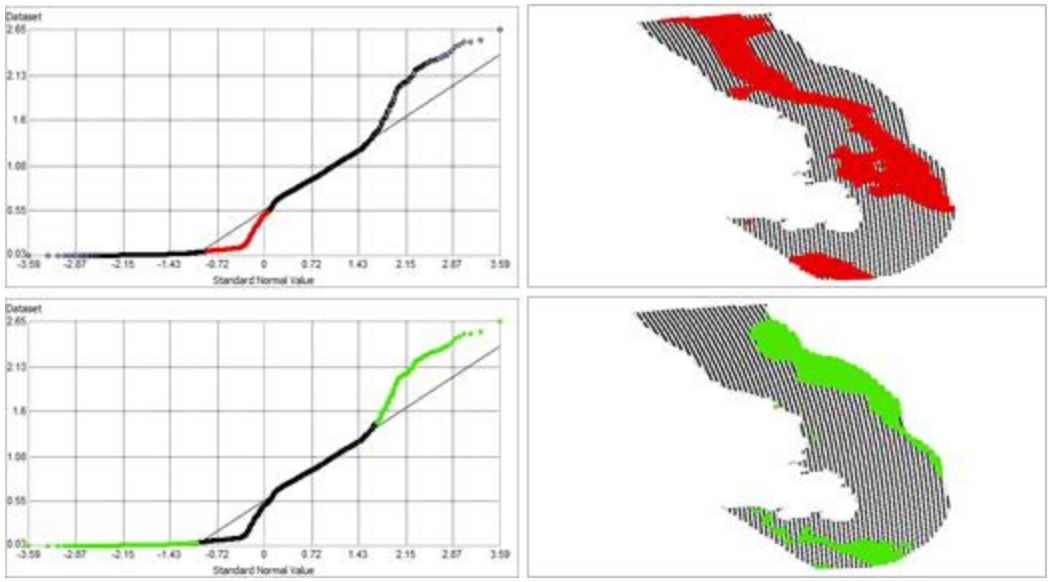

Figure 75. Normal Q-Q plot for data values of Bottom Salinity Range. Points falling under (upper panel) and over (bottom panel) the reference line are mapped.

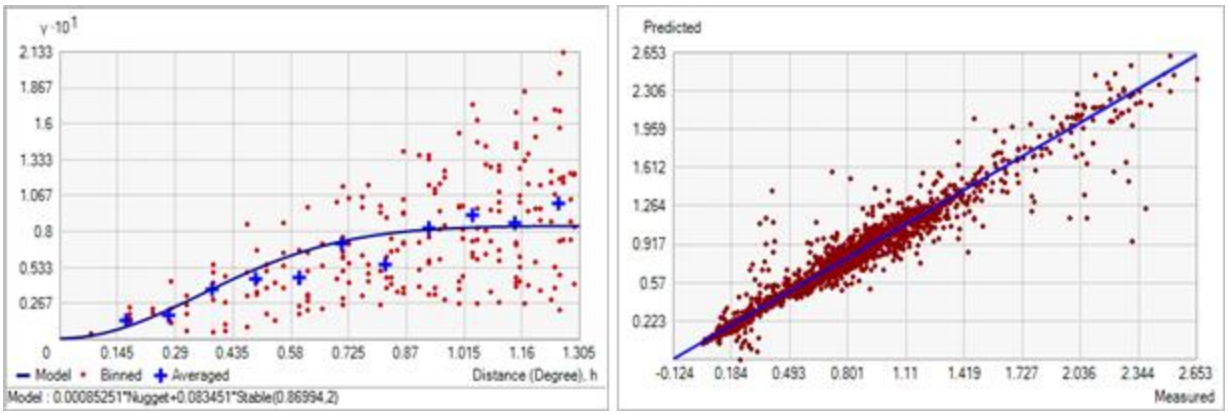

Figure 76. Left panel: Semivariogram of Bottom Salinity Range. Binned values are shown as red dots; average points are shown as blue crosses; the model fit to the averaged values is shown as a blue line. Lag size: 0.109 degrees; number of lags: 12; Parameter: 2; Range: 0.870 degrees; Partial Sill: 0.083. Right panel: Scatterplot of predicted values versus observed values for the model of Bottom Salinity Range.

Table 38. Results of cross-validation of the kriged model for Bottom Salinity Range.

Prediction error	**Value**
Number of Observations	2975
Overall Mean Error	-1.476×10^{-4}
Root Mean Square Prediction Error	0.100
Standardized Mean	-1.671×10^{-3}
Standardized Root Mean Square Prediction Error	2.403
Average Standard Error	0.042

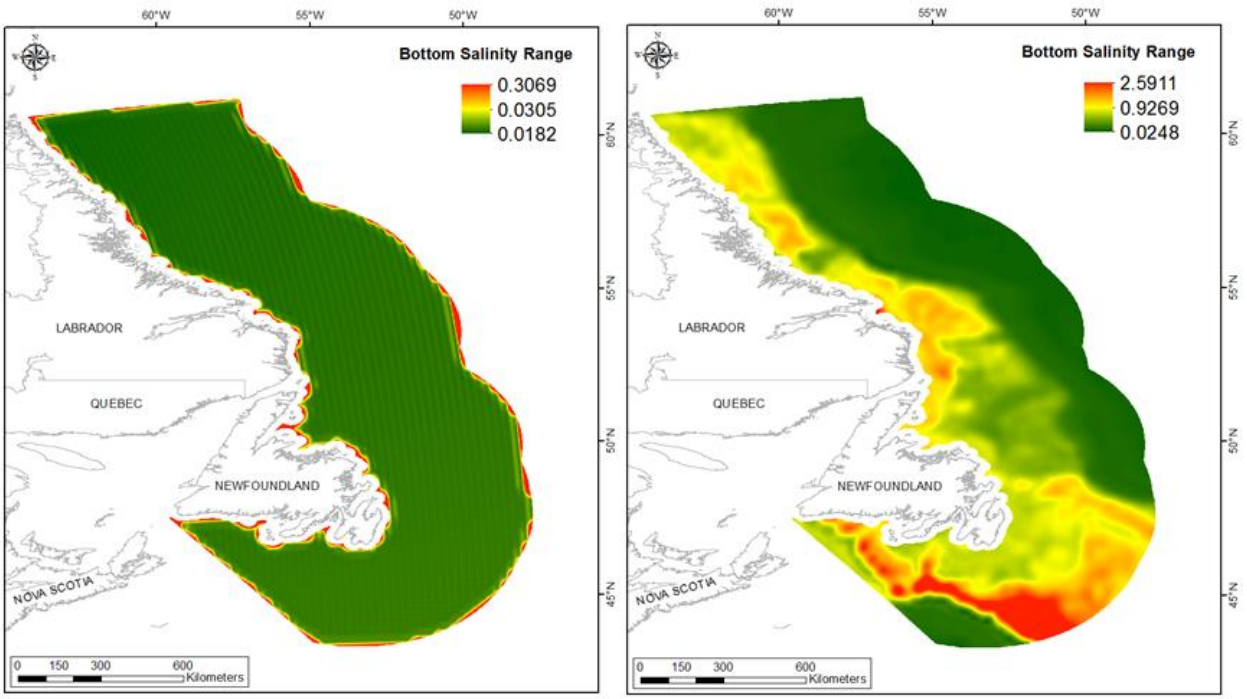

Figure 77. Left panel: Prediction standard error surface of Bottom Salinity Range. Right panel: Interpolated prediction surface of Bottom Salinity Range.

Bottom Salinity Average Minimum

This variable displayed a left-skewed distribution prior to modeling (Table 39, Figure 78). The data were lower than predicted by a normal distribution at mid-range and high values (Figure 79). Upper mid-range and low values were slightly higher than the reference line. There was a strong spatial pattern to the under- and over-prediction with the entire extent falling into one or other bias (Figure 79).

The semivariogram showed weak autocorrelation present in the data and there was a good predictive fit (Figure 80). The kriged model showed fair cross-validation statistics (Table 40). The error map showed a 'bullseye' pattern with error increasing with distance from data points (Figure 81). The kriged surface is presented in Figure 81.

Table 39. Distributional properties of Bottom Salinity Average Minimum.

Property	Value
Number of Observations	2975
Minimum	32.054
Maximum	34.924
Mean	34.205
Median	34.631
Standard Deviation	0.793
Skewness	-0.780
Kurtosis	2.125

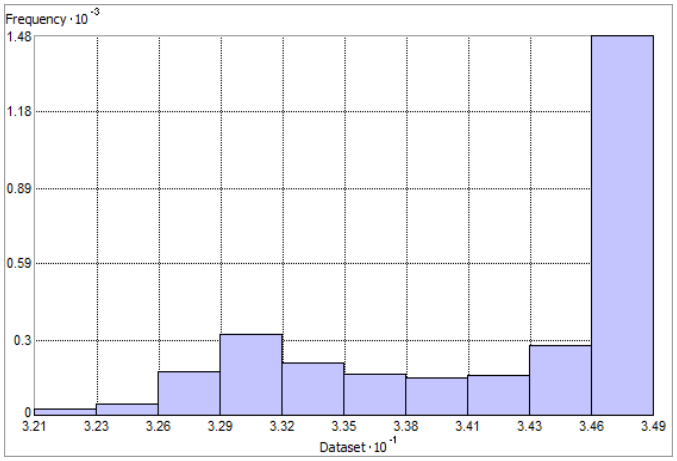

Figure 78. Distribution of Bottom Salinity Average Minimum. Histogram was illustrated using 10 bins. X axis is shown at 10^{-1} Y axis is shown at 10^{-3}.

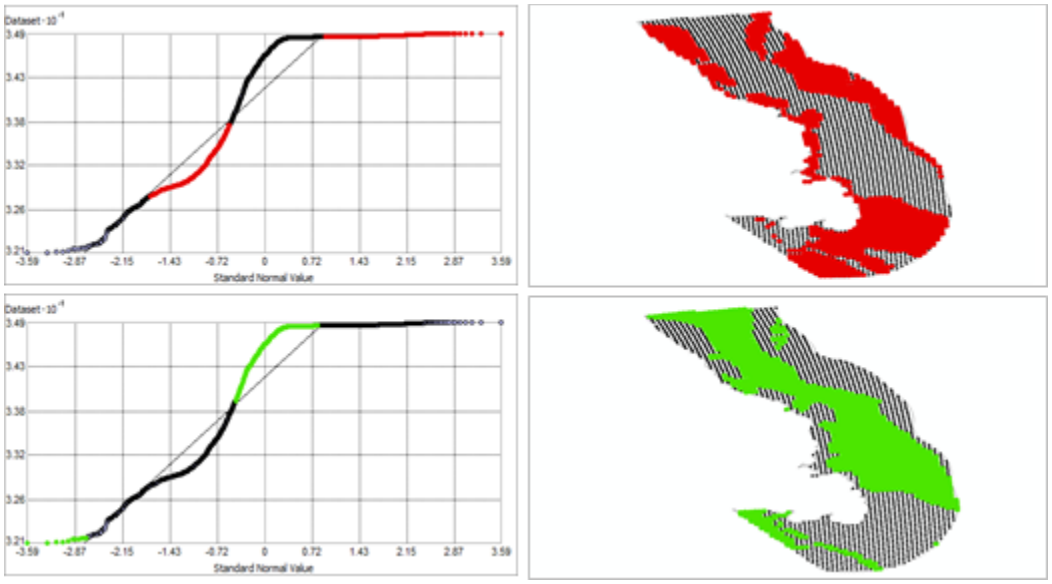

Figure 79. Normal Q-Q plot for data values of Bottom Salinity Average Minimum. Points falling under (upper panel) and over (bottom panel) the reference line are mapped.

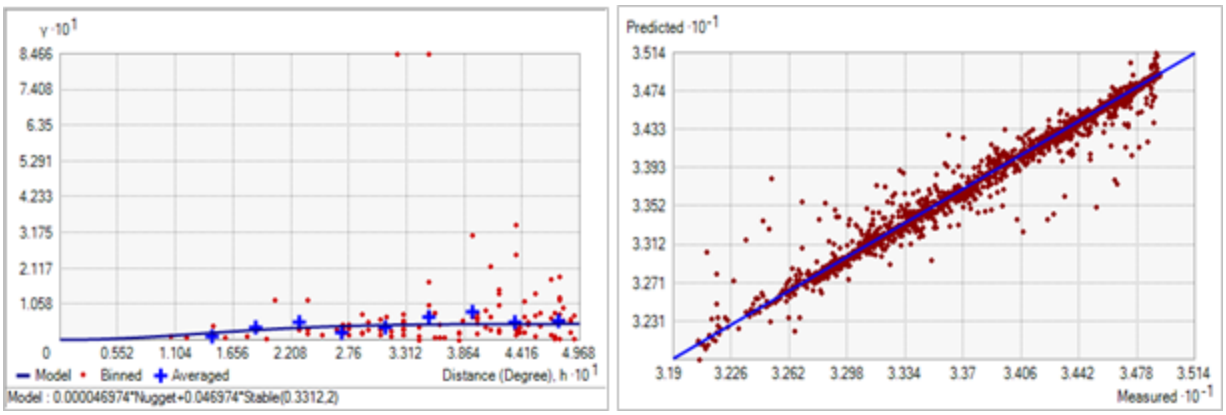

Figure 80. Left panel: Semivariogram of Bottom Salinity Average Minimum. Binned values are shown as red dots; average points are shown as blue crosses; the model fit to the averaged values is shown as a blue line. Lag size: 0.041 degrees; number of lags: 12; Parameter: 2; Range: 0.331 degrees; Partial Sill: 0.047. Right panel: Scatterplot of predicted values versus observed values for the model of Bottom Salinity Average Minimum.

Table 40. Results of cross-validation of the kriged model for Bottom Salinity Average Minimum.

Prediction error	**Value**
Number of Observations	2975
Overall Mean Error	6.620×10^{-4}
Root Mean Square Prediction Error	0.101
Standardized Mean	1.598×10^{-3}
Standardized Root Mean Square Prediction Error	0.653
Average Standard Error	0.144

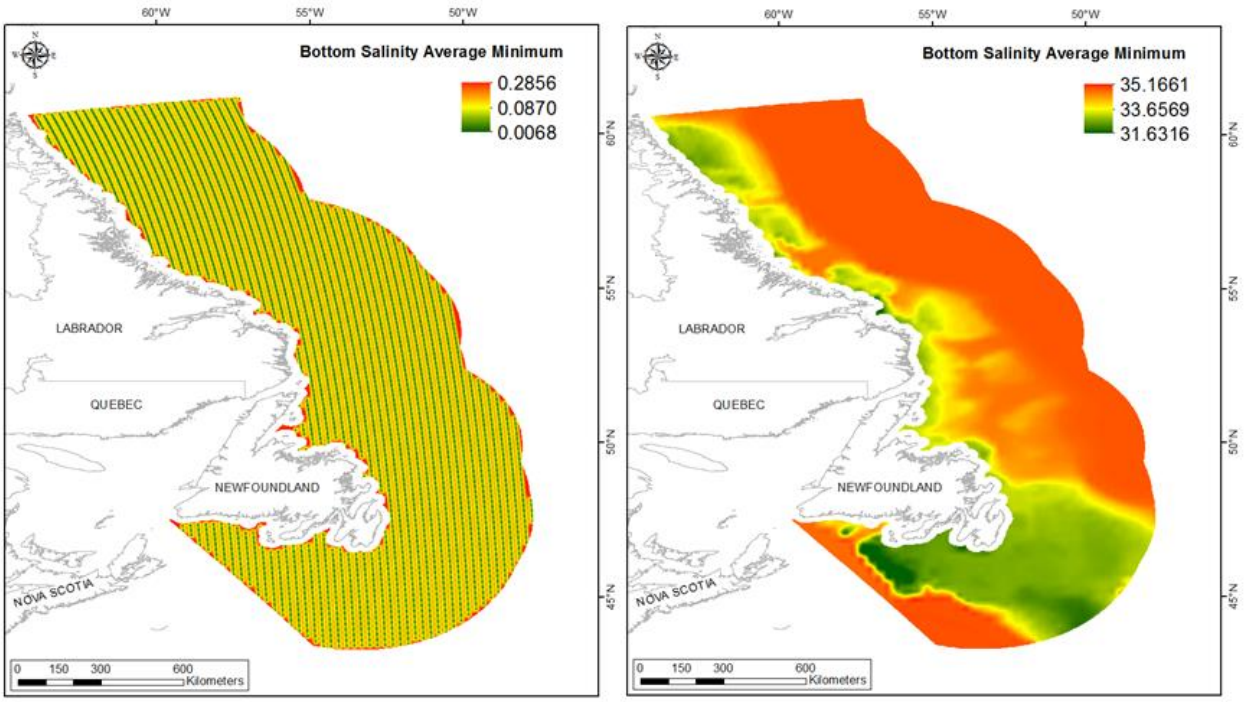

Figure 81. Left panel: Prediction standard error surface of Bottom Salinity Average Minimum. Right panel: Interpolated prediction surface of Bottom Salinity Average Minimum.

Bottom Salinity Average Maximum

This variable displayed a left-skewed distribution prior to modeling (Table 41, Figure 82). The data were lower than predicted by a normal distribution at low and high values (Figure 83). Mid-range and the lowest values were higher than the reference line. There was a strong spatial cohesion to the under- and over-prediction areas with the full spatial extent falling into one or other category (Figure 83).

The semivariogram showed moderate autocorrelation present in the data and there was a good predictive fit (Figure 84). The kriged model showed good cross-validation statistics (Table 42) indicating that it was good at prediction. The error map showed a 'bullseye' pattern with error increasing with distance from data points (Figure 85). The kriged surface is presented in Figure 85.

Table 41. Distributional properties of Bottom Salinity Average Maximum.

Property	Value
Number of Observations	2975
Minimum	32.670
Maximum	35.314
Mean	34.455
Median	34.828
Standard Deviation	0.609
Skewness	-1.063
Kurtosis	2.748

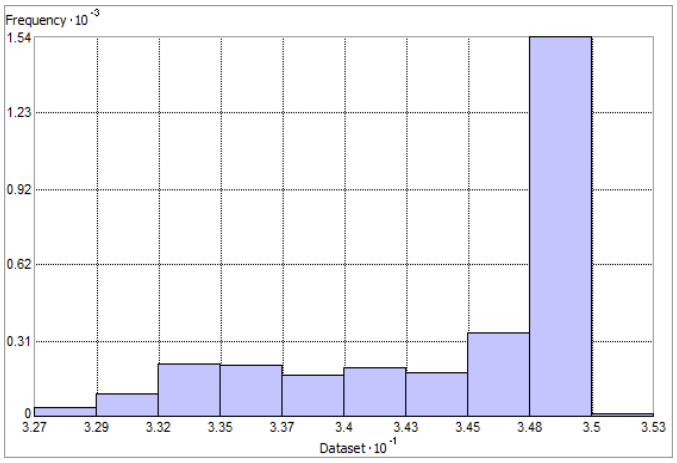

Figure 82. Distribution of Bottom Salinity Average Maximum. Histogram was illustrated using 10 bins. X axis is shown at 10^{-1} Y axis is shown at 10^{-3}.

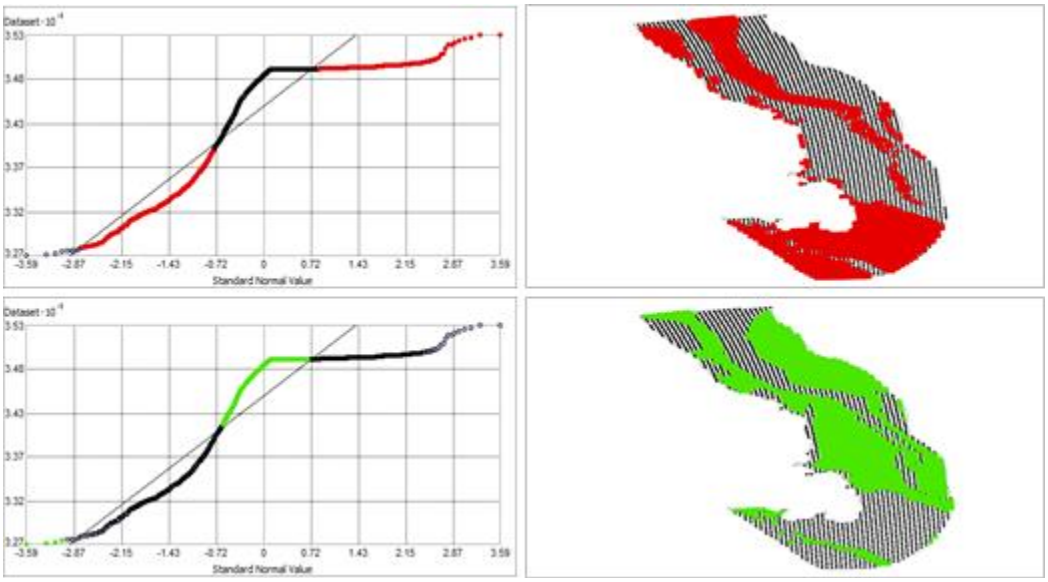

Figure 83. Normal Q-Q plot for data values of Bottom Salinity Average Maximum. Points falling under (upper panel) and over (bottom panel) the reference line are mapped.

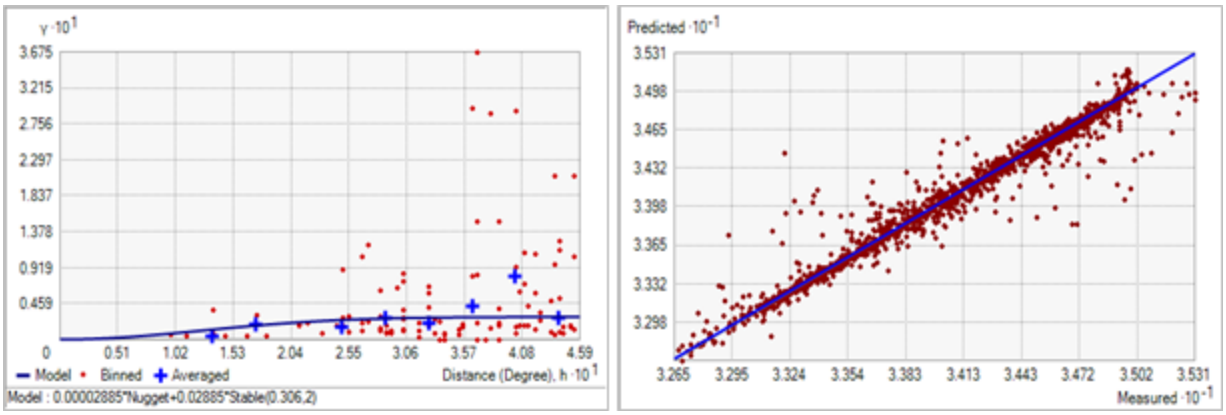

Figure 84. Left panel: Semivariogram of Bottom Salinity Average Maximum. Binned values are shown as red dots; average points are shown as blue crosses; the model fit to the averaged values is shown as a blue line. Lag size: 0.038 degrees; number of lags: 12; Parameter: 2; Range: 0.306 degrees; Partial Sill: 0.029. Right panel: Scatterplot of predicted values versus observed values for the model of Bottom Salinity Average Maximum.

Table 42. Results of cross-validation of the kriged model for Bottom Salinity Average Maximum.

Prediction error	**Value**
Number of Observations	2975
Overall Mean Error	4.839×10^{-4}
Root Mean Square Prediction Error	0.091
Standardized Mean	1.676×10^{-3}
Standardized Root Mean Square Prediction Error	0.667
Average Standard Error	0.126

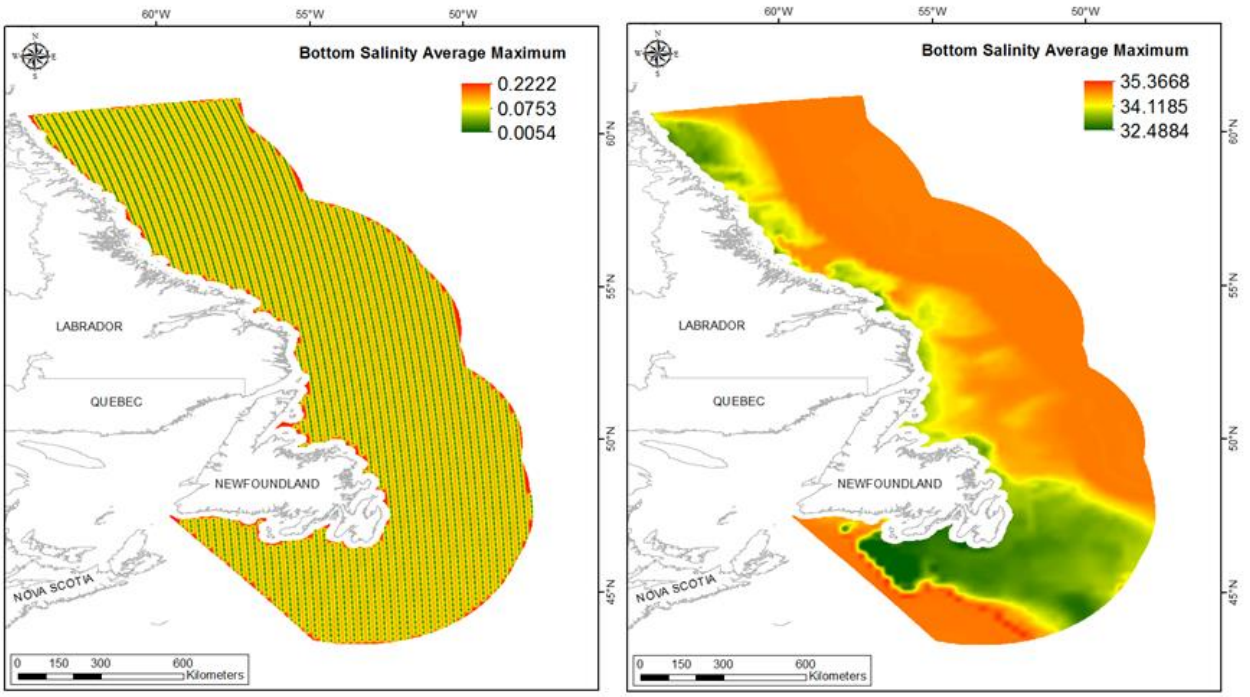

Figure 85. Left panel: Prediction standard error surface of Bottom Salinity Average Maximum. Right panel: Interpolated prediction surface of Bottom Salinity Average Maximum.

Bottom Salinity Average Range

This variable displayed a right-skewed distribution with kurtosis prior to modeling (Table 43, Figure 86). The data were higher than predicted by a normal distribution at low and high values, and mid-range values were lower than the reference line (Figure 87). There was a strong pattern to the areas of under- and over-prediction (Figure 87).

The semivariogram showed good autocorrelation present in the data, there was a good predictive fit (Figure 88). The kriged model showed good cross-validation statistics (Table 44) indicating that it was good at prediction. The error map showed a 'bullseye' pattern with error increasing with distance from data points (Figure 89). The kriged surface is presented in Figure 89. Negative values resulted in the prediction surface after ordinary kriging of this variable. This possibly resulted from the highly right-skewed nature exhibited in the raw data (see Figure 86). Of the 533592 raster cells in the study extent, only 20 contained negative values (see Table A1). These were located in an isolated patch along the southern edge of the study extent (see Figure A1).

Table 43. Distributional properties of Bottom Salinity Average Range.

Property	Value
Number of Observations	2975
Minimum	0.009
Maximum	1.259
Mean	0.250
Median	0.191
Standard Deviation	0.240
Skewness	1.003
Kurtosis	3.709

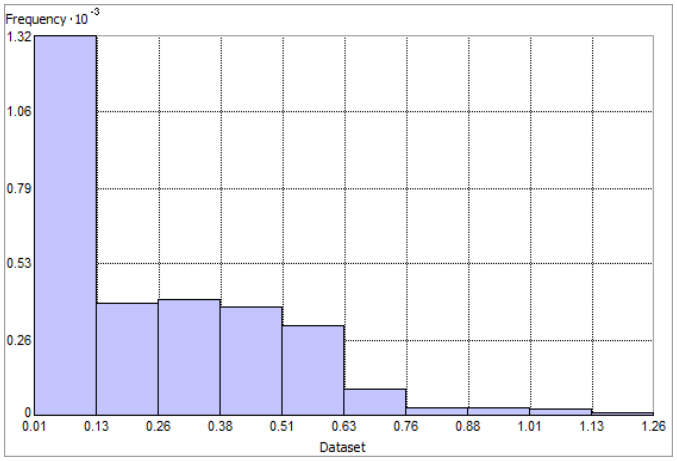

Figure 86. Distribution of Bottom Salinity Average Range. Histogram was illustrated using 10 bins. Y axis is shown at 10^{-3}.

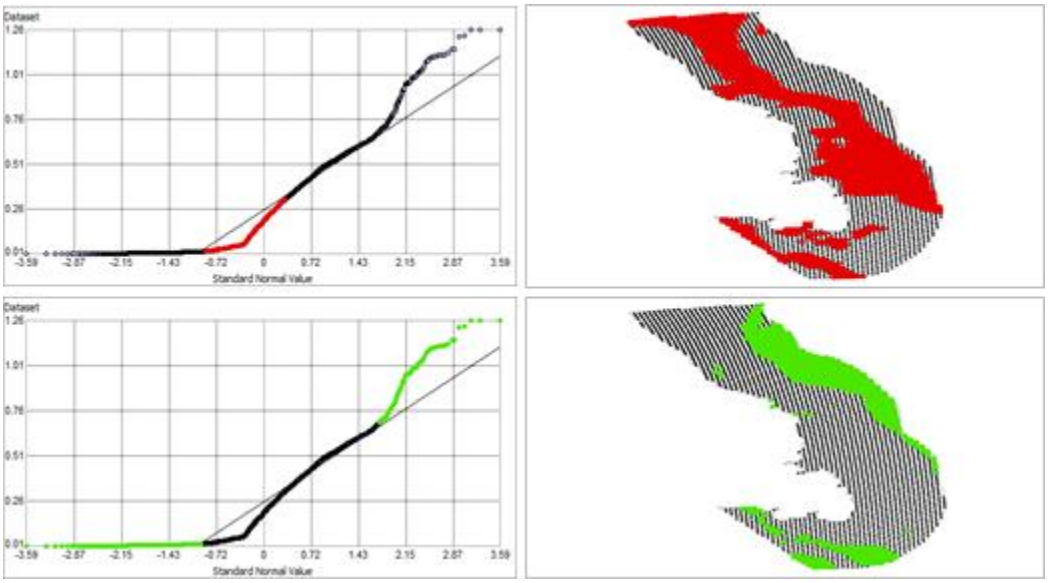

Figure 87. Normal Q-Q plot for data values of Bottom Salinity Average Range. Points falling under (upper panel) and over (bottom panel) the reference line are mapped.

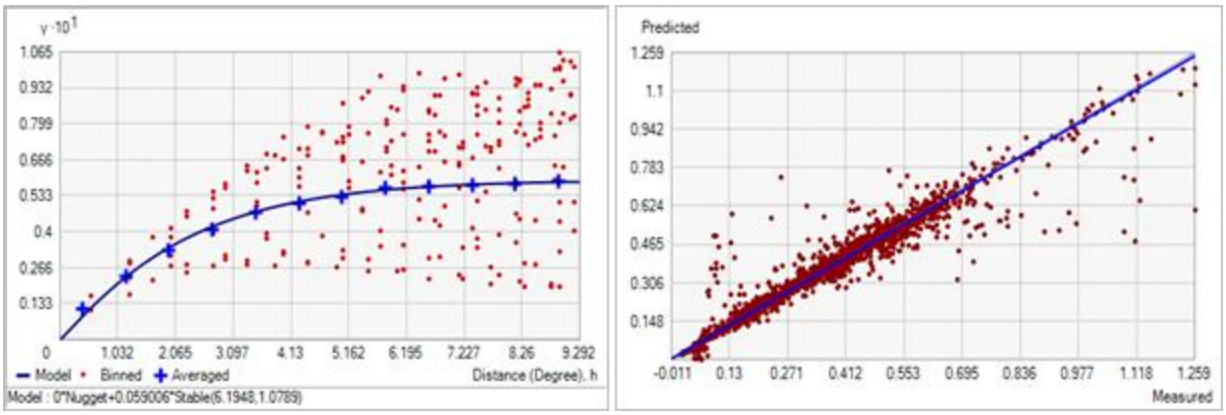

Figure 88. Left panel: Semivariogram of Bottom Salinity Average Range. Binned values are shown as red dots; average points are shown as blue crosses; the model fit to the averaged values is shown as a blue line. Lag size: 0.774 degrees; number of lags: 12; Parameter: 1.079; Range: 6.195 degrees; Partial Sill: 0.059. Right panel: Scatterplot of predicted values versus observed values for the model of Bottom Salinity Average Range.

Table 44. Results of cross-validation of the kriged model for Bottom Salinity Average Range.

Prediction error	**Value**
Number of Observations	2975
Overall Mean Error	-1.312×10^{-4}
Root Mean Square Prediction Error	0.051
Standardized Mean	-1.140×10^{-3}
Standardized Root Mean Square Prediction Error	0.893
Average Standard Error	0.055

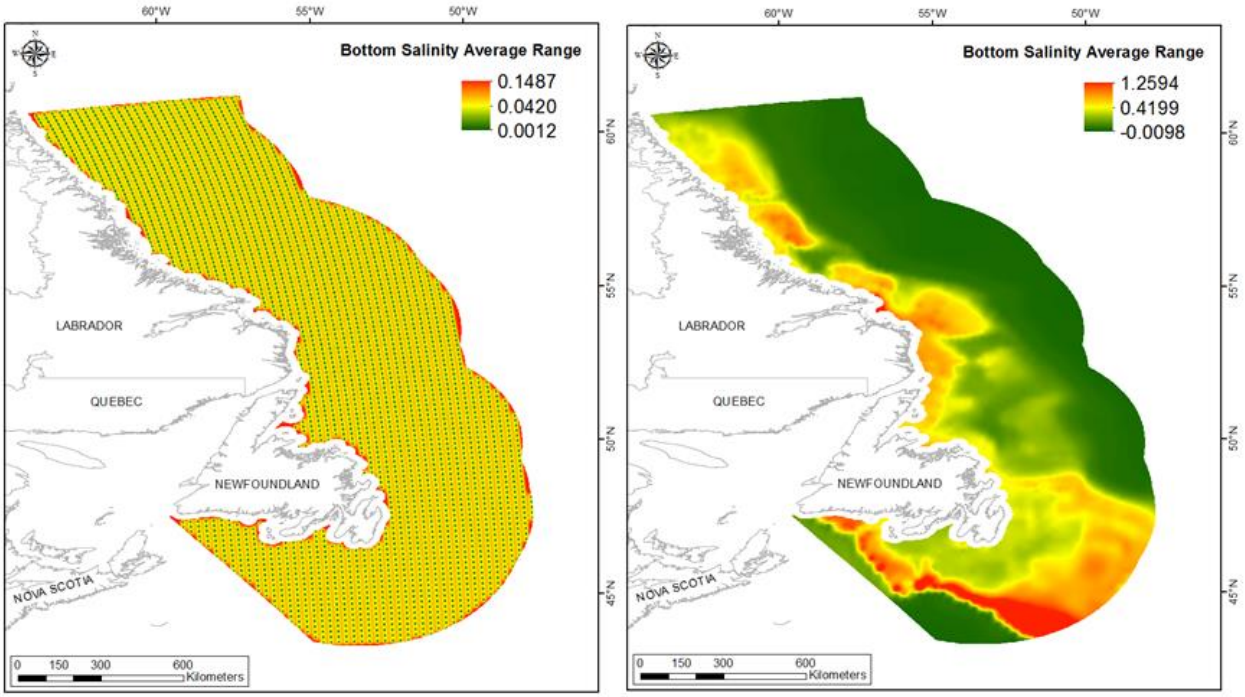

Figure 89. Left panel: Prediction standard error surface of Bottom Salinity Average Range. Right panel: Interpolated prediction surface of Bottom Salinity Average Range.

Surface Salinity Mean

This variable displayed a bimodal distribution prior to modeling (Table 45, Figure 90). The data were lower than predicted by a normal distribution at mid-range and high values (Figure 91). Low and upper mid values were higher than the reference line. There was a spatial pattern to the under- and over-prediction with the entire spatial extent falling into one or other bias (Figure 91).

The semivariogram showed good autocorrelation present in the data (Figure 92). There was an excellent predictive fit (Figure 92). The kriged model showed an excellent cross-validation statistics (Table 46). The error map showed a 'bullseye' pattern with error increasing with distance from data points (Figure 93). The kriged surface is presented in Figure 93.

Table 45. Distributional properties of Surface Salinity Mean.

Property	Value
Number of Observations	2975
Minimum	30.831
Maximum	34.482
Mean	33.012
Median	32.844
Standard Deviation	0.920
Skewness	0.041
Kurtosis	1.731

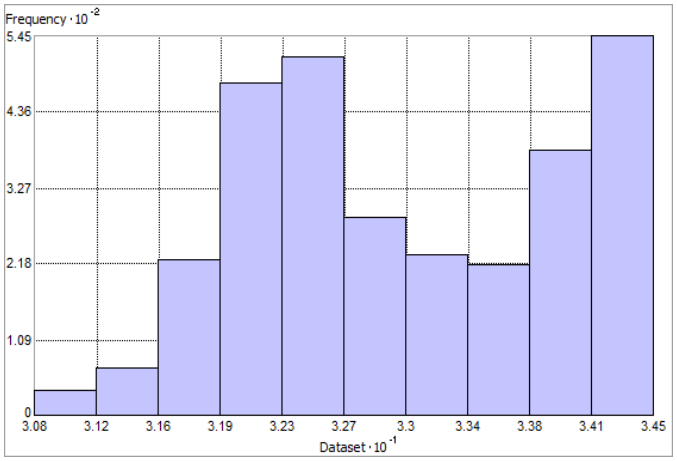

Figure 90. Distribution of Surface Salinity Mean. Histogram was illustrated using 10 bins. X axis is shown at 10^{-1}. Y axis is shown at 10^{-2}.

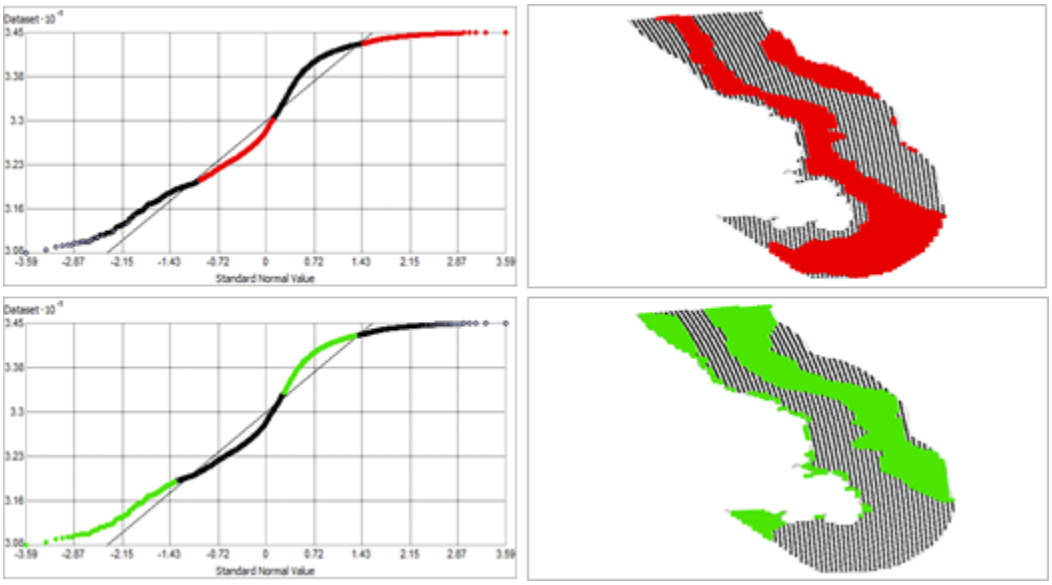

Figure 91. Normal Q-Q plot for data values of Surface Salinity Mean. Points falling under (upper panel) and over (bottom panel) the reference line are mapped.

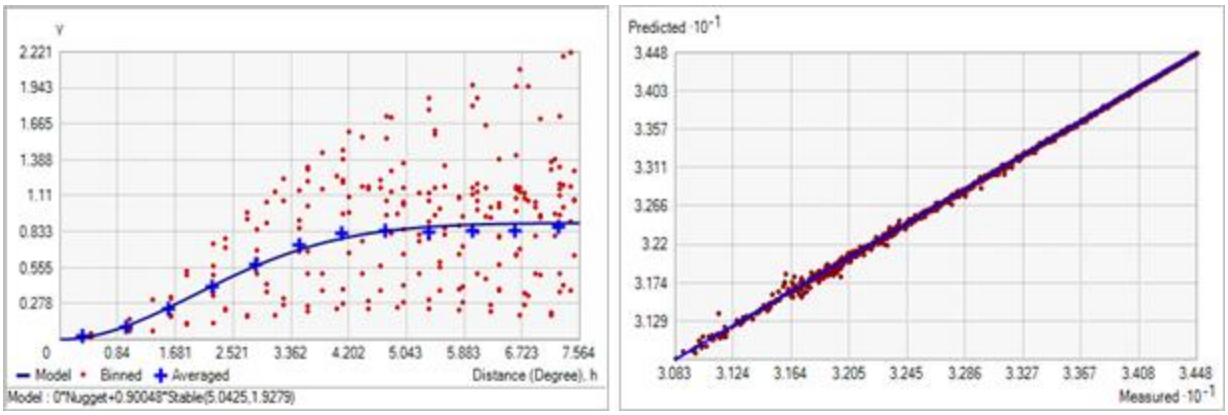

Figure 92. Left panel: Semivariogram of Surface Salinity Mean. Binned values are shown as red dots; average points are shown as blue crosses; the model fit to the averaged values is shown as a blue line. Lag size: 0.630 degrees; number of lags: 12; Parameter: 1.928; Range: 5.043 degrees; Partial Sill: 0.900. Right panel: Scatterplot of predicted values versus observed values for the model of Surface Salinity Mean.

Table 46. Results of cross-validation of the kriged model for Surface Salinity Mean.

Prediction error	**Value**
Number of Observations	2975
Overall Mean Error	2.392×10^{-4}
Root Mean Square Prediction Error	0.017
Standardized Mean	8.179×10^{-3}
Standardized Root Mean Square Prediction Error	0.958
Average Standard Error	0.017

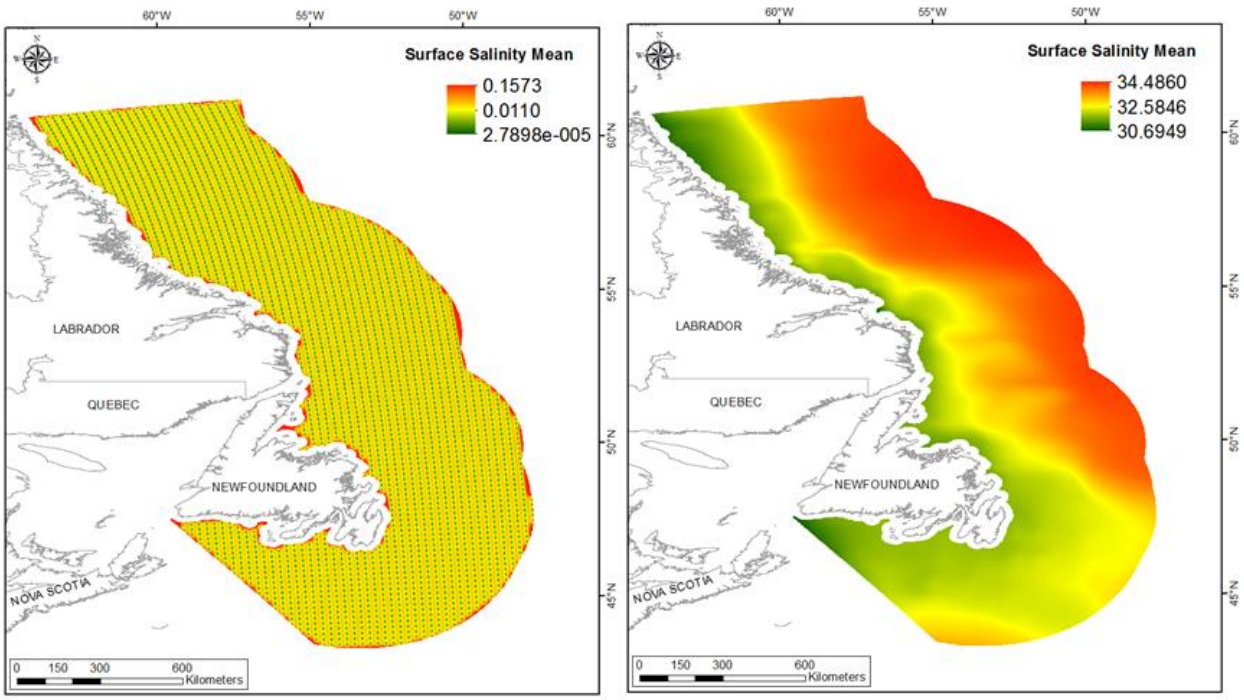

Figure 93. Left panel: Prediction standard error surface of Surface Salinity Mean. Right panel: Interpolated prediction surface of Surface Salinity Mean.

Surface Salinity Minimum

This variable displayed a slightly left-skewed distribution with kurtosis prior to modeling (Table 47, Figure 94). The data were lower than predicted by a normal distribution at low and high values (Figure 95). Mid-range values were slightly higher than the reference line. There was a strong spatial pattern to the under- and over-prediction (Figure 95).

The semivariogram showed weak autocorrelation present in the data (Figure 96). The kriged model showed an excellent fit between predicted and measured values (Figure 96) and an excellent cross-validation statistics (Table 46). The error map showed a 'bullseye' pattern with error increasing with distance from data points (Figure 97). The kriged surface is presented in Figure 97.

Table 47. Distributional properties of Surface Salinity Minimum.

Property	Value
Number of Observations	2975
Minimum	27.543
Maximum	33.670
Mean	31.624
Median	31.633
Standard Deviation	0.989
Skewness	-0.663
Kurtosis	4.036

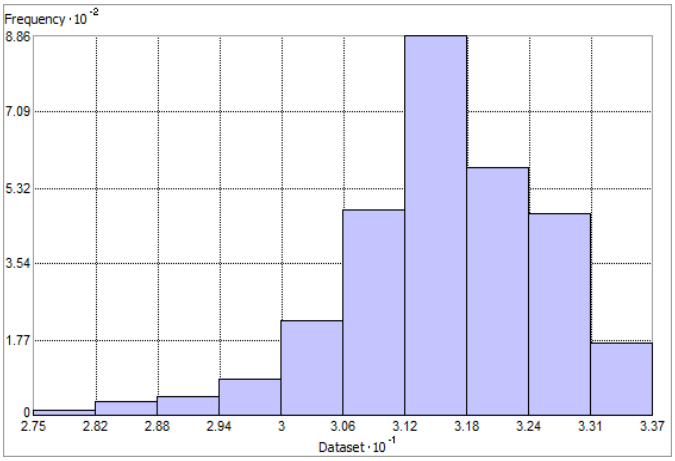

Figure 94. Distribution of Surface Salinity Minimum. Histogram was illustrated using 10 bins. X axis is shown at 10^{-1}; Y axis is shown at 10^{-2}.

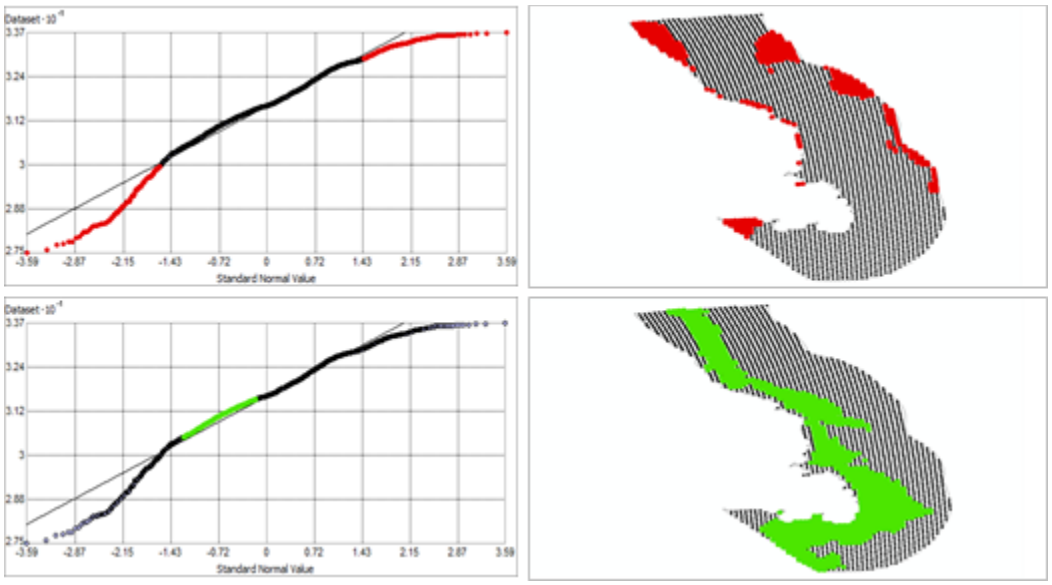

Figure 95. Normal Q-Q plot for data values of Surface Salinity Minimum. Points falling under (upper panel) and over (bottom panel) the reference line are mapped.

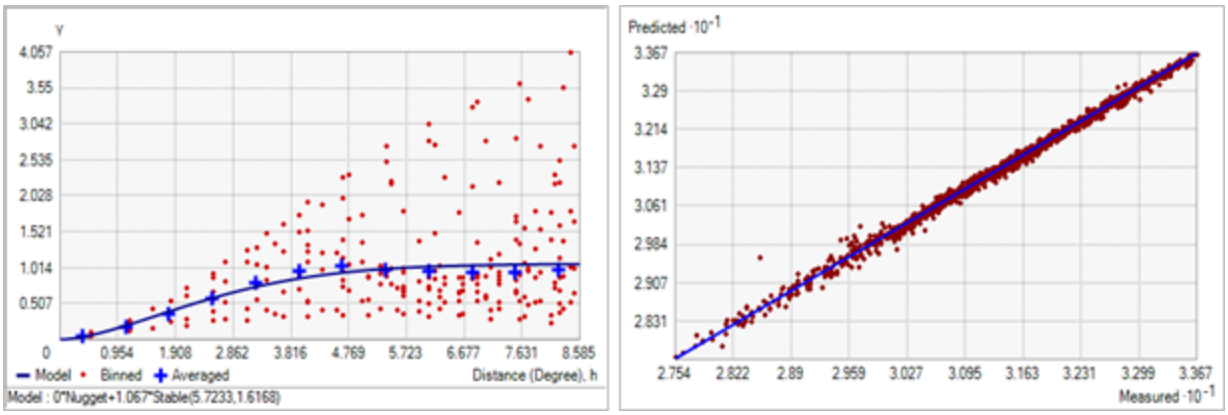

Figure 96. Left panel: Semivariogram of Surface Salinity Minimum. Binned values are shown as red dots; average points are shown as blue crosses; the model fit to the averaged values is shown as a blue line. Lag size: 0.715 degrees; number of lags: 12; Parameter: 1.617; Range: 5.723 degrees; Partial Sill: 1.067. Right panel: Scatterplot of predicted values versus observed values for the model of Surface Salinity Minimum.

Table 48. Results of cross-validation of the kriged model for Surface Salinity Minimum.

Prediction error	**Value**
Number of Observations	2975
Overall Mean Error	7.597×10^{-4}
Root Mean Square Prediction Error	0.060
Standardized Mean	5.610×10^{-3}
Standardized Root Mean Square Prediction Error	0.897
Average Standard Error	0.063

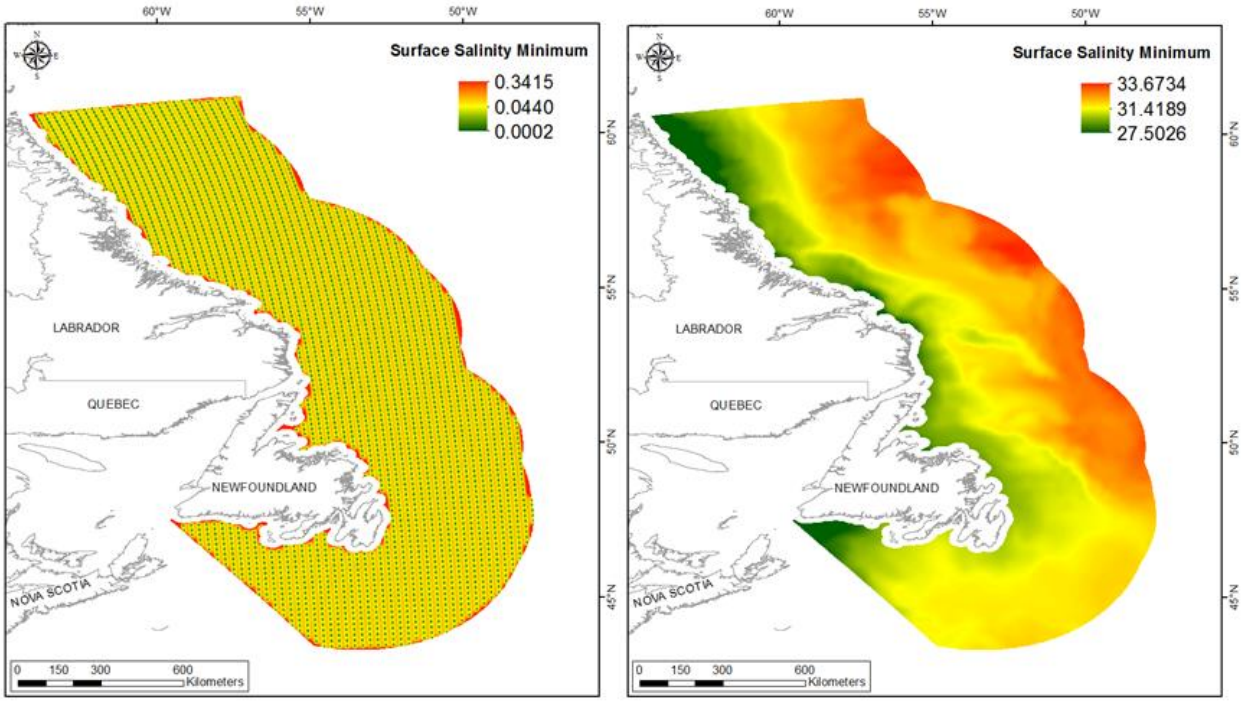

Figure 97. Left panel: Prediction standard error surface of Surface Salinity Minimum. Right panel: Interpolated prediction surface of Surface Salinity Minimum.

Surface Salinity Maximum

This variable displayed a bimodal distribution prior to modeling (Table 49, Figure 98). The data were lower than predicted by a normal distribution at mid-range and high values (Figure 99). Upper mid-range and low values were higher than the reference line. There was a spatial pattern to the under- and over-prediction (Figure 99).

The semivariogram showed weak autocorrelation present in the data and an excellent predictive fit (Figure 100). The model showed good cross-validation statistics (Table 50) indicating that it was good at prediction, although the standardized root mean square was less than 1 indicating that variability in the predictions has been overestimated. The error map showed a 'bullseye' pattern with error increasing with distance from data points (Figure 101). The kriged surface is presented in Figure 101.

Table 49. Distributional properties of Surface Salinity Maximum.

Property	Value
Number of Observations	2975
Minimum	32.267
Maximum	35.207
Mean	33.943
Median	33.908
Standard Deviation	0.760
Skewness	-0.183
Kurtosis	1.662

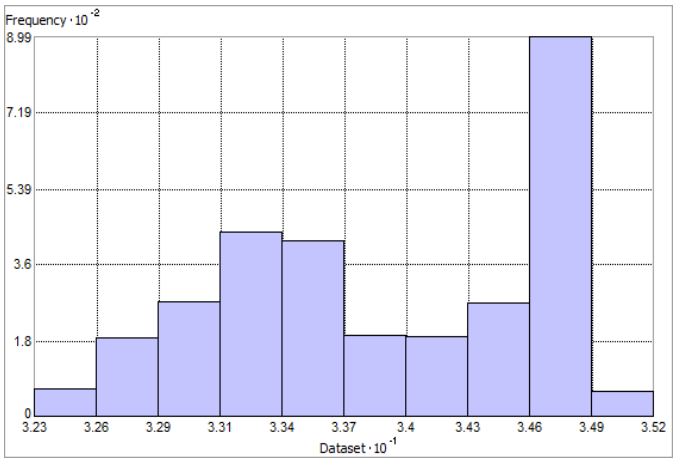

Figure 98. Distribution of Surface Salinity Maximum. Histogram was illustrated using 10 bins. X axis is shown at 10^{-1}; Y axis is shown at 10^{-2}.

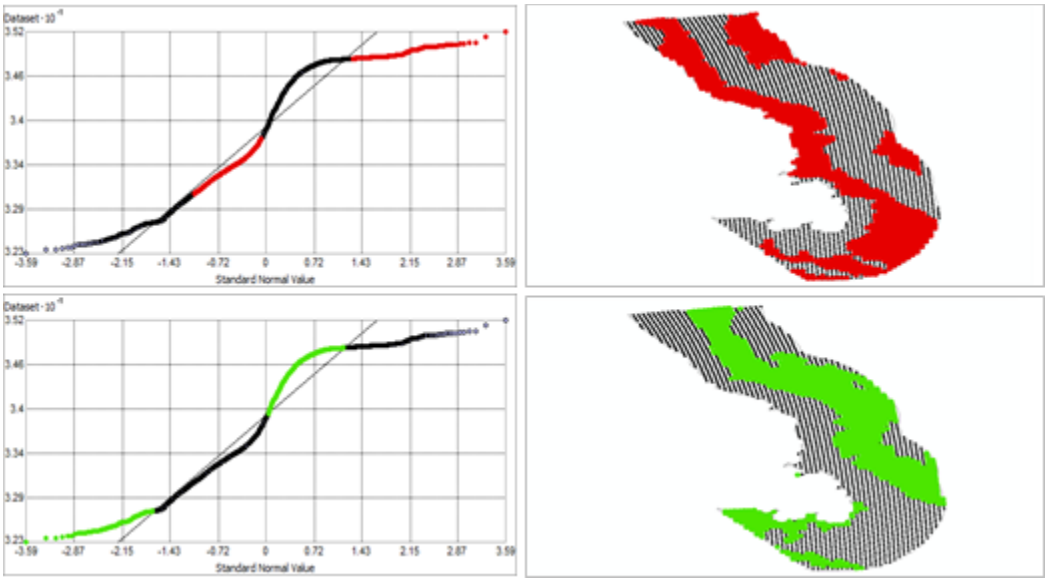

Figure 99. Normal Q-Q plot for data values of Surface Salinity Maximum. Points falling under (upper panel) and over (bottom panel) the reference line are mapped.

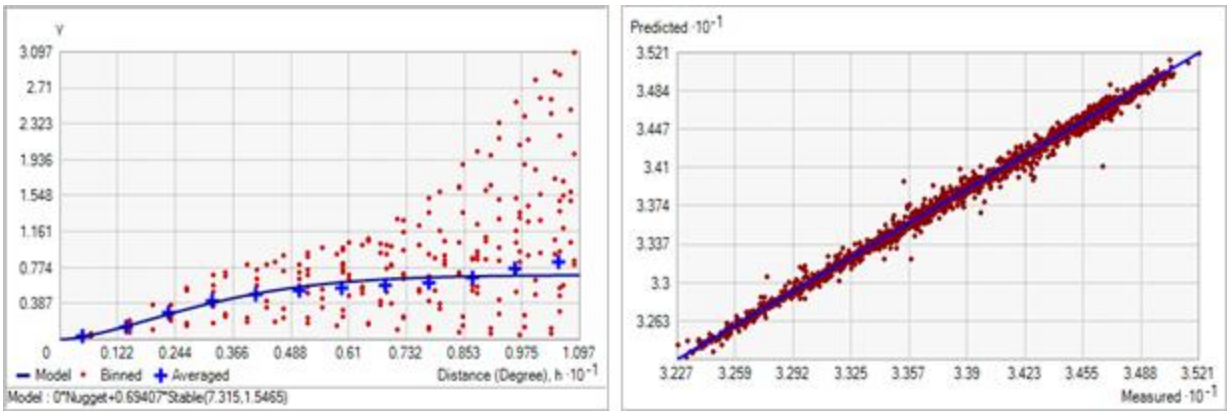

Figure 100. Left panel: Semivariogram of Surface Salinity Maximum. Binned values are shown as red dots; average points are shown as blue crosses; the model fit to the averaged values is shown as a blue line. Lag size: 0.914 degrees; number of lags: 12; Parameter: 1.546; Range: 7.315 degrees; Partial Sill: 0.694. Right panel: Scatterplot of predicted values versus observed values for the model of Surface Salinity Maximum.

Table 50. Results of cross-validation of the kriged model for Surface Salinity Maximum.

Prediction error	**Value**
Number of Observations	2975
Overall Mean Error	5.157×10^{-5}
Root Mean Square Prediction Error	0.041
Standardized Mean	4.726×10^{-4}
Standardized Root Mean Square Prediction Error	0.794
Average Standard Error	0.052

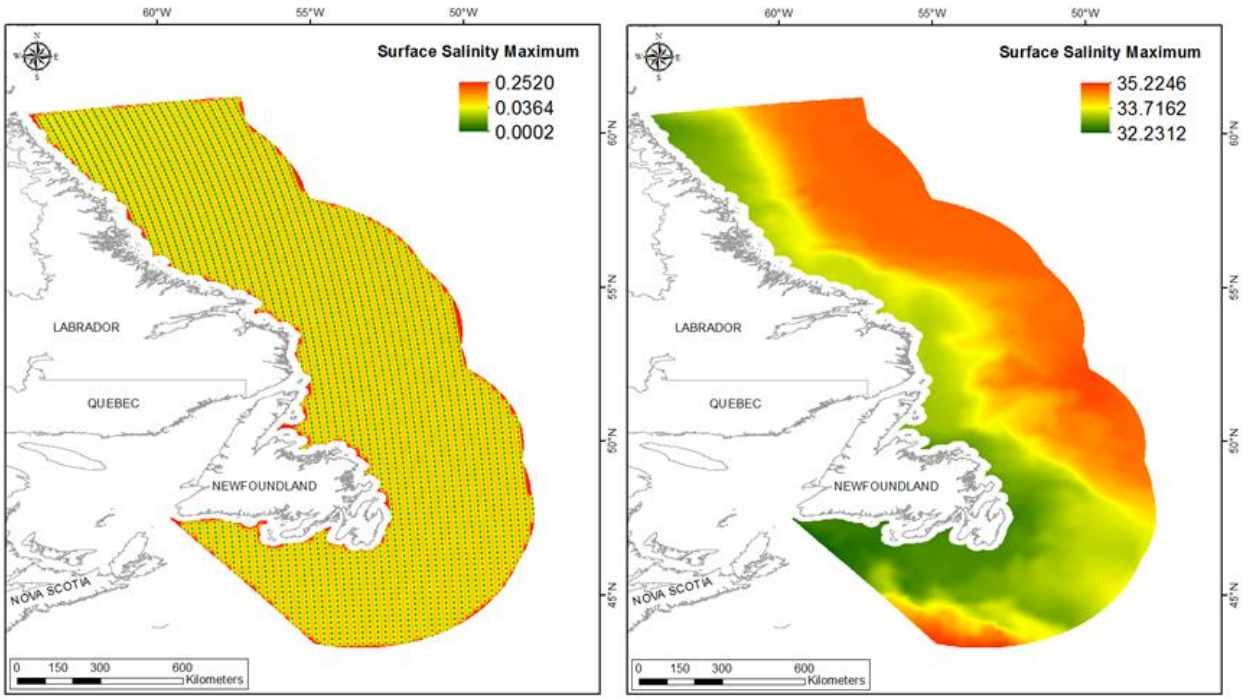

Figure 101. Left panel: Prediction standard error surface of Surface Salinity Maximum. Right panel: Interpolated prediction surface of Surface Salinity Maximum.

Surface Salinity Range

This variable displayed a right-skewed distribution with kurtosis prior to modeling (Table 51, Figure 102). The data were higher than predicted by a normal distribution at low and high values (Figure 103), with mid-range values falling slightly lower than the reference line. There was no strong spatial pattern to the under- and over-prediction (Figure 103).

The semivariogram showed moderate autocorrelation present in the data (Figure 104). The model showed a good fit between measured and predicted values (Figure 104) but poor cross-validation statistics indicating that it was poor at prediction (Table 52). The standardized root mean square was greater than 1 indicating that variability in the predictions has been underestimated. The error map showed low error and no strong spatial pattern over the spatial extent although error was highest along the coast (Figure 105). The kriged surface is presented in Figure 105.

Table 51. Distributional properties of Surface Salinity Range.

Property	Value
Number of Observations	2975
Minimum	1.164
Maximum	5.423
Mean	2.319
Median	2.290
Standard Deviation	0.604
Skewness	0.924
Kurtosis	5.081

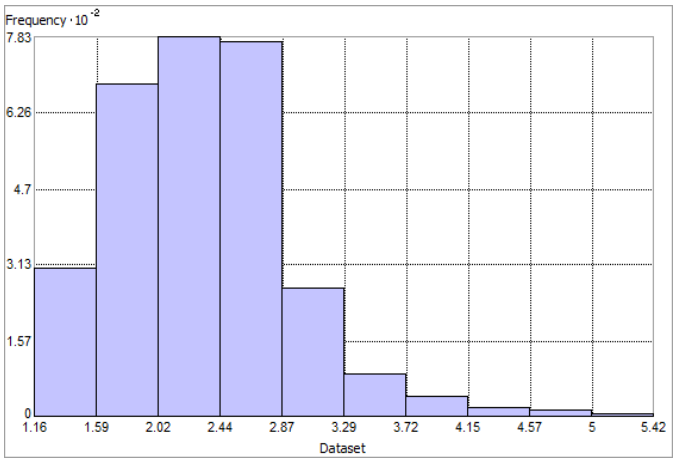

Figure 102. Distribution of Surface Salinity Range. Histogram was illustrated using 10 bins. Y axis is shown at 10^{-2}.

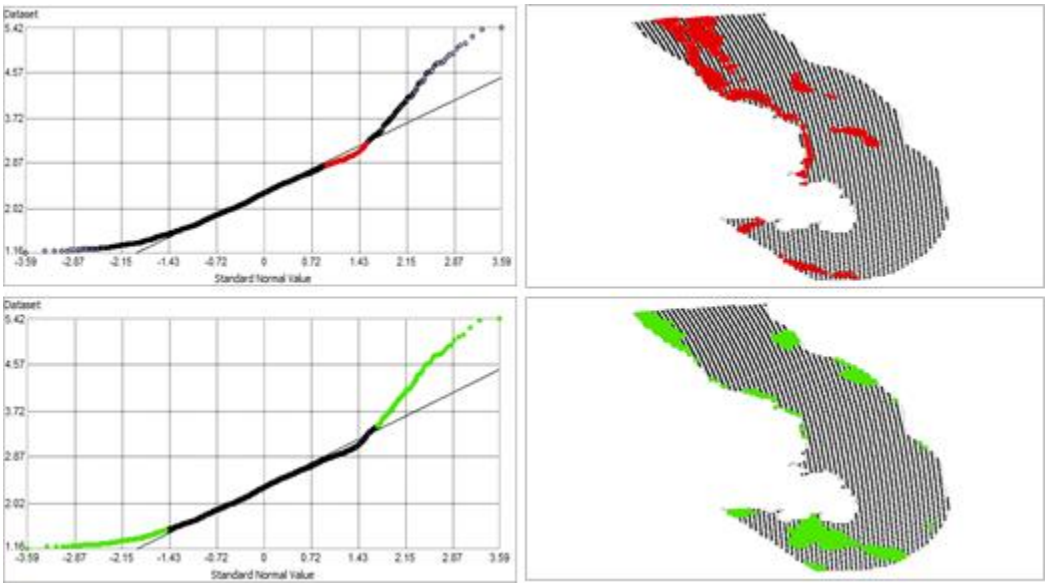

Figure 103. Normal Q-Q plot for data values of Surface Salinity Range. Points falling under (upper panel) and over (bottom panel) the reference line are mapped.

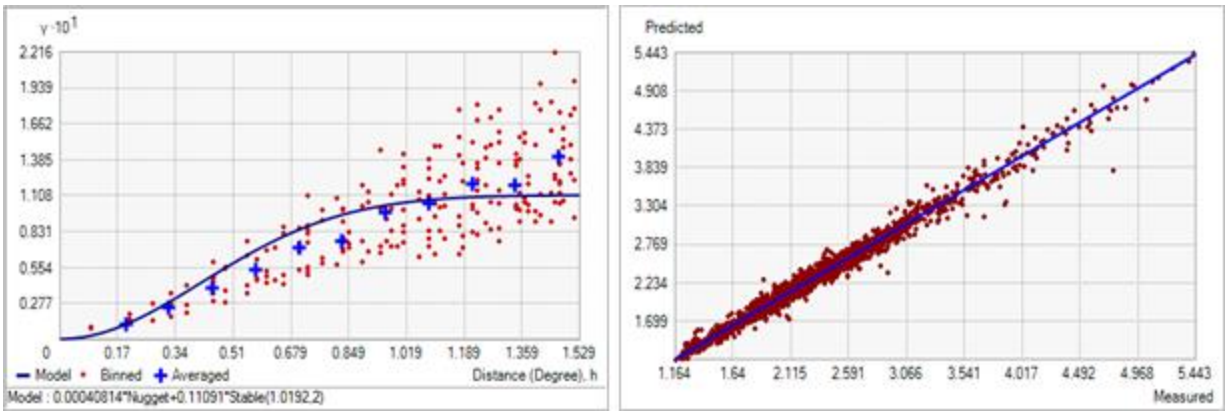

Figure 104. Left panel: Semivariogram of Surface Salinity Range. Binned values are shown as red dots; average points are shown as blue crosses; the model fit to the averaged values is shown as a blue line. Lag size: 0.127 degrees; number of lags: 12; Parameter: 2; Range: 1.019 degrees; Partial Sill: 0.111. Right panel: Scatterplot of predicted values versus observed values for the model of Surface Salinity Range.

Table 52. Results of cross-validation of the kriged model for Surface Salinity Range.

Prediction error	**Value**
Number of Observations	2975
Overall Mean Error	-1.441×10^{-3}
Root Mean Square Prediction Error	0.073
Standardized Mean	-0.026
Standardized Root Mean Square Prediction Error	2.465
Average Standard Error	0.029

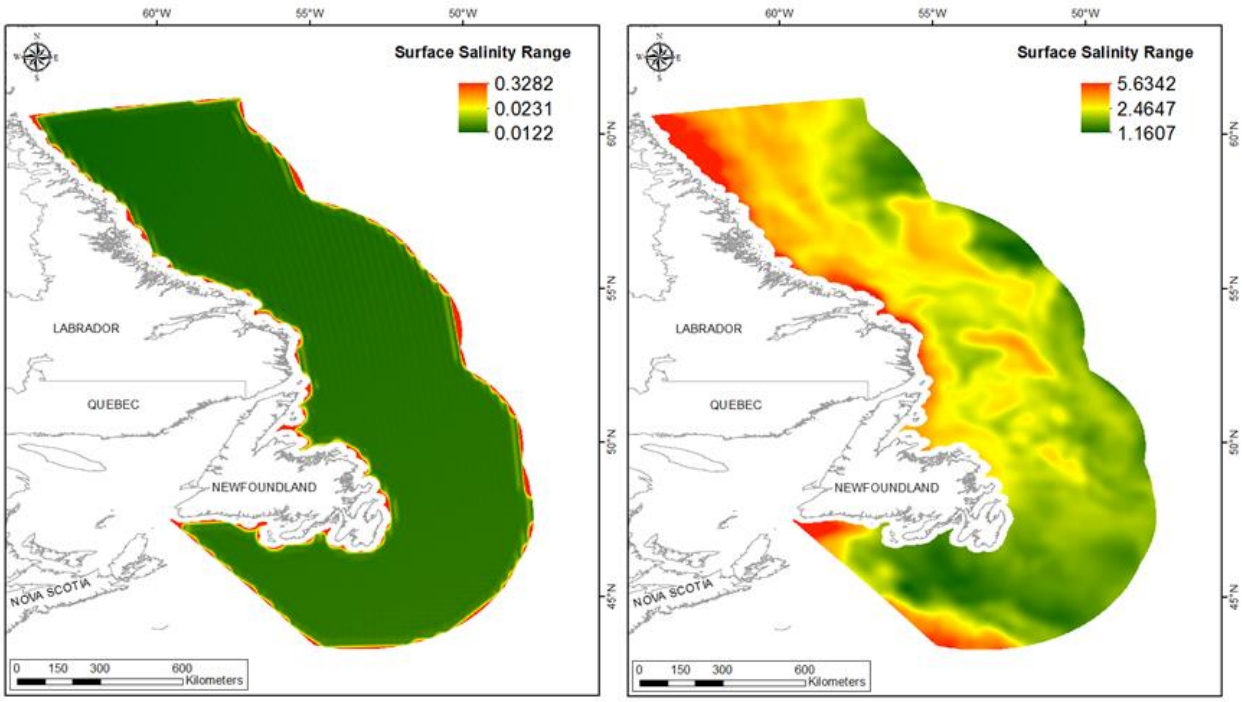

Figure 105. Left panel: Prediction standard error surface of Surface Salinity Range. Right panel: Interpolated prediction surface of Surface Salinity Range.

Surface Salinity Average Minimum

This variable displayed a slightly left-skewed distribution prior to the modeling (Table 53, Figure 106). The data were lower than predicted by a normal distribution at low, high and mid-range values (Figure 107). The lowest values were slightly higher than the reference line. There was a strong spatial pattern to the under- and over-prediction (Figure 107).

The semivariogram showed moderated autocorrelation present in the data, but excellent predictive fit (Figure 108). The model showed excellent cross-validation statistics indicating it was good at prediction (Table 54). The error map showed a 'bullseye' pattern with error increasing with distance from data points (Figure 109). The kriged surface is presented in Figure 109.

Table 53. Distributional properties of Surface Salinity Average Minimum.

Property	Value
Number of Observations	2975
Minimum	28.978
Maximum	34.198
Mean	32.309
Median	32.145
Standard Deviation	1.028
Skewness	-0.087
Kurtosis	2.480

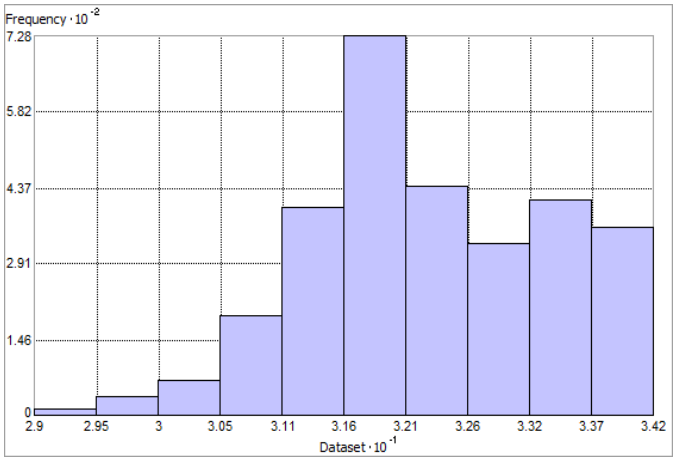

Figure 106. Distribution of Surface Salinity Average Minimum. Histogram was illustrated using 10 bins. X axis is shown at 10^{-1}; Y axis is shown at 10^{-2}.

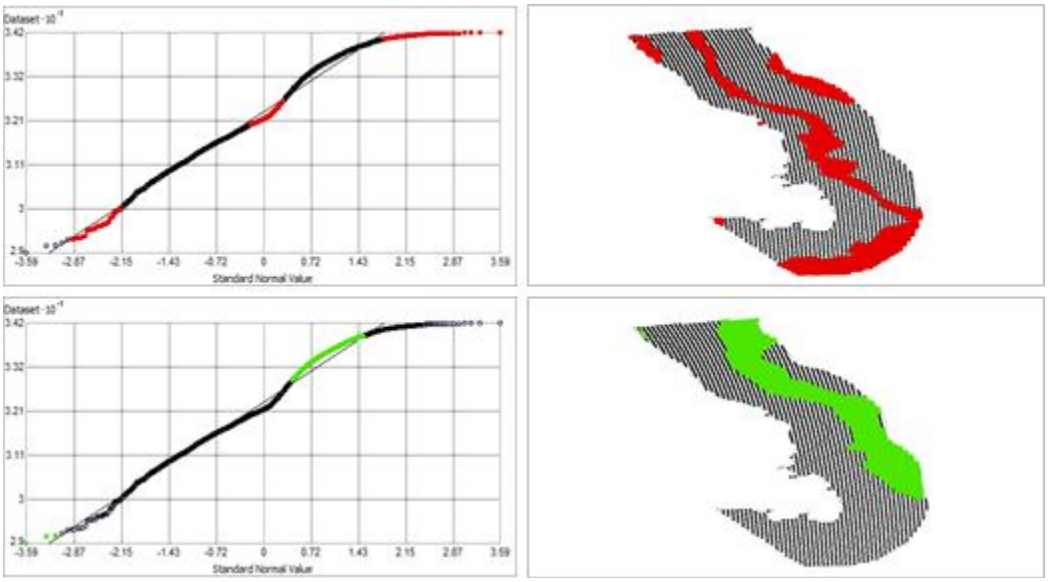

Figure 107. Normal Q-Q plot for data values of Surface Salinity Average Minimum. Points falling under (upper panel) and over (bottom panel) the reference line are mapped.

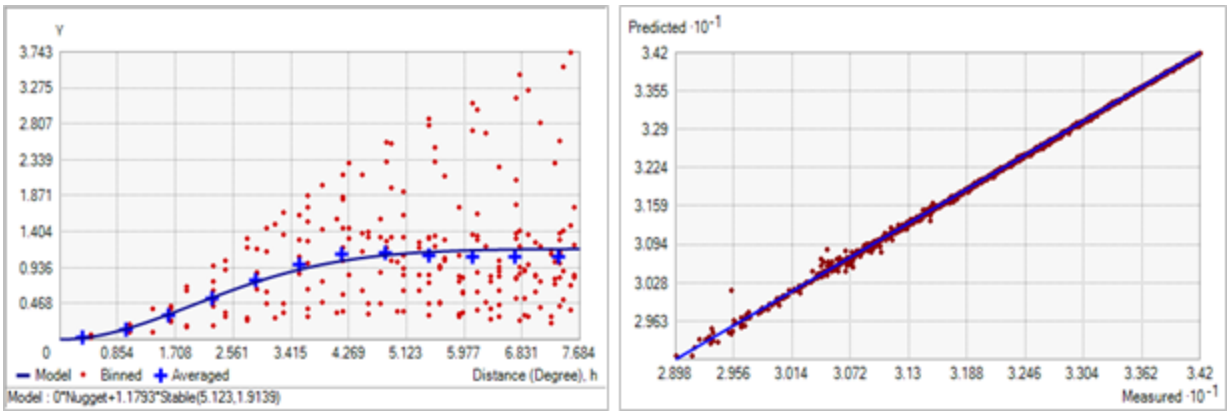

Figure 108. Left panel: Semivariogram of Surface Salinity Average Minimum. Binned values are shown as red dots; average points are shown as blue crosses; the model fit to the averaged values is shown as a blue line. Lag size: 0.640 degrees; number of lags: 12; Parameter: 1.914; Range: 5.123 degrees; Partial Sill: 1.179. Right panel: Scatterplot of predicted values versus observed values for the model of Surface Salinity Average Minimum.

Table 54. Results of cross-validation of the kriged model for Surface Salinity Average Minimum.

Prediction error	**Value**
Number of Observations	2975
Overall Mean Error	4.792×10^{-4}
Root Mean Square Prediction Error	0.025
Standardized Mean	0.011
Standardized Root Mean Square Prediction Error	1.008
Average Standard Error	0.075

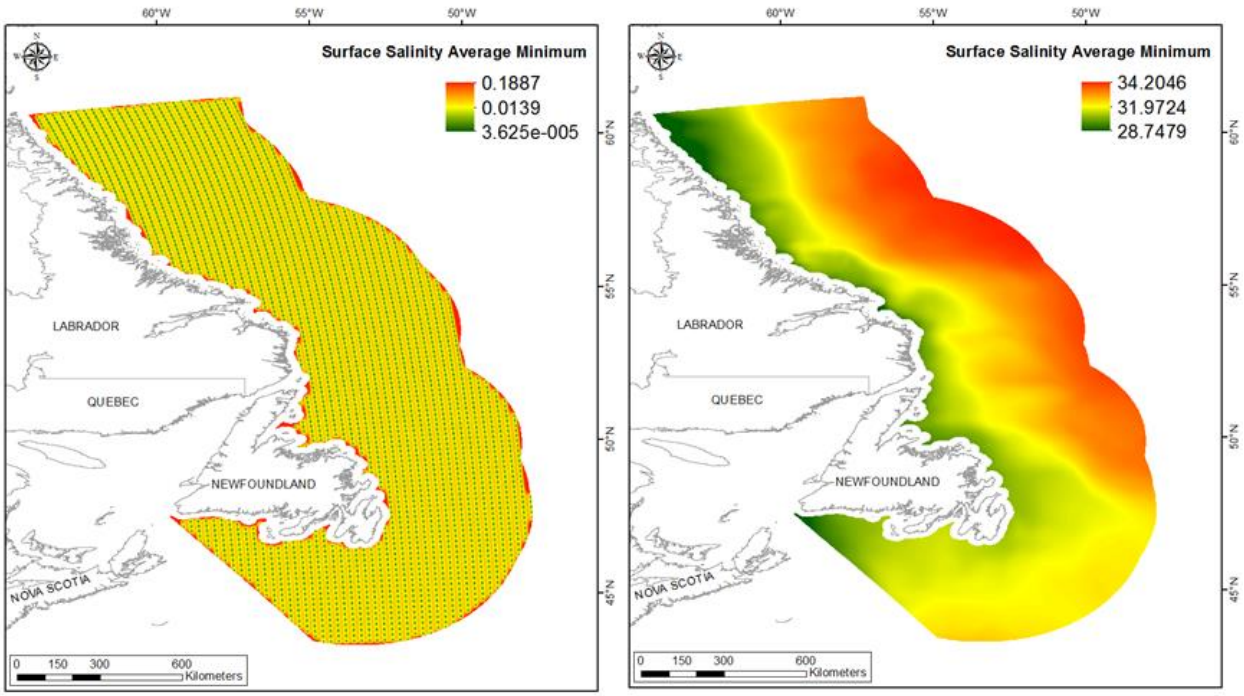

Figure 109. Left panel: Prediction standard error surface of Surface Salinity Average Minimum. Right panel: Interpolated prediction surface of Surface Salinity Average Minimum.

Surface Salinity Average Maximum

This variable displayed a left-skewed and bimodal distribution (Table 55, Figure 110). The data were higher than predicted by a normal distribution with the former occurring at low and upper mid-range values of the distribution and lower than predicted at mid-range and high values (Figure 111). There was a spatial pattern to the under- and over-prediction with the entire surface falling into one or other bias (Figure 111).

The semivariogram showed weak autocorrelation present in the data but excellent predictive fit (Figure 112). The model showed poor cross-validation statistics (Table 56). The standardized root mean square was greater than 1 indicating that variability in the predictions has been underestimated. The error map showed low error and no strong spatial pattern over the spatial extent but was higher along the coast (Figure 113). The kriged surface is presented in Figure 113.

Table 55. Distributional properties of Surface Salinity Average Maximum.

Property	Value
Number of Observations	2975
Minimum	31.847
Maximum	34.762
Mean	33.595
Median	33.534
Standard Deviation	0.841
Skewness	-0.043
Kurtosis	1.531

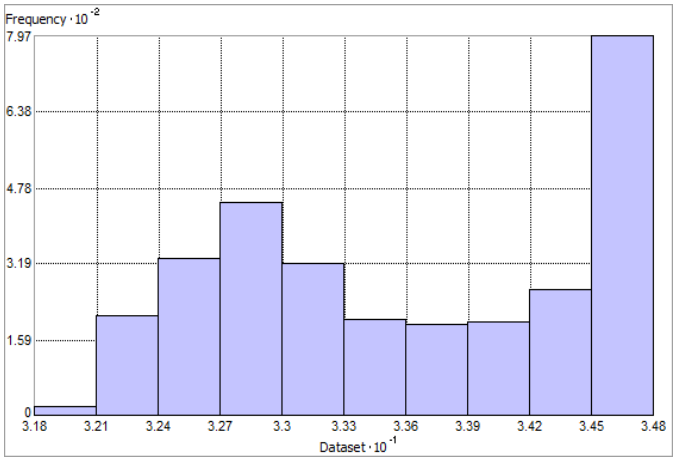

Figure 110. Distribution of Surface Salinity Average Maximum. Histogram was illustrated using 10 bins. X axis is shown at 10^{-1}; Y axis is shown at 10^{-2}.

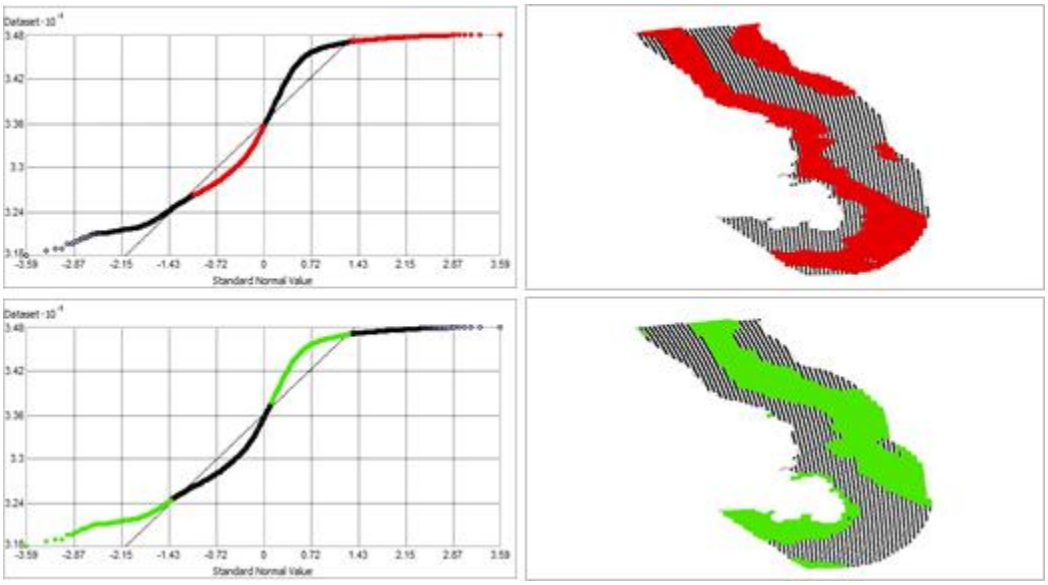

Figure 111. Normal Q-Q plot for data values of Surface Salinity Average Maximum. Points falling under (upper panel) and over (bottom panel) the reference line are mapped.

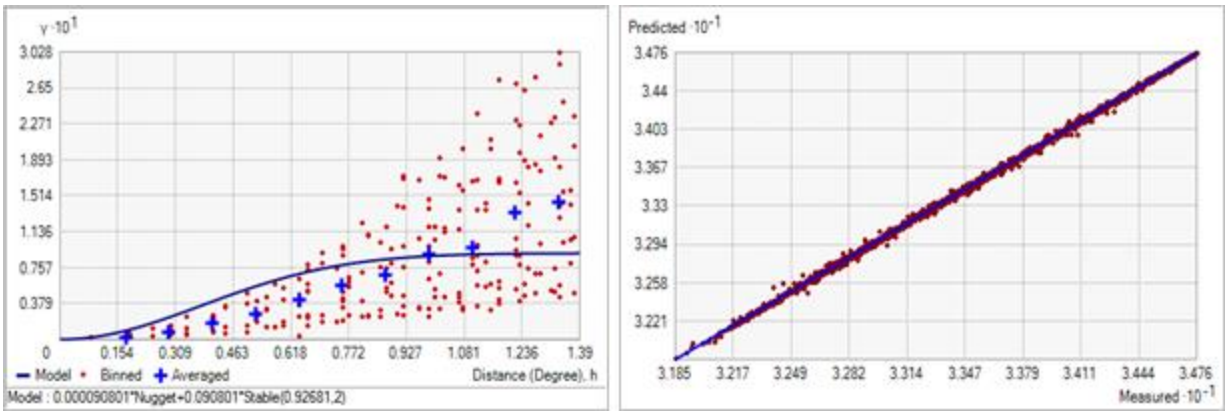

Figure 112. Left panel: Semivariogram of Surface Salinity Average Maximum. Binned values are shown as red dots; average points are shown as blue crosses; the model fit to the averaged values is shown as a blue line. Lag size: 0.312 degrees; number of lags: 12; Parameter: 2; Range: 2.499 degrees; Partial Sill: 1.977. Right panel: Scatterplot of predicted values versus observed values for the model of Surface Salinity Average Maximum.

Table 56. Results of cross-validation of the kriged model for Surface Salinity Average Maximum.

Prediction error	**Value**
Number of Observations	606
Overall Mean Error	-0.001
Root Mean Square Prediction Error	0.131
Standardized Mean	-0.002
Standardized Root Mean Square Prediction Error	2.266
Average Standard Error	0.053

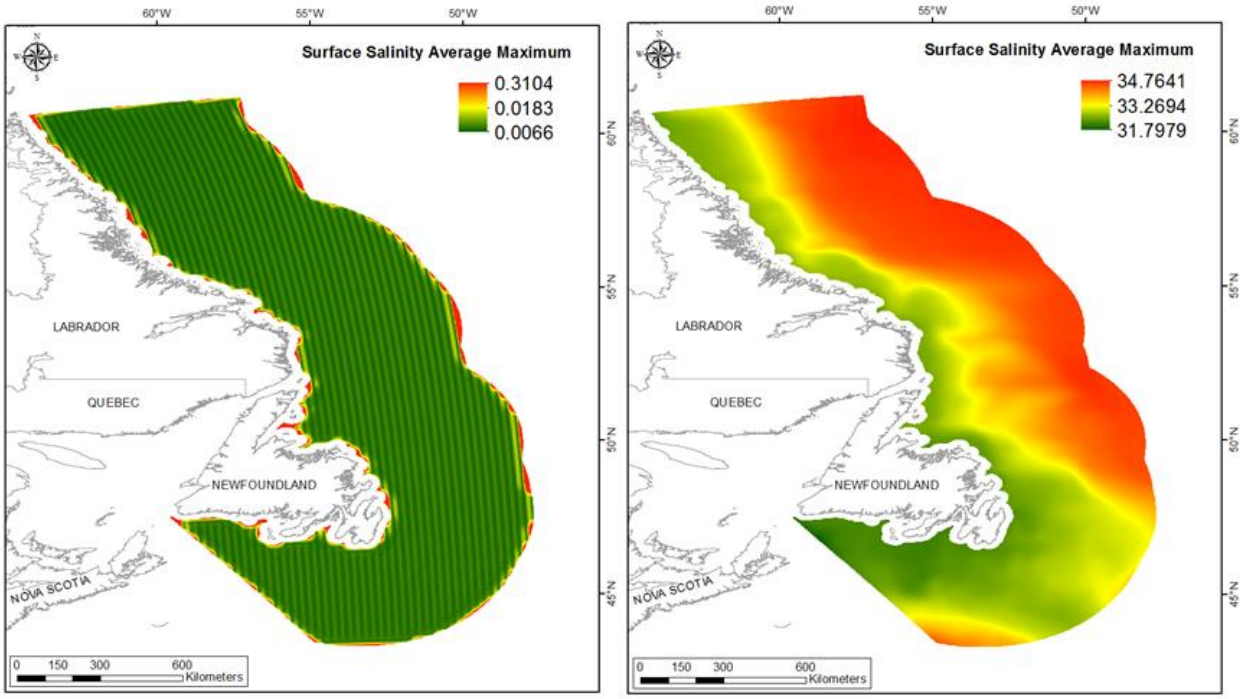

Figure 113. Left panel: Prediction standard error surface of Surface Salinity Average Maximum. Right panel: Interpolated prediction surface of Surface Salinity Average Maximum.

Surface Salinity Average Range

This variable displayed a right-skewed distribution with kurtosis prior to modelling (Table 57, Figure 114). The data were higher than predicted by a normal distribution at low and high values (Figure 127), with mid-range values falling slightly lower than the reference line (Figure 115). There was a strong spatial pattern to the under- and over-predicted values (Figure 115).

The semivariogram showed moderate autocorrelation but an excellent predictive fit of the model (Figure 116). The model showed fair cross-validation statistics (Table 58). The standardized root mean square was greater than 1 indicating that variability in the predictions has been underestimated. The error map showed low error and no strong spatial pattern over the spatial extent but was higher along the coast (Figure 117). The kriged surface is presented in Figure 117.

Table 57. Distributional properties of Surface Salinity Average Range.

Property	Value
Number of Observations	2975
Minimum	0.490
Maximum	3.459
Mean	1.286
Median	1.268
Standard Deviation	0.455
Skewness	0.844
Kurtosis	4.557

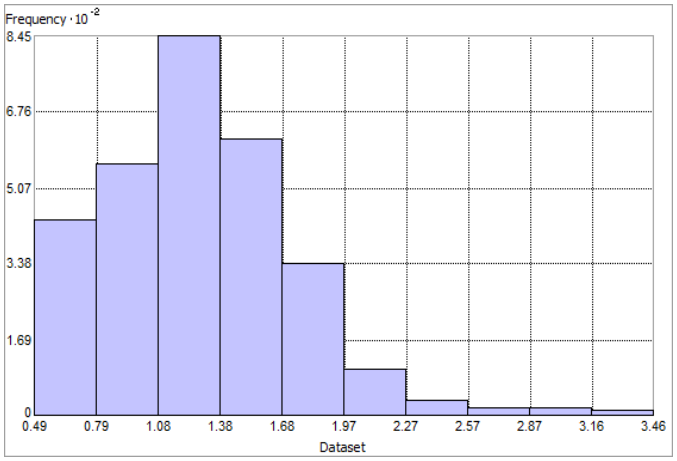

Figure 114. Distribution of Surface Salinity Average Range. Histogram was illustrated using 10 bins. Y axis is shown at 10^{-2}.

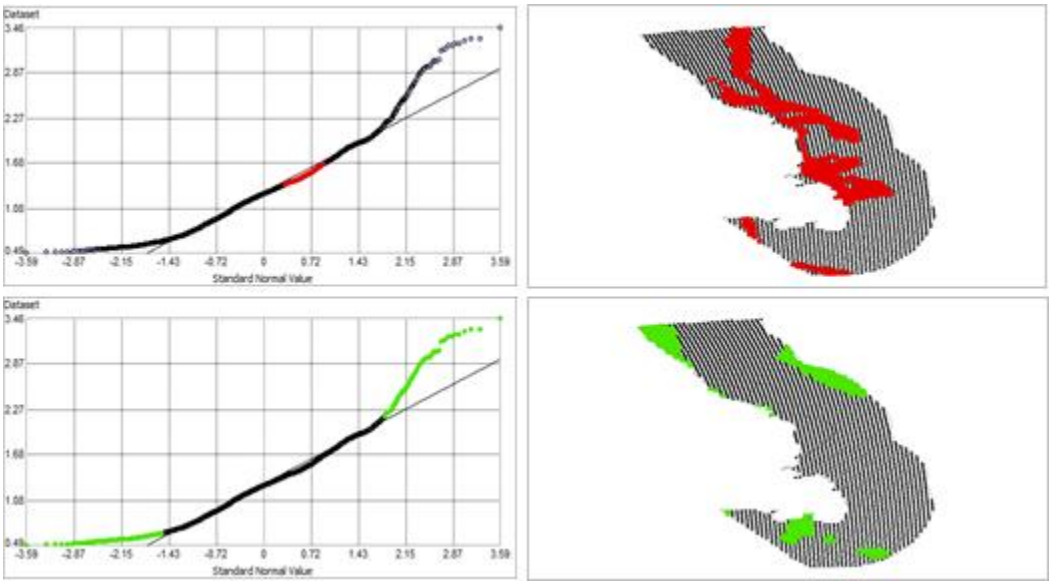

Figure 115. Normal Q-Q plot for data values of Surface Salinity Average Range. Points falling under (upper panel) and over (bottom panel) the reference line are mapped.

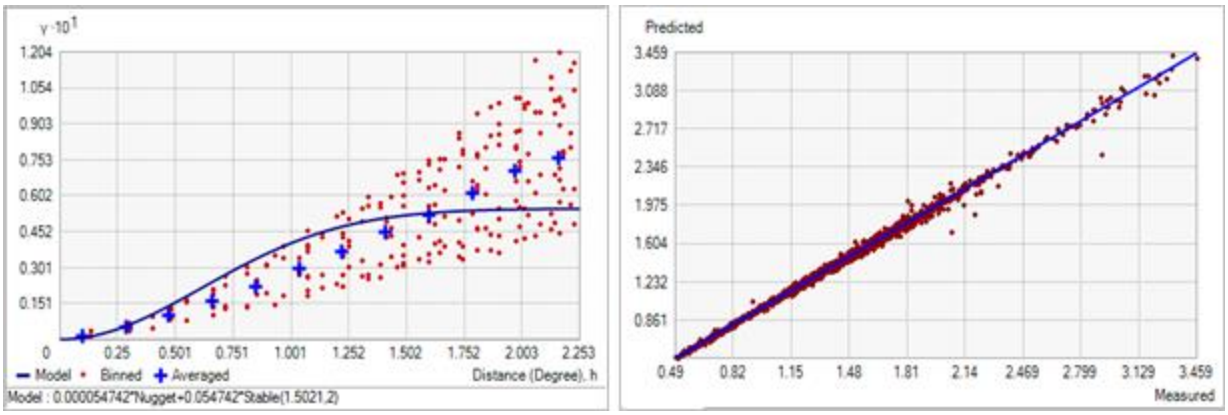

Figure 116. Left panel: Semivariogram of Surface Salinity Average Range. Binned values are shown as red dots; average points are shown as blue crosses; the model fit to the averaged values is shown as a blue line. Lag size: 0.188 degrees; number of lags: 12; Parameter: 2; Range: 1.502 degrees; Partial Sill: 0.055. Right panel: Scatterplot of predicted values versus observed values for the model of Surface Salinity Average Range.

Table 58. Results of cross-validation of the kriged model for Surface Salinity Average Range.

Prediction error	**Value**
Number of Observations	2975
Overall Mean Error	-6.240×10^{-4}
Root Mean Square Prediction Error	0.024
Standardized Mean	-0.040
Standardized Root Mean Square Prediction Error	2.220
Average Standard Error	9.503×10^{-3}

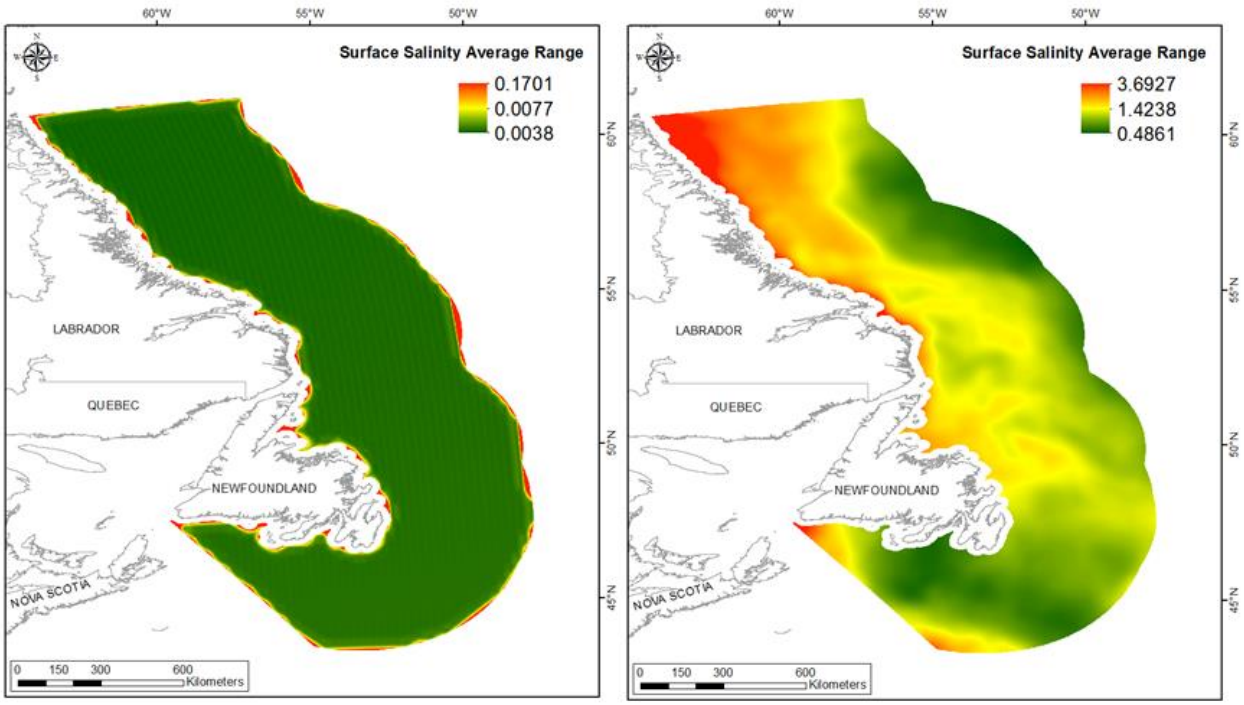

Figure 117. Left panel: Prediction standard error surface of Surface Salinity Average Range. Right panel: Interpolated prediction surface of Surface Salinity Average Range.

Current Speed

Currents move water and heat around in the world's oceans and influence the chemical composition of the water column. Upwelling and downwelling currents strongly influence the distribution and abundance of marine life. Similarly, current speed determines the rate at which food particles reach benthic species through both vertical and horizontal transmission and consequently influences the distribution of filter-feeding species. Upwelling currents enhance productivity in the water column, while downwelling currents bring food and oxygen to the sea floor. Organisms also use currents for active and passive transport for migration and dispersal. Current speed can influence morphology, especially of marine macrophytes.

Bottom Current Mean

This variable displayed a right-skewed distribution with high kurtosis prior to modeling (Table 59, Figure 118). The data were higher than predicted by a normal distribution at the tails, particularly at high values (Figure 119). Mid-range values were slightly lower than the reference line. The areas of over- and under-prediction did not show spatial pattern with both error types distributed through the spatial extent, however, the entire surface was biased and more towards under-prediction than over-prediction (Figure 119).

The semivariogram showed weak autocorrelation present in the data and there was a poor fit between measured and predicted values (Figure 120). Nevertheless, the model showed good

cross-validation statistics (Table 60) indicating that it was good at prediction. The error map showed a 'bullseye' pattern with error increasing with distance from data points (Figure 121). The kriged surface is presented in Figure 121.

Table 59. Distributional properties of Bottom Current Mean (m s^{-1}).

Property	Value
Number of Observations	2948
Minimum	0.002
Maximum	0.257
Mean	0.036
Median	0.029
Standard Deviation	0.027
Skewness	1.676
Kurtosis	48.210

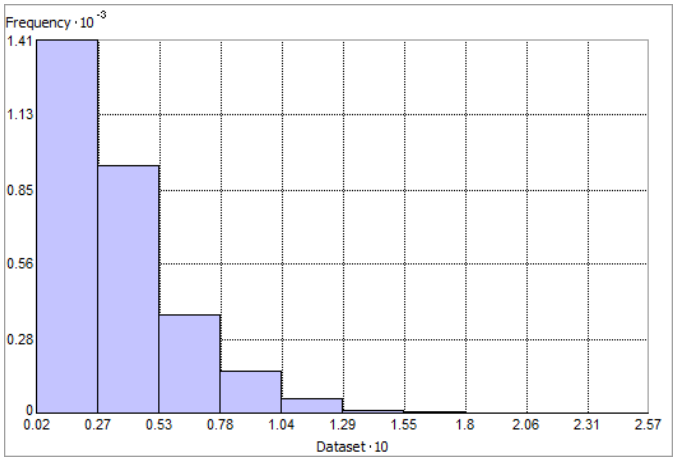

Figure 118. Distribution of Bottom Current Mean (m s^{-1}). Histogram was illustrated using 10 bins. X axis is shown at 10; Y axis is shown at 10^{-3}.

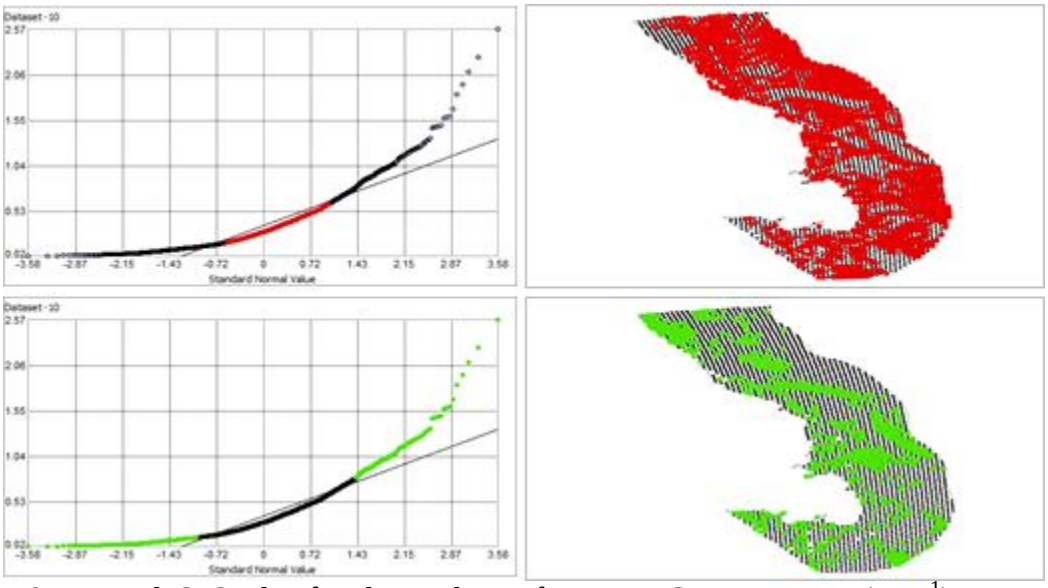

Figure 119. Normal Q-Q plot for data values of Bottom Current Mean (m s^{-1}). Points falling under (upper panel) and over (bottom panel) the reference line are mapped.

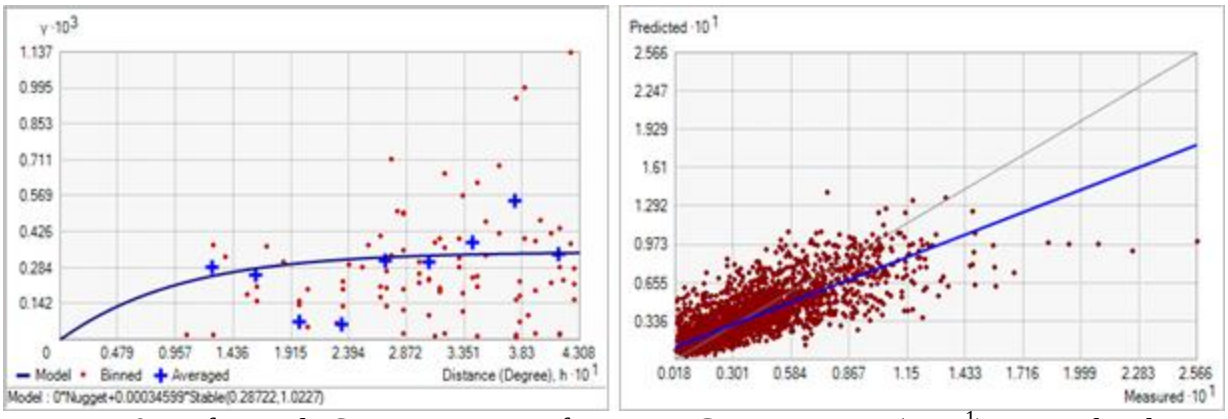

Figure 120. Left panel: Semivariogram of Bottom Current Mean (m s^{-1}). Binned values are shown as red dots; average points are shown as blue crosses; the model fit to the averaged values is shown as a blue line. Lag size: 0.036 degrees; number of lags: 12; Parameter: 1.023; Range: 0.287 degrees; Partial Sill: 3.460 x 10^{-4}. Right panel: Scatterplot of predicted values versus observed values for the model of Bottom Current Mean (m s^{-1}).

Table 60. Results of cross-validation of the kriged model for Bottom Current Mean (m s^{-1}).

Prediction error	**Value**
Number of Observations	2948
Overall Mean Error	-6.404 x 10^{-6}
Root Mean Square Prediction Error	0.017
Standardized Mean	-4.272 x 10^{-4}
Standardized Root Mean Square Prediction Error	0.917
Average Standard Error	0.018

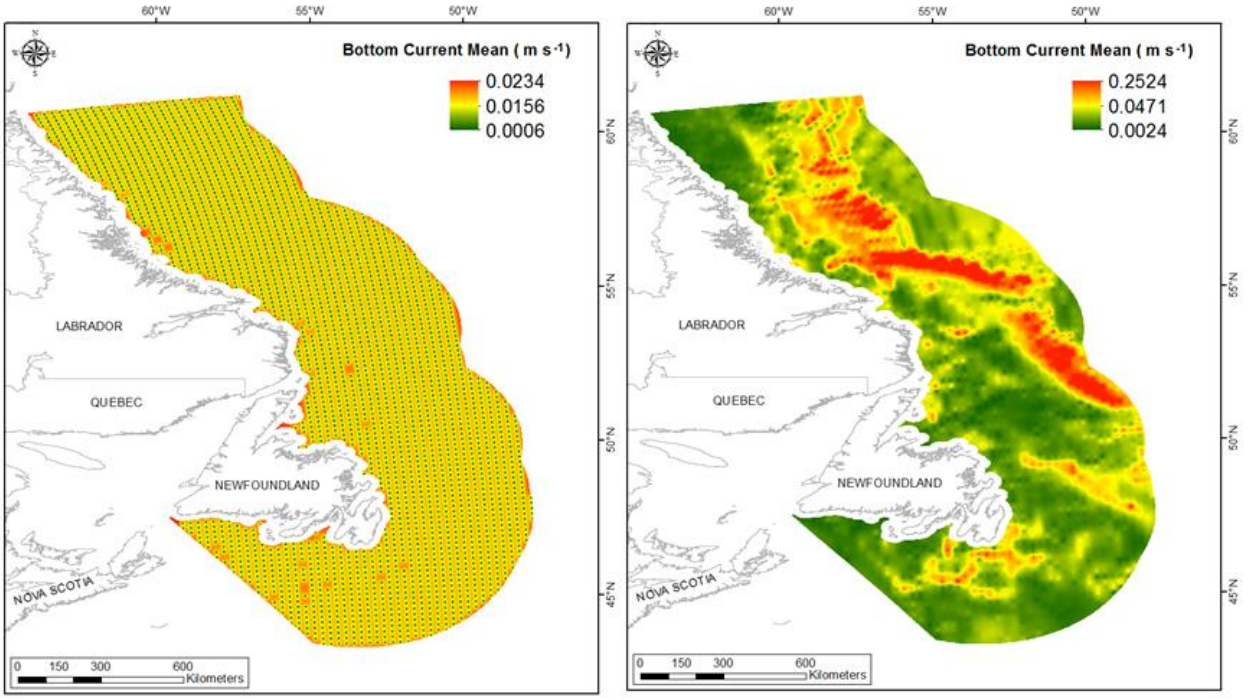

Figure 121. Left panel: Prediction standard error surface of Bottom Current Mean (m s^{-1}). Right panel: Interpolated prediction surface of Bottom Current Mean (m s^{-1}).

Bottom Current Minimum

This variable displayed a right-skewed distribution with kurtosis and outlying data in the lower range (Table 61, Figure 122). The data were higher than predicted by a normal distribution at low and high values and lower than predicted at mid-range values (Figure 123). The areas of over- and under-prediction did not show spatial pattern with both error types distributed throughout the spatial extent (Figure 123).

The semivariogram showed moderate autocorrelation present in the data and poor fit between measured and predicted values of the model (Figure 124). Nevertheless, the model showed excellent cross-validation statistics (Table 62) indicating that it was very good at prediction. The error map showed low error and no strong spatial pattern over the spatial extent but was higher along the coast (Figure 125). The kriged surface is presented in Figure 125. Negative values resulted in the prediction surface after ordinary kriging of this variable. This possibly resulted from the highly right-skewed nature of the raw data and large outlying data points (see Figure 122). Of the 533592 raster cells in the study extent, 5882 contained negative values (see Table A2). These were located in small patches distributed across the Newfoundland and Labrador shelf and in deep water beyond the slope (see Figure A2).

Table 61. Distributional properties of Bottom Current Minimum (m s^{-1}).

Property	Value
Number of Observations	2948
Minimum	1.000 x 10^{-6}
Maximum	0.139
Mean	5.995 x 10^{-3}
Median	1.634 x 10^{-3}
Standard Deviation	0.012
Skewness	3.779
Kurtosis	21.915

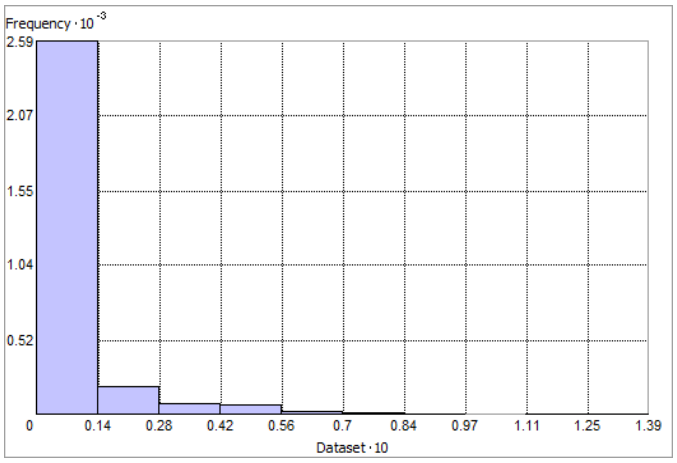

Figure 122. Distribution of Bottom Current Minimum (m s^{-1}). Histogram was illustrated using 10 bins. X axis is shown at 10; Y axis is shown at 10^{-3}.

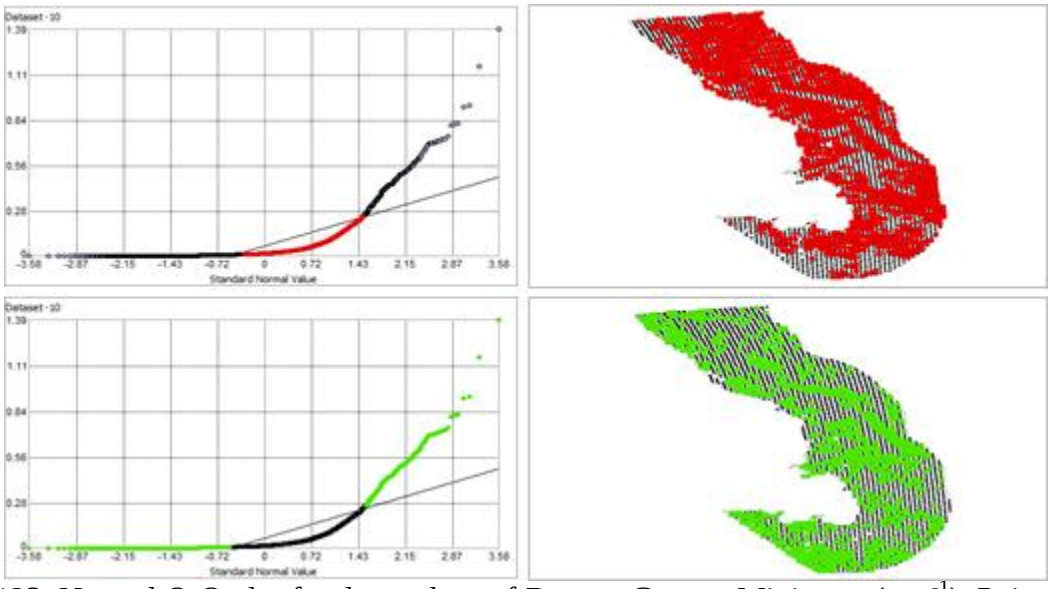

Figure 123. Normal Q-Q plot for data values of Bottom Current Minimum (m s^{-1}). Points falling under (upper panel) and over (bottom panel) the reference line are mapped.

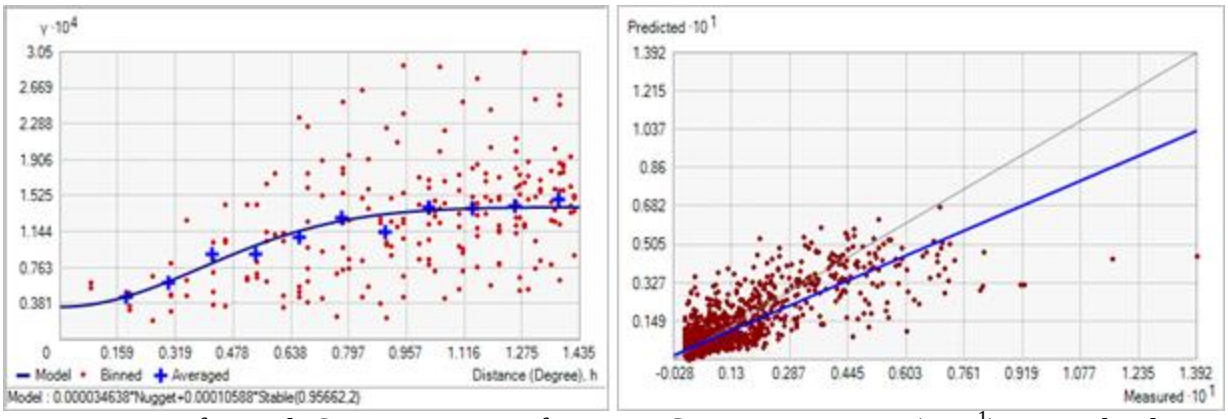

Figure 124. Left panel: Semivariogram of Bottom Current Minimum (m s^{-1}). Binned values are shown as red dots; average points are shown as blue crosses; the model fit to the averaged values is shown as a blue line. Lag size: 0.120 degrees; number of lags: 12; Parameter: 2; Range: 0.957 degrees; Partial Sill: 1.059 x 10^{-4}. Right panel: Scatterplot of predicted values versus observed values for the model of Bottom Current Minimum (m s^{-1}).

Table 62. Results of cross-validation of the kriged model for Bottom Current Minimum (m s^{-1}).

Prediction error	**Value**
Number of Observations	2948
Overall Mean Error	7.895 x 10^{-6}
Root Mean Square Prediction Error	6.471 x 10^{-3}
Standardized Mean	8.904 x 10^{-4}
Standardized Root Mean Square Prediction Error	0.983
Average Standard Error	6.649 x 10^{-3}

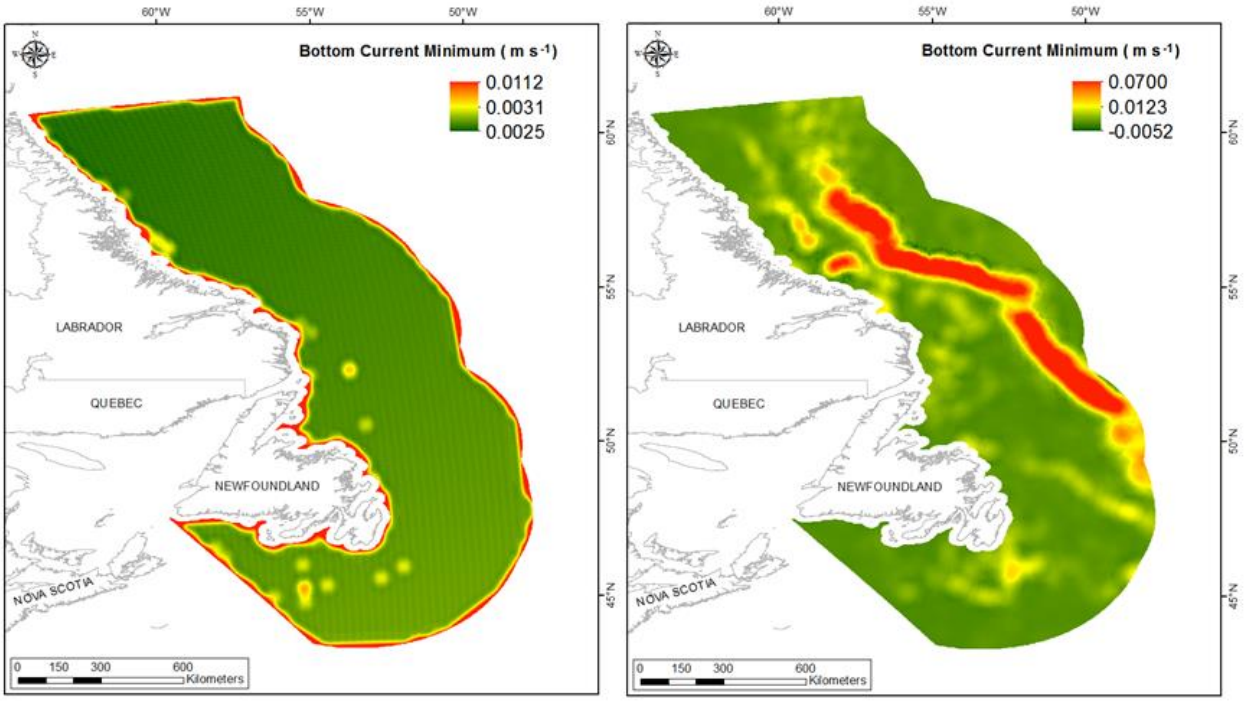

Figure 125. Left panel: Prediction standard error surface of Bottom Current Minimum (m s^{-1}). Right panel: Interpolated prediction surface of Bottom Current Minimum (m s^{-1}).

Bottom Current Maximum

This variable displayed a right-skewed distribution with kurtosis prior to modeling (Table 63, Figure 126). The data were higher than predicted by a normal distribution at high and low values (Figure 127). Mid-range values were slightly lower than the reference line. The areas of over- and under-prediction did not show spatial pattern with both error types distributed through the spatial extent but with no large area unbiased in one or other direction (Figure 127).

The semivariogram showed moderate autocorrelation present in the data and the kriged model show poor fit between measured and predicted values (Figure 128). Nevertheless, the model showed excellent cross-validation statistics (Table 64) indicating that it was very good at prediction. The error map showed a 'bullseye' pattern with error increasing with distance from data points (Figure 129). The kriged surface is presented in Figure 129.

Table 63. Distributional properties of Bottom Current Maximum (m s^{-1}).

Property	Value
Number of Observations	2948
Minimum	0.009
Maximum	0.365
Mean	0.085
Median	0.075
Standard Deviation	0.050
Skewness	0.988
Kurtosis	4.119

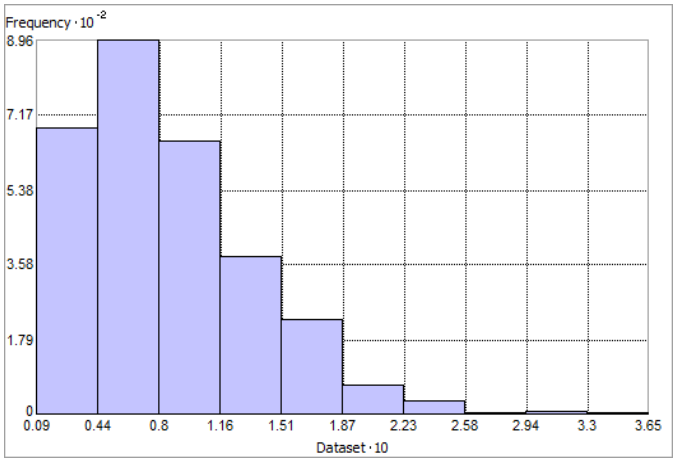

Figure 126. Distribution of Bottom Current Maximum (m s^{-1}). Histogram was illustrated using 10 bins. X axis is shown at 10; Y axis is shown at 10^{-2}.

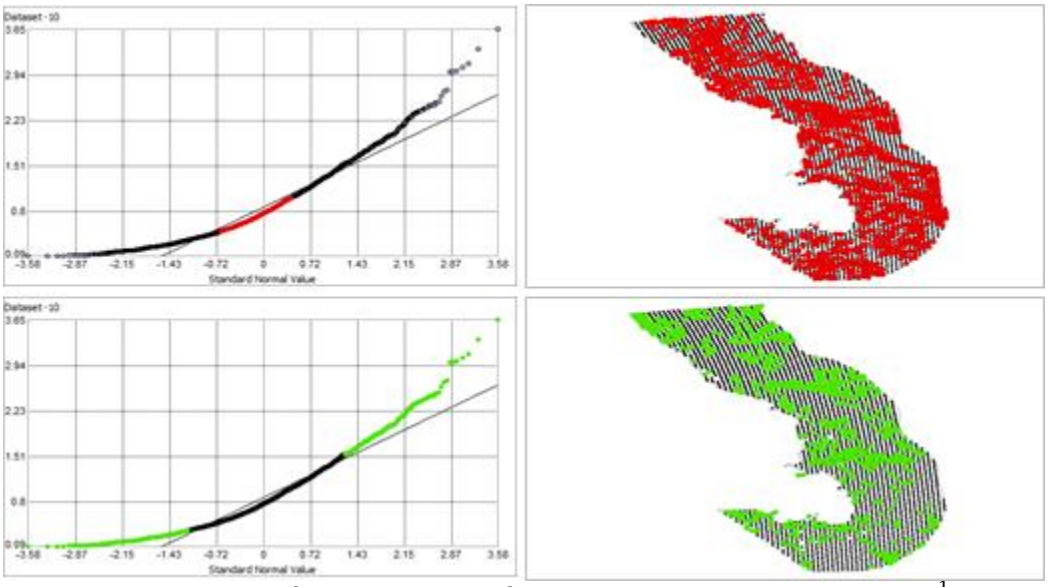

Figure 127. Normal Q-Q plot for data values of Bottom Current Maximum (m s^{-1}). Points falling under (upper panel) and over (bottom panel) the reference line are mapped.

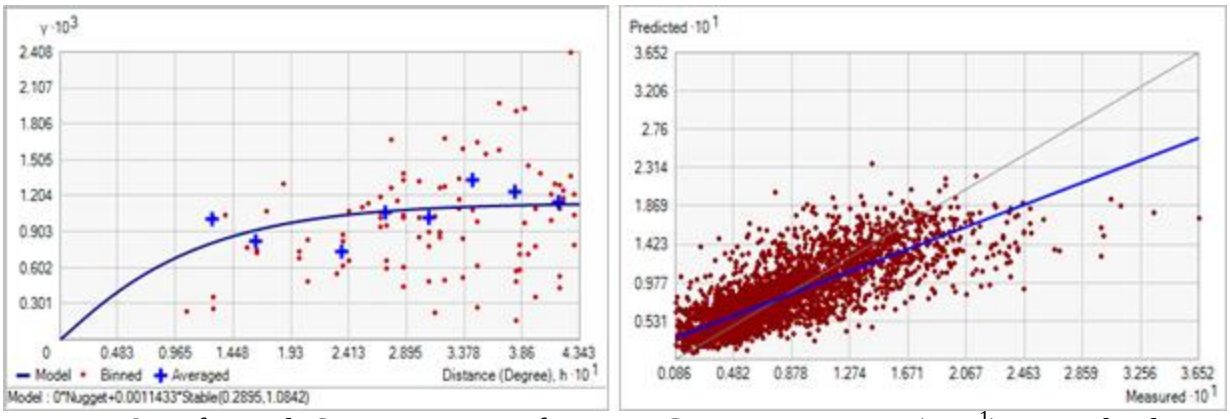

Figure 128. Left panel: Semivariogram of Bottom Current Maximum (m s^{-1}). Binned values are shown as red dots; average points are shown as blue crosses; the model fit to the averaged values is shown as a blue line. Lag size: 0.036 degrees; number of lags: 12; Parameter: 1.084; Range: 0.289 degrees; Partial Sill: 0.001. Right panel: Scatterplot of predicted values versus observed values for the model of Bottom Current Maximum (m s^{-1}).

Table 64. Results of cross-validation of the kriged model for Bottom Current Maximum (m s^{-1}).

Prediction error	**Value**
Number of Observations	2948
Overall Mean Error	-9.792×10^{-6}
Root Mean Square Prediction Error	0.031
Standardized Mean	-3.409×10^{-4}
Standardized Root Mean Square Prediction Error	0.945
Average Standard Error	0.033

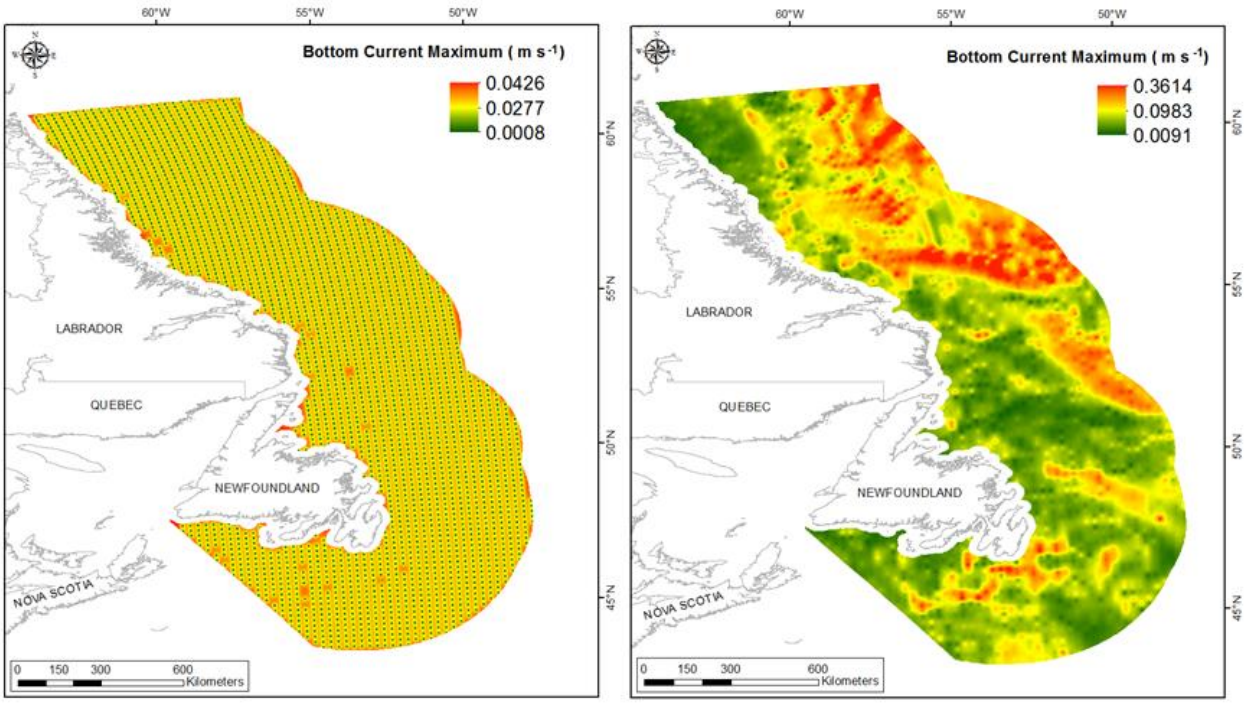

Figure 129. Left panel: Prediction standard error surface of Bottom Current Maximum (m s^{-1}). Right panel: Interpolated prediction surface of Bottom Current Maximum (m s^{-1}).

Bottom Current Range

This variable displayed a right-skewed distribution with kurtosis prior to modeling (Table 65, Figure 130). The data were higher than predicted by a normal distribution at high and low values (Figure 131). Mid-range values were slightly lower than the reference line. The areas of over- and under-prediction did not show a strong spatial pattern with both error types distributed through the spatial extent (Figure 131).

The semivariogram showed weak autocorrelation present in the data and the models showed fair fit between the measured and predicted values (Figure 132). Nevertheless, the model showed good cross-validation statistics (Table 66) indicating that it was good at prediction. The error map showed no spatial pattern over the study extent except for along the coast where it was high (Figure 133). The kriged surface is presented in Figure 133.

Table 65. Distributional properties of Bottom Current Range (m s^{-1}).

Property	Value
Number of Observations	2948
Minimum	0.009
Maximum	0.270
Mean	0.079
Median	0.071
Standard Deviation	0.045
Skewness	0.965
Kurtosis	3.865

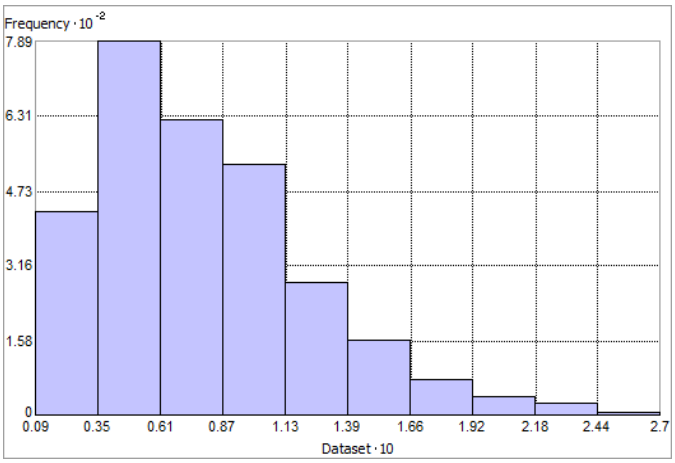

Figure 130. Distribution of Bottom Current Range (m s^{-1}). Histogram was illustrated using 10 bins. X axis is shown at 10; Y axis is shown at 10^{-2}.

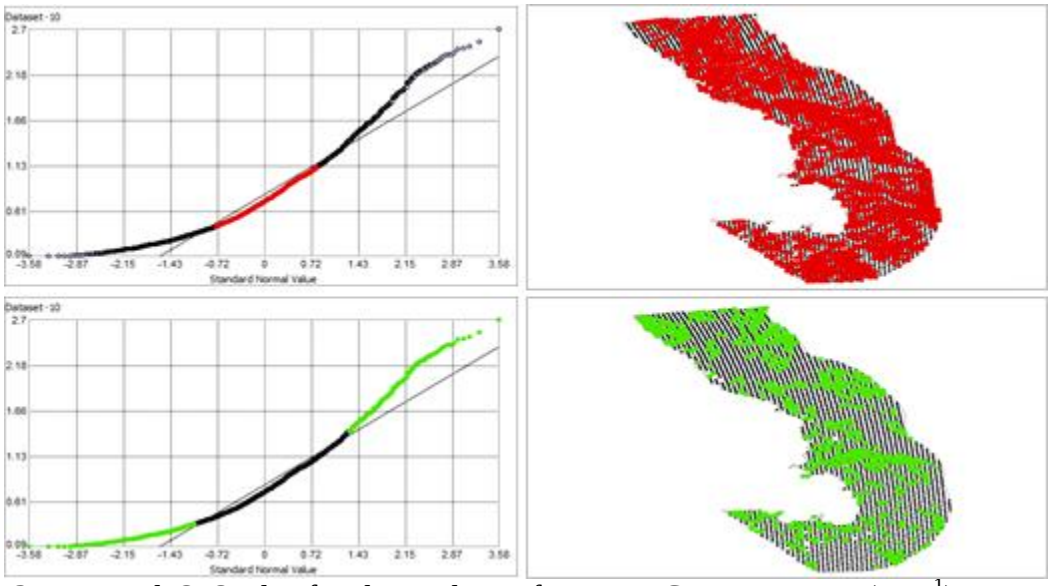

Figure 131. Normal Q-Q plot for data values of Bottom Current Range (m s^{-1}). Points falling under (upper panel) and over (bottom panel) the reference line are mapped.

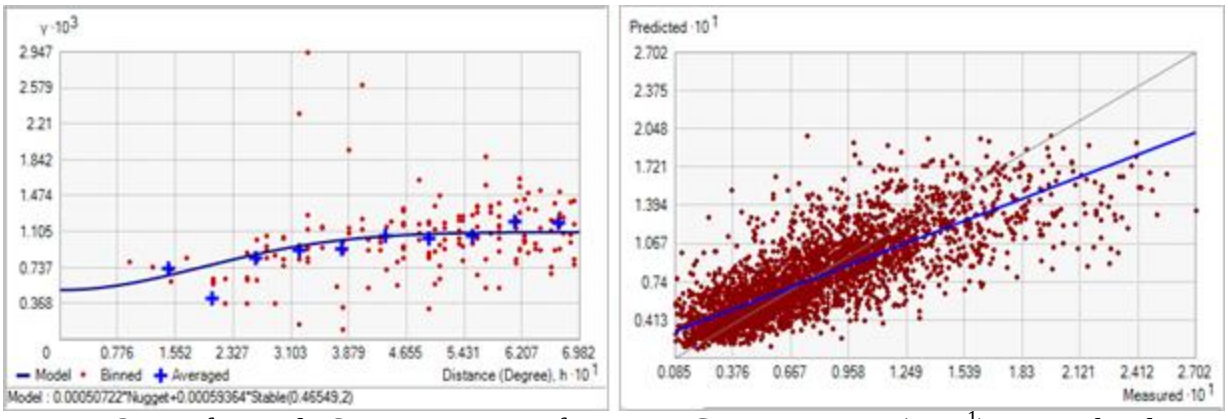

Figure 132. Left panel: Semivariogram of Bottom Current Range (m s^{-1}). Binned values are shown as red dots; average points are shown as blue crosses; the model fit to the averaged values is shown as a blue line. Lag size: 0.058 degrees; number of lags: 12; Parameter: 2; Range: 0.465 degrees; Partial Sill: 5.936 x 10^{-4}. Right panel: Scatterplot of predicted values versus observed values for the model of Bottom Current Range (m s^{-1}).

Table 66. Results of cross-validation of the kriged model for Bottom Current Range (m s^{-1}).

Prediction error	**Value**
Number of Observations	2948
Overall Mean Error	1.033 x 10^{-5}
Root Mean Square Prediction Error	0.028
Standardized Mean	2.849 x 10^{-4}
Standardized Root Mean Square Prediction Error	1.001
Average Standard Error	0.028

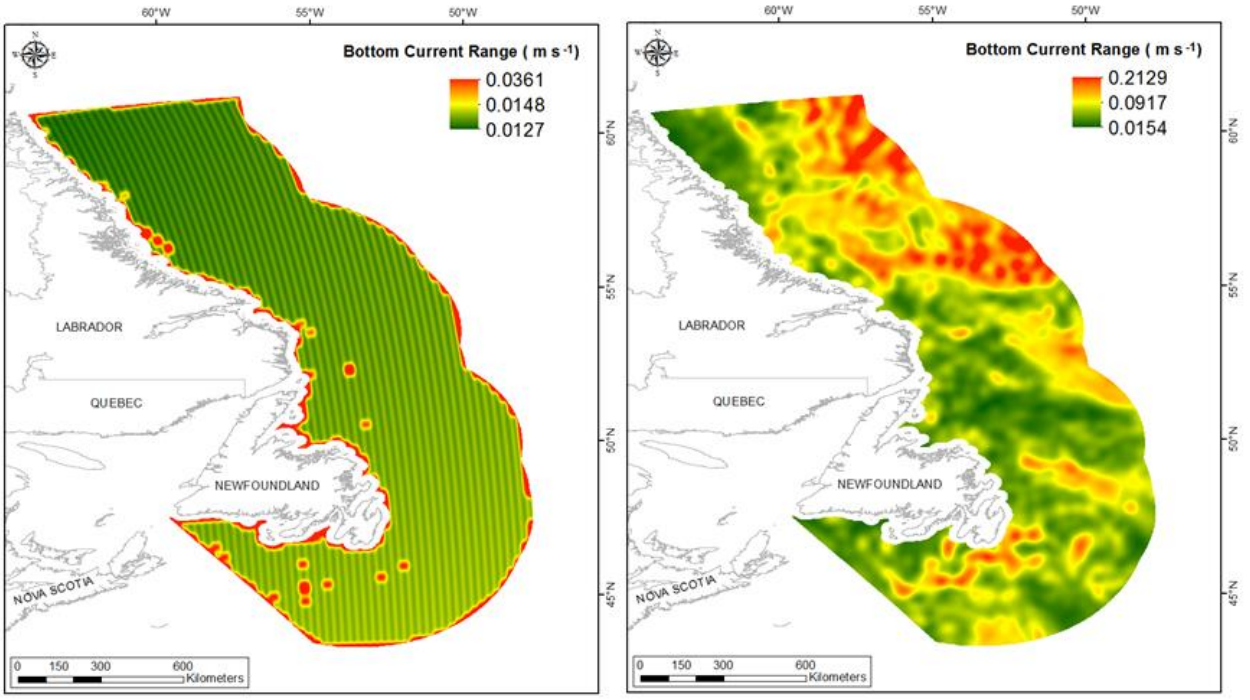

Figure 133. Left panel: Prediction standard error surface of Bottom Current Range (m s^{-1}). Right panel: Interpolated prediction surface of Bottom Current Range (m s^{-1}).

Bottom Current Average Minimum

This variable displayed a right-skewed distribution with kurtosis prior to modeling (Table 67, Figure 134). The data were higher than predicted by a normal distribution at high values (Figure 135). Mid-range values were slightly lower than the reference line. The areas of over- and under-prediction did not show a strong spatial pattern with both error types distributed across the spatial extent (Figure 135).

The semivariogram showed moderate autocorrelation present in the data and the model showed fair fit between measured and predicted values (Figure 136). Nevertheless, the model showed very good cross-validation statistics (Table 68) indicating that it was good at prediction. The error map showed no spatial pattern over the study extent except for along the coast where it was high (Figure 137). The kriged surface is presented in Figure 137.

Table 67. Distributional properties of Bottom Current Average Minimum (m s^{-1}).

Property	Value
Number of Observations	2948
Minimum	1.850 x 10^{-4}
Maximum	0.191
Mean	0.016
Median	8.882 x 10^{-3}
Standard Deviation	0.019
Skewness	2.419
Kurtosis	11.207

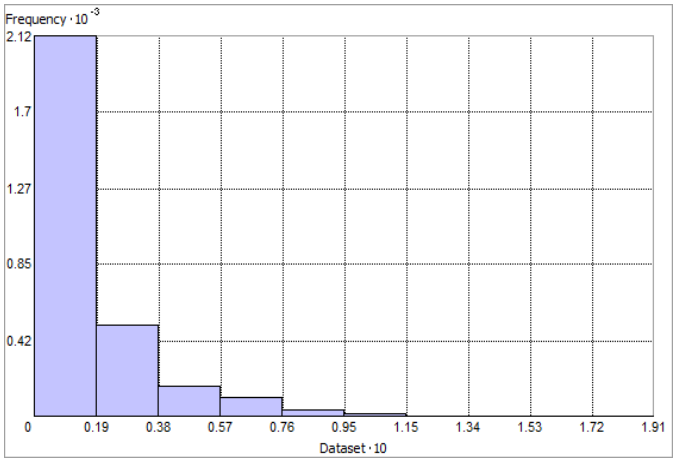

Figure 134. Distribution of Bottom Current Average Minimum (m s^{-1}). Histogram was illustrated using 10 bins. X axis is shown at 10; Y axis is shown at 10^{-3}.

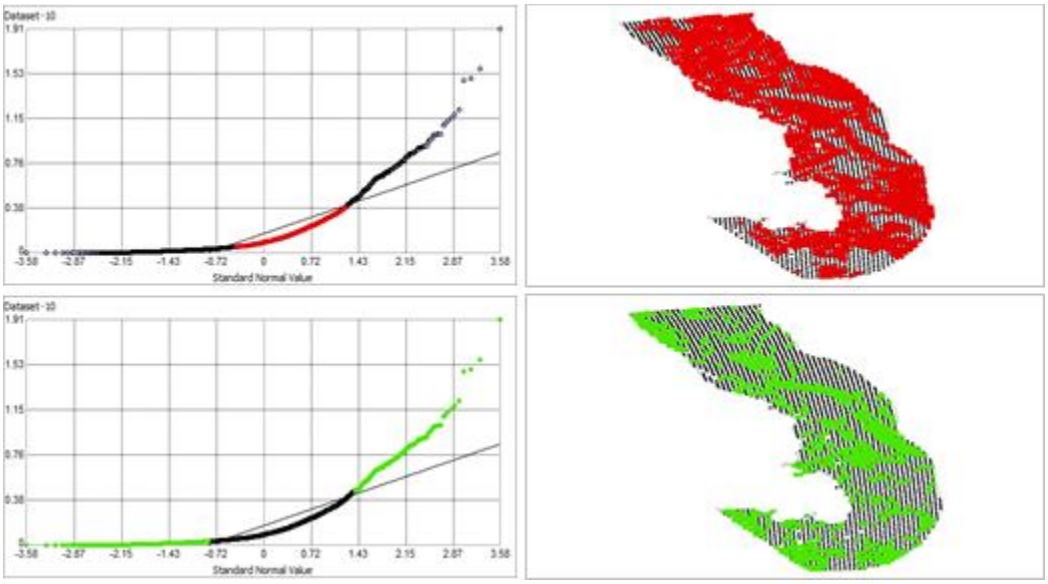

Figure 135. Normal Q-Q plot for data values of Bottom Current Average Minimum (m s^{-1}). Points falling under (upper panel) and over (bottom panel) the reference line are mapped.

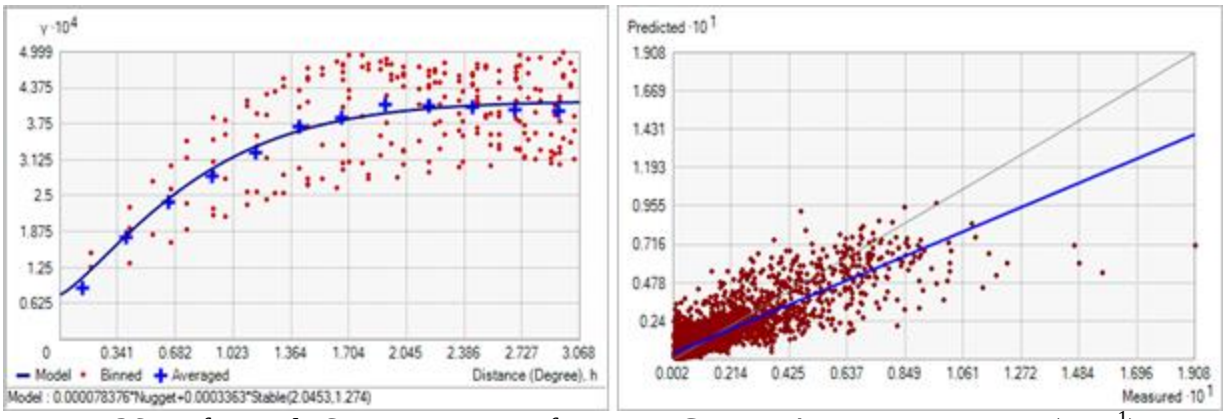

Figure 136. Left panel: Semivariogram of Bottom Current Average Minimum (m s^{-1}). Binned values are shown as red dots; average points are shown as blue crosses; the model fit to the averaged values is shown as a blue line. Lag size: 0.256 degrees; number of lags: 12; Parameter: 1.274; Range: 2.045 degrees; Partial Sill: 3.363 x 10^{-4}. Right panel: Scatterplot of predicted values versus observed values for the model of Bottom Current Average Minimum (m s^{-1}).

Table 68. Results of cross-validation of the kriged model for Bottom Current Average Minimum (m s^{-1}).

Prediction error	**Value**
Number of Observations	2948
Overall Mean Error	6.784 x 10^{-6}
Root Mean Square Prediction Error	0.011
Standardized Mean	3.595 x 10^{-4}
Standardized Root Mean Square Prediction Error	0.952
Average Standard Error	0.011

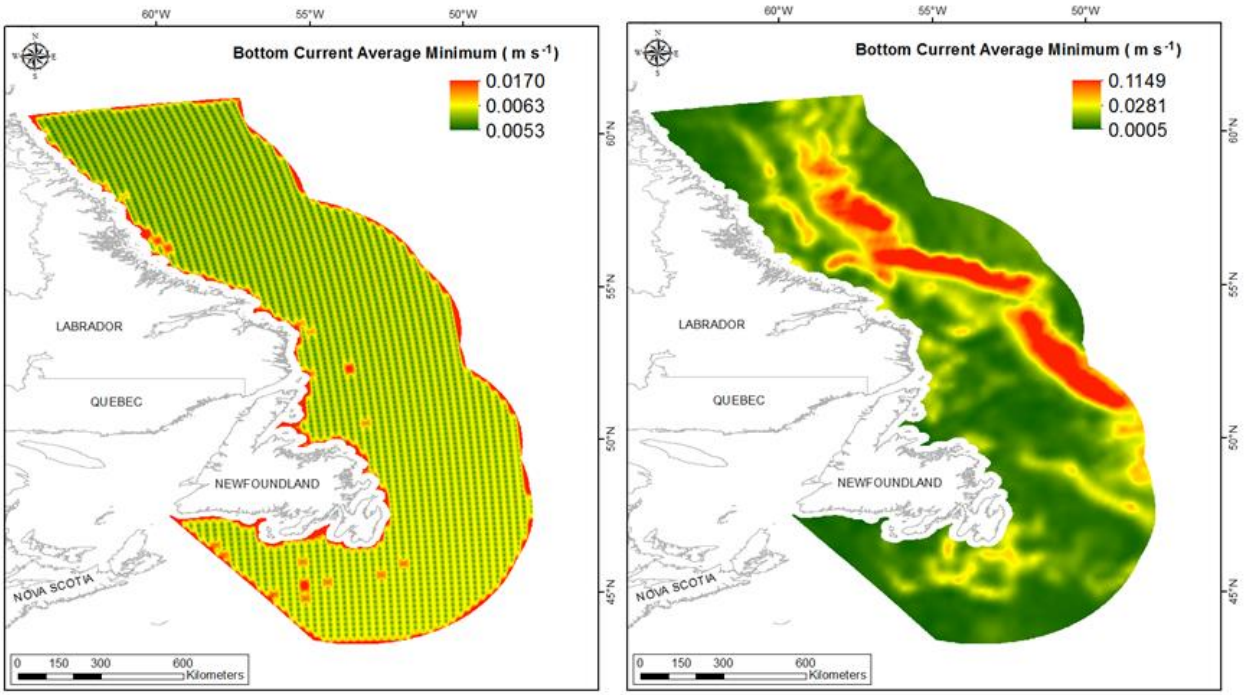

Figure 137. Left panel: Prediction standard error surface of Bottom Current Average Minimum (m s^{-1}). Right panel: Interpolated prediction surface of Bottom Current Average Minimum (m s^{-1}).

Bottom Current Average Maximum

This variable displayed a right-skewed distribution with kurtosis and outlying data in the upper range (Table 69, Figure 138). The data were higher than predicted by a normal distribution at high values and lower at mid-range values (Figure 139). The areas of over- and under-prediction did not show a strong spatial pattern with both error types distributed across the spatial extent (Figure 139).

The semivariogram showed weak autocorrelation present in the data and the model showed fair fit between measured and predicted values (Figure 140). Nevertheless, the model showed good cross-validation statistics (Table 70) indicating that it was good at prediction. The error map showed a 'bullseye' pattern with error increasing with distance from data points (Figure 141). The kriged surface is presented in Figure 141.

Table 69. Distributional properties of Bottom Current Average Maximum (m s^{-1}).

Property	Value
Number of Observations	2948
Minimum	4.90 x 10^{-3}
Maximum	0.318
Mean	0.060
Median	0.053
Standard Deviation	0.037
Skewness	1.194
Kurtosis	5.523

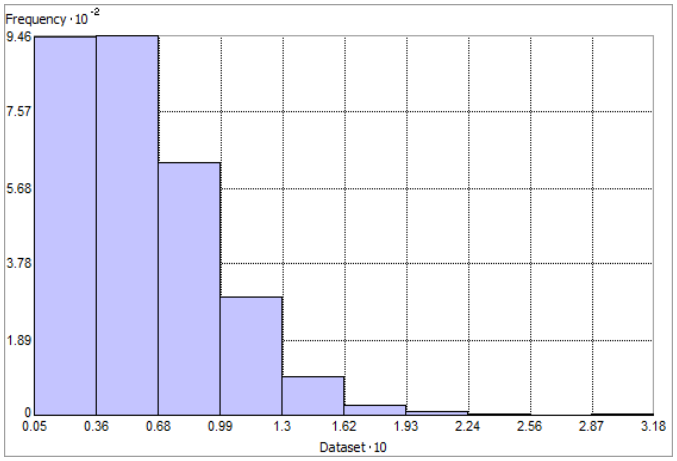

Figure 138. Distribution of Bottom Current Average Maximum (m s^{-1}). Histogram was illustrated using 10 bins. X axis is shown at 10; Y axis is shown at 10^{-2}.

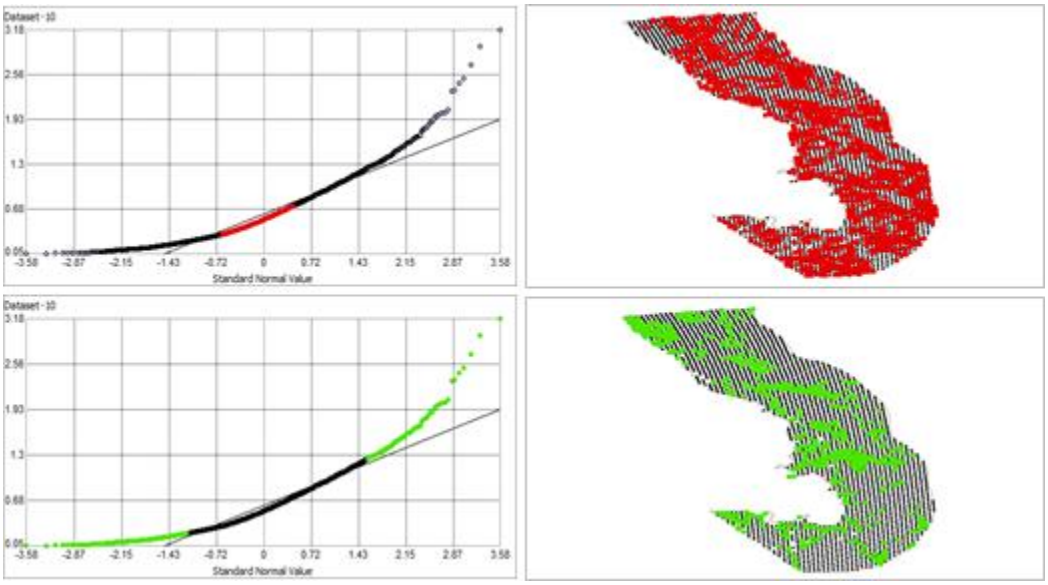

Figure 139. Normal Q-Q plot for data values of Bottom Current Average Maximum (m s^{-1}). Points falling under (upper panel) and over (bottom panel) the reference line are mapped.

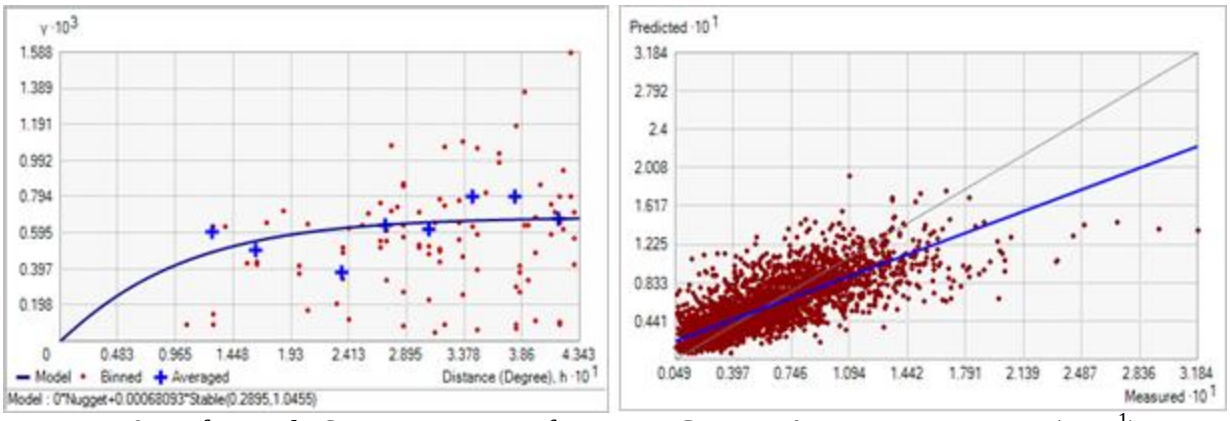

Figure 140. Left panel: Semivariogram of Bottom Current Average Maximum (m s^{-1}). Binned values are shown as red dots; average points are shown as blue crosses; the model fit to the averaged values is shown as a blue line. Lag size: 0.036 degrees; number of lags: 12; Parameter: 1.046; Range: 0.290 degrees; Partial Sill: 6.089 x 10^{-4}. Right panel: Scatterplot of predicted values versus observed values for the model of Bottom Current Average Maximum (m s^{-1}).

Table 70. Results of cross-validation of the kriged model for Bottom Current Average Maximum (m s^{-1}).

Prediction error	**Value**
Number of Observations	2948
Overall Mean Error	-1.395 x 10^{-5}
Root Mean Square Prediction Error	0.024
Standardized Mean	-6.135 x 10^{-4}
Standardized Root Mean Square Prediction Error	0.937
Average Standard Error	0.025

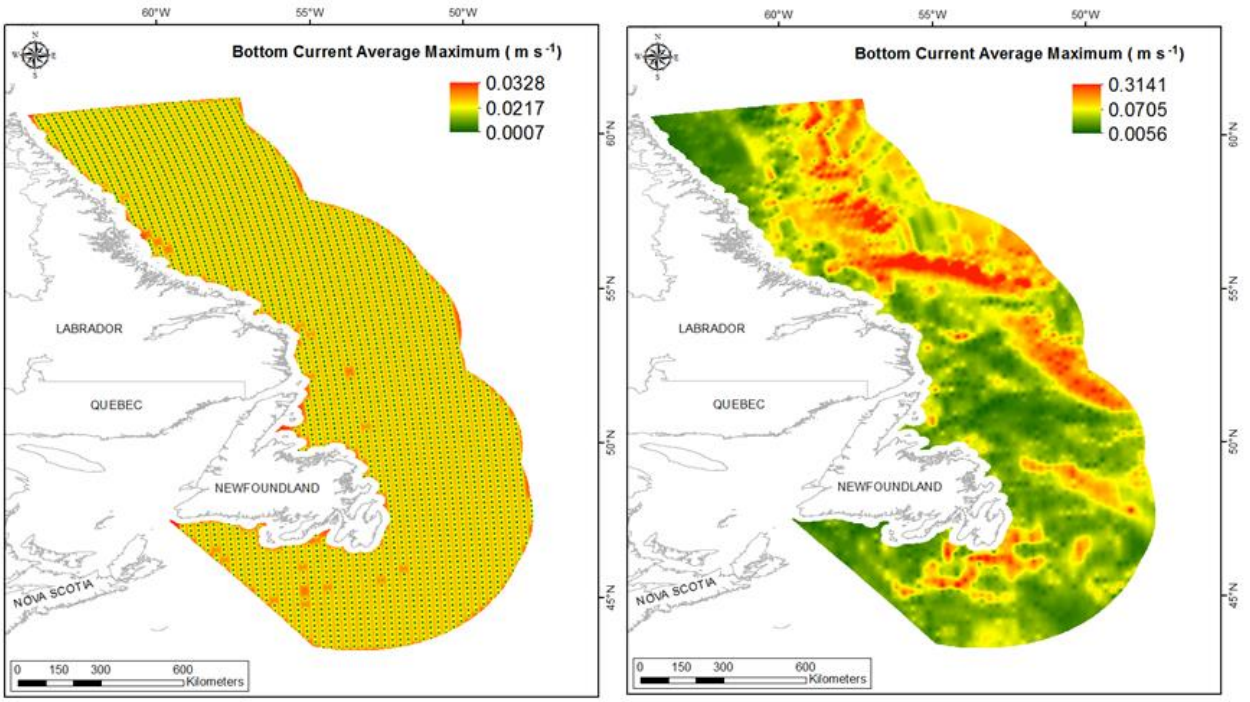

Figure 141. Left panel: Prediction standard error surface of Bottom Current Average Maximum (m s^{-1}). Right panel: Interpolated prediction surface of Bottom Current Average Maximum (m s^{-1}).

Bottom Current Average Range

This variable displayed a right-skewed distribution with kurtosis prior to modeling (Table 71, Figure 142). The data were higher than predicted by a normal distribution at high and low values (Figure 143). Mid-range values were slightly lower than the reference line. The areas of over- and under-prediction did not show a strong spatial pattern with both error types distributed across the spatial extent, however all of the area was biased with most areas under-predicting (Figure 143).

The semivariogram showed very weak autocorrelation present in the data but showed fair fit between measured and predicted values (Figure 144). Nevertheless, the model showed excellent cross-validation statistics (Table 72) indicating that it was good at prediction. The error map showed no spatial pattern over the study extent except for along the coast where it was high (Figure 145). The kriged surface is presented in Figure 145.

Table 71. Distributional properties of Bottom Current Average Range (m s^{-1}).

Property	Value
Number of Observations	2948
Minimum	0.005
Maximum	0.143
Mean	0.044
Median	0.039
Standard Deviation	0.024
Skewness	0.904
Kurtosis	3.717

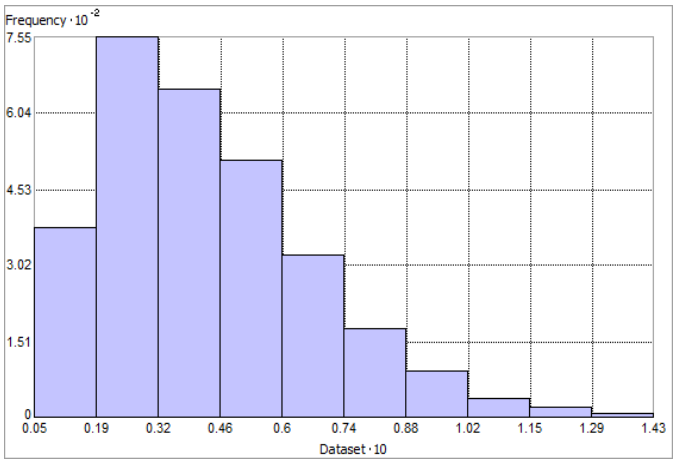

Figure 142. Distribution of Bottom Current Average Range (m s^{-1}). Histogram was illustrated using 10 bins. X axis is shown at 10; Y axis is shown at 10^{-2}.

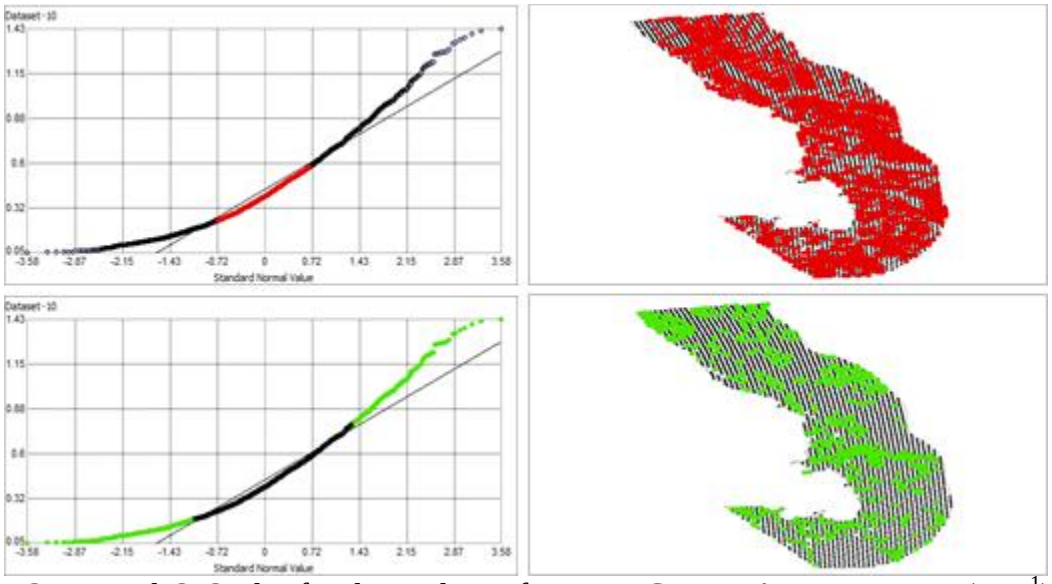

Figure 143. Normal Q-Q plot for data values of Bottom Current Average Range (m s^{-1}). Points falling under (upper panel) and over (bottom panel) the reference line are mapped.

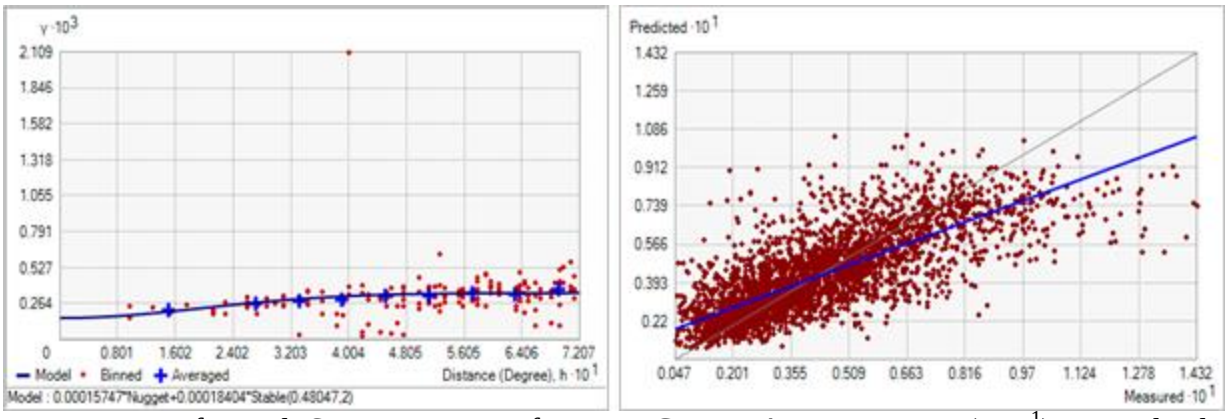

Figure 144. Left panel: Semivariogram of Bottom Current Average Range (m s^{-1}). Binned values are shown as red dots; average points are shown as blue crosses; the model fit to the averaged values is shown as a blue line. Lag size: 0.060 degrees; number of lags: 12; Parameter: 2; Range: 0.480 degrees; Partial Sill: 1.840 x 10^{-4}. Right panel: Scatterplot of predicted values versus observed values for the model of Bottom Current Average Range (m s^{-1}).

Table 72. Results of cross-validation of the kriged model for Bottom Current Average Range (m s^{-1}).

Prediction error	**Value**
Number of Observations	2948
Overall Mean Error	-2.799 x 10^{-6}
Root Mean Square Prediction Error	0.016
Standardized Mean	-2.647 x 10^{-4}
Standardized Root Mean Square Prediction Error	1.005
Average Standard Error	0.016

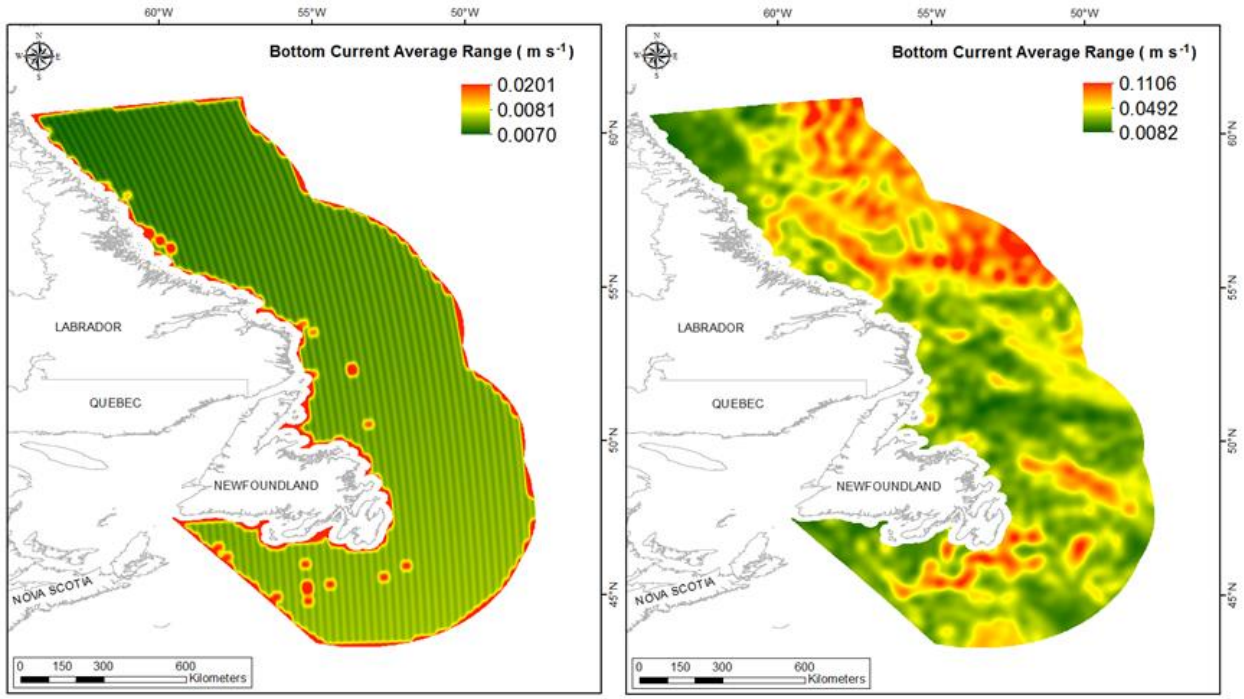

Figure 145. Left panel: Prediction standard error surface of Bottom Current Average Range (m s^{-1}). Right panel: Interpolated prediction surface of Bottom Current Average Range (m s^{-1}).

Surface Current Mean

This variable displayed a right-skewed distribution with kurtosis prior to modeling (Table 73, Figure 146). The data were higher than predicted by a normal distribution at high values (Figure 147). Mid-range values were slightly lower than the reference line. The areas of over- and under-prediction showed a spatial pattern (Figure 147).

The semivariogram showed moderate autocorrelation in the data but showed excellent fit between measured and observed values (Figure 148). The model showed good cross-validation statistics (Table 74) indicating that it was good at prediction. The error map showed a 'bullseye' pattern with error increasing with distance from data points (Figure 149). The kriged surface is presented in Figure 149.

Table 73. Distributional properties of Surface Current Mean (m s^{-1}).

Property	Value
Number of Observations	2975
Minimum	0.030
Maximum	0.455
Mean	0.125
Median	0.110
Standard Deviation	0.070
Skewness	0.935
Kurtosis	3.676

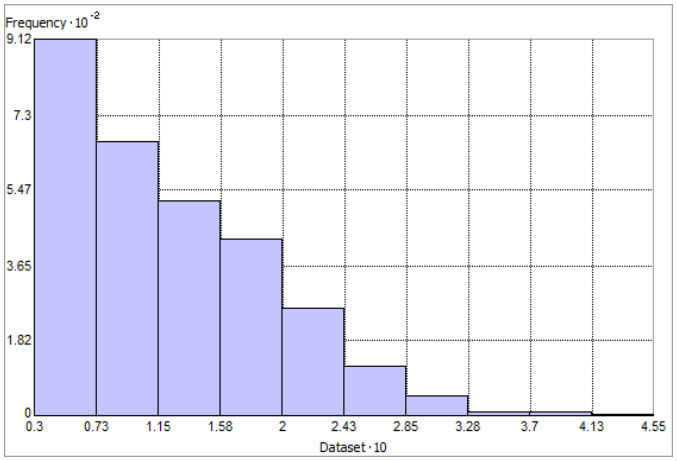

Figure 146. Distribution of Surface Current Mean (m s^{-1}). Histogram was illustrated using 10 bins. X axis is shown at 10; Y axis is shown at 10^{-2}.

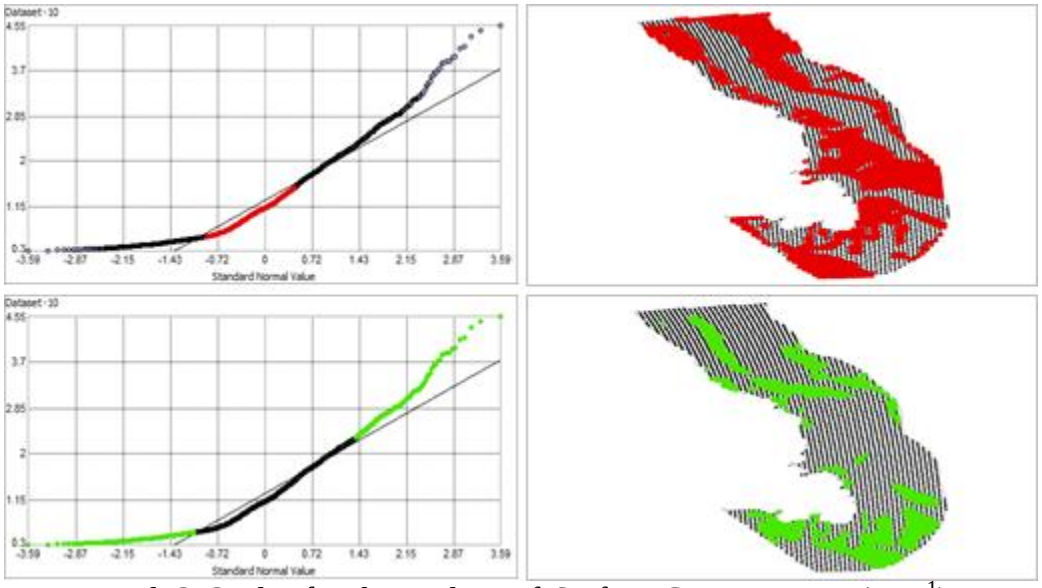

Figure 147. Normal Q-Q plot for data values of Surface Current Mean (m s^{-1}). Points falling under (upper panel) and over (bottom panel) the reference line are mapped.

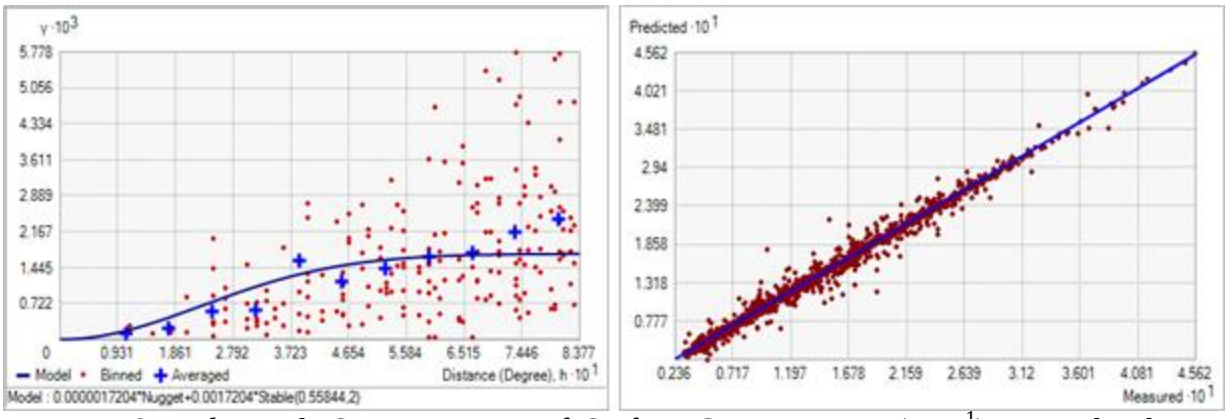

Figure 148. Left panel: Semivariogram of Surface Current Mean (m s^{-1}). Binned values are shown as red dots; average points are shown as blue crosses; the model fit to the averaged values is shown as a blue line. Lag size: 0.070 degrees; number of lags: 12; Parameter: 2; Range: 0.558 degrees; Partial Sill: 1.720 x 10^{-3}. Right panel: Scatterplot of predicted values versus observed values for the model of Surface Current Mean (m s^{-1}).

Table 74. Results of cross-validation of the kriged model for Surface Current Mean (m s^{-1}).

Prediction error	**Value**
Number of Observations	2975
Overall Mean Error	-2.118 x 10^{-5}
Root Mean Square Prediction Error	0.007
Standardized Mean	-5.350 x 10^{-4}
Standardized Root Mean Square Prediction Error	1.328
Average Standard Error	6.062 x 10^{-3}

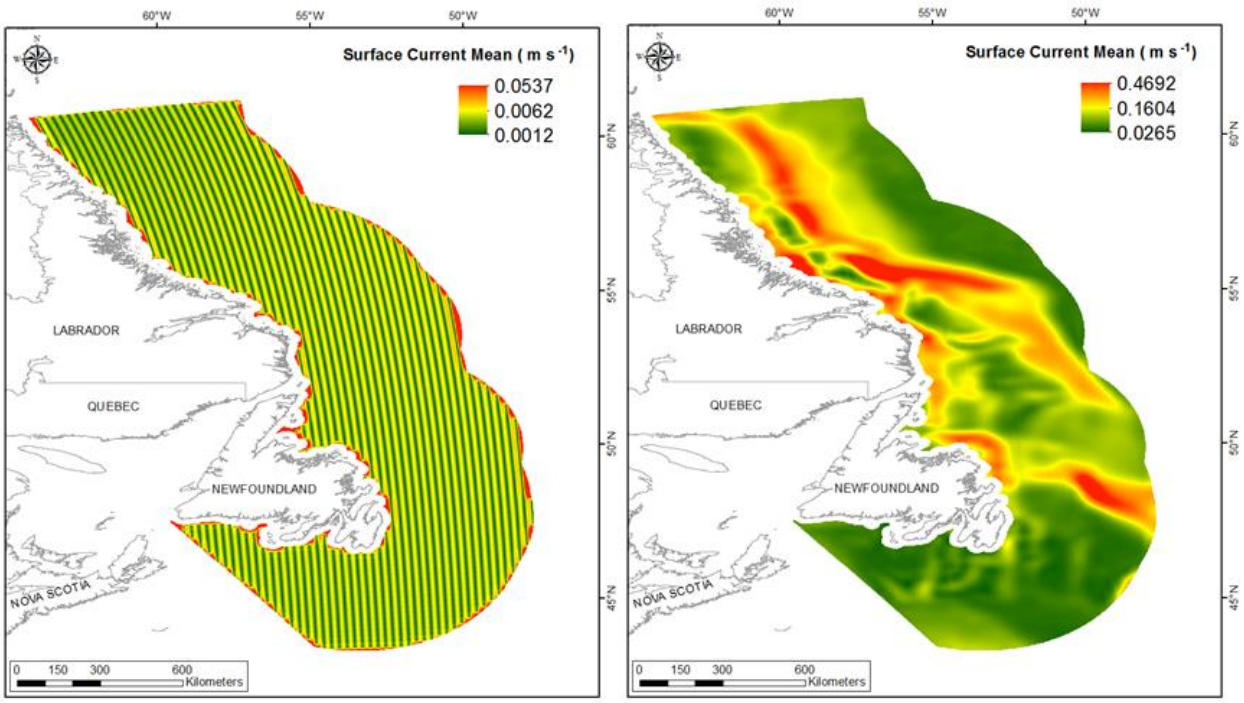

Figure 149. Left panel: Prediction standard error surface of Surface Current Mean (m s^{-1}). Right panel: Interpolated prediction surface of Surface Current Mean (m s^{-1}).

Surface Current Minimum

This variable displayed a right-skewed distribution with kurtosis prior to modeling (Table 75, Figure 150). The data were higher than predicted by a normal distribution at high values (Figure 151). Mid-range values were lower than the reference line. The areas of over- and under-prediction did not show a strong spatial pattern with both error types distributed across the spatial extent, however the whole area was either under or over predicted (Figure 151).

The semivariogram showed autocorrelation present in the data and the model showed fair fit between measured and predicted values (Figure 152). Nevertheless, the model showed excellent cross-validation statistics (Table 76) indicating that it was very good at prediction. The error map showed a 'bullseye' pattern with error increasing with distance from data points (Figure 153). The kriged surface is presented in Figure 153. Negative values resulted in the prediction surface after ordinary kriging of this variable. This possibly resulted from the highly right-skewed nature of the raw data (see Figure 150). Of the 533592 raster cells in the study extent, 353 contained negative values (see Table A3). These occurred in 5 small patches that were located on the Labrador Shelf and in the deeper waters off Newfoundland (see Figure A3).

Table 75. Distributional properties of Surface Current Minimum (m s^{-1}).

Property	Value
Number of Observations	2975
Minimum	2.100 x 10^{-5}
Maximum	0.217
Mean	0.024
Median	0.010
Standard Deviation	0.029
Skewness	1.864
Kurtosis	6.659

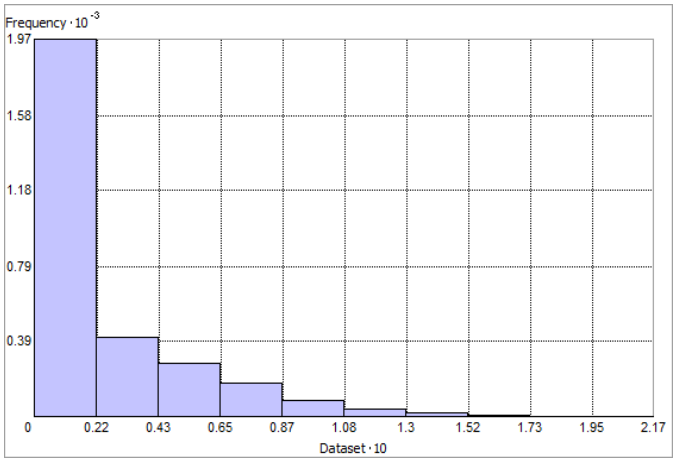

Figure 150. Distribution of Surface Current Minimum (m s^{-1}). Histogram was illustrated using 10 bins. X axis shown at 10; Y axis shown at 10^{-3}.

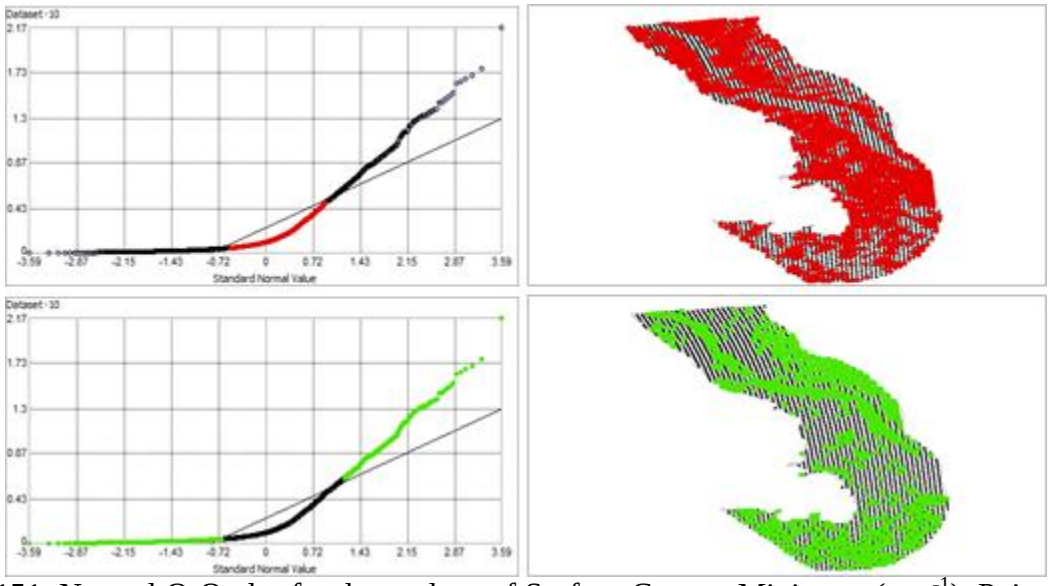

Figure 151. Normal Q-Q plot for data values of Surface Current Minimum (m s^{-1}). Points falling under (upper panel) and over (bottom panel) the reference line are mapped.

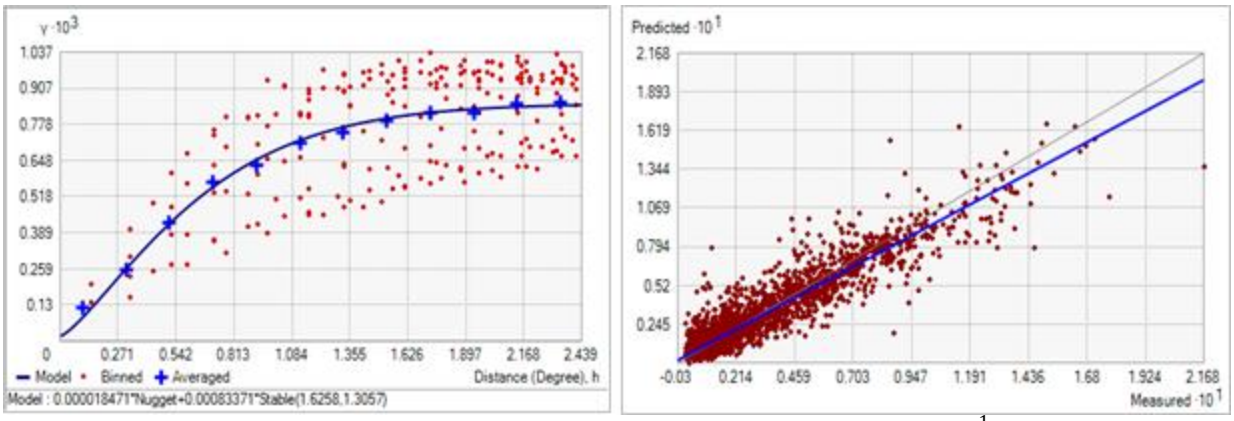

Figure 152. Left panel: Semivariogram of Surface Current Minimum (m s^{-1}). Binned values are shown as red dots; average points are shown as blue crosses; the model fit to the averaged values is shown as a blue line. Lag size: 0.203 degrees; number of lags: 12; Parameter: 1.306; Range: 1.626 degrees; Partial Sill: 8.337 x 10^{-4}. Right panel: Scatterplot of predicted values versus observed values for the model of Surface Current Minimum (m s^{-1}).

Table 76. Results of cross-validation of the kriged model for Surface Current Minimum (m s^{-1}).

Prediction error	**Value**
Number of Observations	2975
Overall Mean Error	2.233 x 10^{-5}
Root Mean Square Prediction Error	0.010
Standardized Mean	8.159 x 10^{-4}
Standardized Root Mean Square Prediction Error	0.923
Average Standard Error	0.011

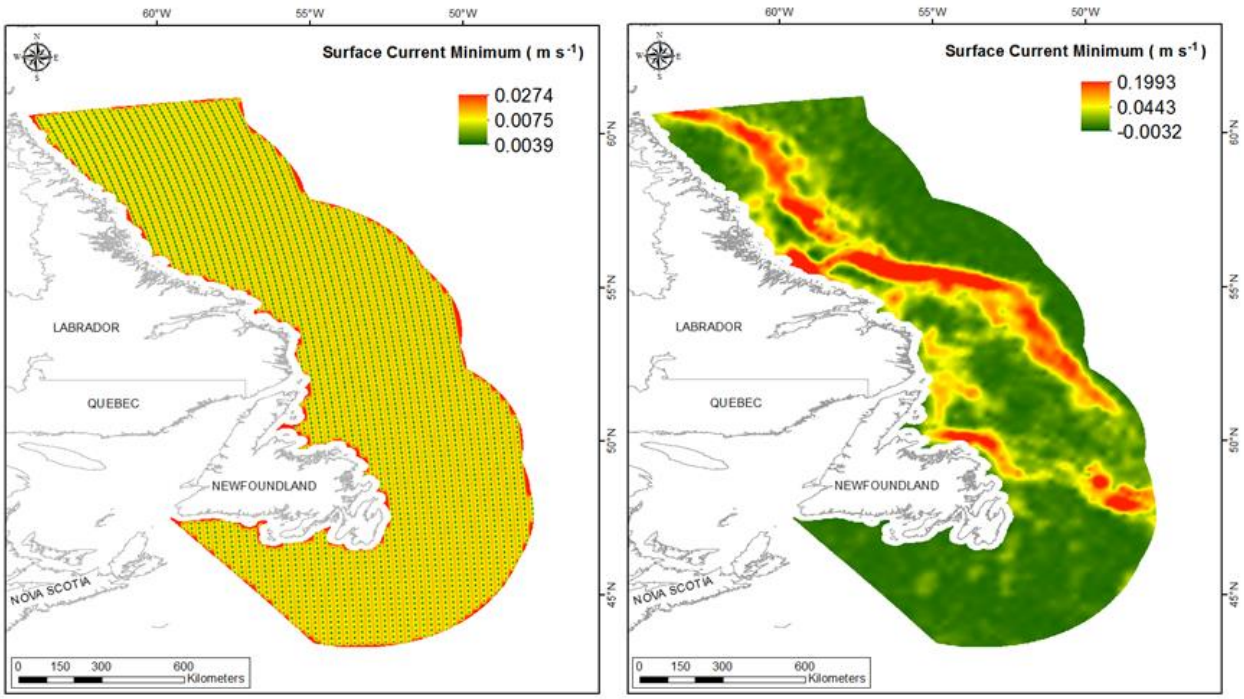

Figure 153. Left panel: Prediction standard error surface of Surface Current Minimum (m s^{-1}). Right panel: Interpolated prediction surface of Surface Current Minimum (m s^{-1}).

Surface Current Maximum

This variable displayed a slightly right-skewed distribution with kurtosis prior to modeling (Table 77, Figure 154). The data were higher than predicted by a normal distribution at low and high values (Figure 155). Mid-range values were slightly lower than the reference line. The areas of over- and under-prediction did not show a strong spatial pattern (Figure 155).

The semivariogram showed moderate autocorrelation present in the data and the model showed good fit between measured and predicted values (Figure 156). The model showed good cross-validation statistics (Table 78) indicating that it was very good at prediction. The error map showed no spatial pattern over the study extent except for along the coast where it was high (Figure 157). The kriged surface is presented in Figure 157.

Table 77. Distributional properties of Surface Current Maximum (m s^{-1}).

Property	Value
Number of Observations	2975
Minimum	0.065
Maximum	0.800
Mean	0.269
Median	0.265
Standard Deviation	0.108
Skewness	0.537
Kurtosis	3.319

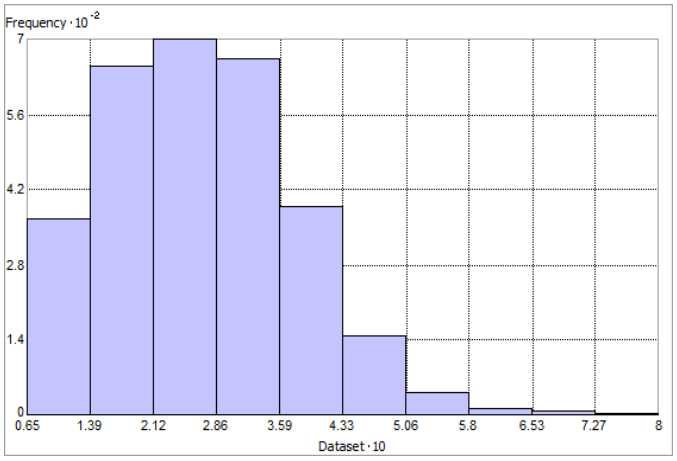

Figure 154. Distribution of Surface Current Maximum (m s^{-1}). Histogram was illustrated using 10 bins. X axis is shown at 10; Y axis is shown at 10^{-2}.

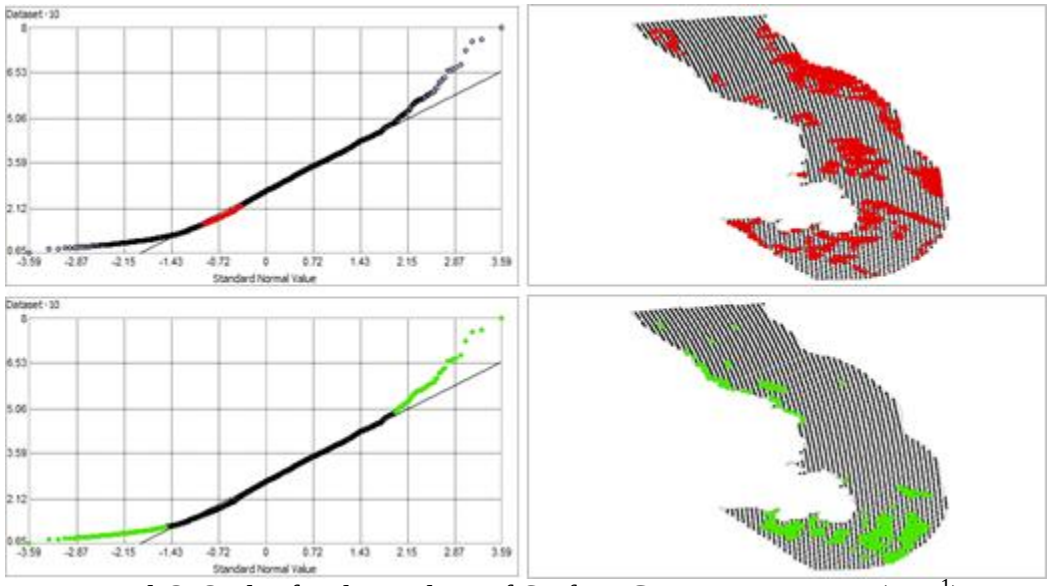

Figure 155. Normal Q-Q plot for data values of Surface Current Maximum (m s^{-1}). Points falling under (upper panel) and over (bottom panel) the reference line are mapped.

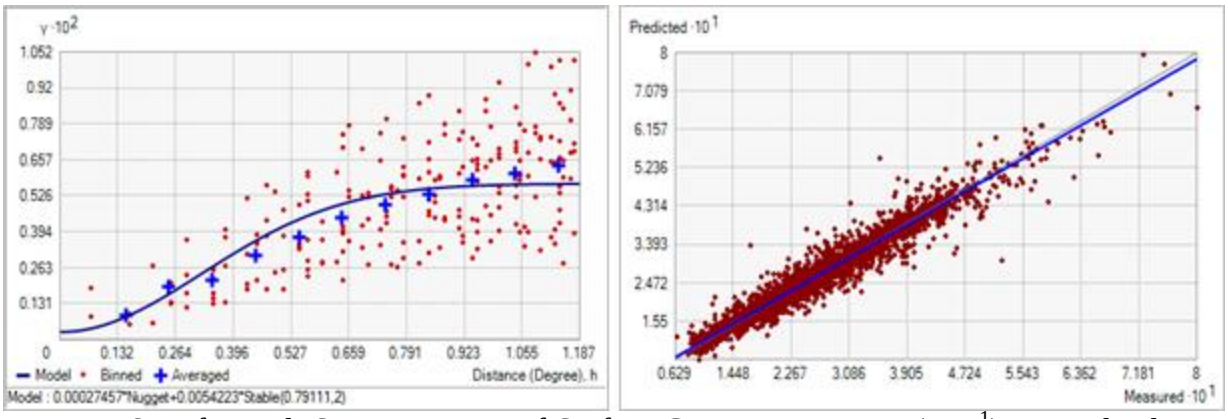

Figure 156. Left panel: Semivariogram of Surface Current Maximum (m s^{-1}). Binned values are shown as red dots; average points are shown as blue crosses; the model fit to the averaged values is shown as a blue line. Lag size: 0.099 degrees; number of lags: 12; Parameter: 2; Range: 0.791 degrees; Partial Sill: 0.005. Right panel: Scatterplot of predicted values versus observed values for the model of Surface Current Maximum (m s^{-1}).

Table 78. Results of cross-validation of the kriged model for Surface Current Maximum (m s^{-1}).

Prediction error	**Value**
Number of Observations	2975
Overall Mean Error	-1.996×10^{-4}
Root Mean Square Prediction Error	0.025
Standardized Mean	-7.835×10^{-3}
Standardized Root Mean Square Prediction Error	1.127
Average Standard Error	0.022

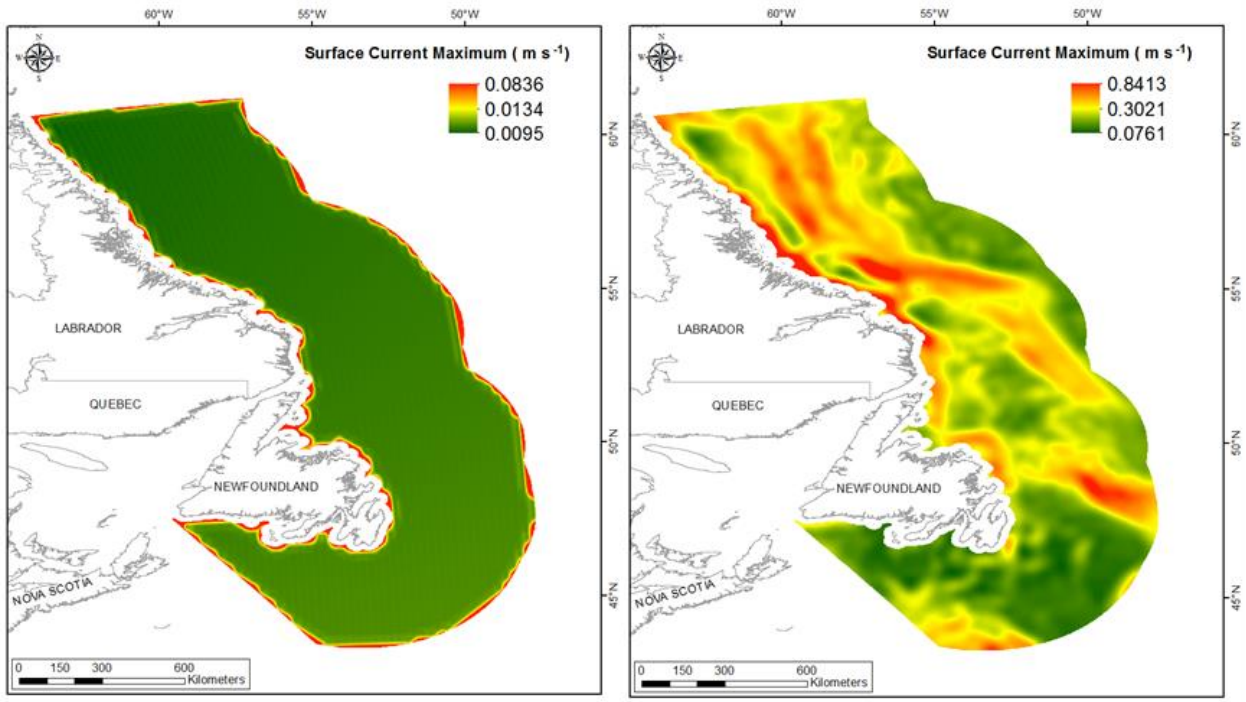

Figure 157. Left panel: Prediction standard error surface of Surface Current Maximum (m s^{-1}). Right panel: Interpolated prediction surface of Surface Current Maximum (m s^{-1}).

Surface Current Range

This variable displayed a bell-shaped distribution prior to modeling (Table 79, Figure 158). The data were higher than predicted by a normal distribution at low and high values with the rest of the data following the prediction line (Figure 159).

The semivariogram showed moderate autocorrelation present in the data and the model showed good fit between measured and predicted values (Figure 160). Nevertheless, the model showed excellent cross-validation statistics (Table 80) indicating that it was very good at prediction. The error map showed no spatial pattern over the study extent except for some areas along the coast where it was high (Figure 161). The kriged surface is presented in Figure 161.

Table 79. Distributional properties of Surface Current Range (m s^{-1}).

Property	Value
Number of Observations	2975
Minimum	0.062
Maximum	0.633
Mean	0.245
Median	0.246
Standard Deviation	0.090
Skewness	0.454
Kurtosis	3.282

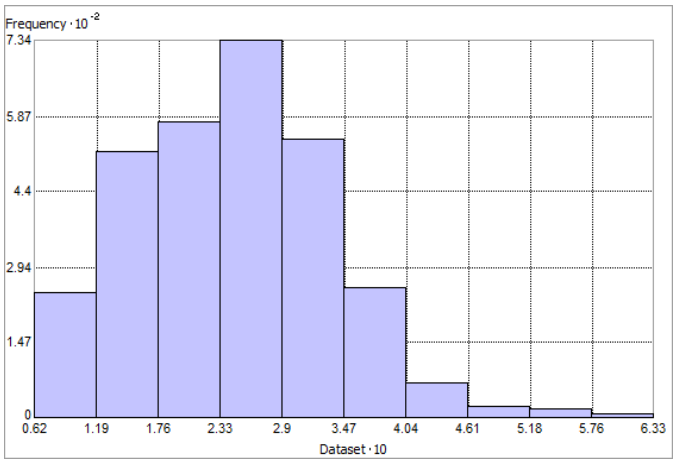

Figure 158. Distribution of Surface Current Range (m s^{-1}). Histogram was illustrated using 10 bins. X axis is shown at 10; Y axis is shown at 10^{-2}.

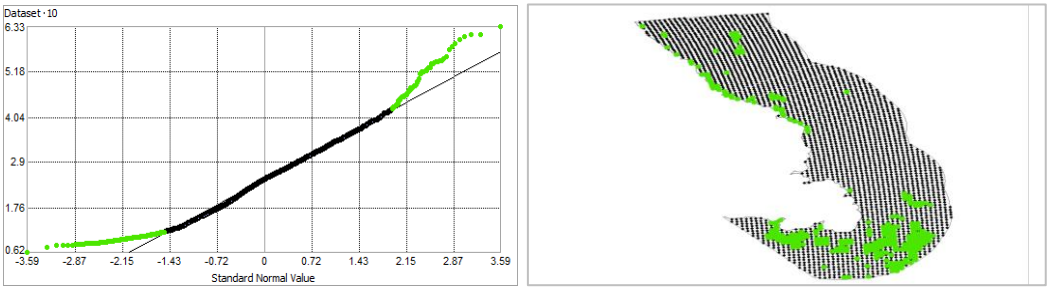

Figure 159. Normal Q-Q plot for data values of Surface Current Range (m s^{-1}). Points falling over the reference line are mapped.

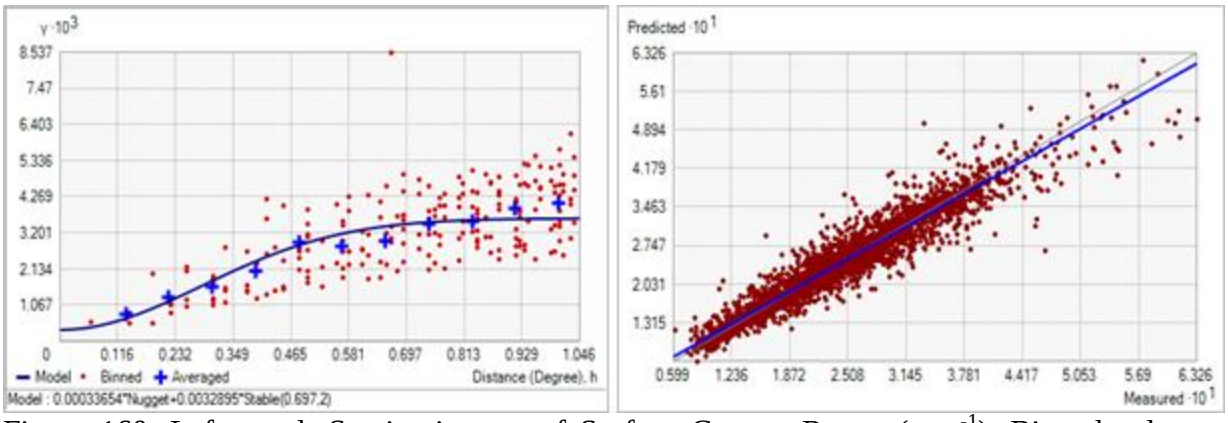

Figure 160. Left panel: Semivariogram of Surface Current Range (m s^{-1}). Binned values are shown as red dots; average points are shown as blue crosses; the model fit to the averaged values is shown as a blue line. Lag size: 0.087 degrees; number of lags: 12; Parameter: 2; Range: 0.697 degrees; Partial Sill: 3.289 x 10^{-3}. Right panel: Scatterplot of predicted values versus observed values for the model of Surface Current Range (m s^{-1}).

Table 80. Results of cross-validation of the kriged model for Surface Current Range (m s^{-1}).

Prediction error	Value
Number of Observations	2975
Overall Mean Error	-2.392×10^{-4}
Root Mean Square Prediction Error	0.026
Standardized Mean	-7.019×10^{-3}
Standardized Root Mean Square Prediction Error	1.066
Average Standard Error	0.024

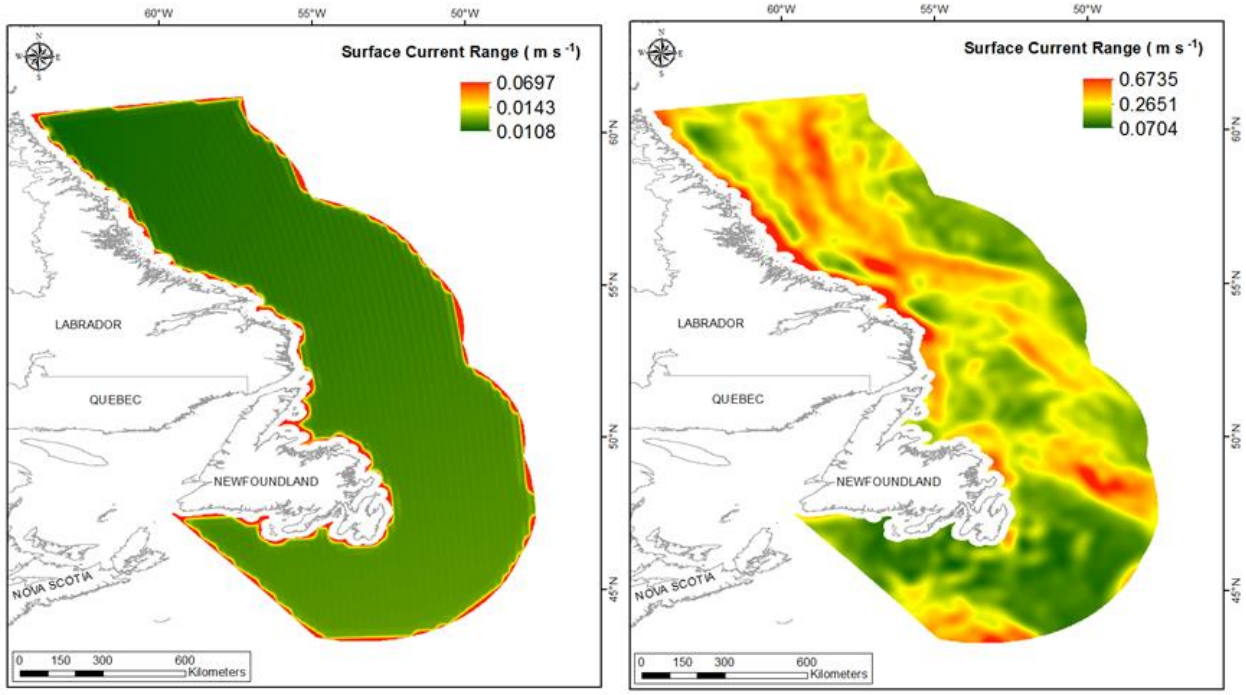

Figure 161. Left panel: Prediction standard error surface of Surface Current Range (m s^{-1}). Right panel: Interpolated prediction surface of Surface Current Range (m s^{-1}).

Surface Current Average Minimum

This variable displayed a right-skewed distribution with kurtosis prior to modeling (Table 81, Figure 162). The data were higher than predicted by a normal distribution at high values (Figure 163). Mid-range values were lower than the reference line. The areas of over- and under-prediction showed a spatial pattern and the entire area was either under- or over-predicted (Figure 163).

The semivariogram showed weak autocorrelation present in the data; however, the model showed very good fit between measured and predicted values (Figure 164). Nevertheless, the

model showed fair cross-validation statistics (Table 82). The error map showed a 'bullseye' pattern with error increasing with distance from data points (Figure 165). The kriged surface is presented in Figure 165. Negative values resulted in the prediction surface after ordinary kriging of this variable. This possibly resulted from the highly right-skewed nature of the raw data (see Figure 162). Of the 533592 raster cells in the study extent, only 65 contained negative values (see Table A4). These occurred in a single patch located on the Labrador Shelf (see Figure A4).

Table 81. Distributional properties of Surface Current Average Minimum (m s^{-1}).

Property	Value
Number of Observations	2975
Minimum	0.008
Maximum	0.327
Mean	0.061
Median	0.044
Standard Deviation	0.051
Skewness	1.345
Kurtosis	4.809

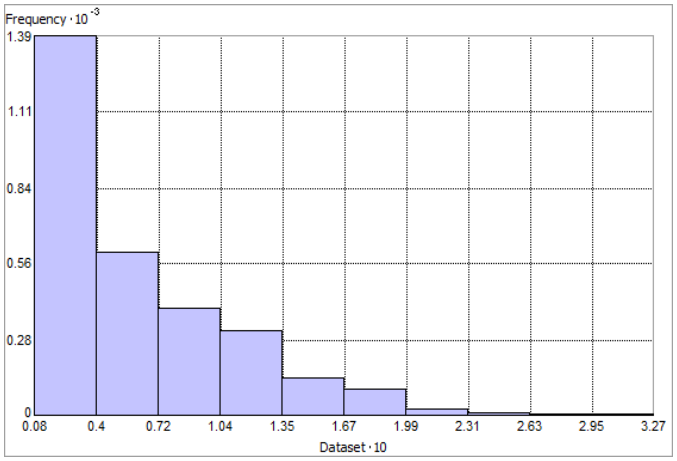

Figure 162. Distribution of Surface Current Average Minimum (m s^{-1}). Histogram was illustrated using 10 bins. X axis shown at 10; Y axis shown at 10^{-3}.

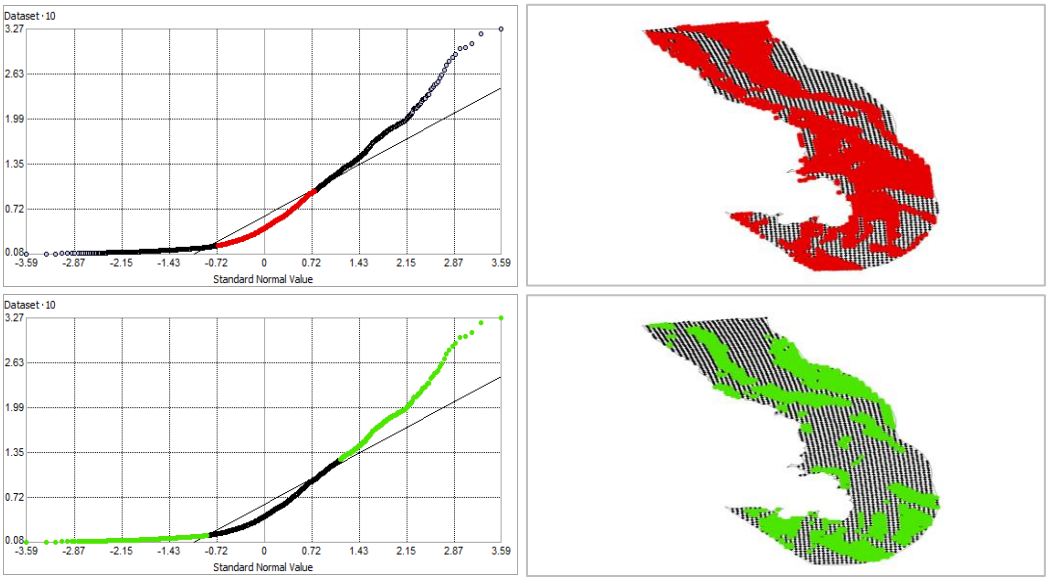

Figure 163. Normal Q-Q plot for data values of Surface Current Average Minimum (m s^{-1}). Points falling under (upper panel) and over (bottom panel) the reference line are mapped.

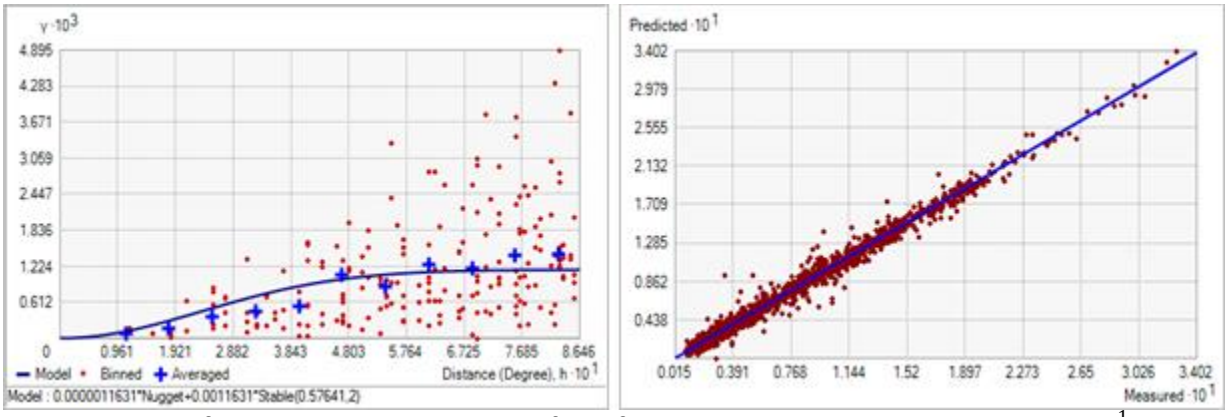

Figure 164. Left panel: Semivariogram of Surface Current Average Minimum (m s^{-1}). Binned values are shown as red dots; average points are shown as blue crosses; the model fit to the averaged values is shown as a blue line. Lag size: 0.072 degrees; number of lags: 12; Parameter: 2; Range: 0.576 degrees; Partial Sill: 1.163 x 10^{-3}. Right panel: Scatterplot of predicted values versus observed values for the model of Surface Current Average Minimum (m s^{-1}).

Table 82. Results of cross-validation of the kriged model for Surface Current Average Minimum (m s^{-1}).

Prediction error	**Value**
Number of Observations	2975
Overall Mean Error	4.100 x 10^{-5}
Root Mean Square Prediction Error	5.256 x 10^{-3}
Standardized Mean	2.103 x 10^{-3}
Standardized Root Mean Square Prediction Error	1.527
Average Standard Error	4.542 x 10^{-3}

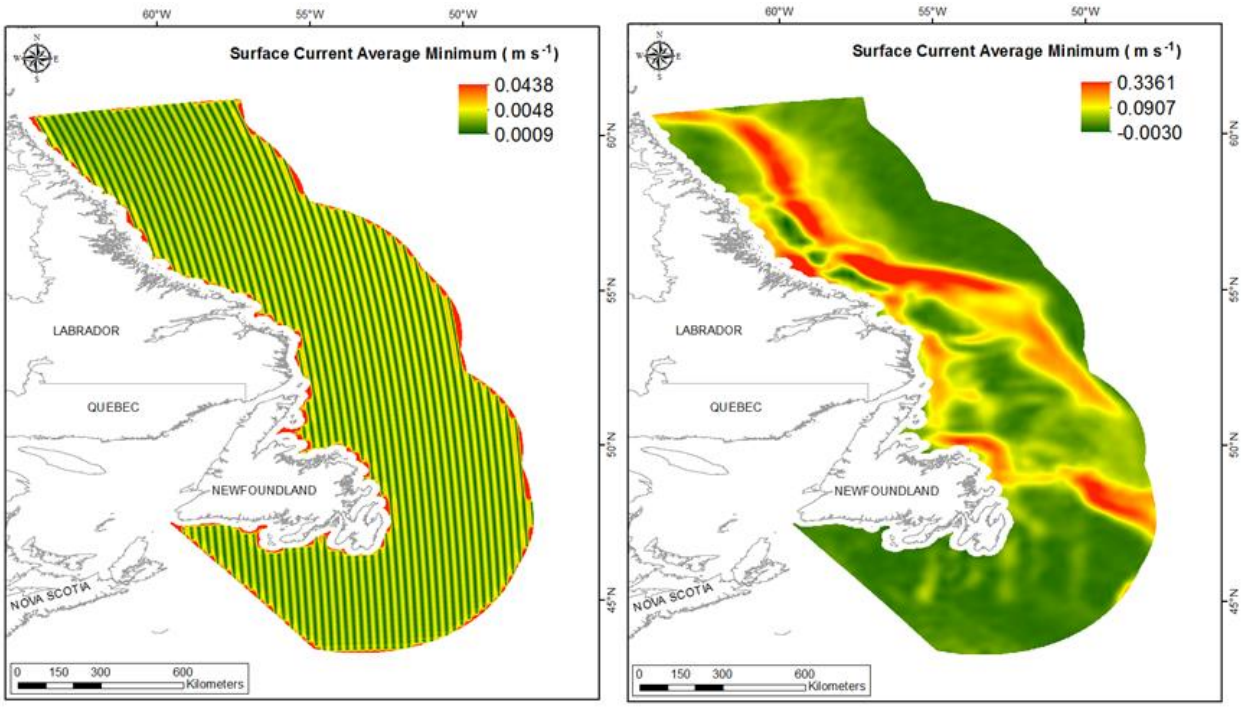

Figure 165. Left panel: Prediction standard error surface of Surface Current Average Minimum (m s^{-1}). Right panel: Interpolated prediction surface of Surface Current Average Minimum (m s^{-1}).

Surface Current Average Maximum

This variable displayed a bell-shaped right-skewed distribution prior to modeling (Table 83, Figure 166). The data were higher than predicted by a normal distribution at low and high values (Figure 167). Mid-range values were slightly lower than the reference line. The areas of over- and under-prediction showed spatial pattern (Figure 167).

The semivariogram showed weak autocorrelation present in the data and the model showed good fit between measured and predicted values (Figure 168). Nevertheless, the model showed fair cross-validation statistics (Table 84). The error map showed a 'bullseye' pattern with error increasing with distance from data points (Figure 169). The kriged surface is presented in Figure 169.

Table 83. Distributional properties of Surface Current Average Maximum (m s^{-1}).

Property	Value
Number of Observations	2975
Minimum	0.054
Maximum	0.573
Mean	0.200
Median	0.191
Standard Deviation	0.089
Skewness	0.626
Kurtosis	3.086

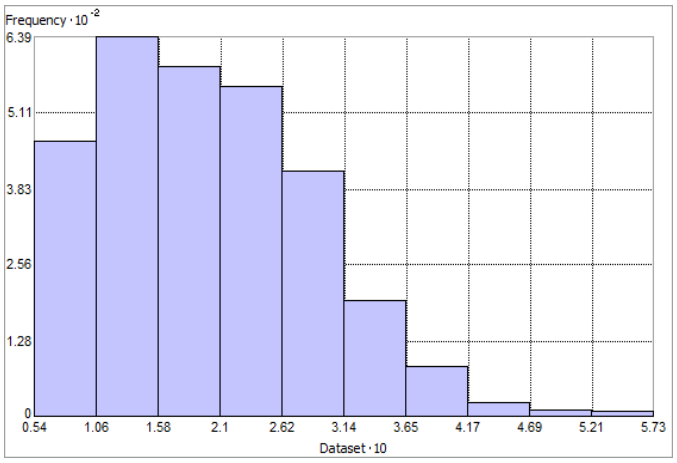

Figure 166. Distribution of Surface Current Average Maximum (m s^{-1}). Histogram was illustrated using 10 bins. X axis is shown at 10; Y axis is shown at 10^{-2}.

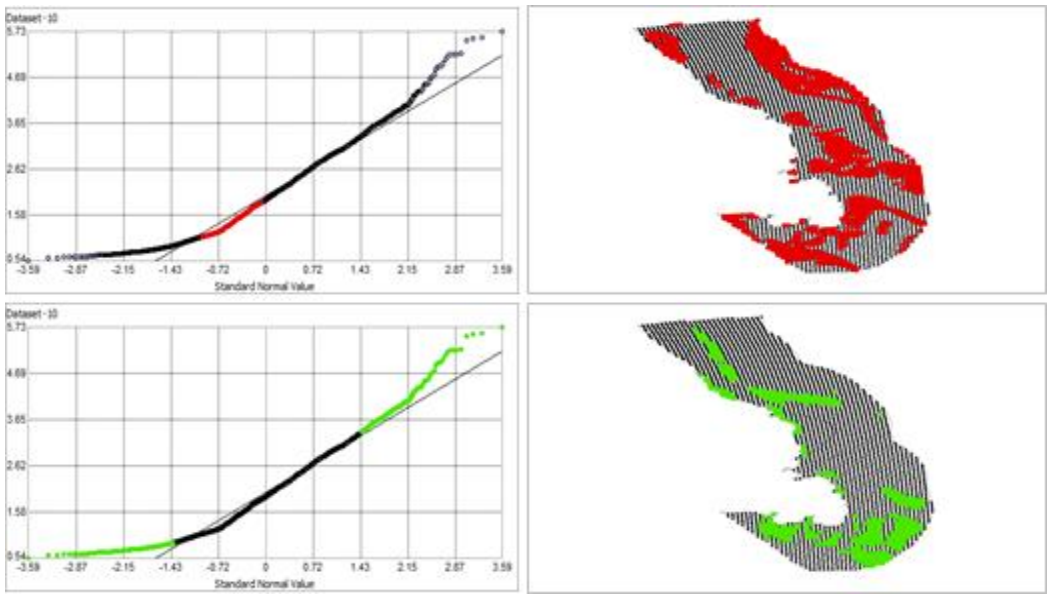

Figure 167. Normal Q-Q plot for data values of Surface Current Average Maximum (m s^{-1}). Points falling under (upper panel) and over (bottom panel) the reference line are mapped.

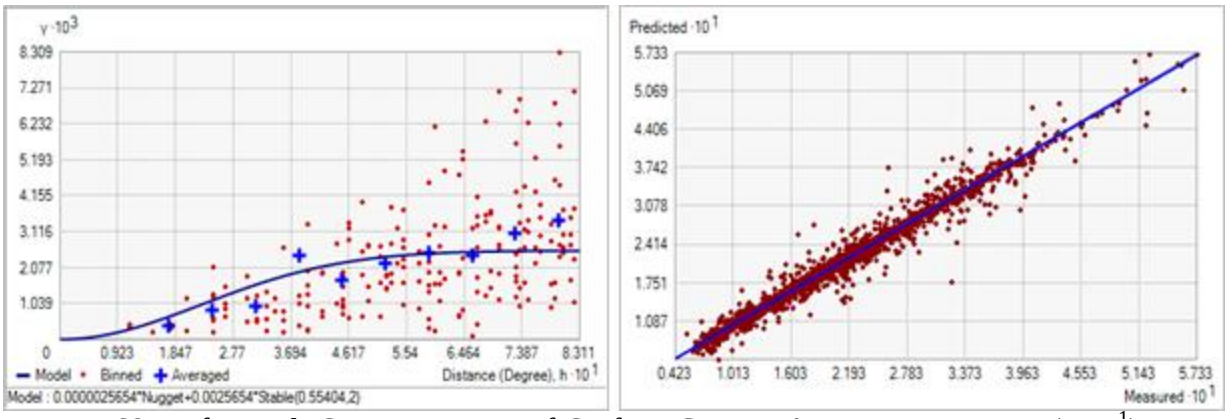

Figure 168. Left panel: Semivariogram of Surface Current Average Maximum (m s^{-1}). Binned values are shown as red dots; average points are shown as blue crosses; the model fit to the averaged values is shown as a blue line. Lag size: 0.069 degrees; number of lags: 12; Parameter: 2; Range: 0.554 degrees; Partial Sill: 2.565 x 10^{-3}. Right panel: Scatterplot of predicted values versus observed values for the model of Surface Current Average Maximum (m s^{-1}).

Table 84. Results of cross-validation of the kriged model for Surface Current Average Maximum (m s^{-1}).

Prediction error	**Value**
Number of Observations	2975
Overall Mean Error	-1.646 x 10^{-4}
Root Mean Square Prediction Error	0.012
Standardized Mean	-4.989 x 10^{-3}
Standardized Root Mean Square Prediction Error	1.942
Average Standard Error	7.581 x 10^{-3}

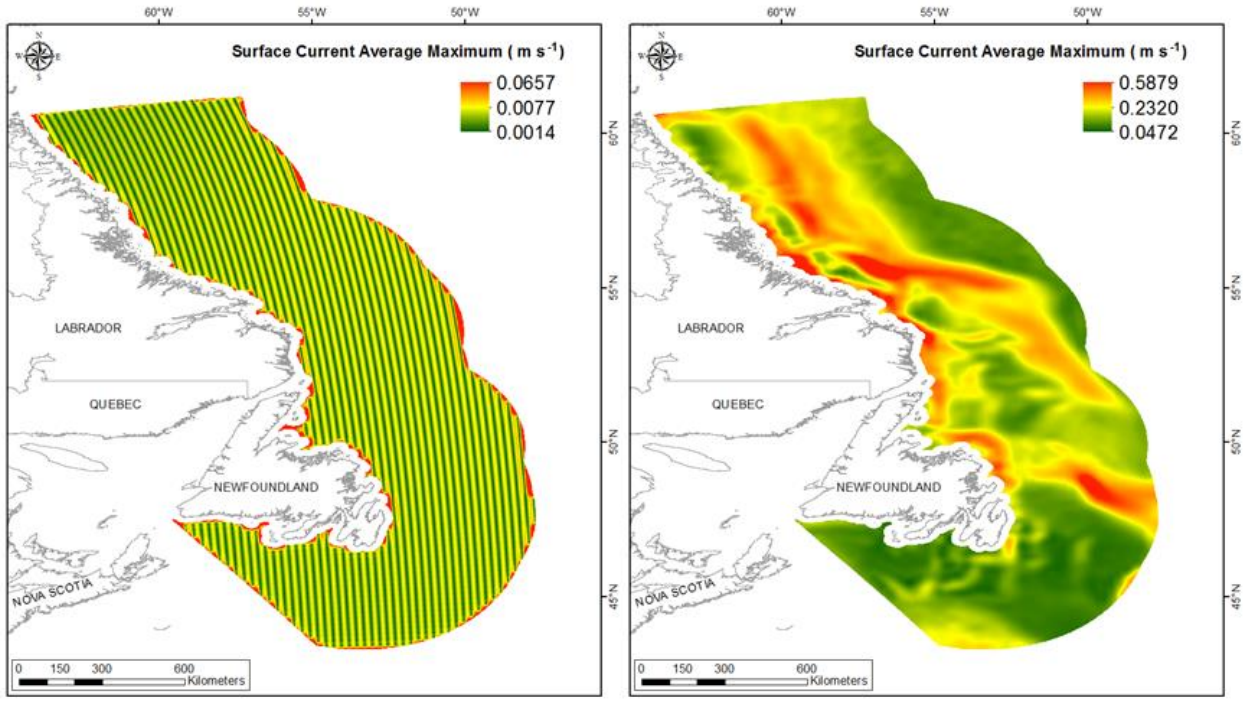

Figure 169. Left panel: Prediction standard error surface of Surface Current Average Maximum (m s^{-1}). Right panel: Interpolated prediction surface of Surface Current Average Maximum (m s^{-1}).

Surface Current Average Range

This variable displayed a bell-shaped prior to modeling (Table 85, Figure 170). The data were higher than predicted by a normal distribution at low and high values (Figure 171). Mid-range values were slightly lower than the reference line. The areas of over- and under-prediction showed no strong spatial pattern and the degree of under-prediction was relatively low (Figure 171).

The semivariogram showed moderate autocorrelation present in the data and the model showed good fit between measured and predicted values (Figure 172). The model showed good cross-validation statistics (Table 86) indicating that it was very good at prediction. The error map showed low error and no strong spatial pattern over the spatial extent but was higher along the coast (Figure 173). The kriged surface is presented in Figure 173.

Table 85. Distributional properties of Surface Current Average Range (m s^{-1}).

Property	Value
Number of Observations	2975
Minimum	0.044
Maximum	0.333
Mean	0.139
Median	0.141
Standard Deviation	0.047
Skewness	0.247
Kurtosis	2.750

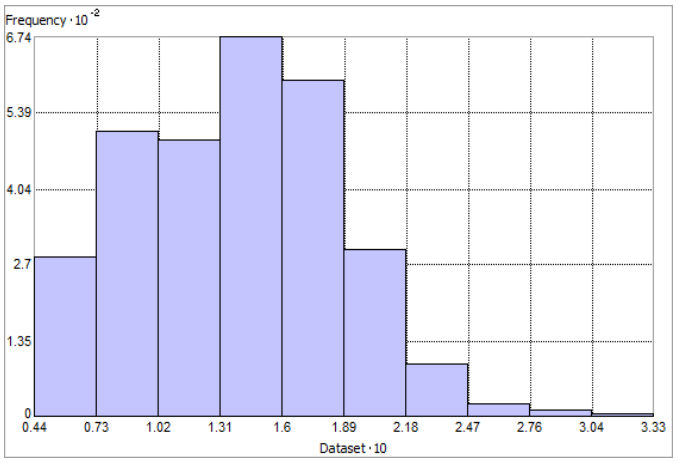

Figure 170. Distribution of Surface Current Average Range (m s^{-1}). Histogram was illustrated using 10 bins. X axis shown at 10; Y axis shown at 10^{-2}.

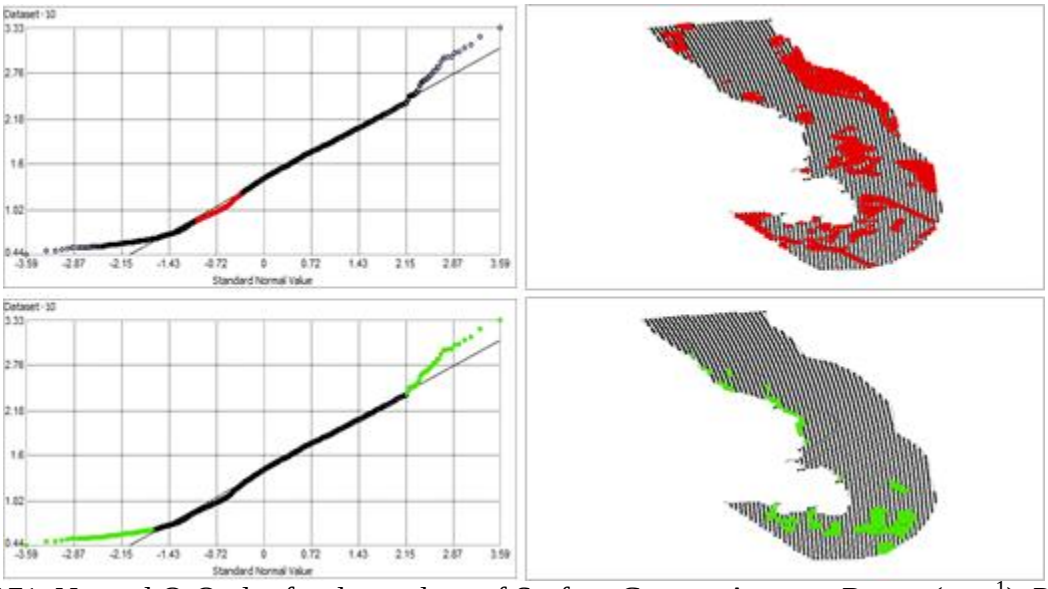

Figure 171. Normal Q-Q plot for data values of Surface Current Average Range (m s^{-1}). Points falling under (upper panel) and over (bottom panel) the reference line are mapped.

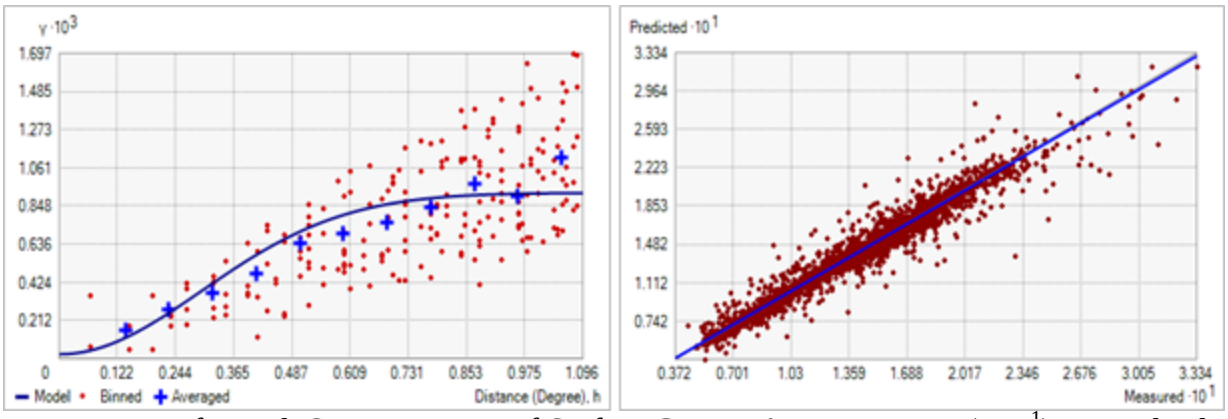

Figure 172. Left panel: Semivariogram of Surface Current Average Range (m s^{-1}). Binned values are shown as red dots; average points are shown as blue crosses; the model fit to the averaged values is shown as a blue line. Lag size: 0.091 degrees; number of lags: 12; Parameter: 2; Range: 0.731 degrees; Partial Sill: 8.970 x 10^{-4}. Right panel: Scatterplot of predicted values versus observed values for the model of Surface Current Average Range (m s^{-1}).

Table 86. Results of cross-validation of the kriged model for Surface Current Average Range (m s^{-1}).

Prediction error	**Value**
Number of Observations	2975
Overall Mean Error	-1.132 x 10^{-4}
Root Mean Square Prediction Error	0.010
Standardized Mean	-0.010
Standardized Root Mean Square Prediction Error	1.338
Average Standard Error	7.246 x 10^{-3}

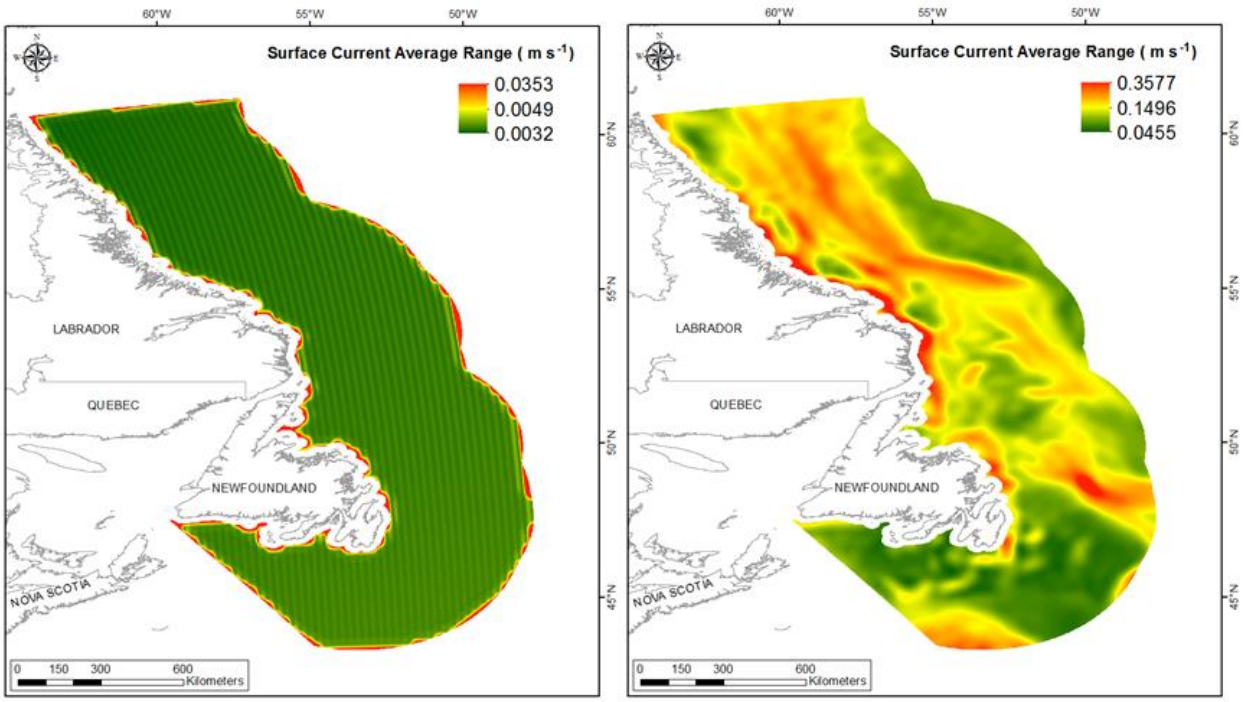

Figure 173. Left panel: Prediction standard error surface of Surface Current Average Range (m s^{-1}). Right panel: Interpolated prediction surface of Surface Current Average Range (m s^{-1}).

Maximum Seasonal Mixed Layer Depth

Maximum mixed layer depth, or, the depth at which surface vertical mixing dissipates, is a near-universal feature of the open ocean (de Boyer Montégut et al. 2004). Within this mixed layer, salinity, temperature, or density are nearly uniform, a phenonmenon caused by surface forcing, lateral advection, and internal wave processes that vary on diurnal, intra-seasonal, seasonal, and inter-annual scales (de Boyer Montégut et al. 2004). The depth of this mixed zone can show large spatial variability, ranging from less than 20 m in the summer hemisphere, to more than 500 m in the winter hemisphere at subpolar latitudes (de Boyer Montégut et al. 2004). The mixed layer depth has a significant influence on primary production in the surface waters. As the mixed layer depth increases it entrains nutrients from deeper waters below, supplying additional nutrients for primary production (Polovina et al., 1995, Carstensen et al. 2002).

Maximum Spring Mixed Layer Depth

This variable displayed a severely right-skewed distribution with kurtosis prior to modeling (Table 87, Figure 174). The data were higher than predicted by a normal distribution at low and high values (Figure 175). Mid-range values deviated considerably from the reference line. All areas of the spatial extent were either over- or under-predicted (Figure 175).

The semivariogram showed moderate autocorrelation present in the data and the model showed a good fit between measured and predicted values (Figure 176). The model showed good cross-validation statistics (Table 88) indicating that it was very good at prediction. The error map showed a 'bullseye' pattern with error increasing with distance from data points (Figure 177). The kriged surface is presented in Figure 177.

Table 87. Distributional properties of Maximum Spring Mixed Layer Depth (m).

Property	Value
Number of Observations	2975
Minimum	20.978
Maximum	1821.900
Mean	168.870
Median	45.481
Standard Deviation	271.860
Skewness	2.899
Kurtosis	12.246

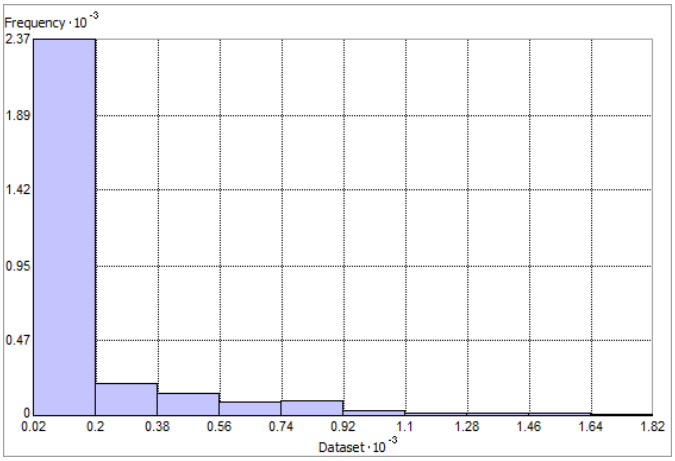

Figure 174. Distribution of Maximum Spring Mixed Layer Depth (m). Histogram was illustrated using 10 bins. X and Y axes are shown at 10^{-3}.

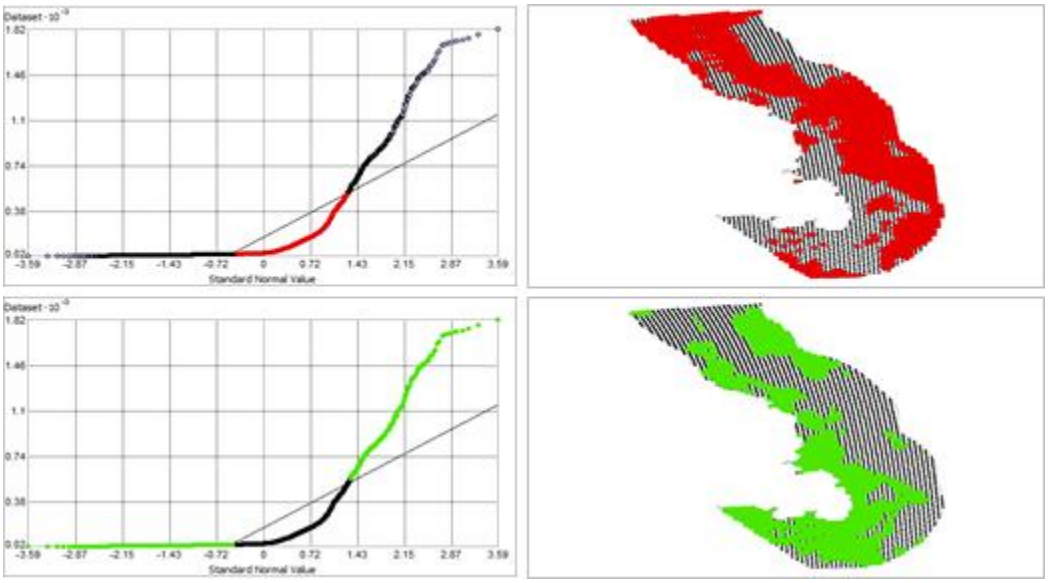

Figure 175. Normal Q-Q plot for data values of Maximum Spring Mixed Layer Depth (m). Points falling under (upper panel) and over (bottom panel) the reference line are mapped.

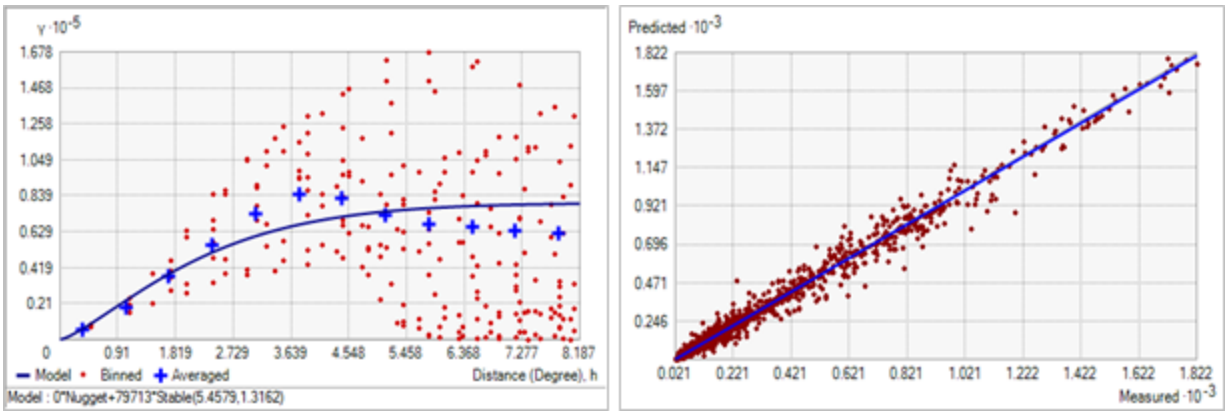

Figure 176. Left panel: Semivariogram of Maximum Spring Mixed Layer Depth (m). Binned values are shown as red dots; average points are shown as blue crosses; the model fit to the averaged values is shown as a blue line. Lag size: 0.682 degrees; number of lags: 12; Parameter: 1.316; Range: 5.458 degrees; Partial Sill: 79712.74. Right panel: Scatterplot of predicted values versus observed values for the model of Maximum Spring Mixed Layer Depth (m).

Table 88. Results of cross-validation of the kriged model for Maximum Spring Mixed Layer Depth (m).

Prediction error	**Value**
Number of Observations	2975
Overall Mean Error	-0.028
Root Mean Square Prediction Error	30.130
Standardized Mean	-6.324×10^{-4}
Standardized Root Mean Square Prediction Error	0.787
Average Standard Error	39.897

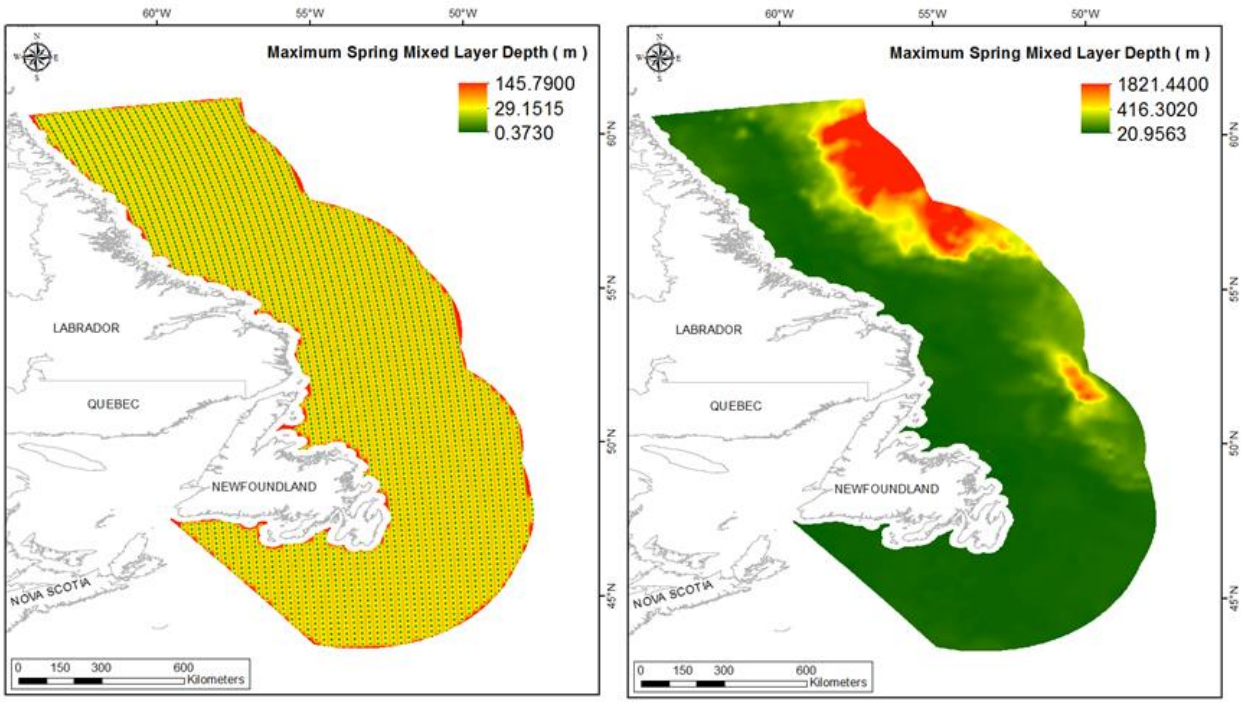

Figure 177. Left panel: Prediction standard error surface of Maximum Spring Mixed Layer Depth (m). Right panel: Interpolated prediction surface of Maximum Spring Mixed Layer Depth (m).

Maximum Summer Mixed Layer Depth

This variable displayed a severely right-skewed distribution with high kurtosis prior to modeling (Table 89, Figure 178). The data were higher than predicted by a normal distribution at low and high values (Figure 179). Mid-range values deviated from the reference line. The areas of over- and under-prediction showed a strong spatial pattern with all area biased on one direction or the other (Figure 179).

The semivariogram showed moderate autocorrelation present in the data and the model showed a good fit between measured and predicted values (Figure 180). The model showed good cross-validation statistics (Table 90) indicating that it was very good at prediction. The error map showed no spatial pattern over the study extent except for some areas along the coast where it was high (Figure 181). The kriged surface is presented in Figure 181. Negative values resulted in the prediction surface after ordinary kriging of this variable. This possibly resulted from the extremely right-skewed nature of the raw data (see Figure 178). Of the 533592 raster cells in the study extent, 235 contained negative values (see Table A5). These occurred in two small patches in deep water northeast of Newfoundland and surrounded the area predicted to have a high summer mixed layer depth (see Figure A5).

Table 89. Distributional properties of Maximum Summer Mixed Layer Depth (m).

Property	Value
Number of Observations	2975
Minimum	12.301
Maximum	551.300
Mean	34.874
Median	22.010
Standard Deviation	47.298
Skewness	6.109
Kurtosis	46.208

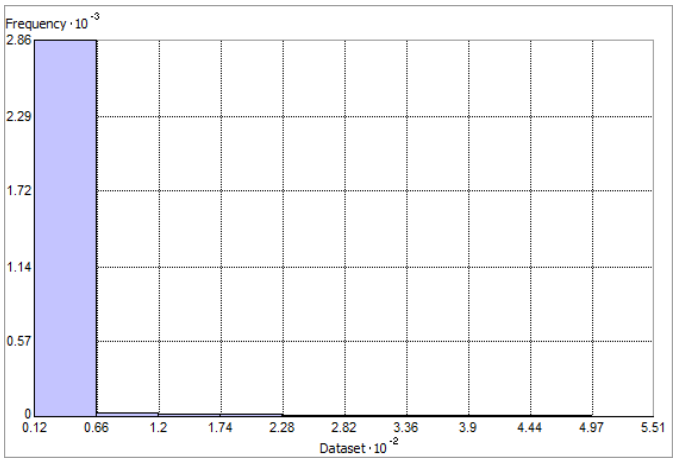

Figure 178. Distribution of Maximum Summer Mixed Layer Depth (m). Histogram was illustrated using 10 bins. X axis shown at 10^{-2}; Y axis shown at 10^{-3}.

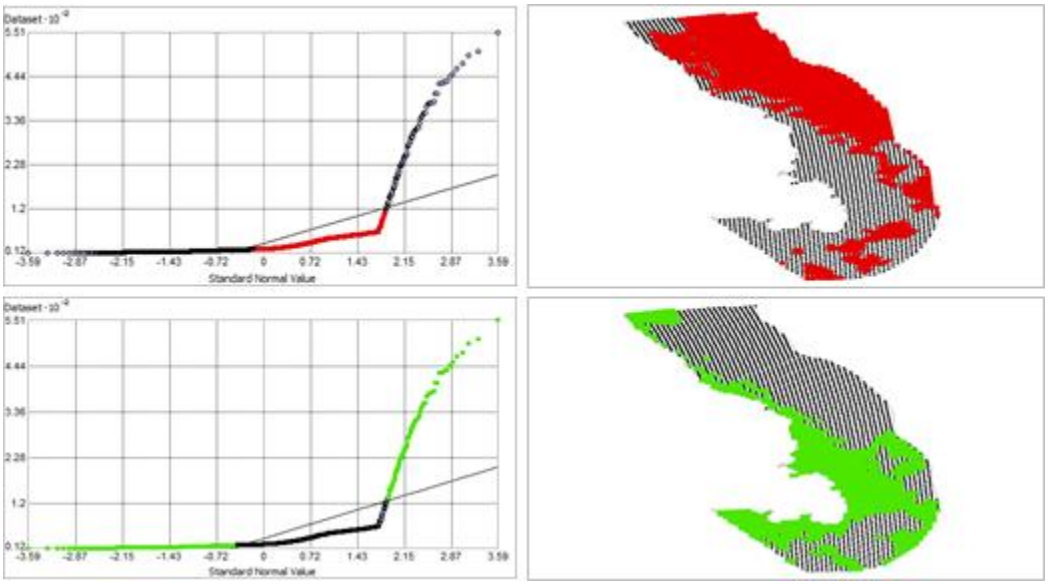

Figure 179. Normal Q-Q plot for data values of Maximum Summer Mixed Layer Depth (m). Points falling under (upper panel) and over (bottom panel) the reference line are mapped.

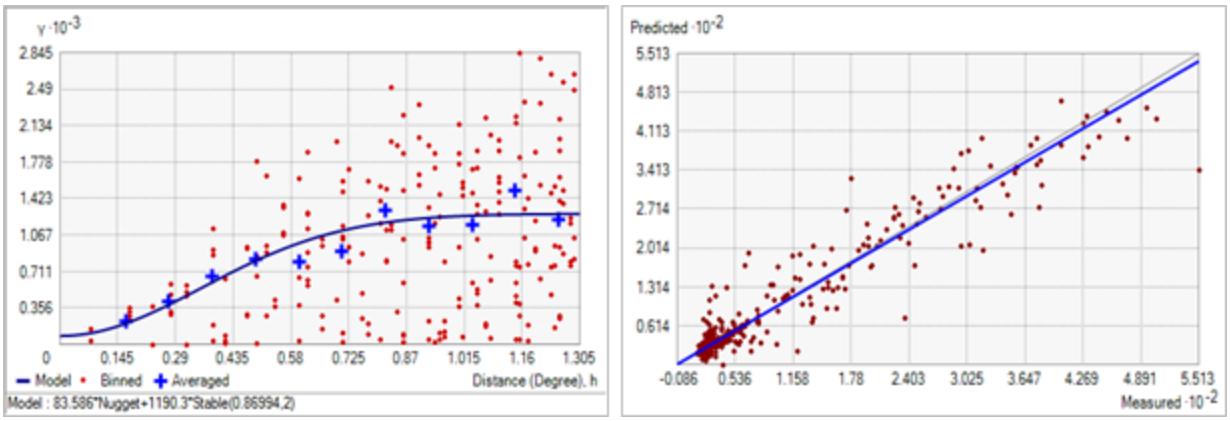

Figure 180. Left panel: Semivariogram of Maximum Summer Mixed Layer Depth (m). Binned values are shown as red dots; average points are shown as blue crosses; the model fit to the averaged values is shown as a blue line. Lag size: 0.109 degrees; number of lags: 12; Parameter: 2; Range: 0.870 degrees; Partial Sill: 1190.328. Right panel: Scatterplot of predicted values versus observed values for the model of Maximum Summer Mixed Layer Depth (m).

Table 90. Results of cross-validation of the kriged model for Maximum Summer Mixed Layer Depth (m).

Prediction error	**Value**
Number of Observations	2975
Overall Mean Error	0.042
Root Mean Square Prediction Error	11.793
Standardized Mean	2.609×10^{-3}
Standardized Root Mean Square Prediction Error	1.055
Average Standard Error	11.272

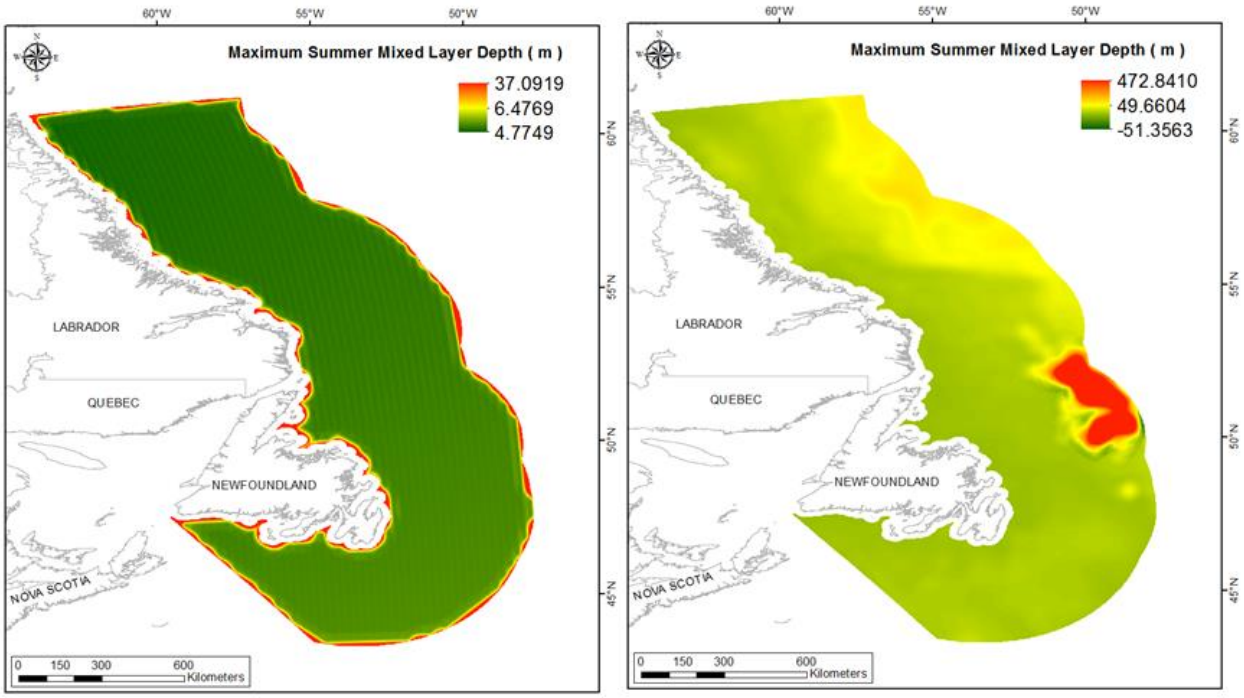

Figure 181. Left panel: Prediction standard error surface of Maximum Summer Mixed Layer Depth (m). Right panel: Interpolated prediction surface of Maximum Summer Mixed Layer Depth (m).

Maximum Fall Mixed Layer Depth

This variable displayed a right-skewed, bimodal distribution prior to modeling (Table 91, Figure 182). The data were higher than predicted by a normal distribution at low and upper mid-range values and mid-range and the highest values were lower than predicted (Figure 183). The data rarely followed the predicted line and so all areas were either over- or under-predicted with a strong spatial pattern bias (Figure 183).

The semivariogram showed weak autocorrelation present in the data and the model showed a good fit between measured and predicted values (Figure 184). The model showed poor cross-validation statistics (Table 92). The error map showed a 'bullseye' pattern with error increasing with distance from data points (Figure 185). The kriged surface is presented in Figure 185.

Table 91. Distributional properties of Maximum Fall Mixed Layer Depth (m).

Property	Value
Number of Observations	2975
Minimum	24.690
Maximum	228.510
Mean	85.294
Median	57.984
Standard Deviation	50.556
Skewness	0.829
Kurtosis	2.195

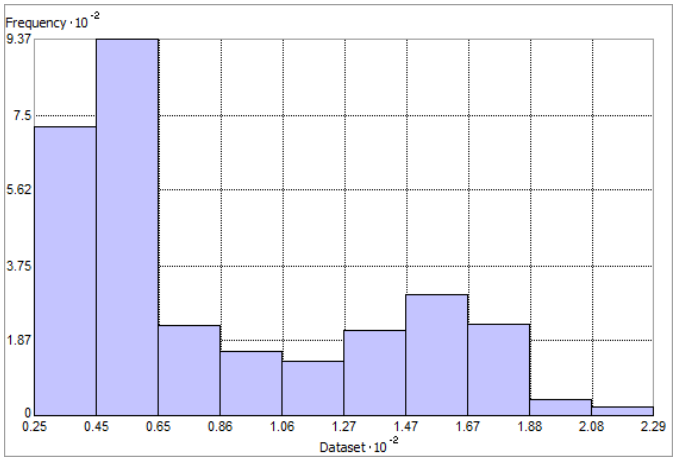

Figure 182. Distribution of Maximum Fall Mixed Layer Depth (m). Histogram was illustrated using 10 bins. X and Y axes are shown at 10^{-2}.

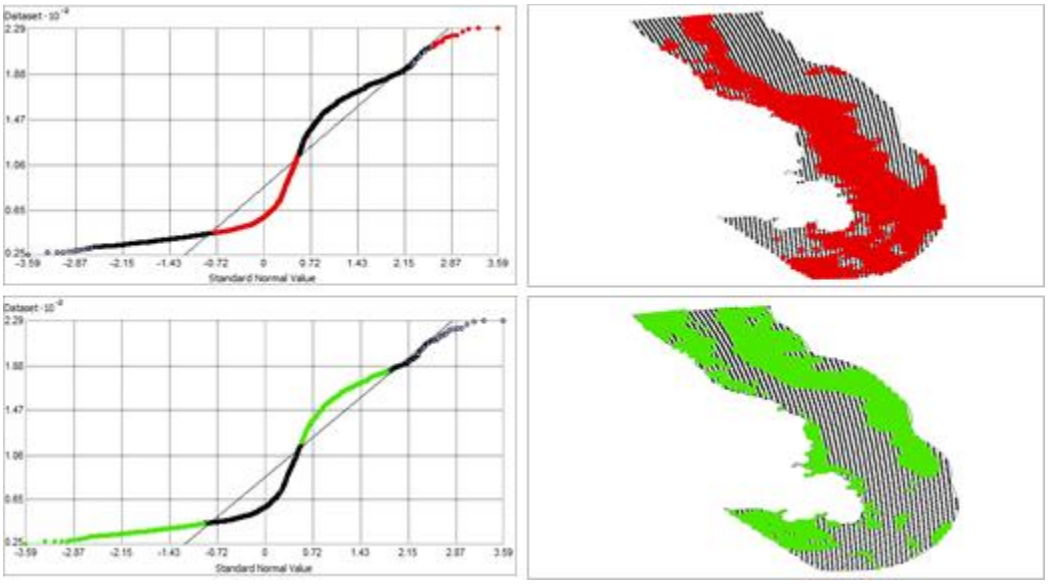

Figure 183. Normal Q-Q plot for data values of Maximum Fall Mixed Layer Depth (m). Points falling under (upper panel) and over (bottom panel) the reference line are mapped.

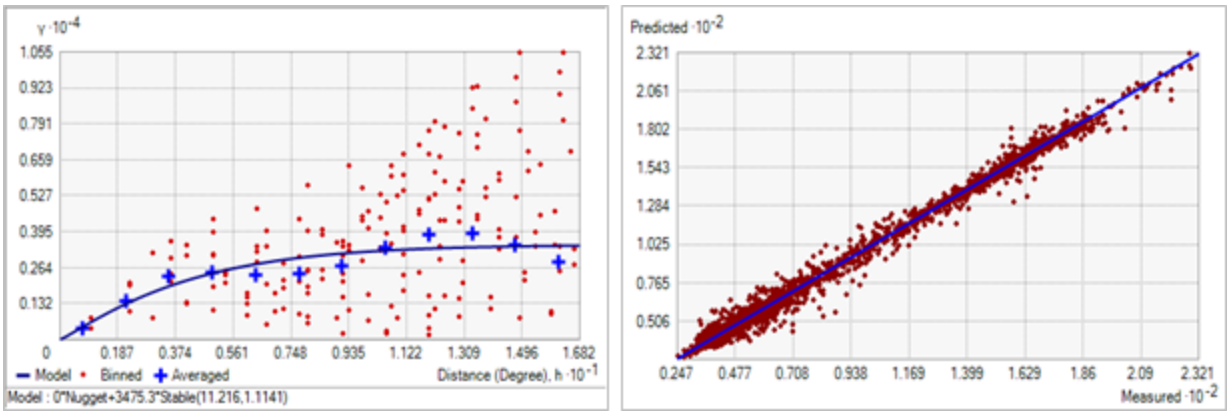

Figure 184. Left panel: Semivariogram of Maximum Fall Mixed Layer Depth (m). Binned values are shown as red dots; average points are shown as blue crosses; the model fit to the averaged values is shown as a blue line. Lag size: 1.402 degrees; number of lags: 12; Parameter: 1.114; Range: 11.216 degrees; Partial Sill: 3475.272. Right panel: Scatterplot of predicted values versus observed values for the model of Maximum Fall Mixed Layer Depth (m).

Table 92. Results of cross-validation of the kriged model for Maximum Fall Mixed Layer Depth (m).

Prediction error	**Value**
Number of Observations	2975
Overall Mean Error	-0.011
Root Mean Square Prediction Error	4.370
Standardized Mean	-7.510×10^{-4}
Standardized Root Mean Square Prediction Error	0.503
Average Standard Error	8.793

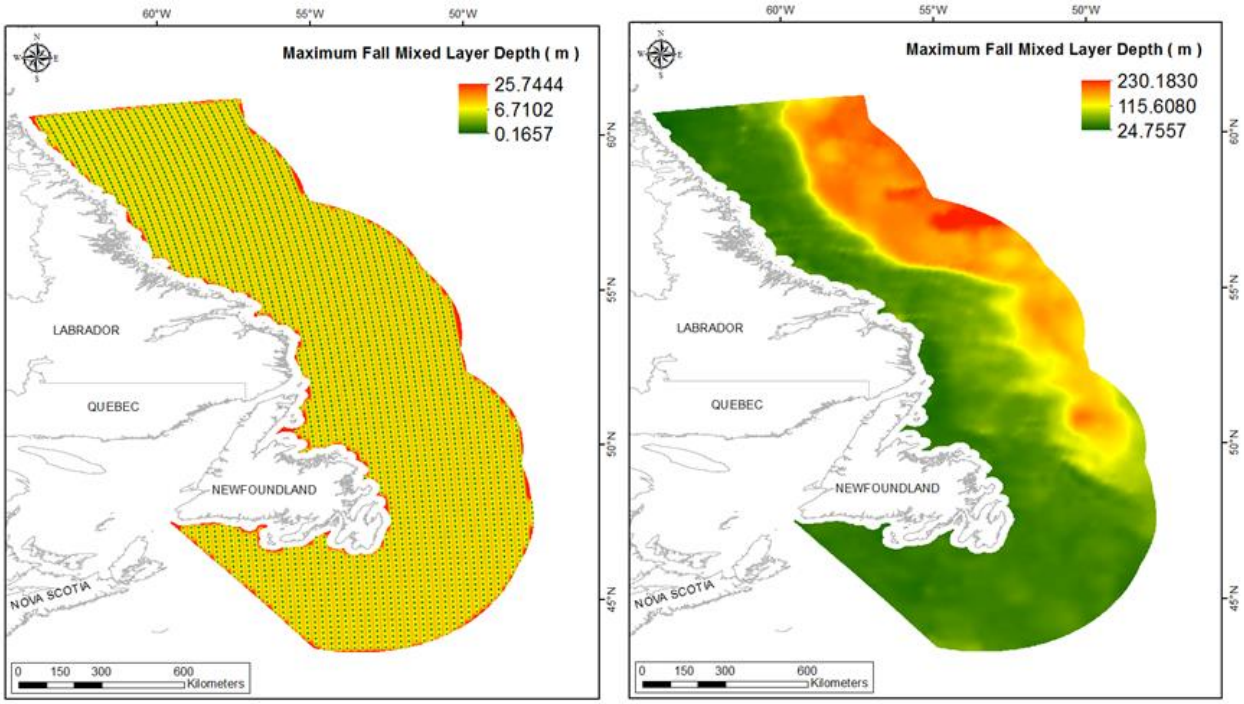

Figure 185. Left panel: Prediction standard error surface of Maximum Fall Mixed Layer Depth (m). Right panel: Interpolated prediction surface of Maximum Fall Mixed Layer Depth (m).

Maximum Winter Mixed Layer Depth

This variable displayed a severely right-skewed distribution with kurtosis (Table 93, Figure 186). The data were higher than predicted by a normal distribution at low and high values (Figure 187). Mid-range values deviated considerably from the reference line. The areas of over- and under-prediction showed a strong spatial pattern with all areas either under- or over- predicted (Figure 187).

The semivariogram showed moderate autocorrelation present in the data and the model showed a good fit between measured and predicted values (Figure 188). The model showed poor cross-validation statistics (Table 94). The error map showed a 'bullseye' pattern with error increasing with distance from data points (Figure 189). The kriged surface is presented in Figure 189.

Table 93. Distributional properties of Maximum Winter Mixed Layer Depth (m).

Property	Value
Number of Observations	2975
Minimum	33.255
Maximum	2590.500
Mean	400.270
Median	85.868
Standard Deviation	646.310
Skewness	1.888
Kurtosis	5.061

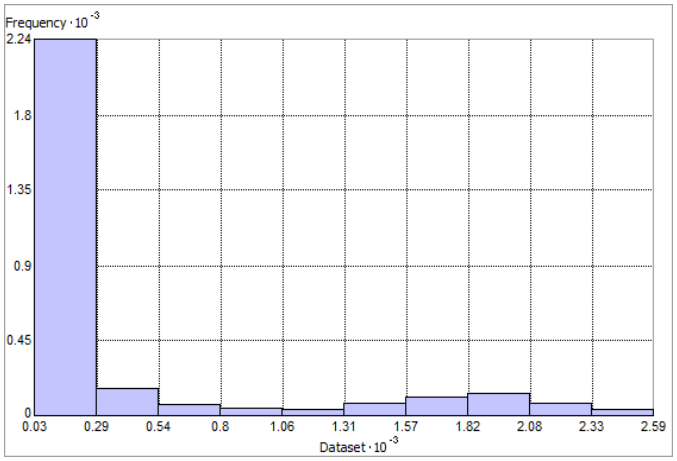

Figure 186. Distribution of Maximum Winter Mixed Layer Depth (m). Histogram was illustrated using 10 bins. X and Y axes are shown at 10^{-3}.

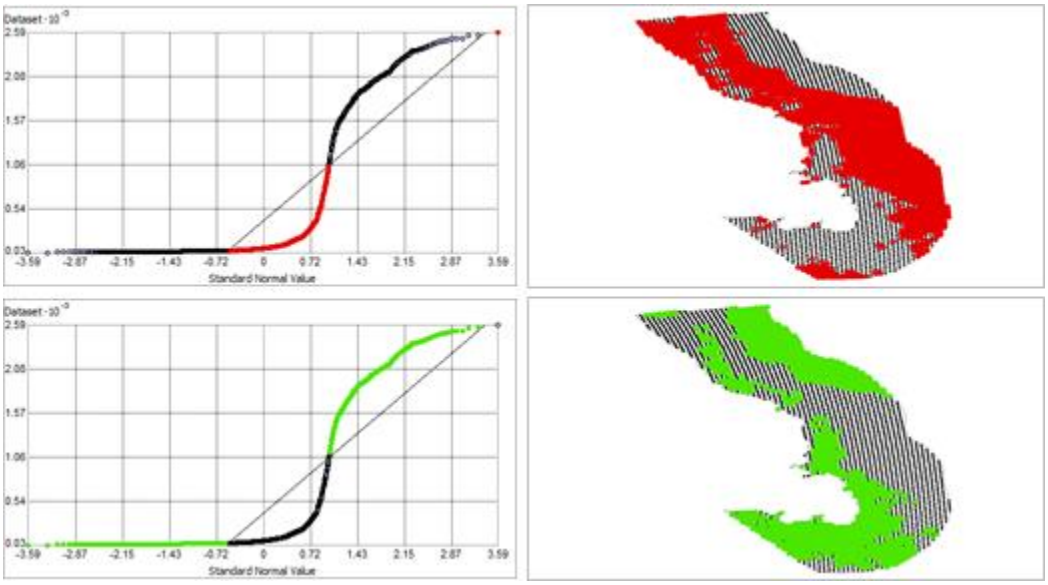

Figure 187. Normal Q-Q plot for data values of Maximum Winter Mixed Layer Depth (m). Points falling under (upper panel) and over (bottom panel) the reference line are mapped.

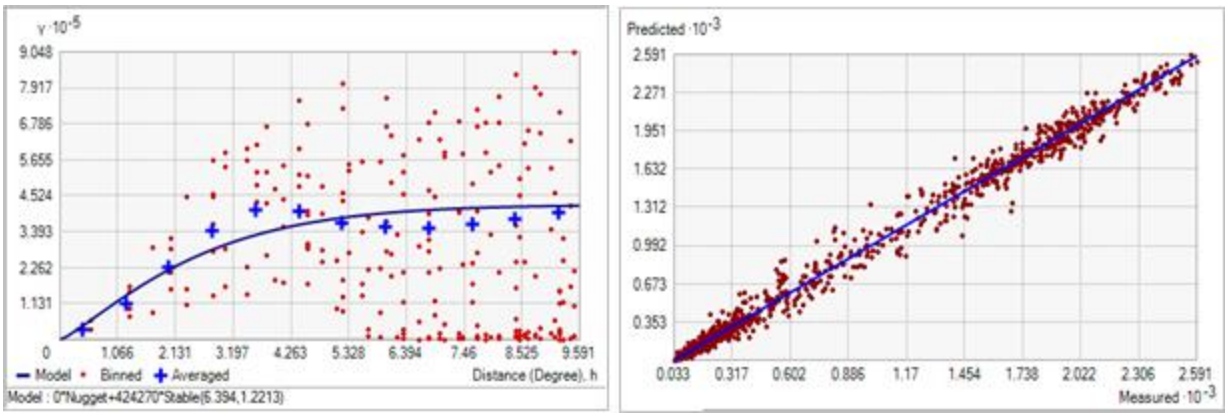

Figure 188. Left panel: Semivariogram of Maximum Winter Mixed Layer Depth (m). Binned values are shown as red dots; average points are shown as blue crosses; the model fit to the averaged values is shown as a blue line. Lag size: 0.799 degrees; number of lags: 12; Parameter: 1.221; Range: 6.394 degrees; Partial Sill: 424273.100. Right panel: Scatterplot of predicted values versus observed values for the model of Maximum Winter Mixed Layer Depth (m).

Table 94. Results of cross-validation of the kriged model for Maximum Winter Mixed Layer Depth (m).

Prediction error	**Value**
Number of Observations	2975
Overall Mean Error	0.095
Root Mean Square Prediction Error	46.797
Standardized Mean	2.692×10^{-4}
Standardized Root Mean Square Prediction Error	0.470
Average Standard Error	104.050

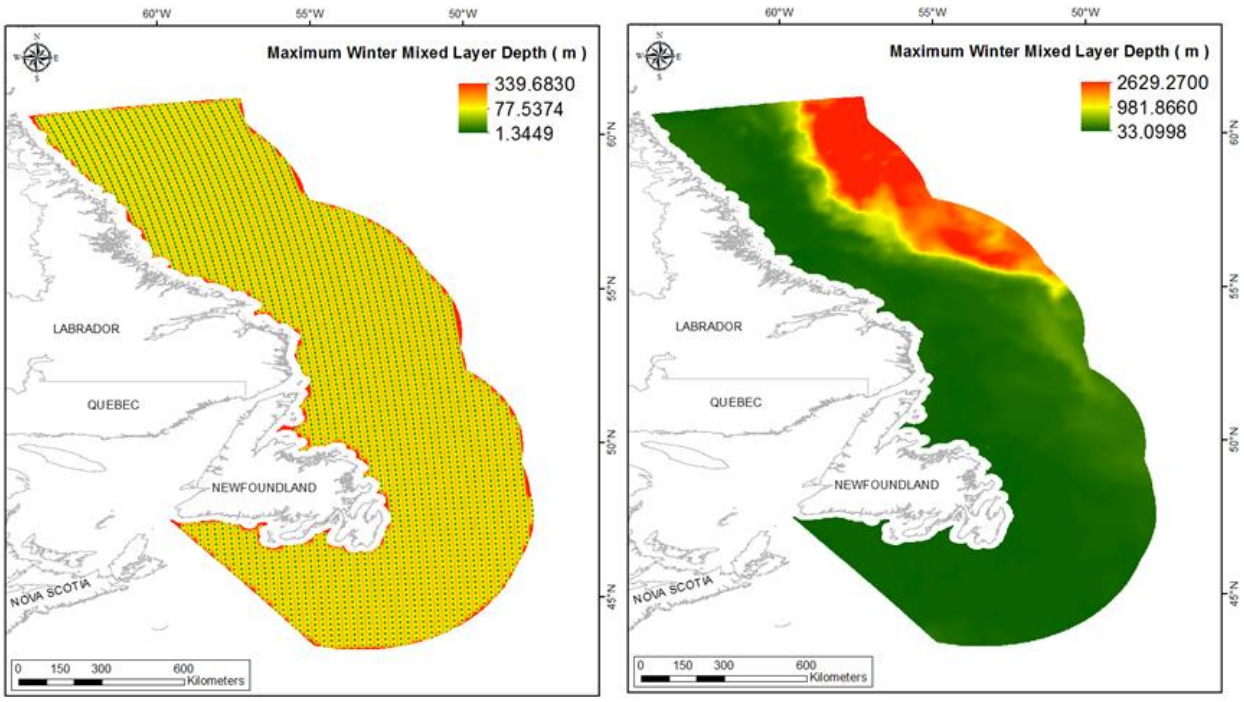

Figure 189. Left panel: Prediction standard error surface of Maximum Winter Mixed Layer Depth (m). Right panel: Interpolated prediction surface of Maximum Winter Mixed Layer Depth (m).

Maximum Average Spring Mixed Layer Depth

This variable displayed a right-skewed distribution with kurtosis prior to modeling (Table 95, Figure 190). The data were higher than predicted by a normal distribution at low and high values (Figure 191). Mid-range values deviated considerably from the reference line. The areas of over- and under-prediction showed no strong spatial pattern (Figure 191).

The semivariogram showed moderate autocorrelation present in the data and the model showed a very good fit between measured and predicted values (Figure 192). The model showed good cross-validation statistics (Table 96) indicating that it was very good at prediction. The error map showed a 'bullseye' pattern with error increasing with distance from data points (Figure 193). The kriged surface is presented in Figure 193.

Table 95. Distributional properties of Maximum Average Spring Mixed Layer Depth (m).

Property	Value
Number of Observations	2975
Minimum	15.334
Maximum	355.330
Mean	55.406
Median	27.206
Standard Deviation	58.759
Skewness	2.416
Kurtosis	8.867

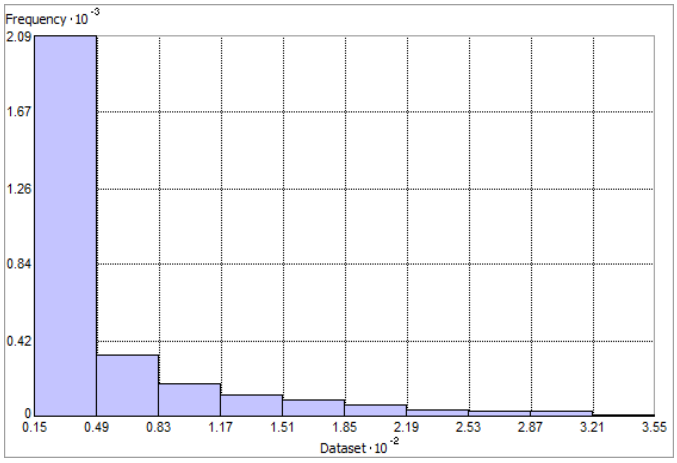

Figure 190. Distribution of Maximum Average Spring Mixed Layer Depth (m). Histogram was illustrated using 10 bins. X axis is shown at 10^{-2}; Y axis is shown at 10^{-3}.

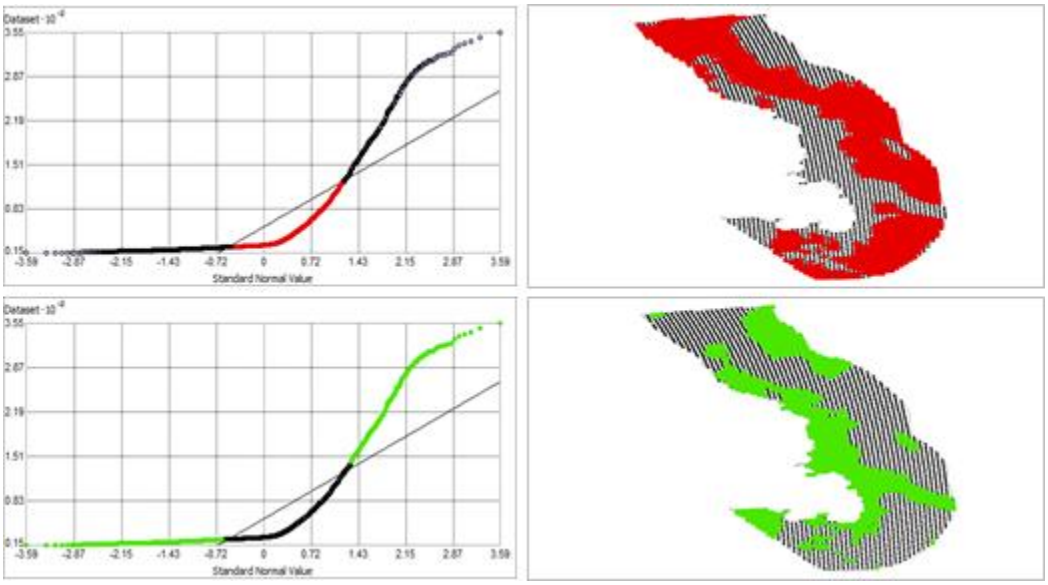

Figure 191. Normal Q-Q plot for data values of Maximum Average Spring Mixed Layer Depth (m). Points falling under (upper panel) and over (bottom panel) the reference line are mapped.

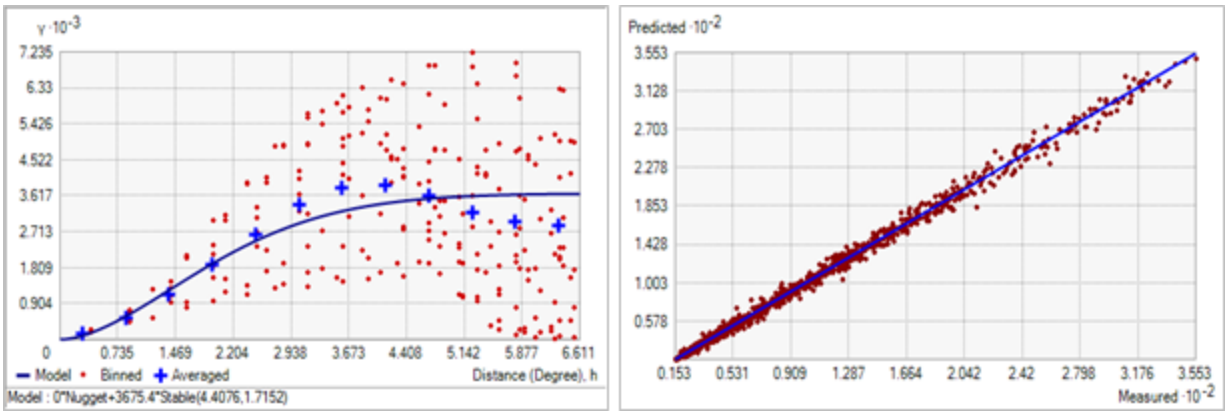

Figure 192. Left panel: Semivariogram of Maximum Average Spring Mixed Layer Depth (m). Binned values are shown as red dots; average points are shown as blue crosses; the model fit to the averaged values is shown as a blue line. Lag size: 0.551 degrees; number of lags: 12; Parameter: 1.715; Range: 4.408 degrees; Partial Sill: 3675.363. Right panel: Scatterplot of predicted values versus observed values for the model of Maximum Average Spring Mixed Layer Depth (m).

Table 96. Results of cross-validation of the kriged model for Maximum Average Spring Mixed Layer Depth (m).

Prediction error	**Value**
Number of Observations	2975
Overall Mean Error	-0.014
Root Mean Square Prediction Error	3.159
Standardized Mean	-1.966×10^{-3}
Standardized Root Mean Square Prediction Error	0.982
Average Standard Error	3.400

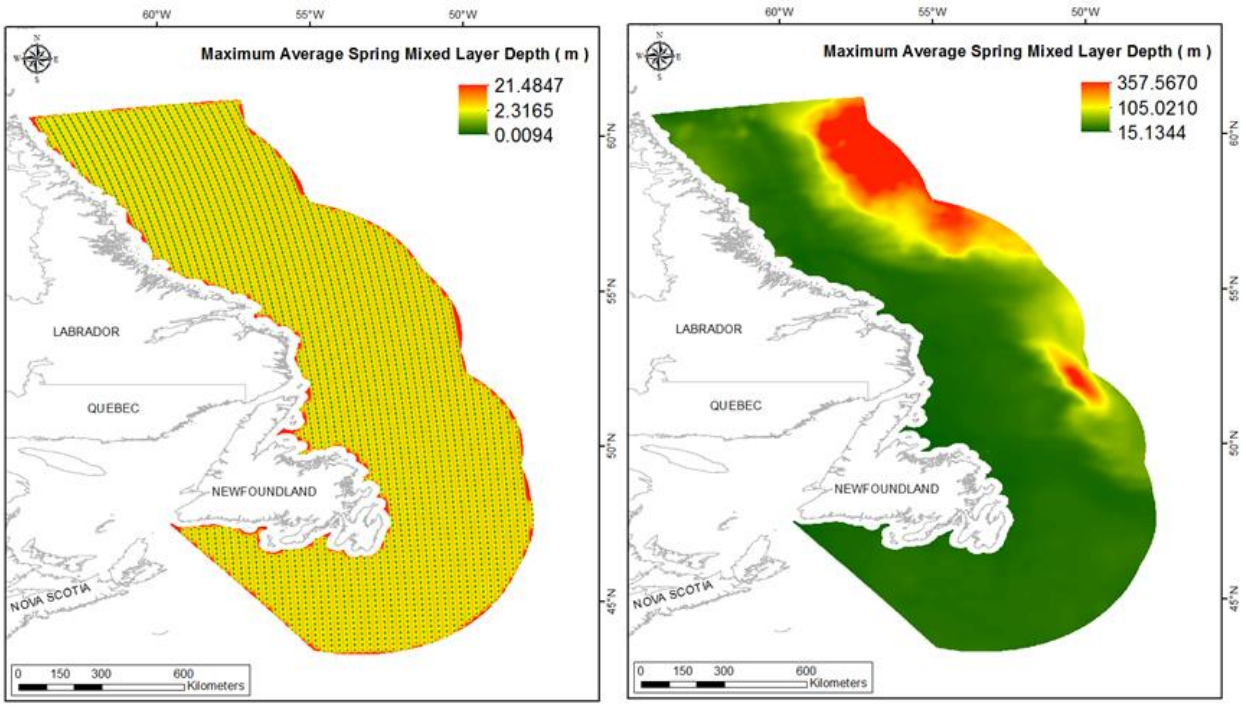

Figure 193. Left panel: Prediction standard error surface of Maximum Average Spring Mixed Layer Depth (m). Right panel: Interpolated prediction surface of Maximum Average Spring Mixed Layer Depth (m).

Maximum Average Summer Mixed Layer Depth

This variable displayed a right-skewed distribution with kurtosis prior the modeling (Table 97, Figure 194). The data were higher than predicted by a normal distribution at low and high values (Figure 195). Mid-range values deviated slightly from the reference line. The areas of over- and under-prediction showed a very strong spatial pattern (Figure 195).

The semivariogram showed moderate autocorrelation present in the data and the model showed a good fit between measured and predicted values (Figure 196). The model showed fair cross-validation statistics (Table 98) indicating that it was fair at prediction. The error map showed a 'bullseye' pattern with error increasing with distance from data points (Figure 197). The kriged surface is presented in Figure 197.

Table 97. Distributional properties of Maximum Average Summer Mixed Layer Depth (m).

Property	Value
Number of Observations	2975
Minimum	11.194
Maximum	71.450
Mean	19.071
Median	15.891
Standard Deviation	7.391
Skewness	1.683
Kurtosis	7.015

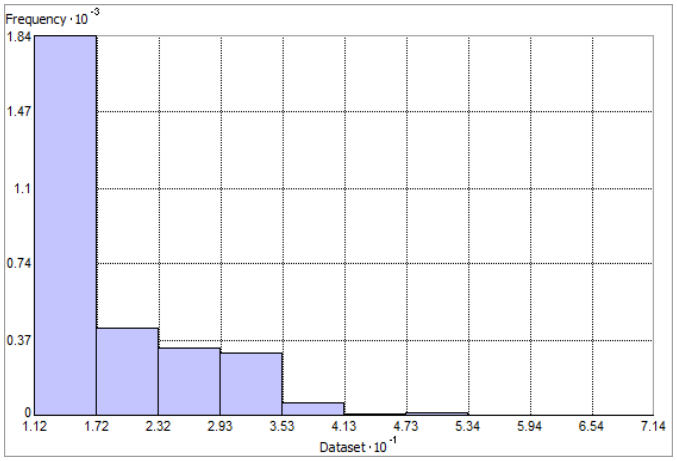

Figure 194. Distribution of Maximum Average Summer Mixed Layer Depth (m). Histogram was illustrated using 10 bins. X axis is shown at 10^{-1}; Y axis is shown at 10^{-3}.

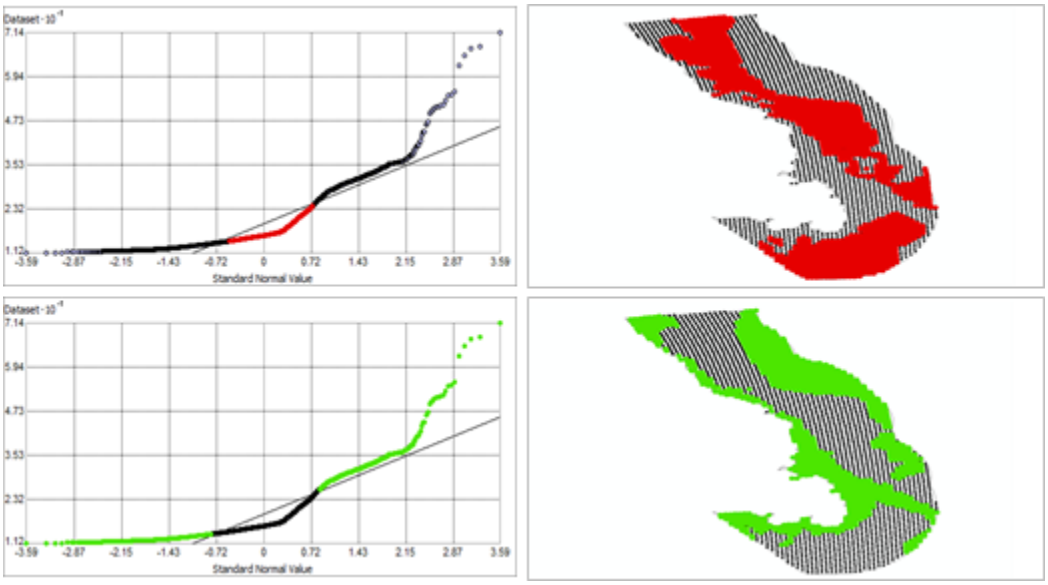

Figure 195. Normal Q-Q plot for data values of Maximum Average Summer Mixed Layer Depth (m). Points falling under (upper panel) and over (bottom panel) the reference line are mapped.

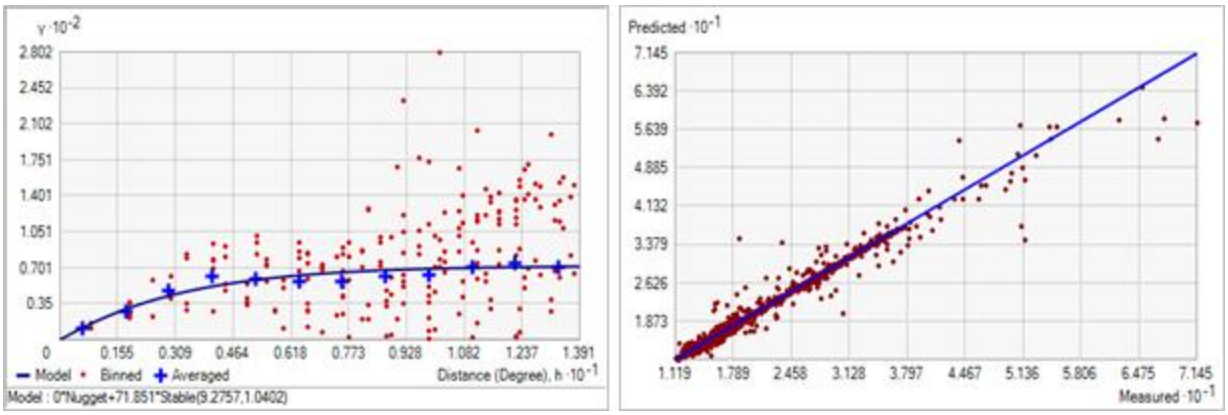

Figure 196. Left panel: Semivariogram of Maximum Average Summer Mixed Layer Depth (m). Binned values are shown as red dots; average points are shown as blue crosses; the model fit to the averaged values is shown as a blue line. Lag size: 1.159 degrees; number of lags: 12; Parameter: 1.040; Range: 9.276 degrees; Partial Sill: 71.851. Right panel: Scatterplot of predicted values versus observed values for the model of Maximum Average Summer Mixed Layer Depth (m).

Table 98. Results of cross-validation of the kriged model for Maximum Average Summer Mixed Layer Depth (m).

Prediction error	**Value**
Number of Observations	2975
Overall Mean Error	1.853×10^{-3}
Root Mean Square Prediction Error	0.985
Standardized Mean	4.544×10^{-4}
Standardized Root Mean Square Prediction Error	0.586
Average Standard Error	1.679

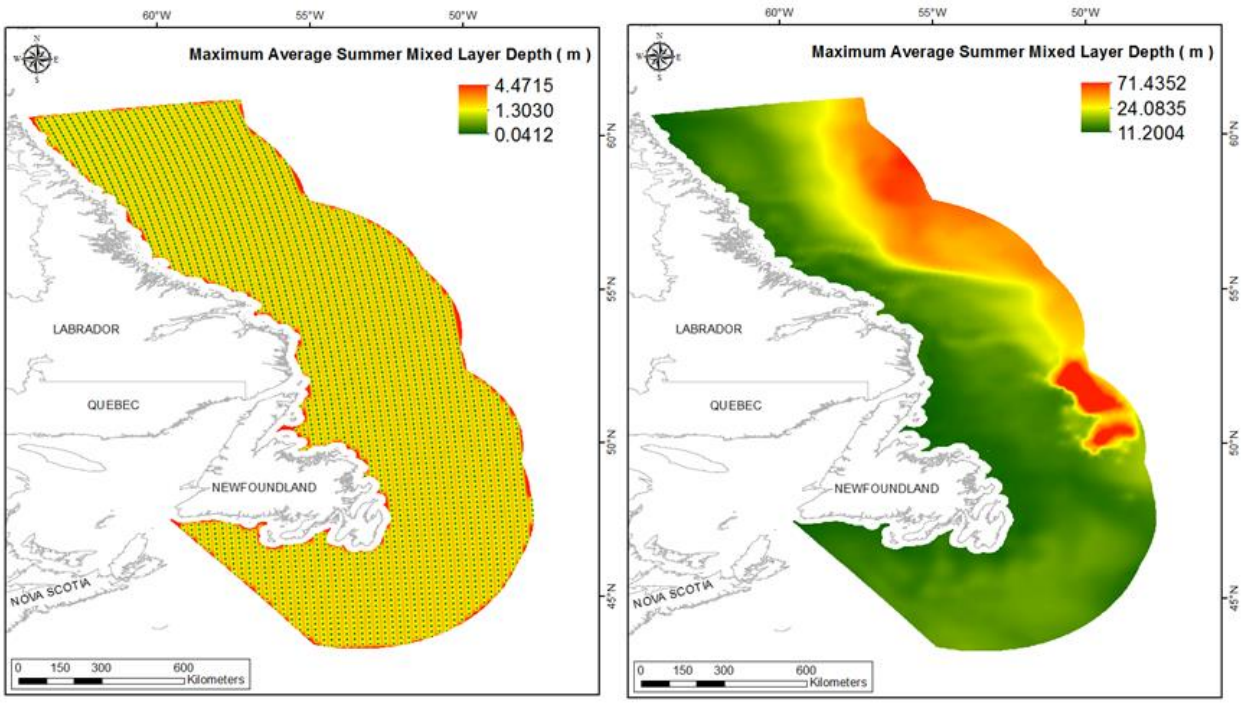

Figure 197. Left panel: Prediction standard error surface of Maximum Average Summer Mixed Layer Depth (m). Right panel: Interpolated prediction surface of Maximum Average Summer Mixed Layer Depth (m).

Maximum Average Fall Mixed Layer Depth

This variable displayed a right-skewed distribution prior to modeling (Table 99, Figure 198). The data were higher than predicted by a normal distribution at low and upper mid-range values (Figure 199). High and mid-range values were slower than predicted by a normal distribution. The areas of over- and under-prediction showed a very strong spatial pattern with all areas biased in one direction or the other (Figure 199).

The semivariogram showed moderate autocorrelation present in the data and the model showed a really good fit between measured and predicted values (Figure 200). The model showed weak cross-validation statistics (Table 100) indicating that it was not good at prediction. The error map showed a 'bullseye' pattern with error increasing with distance from data points (Figure 201). The kriged surface is presented in Figure 201.

Table 99. Distributional properties of Maximum Average Fall Mixed Layer Depth (m).

Property	Value
Number of Observations	2975
Minimum	17.273
Maximum	116.810
Mean	54.755
Median	39.797
Standard Deviation	27.104
Skewness	0.770
Kurtosis	2.045

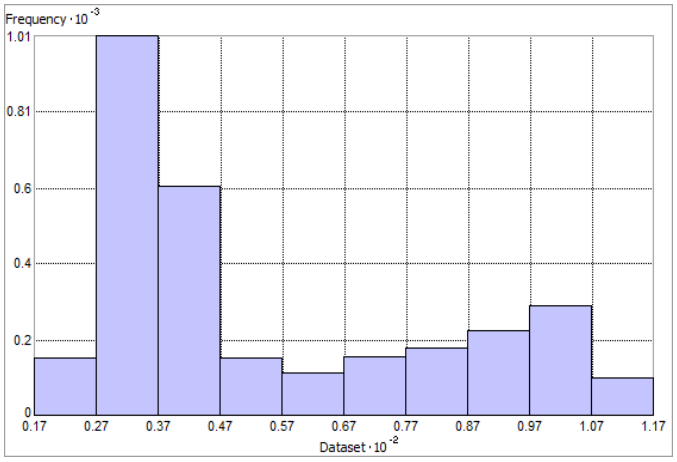

Figure 198. Distribution of Maximum Average Fall Mixed Layer Depth (m). Histogram was illustrated using 10 bins. X axis is shown at 10^{-2}; Y axis is shown at 10^{-3}.

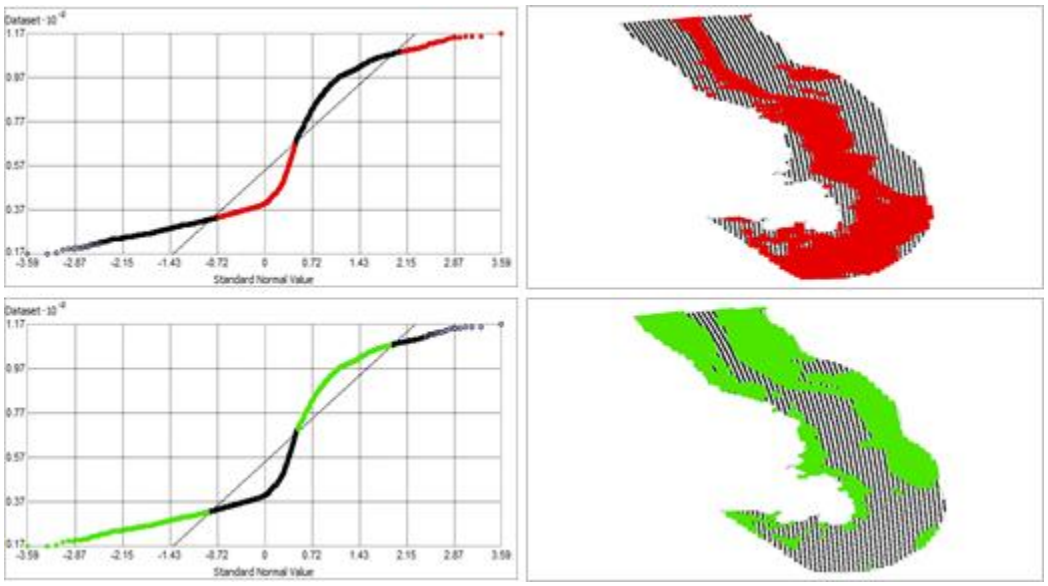

Figure 199. Normal Q-Q plot for data values of Maximum Average Fall Mixed Layer Depth (m). Points falling under (upper panel) and over (bottom panel) the reference line are mapped.

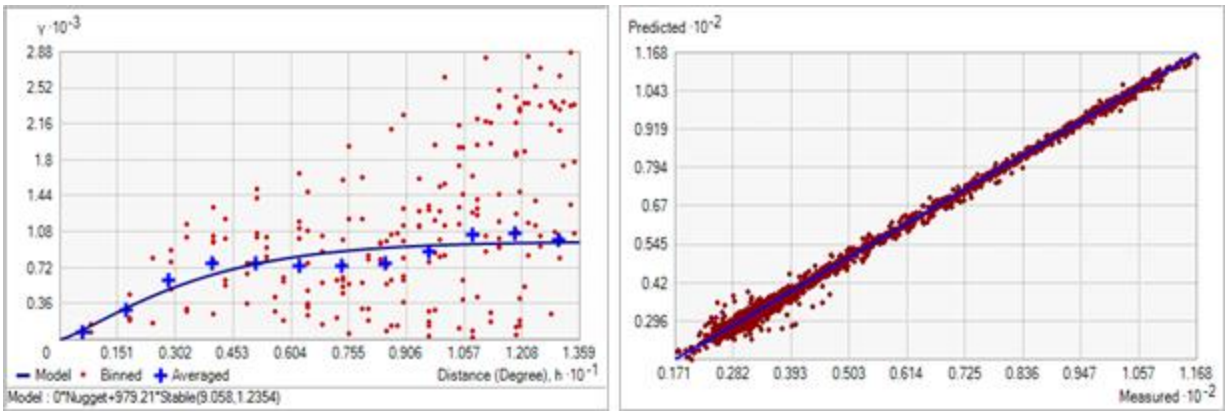

Figure 200. Left panel: Semivariogram of Maximum Average Fall Mixed Layer Depth (m). Binned values are shown as red dots; average points are shown as blue crosses; the model fit to the averaged values is shown as a blue line. Lag size: 1.132 degrees; number of lags: 12; Parameter: 1.235; Range: 9.058 degrees; Partial Sill: 979.210. Right panel: Scatterplot of predicted values versus observed values for the model of Maximum Average Fall Mixed Layer Depth (m).

Table 100. Results of cross-validation of the kriged model for Maximum Average Fall Mixed Layer Depth (m).

Prediction error	**Value**
Number of Observations	2975
Overall Mean Error	-1.199×10^{-4}
Root Mean Square Prediction Error	1.308
Standardized Mean	-9.969×10^{-5}
Standardized Root Mean Square Prediction Error	0.339
Average Standard Error	3.892

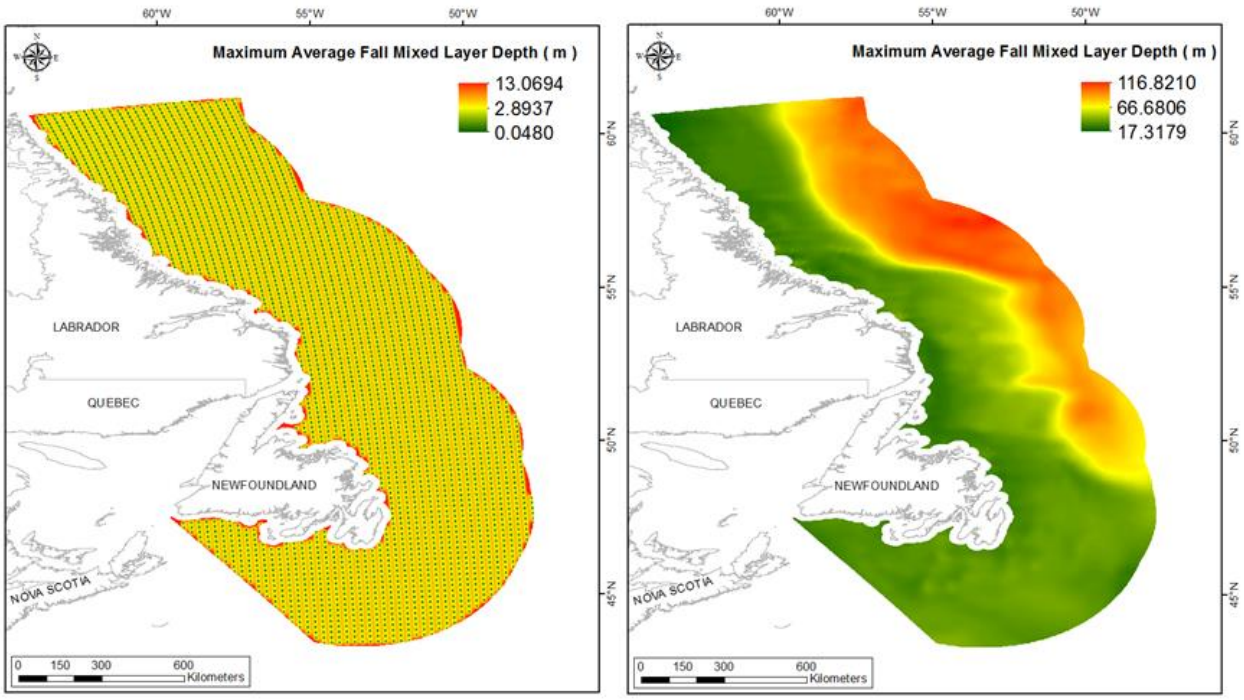

Figure 201. Left panel: Prediction standard error surface of Maximum Average Fall Mixed Layer Depth (m). Right panel: Interpolated prediction surface of Maximum Average Fall Mixed Layer Depth (m).

Maximum Average Winter Mixed Layer Depth

This variable displayed a right-skewed distribution with kurtosis prior to modeling (Table 101, Figure 202). The data were higher than predicted by a normal distribution at low and high values (Figure 203). Mid-range values deviated considerably from the reference line. The areas of over- and under-prediction showed a strong spatial pattern with bias across the full spatial extent (Figure 203).

The semivariogram showed moderate autocorrelation present in the data and the model showed a good fit between measured and predicted values (Figure 204). The model showed weak cross-validation statistics (Table 102) indicating that it was poor at prediction. The error map showed low error in a slight linear pattern over the study extent except for some areas along the coast where it was high (Figure 205). The kriged surface is presented in Figure 205.

Table 101. Distributional properties of Maximum Average Winter Mixed Layer Depth (m).

Property	Valu
Number of Observations	2975
Minimum	26.941
Maximum	931.400
Mean	132.990
Median	53.008
Standard Deviation	172.980
Skewness	2.542
Kurtosis	9.219

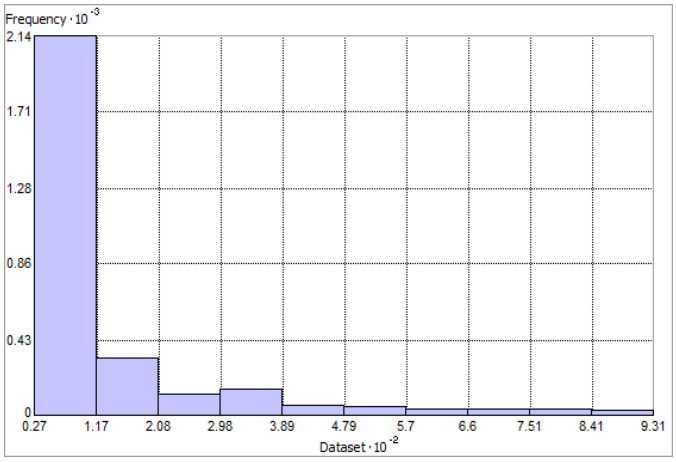

Figure 202. Distribution of Maximum Average Winter Mixed Layer Depth (m). Histogram was illustrated using 10 bins. X axis is shown at 10^{-2}; Y axis is shown at 10^{-3}.

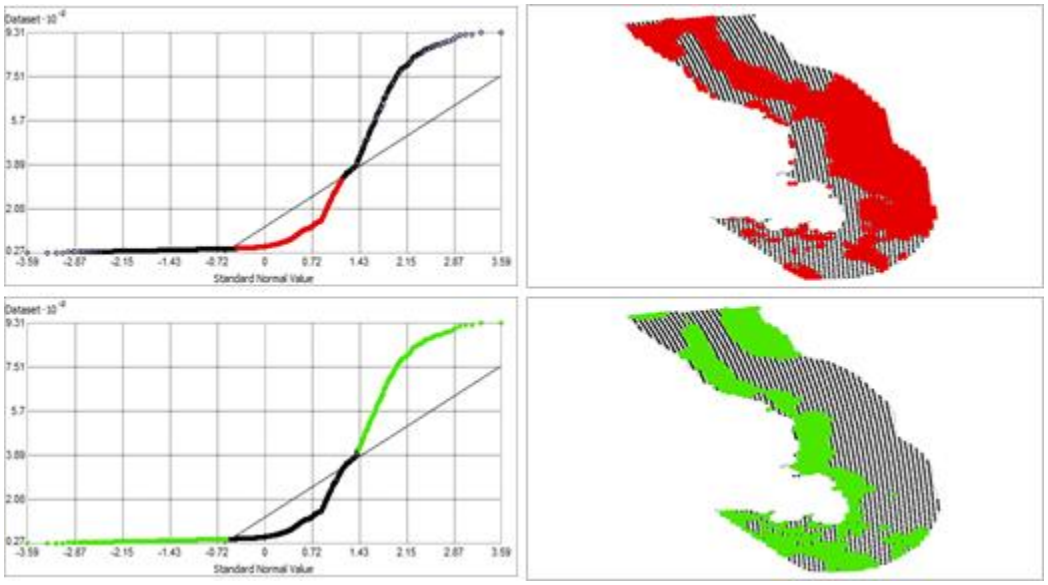

Figure 203. Normal Q-Q plot for data values of Maximum Average Winter Mixed Layer Depth (m). Points falling under (upper panel) and over (bottom panel) the reference line are mapped.

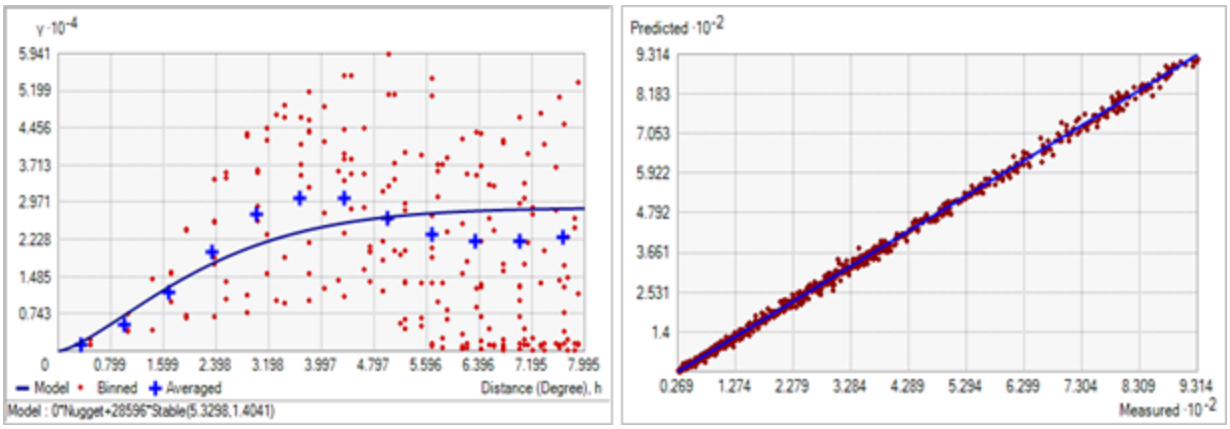

Figure 204. Left panel: Semivariogram of Maximum Average Winter Mixed Layer Depth (m). Binned values are shown as red dots; average points are shown as blue crosses; the model fit to the averaged values is shown as a blue line. Lag size: 0.666 degrees; number of lags: 12; Parameter: 1.404; Range: 5.330 degrees; Partial Sill: 28595.770. Right panel: Scatterplot of predicted values versus observed values for the model of Maximum Average Winter Mixed Layer Depth (m).

Table 102. Results of cross-validation of the kriged model for Maximum Average Winter Mixed Layer Depth (m).

Prediction error	**Value**
Number of Observations	2975
Overall Mean Error	7.599×10^{-3}
Root Mean Square Prediction Error	5.596
Standardized Mean	-1.648×10^{-5}
Standardized Root Mean Square Prediction Error	0.298
Average Standard Error	19.612

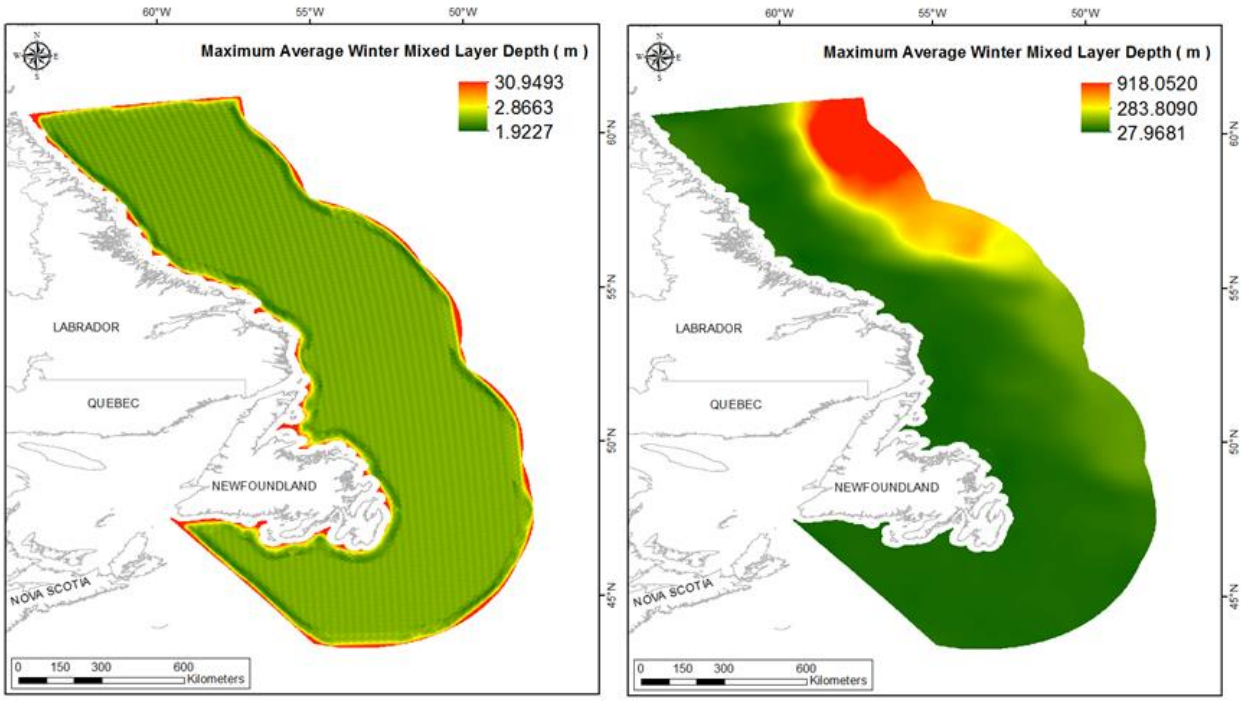

Figure 205. Left panel: Prediction standard error surface of Maximum Average Winter Mixed Layer Depth (m). Right panel: Interpolated prediction surface of Maximum Average Winter Mixed Layer Depth (m).

Bottom Shear

Bottom shear stress is a function of the maximum predicted tidal current and reflects friction pressure on the seabed. Its unit is Pa or pascal, which is equivalent to one newton (1 N) of force over one meter squared. Shear stress near the seabed causes sediment erosion and affects vertical mixing and conditions conducive to sediment deposition (Cheng et al. 1999).

Bottom Shear Mean

This variable displayed a severely right-skewed, discontinuous distribution, with outlying data in the upper range and high kurtosis (Table 103, Figure 206). The data were higher than predicted by a normal distribution at high values (Figure 207). Mid-range values were slightly lower than the reference line. The areas of over- and under-prediction showed no strong spatial pattern although the majority of the spatial extent was either over- or under-predicted (Figure 207).

The semivariogram showed autocorrelation present in the data and the model showed poor fit between measured and predicted values (Figure 208). Nevertheless, the model showed really good cross-validation statistics (Table 104) indicating that it was good at prediction. The error map showed a ‘bullseye’ pattern with error increasing with distance from data points (Figure 209). The kriged surface is presented in Figure 209.

Table 103. Distributional properties of Bottom Shear Mean (Pa).

Property	Value
Number of Observations	2948
Minimum	6.370 x 10^{-4}
Maximum	0.258
Mean	0.016
Median	0.011
Standard Deviation	0.016
Skewness	4.013
Kurtosis	37.308

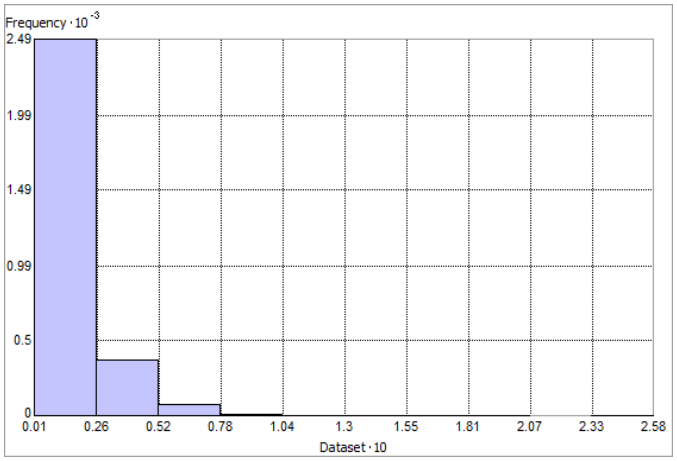

Figure 206. Distribution of Bottom Shear Mean (Pa). Histogram was illustrated using 10 bins. X axis is shown at 10; Y axis is shown at10^{-2}.

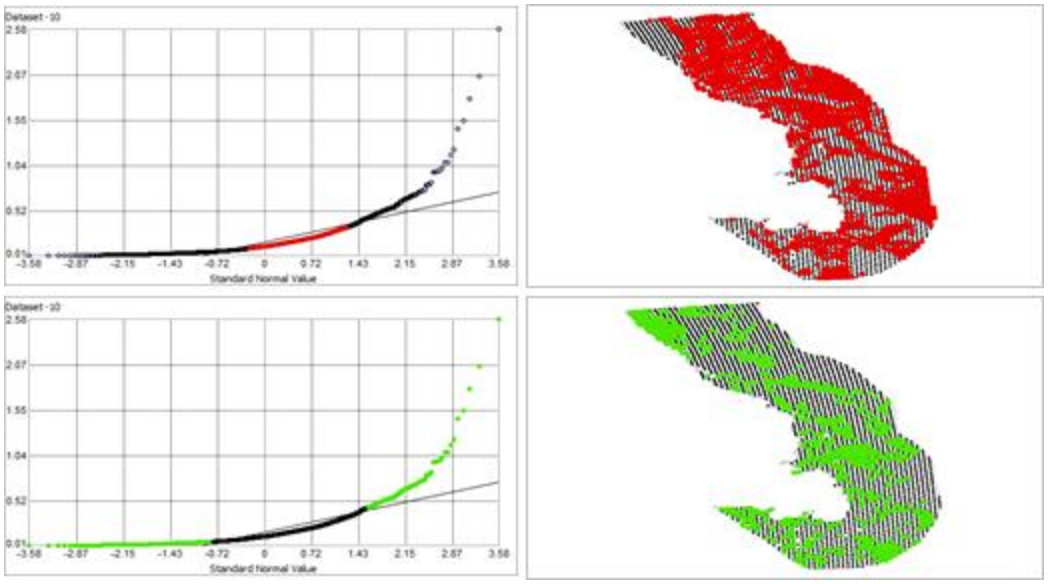

Figure 207. Normal Q-Q plot for data values of Bottom Shear Mean (Pa). Points falling under (upper panel) and over (bottom panel) the reference line are mapped.

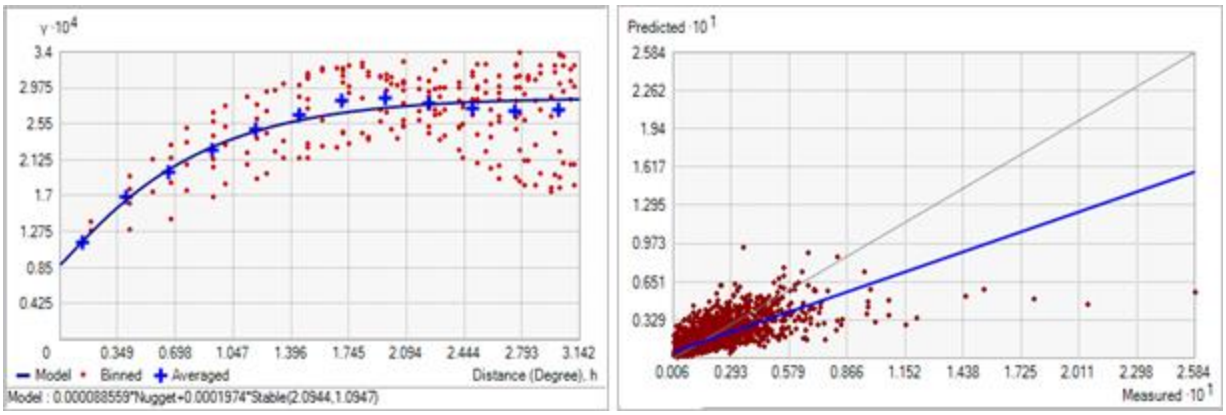

Figure 208. Left panel: Semivariogram of Bottom Shear Mean (Pa). Binned values are shown as red dots; average points are shown as blue crosses; the model fit to the averaged values is shown as a blue line. Lag size: 0.262 degrees; number of lags: 12; Parameter: 1.095; Range: 2.094 degrees; Partial Sill: 1.974 x 10^{-4}. Right panel: Scatterplot of predicted values versus observed values for the model of Bottom Shear Mean (Pa).

Table 104. Results of cross-validation of the kriged model for Bottom Shear Mean (Pa).

Prediction error	**Value**
Number of Observations	2948
Overall Mean Error	6.340 x 10^{-6}
Root Mean Square Prediction Error	0.011
Standardized Mean	3.394 x 10^{-4}
Standardized Root Mean Square Prediction Error	0.956
Average Standard Error	0.012

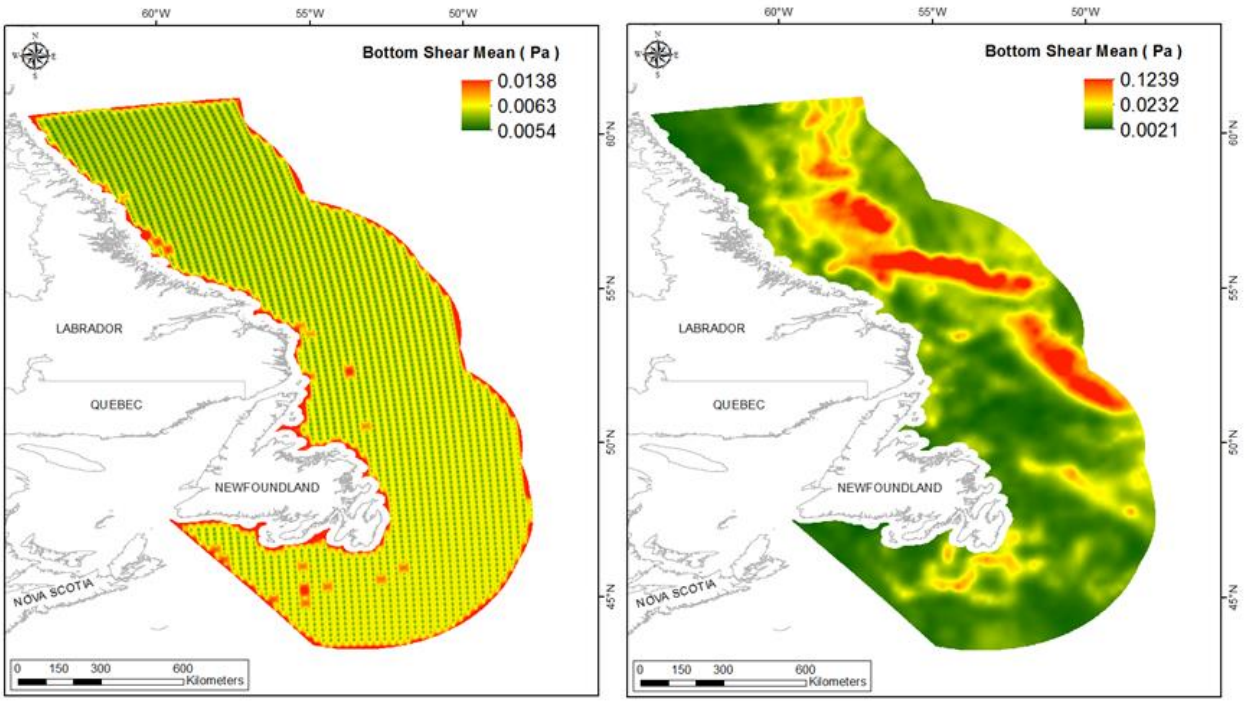

Figure 209. Left panel: Prediction standard error surface of Bottom Shear Mean (Pa). Right panel: Interpolated prediction surface of Bottom Shear Mean (Pa).

Bottom Shear Minimum

This variable displayed a highly right-skewed distribution with kurtosis and outlying data in the upper range prior to modeling (Table 105, Figure 210). The data were higher than predicted by a normal distribution at high values (Figure 211). Mid-range values were slightly lower than the reference line. The areas of over- and under-prediction showed no spatial pattern but as for the previous variable, all areas were either over- or under-predicted (Figure 211).

The semivariogram showed autocorrelation present in the data and the model showed poor fit between measured and predicted values (Figure 212). Nevertheless, the model showed good cross-validation statistics (Table 106) indicating that it was good at prediction. The error map showed low error in a slight linear pattern over the study extent except for some areas along the coast where it was high (Figure 213). The kriged surface is presented in Figure 213. Negative values resulted in the prediction surface after ordinary kriging of this variable. This possibly resulted from the highly right-skewed nature of the raw data and large outlying data points (see Figure 210). Of the 533592 raster cells in the study extent, 4366 contained negative values (see Table A6). These occurred in several patches distributed across the study extent on the shelf, along the slope, and in deep water (see Figure A6).

Table 105. Distributional properties of Bottom Shear Minimum (Pa).

Property	Value
Number of Observations	2948
Minimum	1.000×10^{-6}
Maximum	0.085
Mean	2.269×10^{-3}
Median	5.795×10^{-4}
Standard Deviation	4.96×10^{-3}
Skewness	5.267
Kurtosis	49.505

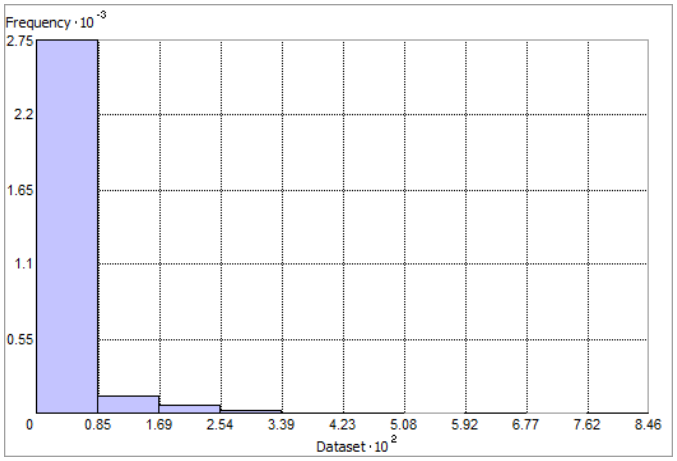

Figure 210. Distribution of Bottom Shear Minimum (Pa). Histogram was illustrated using 10 bins. X axis is shown at 10^{-2}; Y axis is shown at 10^{-3}.

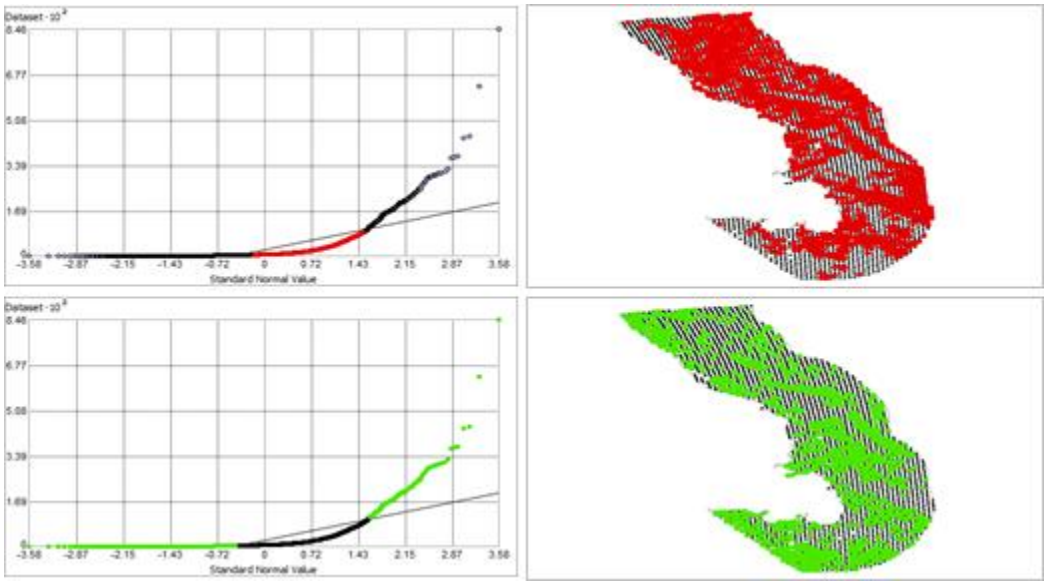

Figure 211. Normal Q-Q plot for data values of Bottom Shear Minimum (Pa). Points falling under (upper panel) and over (bottom panel) the reference line are mapped.

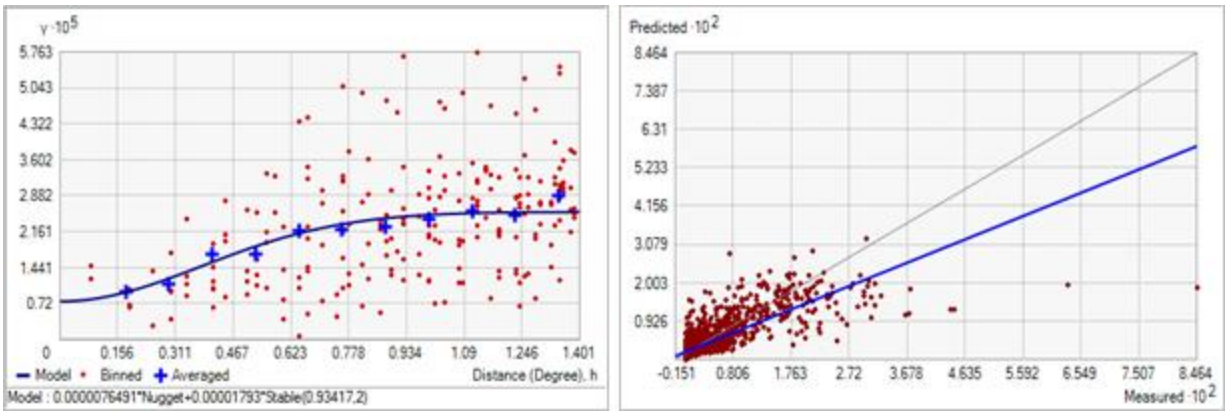

Figure 212. Left panel: Semivariogram of Bottom Shear Minimum (Pa). Binned values are shown as red dots; average points are shown as blue crosses; the model fit to the averaged values is shown as a blue line. Lag size: 0.117 degrees; number of lags: 12; Parameter: 2; Range: 0.934 degrees; Partial Sill: 1.793 x 10^{-5}. Right panel: Scatterplot of predicted values versus observed values for the model of Bottom Shear Minimum (Pa).

Table 106. Results of cross-validation of the kriged model for Bottom Shear Minimum (Pa).

Prediction error	**Value**
Number of Observations	2948
Overall Mean Error	3.374 x 10^{-6}
Root Mean Square Prediction Error	3.018 x 10^{-3}
Standardized Mean	8.442 x 10^{-4}
Standardized Root Mean Square Prediction Error	0.982
Average Standard Error	3.105 x 10^{-3}

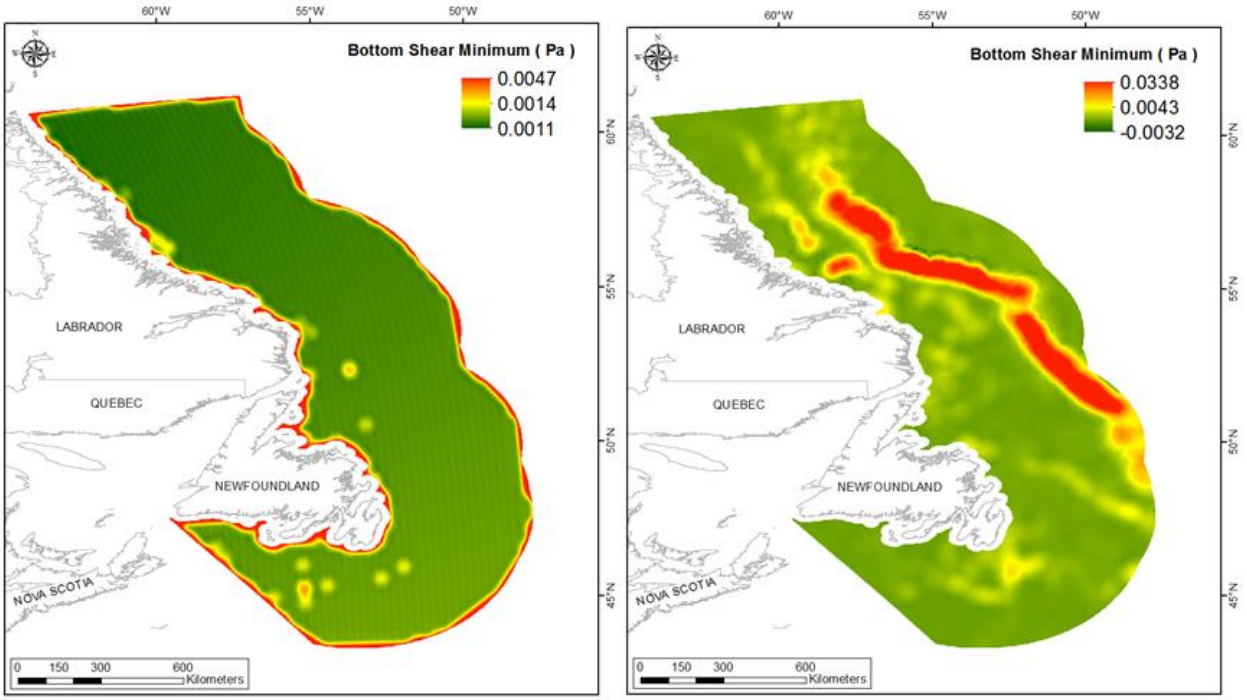

Figure 213. Left panel: Prediction standard error surface of Bottom Shear Minimum (Pa). Right panel: Interpolated prediction surface of Bottom Shear Minimum (Pa).

Bottom Shear Maximum

This variable displayed a severely right-skewed distribution with kurtosis (Table 107, Figure 214). The data were higher than predicted by a normal distribution at high values (Figure 215). Mid-range values were slightly lower than the reference line. The areas of over- and under-prediction showed no strong spatial pattern but all parts of the spatial extent were biased in one direction or the other (Figure 215).

The semivariogram showed weak autocorrelation present in the data and the model showed a poor fit between measured and observed values (Figure 216). However, the model showed strong cross-validation statistics (Table 108) indicating that it was good at prediction. The error map showed no spatial pattern over the study extent except for some areas along the coast where it was high (Figure 217). The kriged surface is presented in Figure 217.

Table 107. Distributional properties of Bottom Shear Maximum (Pa).

Property	Value
Number of Observations	2948
Minimum	3.051 x10^{-3}
Maximum	0.490
Mean	0.047
Median	0.033
Standard Deviation	0.043
Skewness	2.549
Kurtosis	14.612

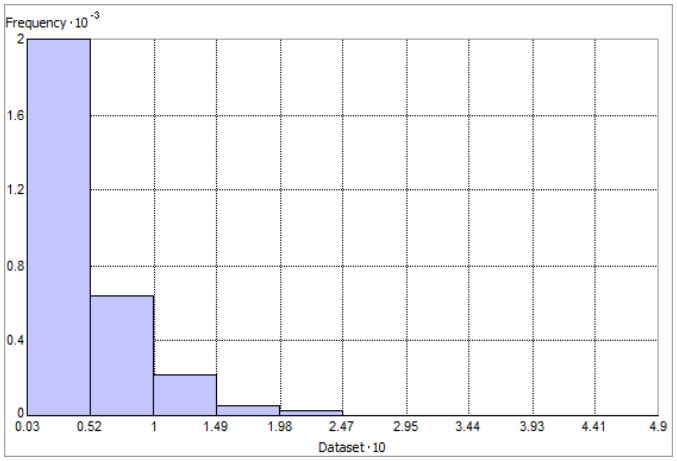

Figure 214. Distribution of Bottom Shear Maximum (Pa). Histogram was illustrated using 10 bins. X axis is shown at 10; Y axis is shown at 10^{-3}.

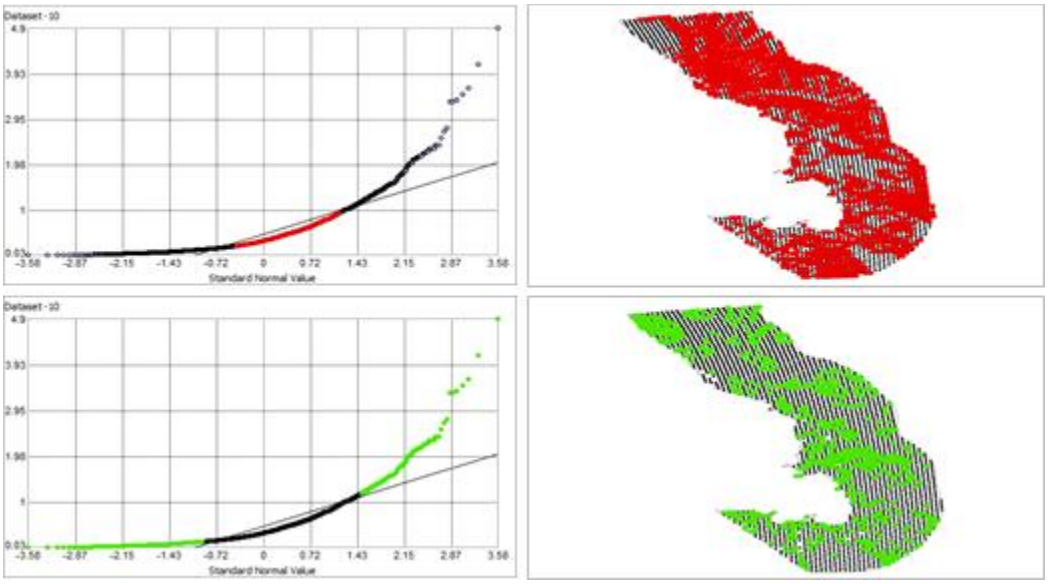

Figure 215. Normal Q-Q plot for data values of Bottom Shear Maximum (Pa). Points falling under (upper panel) and over (bottom panel) the reference line are mapped.

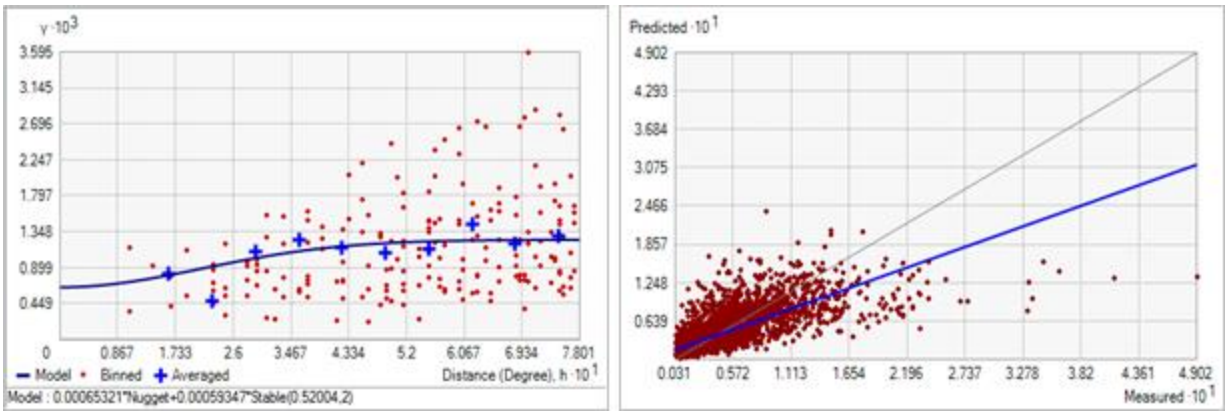

Figure 216. Left panel: Semivariogram of Bottom Shear Maximum (Pa). Binned values are shown as red dots; average points are shown as blue crosses; the model fit to the averaged values is shown as a blue line. Lag size: 0.065 degrees; number of lags: 12; Parameter: 2; Range: 0.520 degrees; Partial Sill: 5.935 x 10^{-4}. Right panel: Scatterplot of predicted values versus observed values for the model of Bottom Shear Maximum (Pa).

Table 108. Results of cross-validation of the kriged model for Bottom Shear Maximum (Pa).

Prediction error	**Value**
Number of Observations	2948
Overall Mean Error	3.122 x 10^{-5}
Root Mean Square Prediction Error	0.030
Standardized Mean	8.247 x 10^{-4}
Standardized Root Mean Square Prediction Error	0.992
Average Standard Error	0.030

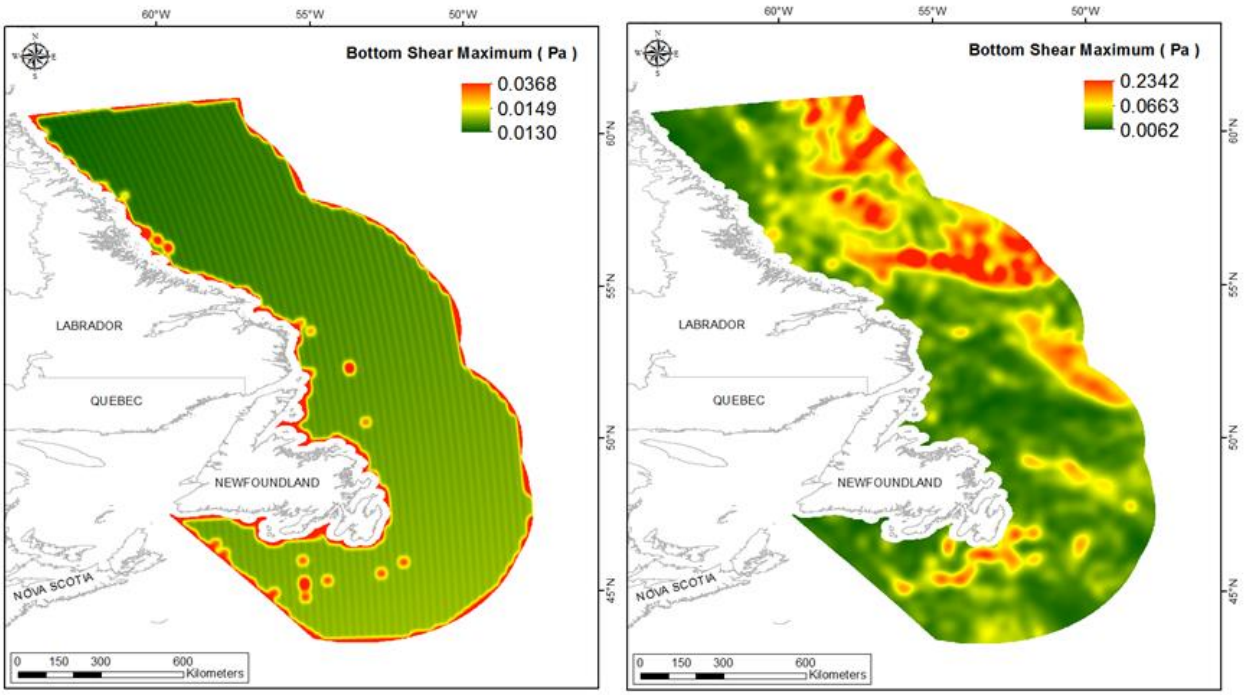

Figure 217. Left panel: Prediction standard error surface of Bottom Shear Maximum (Pa). Right panel: Interpolated prediction surface of Bottom Shear Maximum (Pa).

Bottom Shear Range

This variable displayed a severely right-skewed distribution with kurtosis (Table 109, Figure 218). The data were higher than predicted by a normal distribution at high values (Figure 219). Mid-range values were slightly lower than the reference line. The areas of over- and under-prediction showed no strong spatial pattern but all parts of the spatial extent were either under- or over-predicted (Figure 219).

The semivariogram showed moderate autocorrelation present in the data and the model showed a poor fit between measured and observed values (Figure 220). Nevertheless, the model showed really good cross-validation statistics (Table 110) indicating that it was good at prediction. The error map showed no spatial pattern over the study extent except for some areas along the coast where it was high (Figure 221). The kriged surface is presented in Figure 221.

Table 109. Distributional properties of Bottom Shear Range (Pa).

Property	Value
Number of Observations	2948
Minimum	3.042 x 10^{-3}
Maximum	0.406
Mean	0.045
Median	0.032
Standard Deviation	0.040
Skewness	2.418
Kurtosis	12.426

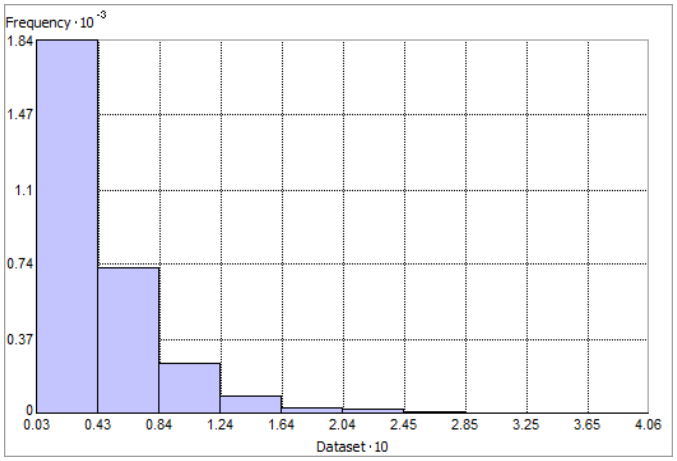

Figure 218. Distribution of Bottom Shear Range (Pa). Histogram was illustrated using 10 bins. X axis is shown at 10; Y axis is shown at 10^{-3}.

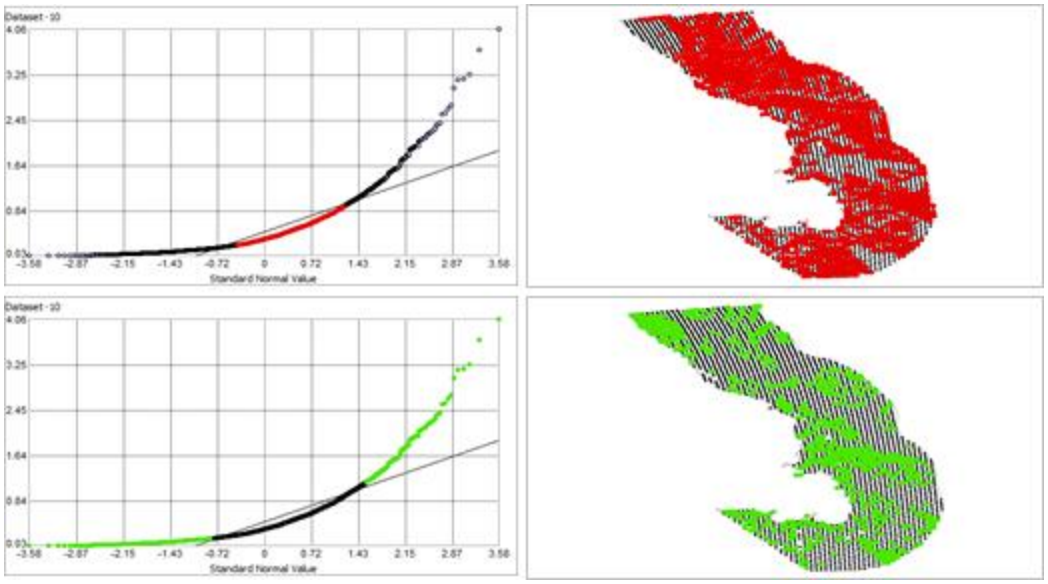

Figure 219. Normal Q-Q plot for data values of Bottom Shear Range (Pa). Points falling under (upper panel) and over (bottom panel) the reference line are mapped.

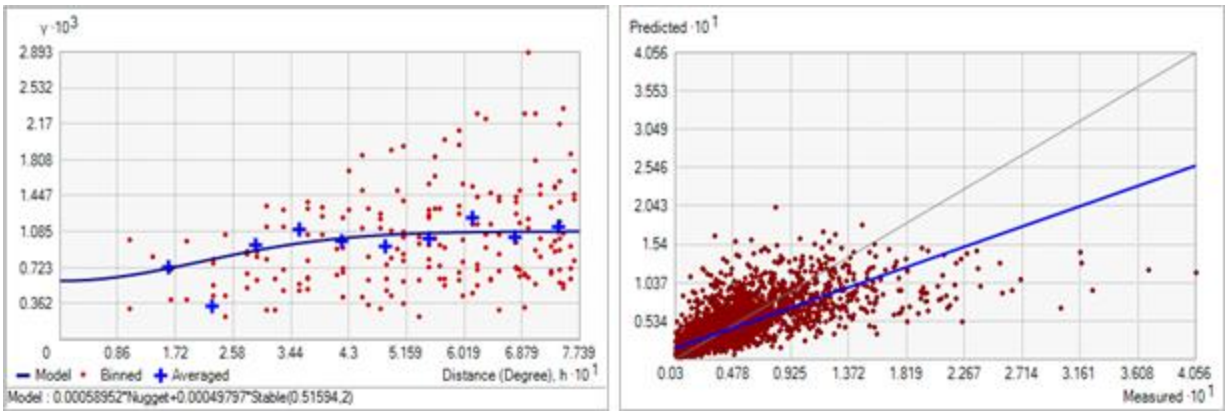

Figure 220. Left panel: Semivariogram of Bottom Shear Range (Pa). Binned values are shown as red dots; average points are shown as blue crosses; the model fit to the averaged values is shown as a blue line. Lag size: 0.064 degrees; number of lags: 12; Parameter: 2; Range: 0.516 degrees; Partial Sill: 4.980 x 10^{-4}. Right panel: Scatterplot of predicted values versus observed values for the model of Bottom Shear Range (Pa).

Table 110. Results of cross-validation of the kriged model for Bottom Shear Range (Pa).

Prediction error	**Value**
Number of Observations	2948
Overall Mean Error	2.306 x 10^{-5}
Root Mean Square Prediction Error	0.028
Standardized Mean	6.293 x 10^{-4}
Standardized Root Mean Square Prediction Error	0.990
Average Standard Error	0.029

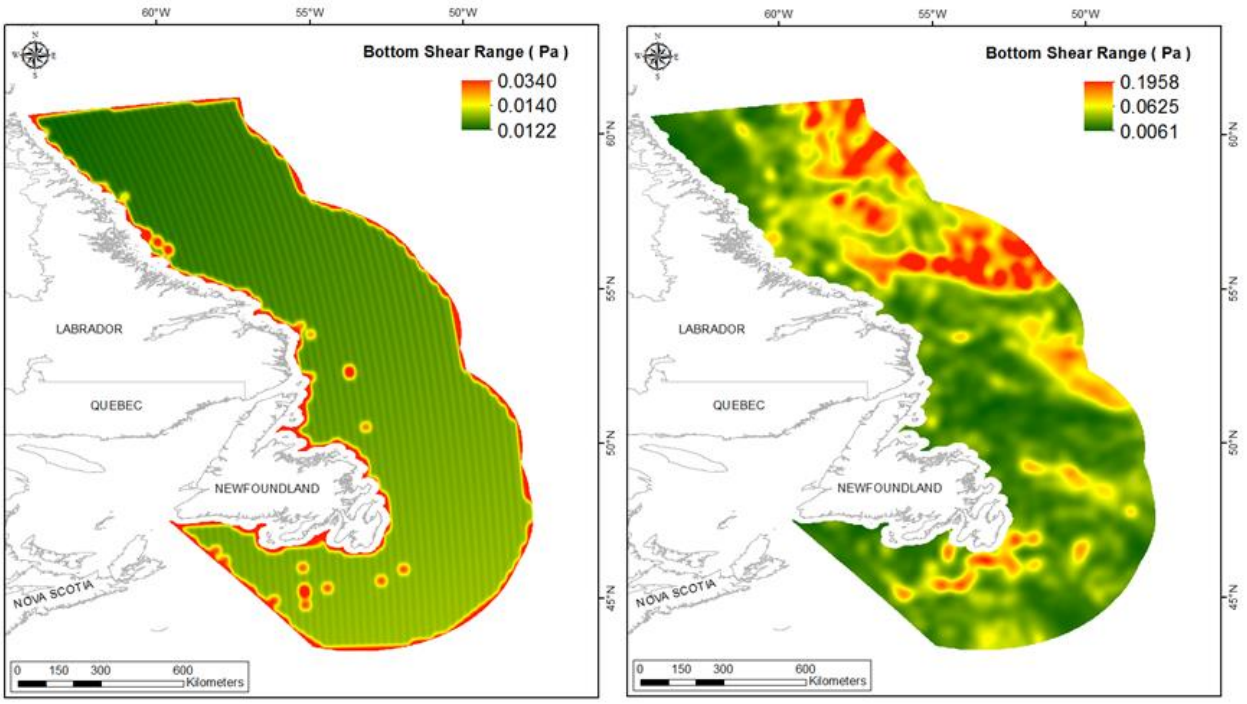

Figure 221. Left panel: Prediction standard error surface of Bottom Shear Range (Pa). Right panel: Interpolated prediction surface of Bottom Shear Range (Pa).

Bottom Shear Average Minimum

This variable displayed a severely right-skewed distribution with outlying data in the upper range and kurtosis (Table 111, Figure 222). The data were higher than predicted by a normal distribution at high values (Figure 223). Mid-range values were slightly lower than the reference line. The areas of over- and under-prediction showed no strong spatial pattern but the spatial extent was either over- or under-predicted in the majority of areas (Figure 223).

The semivariogram showed moderate autocorrelation present in the data and the model showed a poor fit between measured and observed values (Figure 224). Nevertheless, the model showed good cross-validation statistics (Table 112) indicating that it was good at prediction. The error map showed no spatial pattern over the study extent except for some areas along the coast where it was high (Figure 225). The kriged surface is presented in Figure 225. Negative values resulted in the prediction surface after ordinary kriging of this variable. This possibly resulted from the highly right-skewed nature of the raw data and large outlying data points (see Figure 222). Of the 533592 raster cells in the study extent, only 153 contained negative values (see Table A7). These occurred in a few small patches along the coastal edge of the study extent, northeast of Newfoundland, on the Newfoundland Shelf, and just beyond the slope south and east of Newfoundland and Labrador (see Figure A7).

Table 111. Distributional properties of Bottom Shear Average Minimum (Pa).

Property	Value
Number of Observations	2948
Minimum	6.600×10^{-5}
Maximum	0.150
Mean	6.541×10^{-3}
Median	3.170×10^{-3}
Standard Deviation	9.338×10^{-3}
Skewness	4.271
Kurtosis	37.680

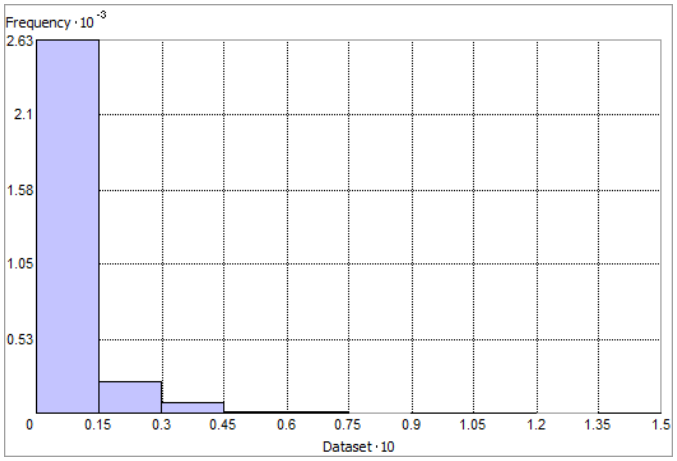

Figure 222. Distribution of Bottom Shear Average Minimum (Pa). Histogram was illustrated using 10 bins. X axis is shown at 10; Y axis is shown at 10^{-3}.

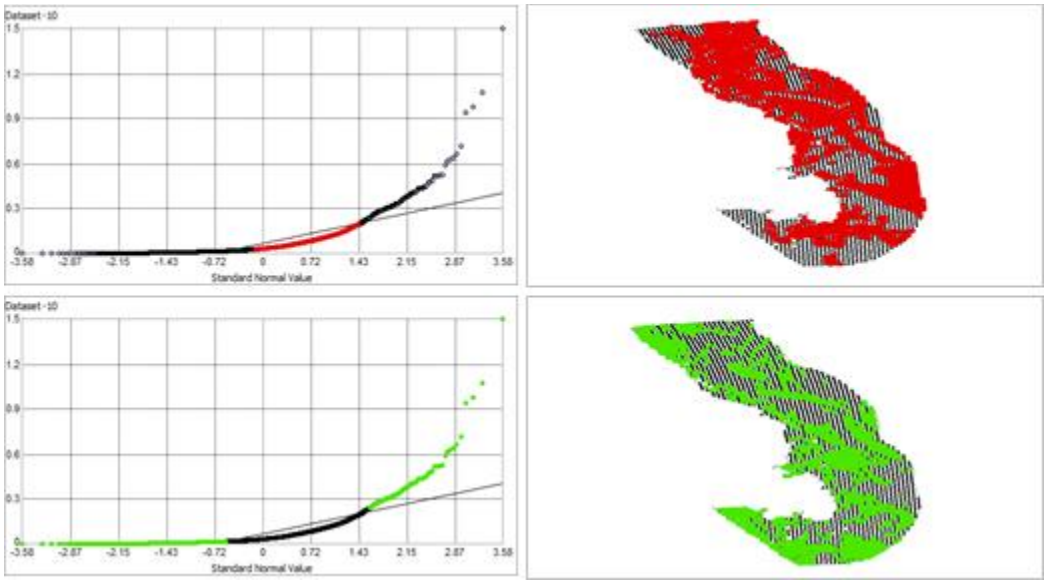

Figure 223. Normal Q-Q plot for data values of Bottom Shear Average Minimum (Pa). Points falling under (upper panel) and over (bottom panel) the reference line are mapped.

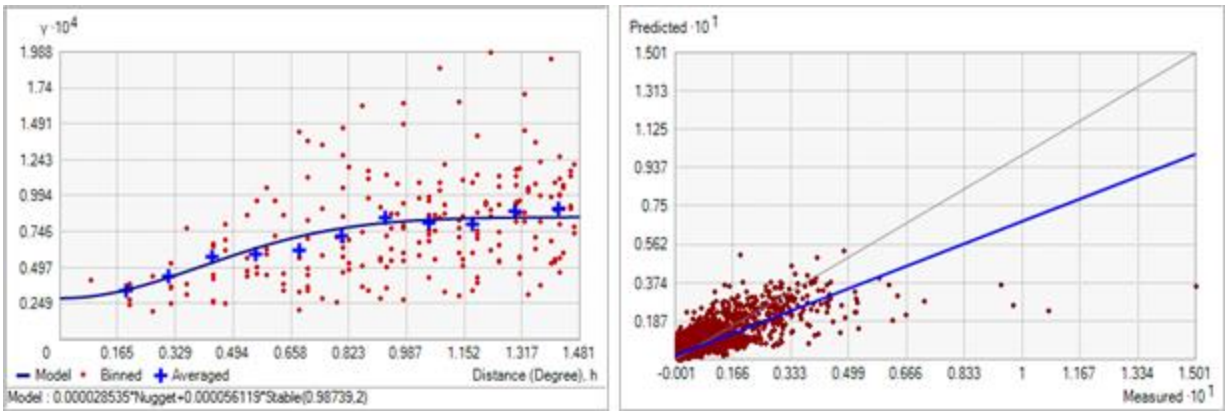

Figure 224. Left panel: Semivariogram of Bottom Shear Average Minimum (Pa). Binned values are shown as red dots; average points are shown as blue crosses; the model fit to the averaged values is shown as a blue line. Lag size: 0.123 degrees; number of lags: 12; Parameter: 2; Range: 0.987 degrees; Partial Sill: 5.612 x 10^{-5}. Right panel: Scatterplot of predicted values versus observed values for the model of Bottom Shear Average Minimum (Pa).

Table 112. Results of cross-validation of the kriged model for Bottom Shear Average Minimum (Pa).

Prediction error	**Value**
Number of Observations	2948
Overall Mean Error	4.485 x 10^{-6}
Root Mean Square Prediction Error	5.802 x 10^{-3}
Standardized Mean	5.551 x 10^{-4}
Standardized Root Mean Square Prediction Error	0.988
Average Standard Error	5.917 x 10^{-3}

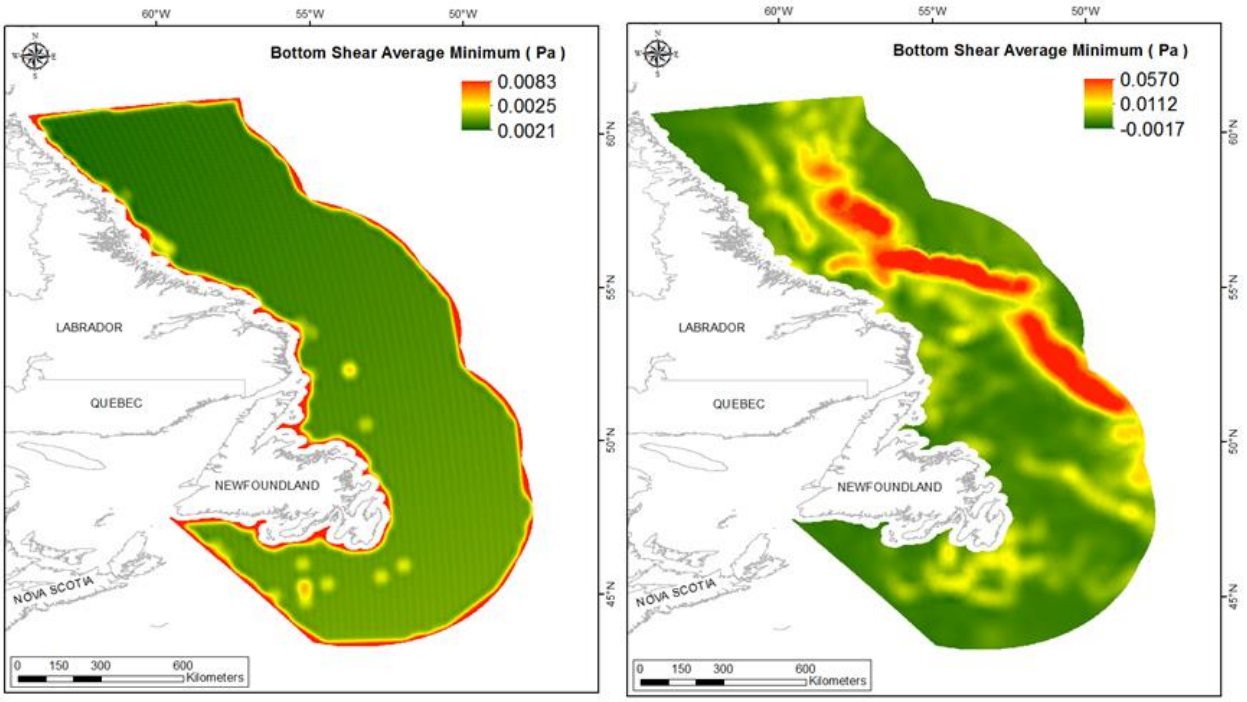

Figure 225. Left panel: Prediction standard error surface of Bottom Shear Average Minimum (Pa). Right panel: Interpolated prediction surface of Bottom Shear Average Minimum (Pa).

Bottom Shear Average Maximum

This variable displayed a severely right-skewed distribution with kurtosis (Table 113, Figure 226). The data were higher than predicted by a normal distribution at high values (Figure 227). Mid-range values were slightly lower than the reference line. The areas of over- and under-prediction showed no strong spatial pattern (Figure 227).

The semivariogram showed weak autocorrelation present in the data and the model showed a poor fit between measured and observed values (Figure 228). Nevertheless, the model showed good cross-validation statistics (Table 114) indicating that it was good at prediction. The error map showed a 'bullseye' pattern with error increasing with distance from data points (Figure 229). The kriged surface is presented in Figure 229.

Table 113. Distributional properties of Bottom Shear Average Maximum (Pa).

Property	Value
Number of Observations	2948
Minimum	1.741 x 10^{-3}
Maximum	0.379
Mean	0.029
Median	0.021
Standard Deviation	0.026
Skewness	3.417
Kurtosis	28.076

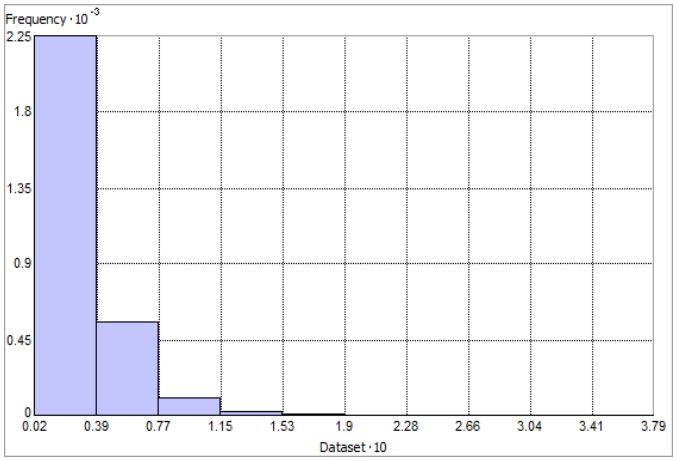

Figure 226. Distribution of Bottom Shear Average Maximum (Pa). Histogram was illustrated using 10 bins. X axis is shown at 10; Y axis is shown at 10^{-3}.

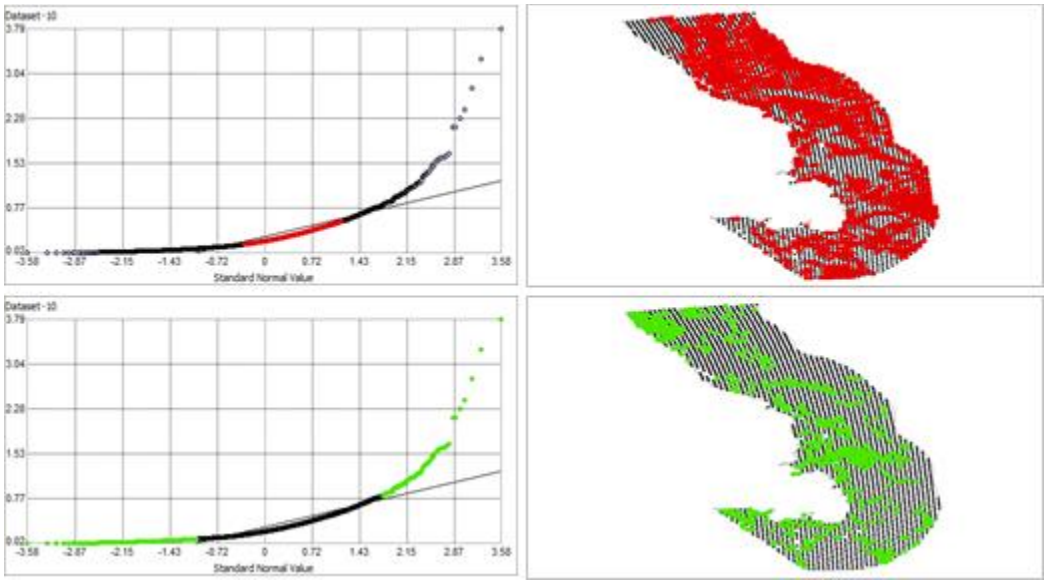

Figure 227. Normal Q-Q plot for data values of Bottom Shear Average Maximum (Pa). Points falling under (upper panel) and over (bottom panel) the reference line are mapped.

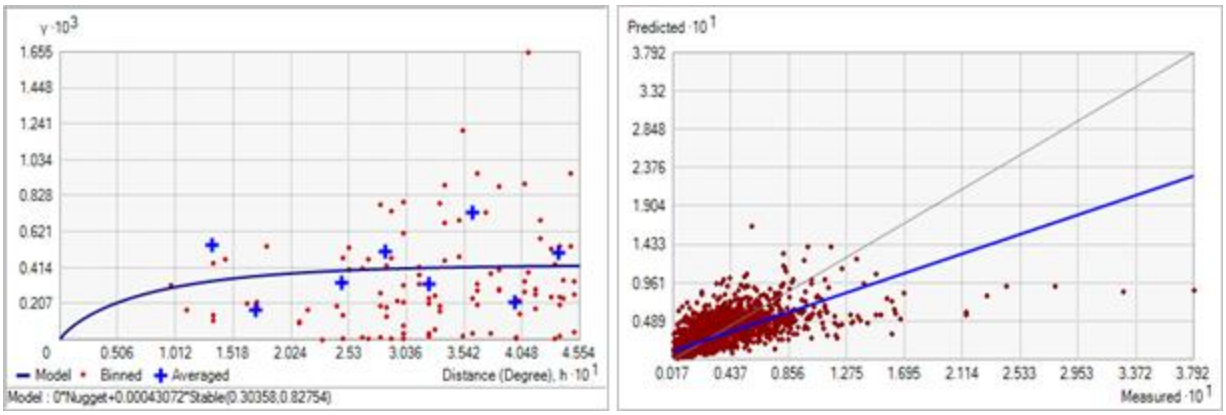

Figure 228. Left panel: Semivariogram of Bottom Shear Average Maximum (Pa). Binned values are shown as red dots; average points are shown as blue crosses; the model fit to the averaged values is shown as a blue line. Lag size: 0.038 degrees; number of lags: 12; Parameter: 0.828; Range: 0.306 degrees; Partial Sill: 4.307 x 10-4. Right panel: Scatterplot of predicted values versus observed values for the model of Bottom Shear Average Maximum (Pa).

Table 114. Results of cross-validation of the kriged model for Bottom Shear Average Maximum (Pa).

Prediction error	**Value**
Number of Observations	2948
Overall Mean Error	-2.836×10^{-6}
Root Mean Square Prediction Error	0.019
Standardized Mean	-2.228×10^{-4}
Standardized Root Mean Square Prediction Error	0.931
Average Standard Error	0.021

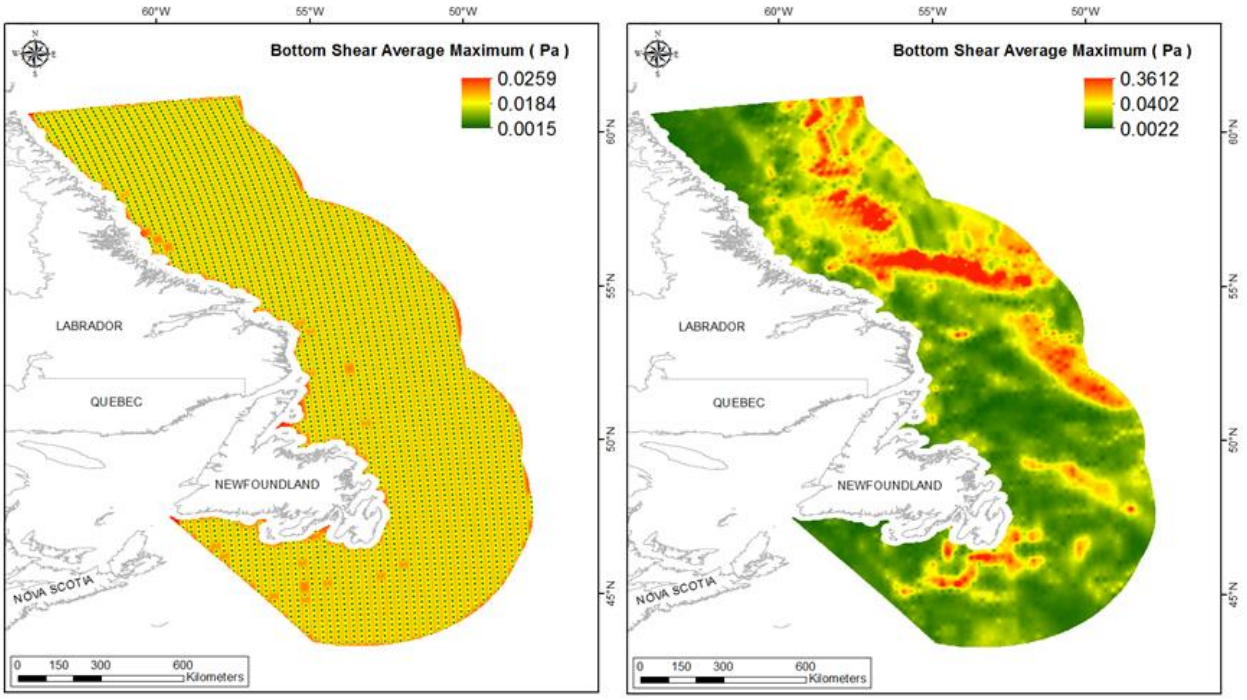

Figure 229. Left panel: Prediction standard error surface of Bottom Shear Average Maximum (Pa). Right panel: Interpolated prediction surface of Bottom Shear Average Maximum (Pa).

Bottom Shear Average Range

This variable displayed a severely right-skewed distribution with outlying data in the upper range (Table 115, Figure 230). The data were higher than predicted by a normal distribution at high values (Figure 231). Mid-range values were slightly lower than the reference line. The areas of over- and under-prediction covered the full spatial extent but showed no strong spatial pattern between them (Figure 231).

The semivariogram showed weak autocorrelation present in the data and the model showed a poor fit between measured and observed values (Figure 232). Nevertheless, the model showed good cross-validation statistics (Table 116) indicating that it was very good at prediction. The error map showed no spatial pattern over the study extent except for some areas along the coast where it was high (Figure 233). The kriged surface is presented in Figure 233.

Table 115. Distributional properties of Bottom Shear Average Range (Pa).

Property	Value
Number of Observations	2948
Minimum	1.676 x 10^{-3}
Maximum	0.230
Mean	0.022
Median	0.017
Standard Deviation	0.019
Skewness	2.871
Kurtosis	19.212

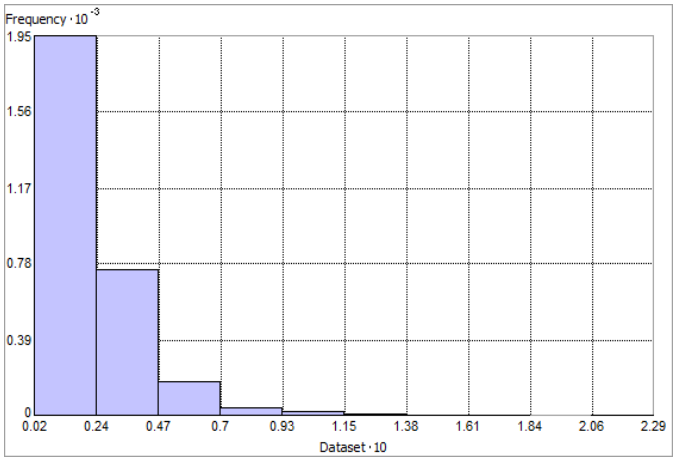

Figure 230. Distribution of Bottom Shear Average Range (Pa). Histogram was illustrated using 10 bins. X axis is shown at 10; Y axis is shown at 10^{-3}.

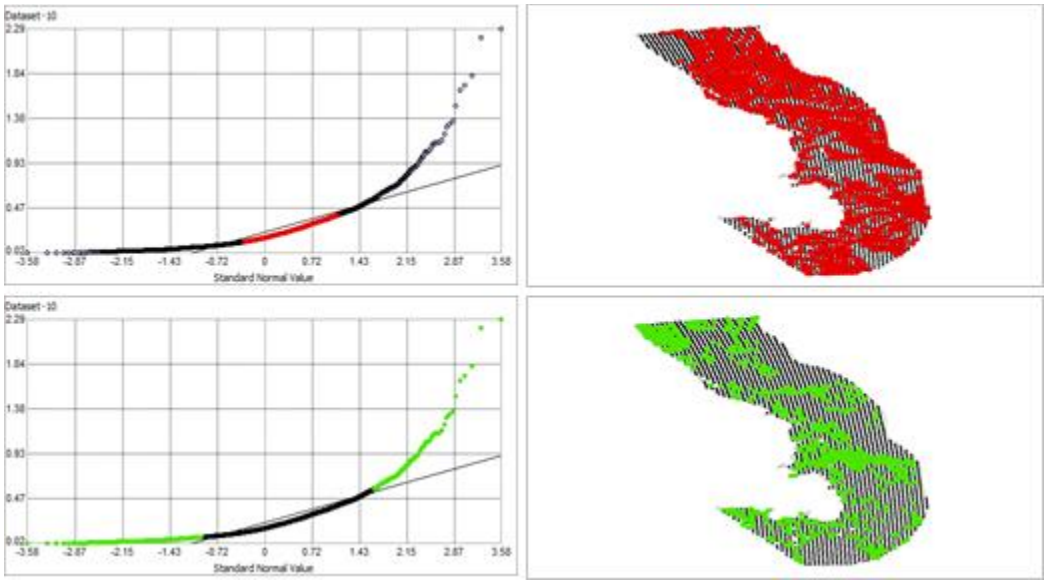

Figure 231. Normal Q-Q plot for data values of Bottom Shear Average Range (Pa). Points falling under (upper panel) and over (bottom panel) the reference line are mapped.

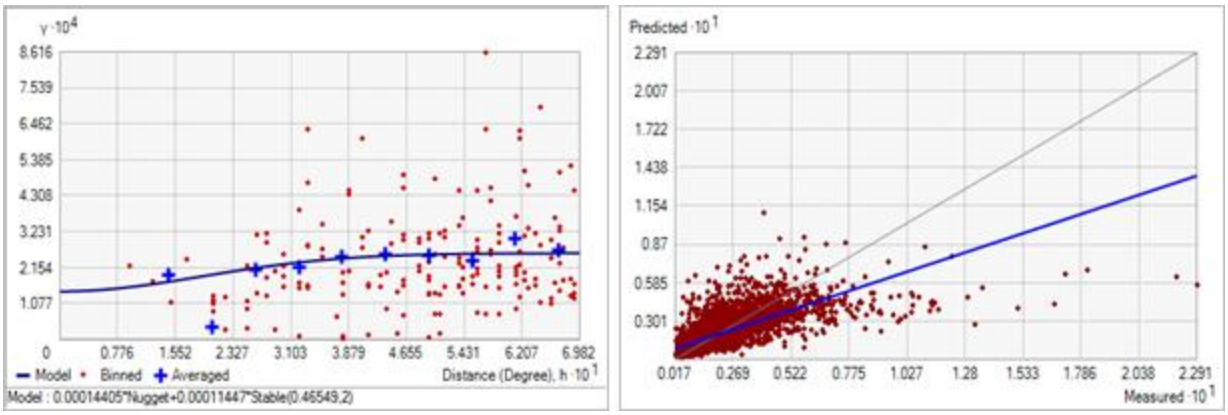

Figure 232. Left panel: Semivariogram of Bottom Shear Average Range (Pa). Binned values are shown as red dots; average points are shown as blue crosses; the model fit to the averaged values is shown as a blue line. Lag size: 0.058 degrees; number of lags: 12; Parameter: 2; Range: 0.465 degrees; Partial Sill: 1.145 x 10^{-4}. Right panel: Scatterplot of predicted values versus observed values for the model of Bottom Shear Average Range (Pa).

Table 116. Results of cross-validation of the kriged model for Bottom Shear Average Range (Pa).

Prediction error	**Value**
Number of Observations	2948
Overall Mean Error	3.663 x 10^{-6}
Root Mean Square Prediction Error	0.014
Standardized Mean	1.200 x 10^{-4}
Standardized Root Mean Square Prediction Error	0.982
Average Standard Error	0.014

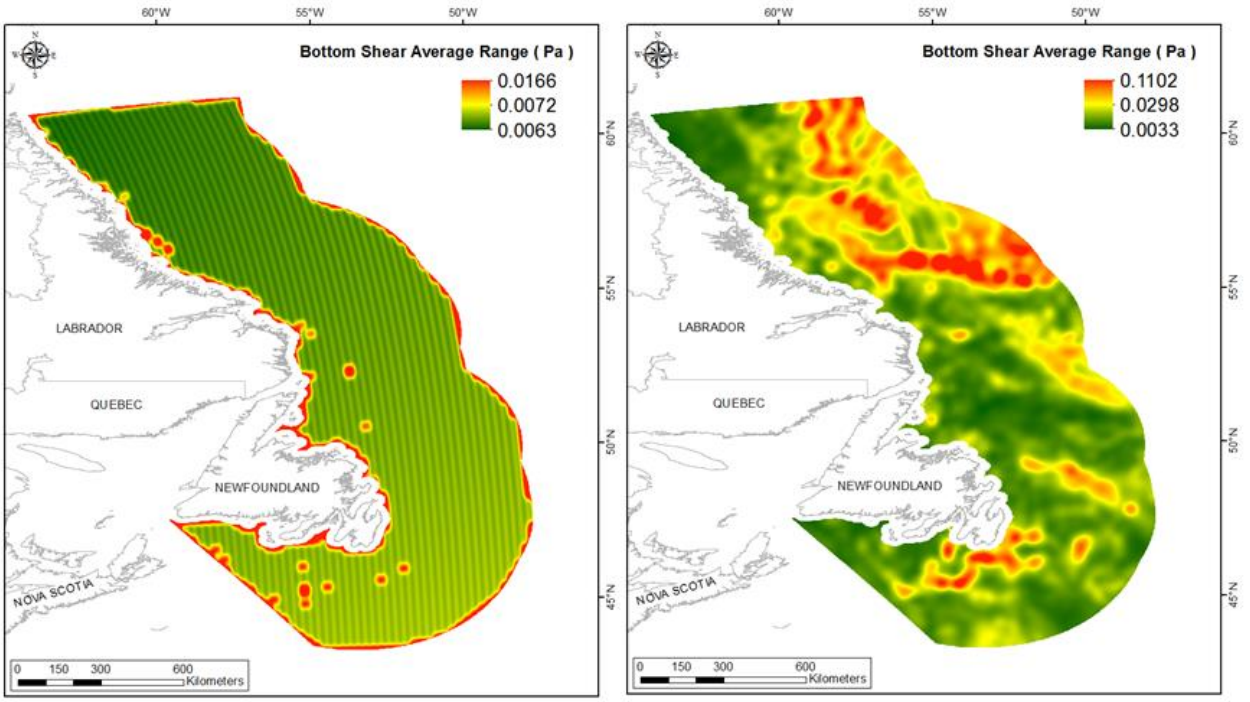

Figure 233. Left panel: Prediction standard error surface of Bottom Shear Average Range (Pa). Right panel: Interpolated prediction surface of Bottom Shear Average Range (Pa).

Sea Surface Chlorophyll *a*

Sea surface chlorophyll *a* concentration is a proxy for phytoplankton biomass and is therefore related to the vertical flux of particulate organic carbon and food supply to the seafloor (Lutz et al. 2007). Gradients in food supply have often been identified as the main factor in controlling changes in benthic biomass, diversity, distribution, and zonation in the deep sea (Levin et al. 2001, Carney 2005, Soltwedel et al. 2009, MacDonald et al. 2010, Papiol et al. 2012). In the northwest Atlantic, surface chlorophyll *a* has shown to be an important determinant in generalized linear models of megafaunal abundance and richness (Beazley et al. 2013) and was an important variable in random forest models predicting the presence of *Geodia* sponge and sponge grounds (Knudby et al. 2013). The spring phytoplankton bloom is thought to be a controlling factor in the reproductive cycles of several deep-sea corals (Sun et al. 2010a, 2010b, 2011, Mercier and Hamel 2011) and sponges (Spetland et al. 2007) in the north Atlantic. Therefore, we expect that seasonal over annual measures of chlorophyll *a* will be more important in species distribution models.

Spring Chlorophyll *a* Mean

This variable displayed a right-skewed distribution with kurtosis and outlying data in the upper range (Table 117, Figure 234). The data were higher than predicted by a normal distribution at low and high values (Figure 235). No data fell under the reference line. The areas over-predicted

showed no strong spatial pattern over the spatial extent but were more common in the north (Figure 235).

The semivariogram showed autocorrelation present in the data and the model showed a fair fit between measured and predicted values (Figure 236). The model showed fair cross-validation statistics (Table 118). The error map showed medium to high error in a grid-like pattern over the study extent (Figure 237). The kriged surface is presented in Figure 237.

Table 117. Distributional properties of Spring Chlorophyll *a* Mean (mg m^{-3}).

Property	Value
Number of Observations	17048
Minimum	0.562
Maximum	9.278
Mean	1.147
Median	1.086
Standard Deviation	0.389
Skewness	4.780
Kurtosis	70.121

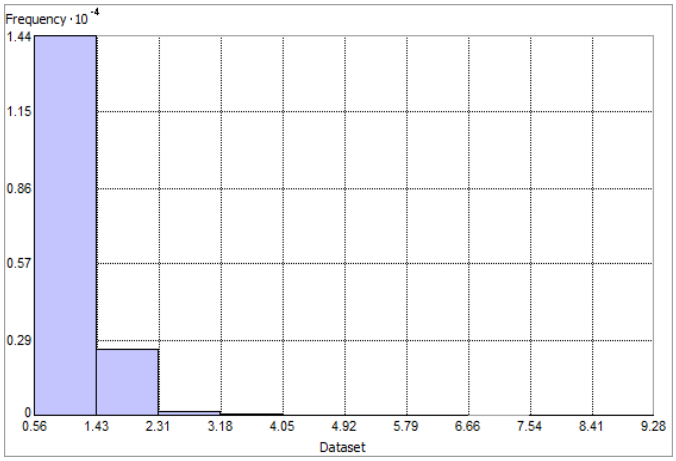

Figure 234. Distribution of Spring Chlorophyll *a* Mean (mg m^{-3}). Histogram was illustrated using 10 bins. Y axis is shown at 10^{-4}.

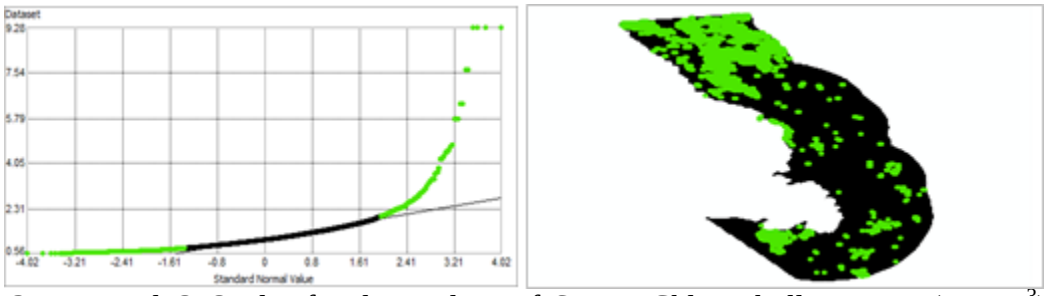

Figure 235. Normal Q-Q plot for data values of Spring Chlorophyll *a* Mean (mg m^{-3}). Points falling over (bottom panel) the reference line are mapped.

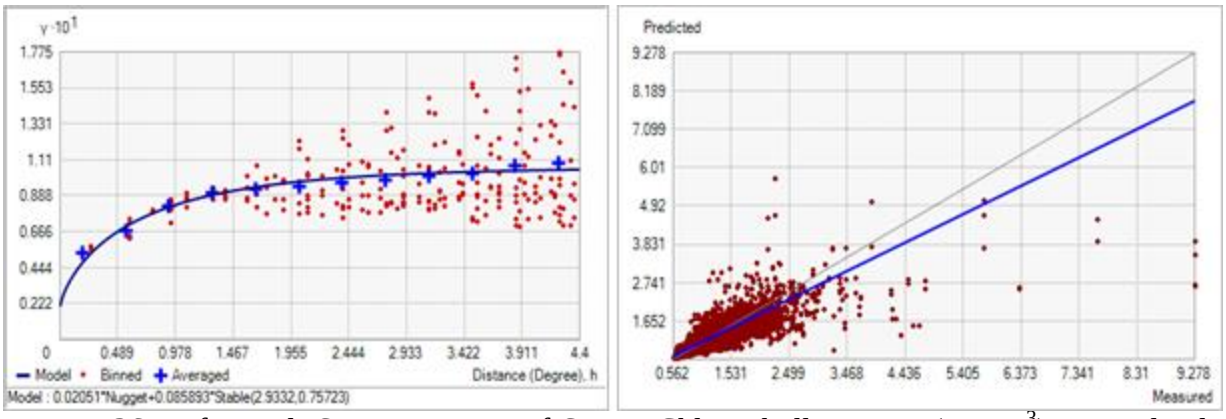

Figure 236. Left panel: Semivariogram of Spring Chlorophyll *a* Mean (mg m^{-3}). Binned values are shown as red dots; average points are shown as blue crosses; the model fit to the averaged values is shown as a blue line. Lag size: 0.367 degrees; number of lags: 12; Parameter: 0.757; Range: 2.933 degrees; Partial Sill: 0.086. Right panel: Scatterplot of predicted values versus observed values for the model of Spring Chlorophyll *a* Mean (mg m^{-3}).

Table 118. Results of cross-validation of the kriged model for Spring Chlorophyll *a* Mean (mg m^{-3}).

Prediction error	**Value**
Number of Observations	17048
Overall Mean Error	-8.929×10^{-5}
Root Mean Square Prediction Error	0.219
Standardized Mean	-3.155×10^{-4}
Standardized Root Mean Square Prediction Error	1.113
Average Standard Error	0.197

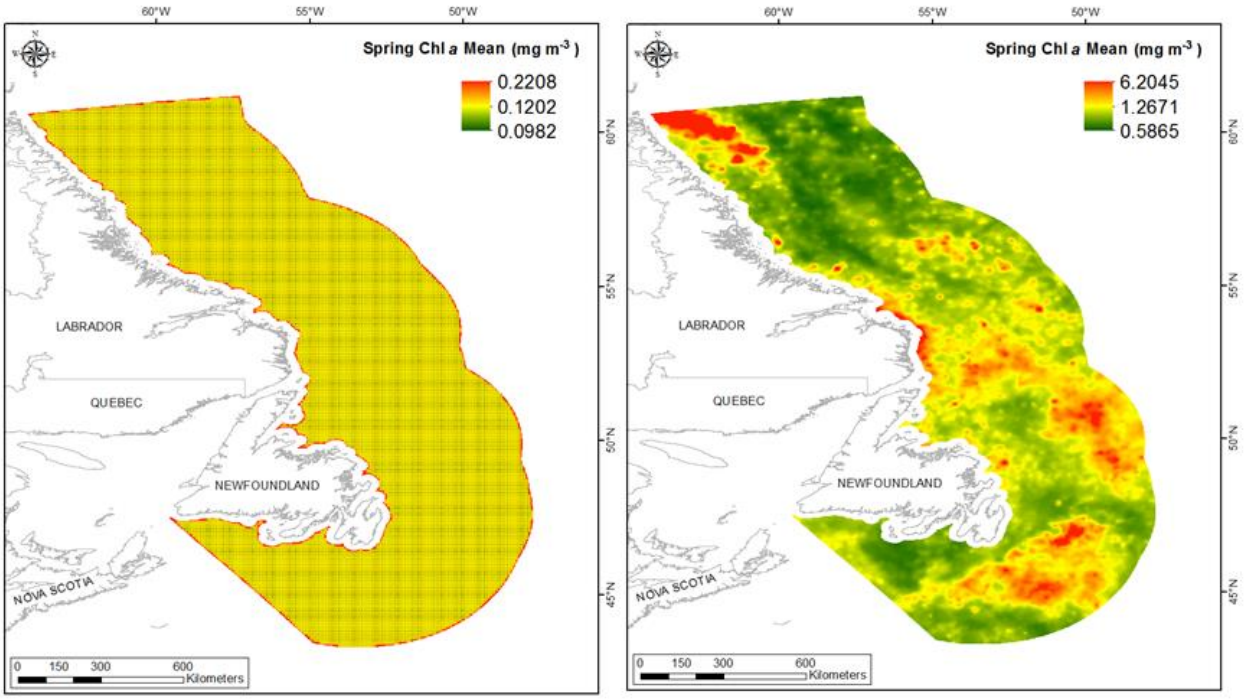

Figure 237. Left panel: Prediction standard error surface of Spring Chlorophyll *a* Mean (mg m^{-3}). Right panel: Interpolated prediction surface of Spring Chlorophyll *a* Mean (mg m^{-3}).

Spring Chlorophyll *a* Minimum

This variable displayed a right-skewed distribution with kurtosis prior to modeling (Table 119, Figure 238). The data were higher than predicted by a normal distribution at high values and slightly lower than predicted at mid values (Figure 239). The areas of under- and over-prediction showed a strong differential spatial pattern over the spatial extent (Figure 239).

The semivariogram showed very weak autocorrelation present in the data and the model showed a moderate fit between measured and predicted values (Figure 240). The model showed fair cross-validation statistics (Table 120). The error map showed low error over most of the study extent except for along the coast where it was high (Figure 241). The kriged surface is presented in Figure 241.

Table 119. Distributional properties of Spring Chlorophyll *a* Minimum (mg m^{-3}).

Property	Value
Number of Observations	17048
Minimum	0.096
Maximum	2.357
Mean	0.260
Median	0.244
Standard Deviation	0.110
Skewness	5.819
Kurtosis	74.345

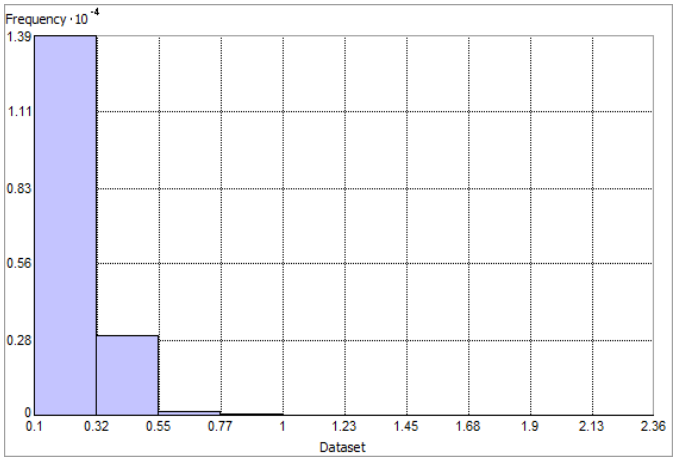

Figure 238. Distribution of Spring Chlorophyll *a* Minimum (mg m^{-3}). Histogram was illustrated using 10 bins. Y axis is shown at 10^{-4}.

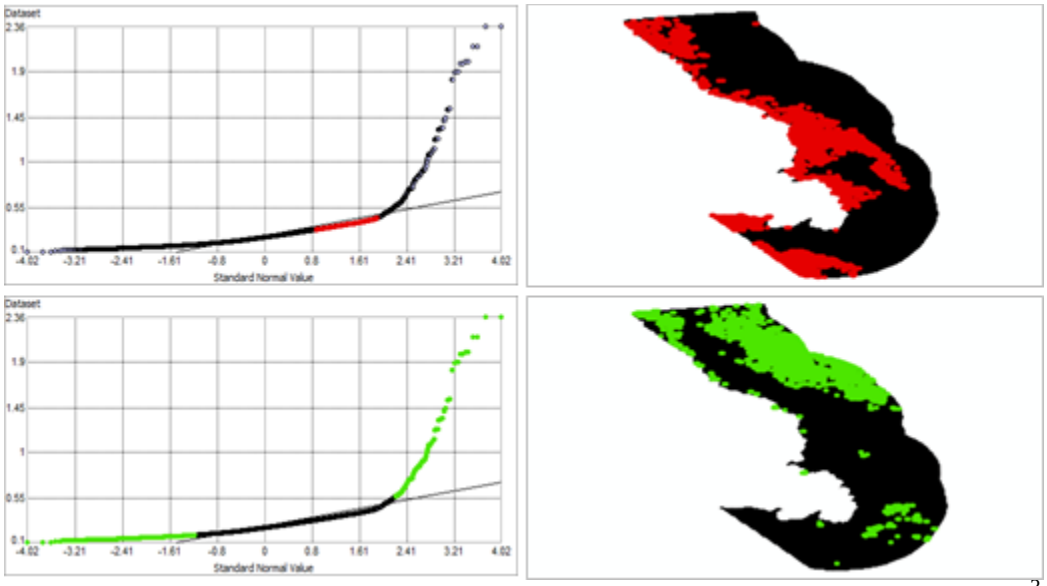

Figure 239. Normal Q-Q plot for data values of Spring Chlorophyll *a* Minimum (mg m^{-3}). Points falling under (upper panel) and over (bottom panel) the reference line are mapped.

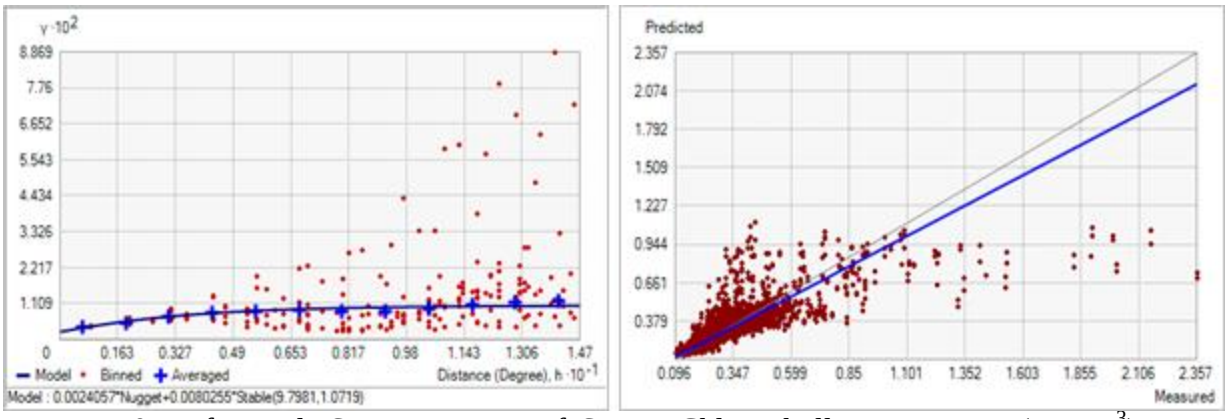

Figure 240. Left panel: Semivariogram of Spring Chlorophyll *a* Minimum (mg m^{-3}). Binned values are shown as red dots; average points are shown as blue crosses; the model fit to the averaged values is shown as a blue line. Lag size: 1.225 degrees; number of lags: 12; Parameter: 1.072; Range: 9.798 degrees; Partial Sill: 8.025 x 10^{-3}. Right panel: Scatterplot of predicted values versus observed values for the variable Spring Chlorophyll *a* Minimum.

Table 120. Results of cross-validation of the kriged model for Spring Chlorophyll *a* Minimum (mg m^{-3}).

Prediction error	**Value**
Number of Observations	17048
Overall Mean Error	2.820 x 10^{-5}
Root Mean Square Prediction Error	0.057
Standardized Mean	5.975 x 10^{-4}
Standardized Root Mean Square Prediction Error	1.086
Average Standard Error	0.052

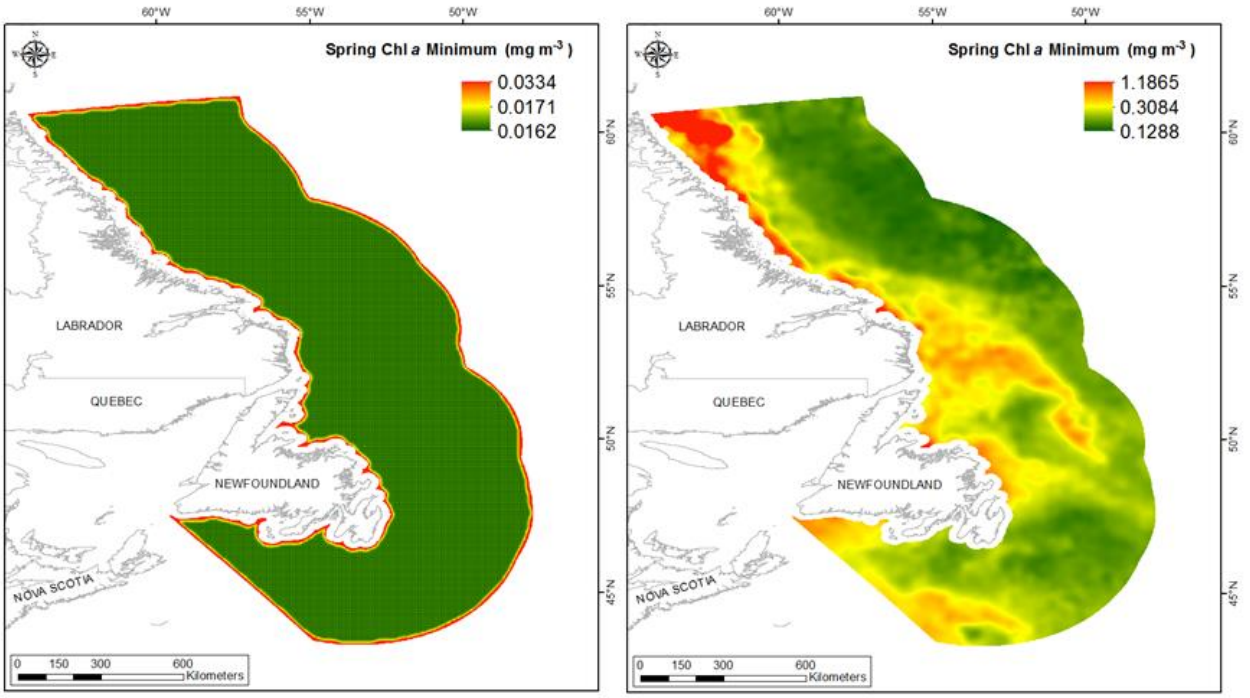

Figure 241. Left panel: Prediction standard error surface of Spring Chlorophyll *a* Minimum (mg m^{-3}). Right panel: Interpolated prediction surface of Spring Chlorophyll *a* Minimum (mg m^{-3}).

Spring Chlorophyll *a* Maximum

This variable displayed a right-skewed distribution with kurtosis prior to modeling (Table 121, Figure 242). The data were higher than predicted by a normal distribution at high values. Mid-range values were slightly lower than the reference line (Figure 243). The areas of under- and over-prediction showed a no strong spatial pattern over the spatial extent (Figure 243).

The semivariogram showed autocorrelation present in the data and the model showed poor fit between measured and predicted values (Figure 244). The model showed fair cross-validation statistics (Table 122). The error map showed medium to high error in a grid-like pattern over the study extent (Figure 245). The kriged surface is presented in Figure 245.

Table 121. Distributional properties of Spring Chlorophyll *a* Maximum (mg m^{-3}).

Property	Value
Number of Observations	17048
Minimum	1.064
Maximum	85.393
Mean	5.054
Median	3.967
Standard Deviation	4.131
Skewness	5.738
Kurtosis	69.636

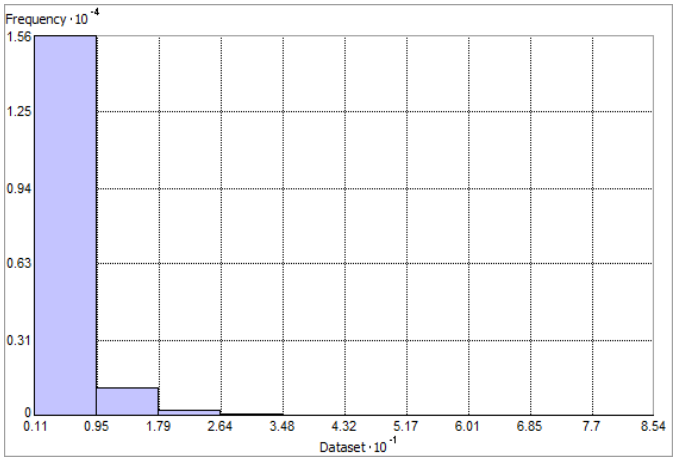

Figure 242. Distribution of Spring Chlorophyll *a* Maximum (mg m^{-3}). Histogram was illustrated using 10 bins. X axis is show at $10^{-1}$and Y axis is shown at 10^{-4}.

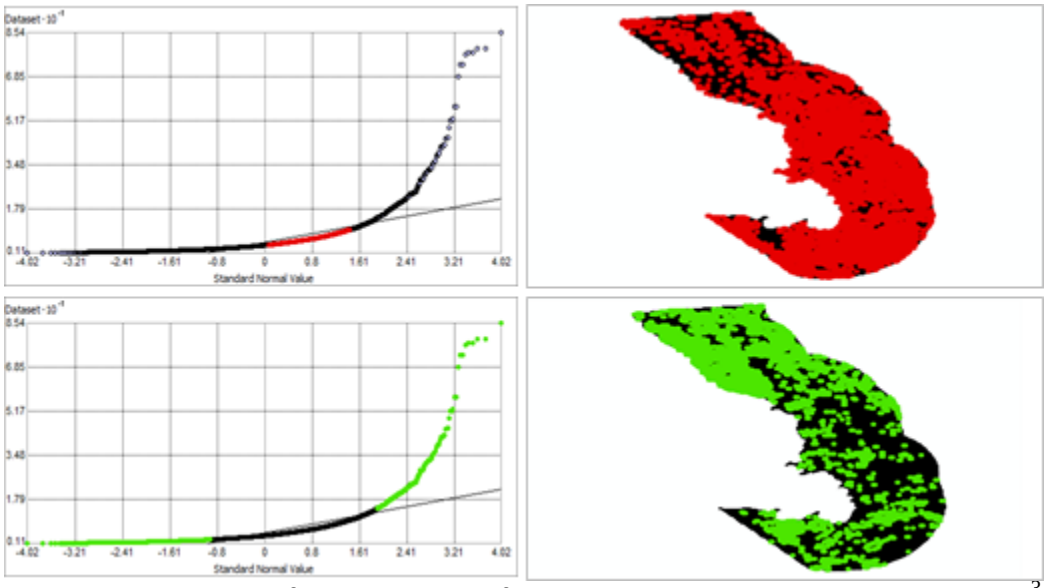

Figure 243. Normal Q-Q plot for data values of Spring Chlorophyll *a* Maximum (mg m^{-3}). Points falling under (upper panel) and over (lower panel) the reference line are mapped.

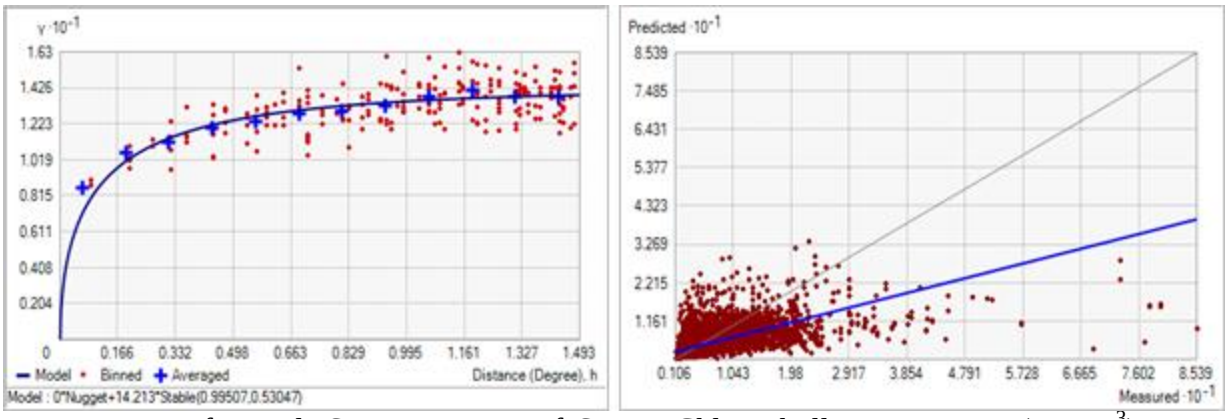

Figure 244. Left panel: Semivariogram of Spring Chlorophyll *a* Maximum (mg m^{-3}). Binned values are shown as red dots; average points are shown as blue crosses; the model fit to the averaged values is shown as a blue line. Lag size: 0.124 degrees; number of lags: 12; Parameter: 0.530; Range: 0.995 degrees; Partial Sill: 14.213. Right panel: Scatterplot of predicted values versus observed values for the variable Spring Chlorophyll *a* Maximum (mg m^{-3}).

Table 122. Results of cross-validation of the kriged model for Spring Chlorophyll *a* Maximum (mg m^{-3}).

Prediction error	**Value**
Number of Observations	17048
Overall Mean Error	-6.584×10^{-4}
Root Mean Square Prediction Error	3.285
Standardized Mean	-1.697×10^{-4}
Standardized Root Mean Square Prediction Error	1.129
Average Standard Error	2.912

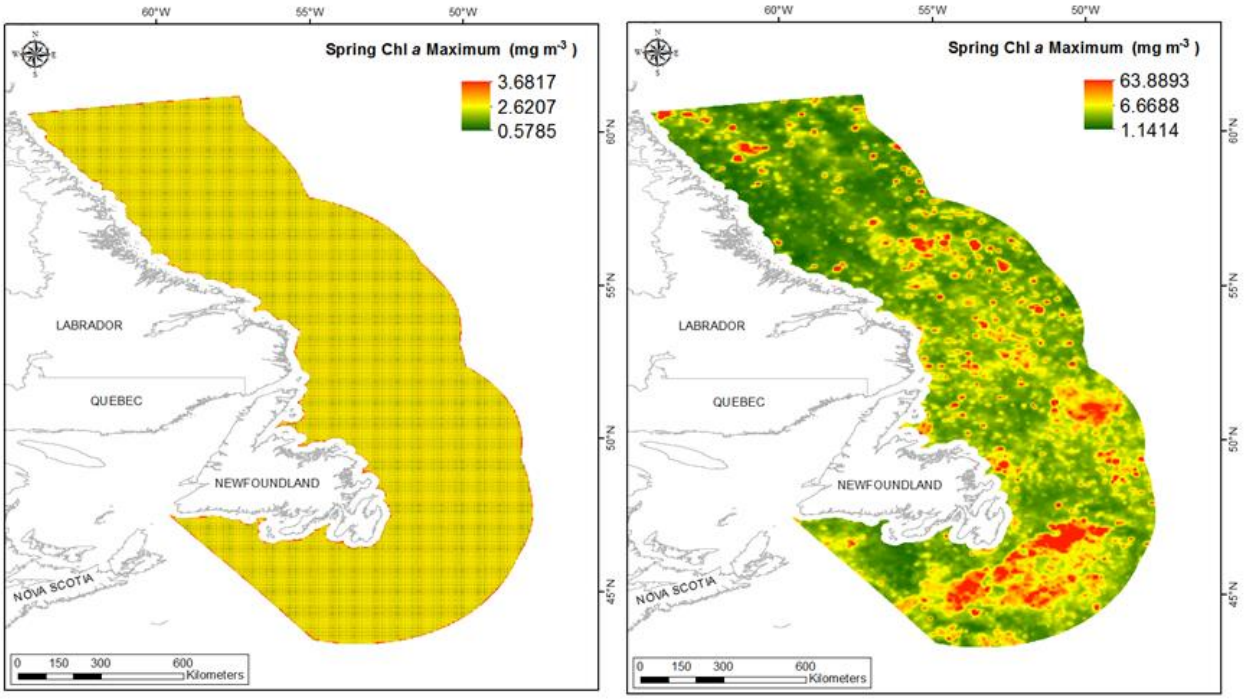

Figure 245. Left panel: Prediction standard error surface of Spring Chlorophyll *a* Maximum (mg m^{-3}). Right panel: Interpolated prediction surface of Spring Chlorophyll *a* Maximum (mg m^{-3}).

Spring Chlorophyll *a* Range

This variable displayed a right-skewed distribution with kurtosis and outlying data in the upper range (Table 123, Figure 246). The data were higher than predicted by a normal distribution at high values and lower at mid-range values (Figure 247). The areas of under- and over-prediction showed no spatial pattern over the spatial extent (Figure 247).

The semivariogram showed high autocorrelation present in the data and the model showed poor fit between measured and predicted values (Figure 248). The model showed fair cross-validation statistics (Table 124) indicating that it was good at prediction. The error map showed medium to high error in a grid-like pattern over the study extent (Figure 249). The kriged surface is presented in Figure 249.

Table 123. Distributional properties of Spring Chlorophyll *a* Range (mg m^{-3}).

Property	Value
Number of Observations	17048
Minimum	0.453
Maximum	85.068
Mean	4.794
Median	3.701
Standard Deviation	4.132
Skewness	5.738
Kurtosis	69.609

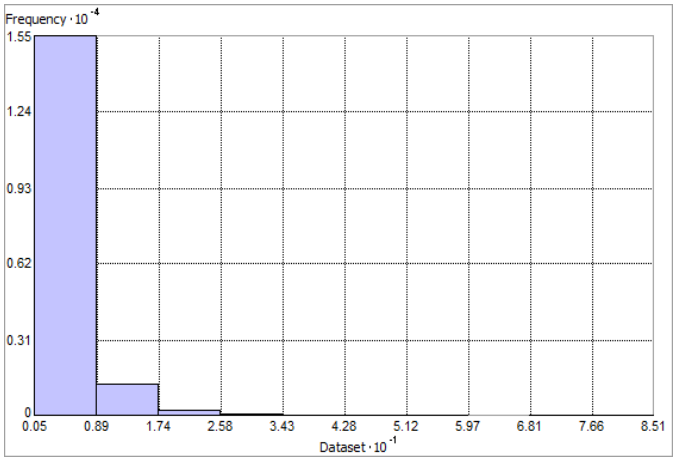

Figure 246. Distribution of Spring Chlorophyll *a* Range (mg m^{-3}). Histogram was illustrated using 10 bins. X and Y axes are shown at 10^{-1} and 10^{-4} respectively.

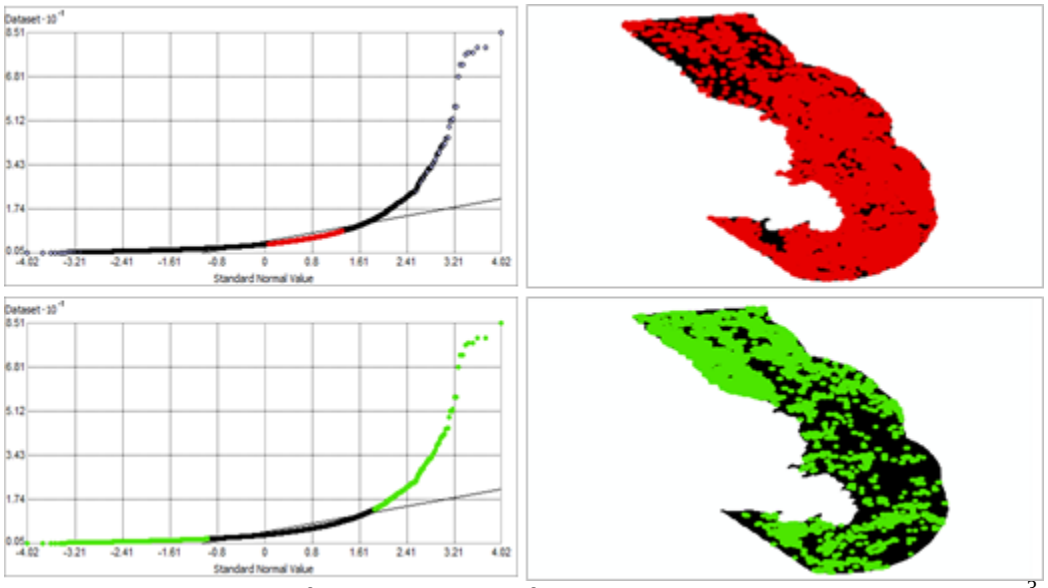

Figure 247. Normal Q-Q plot for data values of Spring Chlorophyll *a* Range (mg m^{-3}). Points falling under (upper panel) and over (bottom panel) the reference line are mapped.

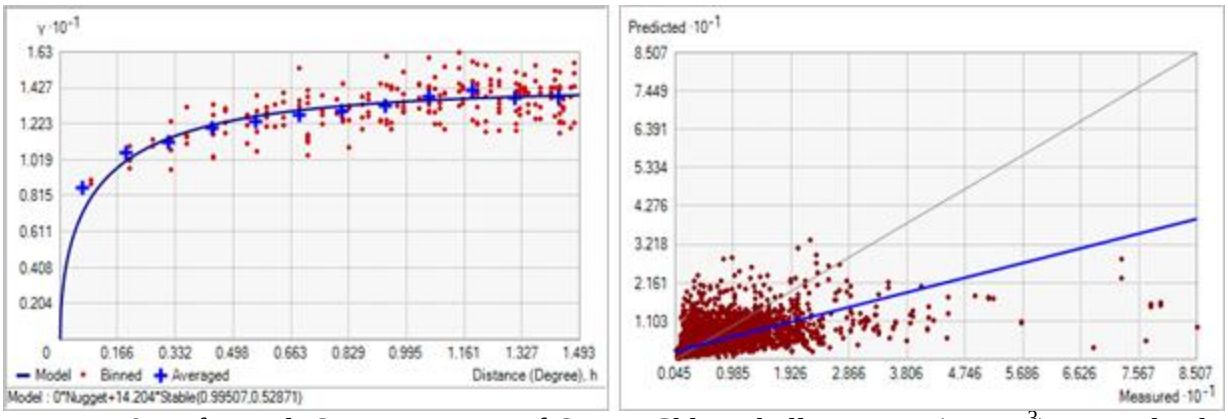

Figure 248. Left panel: Semivariogram of Spring Chlorophyll *a* Range (mg m^{-3}). Binned values are shown as red dots; average points are shown as blue crosses; the model fit to the averaged values is shown as a blue line. Lag size: 0.124 degrees; number of lags: 12; Parameter: 0.529; Range: 0.995 degrees; Partial Sill: 14.204. Right panel: Scatterplot of predicted values versus observed values for the variable Spring Chlorophyll *a* Range (mg m^{-3}).

Table 124. Results of cross-validation of the kriged model for Spring Chlorophyll *a* Range (mg m^{-3}).

Prediction error	**Value**
Number of Observations	17048
Overall Mean Error	-6.366×10^{-4}
Root Mean Square Prediction Error	3.288
Standardized Mean	-1.643×10^{-4}
Standardized Root Mean Square Prediction Error	1.128
Average Standard Error	2.915

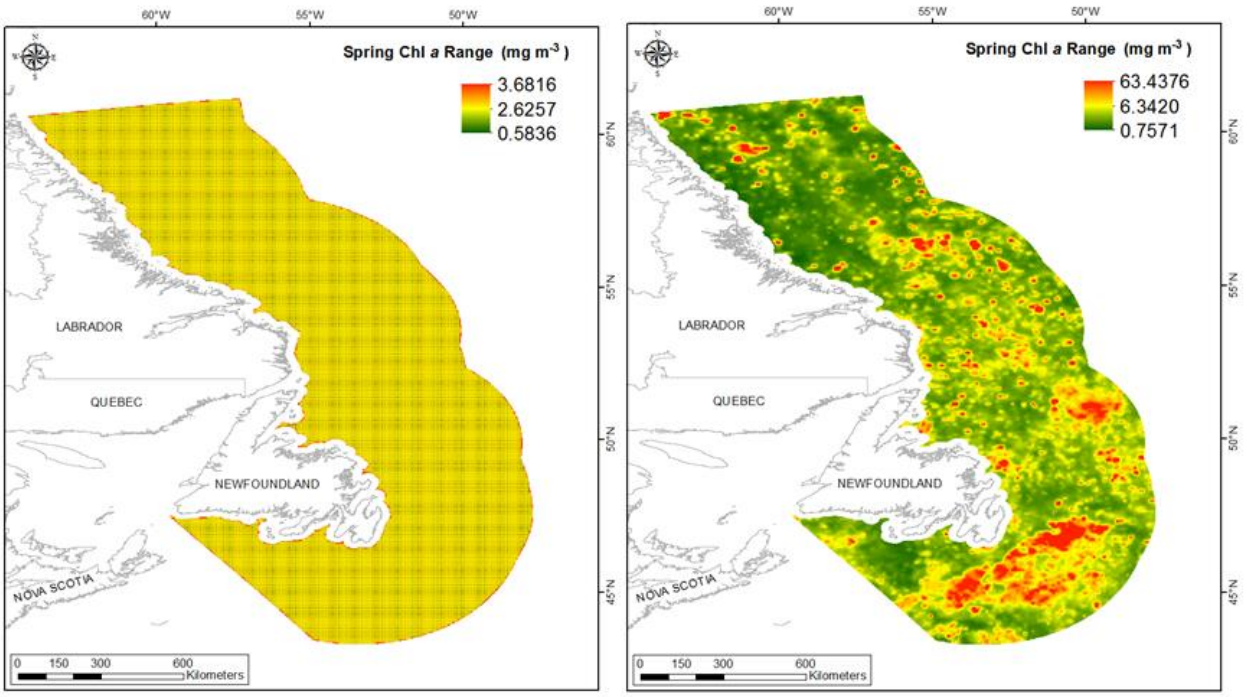

Figure 249. Left panel: Prediction standard error surface of Spring Chlorophyll *a* Range (mg m^{-3}). Right panel: Interpolated prediction surface of Spring Chlorophyll *a* Range (mg m^{-3}).

Summer Chlorophyll *a* Mean

This variable displayed a right-skewed distribution with kurtosis and outlying data in the upper range (Table 125, Figure 250). The data were higher than predicted by a normal distribution at the upper range and lower than predicted at mid values (Figure 251). The areas of under- and over-prediction showed some spatial patterning over the spatial extent with a tendency for over-prediction to the south (Figure 251).

The semivariogram showed moderate autocorrelation present in the data and the model showed a good fit between measured and predicted values (Figure 252). The model showed fair cross-validation statistics (Table 126). The error map showed low error over the study extent with higher error around the coast (Figure 253). The kriged surface is presented in Figure 253.

Table 125. Distributional properties of Summer Chlorophyll *a* Mean (mg m^{-3}).

Property	Value
Number of Observations	17048
Minimum	0.235
Maximum	3.770
Mean	0.587
Median	0.503
Standard Deviation	0.278
Skewness	1.687
Kurtosis	9.860

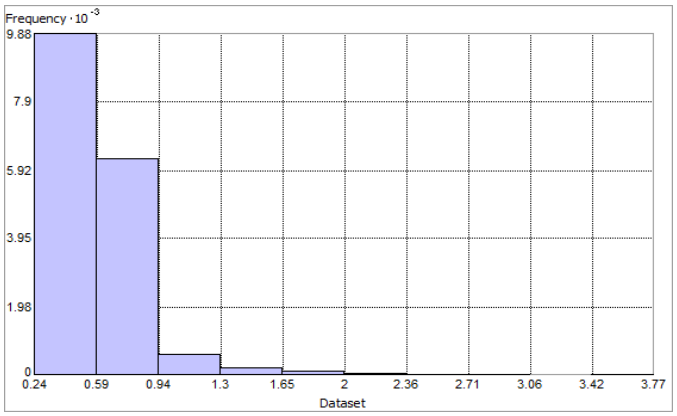

Figure 250. Distribution of Summer Chlorophyll *a* Mean (mg m^{-3}). Histogram was illustrated using 10 bins. Y axis is shown at 10^{-3}.

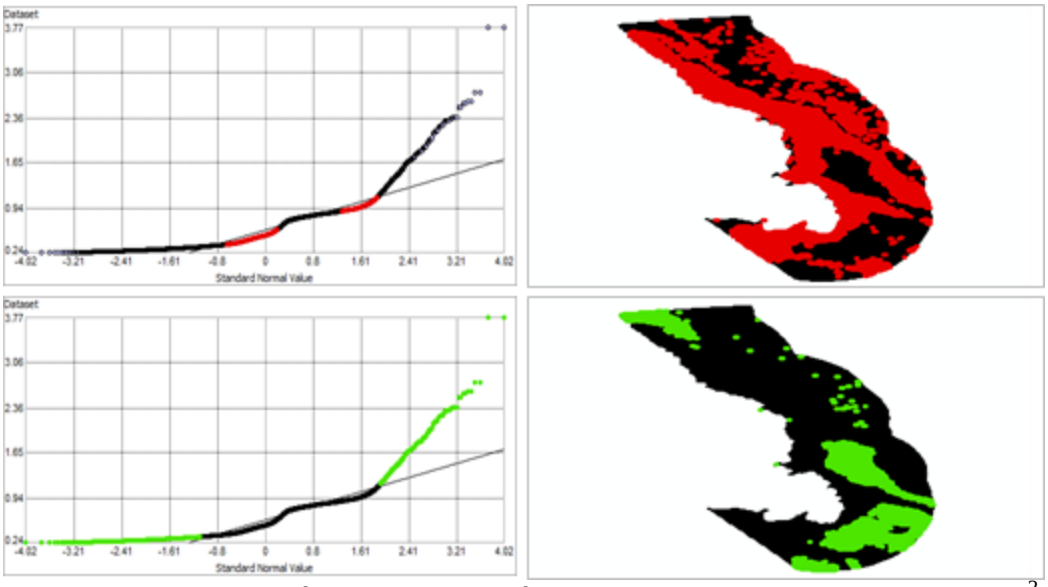

Figure 251. Normal Q-Q plot for data values of Summer Chlorophyll *a* Mean (mg m^{-3}). Points falling under (upper panel) and over (bottom panel) the reference line are mapped.

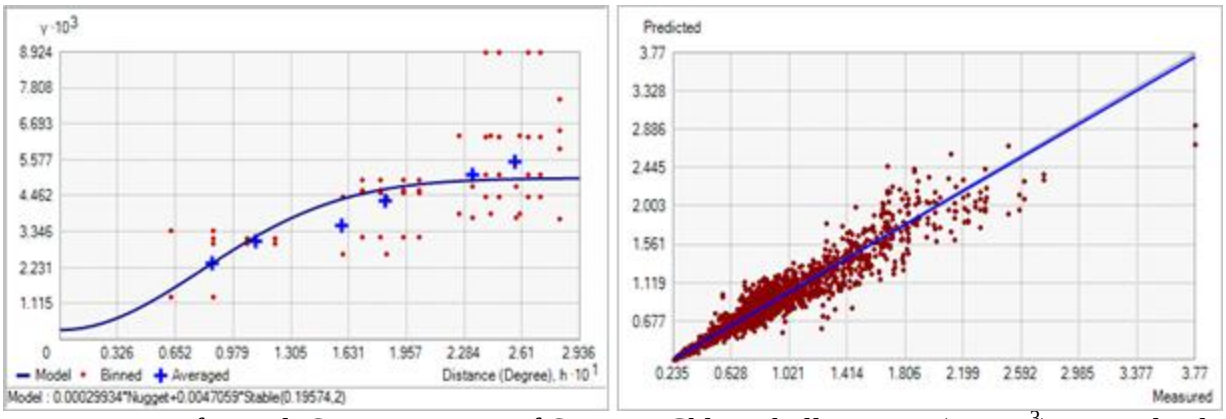

Figure 252. Left panel: Semivariogram of Summer Chlorophyll *a* Mean (mg m^{-3}). Binned values are shown as red dots; average points are shown as blue crosses; the model fit to the averaged values is shown as a blue line. Lag size: 0.024 degrees; number of lags: 12; Parameter: 2; Range: 0.196 degrees; Partial Sill: 4.706 x 10^{-3}. Right panel: Scatterplot of predicted values versus observed values for the variable Summer Chlorophyll *a* Mean (mg m^{-3}).

Table 126. Results of cross-validation of the kriged model for Summer Chlorophyll *a* Mean (mg m^{-3}).

Prediction error	**Value**
Number of Observations	17048
Overall Mean Error	-1.825 x 10^{-4}
Root Mean Square Prediction Error	0.052
Standardized Mean	-4.129 x 10^{-3}
Standardized Root Mean Square Prediction Error	1.471
Average Standard Error	0.035

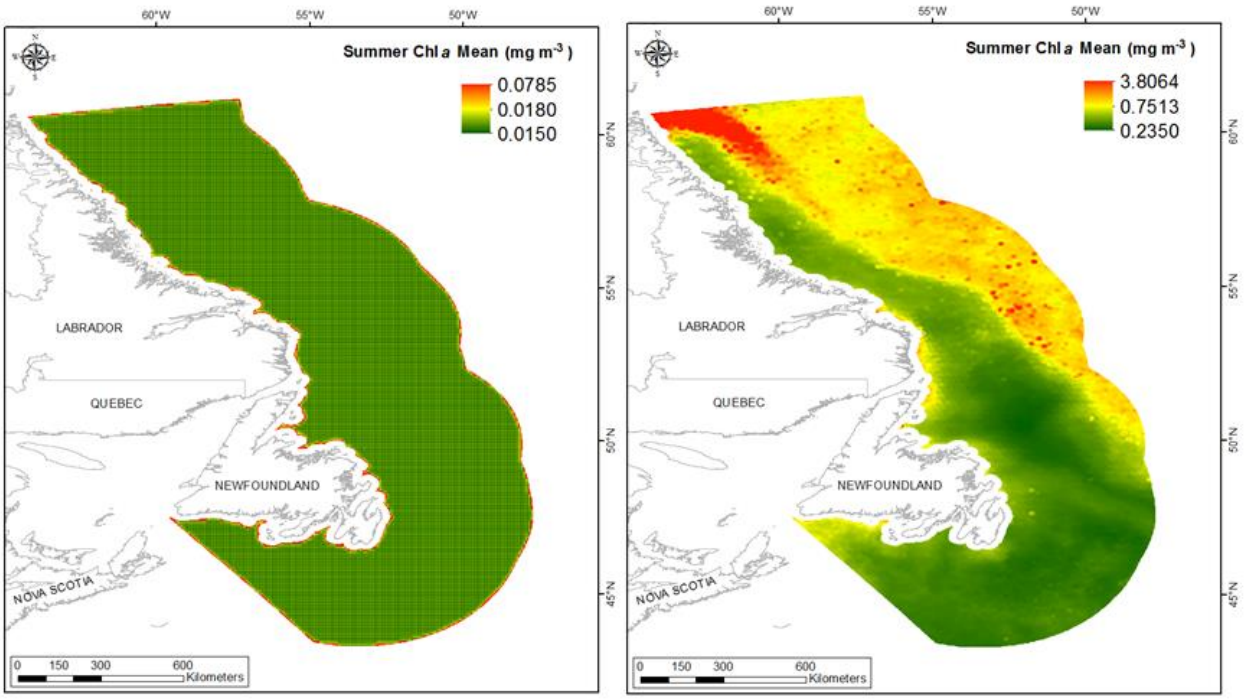

Figure 253. Left panel: Prediction standard error surface of Summer Chlorophyll *a* Mean (mg m^{-3}). Right panel: Interpolated prediction surface of Summer Chlorophyll *a* Mean (mg m^{-3}).

Summer Chlorophyll *a* Minimum

This variable displayed a right-skewed distribution with kurtosis prior to modeling (Table 127, Figure 254). The data were higher than predicted by a normal distribution at high and low values (Figure 255). Over-predicted data points were more prevalent in the south and north of the spatial extent and there were no areas of under-prediction (Figure 255).

The semivariogram showed autocorrelation present in the data and the model showed a good fit between measured and predicted values (Figure 256). The model showed good cross-validation statistics (Table 128) indicating that it was good at prediction. The error map showed medium to high error in a grid-like pattern over the study extent (Figure 257). The kriged surface is presented in Figure 257.

Table 127. Distributional properties of Summer Chlorophyll *a* Minimum (mg m^{-3}).

Property	Value
Number of Observations	17048
Minimum	0.103
Maximum	1.246
Mean	0.311
Median	0.303
Standard Deviation	0.099
Skewness	1.627
Kurtosis	9.903

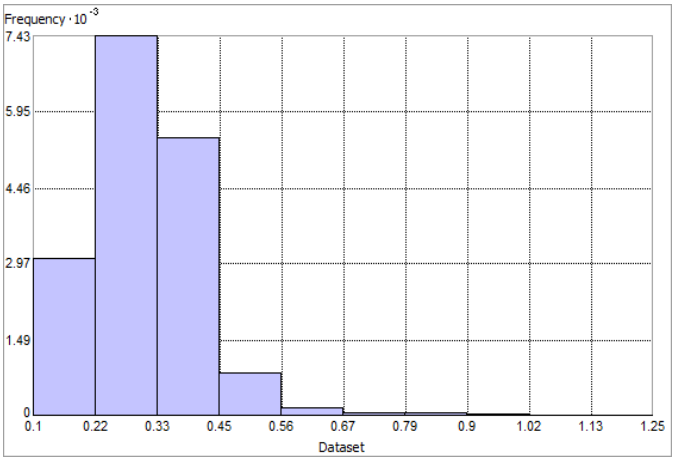

Figure 254. Distribution of Summer Chlorophyll *a* Minimum (mg m^{-3}). Histogram was illustrated using 10 bins. Y axis is shown at 10^{-3}.

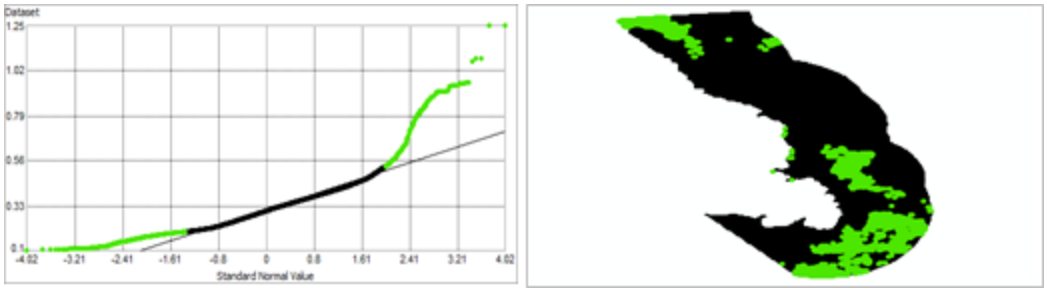

Figure 255. Normal Q-Q plot for data values of Summer Chlorophyll *a* Minimum (mg m^{-3}). Points falling over (bottom panel) the reference line are mapped.

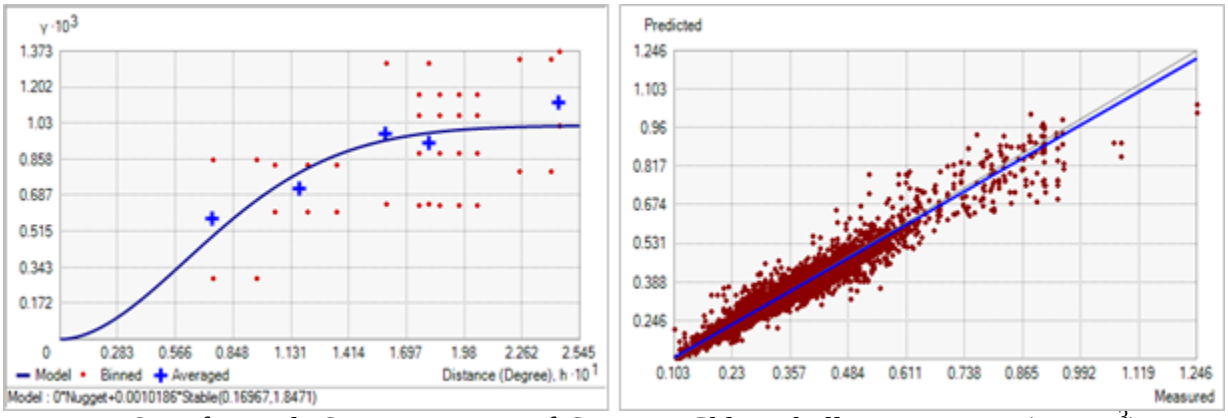

Figure 256. Left panel: Semivariogram of Summer Chlorophyll *a* Minimum (mg m^{-3}). Binned values are shown as red dots; average points are shown as blue crosses; the model fit to the averaged values is shown as a blue line. Lag size: 0.021 degrees; number of lags: 12; Parameter: 1.847; Range: 0.170 degrees; Partial Sill: 1.019 x 10^{-3}. Right panel: Scatterplot of predicted values versus observed values for the variable Summer Chlorophyll *a* Minimum (mg m^{-3}).

Table 128. Results of cross-validation of the kriged model for Summer Chlorophyll *a* Minimum (mg m^{-3}).

Prediction error	**Value**
Number of Observations	17048
Overall Mean Error	-7.844×10^{-5}
Root Mean Square Prediction Error	0.021
Standardized Mean	-3.063×10^{-3}
Standardized Root Mean Square Prediction Error	1.014
Average Standard Error	0.020

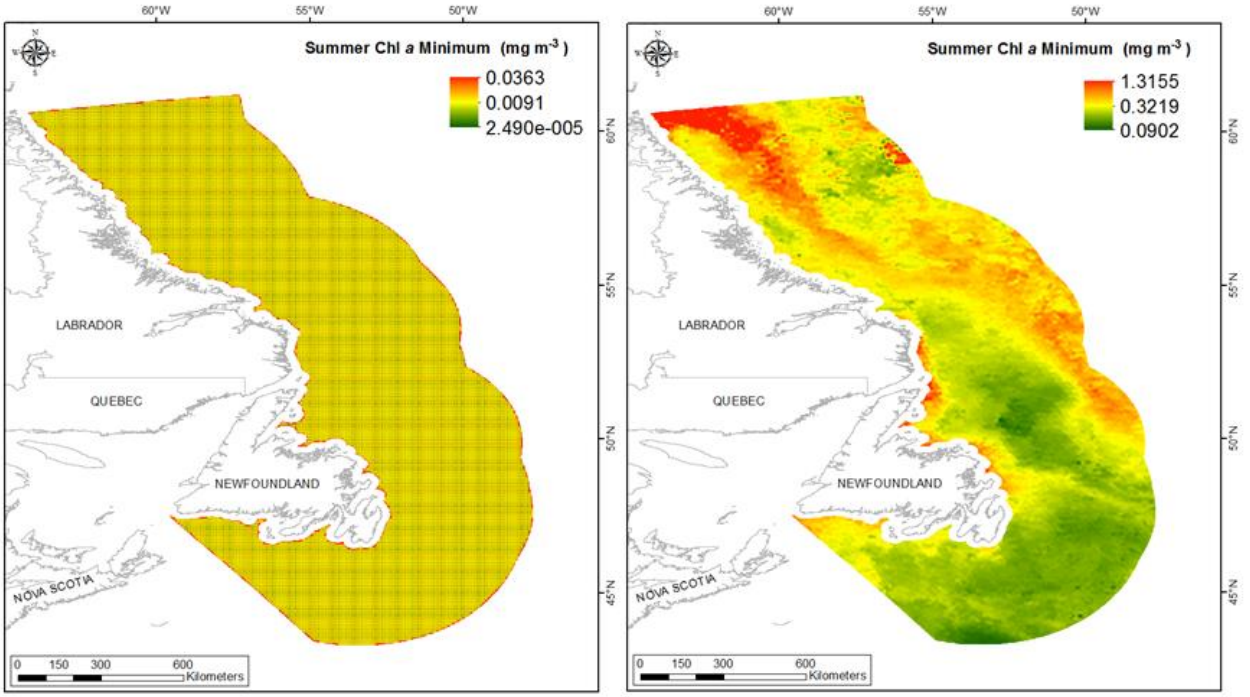

Figure 257. Left panel: Prediction standard error surface of Summer Chlorophyll *a* Minimum (mg m^{-3}). Right panel: Interpolated prediction surface of Summer Chlorophyll *a* Minimum (mg m^{-3}).

Summer Chlorophyll *a* Maximum

This variable displayed a right-skewed distribution with high kurtosis and outlying data in the upper range (Table 129, Figure 258). The data were higher than predicted by a normal distribution at high values and slightly lower than predicted at mid values (Figure 259). The areas of under- and over-prediction showed a strong spatial pattern over the spatial extent (Figure 259).

The semivariogram showed autocorrelation present in the data and the model showed fair fit between measured and predicted values (Figure 260). The model showed fair cross-validation

statistics (Table 130). The error map showed medium to high error in a grid-like pattern over the study extent (Figure 261). The kriged surface is presented in Figure 261.

Table 129. Distributional properties of Summer Chlorophyll *a* Maximum (mg m^{-3}).

Property	Value
Number of Observations	17048
Minimum	0.302
Maximum	40.122
Mean	1.260
Median	0.940
Standard Deviation	1.288
Skewness	8.329
Kurtosis	149.85

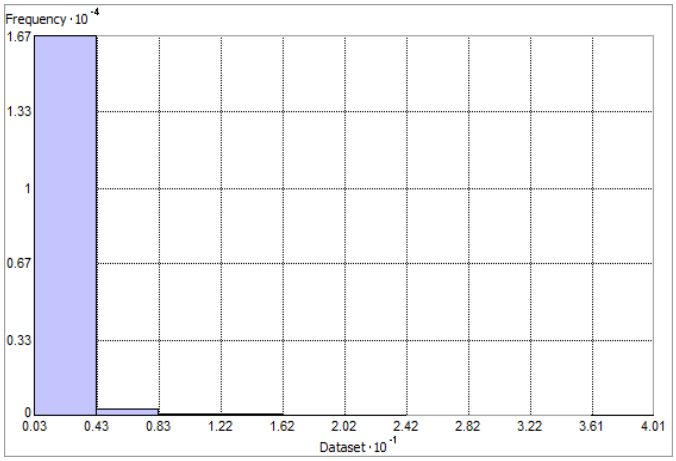

Figure 258. Distribution of Summer Chlorophyll *a* Maximum (mg m^{-3}). Histogram was illustrated using 10 bins. X is shown at 10^{-1}; Y axis is shown at 10^{-4}.

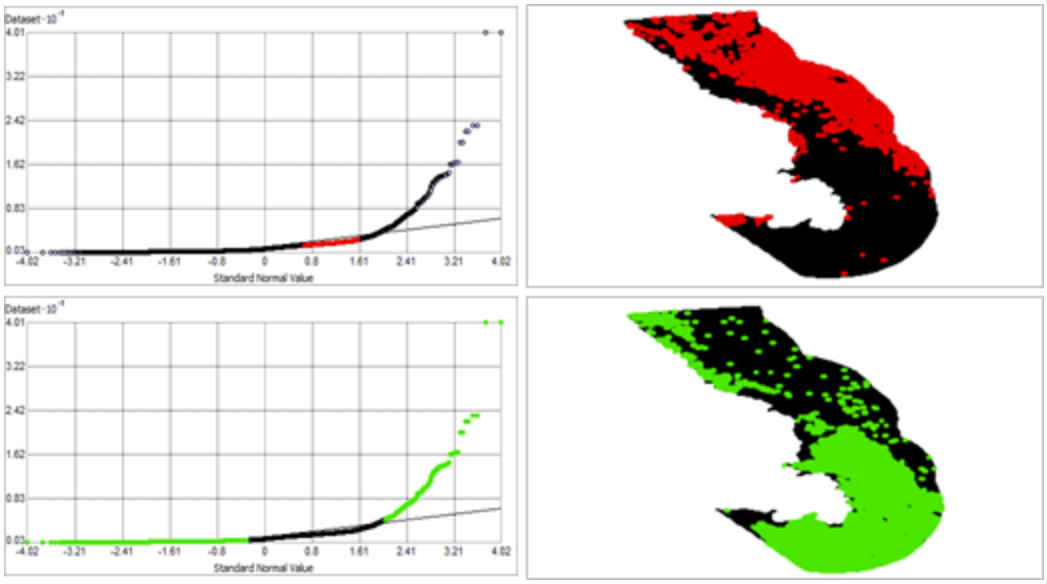

Figure 259. Normal Q-Q plot for data values of Summer Chlorophyll *a* Maximum (mg m^{-3}). Points falling under (upper panel) and over (bottom panel) the reference line are mapped.

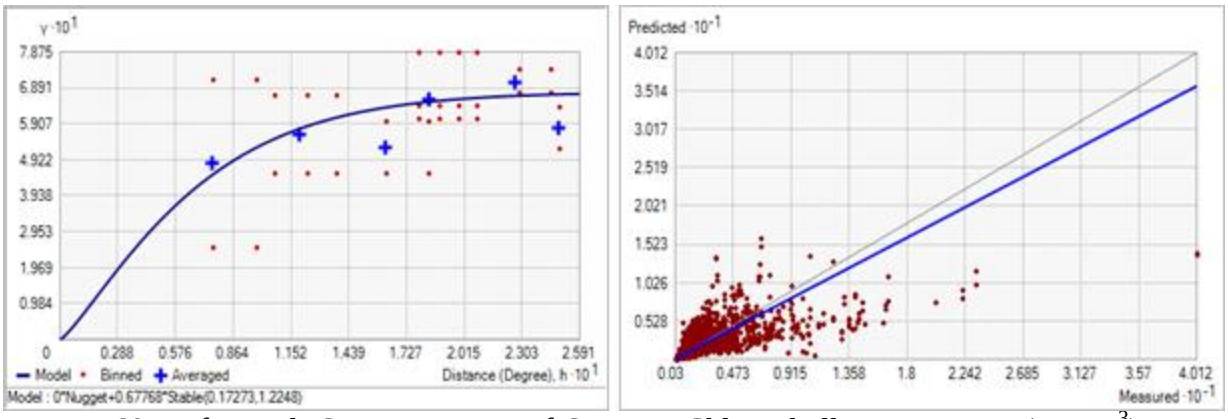

Figure 260. Left panel: Semivariogram of Summer Chlorophyll *a* Maximum (mg m^{-3}). Binned values are shown as red dots; average points are shown as blue crosses; the model fit to the averaged values is shown as a blue line. Lag size: 0.022 degrees; number of lags: 12; Parameter: 1.225; Range: 0.173 degrees; Partial Sill: 0.678. Right panel: Scatterplot of predicted values versus observed values for the variable Summer Chlorophyll *a* Maximum (mg m^{-3}).

Table 130. Results of cross-validation of the kriged model for Summer Chlorophyll *a* Maximum (mg m^{-3}).

Prediction error	**Value**
Number of Observations	17048
Overall Mean Error	4.148×10^{-5}
Root Mean Square Prediction Error	0.814
Standardized Mean	4.760×10^{-5}
Standardized Root Mean Square Prediction Error	1.137
Average Standard Error	0.715

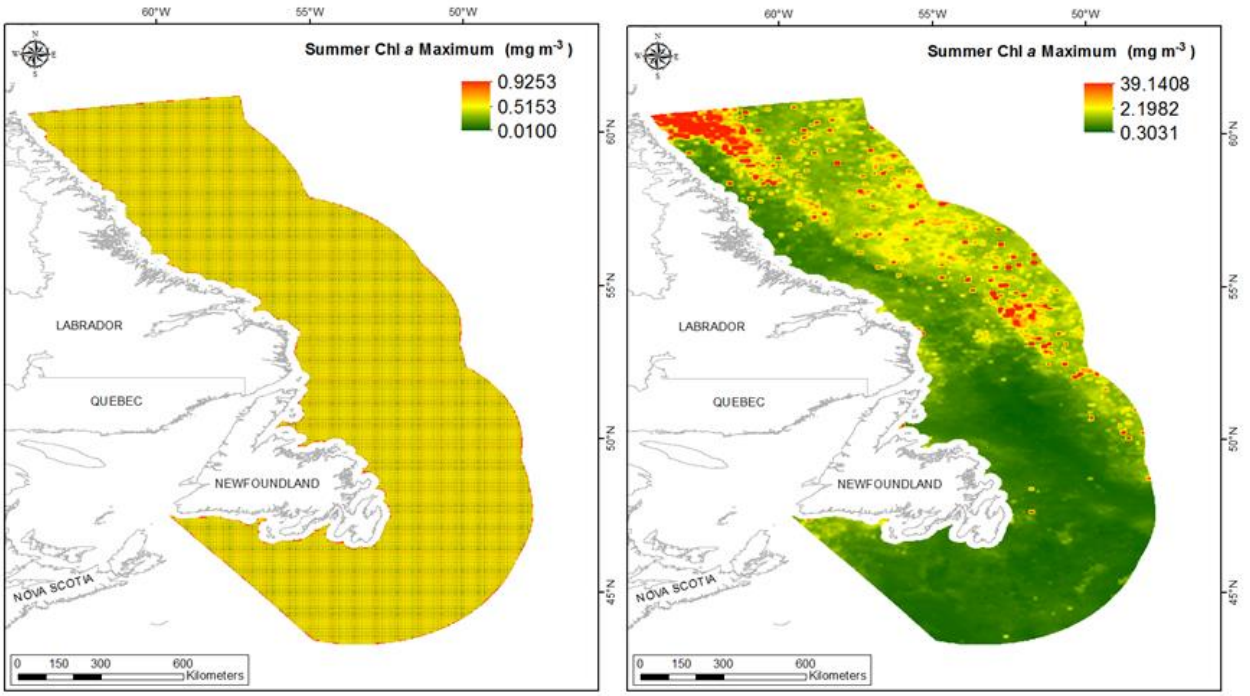

Figure 261. Left panel: Prediction standard error surface of Summer Chlorophyll *a* Maximum (mg m^{-3}). Right panel: Interpolated prediction surface of Summer Chlorophyll *a* Maximum (mg m^{-3}).

Summer Chlorophyll *a* Range

This variable displayed a right-skewed distribution with severe kurtosis and outlying data in the upper range (Table 131, Figure 262). The data were higher than predicted by a normal distribution at the upper range and slightly lower than predicted at mid values (Figure 263). The areas of under- and over-prediction showed spatial pattern over the spatial extent (Figure 263).

The semivariogram showed high autocorrelation present in the data and the model showed fair fit between measured and predicted values (Figure 264). The model showed fair cross-validation statistics (Table 132). The error map showed medium to high error in a grid-like pattern over the study extent (Figure 265). The kriged surface is presented in Figure 265.

Table 131. Distributional properties of Summer Chlorophyll *a* Range (mg m^{-3}).

Property	Value
Number of Observations	17048
Minimum	0.106
Maximum	39.311
Mean	0.949
Median	0.620
Standard Deviation	1.235
Skewness	8.913
Kurtosis	166.200

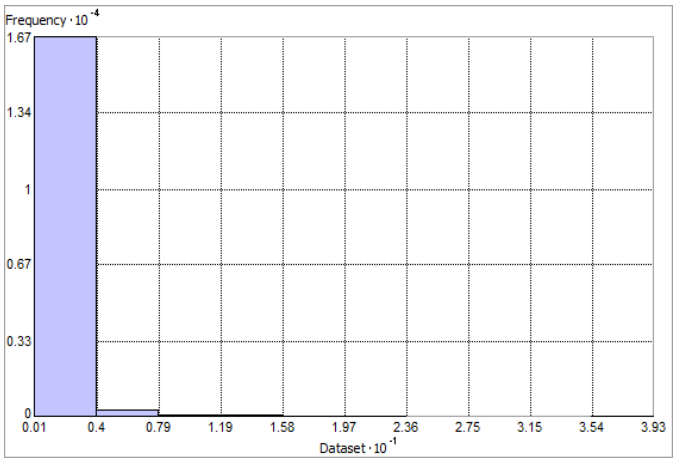

Figure 262. Distribution of Summer Chlorophyll *a* Range (mg m^{-3}). Histogram was illustrated using 10 bins. X axis is shown at 10^{-1}; Y axis is shown at 10^{-4}.

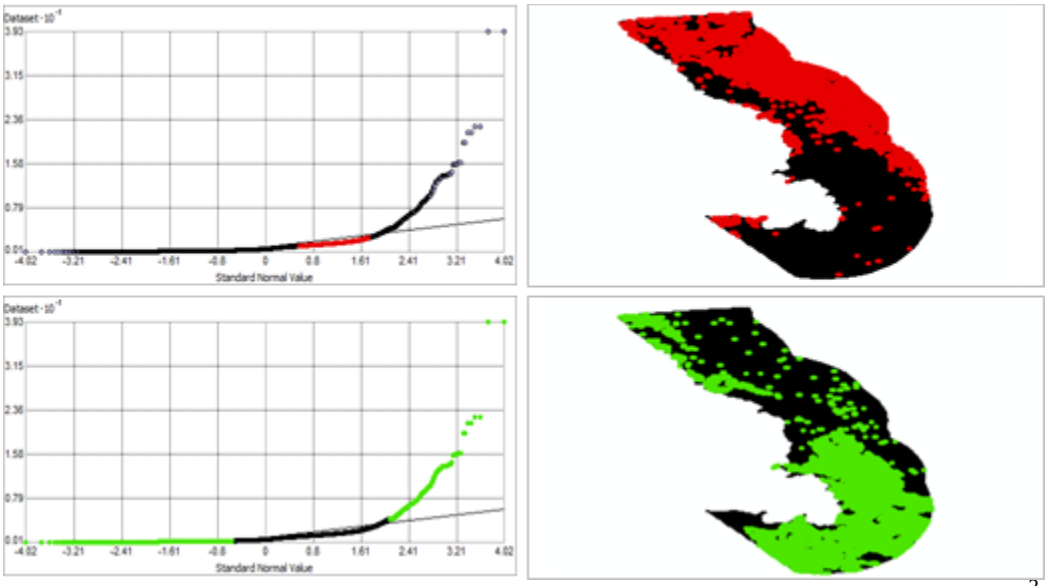

Figure 263. Normal Q-Q plot for data values of Summer Chlorophyll *a* Range (mg m^{-3}). Points falling under (upper panel) and over (bottom panel) the reference line are mapped.

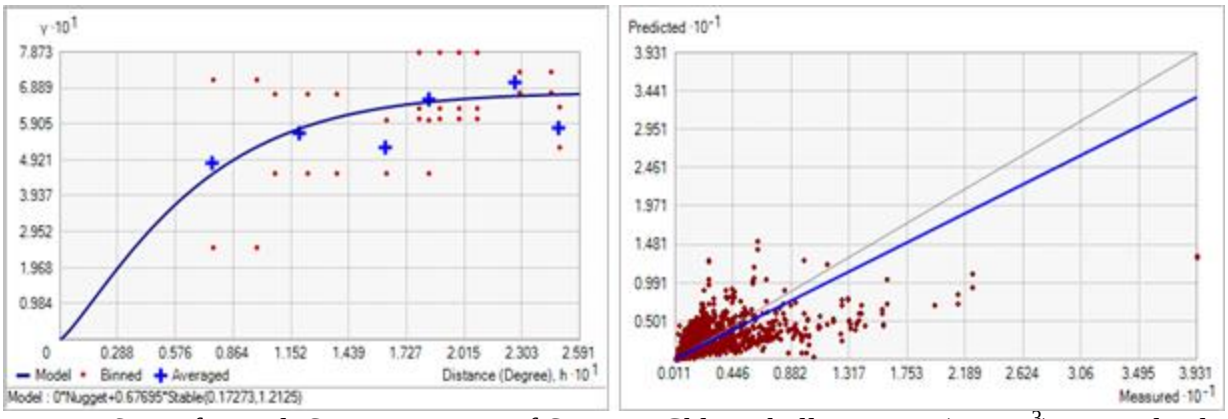

Figure 264. Left panel: Semivariogram of Summer Chlorophyll *a* Range (mg m^{-3}). Binned values are shown as red dots; average points are shown as blue crosses; the model fit to the averaged values is shown as a blue line. Lag size: 0.022 degrees; number of lags: 12; Parameter: 1.213; Range: 0.173 degrees; Partial Sill: 0.677. Right panel: Scatterplot of predicted values versus observed values for the variable Summer Chlorophyll *a* Range (mg m^{-3}).

Table 132. Results of cross-validation of the kriged model for Summer Chlorophyll *a* Range (mg m^{-3}).

Prediction error	**Value**
Number of Observations	17048
Overall Mean Error	9.347×10^{-5}
Root Mean Square Prediction Error	0.814
Standardized Mean	1.099×10^{-4}
Standardized Root Mean Square Prediction Error	1.135
Average Standard Error	0.717

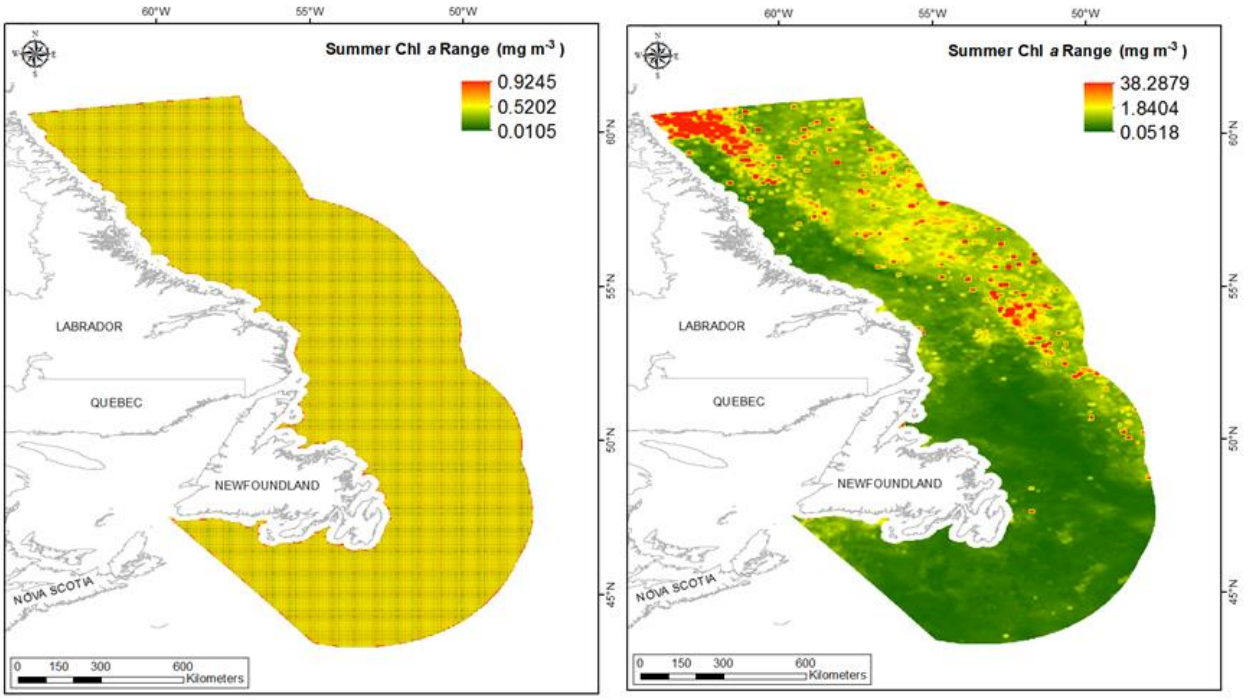

Figure 265. Left panel: Prediction standard error surface of Summer Chlorophyll *a* Range (mg m^{-3}). Right panel: Interpolated prediction surface of Summer Chlorophyll *a* Range (mg m^{-3}).

Fall Chlorophyll *a* Mean

This variable displayed a right-skewed distribution with kurtosis and several outlying points in the upper range (Table 133, Figure 266). The data were higher than predicted by a normal distribution at the upper values (Figure 267). The areas of over-prediction were more prevalent in the southern portion of the spatial extent (Figure 267).

The semivariogram showed weak autocorrelation present in the data and the model showed fair fit between measured and predicted values (Figure 268). The model showed fair cross-validation statistics (Table 134). The error map showed low error in a slight linear pattern over the study extent except for some areas along the coast where it was high (Figure 269). The kriged surface is presented in Figure 269.

Table 133. Distributional properties of Fall Chlorophyll *a* Mean (mg m^{-3}).

Property	Value
Number of Observations	17048
Minimum	0.375
Maximum	4.712
Mean	0.691
Median	0.671
Standard Deviation	0.137
Skewness	5.037
Kurtosis	107.500

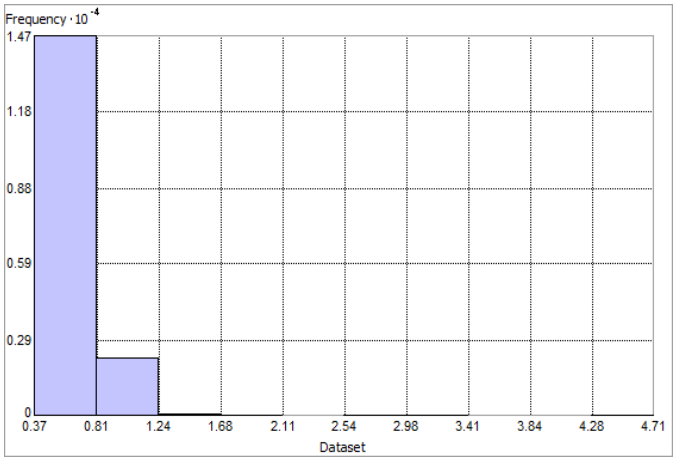

Figure 266. Distribution of Fall Chlorophyll *a* Mean (mg m^{-3}). Histogram was illustrated using 10 bins. Y axis is shown at 10^{-4}.

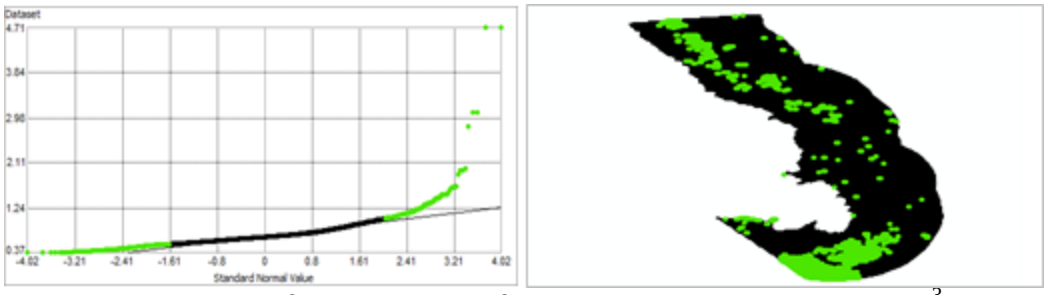

Figure 267. Normal Q-Q plot for data values of Fall Chlorophyll *a* Mean (mg m^{-3}). Points falling over (bottom panel) the reference line are mapped.

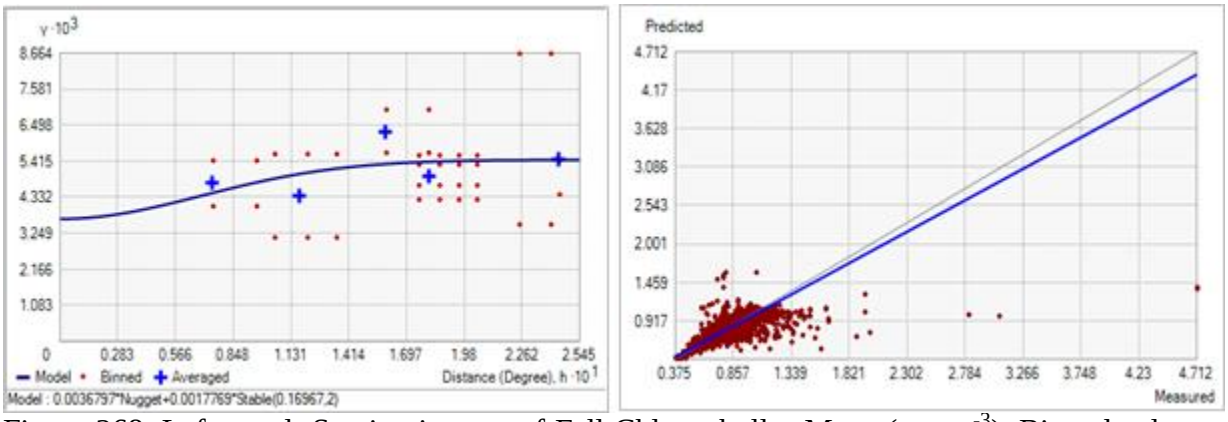

Figure 268. Left panel: Semivariogram of Fall Chlorophyll *a* Mean (mg m^{-3}). Binned values are shown as red dots; average points are shown as blue crosses; the model fit to the averaged values is shown as a blue line. Lag size: 0.021 degrees; number of lags: 12; Parameter: 2; Range: 0.170 degrees; Partial Sill: 1.777 x 10^{-3}. Right panel: Scatterplot of predicted values versus observed values for the variable Fall Chlorophyll *a* Mean (mg m^{-3}).

Table 134. Results of cross-validation of the kriged model for Fall Chlorophyll *a* Mean (mg m^{-3}).

Prediction error	Value
Number of Observations	17048
Overall Mean Error	-1.355×10^{-4}
Root Mean Square Prediction Error	0.073
Standardized Mean	-1.754×10^{-3}
Standardized Root Mean Square Prediction Error	1.028
Average Standard Error	0.071

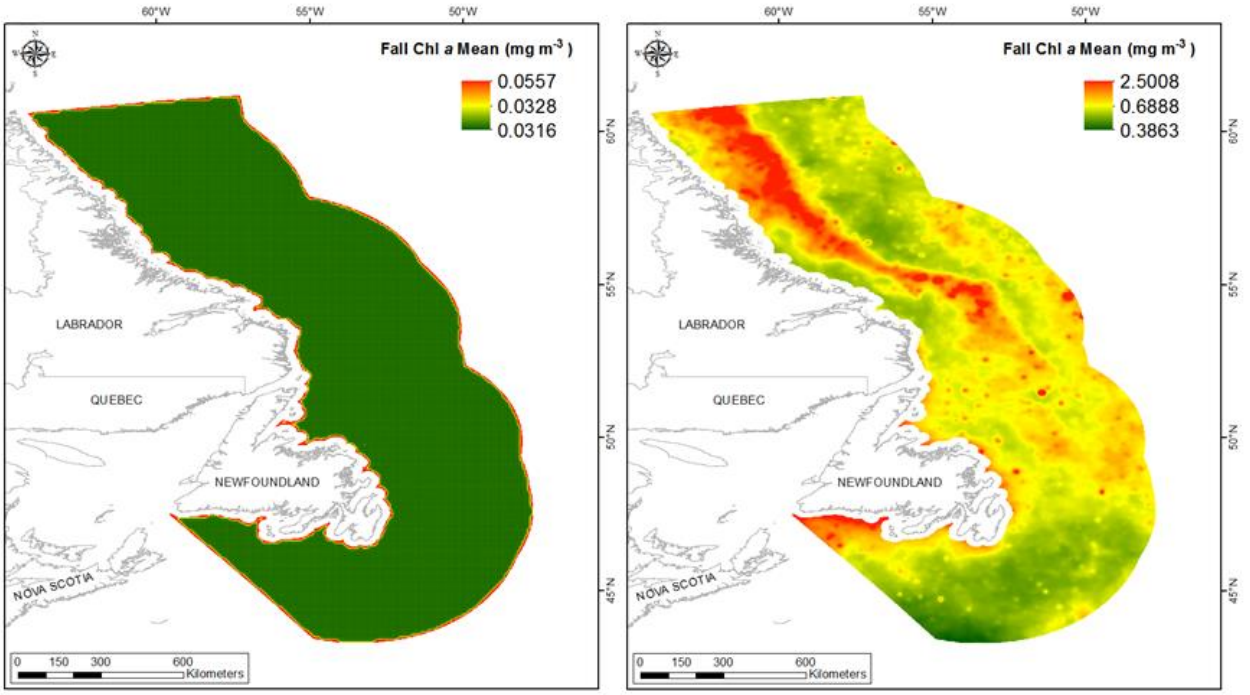

Figure 269. Left panel: Prediction standard error surface of Fall Chlorophyll *a* Mean (mg m^{-3}). Right panel: Interpolated prediction surface of Fall Chlorophyll *a* Mean (mg m^{-3}).

Fall Chlorophyll *a* Minimum

This variable displayed a near normal distribution prior to modeling (Table 135, Figure 270). The data were higher than predicted by a normal distribution at the high values (Figure 271). The areas of over-prediction showed no spatial pattern over the spatial extent (Figure 271).

The semivariogram showed autocorrelation present in the data and the model showed a good fit between measured and predicted values (Figure 272). The model showed good cross-validation statistics (Table 136) indicating that it was good at prediction. The error map showed medium to high error in a grid-like pattern over the study extent (Figure 273). The kriged surface is presented in Figure 273.

Table 135. Distributional properties of Fall Chlorophyll *a* Minimum (mg m^{-3}).

Property	Value
Number of Observations	17048
Minimum	0.139
Maximum	0.795
Mean	0.367
Median	0.366
Standard Deviation	0.077
Skewness	0.303
Kurtosis	3.612

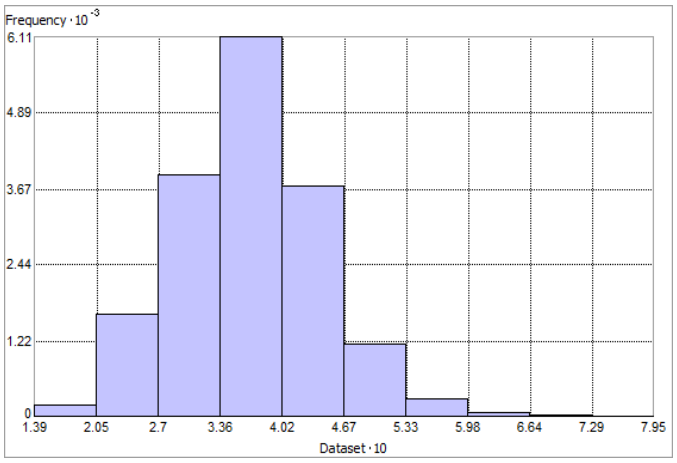

Figure 270. Distribution of Fall Chlorophyll *a* Minimum (mg m^{-3}). Histogram was illustrated using 10 bins. X axis is shown at 10; Y axis is shown at 10^{-3}.

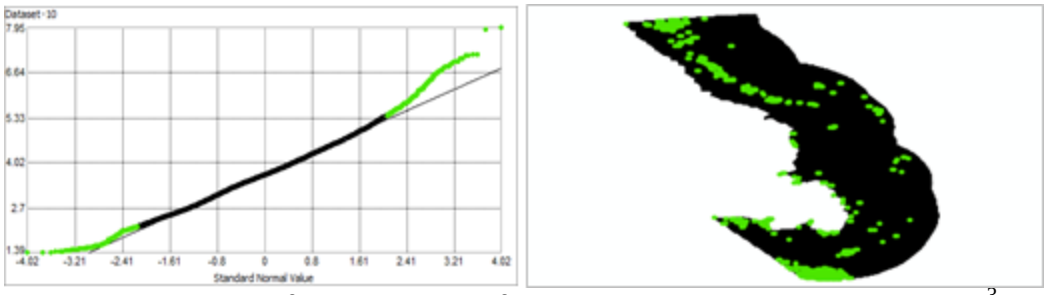

Figure 271. Normal Q-Q plot for data values of Fall Chlorophyll *a* Minimum (mg m^{-3}). Points falling over (bottom panel) the reference line are mapped.

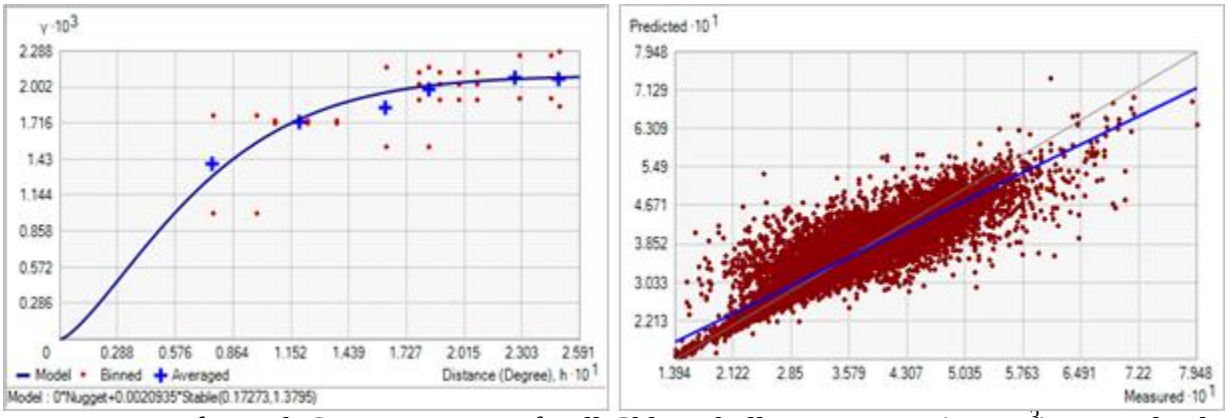

Figure 272. Left panel: Semivariogram of Fall Chlorophyll *a* Minimum (mg m^{-3}). Binned values are shown as red dots; average points are shown as blue crosses; the model fit to the averaged values is shown as a blue line. Lag size: 0.022 degrees; number of lags: 12; Parameter: 1.379; Range: 0.173 degrees; Partial Sill: 2.094 x 10^{-3}. Right panel: Scatterplot of predicted values versus observed values for the variable Fall Chlorophyll *a* Minimum (mg m^{-3}).

Table 136. Results of cross-validation of the kriged model for Fall Chlorophyll *a* Minimum (mg m^{-3}).

Prediction error	**Value**
Number of Observations	17048
Overall Mean Error	-6.308×10^{-5}
Root Mean Square Prediction Error	0.036
Standardized Mean	-1.359×10^{-3}
Standardized Root Mean Square Prediction Error	0.962
Average Standard Error	0.038

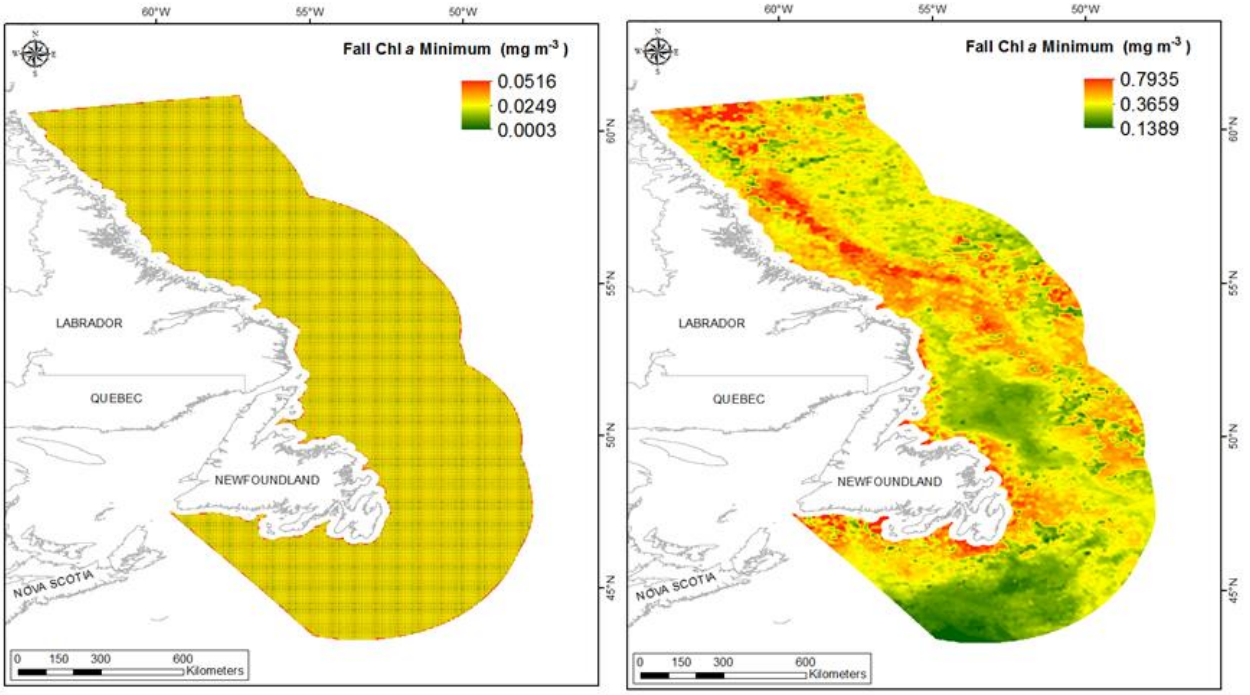

Figure 273. Left panel: Prediction standard error surface of Fall Chlorophyll *a* Minimum (mg m^{-3}). Right panel: Interpolated prediction surface of Fall Chlorophyll *a* Minimum (mg m^{-3}).

Fall Chlorophyll *a* Maximum

This variable displayed a right-skewed distribution with extreme kurtosis and several outlying points in the upper range (Table 137, Figure 274). The data were higher than predicted by a normal distribution at the upper range and lower than predicted at mid values (Figure 275). The areas of under- and over-prediction showed no spatial pattern over the spatial extent (Figure 275).

The semivariogram showed weak autocorrelation present in the data and the model showed a very poor fit between measured and predicted values (Figure 276). Nevertheless, the model

showed fair cross-validation statistics (Table 138). The error map showed medium to high error in a grid-like pattern over the study extent (Figure 277). The kriged surface is presented in Figure 277.

Table 137. Distributional properties of Fall Chlorophyll *a* Maximum (mg m^{-3}).

Property	Value
Number of Observations	17048
Minimum	0.624
Maximum	49.819
Mean	1.414
Median	1.199
Standard Deviation	1.226
Skewness	19.468
Kurtosis	623.500

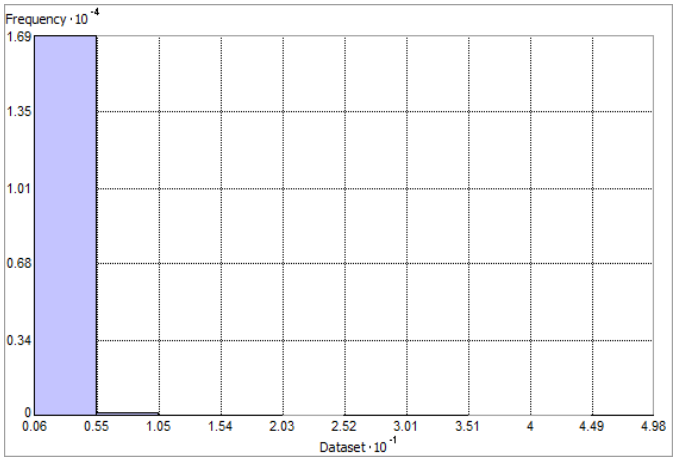

Figure 274. Distribution of Fall Chlorophyll *a* Maximum (mg m^{-3}). Histogram was illustrated using 10 bins. X axis is shown at 10^{-1}; Y axis is shown at 10^{-4}.

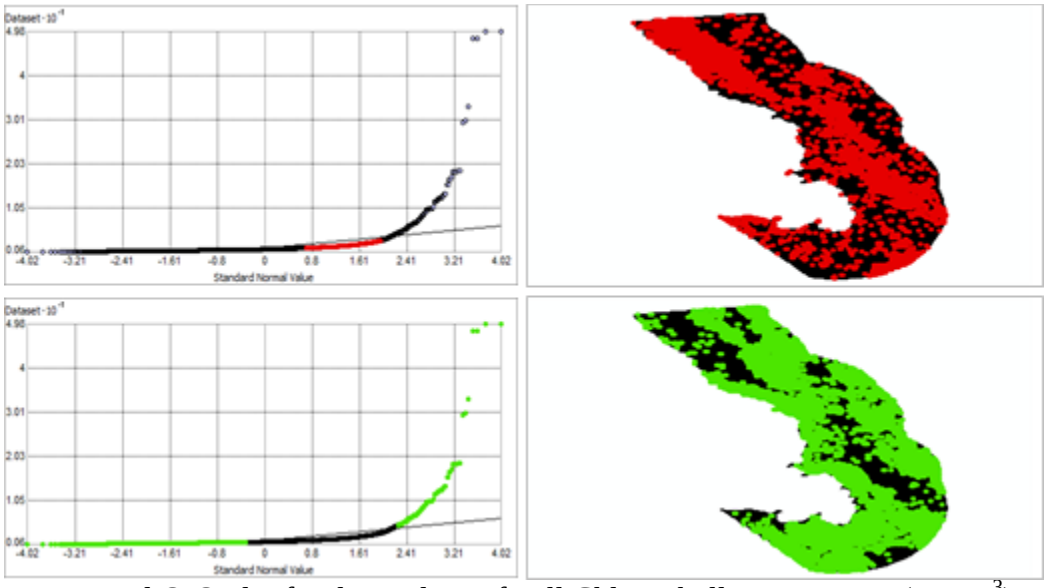

Figure 275. Normal Q-Q plot for data values of Fall Chlorophyll *a* Maximum (mg m^{-3}). Points falling under (upper panel) and over (bottom panel) the reference line are mapped.

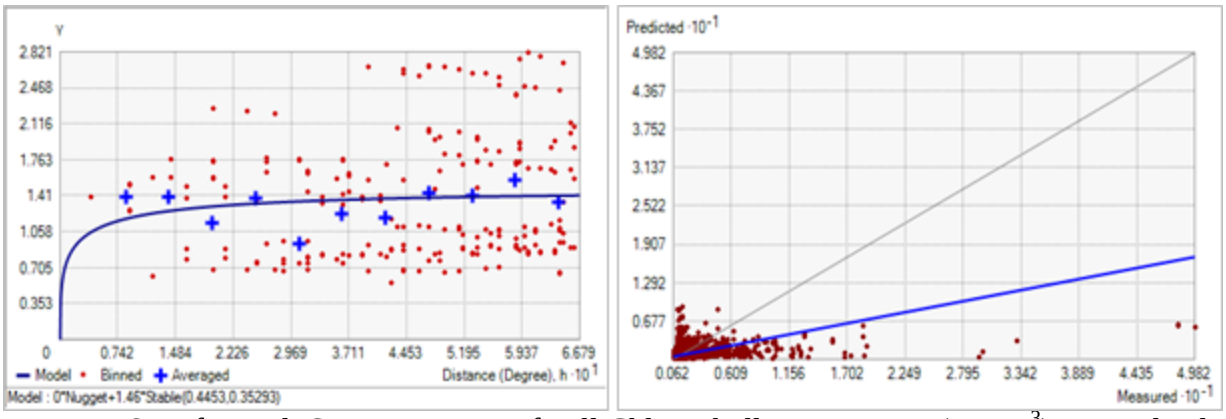

Figure 276. Left panel: Semivariogram of Fall Chlorophyll *a* Maximum (mg m^{-3}). Binned values are shown as red dots; average points are shown as blue crosses; the model fit to the averaged values is shown as a blue line. Lag size: 0.056 degrees; number of lags: 12; Parameter: 0.353; Range: 0.445 degrees; Partial Sill: 1.460. Right panel: Scatterplot of predicted values versus observed values for the variable Fall Chlorophyll *a* Maximum (mg m^{-3}).

Table 138. Results of cross-validation of the kriged model for Fall Chlorophyll *a* Maximum (mg m^{-3}).

Prediction error	**Value**
Number of Observations	17048
Overall Mean Error	3.565×10^{-4}
Root Mean Square Prediction Error	1.140
Standardized Mean	2.996×10^{-4}
Standardized Root Mean Square Prediction Error	1.008
Average Standard Error	1.131

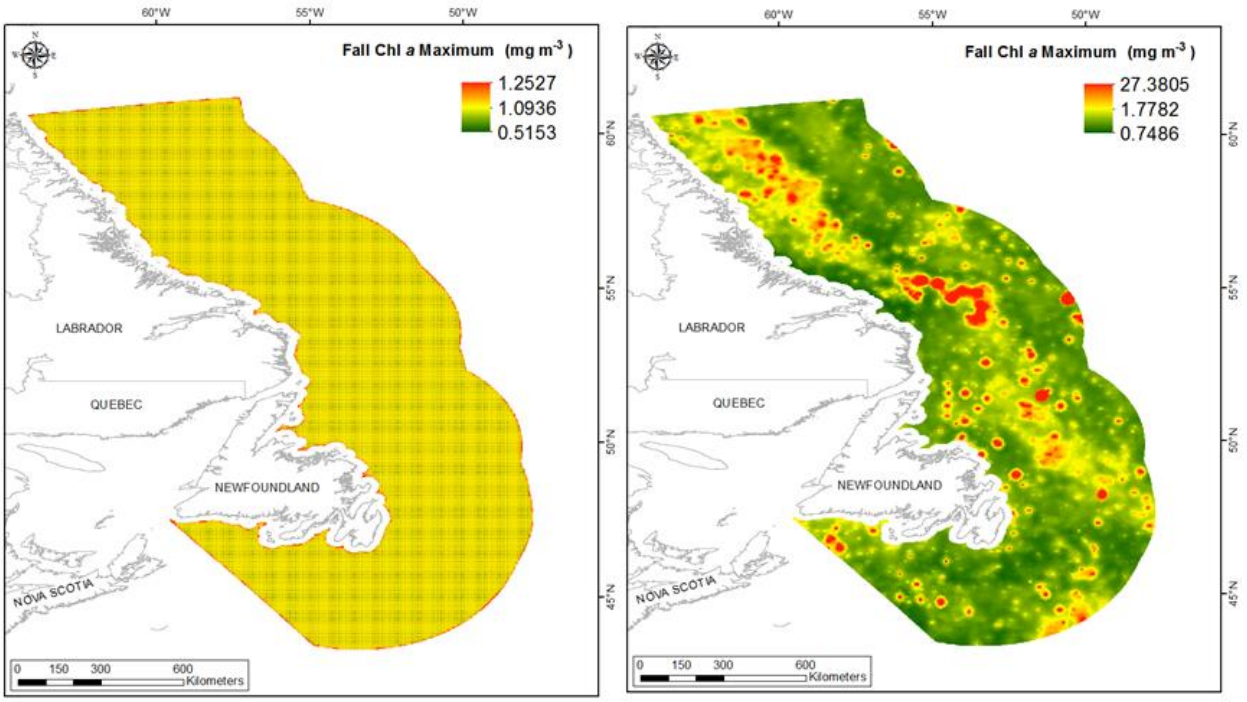

Figure 277. Left panel: Prediction standard error surface of Fall Chlorophyll *a* Maximum (mg m^{-3}). Right panel: Interpolated prediction surface of Fall Chlorophyll *a* Maximum (mg m^3).

Fall Chlorophyll *a* Range

This variable displayed a strongly right-skewed distribution with extreme kurtosis and several outlying points in the upper range prior to modeling (Table 139, Figure 278). The data were higher than predicted by a normal distribution at the upper range and lower than predicted at mid values (Figure 279). The areas of under- and over-prediction showed no strong spatial pattern over the spatial extent (Figure 279).

The semivariogram showed moderate autocorrelation present in the data and the model showed a poor fit between measured and predicted values (Figure 280). The model showed good cross-validation statistics (Table 140) indicating that it was good at prediction. The error map showed medium to high error in a grid-like pattern over the study extent (Figure 281). The kriged surface is presented in Figure 281.

Table 139. Distributional properties of Fall Chlorophyll *a* Range (mg m^{-3}).

Property	Value
Number of Observations	17048
Minimum	0.200
Maximum	49.522
Mean	1.046
Median	0.839
Standard Deviation	1.223
Skewness	19.563
Kurtosis	628.340

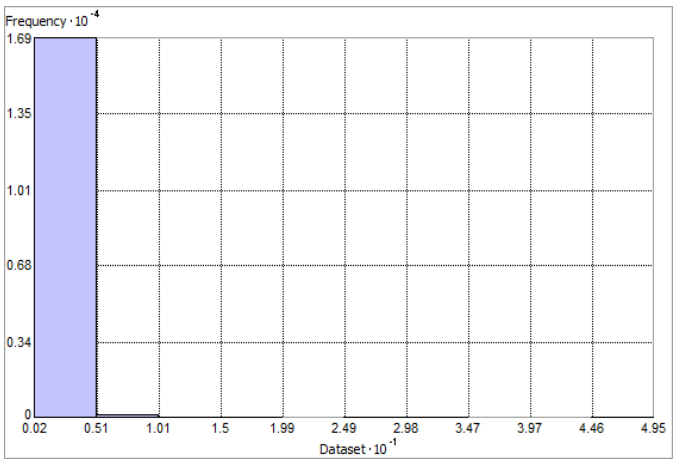

Figure 278. Distribution of Fall Chlorophyll *a* Range (mg m^{-3}). Histogram was illustrated using 10 bins. X and Y axes are shown at 10^{-1} and 10^{-4} respectively.

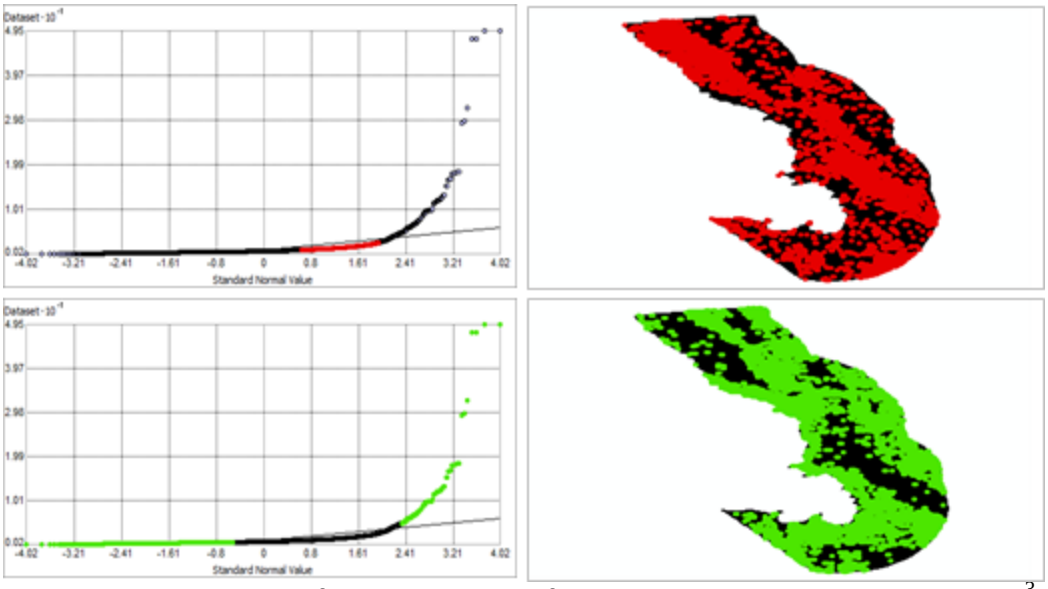

Figure 279. Normal Q-Q plot for data values of Fall Chlorophyll *a* Range (mg m^{-3}). Points falling under (upper panel) and over (bottom panel) the reference line are mapped.

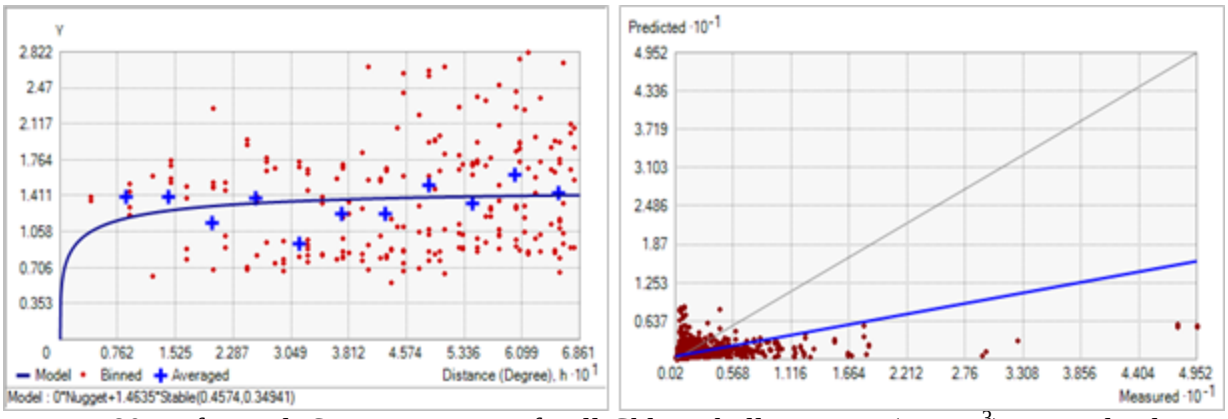

Figure 280. Left panel: Semivariogram of Fall Chlorophyll *a* Range (mg m^{-3}). Binned values are shown as red dots; average points are shown as blue crosses; the model fit to the averaged values is shown as a blue line. Lag size: 0.057 degrees; number of lags: 12; Parameter: 0.349; Range: 0.457 degrees; Partial Sill: 1.463. Right panel: Scatterplot of predicted values versus observed values for the variable Fall Chlorophyll *a* Range (mg m^{-3}).

Table 140. Results of cross-validation of the kriged model for Fall Chlorophyll *a* Range (mg m^{-3}).

Prediction error	**Value**
Number of Observations	17048
Overall Mean Error	4.662×10^{-4}
Root Mean Square Prediction Error	1.141
Standardized Mean	3.905×10^{-4}
Standardized Root Mean Square Prediction Error	1.008
Average Standard Error	1.131

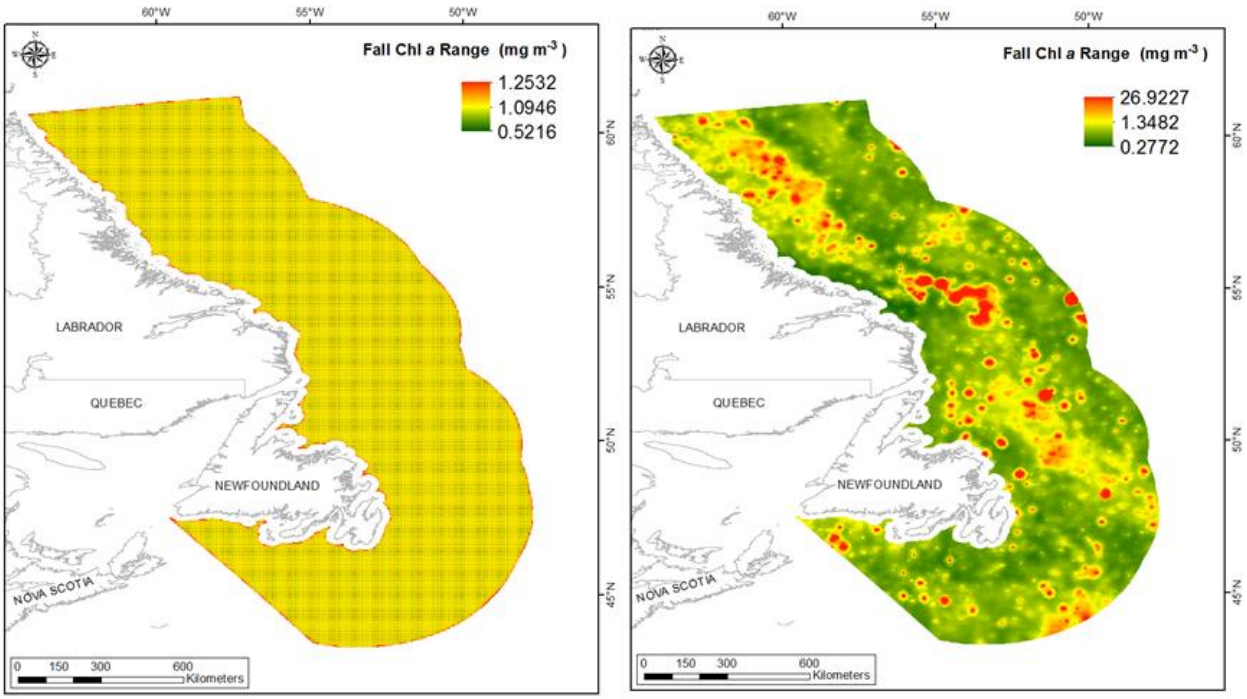

Figure 281. Left panel: Prediction standard error surface of Fall Chlorophyll *a* Range (mg m^{-3}). Right panel: Interpolated prediction surface of Fall Chlorophyll *a* Range (mg m^{-3}).

Annual Chlorophyll *a* Mean

This variable displayed a right-skewed distribution with kurtosis prior to modeling (Table 141, Figure 282). The data were higher than predicted by a normal distribution at the upper and lower range and lower than predicted at mid values (Figure 283). The areas of under- and over-prediction showed no strong spatial pattern over the spatial extent (Figure 283).

The semivariogram showed weak autocorrelation present in the data and the model showed a moderate fit between measured and predicted values (Figure 284). The model showed fair cross-validation statistics (Table 142). The error map showed relatively moderate error in a grid-like pattern over the study extent (Figure 285). The kriged surface is presented in Figure 285.

Table 141. Distributional properties of Annual Chlorophyll *a* Mean (mg m^{-3}).

Property	Value
Number of Observations	17048
Minimum	0.551
Maximum	2.860
Mean	0.806
Median	0.780
Standard Deviation	0.162
Skewness	3.102
Kurtosis	23.397

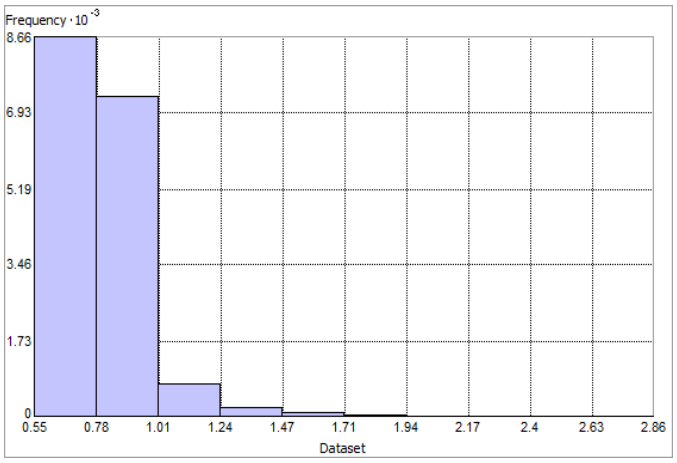

Figure 282. Distribution of Annual Chlorophyll *a* Mean (mg m^{-3}). Histogram was illustrated using 10 bins. Y axis is shown at 10^{-3}.

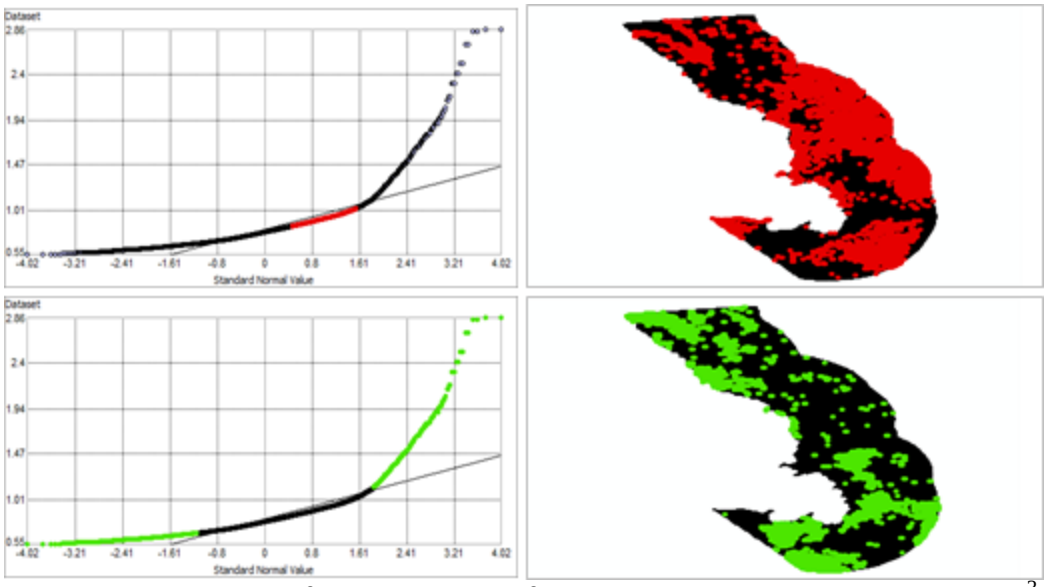

Figure 283. Normal Q-Q plot for data values of Annual Chlorophyll *a* Mean (mg m^{-3}). Points falling under (upper panel) and over (bottom panel) the reference line are mapped.

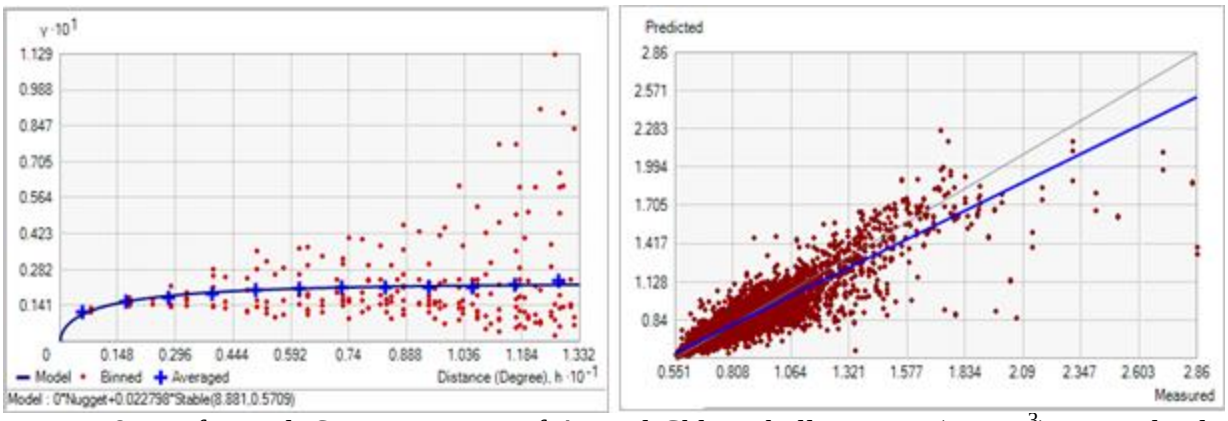

Figure 284. Left panel: Semivariogram of Annual Chlorophyll *a* Mean (mg m^{-3}). Binned values are shown as red dots; average points are shown as blue crosses; the model fit to the averaged values is shown as a blue line. Lag size: 1.110 degrees; number of lags: 12; Parameter: 0.571; Range: 8.881 degrees; Partial Sill: 0.023. Right panel: Scatterplot of predicted values versus observed values for the variable Annual Chlorophyll *a* Mean (mg m^{-3}).

Table 142. Results of cross-validation of the kriged model for Annual Chlorophyll *a* Mean (mg m^{-3}).

Prediction error	**Value**
Number of Observations	17048
Overall Mean Error	-3.757×10^{-5}
Root Mean Square Prediction Error	0.071
Standardized Mean	-2.70×10^{-4}
Standardized Root Mean Square Prediction Error	1.064
Average Standard Error	0.067

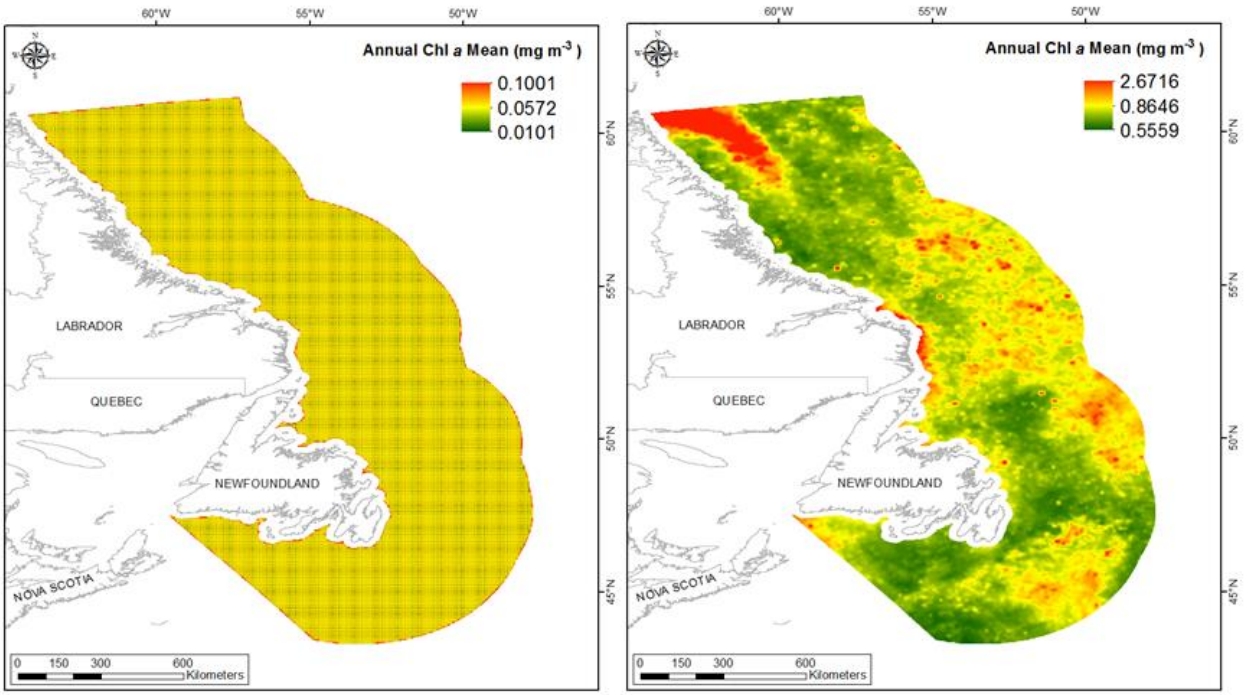

Figure 285. Left panel: Prediction standard error surface of Annual Chlorophyll *a* Mean (mg m^{-3}). Right panel: Interpolated prediction surface of Annual Chlorophyll *a* Mean (mg m^{-3}).

Annual Chlorophyll *a* Minimum

This variable displayed a bell-shaped distribution with right-skewness prior to modeling (Table 143, Figure 286). The data were higher than predicted by a normal distribution at the upper and lower range values (Figure 287). The areas of over-prediction showed spatial bias towards the northern portion of the spatial extent (Figure 287).

The semivariogram showed high autocorrelation present in the data and the model showed a good fit between measured and predicted values (Figure 288). The model showed good cross-validation statistics (Table 144) indicating that it was good at prediction. The error map showed relatively moderate error in a grid-like pattern over the study extent (Figure 289). The kriged surface is presented in Figure 289.

Table 143. Distributional properties of Annual Chlorophyll *a* Minimum (mg m^{-3}).

Property	Value
Number of Observations	17048
Minimum	0.037
Maximum	0.576
Mean	0.211
Median	0.204
Standard Deviation	0.061
Skewness	0.596
Kurtosis	3.576

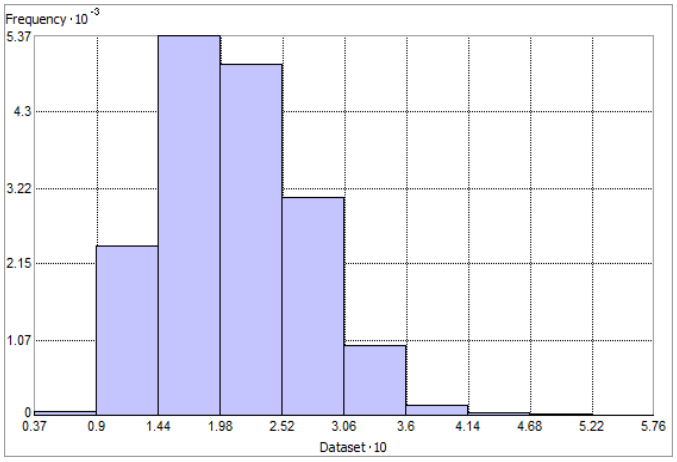

Figure 286. Distribution of Annual Chlorophyll *a* Minimum (mg m^{-3}). Histogram was illustrated using 10 bins. X and Y axes are shown at 10 and 10^{-3} respectively.

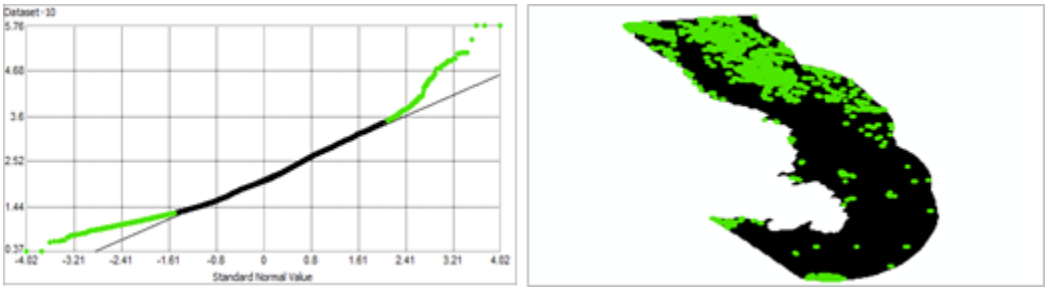

Figure 287. Normal Q-Q plot for data values of Annual Chlorophyll *a* Minimum (mg m^{-3}). Points falling over (bottom panel) the reference line are mapped.

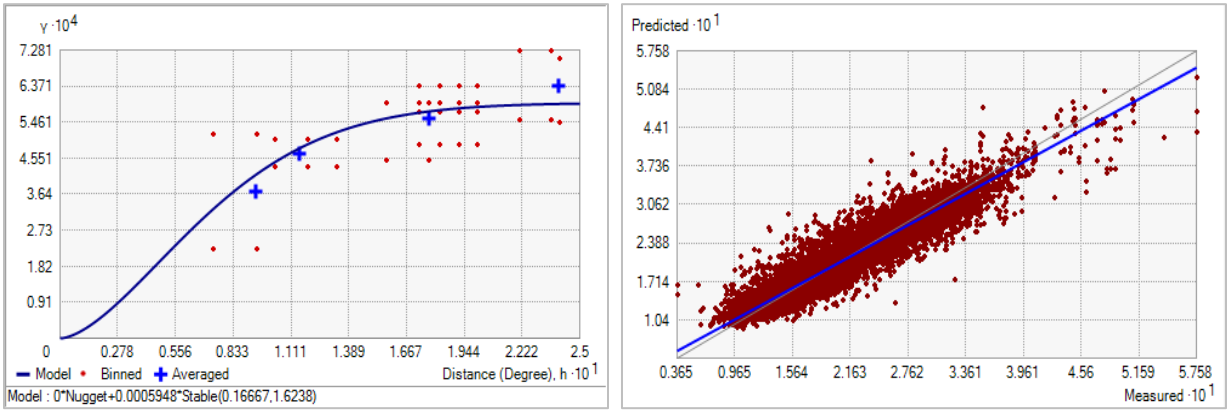

Figure 288. Left panel: Semivariogram of Annual Chlorophyll *a* Minimum (mg m^{-3}). Binned values are shown as red dots; average points are shown as blue crosses; the model fit to the averaged values is shown as a blue line. Lag size: 0.021 degrees; number of lags: 12; Parameter:

1.624; Range: 0.167 degrees; Partial Sill: 5.948 x 10^{-4}. Right panel: Scatterplot of predicted values versus observed values for the variable Annual Chlorophyll *a* Minimum (mg m^{-3}).
Table 144. Results of cross-validation of the kriged model for Annual Chlorophyll *a* Minimum (mg m^{-3}).

Prediction error	Value
Number of Observations	17048
Overall Mean Error	-6.325 x 10^{-6}
Root Mean Square Prediction Error	0.020
Standardized Mean	-1.508 x 10^{-4}
Standardized Root Mean Square Prediction Error	1.063
Average Standard Error	0.019

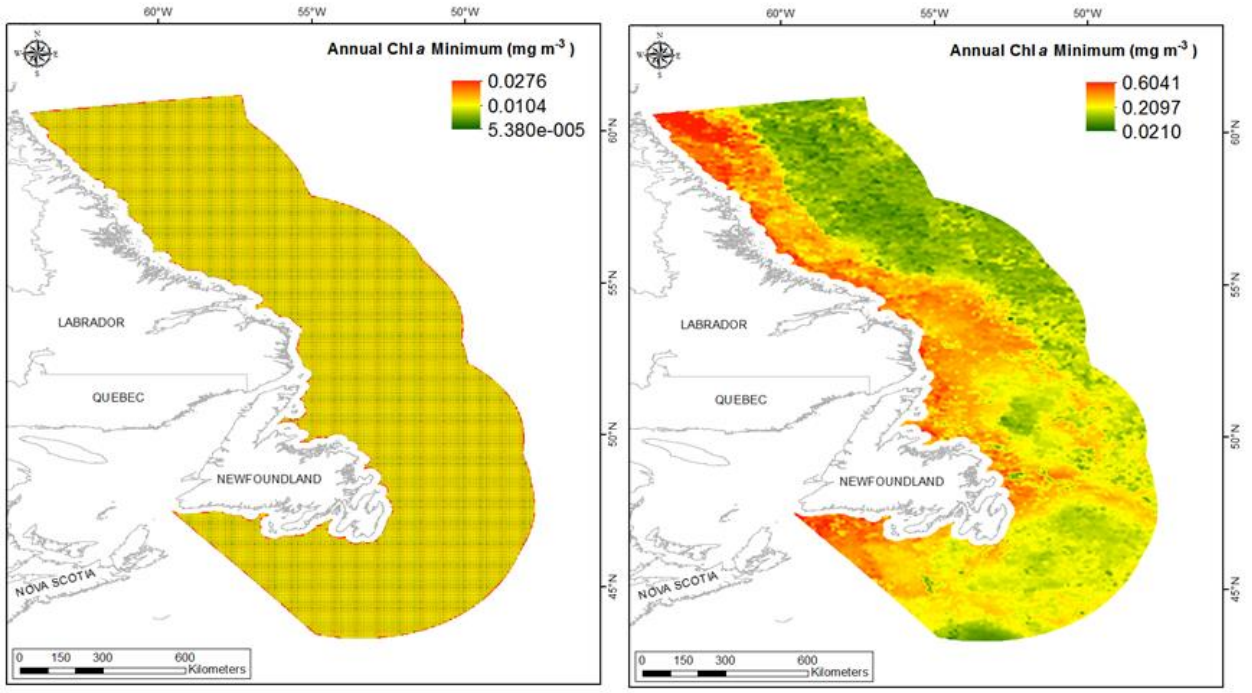

Figure 289. Left panel: Prediction standard error surface of Annual Chlorophyll *a* Minimum (mg m^{-3}). Right panel: Interpolated prediction surface of Annual Chlorophyll *a* Minimum (mg m^{-3}).

Annual Chlorophyll *a* Maximum

This variable displayed a strongly right-skewed distribution with kurtosis prior to modeling (Table 145, Figure 290). The data were higher than predicted by a normal distribution at the upper range and lower than predicted at mid values (Figure 291). The areas of under- and over-prediction showed no strong spatial pattern over the spatial extent (Figure 291).

The semivariogram showed weak autocorrelation present in the data and the model showed a poor fit between measured and predicted values (Figure 292). The model showed moderate

cross-validation statistics (Table 146). The error map showed low error in a grid-like pattern over the study extent (Figure 293). The kriged surface is presented in Figure 293.

Table 145. Distributional properties of Annual Chlorophyll *a* Maximum (mg m^{-3}).

Property	Value
Number of Observations	17048
Minimum	1.156
Maximum	85.393
Mean	5.324
Median	4.163
Standard Deviation	4.357
Skewness	5.555
Kurtosis	63.275

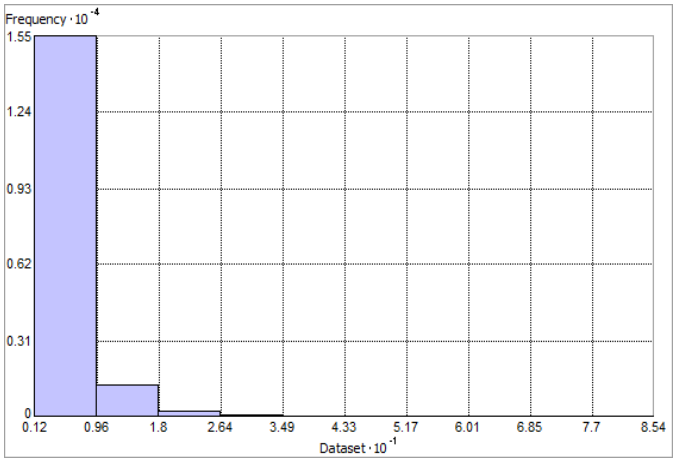

Figure 290. Distribution of Annual Chlorophyll *a* Maximum (mg m^{-3}). Histogram was illustrated using 10 bins. X and Y axes are shown at 10^{-1} and 10^{-4} respectively.

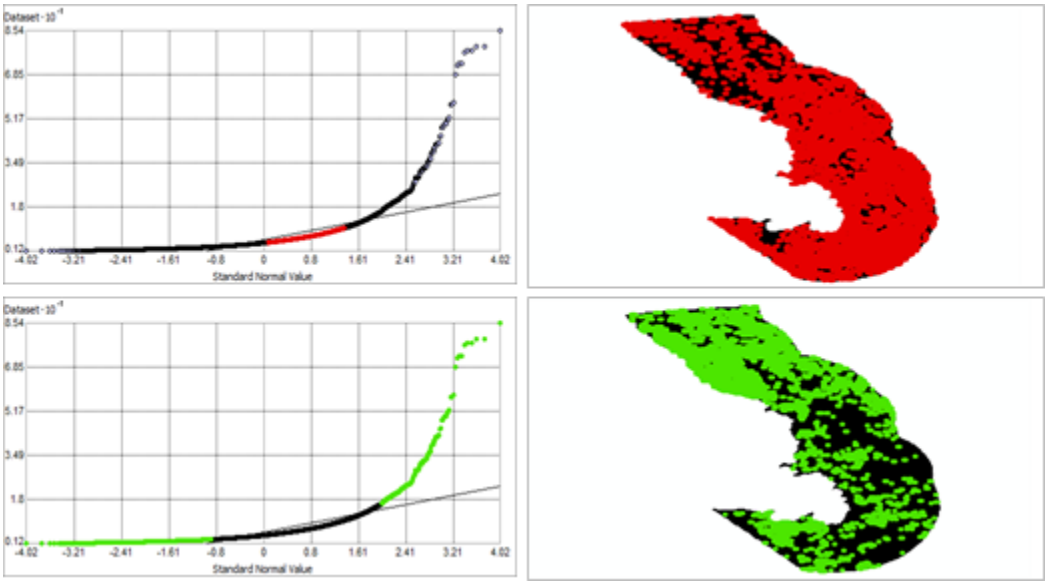

Figure 291. Normal Q-Q plot for data values of Annual Chlorophyll *a* Maximum (mg m^{-3}). Points falling under (upper panel) and over (bottom panel) the reference line are mapped.

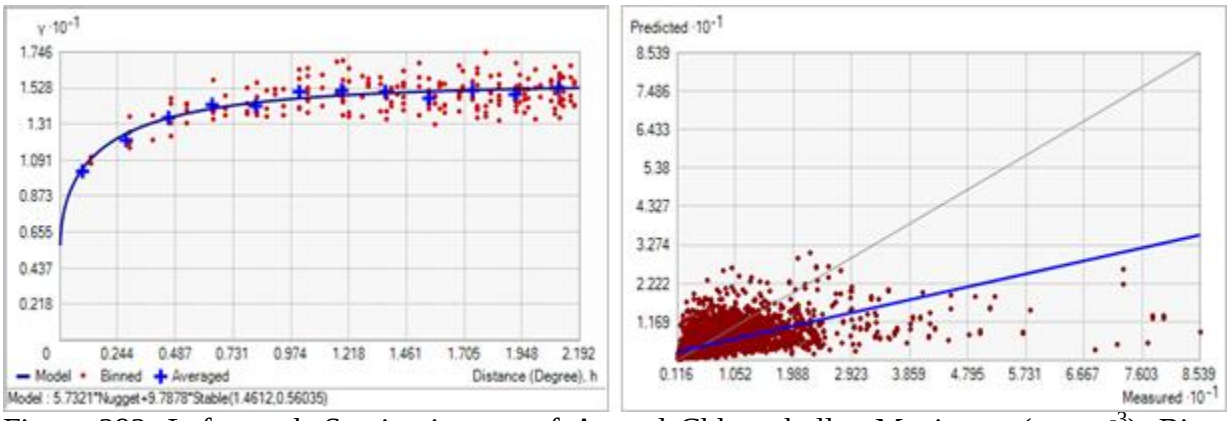

Figure 292. Left panel: Semivariogram of Annual Chlorophyll *a* Maximum (mg m^{-3}). Binned values are shown as red dots; average points are shown as blue crosses; the model fit to the averaged values is shown as a blue line. Lag size: 0.183 degrees; number of lags: 12; Parameter: 0.560; Range: 1.461 degrees; Partial Sill: 9.788. Right panel: Scatterplot of predicted values versus observed values for the variable Annual Chlorophyll *a* Maximum (mg m^{-3}).

Table 146. Results of cross-validation of the kriged model for Annual Chlorophyll *a* Maximum (mg m^{-3}).

Prediction error	**Value**
Number of Observations	17048
Overall Mean Error	9.288×10^{-4}
Root Mean Square Prediction Error	3.579
Standardized Mean	2.669×10^{-4}
Standardized Root Mean Square Prediction Error	1.080
Average Standard Error	3.315

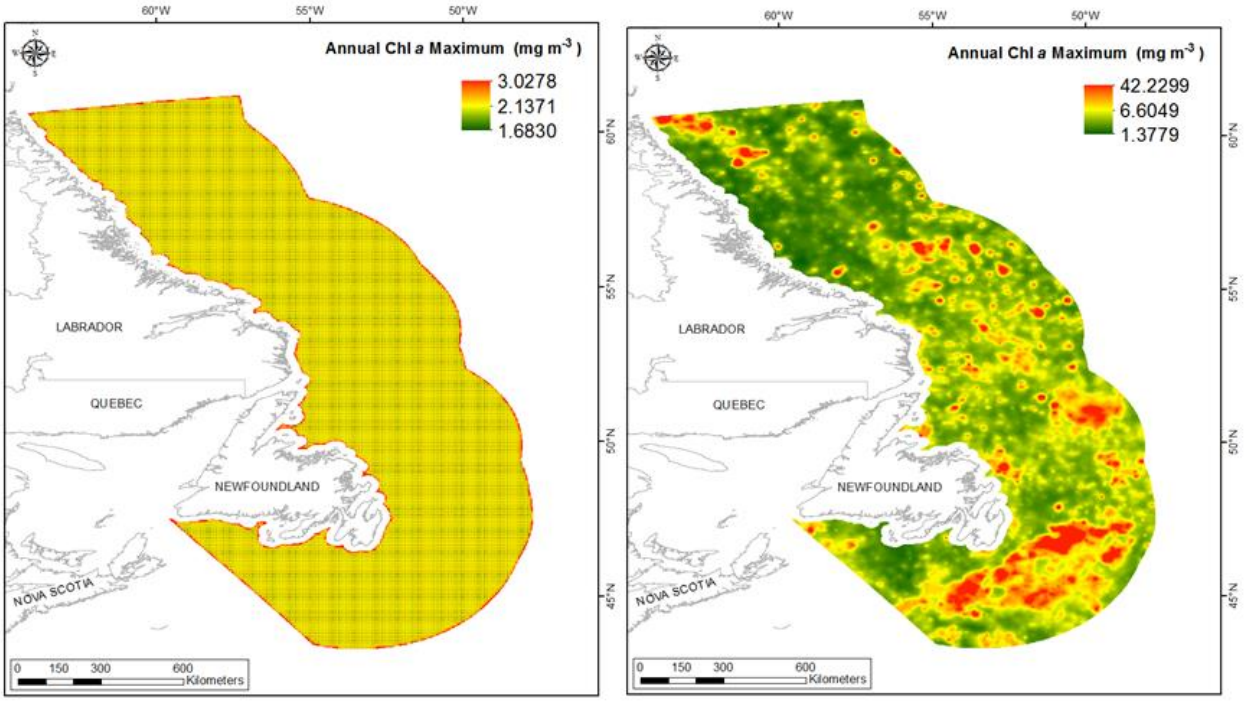

Figure 293. Left panel: Prediction standard error surface of Annual Chlorophyll *a* Maximum (mg m^{-3}). Right panel: Interpolated prediction surface of Annual Chlorophyll *a* Maximum (mg m^{-3}).

Annual Chlorophyll *a* Range

This variable displayed a right-skewed distribution with kurtosis and outlying data in the upper range (Table 147, Figure 294). The data were higher than predicted by a normal distribution at the upper range and lower than predicted at mid values (Figure 295). The areas of under- and over-prediction showed no strong spatial pattern over the spatial extent with most areas showing bias (Figure 295).

The semivariogram showed weak autocorrelation present in the data and the model showed poor fit between measured and predicted values (Figure 296). The model showed fair cross-validation statistics (Table 148). The error map showed medium to high error in a grid-like pattern over the study extent (Figure 297). The kriged surface is presented in Figure 297.

Table 147. Distributional properties of Annual Chlorophyll *a* Range (mg m^{-3}).

Property	Value
Number of Observations	17048
Minimum	0.814
Maximum	85.120
Mean	5.113
Median	3.950
Standard Deviation	4.356
Skewness	5.556
Kurtosis	63.263

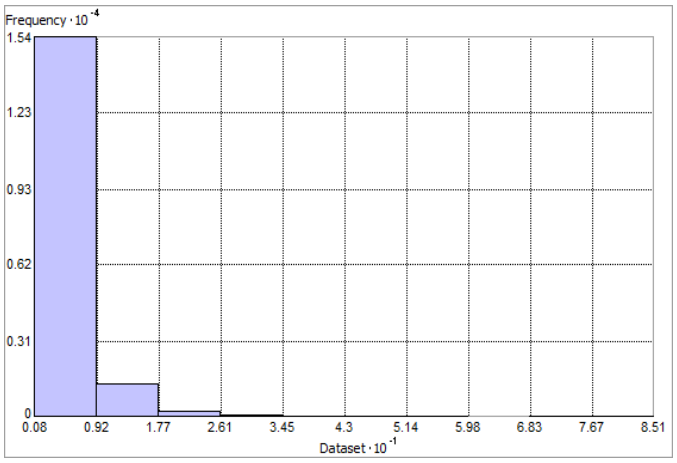

Figure 294. Distribution of Annual Chlorophyll *a* Range (mg m^{-3}). Histogram was illustrated using 10 bins. X axis is shown at 10^{-1}; Y axis is shown at 10^{-4}.

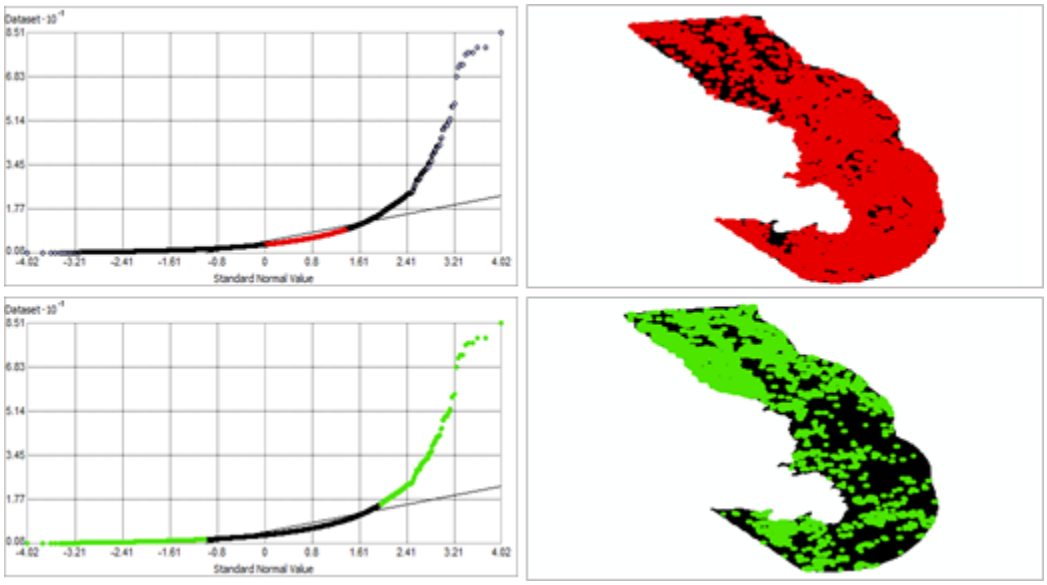

Figure 295. Normal Q-Q plot for data values of Case I Annual Chlorophyll *a* Range (mg m^{-3}). Points falling under (upper panel) and over (bottom panel) the reference line are mapped.

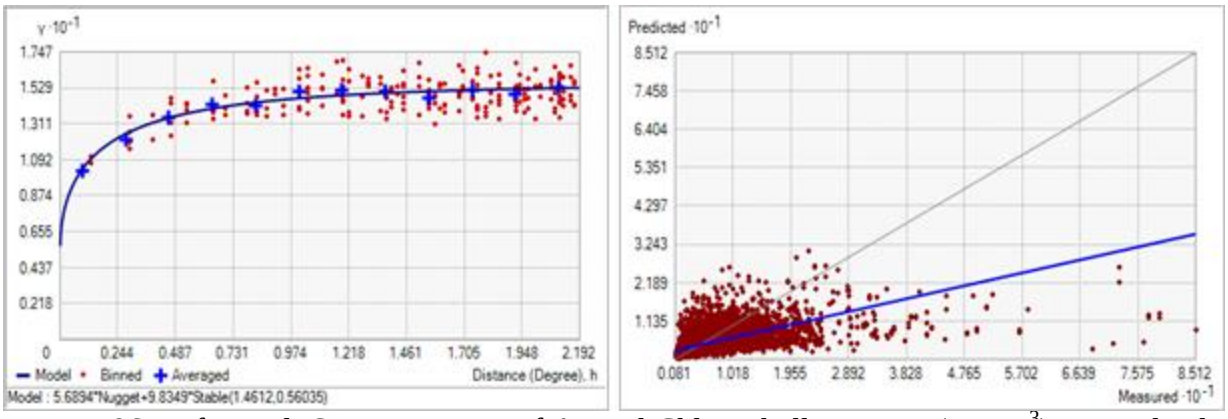

Figure 296. Left panel: Semivariogram of Annual Chlorophyll *a* Range (mg m^{-3}). Binned values are shown as red dots; average points are shown as blue crosses; the model fit to the averaged values is shown as a blue line. Lag size: 0.183 degrees; number of lags: 12; Parameter: 0.560; Range: 1.461 degrees; Partial Sill: 9.835. Right panel: Scatterplot of predicted values versus observed values for the variable Annual Chlorophyll *a* Range (mg m^{-3}).

Table 148. Results of cross-validation of the kriged model for Annual Chlorophyll *a* Range (mg m^{-3}).

Prediction error	**Value**
Number of Observations	17048
Overall Mean Error	9.347×10^{-4}
Root Mean Square Prediction Error	3.579
Standardized Mean	2.684×10^{-4}
Standardized Root Mean Square Prediction Error	1.081
Average Standard Error	3.312

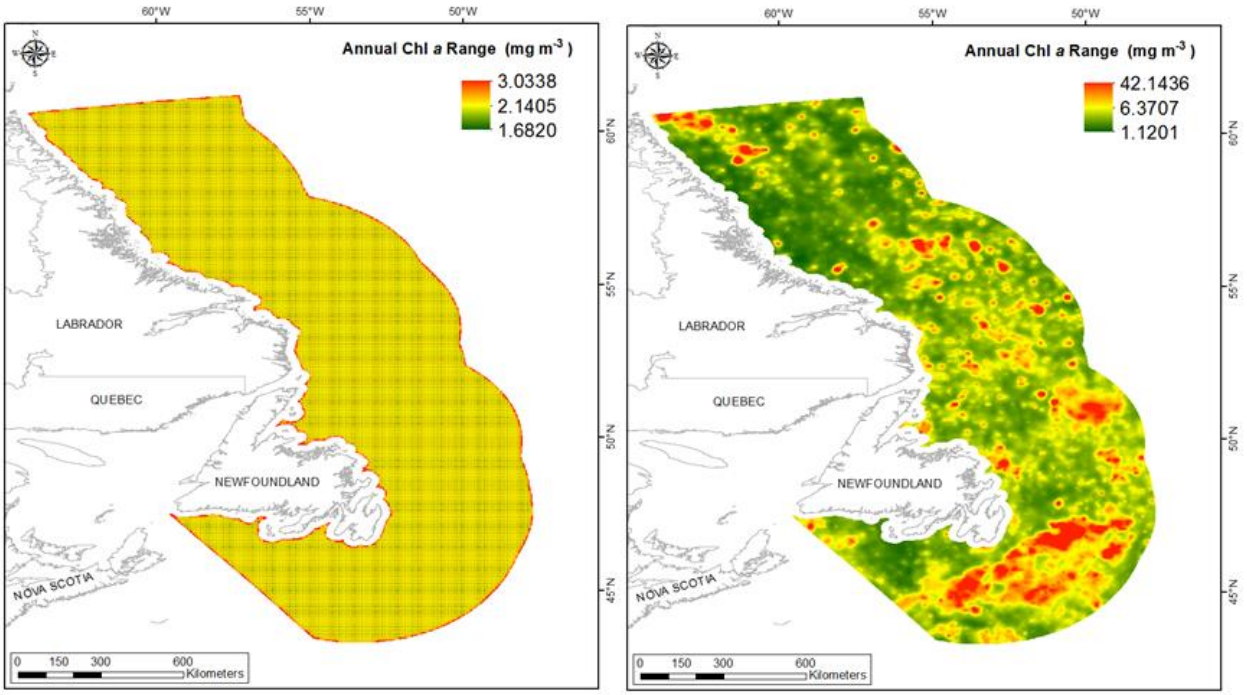

Figure 297. Left panel: Prediction standard error surface of Annual Chlorophyll *a* Range (mg m^{-3}). Right panel: Interpolated prediction surface of Annual Chlorophyll *a* Range (mg m^{-3}).

Primary Production

Primary production measures the rate at which atmospheric or aqueous carbon dioxide is converted to organic carbon by autotrophs (Bender et al. 1987) and relates more directly to the flux of particulate organic carbon and food supply to the seafloor than sea surface chlorophyll *a* concentration. However, as satellite-derived chlorophyll *a* is a main source of data used in the calculation of the primary production variables in this report, we expect these variables to be highly correlated.

Spring Primary Production Mean

This variable displayed a near normal distribution prior to modeling (Table 149, Figure 298). The data were higher than predicted by a normal distribution at low and upper mid-range values however the mid-region was well-predicted (Figure 299). The areas of over- and under-prediction show that where deviations occurred they were over-predicted (Figure 299).

The semivariogram showed weak autocorrelation present in the data and the model showed good fit between measured and predicted values (Figure 300). Although the RMSE and ASE were high, all other errors showed that the model was good at prediction (Table 150). The error map showed high error on Saglek and Nain Banks where no data observations occur (Figure 301). The kriged surface is presented in Figure 301.

Table 149. Distributional properties of Spring Primary Production Mean (mg C m^{-2} day^{-1}).

Property	Value
Number of Observations	9692
Minimum	210.900
Maximum	1272.600
Mean	737.670
Median	730.280
Standard Deviation	123.540
Skewness	0.371
Kurtosis	2.777

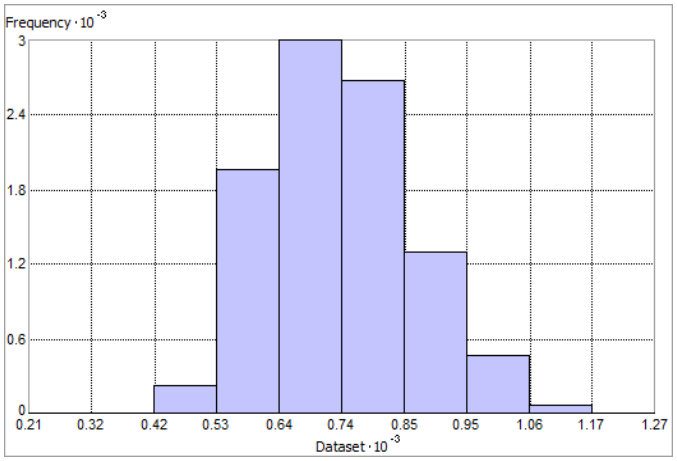

Figure 298. Distribution of Spring Primary Production Mean (mg C m^{-2} day^{-1}). Histogram was illustrated using 10 bins. X and Y axes are shown at 10^{-3}.

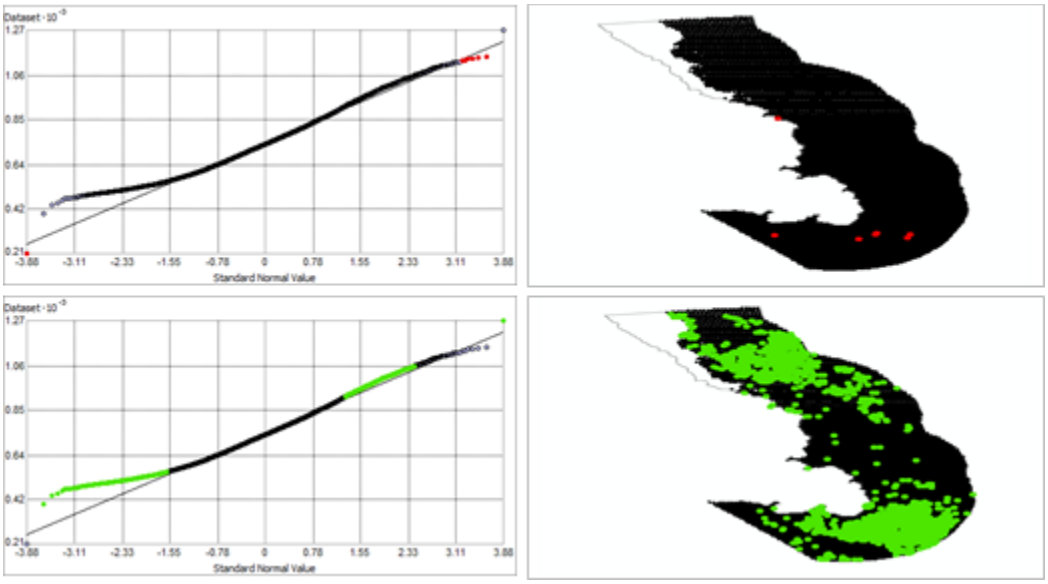

Figure 299. Normal Q-Q plot for data values of Spring Primary Production Mean (mg C m^{-2} day^{-1}). Points falling under (upper panel) and over (bottom panel) the reference line are mapped.

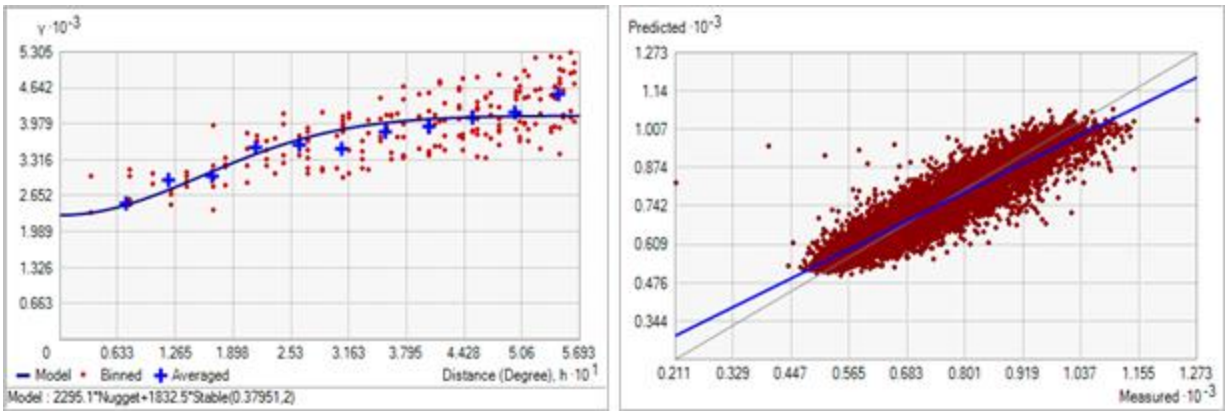

Figure 300. Left panel: Semivariogram of Spring Primary Production Mean (mg C m^{-2} day^{-1}). Binned values are shown as red dots; average points are shown as blue crosses; the model fit to the averaged values is shown as a blue line. Lag size: 0.047 degrees; number of lags: 12; Parameter: 2; Range: 0.380 degrees; Partial Sill: 1832.526. Right panel: Scatterplot of predicted values versus observed values for the model of Spring Primary Production Mean (mg C m^{-2} day^{-1}).

Table 150. Results of cross-validation of the kriged model for Spring Primary Production Mean (mg C m^{-2} day^{-1}).

Prediction error	**Value**
Number of Observations	9692
Overall Mean Error	-5.744×10^{-3}
Root Mean Square Prediction Error	53.520
Standardized Mean	-1.874×10^{-4}
Standardized Root Mean Square Prediction Error	1.004
Average Standard Error	53.318

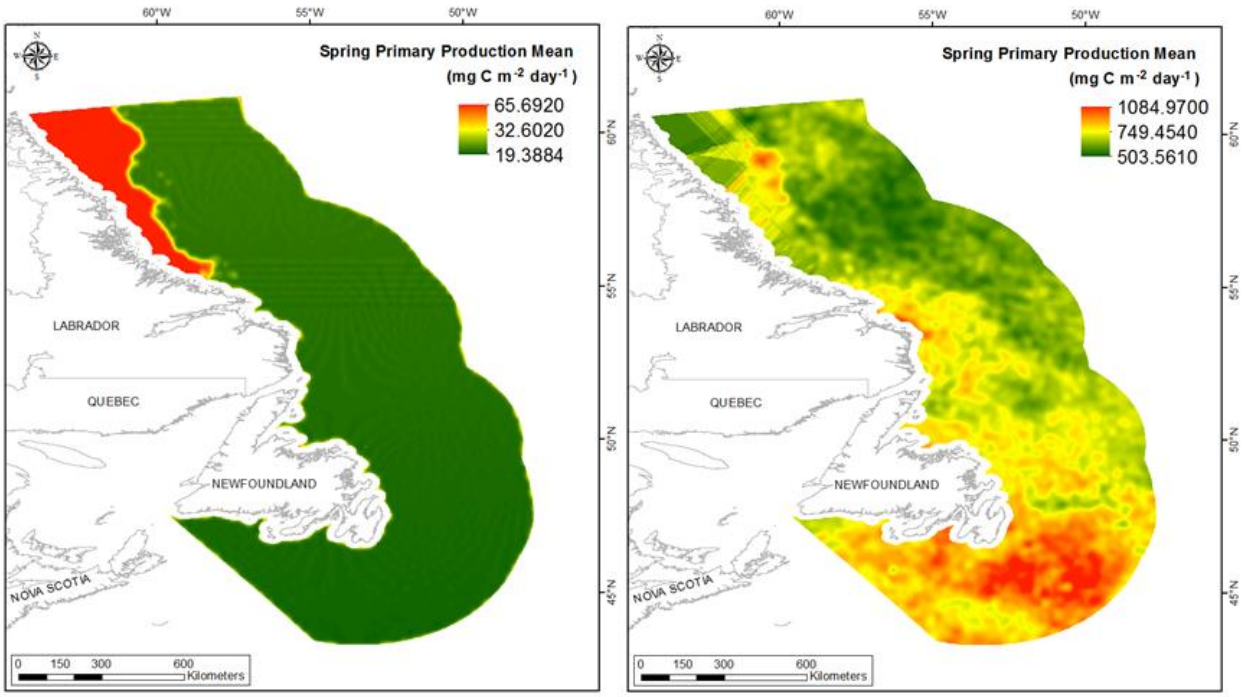

Figure 301. Left panel: Prediction standard error surface of Spring Primary Production Mean (mg C m^{-2} day^{-1}). Right panel: Interpolated prediction surface of Spring Primary Production Mean (mg C m^{-2} day^{-1}).

Spring Primary Production Minimum

This variable displayed a bell-shaped distribution with left-skewness (Table 151, Figure 302). The data were higher than predicted by a normal distribution at low and high values however the mid-region was well-predicted (Figure 303). The areas of over- and under-prediction showed no strong spatial pattern over the spatial extent (Figure 303).

The semivariogram showed weak autocorrelation present in the data and the model showed a fair to poor fit between measured and predicted values (Figure 304). Although the RMSE and ASE were high, all other errors showed that the model was good at prediction (Table 152). The error map showed high error on Saglek and Nain Banks where no data observations occur (Figure 305). The kriged surface is presented in Figure 305.

Table 151. Distributional properties of Spring Primary Production Minimum (mg C m^{-2} day^{-1}).

Property	Value
Number of Observations	9692
Minimum	82.840
Maximum	811.830
Mean	381.610
Median	391.650
Standard Deviation	106.760
Skewness	0.060
Kurtosis	2.471

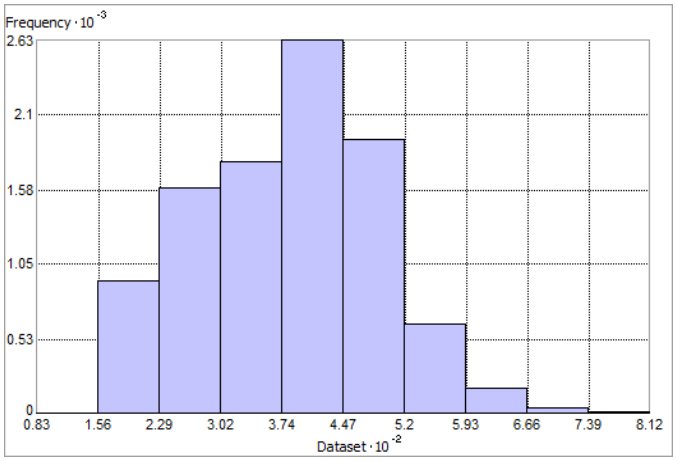

Figure 302. Distribution of Spring Primary Production Minimum (mg C m^{-2} day^{-1}). Histogram was illustrated using 10 bins. X axis is shown at 10^{-2}; Y axis is shown at 10^{-3}.

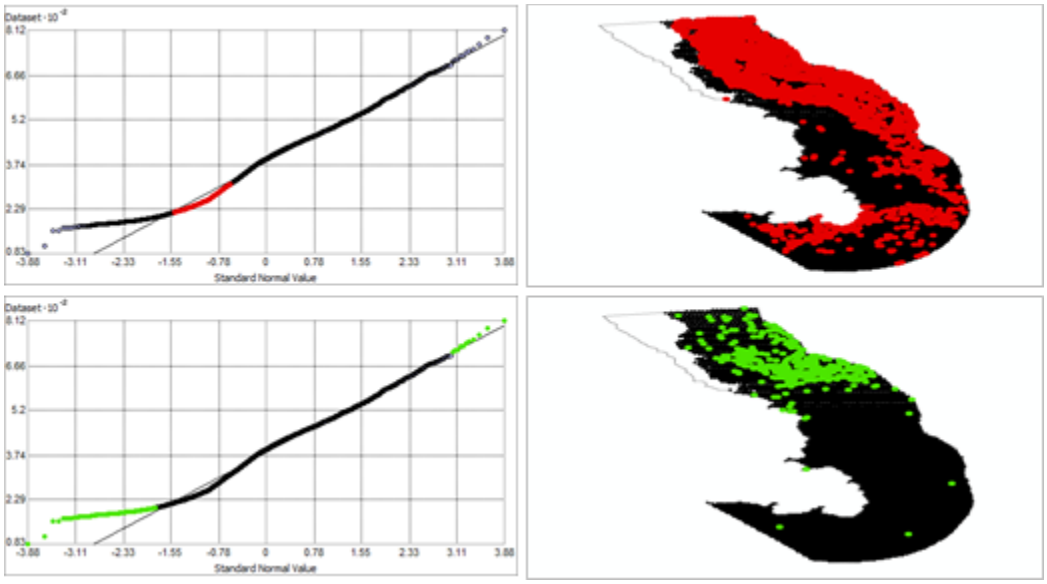

Figure 303. Normal Q-Q plot for data values of Spring Primary Production Minimum (mg C m^{-2} day^{-1}). Points falling under (upper panel) and over (bottom panel) the reference line are mapped.

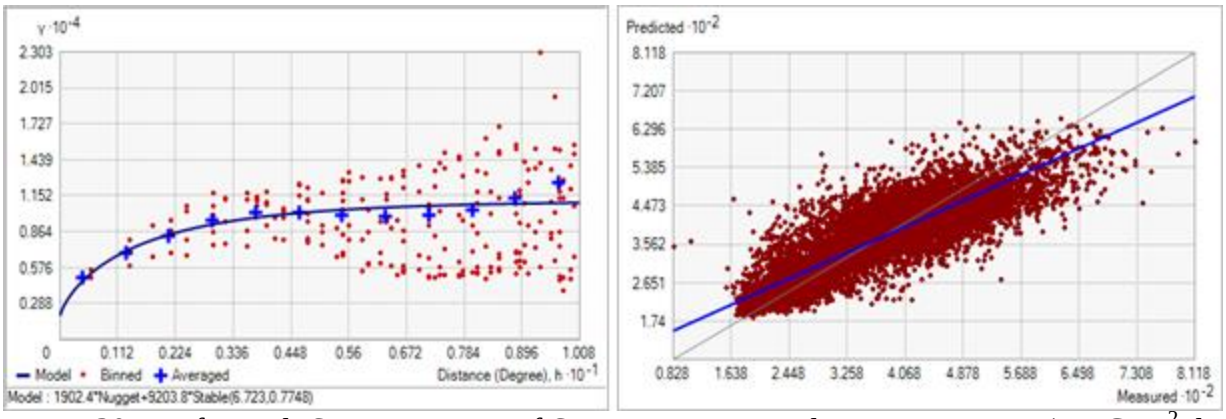

Figure 304. Left panel: Semivariogram of Spring Primary Production Minimum (mg C m^{-2} day^{-1}). Binned values are shown as red dots; average points are shown as blue crosses; the model fit to the averaged values is shown as a blue line. Lag size: 0.840 degrees; number of lags: 12; Parameter: 0.775; Range: 6.723 degrees; Partial Sill: 9203.806. Right panel: Scatterplot of predicted values versus observed values for the model of Spring Primary Production Minimum (mg C m^{-2} day^{-1}).

Table 152. Results of cross-validation of the kriged model for Spring Primary Production Minimum (mg C m^{-2} day^{-1}).

Prediction error	**Value**
Number of Observations	9692
Overall Mean Error	-0.012
Root Mean Square Prediction Error	56.822
Standardized Mean	-2.687×10^{-4}
Standardized Root Mean Square Prediction Error	1.015
Average Standard Error	55.985

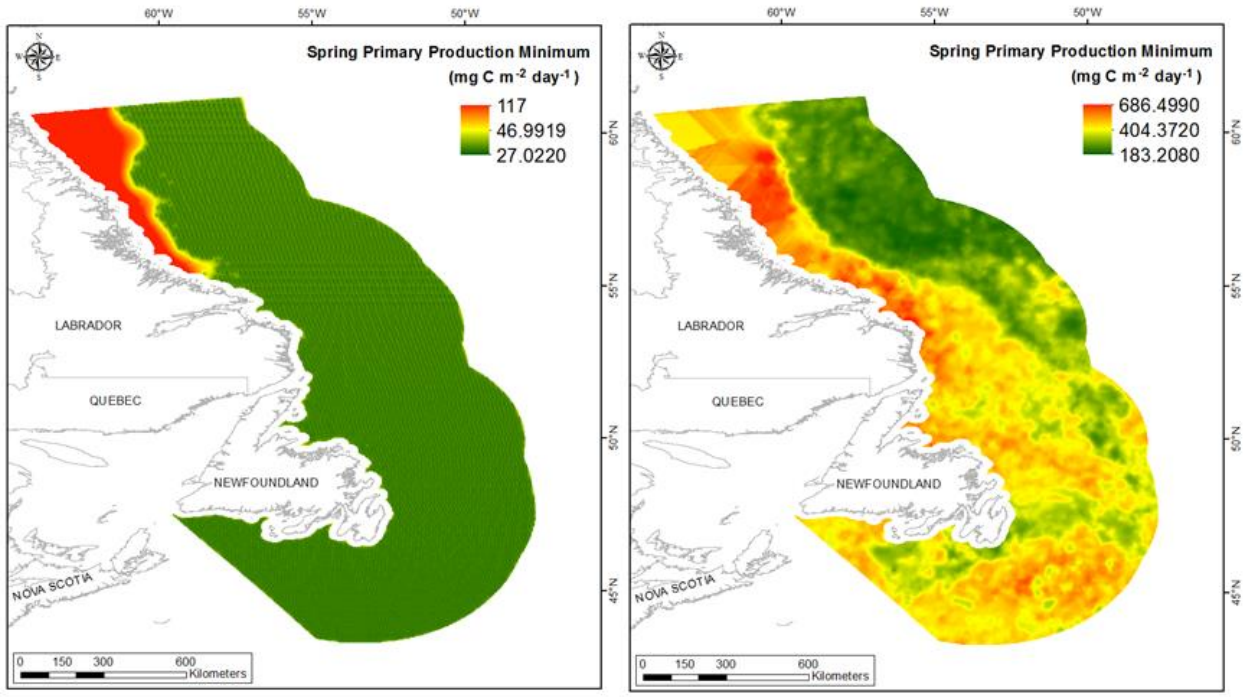

Figure 305. Left panel: Prediction standard error surface of Spring Primary Production Minimum (mg C m^{-2} day^{-1}). Right panel: Interpolated prediction surface of Spring Primary Production Minimum (mg C m^{-2} day^{-1}).

Spring Primary Production Maximum

This variable displayed a bell-shaped distribution with right-skewness (Table 153, Figure 306). The data were higher than predicted by a normal distribution at low and high values, the mid-values were lower than predicted (Figure 307). The areas of over- and under-prediction showed no strong spatial pattern over the spatial extent with most areas either over- or under-predicted (Figure 307).

The semivariogram showed weak autocorrelation present in the data and the model showed a fair to poor fit between measured and predicted values (Figure 308). Although the RMSE and ASE were high, all other errors showed that the model was good at prediction (Table 154). The error map showed high error on Saglek and Nain Banks where no data observations occur (Figure 309). The kriged surface is presented in Figure 309.

Table 153. Distributional properties of Spring Primary Production Maximum (mg C m^{-2} day^{-1}).

Property	Value
Number of Observations	9692
Minimum	337.620
Maximum	2735.300
Mean	1263.400
Median	1200.100
Standard Deviation	330.820
Skewness	0.613
Kurtosis	2.830

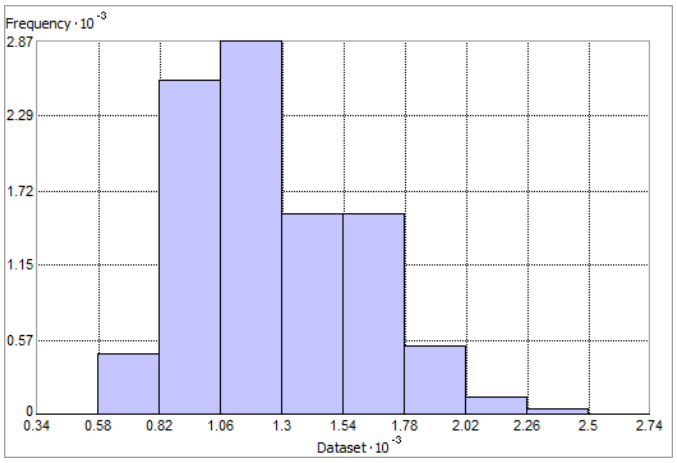

Figure 306. Distribution of Spring Primary Production Maximum (mg C m^{-2} day^{-1}). Histogram was illustrated using 10 bins. X and Y axes are shown at 10^{-3}.

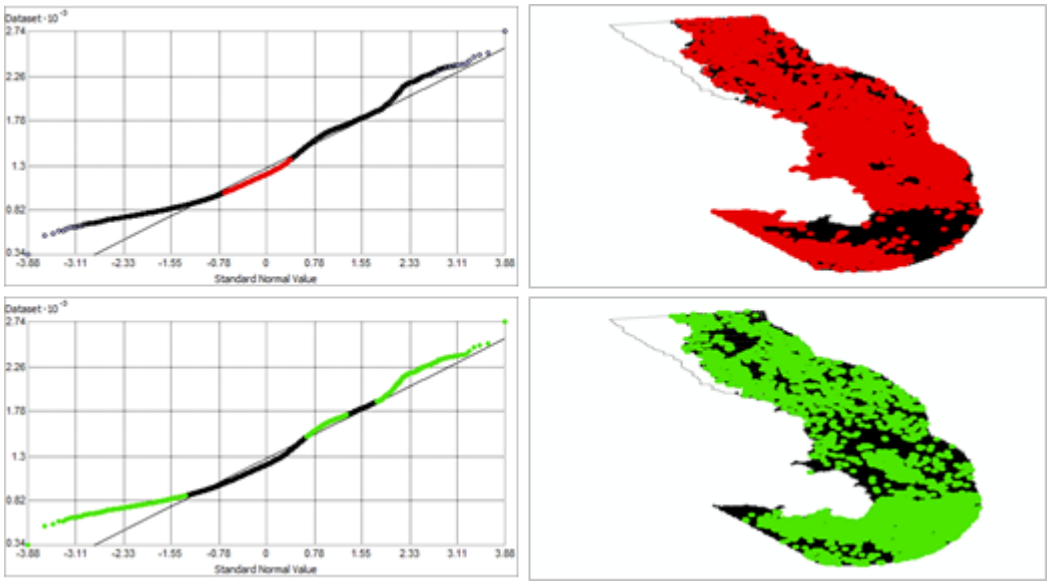

Figure 307. Normal Q-Q plot for data values of Spring Primary Production Maximum (mg C m^{-2} day^{-1}). Points falling under (upper panel) and over (bottom panel) the reference line are mapped.

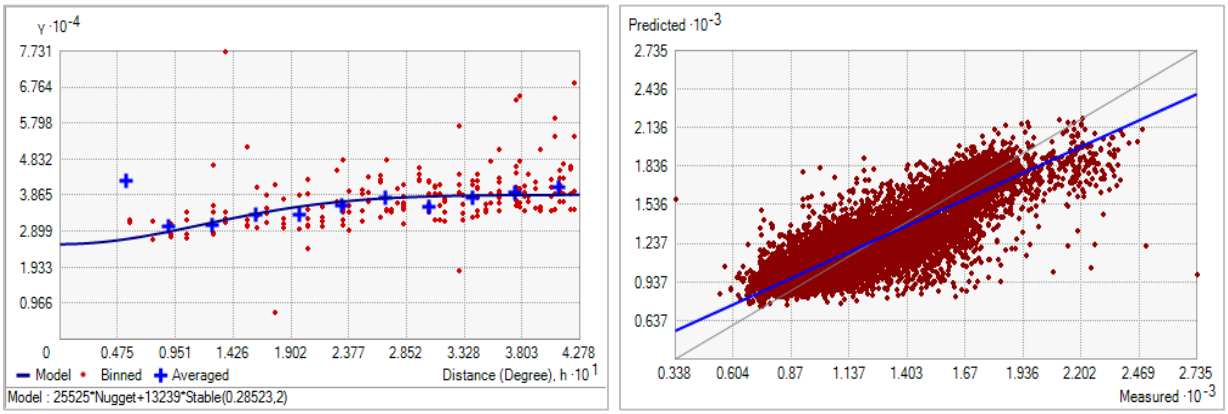

Figure 308. Left panel: Semivariogram of Spring Primary Production Maximum (mg C m^{-2} day^{-1}). Binned values are shown as red dots; average points are shown as blue crosses; the model fit to the averaged values is shown as a blue line. Lag size: 0.036 degrees; number of lags: 12; Parameter: 2; Range: 0.285 degrees; Partial Sill: 13239.500. Right panel: Scatterplot of predicted values versus observed values for the model of Spring Primary Production Maximum (mg C m^{-2} day^{-1}).

Table 154. Results of cross-validation of the kriged model for Spring Primary Production Maximum (mg C m^{-2} day^{-1}).

Prediction error	**Value**
Number of Observations	9692
Overall Mean Error	-0.017
Root Mean Square Prediction Error	180.073
Standardized Mean	-1.218×10^{-3}
Standardized Root Mean Square Prediction Error	0.996
Average Standard Error	180.780

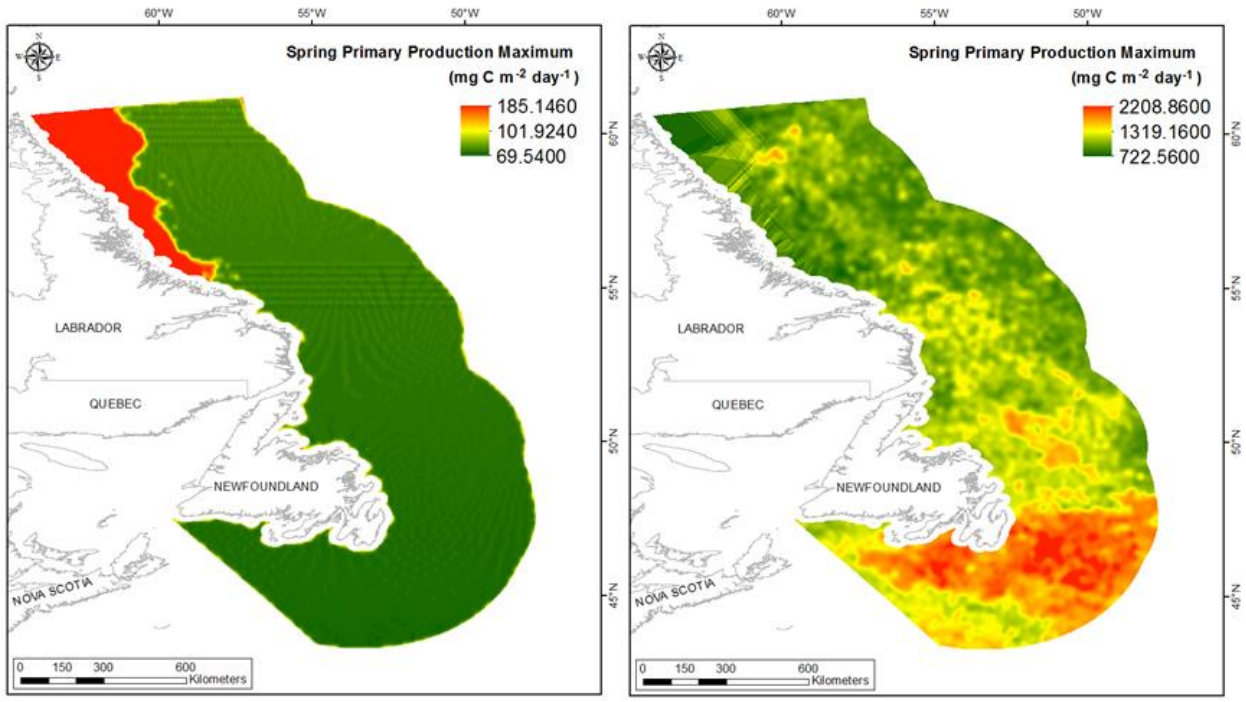

Figure 309. Left panel: Prediction standard error surface of Spring Primary Production Maximum (mg C m^{-2} day^{-1}). Right panel: Interpolated prediction surface of Spring Primary Production Maximum (mg C m^{-2} day^{-1}).

Spring Primary Production Range

This variable displayed a bell-shaped distribution with right-skewness with outlying data in the upper range (Table 155, Figure 310). The data were higher than predicted by a normal distribution at low and high values, the mid-region was slightly lower than predicted (Figure 311). The areas of over and under-prediction showed no strong spatial pattern over the spatial extent (Figure 311).

The semivariogram showed very weak autocorrelation present in the data and the model showed a fair fit between measured and predicted values (Figure 312). Although the RMSE and ASE were very high, all other errors showed that the model was good at prediction (Table 156). The error map showed high error on Saglek and Nain Banks where no data observations occur (Figure 313). The kriged surface is presented in Figure 313.

Table 155. Distributional properties of Spring Primary Production Range (mg C m^{-2} day^{-1}).

Property	Value
Number of Observations	9692
Minimum	54.110
Maximum	2353.600
Mean	881.800
Median	824.820
Standard Deviation	317.230
Skewness	0.584
Kurtosis	3.150

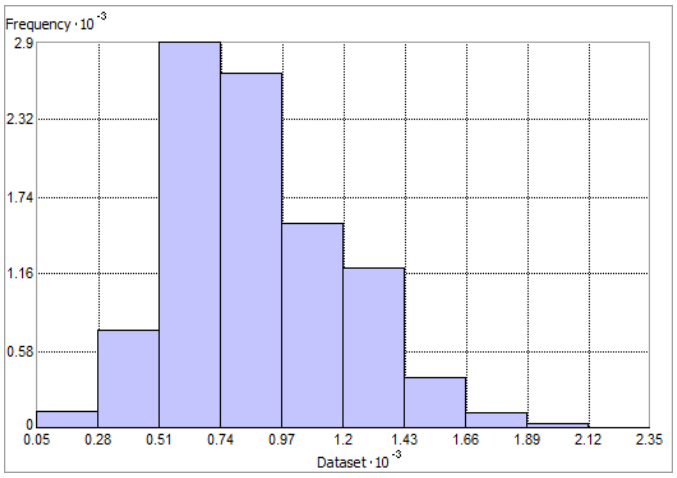

Figure 310. Distribution of Spring Primary Production Range (mg C m^{-2} day^{-1}). Histogram was illustrated using 10 bins. X and Y axes are shown at 10^{-3}.

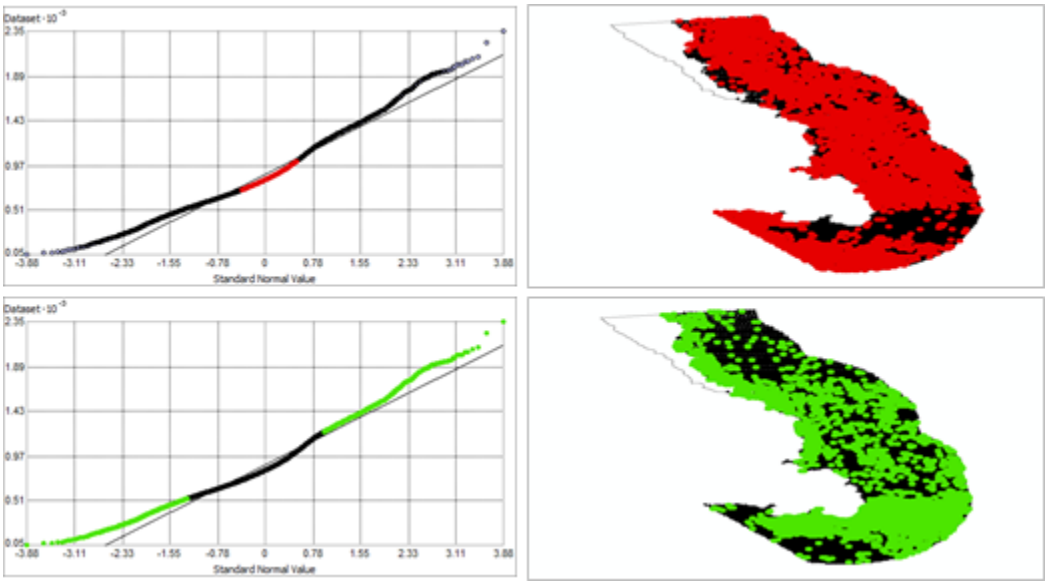

Figure 311. Normal Q-Q plot for data values of Spring Primary Production Range (mg C m^{-2} day^{-1}). Points falling under (upper panel) and over (bottom panel) the reference line are mapped.

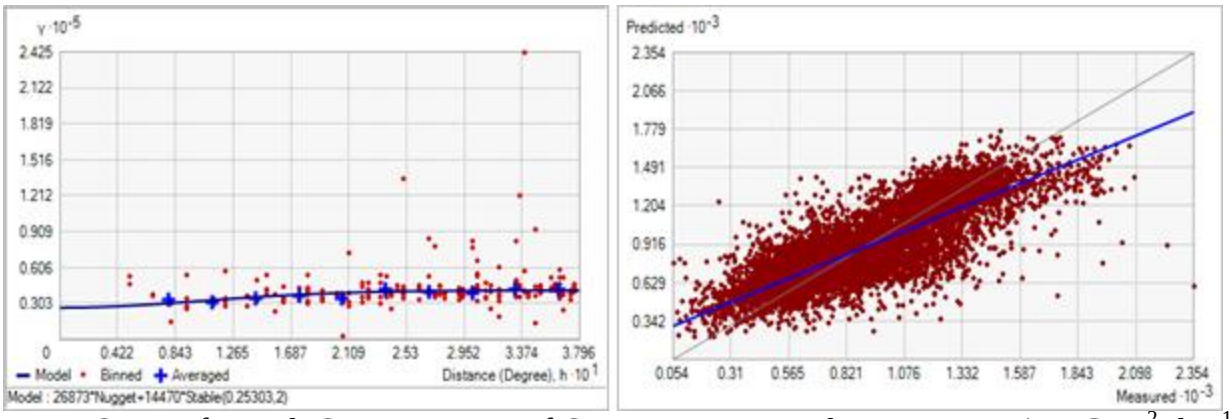

Figure 312. Left panel: Semivariogram of Spring Primary Production Range (mg C m^{-2} day^{-1}). Binned values are shown as red dots; average points are shown as blue crosses; the model fit to the averaged values is shown as a blue line. Lag size: 0.032 degrees; number of lags: 12; Parameter: 2; Range: 0.253 degrees; Partial Sill: 14470.420. Right panel: Scatterplot of predicted values versus observed values for the model of Spring Primary Production Range (mg C m^{-2} day^{-1}).

Table 156. Results of cross-validation of the kriged model for Spring Primary Production Range (mg C m^{-2} day^{-1}).

Prediction error	**Value**
Number of Observations	9692
Overall Mean Error	0.058
Root Mean Square Prediction Error	187.591
Standardized Mean	2.667×10^{-4}
Standardized Root Mean Square Prediction Error	0.990
Average Standard Error	189.366

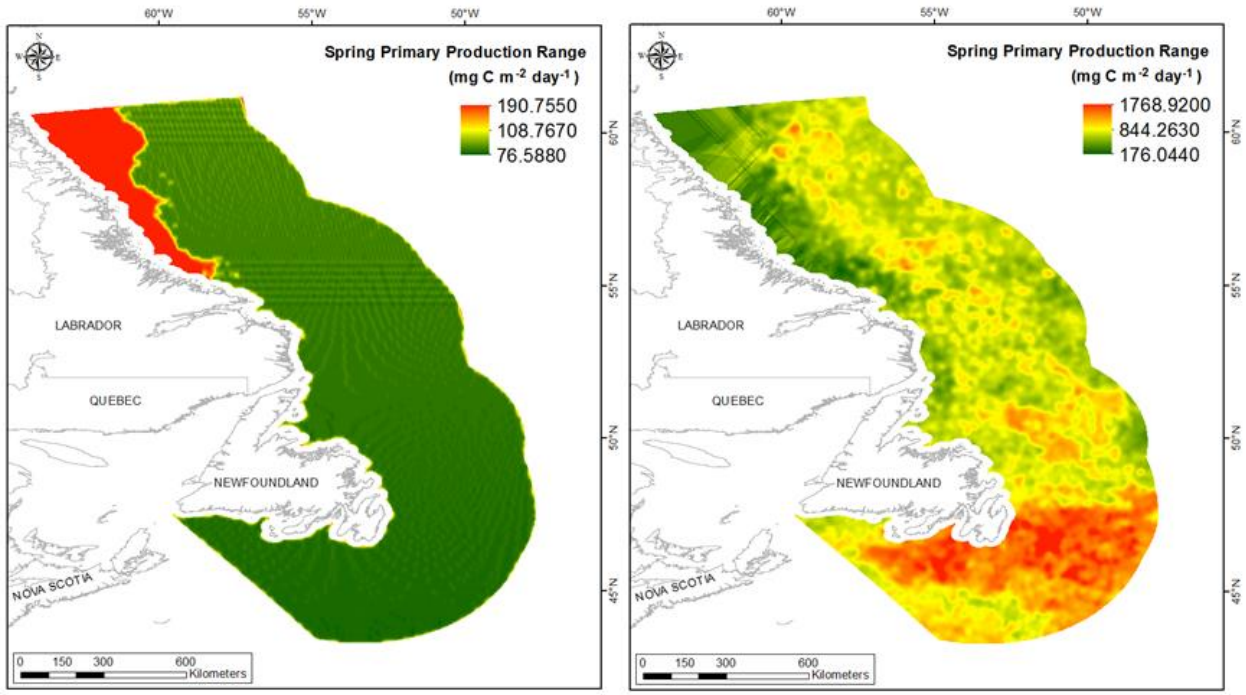

Figure 313. Left panel: Prediction standard error surface of Spring Primary Production Range (mg C m^{-2} day^{-1}). Right panel: Interpolated prediction surface of Spring Primary Production Range (mg C m^{-2} day^{-1}).

Spring Primary Production Average Minimum

This variable displayed a bell-shaped distribution prior to modeling (Table 157, Figure 314). The data were higher than predicted by a normal distribution at low and high values and slightly lower at mid values (Figure 315). The areas of over- and under-prediction showed no strong spatial pattern over the spatial extent (Figure 315).

The semivariogram showed moderate autocorrelation present in the data and the model showed a fair fit between measured and predicted values (Figure 316). Although the RMSE and ASE were high, all other errors showed that the model was good at prediction (Table 158). The error map showed high error on Saglek and Nain Banks where no data observations occur (Figure 317). The kriged surface is presented in Figure 317.

Table 157. Distributional properties of Spring Primary Production Average Minimum (mg C m^{-2} day^{-1}).

Property	Value
Number of Observations	9692
Minimum	161.560
Maximum	1043.600
Mean	525.010
Median	535.100
Standard Deviation	114.350
Skewness	-0.190
Kurtosis	3.042

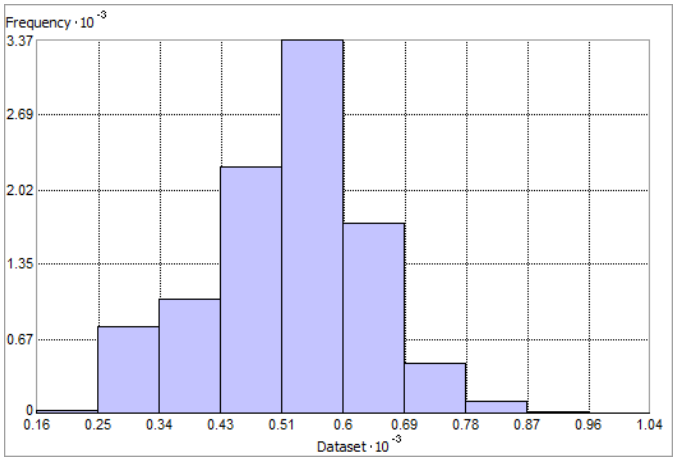

Figure 314. Distribution of Spring Primary Production Average Minimum (mg C m^{-2} day^{-1}). Histogram was illustrated using 10 bins. X and Y axes are shown at 10^{-3}.

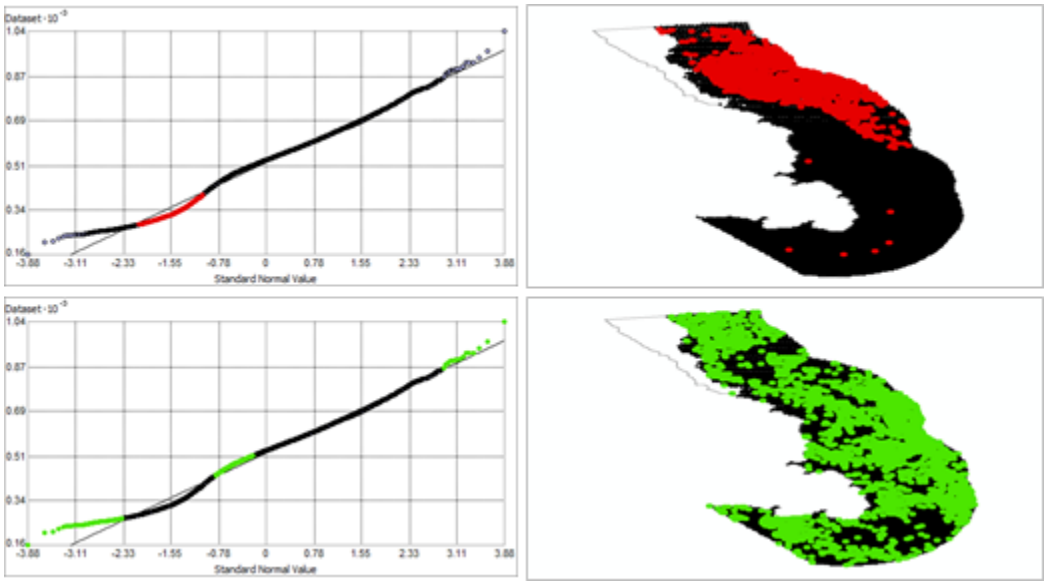

Figure 315. Normal Q-Q plot for data values of Spring Primary Production Average Minimum (mg C m^{-2} day^{-1}). Points falling under (upper panel) and over (bottom panel) the reference line are mapped.

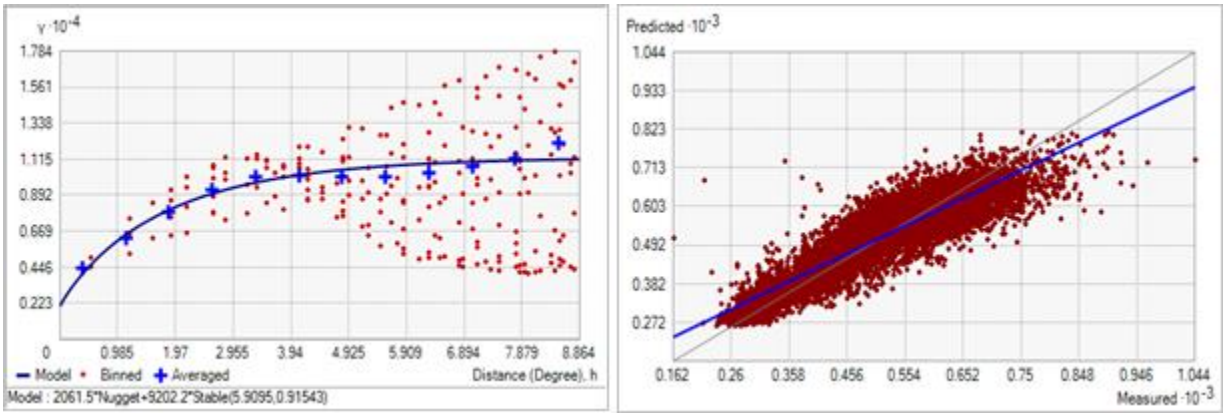

Figure 316. Left panel: Semivariogram of Spring Primary Production Average Minimum (mg C m^{-2} day^{-1}). Binned values are shown as red dots; average points are shown as blue crosses; the model fit to the averaged values is shown as a blue line. Lag size: 0.739 degrees; number of lags: 12; Parameter: 0.915; Range: 5.909 degrees; Partial Sill: 9202.249. Right panel: Scatterplot of predicted values versus observed values for the model of Spring Primary Production Average Minimum (mg C m^{-2} day^{-1}).

Table 158. Results of cross-validation of the kriged model for Spring Primary Production Average Minimum (mg C m^{-2} day^{-1}).

Prediction error	**Value**
Number of Observations	9692
Overall Mean Error	0.013
Root Mean Square Prediction Error	53.846
Standardized Mean	1.026×10^{-4}
Standardized Root Mean Square Prediction Error	0.999
Average Standard Error	53.880

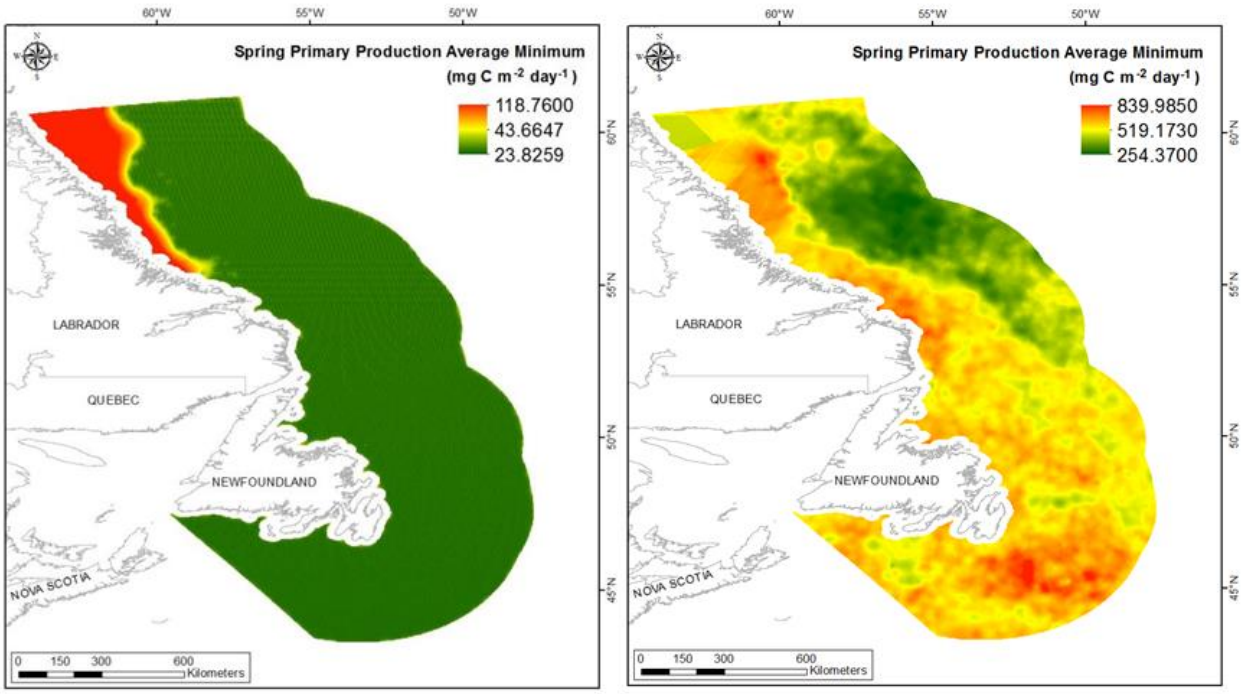

Figure 317. Left panel: Prediction standard error surface of Spring Primary Production Average Minimum (mg C m^{-2} day^{-1}). Right panel: Interpolated prediction surface of Spring Primary Production Average Minimum (mg C m^{-2} day^{-1}).

Spring Primary Production Average Maximum

This variable displayed a bell-shaped distribution with left-skewness prior to modeling (Table 159, Figure 318). The data were higher than predicted by a normal distribution at high and low values, the mid-region was slightly lower than predicted (Figure 319). The areas of over and under-prediction showed no strong spatial pattern over the spatial extent (Figure 319).

The semivariogram showed weak autocorrelation present in the data and the model showed a fair fit between measured and predicted values (Figure 320). Although the RMSE and ASE were high, all other errors showed that the model was good at prediction (Table 160). The error map showed high error on Saglek and Nain Banks where no data observations occur (Figure 321). The kriged surface is presented in Figure 321.

Table 159. Distributional properties of Spring Primary Production Average Maximum (mg C m^{-2} day^{-1}).

Property	Value
Number of Observations	9692
Minimum	276.660
Maximum	1612.900
Mean	960.470
Median	926.180
Standard Deviation	183.310
Skewness	0.660
Kurtosis	2.909

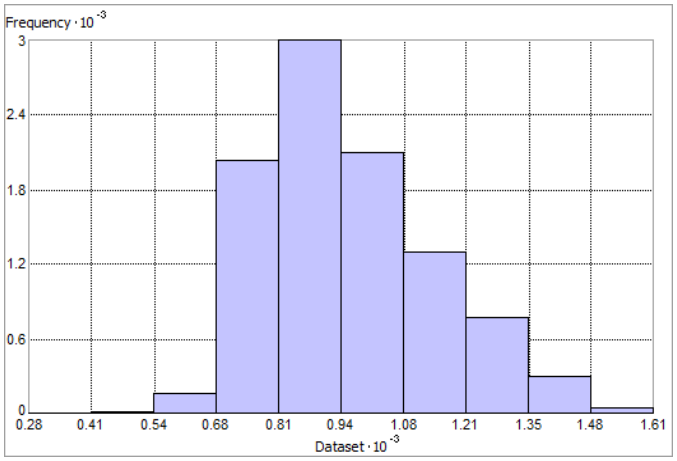

Figure 318. Distribution of Spring Primary Production Average Maximum (mg C m^{-2} day^{-1}). Histogram was illustrated using 10 bins. X and Y axes are shown at 10^{-3}.

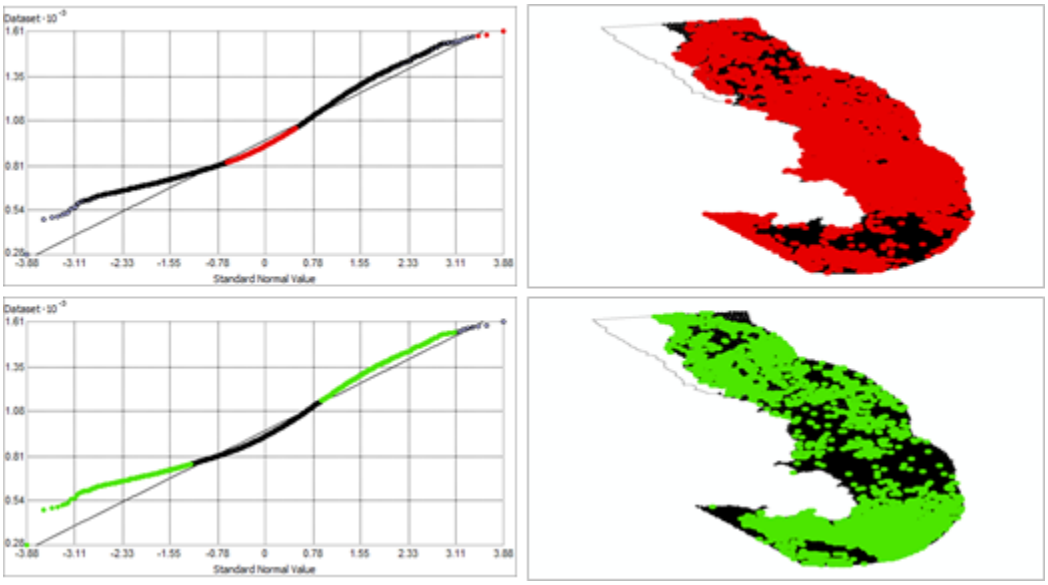

Figure 319. Normal Q-Q plot for data values of Spring Primary Production Average Maximum (mg C m^{-2} day^{-1}). Points falling under (upper panel) and over (bottom panel) the reference line are mapped.

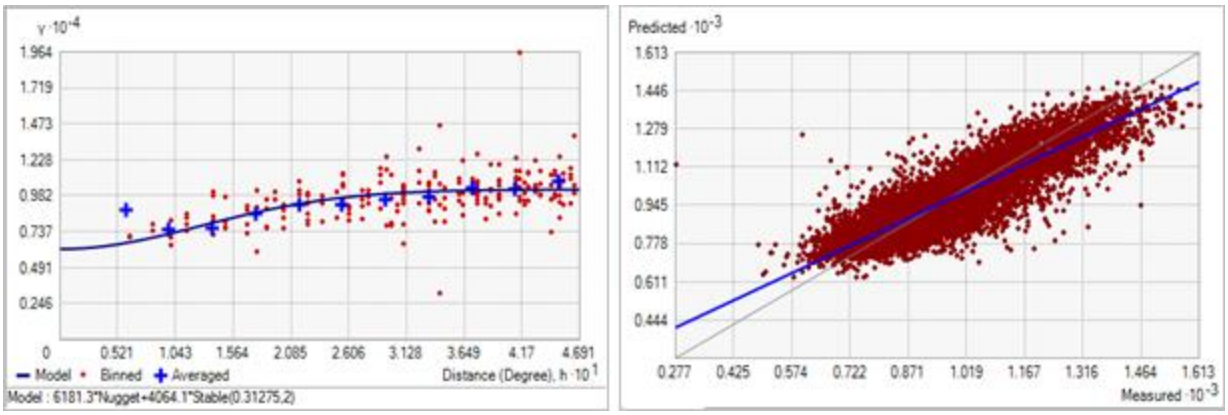

Figure 320. Left panel: Semivariogram of Spring Primary Production Average Maximum (mg C m^{-2} day^{-1}). Binned values are shown as red dots; average points are shown as blue crosses; the model fit to the averaged values is shown as a blue line. Lag size: 0.039 degrees; number of lags: 12; Parameter: 2; Range: 0.313 degrees; Partial Sill: 4064.117. Right panel: Scatterplot of predicted values versus observed values for the model of Spring Primary Production Average Maximum (mg C m^{-2} day^{-1}).

Table 160. Results of cross-validation of the kriged model for Spring Primary Production Average Maximum (mg C m^{-2} day^{-1}).

Prediction error	**Value**
Number of Observations	9692
Overall Mean Error	-8.937×10^{-3}
Root Mean Square Prediction Error	87.963
Standardized Mean	-8.720×10^{-5}
Standardized Root Mean Square Prediction Error	0.9888
Average Standard Error	89.089

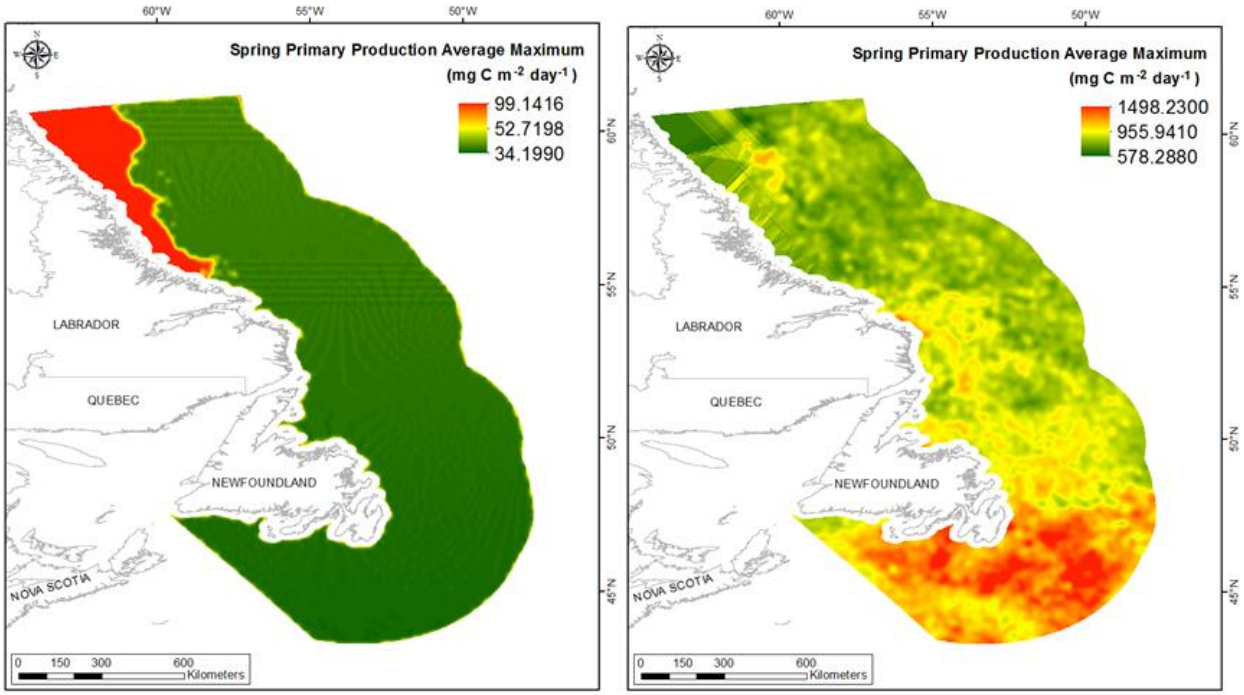

Figure 321. Left panel: Prediction standard error surface of Spring Primary Production Average Maximum (mg C m^{-2} day^{-1}). Right panel: Interpolated prediction surface of Spring Primary Production Average Maximum (mg C m^{-2} day^{-1}).

Spring Primary Production Average Range

This variable displayed a bell-shaped distribution with left-skewness prior the modeling (Table 161, Figure 322). The data were higher than predicted by a normal distribution at low and high values however the mid-region was very well-predicted (Figure 323). No data fell below the reference line. The areas of over-prediction showed no spatial pattern over the spatial extent (Figure 323).

The semivariogram showed moderate autocorrelation present in the data and the model showed a fair to poor fit between measured and predicted values (Figure 324). Although the RMSE and ASE were high, all other errors showed that the model was good at prediction (Table 162). The error map showed high error on Saglek and Nain Banks where no data observations occur (Figure 325). The kriged surface is presented in Figure 325.

Table 161. Distributional properties of Spring Primary Production Average Range (mg C m^{-2} day^{-1}).

Property	Value
Number of Observations	9692
Minimum	4.305
Maximum	1076.600
Mean	435.450
Median	421.220
Standard Deviation	151.590
Skewness	0.448
Kurtosis	3.273

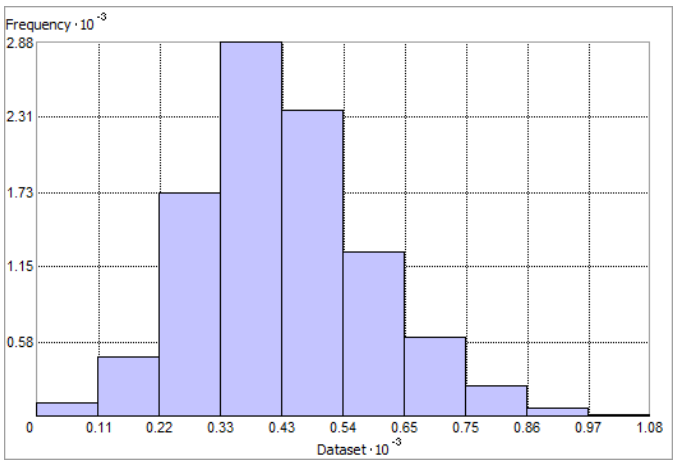

Figure 322. Distribution of Spring Primary Production Average Range (mg C m^{-2} day^{-1}). Histogram was illustrated using 10 bins. X and Y axes are shown at 10^{-3}.

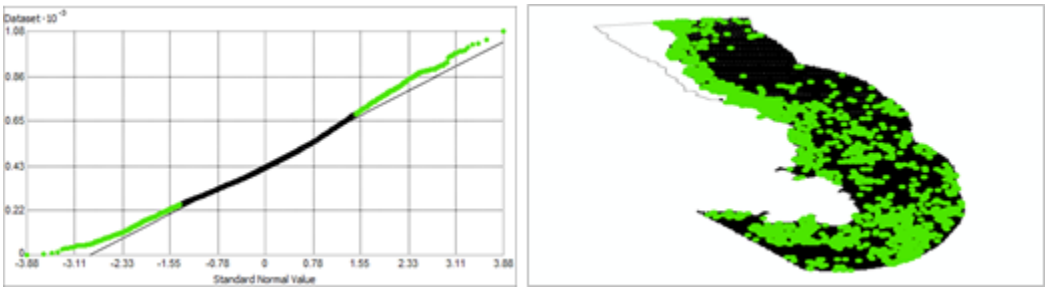

Figure 323. Normal Q-Q plot for data values of Spring Primary Production Average Range (mg C m^{-2} day^{-1}). Points falling over the reference line are mapped; no points fall under the reference line.

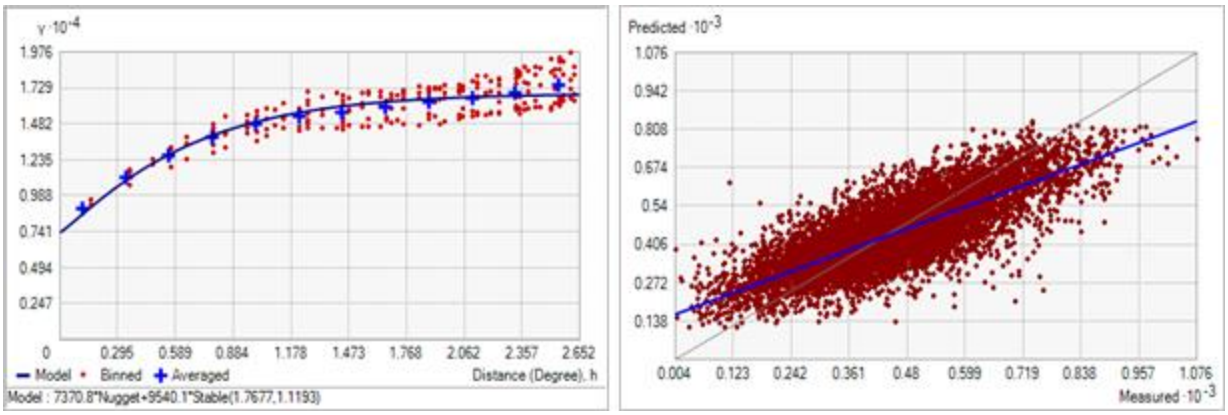

Figure 324. Left panel: Semivariogram of Spring Primary Production Average Range (mg C m^{-2} day^{-1}). Binned values are shown as red dots; average points are shown as blue crosses; the model fit to the averaged values is shown as a blue line. Lag size: 0.044 degrees; number of lags: 12; Parameter: 2; Range: 0.352 degrees; Partial Sill: 3419.920. Right panel: Scatterplot of predicted values versus observed values for the model of Spring Primary Production Average Range (mg C m^{-2} day^{-1}).

Table 162. Results of cross-validation of the kriged model for Spring Primary Production Average Range (mg C m^{-2} day^{-1}).

Prediction error	**Value**
Number of Observations	2204
Overall Mean Error	-0.404
Root Mean Square Prediction Error	90.875
Standardized Mean	-0.004
Standardized Root Mean Square Prediction Error	1.040
Average Standard Error	86.736

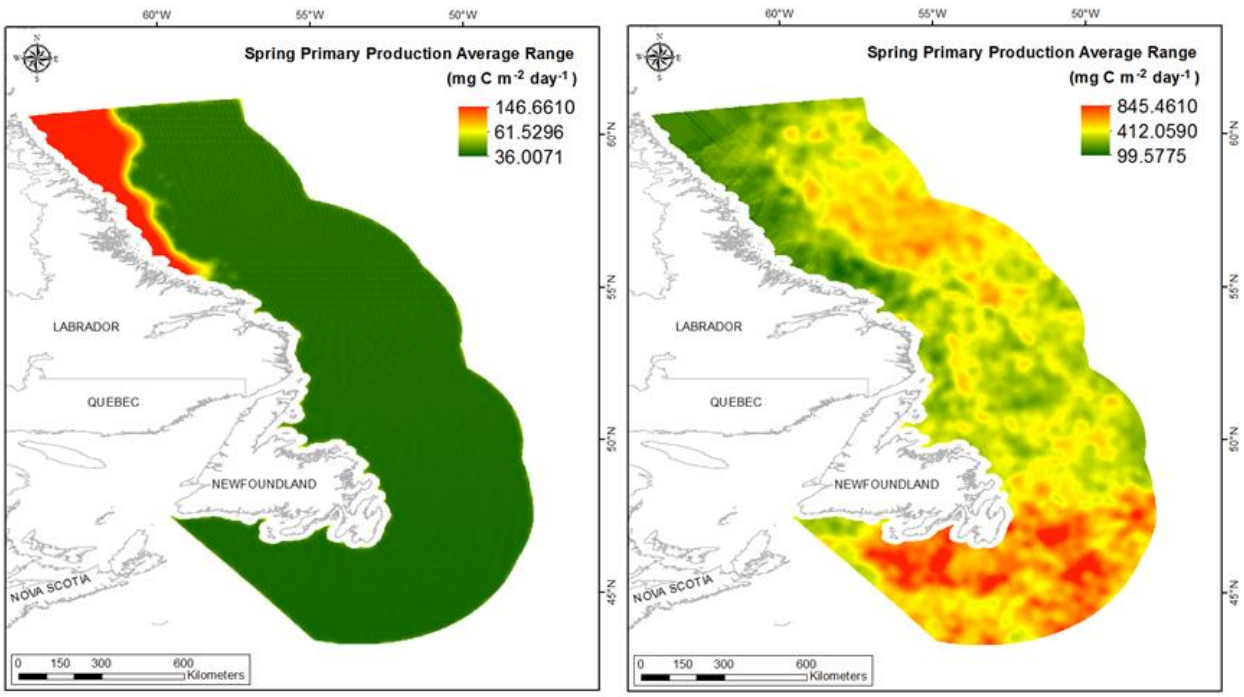

Figure 325. Left panel: Prediction standard error surface of Spring Primary Production Average Range (mg C m^{-2} day^{-1}). Right panel: Interpolated prediction surface of Spring Primary Production Average Range (mg C m^{-2} day^{-1}).

Summer Primary Production Mean

This variable displayed a bell-shaped distribution prior to modeling (Table 163, Figure 326). The data were higher than predicted by a normal distribution at low and upper mid values and lower than predicted at mid and high values (Figure 327). The areas of under- and over-prediction showed no strong spatial pattern over the spatial extent (Figure 327).

The semivariogram showed good autocorrelation present in the data and the model showed a good fit between measured and predicted values (Figure 328). Although the RMSE and ASE were high (Table 164), all other errors showed that the model was good at prediction. The error map showed low to medium error over the study extent with higher error along the edges (Figure 329). The kriged surface is presented in Figure 329.

Table 163. Distributional properties of Summer Primary Production Mean (mg C m^{-2} day^{-1}).

Property	Value
Number of Observations	10374
Minimum	150.910
Maximum	1268.700
Mean	863.750
Median	860.540
Standard Deviation	150.790
Skewness	-2.950 x 10^{-3}
Kurtosis	2.173

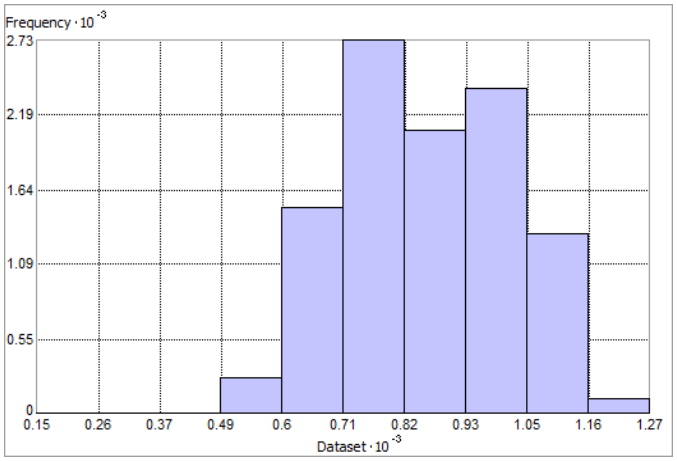

Figure 326. Distribution of Summer Spring Primary Production Mean (mg C m^{-2} day^{-1}). Histogram was illustrated using 10 bins. X and Y axes are shown at 10^{-3}.

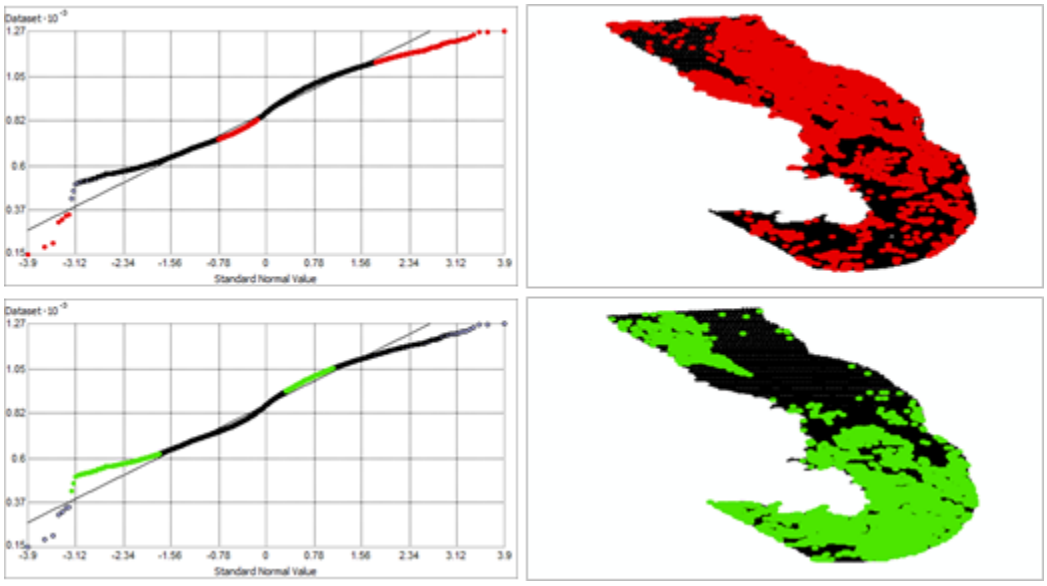

Figure 327. Normal Q-Q plot for data values of Summer Primary Production Mean (mg C m^{-2} day^{-1}). Points falling under (upper panel) and over (bottom panel) the reference line are mapped.

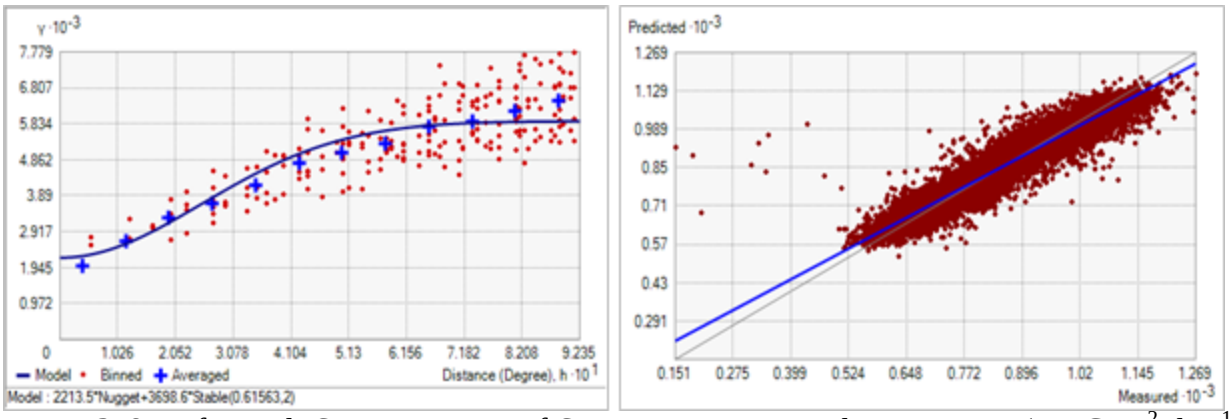

Figure 328. Left panel: Semivariogram of Summer Primary Production Mean (mg C m^{-2} day^{-1}). Binned values are shown as red dots; average points are shown as blue crosses; the model fit to the averaged values is shown as a blue line. Lag size: 0.077 degrees; number of lags: 12; Parameter: 2; Range: 0.616 degrees; Partial Sill: 3698.584. Right panel: Scatterplot of predicted values versus observed values for the model of Summer Primary Production Mean (mg C m^{-2} day^{-1}).

Table 164. Results of cross-validation of the kriged model for Summer Primary Production Mean (mg C m^{-2} day^{-1}).

Prediction error	**Value**
Number of Observations	10374
Overall Mean Error	0.012
Root Mean Square Prediction Error	50.819
Standardized Mean	2.971×10^{-4}
Standardized Root Mean Square Prediction Error	1.000
Average Standard Error	50.840

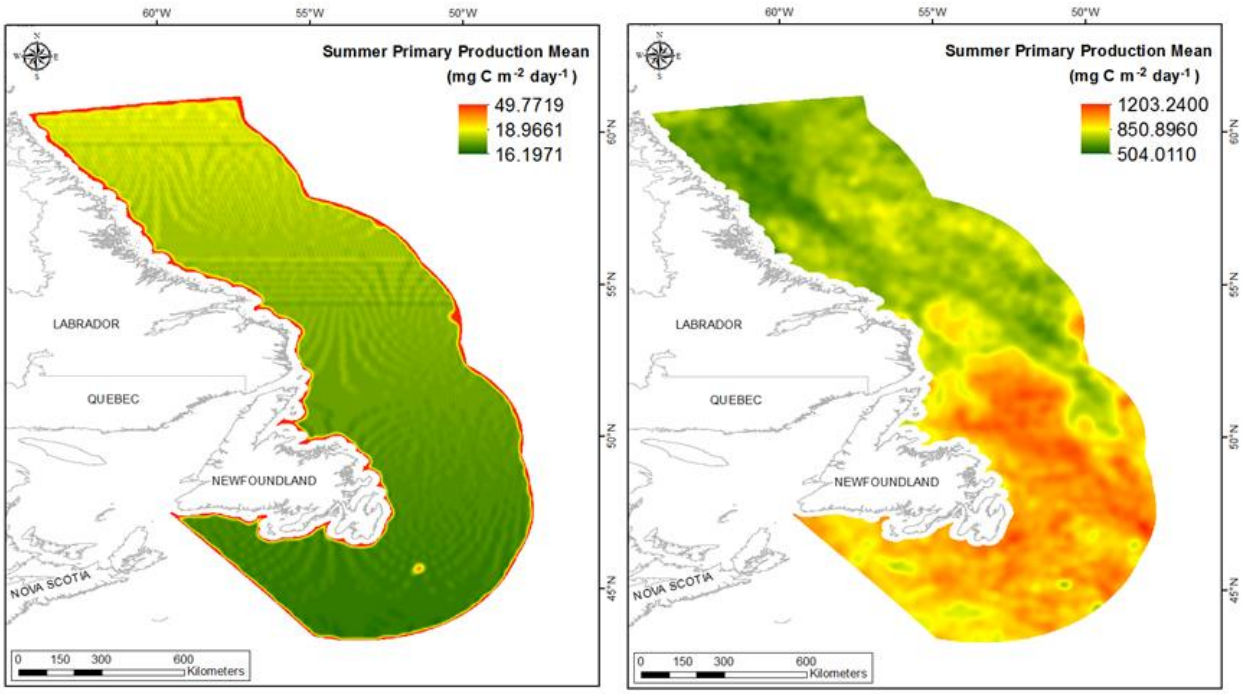

Figure 329. Left panel: Prediction standard error surface of Summer Primary Production Mean (mg C m^{-2} day^{-1}). Right panel: Interpolated prediction surface of Summer Primary Production Mean (mg C m^{-2} day^{-1}).

Summer Primary Production Minimum

This variable displayed a bell-shaped distribution with left-skewness (Table 165, Figure 330). The data were higher and lower than predicted by a normal distribution at low and high values, respectively, however the mid-values deviated only slightly from the reference line (Figure 331). The areas of under- and over-prediction showed no strong spatial pattern over the spatial extent (Figure 331).

The semivariogram showed moderate autocorrelation present in the data and the model showed a fair fit between measured and predicted values (Figure 332). Although the RMSE and ASE were high (Table 166), all other errors showed that the model was good at prediction. The error map showed low to medium error over the study extent with higher error along the edges (Figure 333). The kriged surface is presented in Figure 333.

Table 165. Distributional properties of Summer Primary Production Minimum (mg C m^{-2} day^{-1}).

Property	Value
Number of Observations	2273
Minimum	149.620
Maximum	1359.200
Mean	634.670
Median	641.240
Standard Deviation	129.890
Skewness	0.166
Kurtosis	6.225

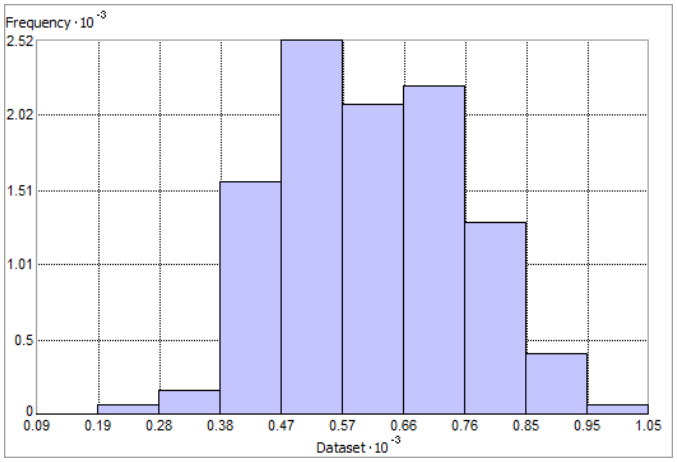

Figure 330. Distribution of Summer Primary Production Minimum (mg C m^{-2} day^{-1}). Histogram was illustrated using 10 bins. X and Y axes are shown at 10^{-3}.

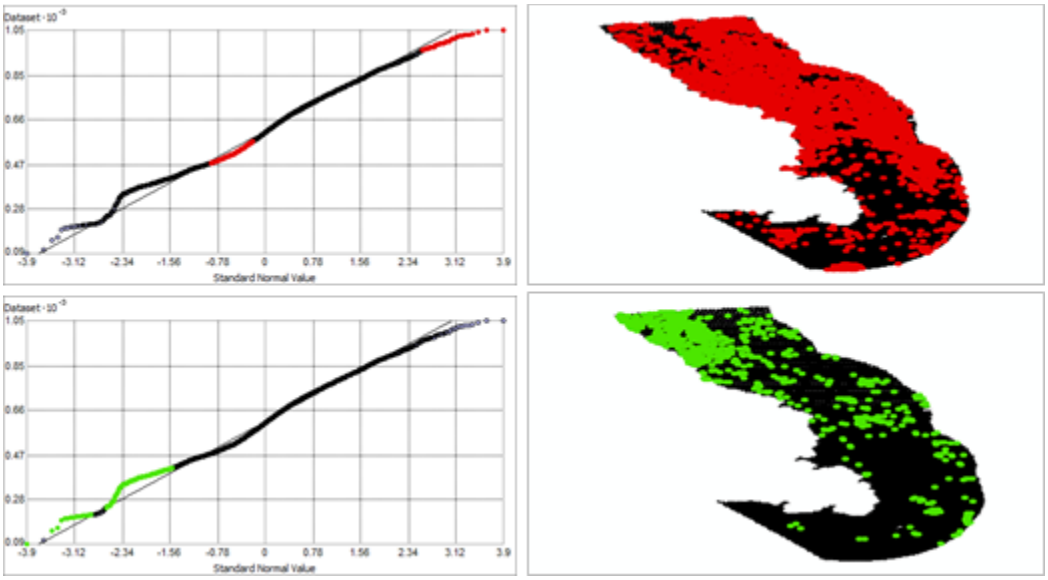

Figure 331. Normal Q-Q plot for data values of Summer Primary Production Minimum (mg C m^{-2} day^{-1}). Points falling under (upper panel) and over (bottom panel) the reference line are mapped.

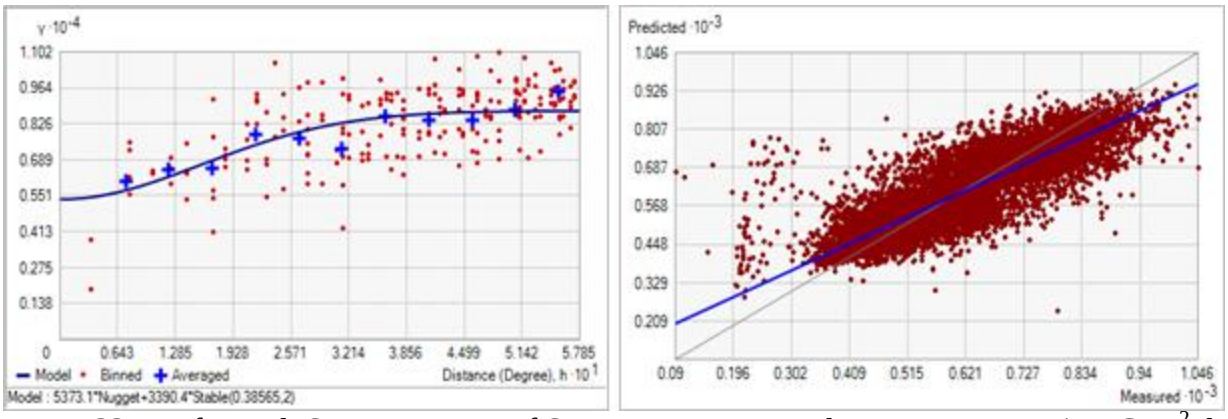

Figure 332. Left panel: Semivariogram of Summer Primary Production Minimum (mg C m^{-2} day^{-1}). Binned values are shown as red dots; average points are shown as blue crosses; the model fit to the averaged values is shown as a blue line. Lag size: 0.048 degrees; number of lags: 12; Parameter: 2; Range: 0.386 degrees; Partial Sill: 3390.435. Right panel: Scatterplot of predicted values versus observed values for the model of Summer Primary Production Minimum (mg C m^{-2} day^{-1}).

Table 166. Results of cross-validation of the kriged model for Summer Primary Production Minimum (mg C m^{-2} day^{-1}).

Prediction error	**Value**
Number of Observations	10374
Overall Mean Error	8.378×10^{-3}
Root Mean Square Prediction Error	76.552
Standardized Mean	1.500×10^{-4}
Standardized Root Mean Square Prediction Error	0.952
Average Standard Error	80.606

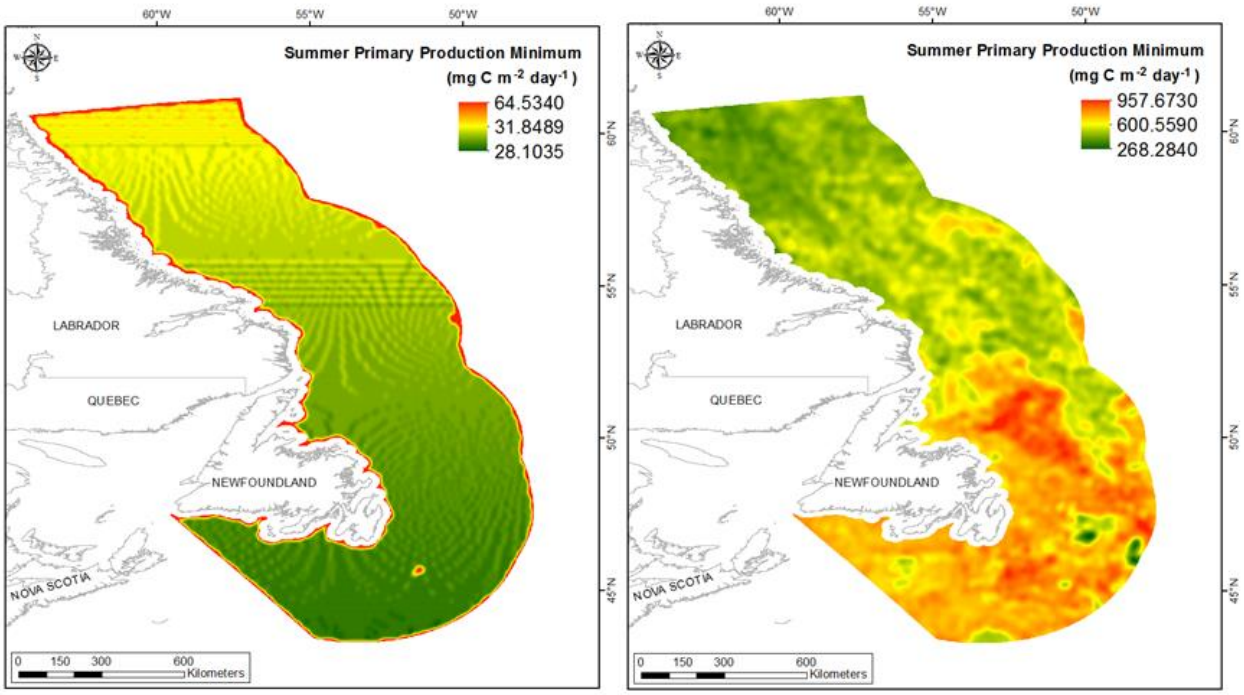

Figure 333. Left panel: Prediction standard error surface of Summer Primary Production Minimum (mg C m^{-2} day^{-1}). Right panel: Interpolated prediction surface of Summer Primary Production Minimum (mg C m^{-2} day^{-1}).

Summer Primary Production Maximum

This variable displayed a near normal distribution prior to modeling (Table 167, Figure 334). The data were higher than predicted by a normal distribution at low and upper mid-values and lower at high values (Figure 335). The areas of under- and over-prediction were relatively minor and showed no strong spatial pattern over the spatial extent (Figure 335).

The semivariogram showed moderate autocorrelation present in the data and the model showed a fair fit between measured and predicted values (Figure 336). Although the RMSE and ASE were high (Table 168), all other errors showed that the model was good at prediction. The error map showed low to medium error over the study extent with higher error along the edges (Figure 337). The kriged surface is presented in Figure 337.

Table 167. Distributional properties of Summer Primary Production Maximum (mg C m^{-2} day^{-1}).

Property	Value
Number of Observations	10374
Minimum	184.060
Maximum	2127.500
Mean	1180.900
Median	1174.200
Standard Deviation	231.400
Skewness	0.214
Kurtosis	2.689

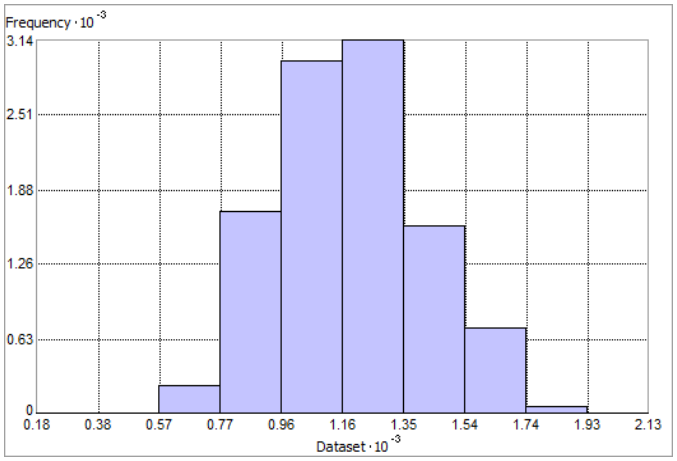

Figure 334. Distribution of Summer Primary Production Maximum (mg C m^{-2} day^{-1}). Histogram was illustrated using 10 bins. X and Y axes are shown at10^{-3}.

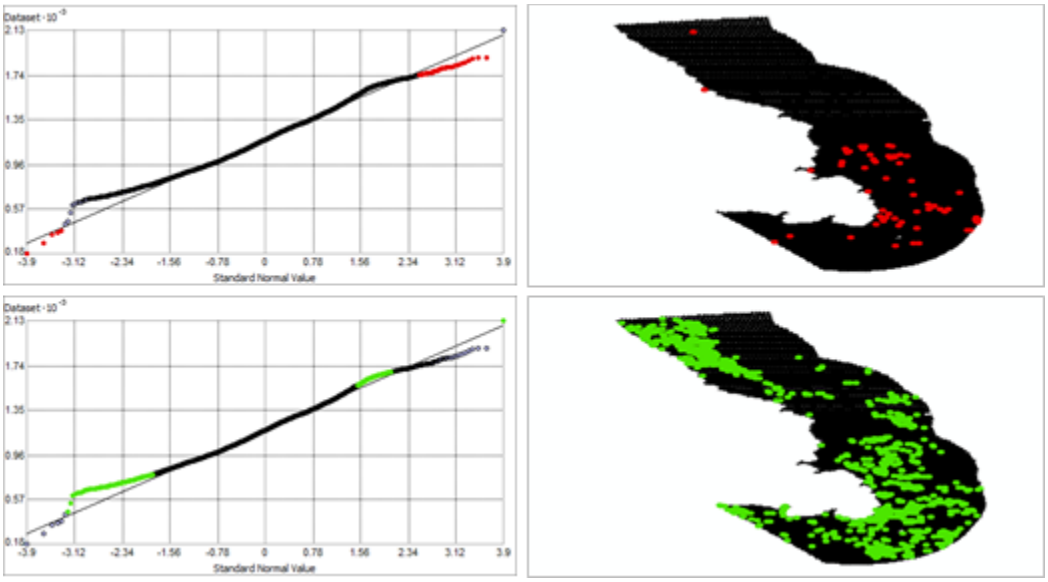

Figure 335. Normal Q-Q plot for data values of Summer Primary Production Maximum (mg C m^{-2} day^{-1}). Points falling under (upper panel) and over (bottom panel) the reference line are mapped.

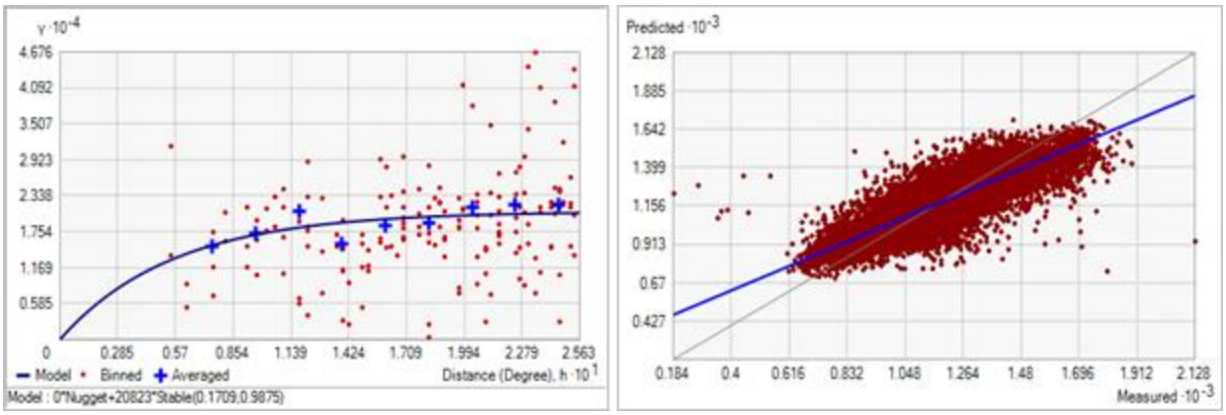

Figure 336. Left panel: Semivariogram of Summer Primary Production Maximum (mg C m^{-2} day^{-1}). Binned values are shown as red dots; average points are shown as blue crosses; the model fit to the averaged values is shown as a blue line. Lag size: 0.021 degrees; number of lags: 12; Parameter: 0.988; Range: 0.171 degrees; Partial Sill: 20823.110. Right panel: Scatterplot of predicted values versus observed values for the model of Summer Primary Production Maximum (mg C m^{-2} day^{-1}).

Table 168. Results of cross-validation of the kriged model for Summer Primary Production Maximum (mg C m^{-2} day^{-1}).

Prediction error	**Value**
Number of Observations	10374
Overall Mean Error	-0.032
Root Mean Square Prediction Error	132.899
Standardized Mean	-1.860×10^{-4}
Standardized Root Mean Square Prediction Error	0.958
Average Standard Error	138.816

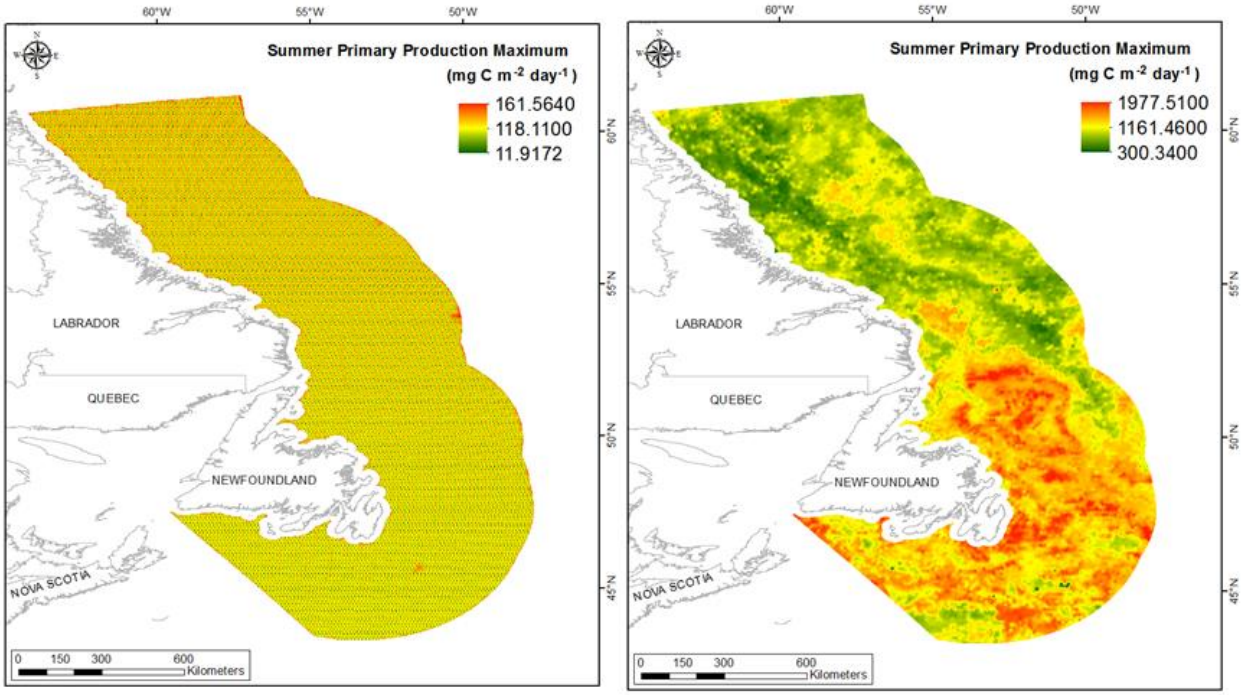

Figure 337. Left panel: Prediction standard error surface of Summer Primary Production Maximum (mg C m^{-2} day^{-1}). Right panel: Interpolated prediction surface of Summer Primary Production Maximum (mg C m^{-2} day^{-1}).

Summer Primary Production Range

This variable displayed a bell-shaped distribution prior to modeling (Table 169, Figure 338). The data were higher than predicted by a normal distribution at low and high values but very well predicted at mid-range values (Figure 339). The areas of over-prediction showed no spatial pattern over the spatial extent (Figure 339). There was little to no under-prediction.

The semivariogram showed weak autocorrelation present in the data and the model showed a poor fit between measured and predicted values (Figure 340). Although the RMSE and ASE were high (Table 170), all other errors showed that the model was good at prediction. The error map showed medium to high error in a grid-like pattern over the study extent (Figure 341). The kriged surface is presented in Figure 341.

Table 169. Distributional properties of Summer Primary Production Range (mg C m^{-2} day^{-1}).

Property	Value
Number of Observations	10374
Minimum	52.220
Maximum	1455.800
Mean	567.190
Median	555.710
Standard Deviation	193.180
Skewness	0.394
Kurtosis	3.084

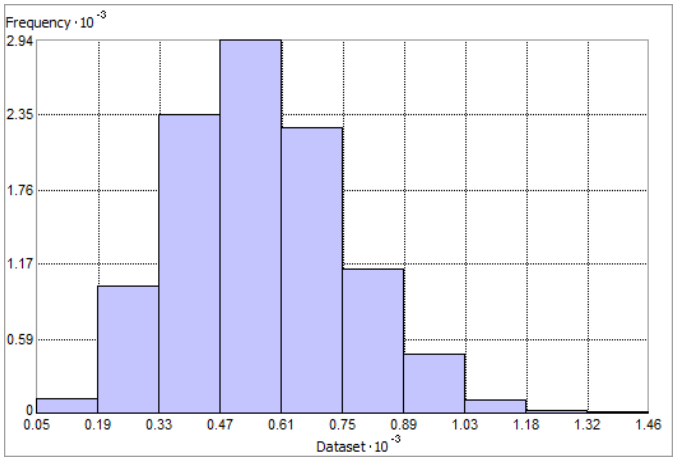

Figure 338. Distribution of Summer Primary Production Range (mg C m^{-2} day^{-1}). Histogram was illustrated using 10 bins. X and Y axes are shown at 10^{-3}:

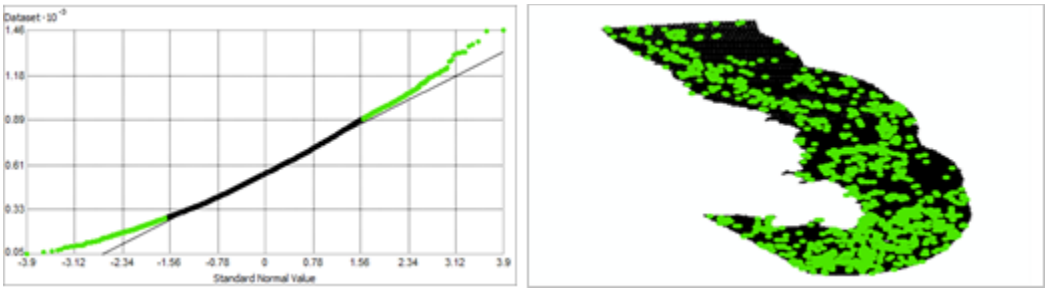

Figure 339. Normal Q-Q plot for data values of Summer Primary Production Range (mg C m^{-2} day^{-1}). Points falling over bottom panel the reference line are mapped; no points fall below the reference line.

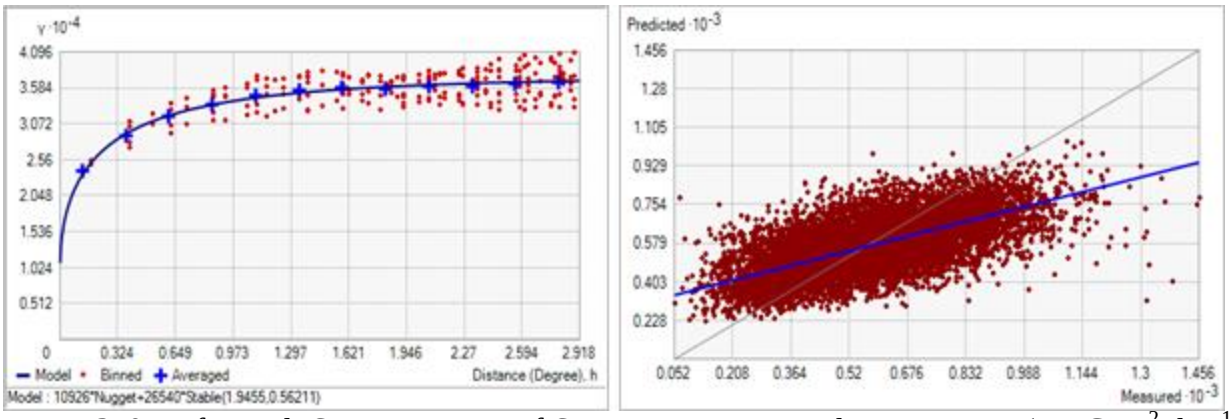

Figure 340. Left panel: Semivariogram of Summer Primary Production Range (mg C m^{-2} day^{-1}). Binned values are shown as red dots; average points are shown as blue crosses; the model fit to the averaged values is shown as a blue line. Lag size: 0.243 degrees; number of lags: 12; Parameter: 0.562; Range: 1.946 degrees; Partial Sill: 26540.090. Right panel: Scatterplot of predicted values versus observed values for the model of Summer Primary Production Range (mg C m^{-2} day^{-1}).

Table 170. Results of cross-validation of the kriged model for Summer Primary Production Range (mg C m^{-2} day^{-1}).

Prediction error	**Value**
Number of Observations	10374
Overall Mean Error	-0.016
Root Mean Square Prediction Error	149.513
Standardized Mean	-9.455×10^{-5}
Standardized Root Mean Square Prediction Error	0.956
Average Standard Error	156.467

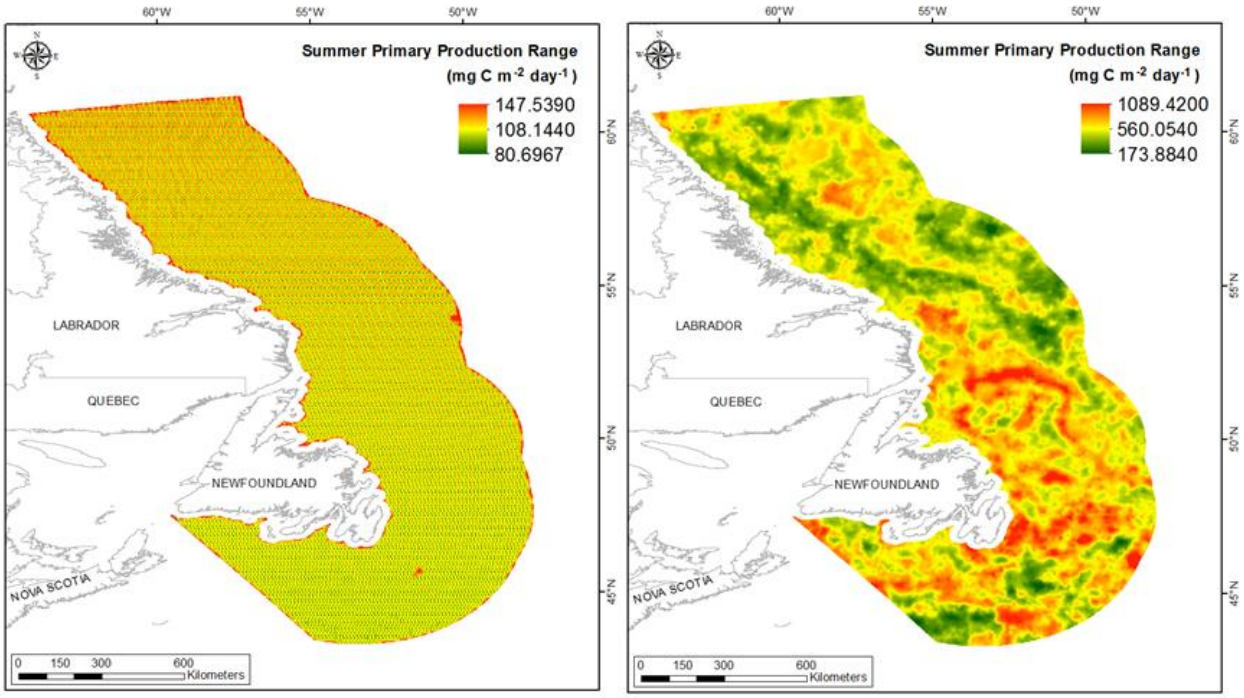

Figure 341. Left panel: Prediction standard error surface of Summer Primary Production Range (mg C m^{-2} day^{-1}). Right panel: Interpolated prediction surface of Summer Primary Production Range (mg C m^{-2} day^{-1}).

Summer Primary Production Average Minimum

This variable displayed a bell-shaped distribution with left skewness (Table 171, Figure 342). The data were lower and higher than predicted by a normal distribution at high and low values, respectively, however mid-range values were well predicted (Figure 343). The areas of under- and over-prediction showed a strong spatial pattern over the study extent with northern areas over-predicted and southern ones under-predicted (Figure 343).

The semivariogram showed moderate autocorrelation present in the data and the model showed a fair fit between measured and predicted values (Figure 344). Although the RMSE and ASE were high (Table 172), all other errors showed that the model was good at prediction. The error map showed low to medium error over the study extent with higher error along the edges (Figure 345). The kriged surface is presented in Figure 345.

Table 171. Distributional properties of Summer Primary Production Average Minimum (mg C m^{-2} day^{-1}).

Property	Value
Number of Observations	10374
Minimum	139.070
Maximum	1122.700
Mean	746.810
Median	747.600
Standard Deviation	136.430
Skewness	-0.018
Kurtosis	2.317

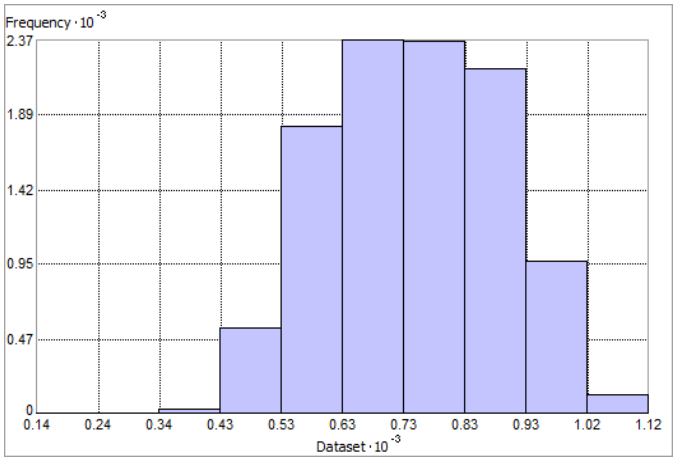

Figure 342. Distribution of Summer Primary Production Average Minimum (mg C m^{-2} day^{-1}). Histogram was illustrated using 10 bins. X and Y axes are shown at 10^{-3}.

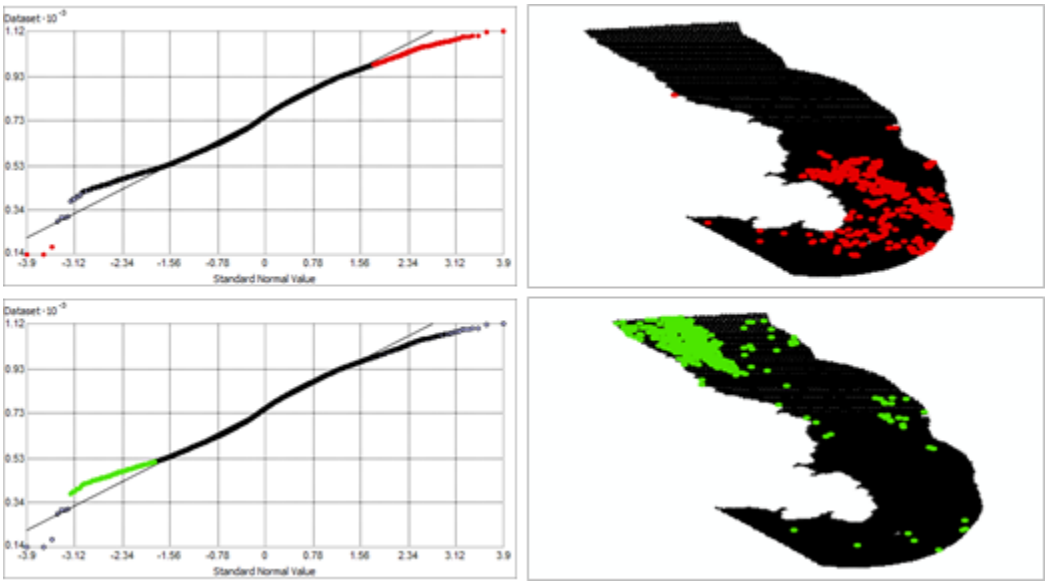

Figure 343. Normal Q-Q plot for data values of Summer Primary Production Average Minimum (mg C m^{-2} day^{-1}). Points falling under (upper panel) and over (bottom panel) the reference line are mapped.

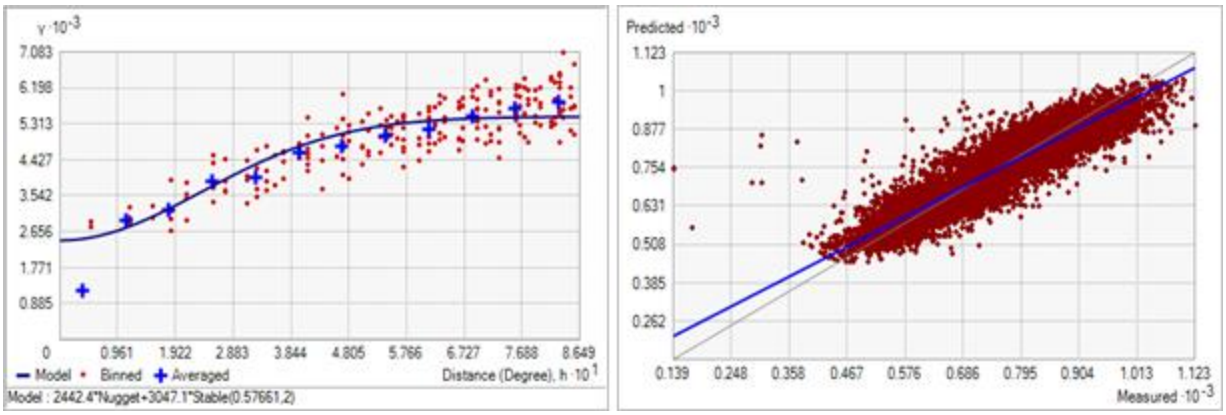

Figure 344. Left panel: Semivariogram of Summer Primary Production Average Minimum (mg C m^{-2} day^{-1}). Binned values are shown as red dots; average points are shown as blue crosses; the model fit to the averaged values is shown as a blue line. Lag size: 0.072 degrees; number of lags: 12; Parameter: 2; Range: 0.577 degrees; Partial Sill: 3047.150. Right panel: Scatterplot of predicted values versus observed values for the model of Summer Primary Production Average Minimum (mg C m^{-2} day^{-1}).

Table 172. Results of cross-validation of the kriged model for Summer Primary Production Average Minimum (mg C m^{-2} day^{-1}).

Prediction error	**Value**
Number of Observations	10374
Overall Mean Error	2.631×10^{-3}
Root Mean Square Prediction Error	53.611
Standardized Mean	1.472×10^{-4}
Standardized Root Mean Square Prediction Error	1.006
Average Standard Error	53.298

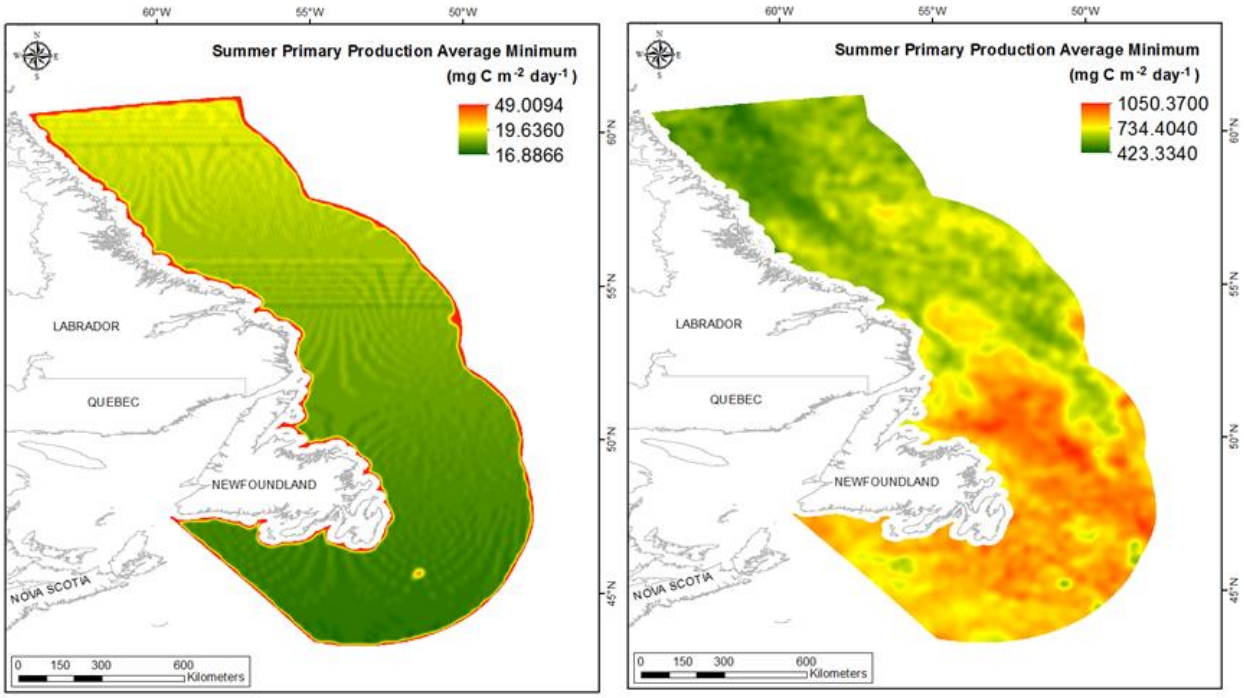

Figure 345. Left panel: Prediction standard error surface of Summer Primary Production Average Minimum (mg C m^{-2} day^{-1}). Right panel: Interpolated prediction surface of Summer Primary Production Average Minimum (mg C m^{-2} day^{-1}).

Summer Primary Production Average Maximum

This variable displayed a bell-shaped distribution with left-skewness (Table 173, Figure 346). The data were higher than predicted by a normal distribution at low values and lower than predicted at high values, however the mid-values deviated only slightly from the reference line (Figure 347). The areas of mild under-prediction were found in the south, while areas of over-prediction showed no strong spatial pattern over the spatial extent (Figure 347).

The semivariogram showed moderate autocorrelation present in the data and the model showed a fair fit between measured and predicted values (Figure 348). Although the RMSE and ASE were high (Table 174), all other errors showed that the model was good at prediction. The error map showed medium to high error in a grid-like pattern over the study extent (Figure 349). The kriged surface is presented in Figure 349.

Table 173. Distributional properties of Summer Primary Production Average Maximum (mg C m^{-2} day^{-1}).

Property	Value
Number of Observations	10374
Minimum	162.760
Maximum	1597.300
Mean	980.690
Median	967.340
Standard Deviation	178.530
Skewness	0.115
Kurtosis	2.305

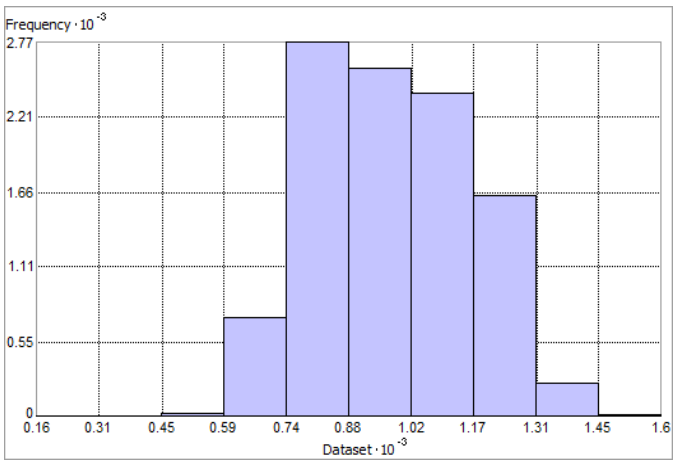

Figure 346. Distribution of Summer Primary Production Average Maximum (mg C m^{-2} day^{-1}). Histogram was illustrated using 10 bins. X and Y axes are shown at 10^{-3}.

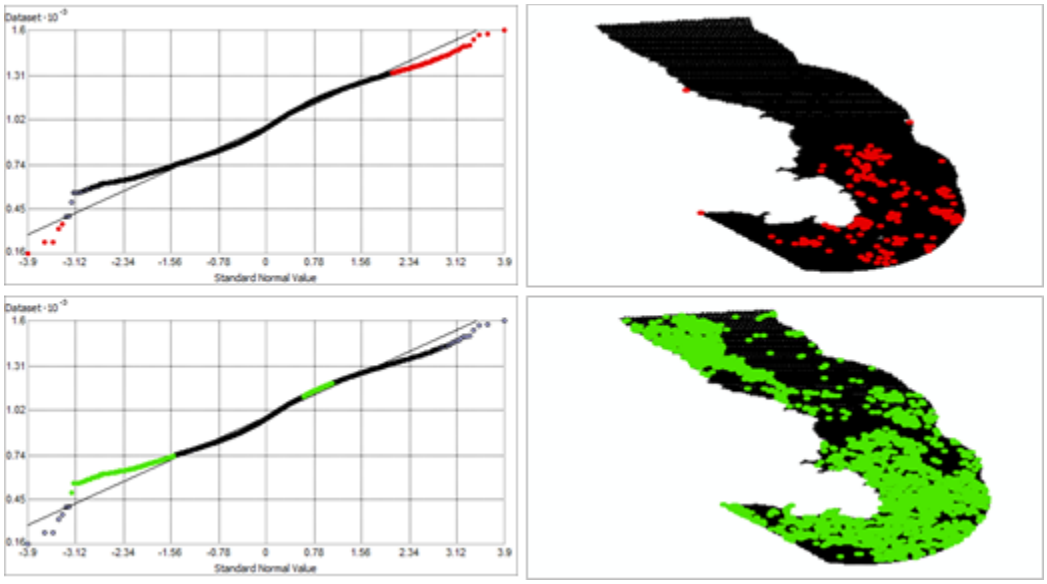

Figure 347. Normal Q-Q plot for data values of Summer Primary Production Average Maximum (mg C m^{-2} day^{-1}). Points falling under (upper panel) and over (bottom panel) the reference line are mapped.

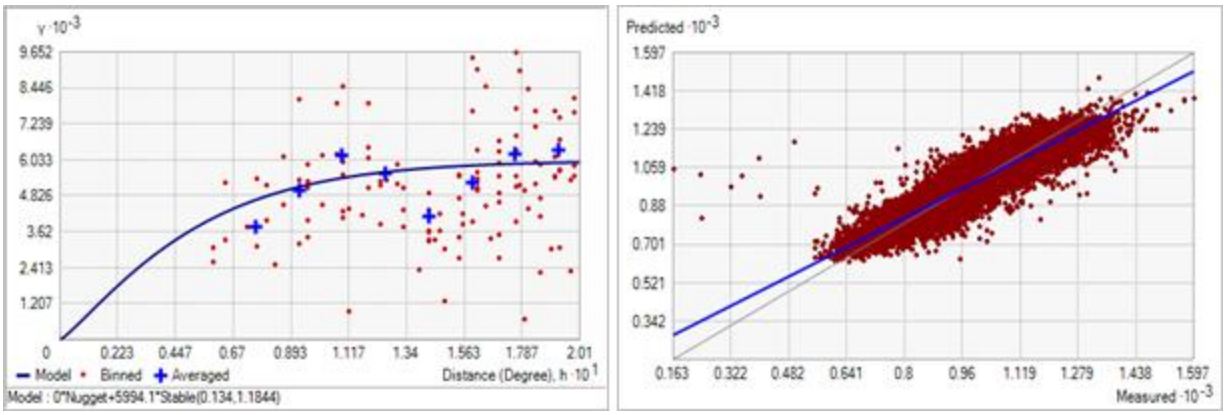

Figure 348. Left panel: Semivariogram of Summer Primary Production Average Maximum (mg C m^{-2} day^{-1}). Binned values are shown as red dots; average points are shown as blue crosses; the model fit to the averaged values is shown as a blue line. Lag size: 0.017 degrees; number of lags: 12; Parameter: 1.184; Range: 0.134 degrees; Partial Sill: 5994.127. Right panel: Scatterplot of predicted values versus observed values for the model of Summer Primary Production Average Maximum (mg C m^{-2} day^{-1}).

Table 174. Results of cross-validation of the kriged model for Summer Primary Production Average Maximum (mg C m^{-2} day^{-1}).

Prediction error	**Value**
Number of Observations	10374
Overall Mean Error	-0.028
Root Mean Square Prediction Error	71.835
Standardized Mean	-2.856×10^{-4}
Standardized Root Mean Square Prediction Error	0.937
Average Standard Error	76.752

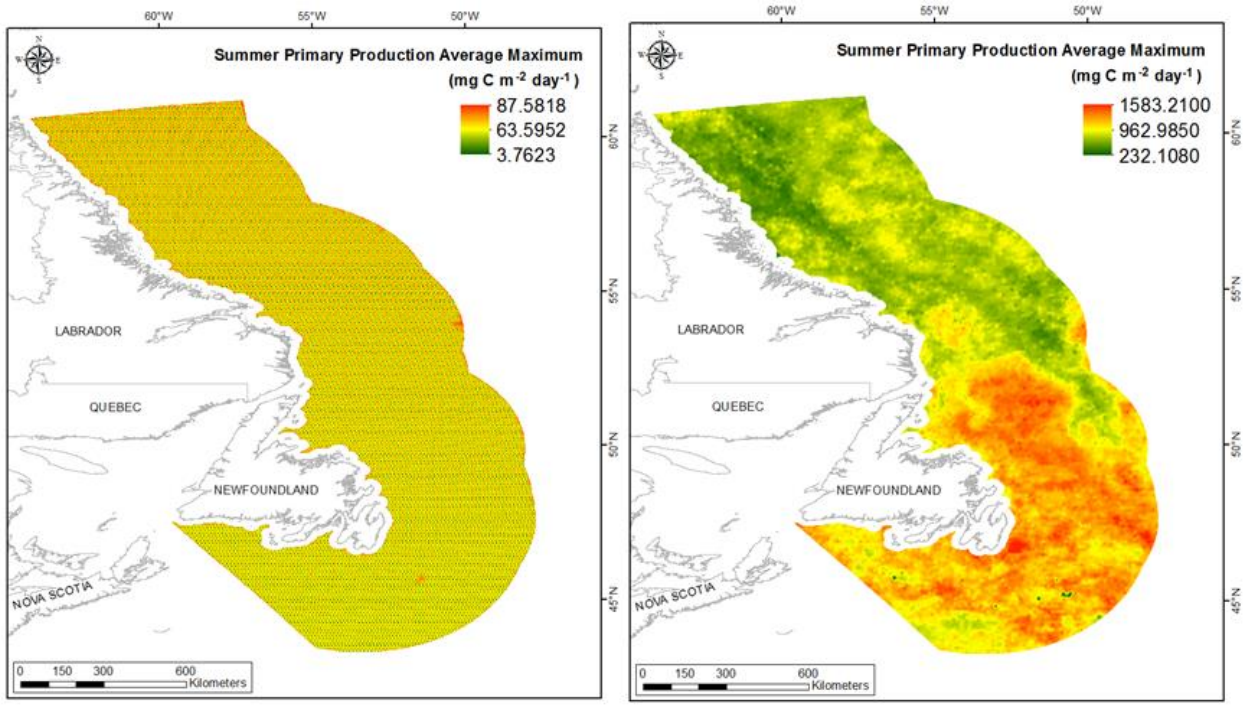

Figure 349. Left panel: Prediction standard error surface of Summer Primary Production Average Maximum (mg C m^{-2} day^{-1}). Right panel: Interpolated prediction surface of Summer Primary Production Average Maximum (mg C m^{-2} day^{-1}).

Summer Primary Production Average Range

This variable displayed a bell-shaped distribution with right-skewness (Table 175, Figure 350). The data were higher than predicted by a normal distribution at low and high values, however mid-values were well predicted (Figure 351). The areas of over-prediction showed no spatial pattern over the spatial extent (Figure 351).

The semivariogram showed moderate autocorrelation present in the data and the model showed a fair to poor fit between measured and predicted values (Figure 352). Although the RMSE and ASE were high (Table 176), all other errors showed that the model was good at prediction. The error map showed medium to high error in a grid-like pattern over the study extent (Figure 353). The kriged surface is presented in Figure 353.

Table 175. Distributional properties of Summer Primary Production Average Range (mg C m^{-2} day^{-1}).

Property	Value
Number of Observations	10374
Minimum	8.415
Maximum	725.890
Mean	233.880
Median	221.680
Standard Deviation	100.090
Skewness	0.652
Kurtosis	3.467

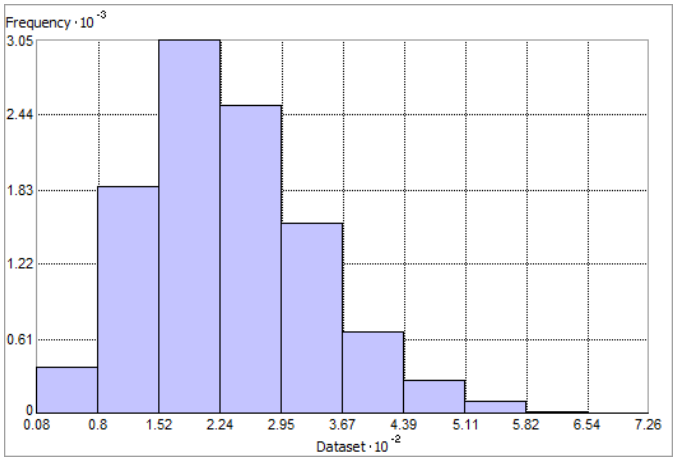

Figure 350. Distribution of Summer Primary Production Average Range (mg C m^{-2} day^{-1}). Histogram was illustrated using 10 bins. X axis is shown at 10^{-2}; Y axis is shown at 10^{-3}.

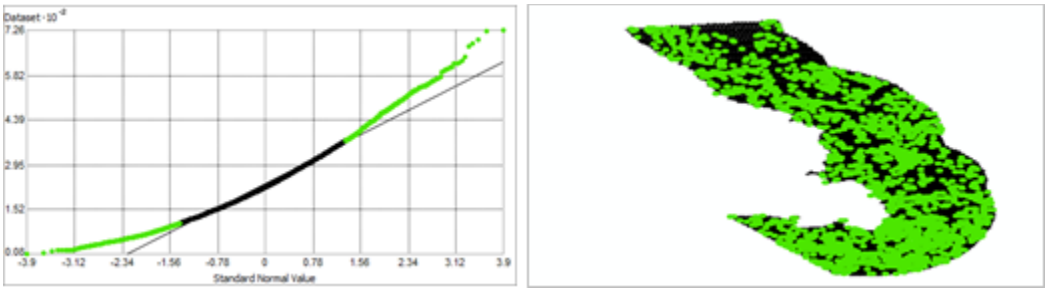

Figure 351. Normal Q-Q plot for data values of Summer Primary Production Average Range (mg C m^{-2} day^{-1}). Points falling over bottom panel the reference line are mapped; no points fall below the reference line.

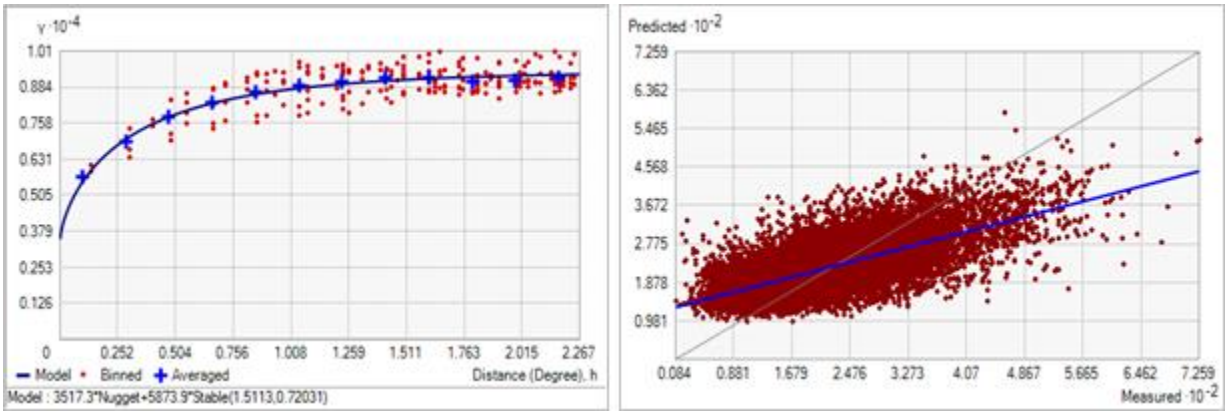

Figure 352. Left panel: Semivariogram of Summer Primary Production Average Range (mg C m^{-2} day^{-1}). Binned values are shown as red dots; average points are shown as blue crosses; the model fit to the averaged values is shown as a blue line. Lag size: 0.189 degrees; number of lags: 12; Parameter: 0.720; Range: 1.511 degrees; Partial Sill: 5873.873. Right panel: Scatterplot of

predicted values versus observed values for the model of Summer Primary Production Average Range (mg C m^{-2} day^{-1}).

Table 176. Results of cross-validation of the kriged model for Summer Primary Production Average Range (mg C m^{-2} day^{-1}).

Prediction error	Value
Number of Observations	10374
Overall Mean Error	-0.013
Root Mean Square Prediction Error	75.254
Standardized Mean	-1.711×10^{-4}
Standardized Root Mean Square Prediction Error	0.968
Average Standard Error	77.821

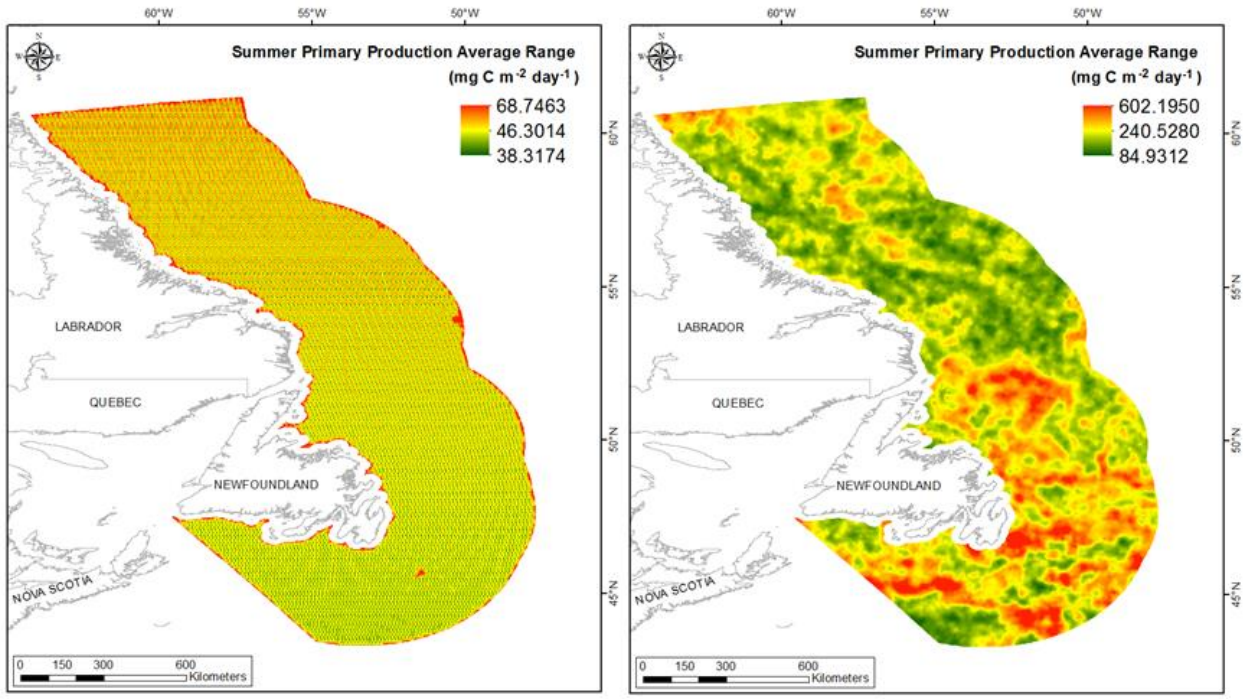

Figure 353. Left panel: Prediction standard error surface of Summer Primary Production Average Range (mg C m^{-2} day^{-1}). Right panel: Interpolated prediction surface of Summer Primary Production Average Range (mg C m^{-2} day^{-1}).

Fall Primary Production Mean

This variable displayed a mild bimodal distribution prior to modeling (Table 177, Figure 354). The data were higher than predicted by a normal distribution at low and upper mid-values and lower at high and mid-values (Figure 355). The areas of under- and over-prediction showed no strong spatial pattern over the spatial extent except for the mid-region of the area where the data were over-predicted (Figure 355).

The semivariogram showed very weak autocorrelation present in the data. However, the model showed a good fit between measured and predicted values (Figure 356). Although the RMSE and ASE were high (Table 178), all other errors showed that the model was good at prediction. The error map showed high error in the deep waters of the northern portion of the study extent where no data observations occur (Figure 357). The kriged surface is presented in Figure 357.

Table 177. Distributional properties of Fall Primary Production Mean (mg C m^{-2} day^{-1}).

Property	Value
Number of Observations	8630
Minimum	103.100
Maximum	772.000
Mean	487.940
Median	490.550
Standard Deviation	122.300
Skewness	-0.127
Kurtosis	1.772

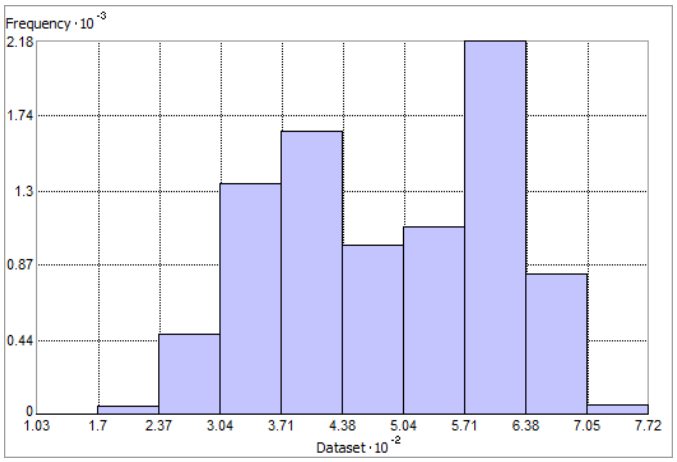

Figure 354. Distribution of Fall Primary Production Mean (mg C m^{-2} day^{-1}). Histogram was illustrated using 10 bins. X axis is shown at 10^{-2}; Y axis is shown at 10^{-3}.

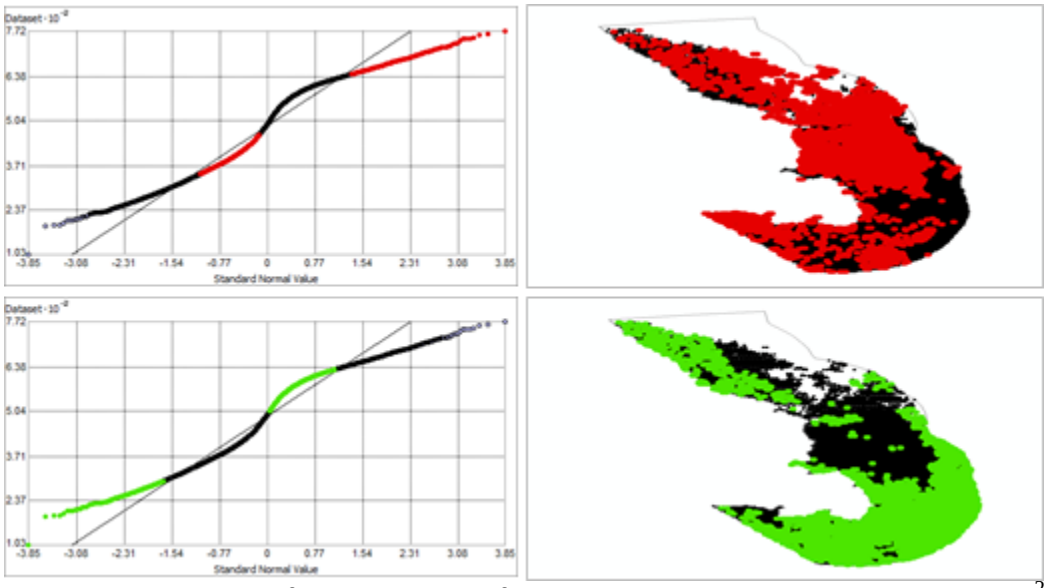

Figure 355. Normal Q-Q plot for data values of Fall Primary Production Mean (mg C m^{-2} day^{-1}). Points falling under (upper panel) and over (bottom panel) the reference line are mapped.

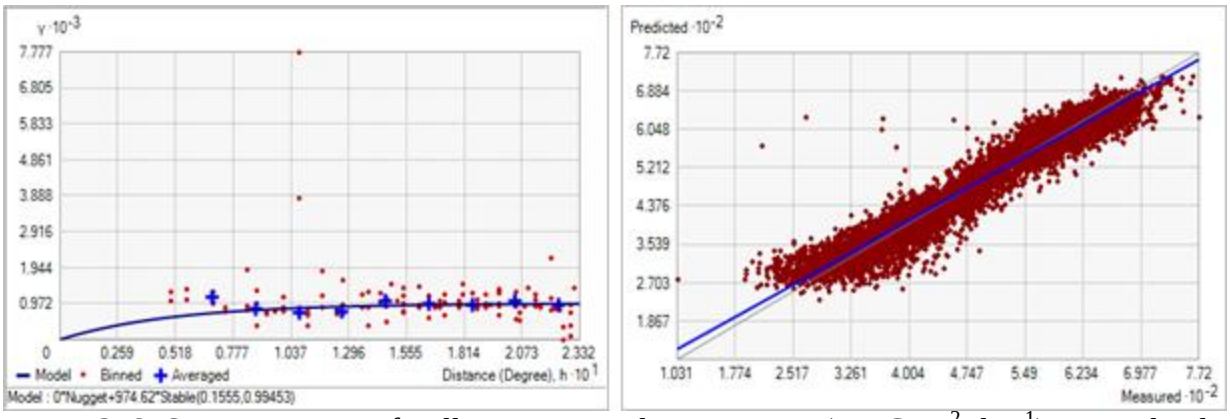

Figure 356. Semivariogram of Fall Primary Production Mean (mg C m^{-2} day^{-1}). Binned values are shown as red dots; average points are shown as blue crosses; the model fit to the averaged values is shown as a blue line. Lag size: 0.019 degrees; number of lags: 12; Parameter: 0.995; Range: 0.155 degrees; Partial Sill: 974.616. Right panel: Scatterplot of predicted values versus observed values for the model of Fall Primary Production Mean (mg C m^{-2} day^{-1}).

Table 178. Results of cross-validation of the kriged model for Fall Primary Production Mean (mg C m^{-2} day^{-1}).

Prediction error	**Value**
Number of Observations	8630
Overall Mean Error	-0.067
Root Mean Square Prediction Error	30.049
Standardized Mean	-1.985×10^{-3}
Standardized Root Mean Square Prediction Error	0.982
Average Standard Error	30.540

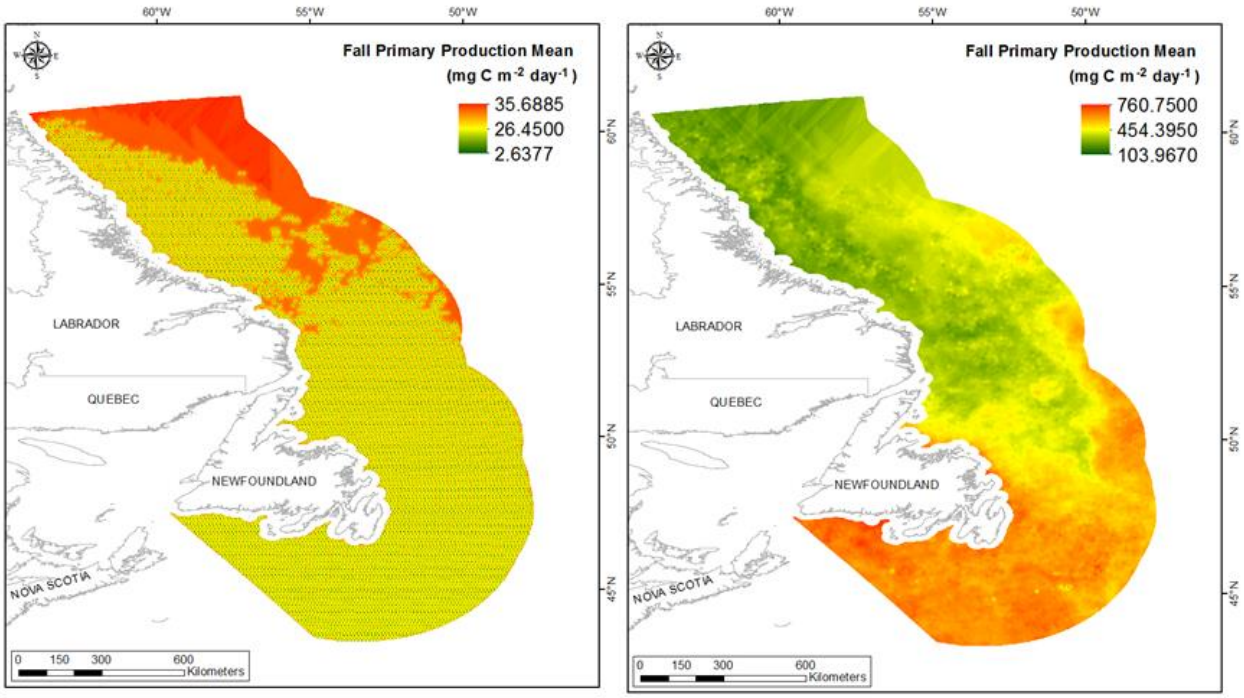

Figure 357. Left panel: Prediction standard error surface of Fall Primary Production Mean (mg C m^{-2} day^{-1}). Right panel: Interpolated prediction surface of Fall Primary Production Mean (mg C m^{-2} day^{-1}).

Fall Primary Production Minimum

This variable displayed a bell-shaped distribution with right-skewness (Table 179, Figure 358). The data were higher than predicted by a normal distribution at low and high values; however the mid-values deviated only slightly from the reference line (Figure 359). The areas of under- and over-prediction showed no strong spatial pattern over the spatial extent (Figure 359).

The semivariogram showed weak autocorrelation present in the data and the model showed a fair fit between measured and predicted values (Figure 360). Although the RMSE and ASE were high (Table 180), all other errors showed that the model was good at prediction. The error map showed high error in the deep waters of the northern portion of the study extent where no data observations occur (Figure 361). The kriged surface is presented in Figure 361.

Table 179. Distributional properties of Fall Primary Production Minimum (mg C m^{-2} day^{-1}).

Property	Value
Number of Observations	8630
Minimum	51.450
Maximum	671.230
Mean	269.410
Median	252.350
Standard Deviation	102.540
Skewness	0.753
Kurtosis	3.154

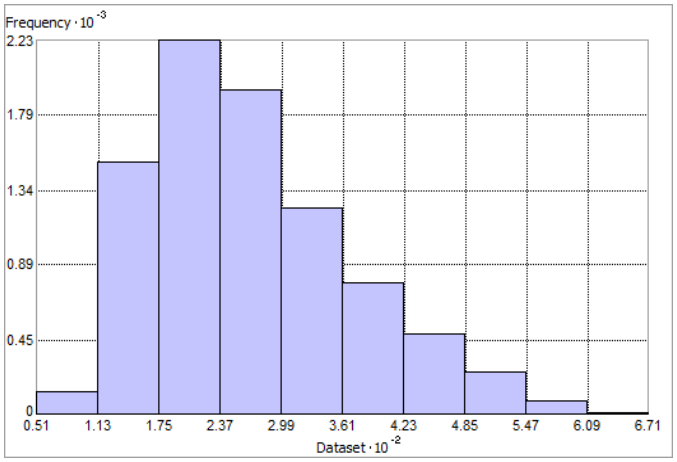

Figure 358. Distribution of Fall Primary Production Minimum (mg C m^{-2} day^{-1}). Histogram was illustrated using 10 bins. X axis is shown at 10^{-2}; Y axis is shown at 10^{-3}.

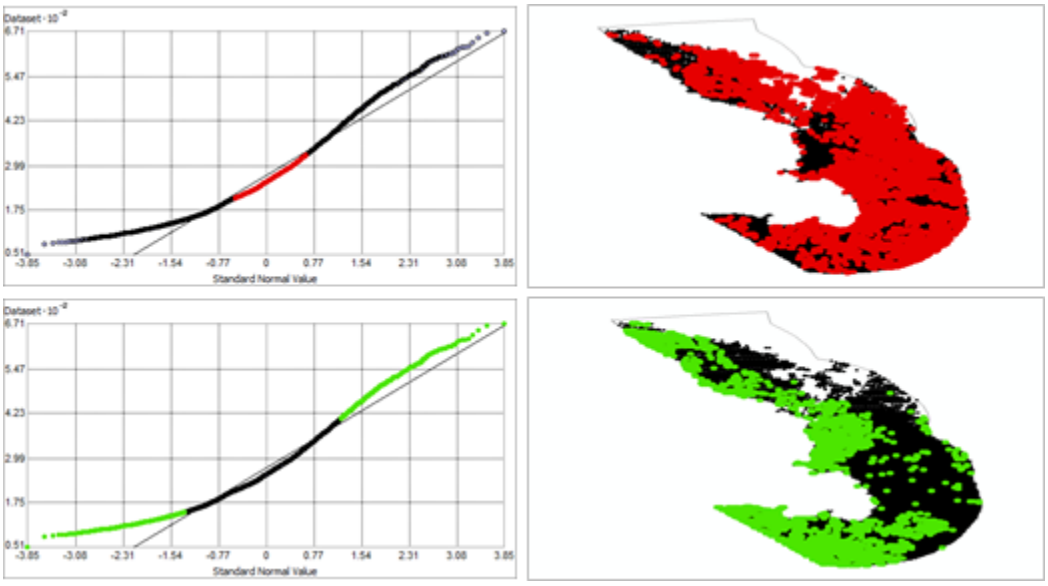

Figure 359. Normal Q-Q plot for data values of Fall Primary Production Minimum (mg C m^{-2} day^{-1}). Points falling under (upper panel) and over (bottom panel) the reference line are mapped.

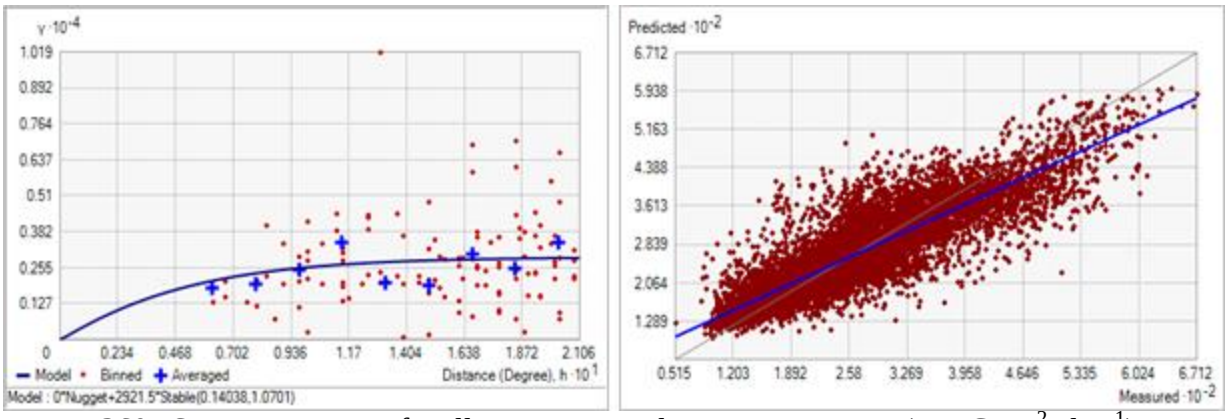

Figure 360. Semivariogram of Fall Primary Production Minimum (mg C m^{-2} day^{-1}). Binned values are shown as red dots; average points are shown as blue crosses; the model fit to the averaged values is shown as a blue line. Lag size: 0.018 degrees; number of lags: 12; Parameter: 1.070; Range: 0.140 degrees; Partial Sill: 2921.550. Right panel: Scatterplot of predicted values versus observed values for the model of Annual Primary Production Minimum (mg C m^{-2} day^{-1}).

Table 180. Results of cross-validation of the kriged model for Fall Primary Production Minimum (mg C m^{-2} day^{-1}).

Prediction error	**Value**
Number of Observations	8630
Overall Mean Error	-0.028
Root Mean Square Prediction Error	51.012
Standardized Mean	-5.867×10^{-4}
Standardized Root Mean Square Prediction Error	0.956
Average Standard Error	53.501

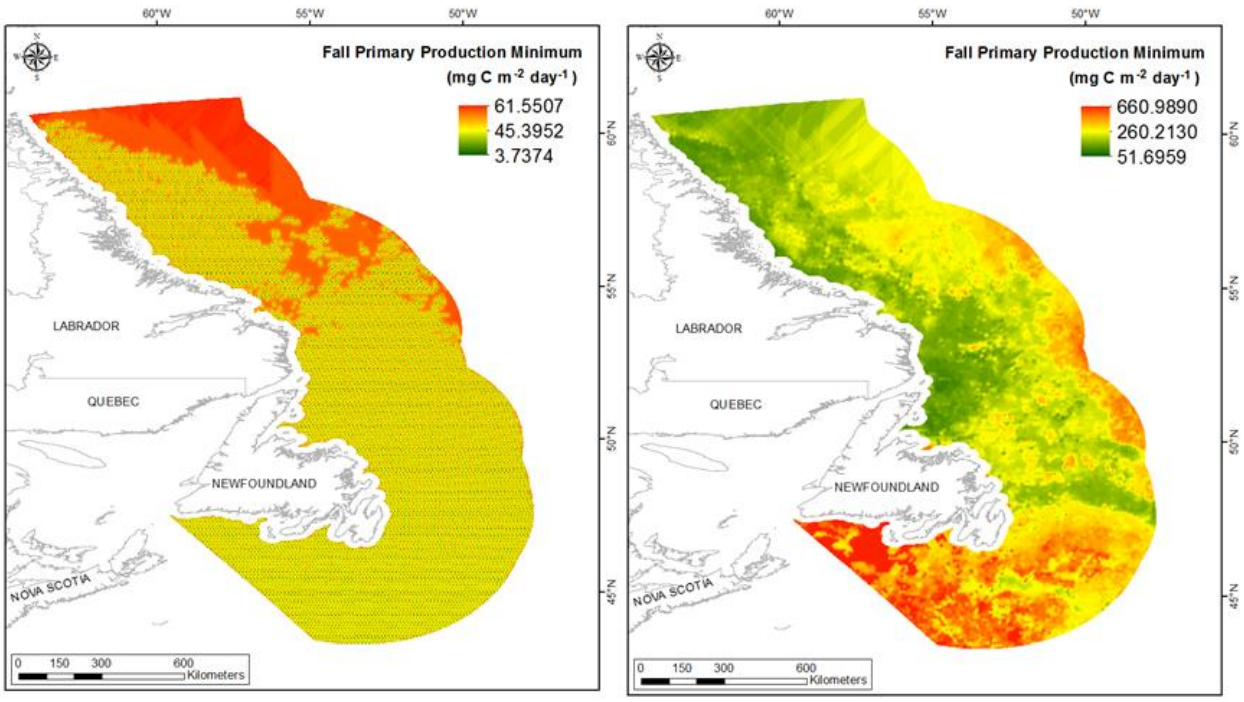

Figure 361. Left panel: Prediction standard error surface of Fall Primary Production Minimum (mg C m^{-2} day^{-1}). Right panel: Interpolated prediction surface of Fall Primary Production Minimum (mg C m^{-2} day^{-1}).

Fall Primary Production Maximum

This variable displayed a bell-shaped distribution with left-skewness (Table 181, Figure 362). The data fit was very good but were slightly higher than predicted by a normal distribution at low, high and mid-values, and slightly lower than predicted at mid upper values (Figure 363). The areas of under- and over-prediction showed no strong spatial pattern over the spatial extent (Figure 363).

The semivariogram showed moderate autocorrelation present in the data and the model showed a fair fit between measured and predicted values (Figure 364). Although the RMSE and ASE were high (Table 182), all other errors showed that the model was good at prediction The error map showed high error in the deep waters of the northern portion of the study extent where no data observations occur (Figure 365). The kriged surface is presented in Figure 365.

Table 181. Distributional properties of Fall Primary Production Maximum (mg C m^{-2} day^{-1}).

Property	Value
Number of Observations	8630
Minimum	138.690
Maximum	1425.800
Mean	709.220
Median	752.430
Standard Deviation	166.630
Skewness	-0.252
Kurtosis	2.648

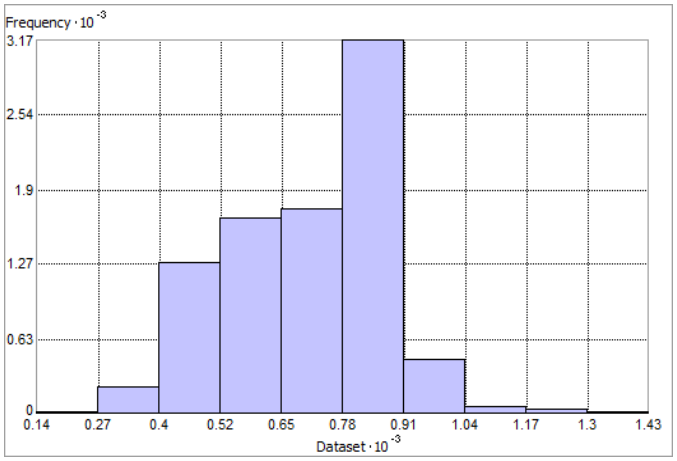

Figure 362. Distribution of Fall Primary Production Maximum (mg C m^{-2} day^{-1}). Histogram was illustrated using 10 bins. X and Y axes are shown at 10^{-3} .

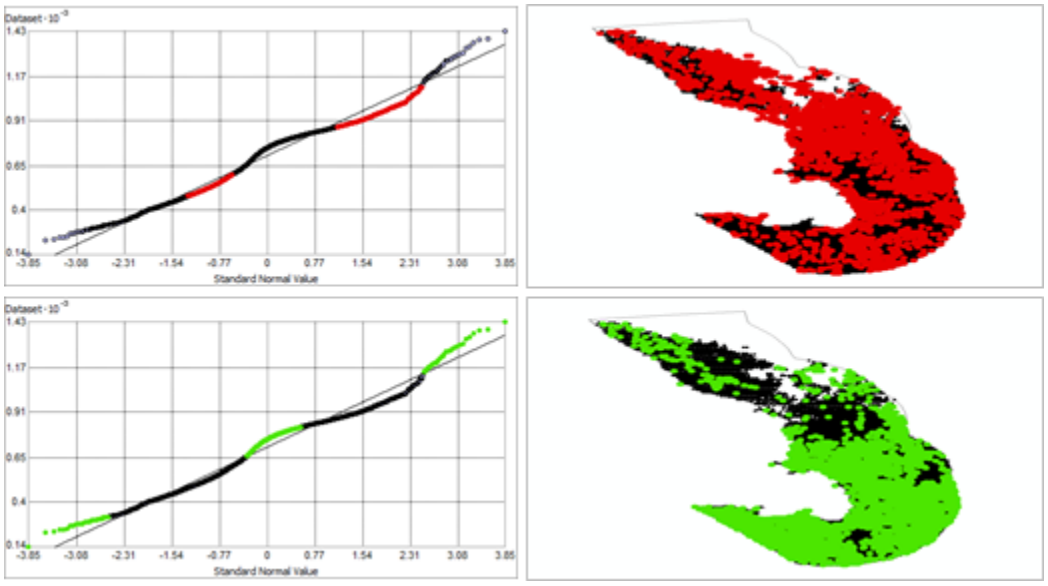

Figure 363. Normal Q-Q plot for data values of Fall Primary Production Maximum (mg C m^{-2} day^{-1}). Points falling under (upper panel) and over (bottom panel) the reference line are mapped.

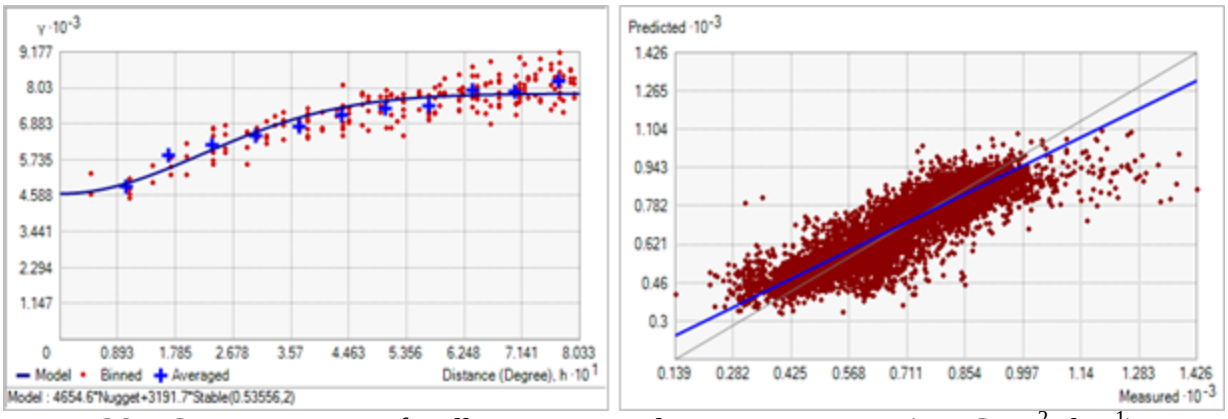

Figure 364. Semivariogram of Fall Primary Production Maximum (mg C m^{-2} day^{-1}). Binned values are shown as red dots; average points are shown as blue crosses; the model fit to the averaged values is shown as a blue line. Lag size: 0.067 degrees; number of lags: 12; Parameter: 2; Range: 0.536 degrees; Partial Sill: 3191.698. Right panel: Scatterplot of predicted values versus observed values for the model of Annual Primary Production Maximum (mg C m^{-2} day^{-1}).

Table 182. Results of cross-validation of the kriged model for Fall Primary Production Maximum (mg C m^{-2} day^{-1}).

Prediction error	**Value**
Number of Observations	8630
Overall Mean Error	-0.040
Root Mean Square Prediction Error	75.388
Standardized Mean	-3.310×10^{-4}
Standardized Root Mean Square Prediction Error	1.032
Average Standard Error	72.923

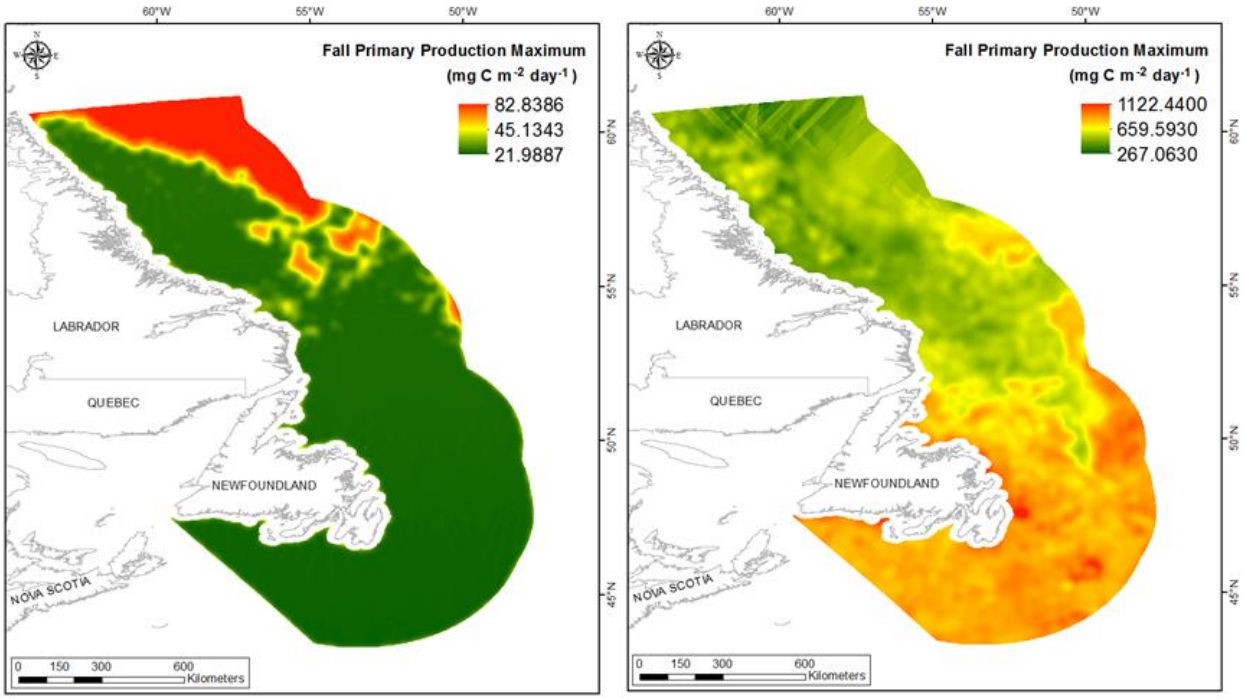

Figure 365. Left panel: Prediction standard error surface of Fall Primary Production Maximum (mg C m^{-2} day^{-1}). Right panel: Interpolated prediction surface of Fall Primary Production Maximum (mg C m^{-2} day^{-1}).

Fall Primary Production Range

This variable displayed a near normal distribution with kurtosis prior to modeling (Table 183, Figure 366). The data were higher than predicted by a normal distribution at low and high values, however the mid-region was well predicted (Figure 367). The areas of over-prediction showed no spatial pattern over the spatial extent (Figure 367).

The semivariogram showed moderate autocorrelation present in the data and the model showed a fair to poor fit between measured and predicted values (Figure 368). Although the RMSE and ASE were high (Table 184), all other errors showed that the model was good at prediction. The error map showed high error in the deep waters of the northern portion of the study extent where no data observations occur (Figure 369). The kriged surface is presented in Figure 369.

Table 183. Distributional properties of Fall Primary Production Range (mg C m^{-2} day^{-1}).

Property	Value
Number of Observations	8630
Minimum	35.190
Maximum	1142.900
Mean	439.810
Median	438.79
Standard Deviation	148.810
Skewness	0.213
Kurtosis	3.113

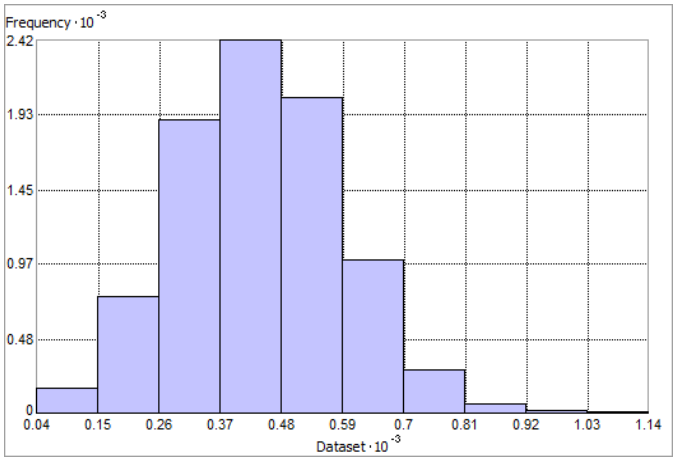

Figure 366. Distribution of Fall Primary Production Range (mg C m^{-2} day^{-1}). Histogram was illustrated using 10 bins. X and Y axes are shown at 10^{-3}.

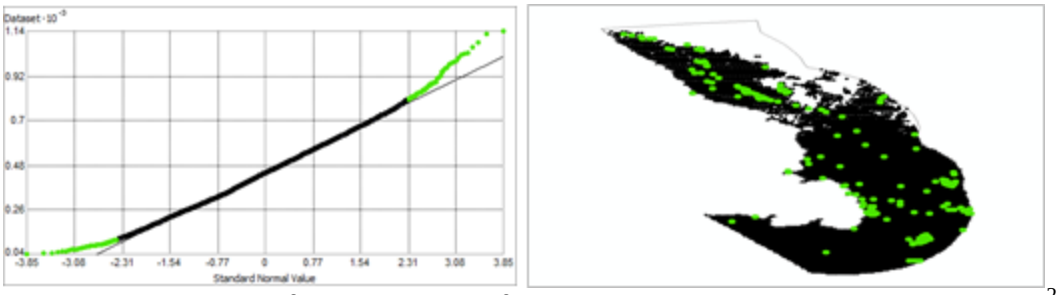

Figure 367. Normal Q-Q plot for data values of Fall Primary Production Range (mg C m^{-2} day^{-1}). Points falling over the reference line are mapped; no points fall under the reference line.

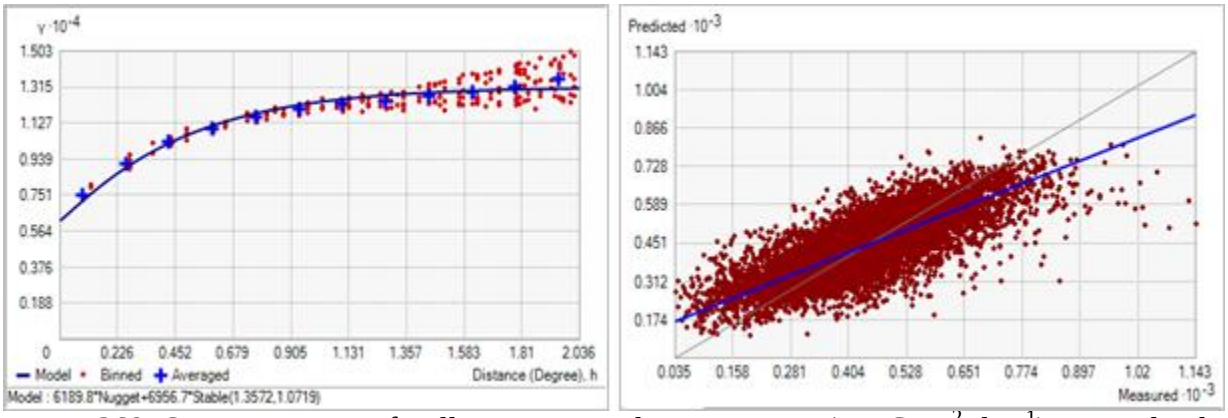

Figure 368. Semivariogram of Fall Primary Production Range (mg C m^{-2} day^{-1}). Binned values are shown as red dots; average points are shown as blue crosses; the model fit to the averaged values is shown as a blue line. Lag size: 0.170 degrees; number of lags: 12; Parameter: 1.072; Range: 1.357 degrees; Partial Sill: 6956.72. Right panel: Scatterplot of predicted values versus observed values for the model of Fall Primary Production Range (mg C m^{-2} day^{-1}).

Table 184. Results of cross-validation of the kriged model for Fall Primary Production Range (mg C m^{-2} day^{-1}).

Prediction error	Value
Number of Observations	8630
Overall Mean Error	-0.023
Root Mean Square Prediction Error	90.709
Standardized Mean	-1.452×10^{-4}
Standardized Root Mean Square Prediction Error	1.016
Average Standard Error	89.242

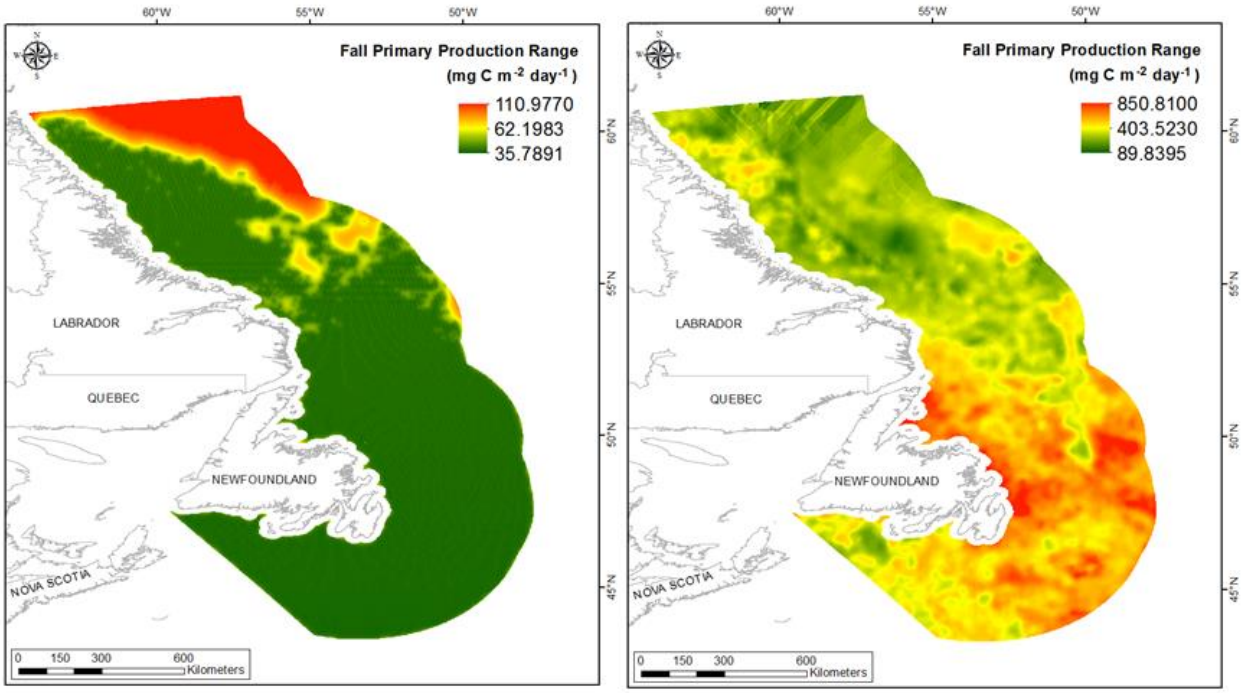

Figure 369. Left panel: Prediction standard error surface of Fall Primary Production Range (mg C m^{-2} day^{-1}). Right panel: Interpolated prediction surface of Fall Primary Production Range (mg C m^{-2} day^{-1}).

Fall Primary Production Average Minimum

This variable displayed a near normal distribution prior to modeling (Table 185, Figure 370). The data were higher than predicted by a normal distribution at low and upper mid-values, and lower than predicted at high and mid-values (Figure 371). The areas of under- and over-prediction showed no strong spatial pattern over the spatial extent (Figure 371).

The semivariogram showed moderate autocorrelation present in the data and the model showed a fair fit between measured and predicted values (Figure 372). Although the RMSE and ASE were high (Table 186), all other errors showed that the model was good at prediction. The error map

showed high error in the deep waters in the northern portion of the study extent where no data observations occur (Figure 373). The kriged surface is presented in Figure 373.

Table 185. Distributional properties of Fall Primary Production Average Minimum (mg C m^{-2} day^{-1}).

Property	Value
Number of Observations	8630
Minimum	73.985
Maximum	699.410
Mean	369.740
Median	360.180
Standard Deviation	117.86
Skewness	0.208
Kurtosis	2.068

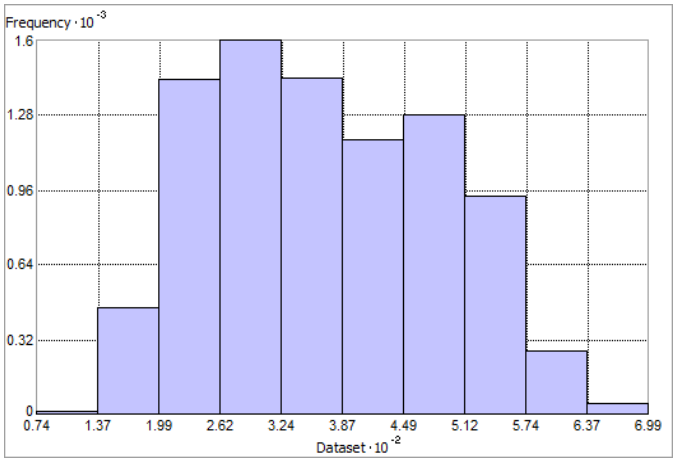

Figure 370. Distribution of Fall Primary Production Average Minimum (mg C m^{-2} day^{-1}). Histogram was illustrated using 10 bins. X axis is shown at 10^{-2}; Y axis is shown at 10^{-3}.

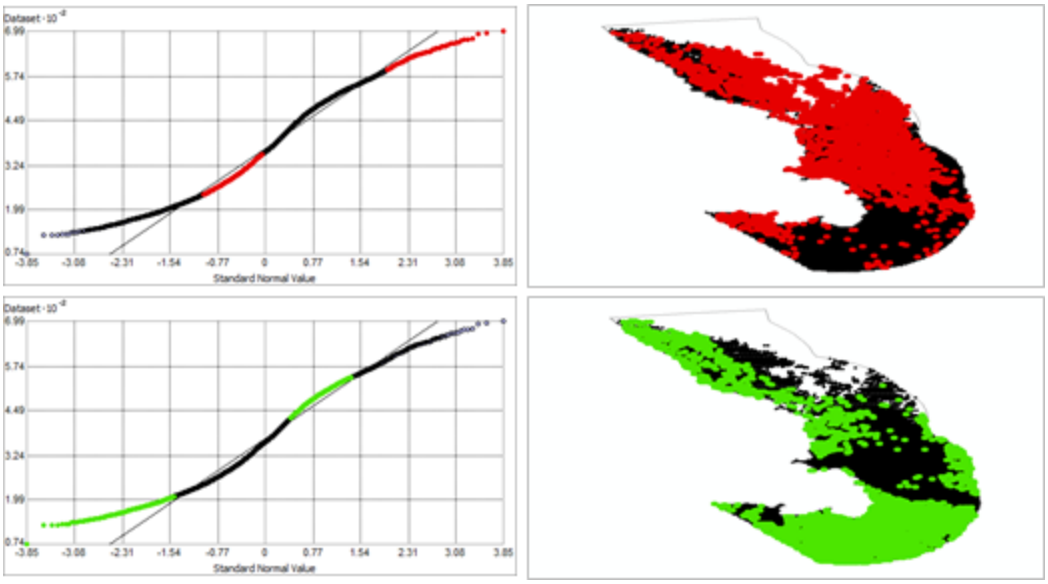

Figure 371. Normal Q-Q plot for data values of Fall Primary Production Average Minimum (mg C m^{-2} day^{-1}). Points falling under (upper panel) and over (bottom panel) the reference line are mapped.

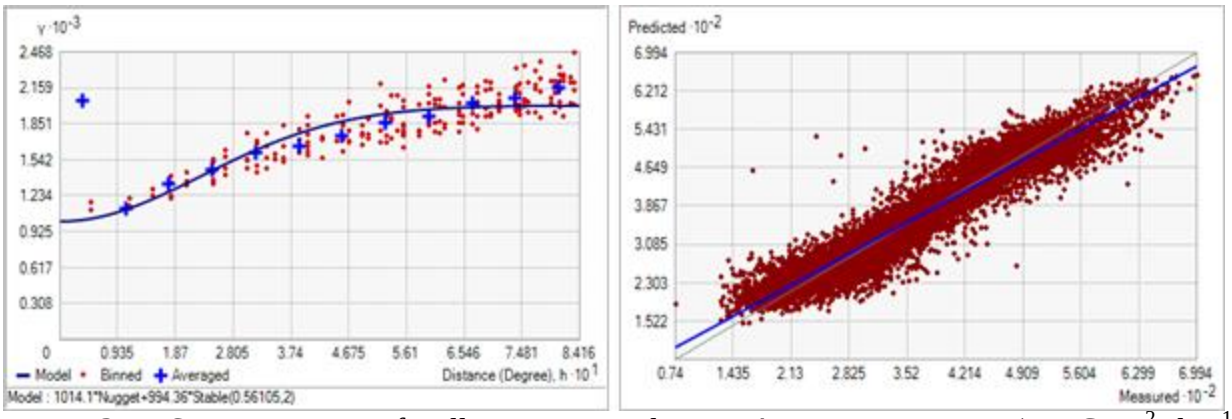

Figure 372. Semivariogram of Fall Primary Production Average Minimum (mg C m^{-2} day^{-1}). Binned values are shown as red dots; average points are shown as blue crosses; the model fit to the averaged values is shown as a blue line. Lag size: 0.070 degrees; number of lags: 12; Parameter: 2; Range: 0.561 degrees; Partial Sill: 994.364. Right panel: Scatterplot of predicted values versus observed values for the model of Fall Primary Production Average Minimum (mg C m^{-2} day^{-1}).

Table 186. Results of cross-validation of the kriged model for Fall Primary Production Average Minimum (mg C m^{-2} day^{-1}).

Prediction error	**Value**
Number of Observations	8630
Overall Mean Error	-0.016
Root Mean Square Prediction Error	34.849
Standardized Mean	-3.739×10^{-4}
Standardized Root Mean Square Prediction Error	1.018
Average Standard Error	34.246

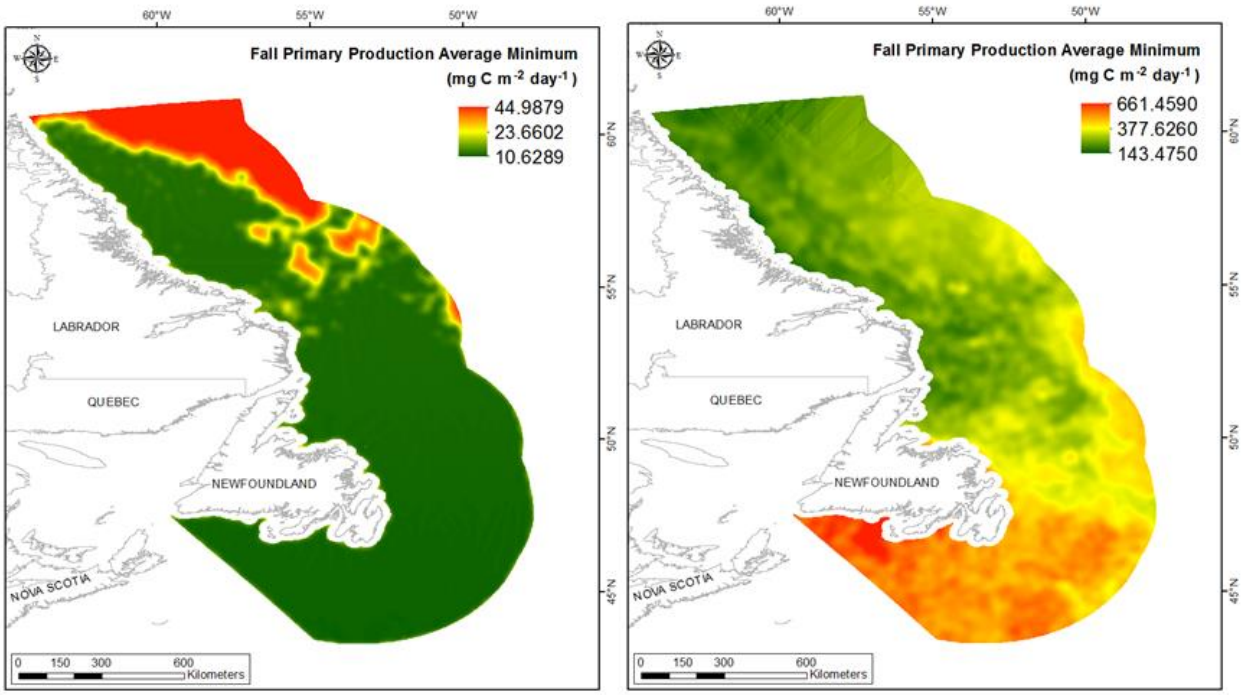

Figure 373. Left panel: Prediction standard error surface of Fall Primary Production Average Minimum (mg C m^{-2} day^{-1}). Right panel: Interpolated prediction surface of Annual Primary Production Average Minimum (mg C m^{-2} day^{-1}).

Fall Primary Production Average Maximum

This variable displayed a bimodal distribution prior to modeling (Table 187, Figure 374). The data were higher than predicted by a normal distribution at low and upper mid-values, and lower than predicted at high and mid-values (Figure 375). The areas of under- and over-prediction did not show a strong spatial pattern over the spatial extent with both types of data spread throughout (Figure 375).

The semivariogram showed weak autocorrelation present in the data and the model showed a fair fit between measured and predicted values (Figure 376). Although the RMSE and ASE were high (Table 188), all other errors showed that the model was good at prediction The error map showed high error in the deep waters in the northern portion of the study extent where no data observations occur (Figure 377). The kriged surface is presented in Figure 377.

Table 187. Distributional properties of Fall Primary Production Average Maximum (mg C m^{-2} day^{-1}).

Property	Value
Number of Observations	8630
Minimum	132.220
Maximum	957.480
Mean	609.310
Median	630.320
Standard Deviation	141.000
Skewness	-0.295
Kurtosis	2.046

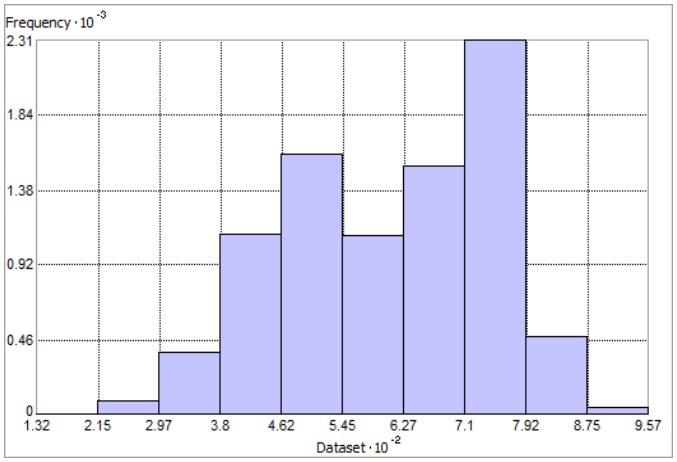

Figure 374. Distribution of Fall Primary Production Average Maximum (mg C m^{-2} day^{-1}). Histogram was illustrated using 10 bins. X axis is shown at 10^{-2}; Y axis is shown at 10^{-3}.

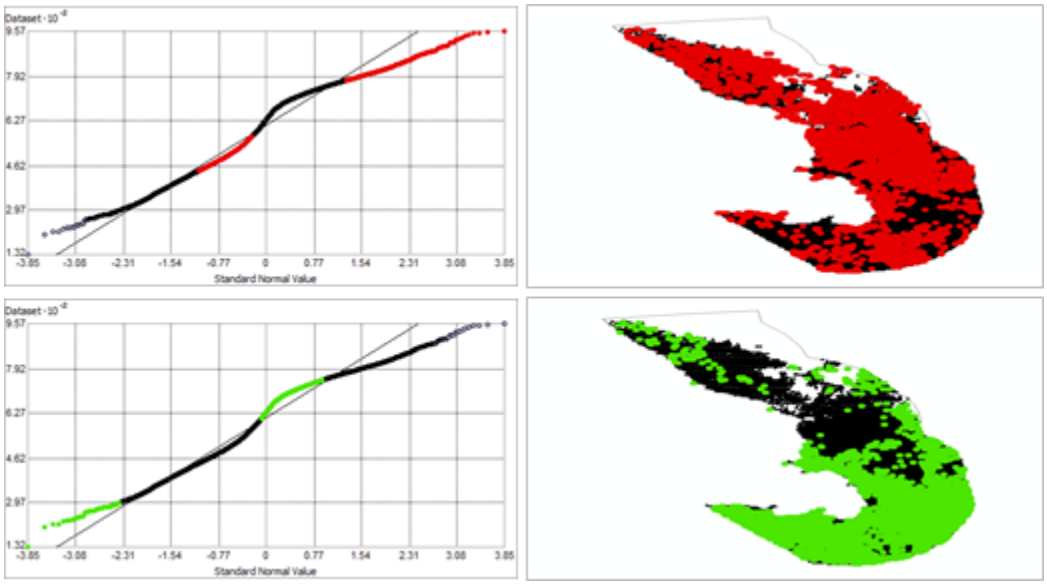

Figure 375. Normal Q-Q plot for data values of Fall Primary Production Average Maximum (mg C m^{-2} day^{-1}). Points falling under (upper panel) and over (bottom panel) the reference line are mapped.

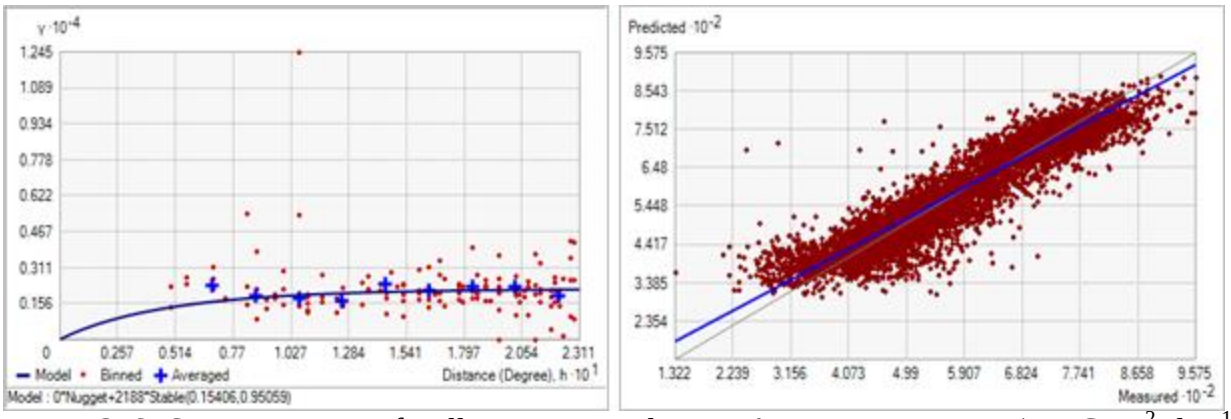

Figure 376. Semivariogram of Fall Primary Production Average Maximum (mg C m^{-2} day^{-1}). Binned values are shown as red dots; average points are shown as blue crosses; the model fit to the averaged values is shown as a blue line. Lag size: 0.019 degrees; number of lags: 12; Parameter: 0.951; Range: 0.154 degrees; Partial Sill: 2187.988. Right panel: Scatterplot of predicted values versus observed values for the model of Fall Primary Production Average Maximum (mg C m^{-2} day^{-1}).

Table 188. Results of cross-validation of the kriged model for Fall Primary Production Average Maximum (mg C m^{-2} day^{-1}).

Prediction error	**Value**
Number of Observations	8630
Overall Mean Error	-0.110
Root Mean Square Prediction Error	46.093
Standardized Mean	-2.131×10^{-3}
Standardized Root Mean Square Prediction Error	0.999
Average Standard Error	45.947

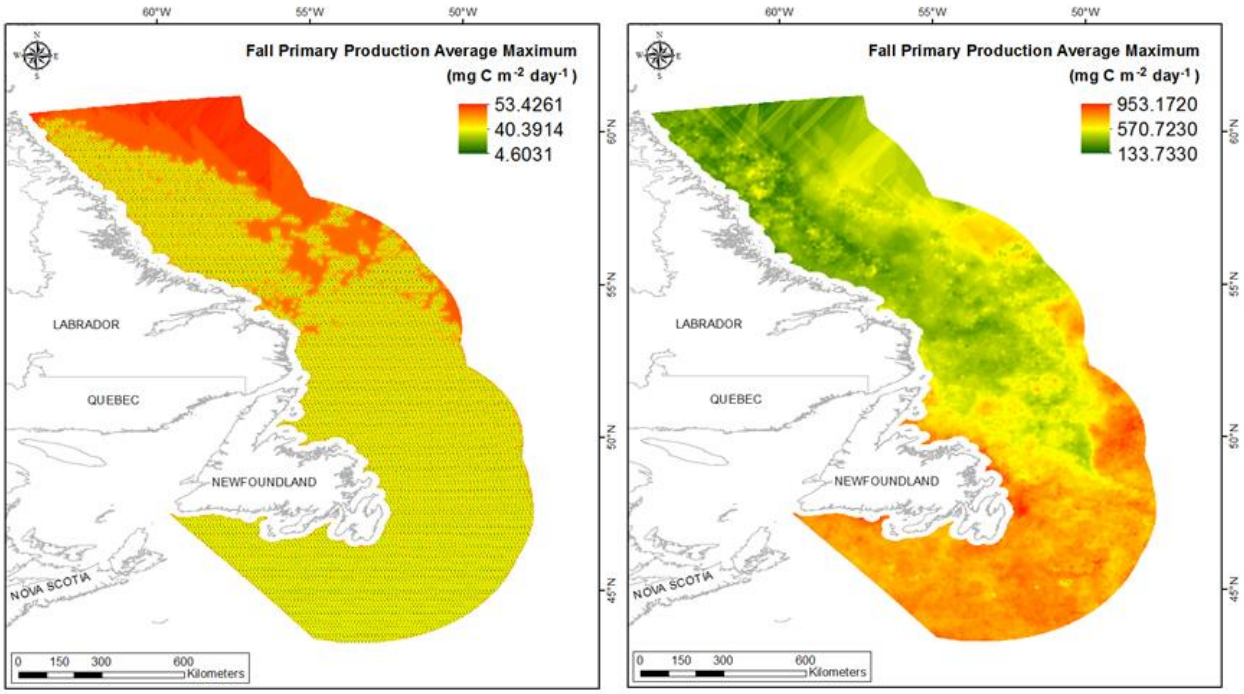

Figure 377. Left panel: Prediction standard error surface of Fall Primary Production Average Maximum (mg C m^{-2} day^{-1}). Right panel: Interpolated prediction surface of Fall Primary Production Average Maximum (mg C m^{-2} day^{-1}).

Fall Primary Production Average Range

This variable displayed a near normal distribution prior to modeling (Table 189, Figure 378). The data were higher than predicted by a normal distribution at low and high values, however the mid-values were well predicted (Figure 379). The areas of over-prediction showed no spatial pattern over the spatial extent (Figure 379).

The semivariogram showed moderate autocorrelation present in the data and the model showed a fair to poor fit between measured and predicted values (Figure 380). Although the RMSE and ASE were high (Table 190), all other errors showed that the model was good at prediction. The error map showed high error in the deep waters in the northern portion of the study extent where no data observations occur (Figure 381). The kriged surface is presented in Figure 381.

Table 189. Distributional properties of Fall Primary Production Average Range (mg C m^{-2} day^{-1}).

Property	Value
Number of Observations	8630
Minimum	3.465
Maximum	608.010
Mean	239.560
Median	236.110
Standard Deviation	84.262
Skewness	0.270
Kurtosis	3.303

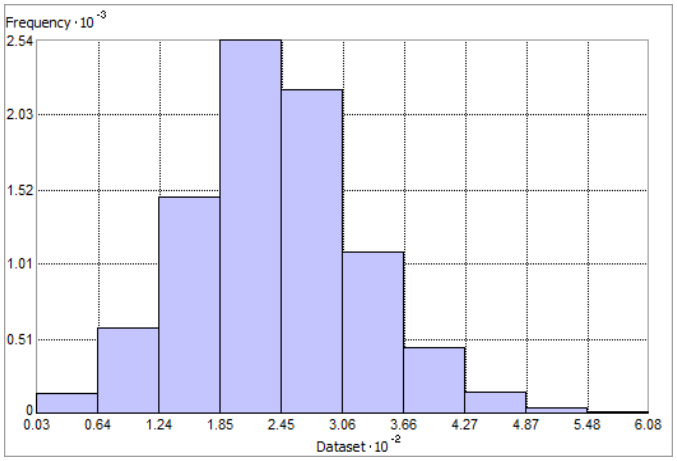

Figure 378. Distribution of Fall Primary Production Average Range (mg C m^{-2} day^{-1}). Histogram was illustrated using 10 bins. X axis is shown at 10^{-2}; Y axis is shown at 10^{-3}.

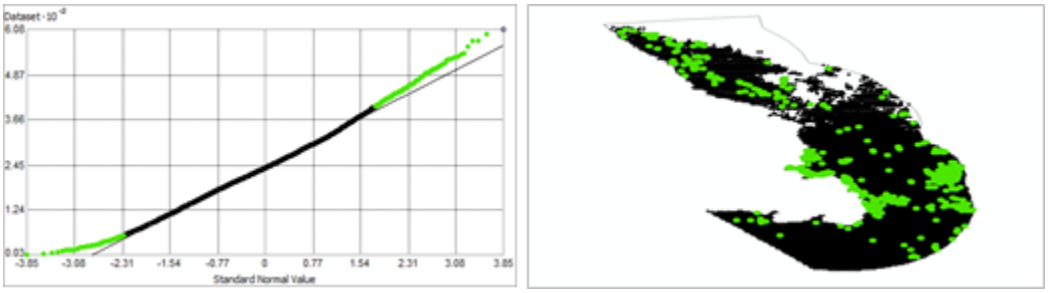

Figure 379. Normal Q-Q plot for data values of Fall Primary Production Average Range (mg C m^{-2} day^{-1}). Points falling over the reference line are mapped; no points fall under the reference line.

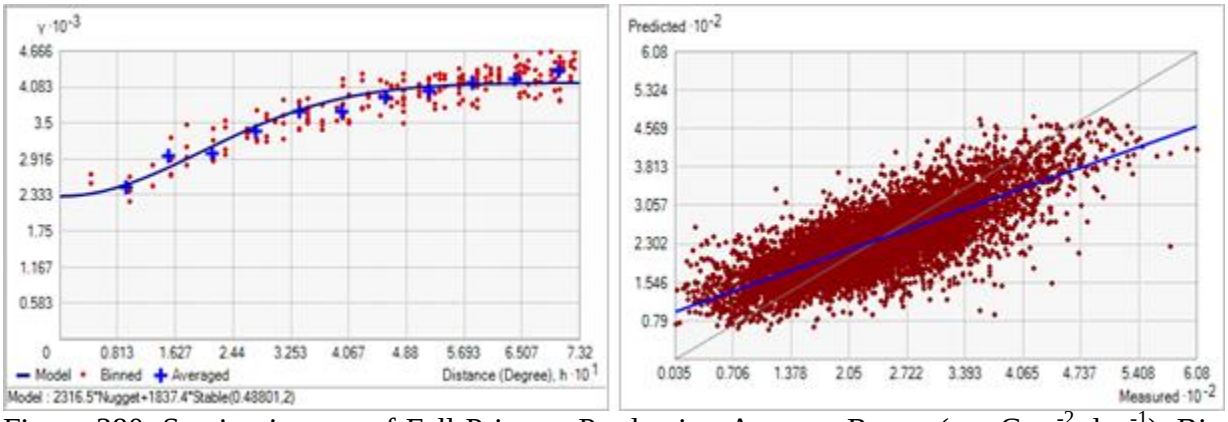

Figure 380. Semivariogram of Fall Primary Production Average Range (mg C m^{-2} day^{-1}). Binned values are shown as red dots; average points are shown as blue crosses; the model fit to the averaged values is shown as a blue line. Lag size: 0.061 degrees; number of lags: 12; Parameter: 2; Range: 0.488 degrees; Partial Sill: 1837.406. Right panel: Scatterplot of predicted values versus observed values for the model of Fall Primary Production Average Range (mg C m^{-2} day^{-1}).

Table 190. Results of cross-validation of the kriged model for Fall Primary Production Average Range (mg C m^{-2} day^{-1}).

Prediction error	Value
Number of Observations	8360
Overall Mean Error	-0.040
Root Mean Square Prediction Error	54.164
Standardized Mean	-4.712×10^{-4}
Standardized Root Mean Square Prediction Error	1.037
Average Standard Error	52.104

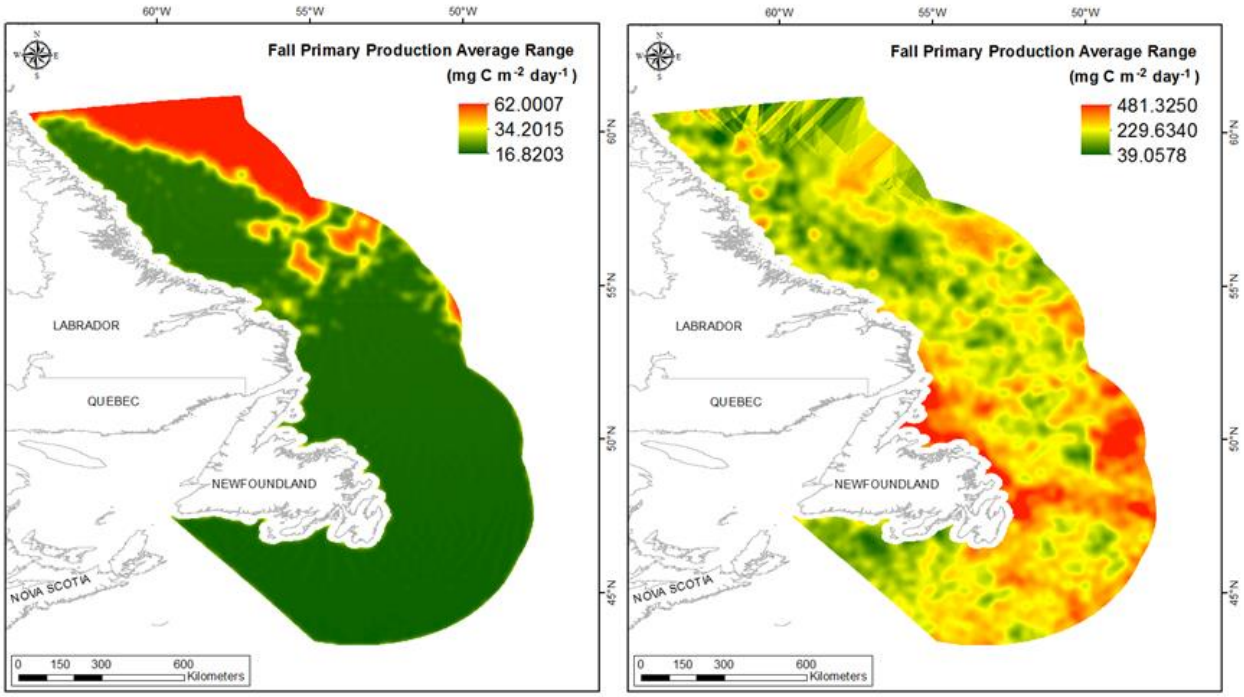

Figure 381. Left panel: Prediction standard error surface of Fall Primary Production Average Range (mg C m^{-2} day^{-1}). Right panel: Interpolated prediction surface of Fall Primary Production Average Range (mg C m^{-2} day^{-1}).

Annual Primary Production Mean

This variable displayed a left skewed distribution prior to modeling (Table 191, Figure 382). The data were slightly higher than predicted by a normal distribution at low values and lower than predicted at high values, however most of the data was very well-predicted (Figure 383). The lowest values fell under the reference line. The areas of under- and over-prediction showed a spatial pattern over the spatial extent but the deviations were minor (Figure 383).

The semivariogram showed weak autocorrelation present in the data and the model showed a fair fit between measured and predicted values (Figure 384). Although the RMSE and ASE were

high (Table 192), all other errors showed that the model was good at prediction. The error map showed medium to high error in a grid-like pattern over the study extent (Figure 385). The kriged surface is presented in Figure 385.

Table 191. Distributional properties of Annual Primary Production Mean (mg C m^{-2} day^{-1}).

Property	Value
Number of Observations	10384
Minimum	186.060
Maximum	898.050
Mean	661.240
Median	665.160
Standard Deviation	69.625
Skewness	-0.164
Kurtosis	3.023

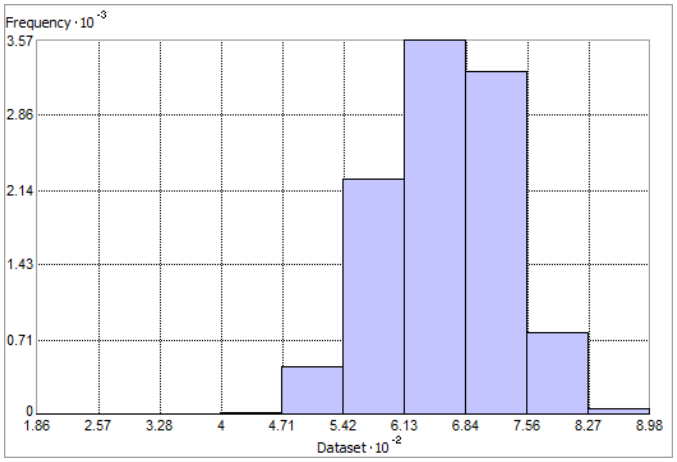

Figure 382. Distribution of Annual Primary Production Mean (mg C m^{-2} day^{-1}). Histogram was illustrated using 10 bins. X axis is shown at 10^{-2}; Y axis is shown at 10^{-3}.

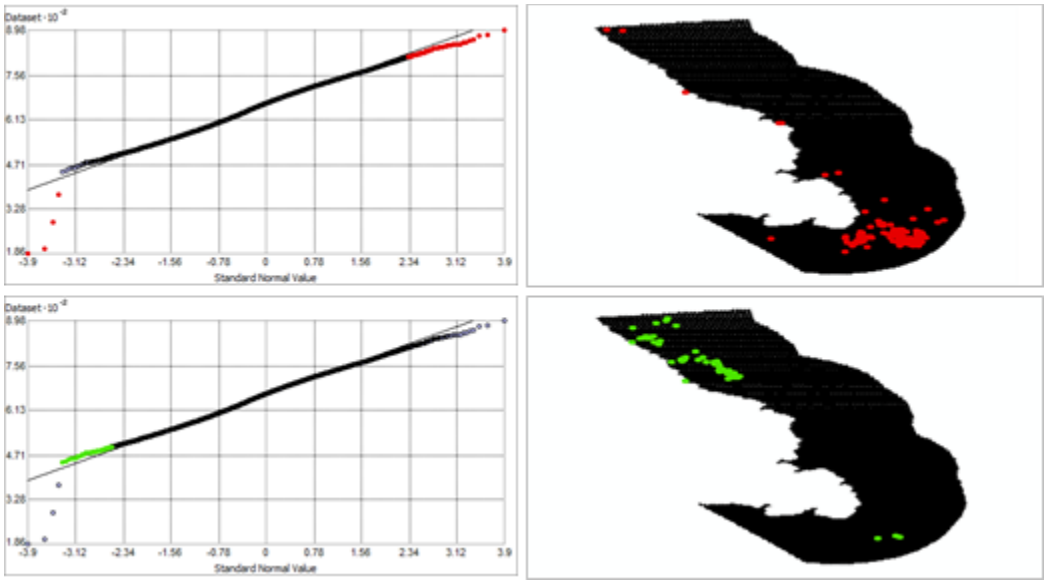

Figure 383. Normal Q-Q plot for data values of Annual Primary Production Mean (mg C m^{-2} day^{-1}). Points falling under (upper panel) and over (bottom panel) the reference line are mapped.

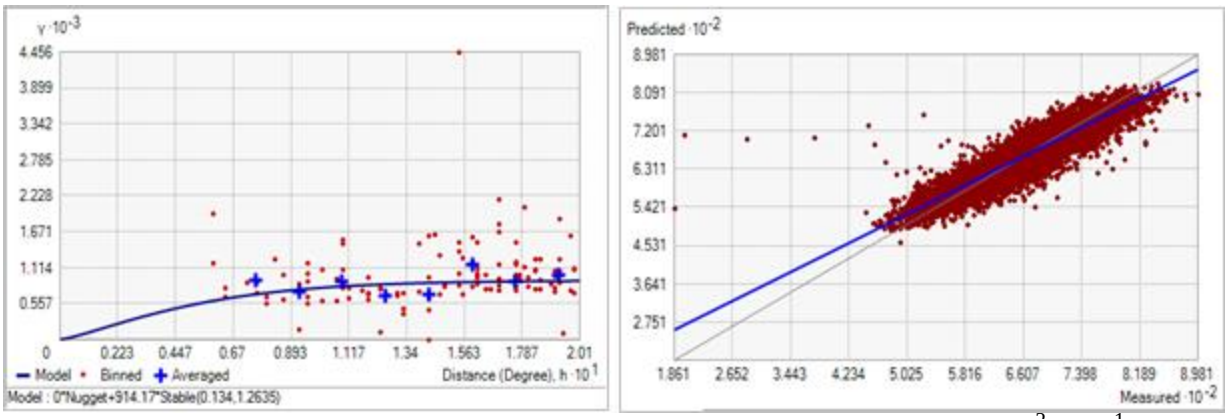

Figure 384. Semivariogram of Annual Primary Production Mean (mg C m^{-2} day^{-1}). Binned values are shown as red dots; average points are shown as blue crosses; the model fit to the averaged values is shown as a blue line. Lag size: 0.017 degrees; number of lags: 12; Parameter: 1.263; Range: 0.134 degrees; Partial Sill: 914.1717. Right panel: Scatterplot of predicted values versus observed values for the model of Annual Primary Production Mean (mg C m^{-2} day^{-1}).

Table 192. Results of cross-validation of the kriged model for Annual Primary Production Mean (mg C m^{-2} day^{-1}).

Prediction error	**Value**
Number of Observations	10384
Overall Mean Error	-5.964×10^{-3}
Root Mean Square Prediction Error	28.645
Standardized Mean	-1.688×10^{-4}
Standardized Root Mean Square Prediction Error	0.958
Average Standard Error	29.876

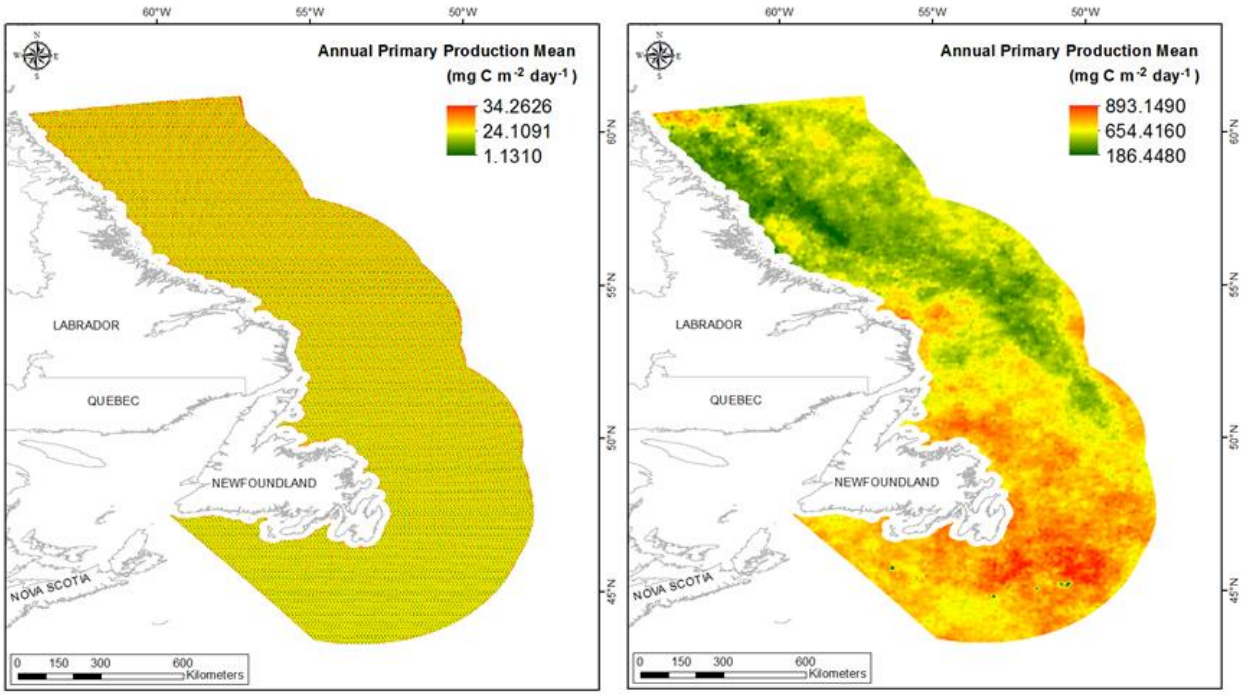

Figure 385. Left panel: Prediction standard error surface of Annual Primary Production Mean (mg C m^{-2} day^{-1}). Right panel: Interpolated prediction surface of Annual Primary Production Mean (mg C m^{-2} day^{-1}).

Annual Primary Production Minimum

This variable displayed a bell-shaped distribution with right-skewness (Table 193, Figure 386). The data were higher than predicted by a normal distribution at low and high values, however, the mid-values deviated only slightly from the reference line (Figure 387). The areas of under- and over-prediction showed little spatial pattern over the spatial extent (Figure 387).

The semivariogram showed moderate autocorrelation present in the data and the model showed a poor fit between measured and predicted values (Figure 388). Although the RMSE and ASE were high (Table 194), all other errors showed that the model was good at prediction. The error map showed medium and low error over most of the study extent but high error around the periphery of the spatial extent (Figure 389). The kriged surface is presented in Figure 389.

Table 193. Distributional properties of Annual Primary Production Minimum (mg C m^{-2} day^{-1}).

Property	Value
Number of Observations	10384
Minimum	23.340
Maximum	446.030
Mean	172.520
Median	168.150
Standard Deviation	40.924
Skewness	0.843
Kurtosis	4.671

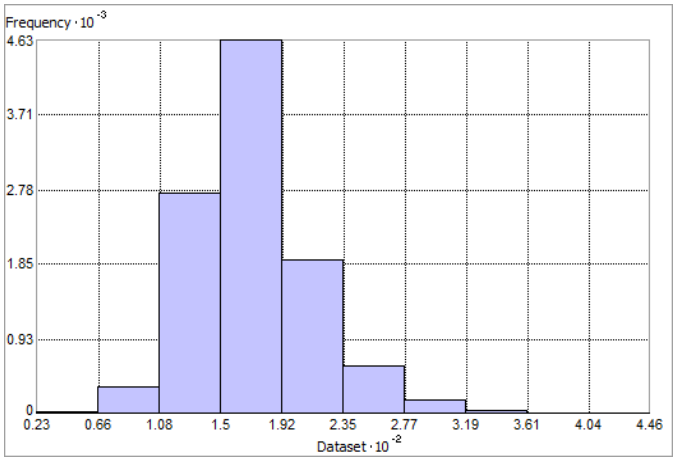

Figure 386. Distribution of Annual Primary Production Minimum (mg C m^{-2} day^{-1}). Histogram was illustrated using 10 bins. X axis is shown at 10^{-2}; Y axis is shown at 10^{-3}.

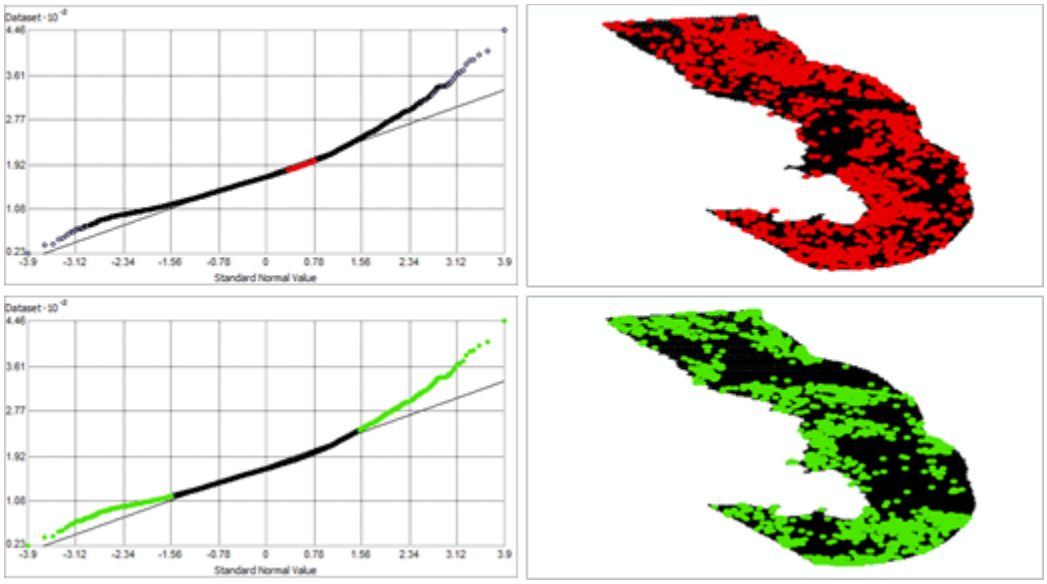

Figure 387. Normal Q-Q plot for data values of Annual Primary Production Minimum (mg C m^{-2} day^{-1}). Points falling under (upper panel) and over (bottom panel) the reference line are mapped.

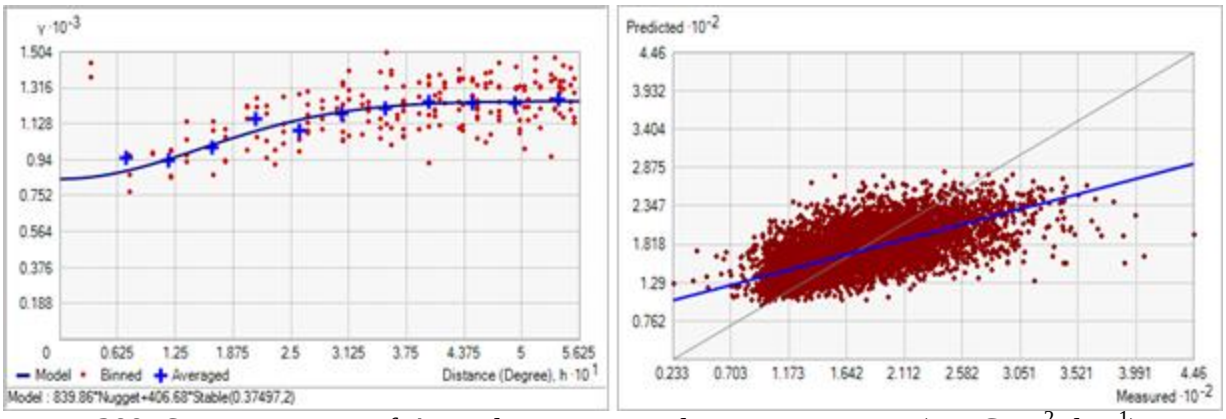

Figure 388. Semivariogram of Annual Primary Production Minimum (mg C m^{-2} day^{-1}). Binned values are shown as red dots; average points are shown as blue crosses; the model fit to the averaged values is shown as a blue line. Lag size: 0.047 degrees; number of lags: 12; Parameter: 2; Range: 0.375 degrees; Partial Sill: 406.680. Right panel: Scatterplot of predicted values versus observed values for the model of Annual Primary Production Minimum (mg C m^{-2} day^{-1}).

Table 194. Results of cross-validation of the kriged model for Annual Primary Production Minimum (mg C m^{-2} day^{-1}).

Prediction error	**Value**
Number of Observations	10384
Overall Mean Error	-3.284×10^{-3}
Root Mean Square Prediction Error	31.673
Standardized Mean	-1.071×10^{-4}
Standardized Root Mean Square Prediction Error	1.001
Average Standard Error	31.614

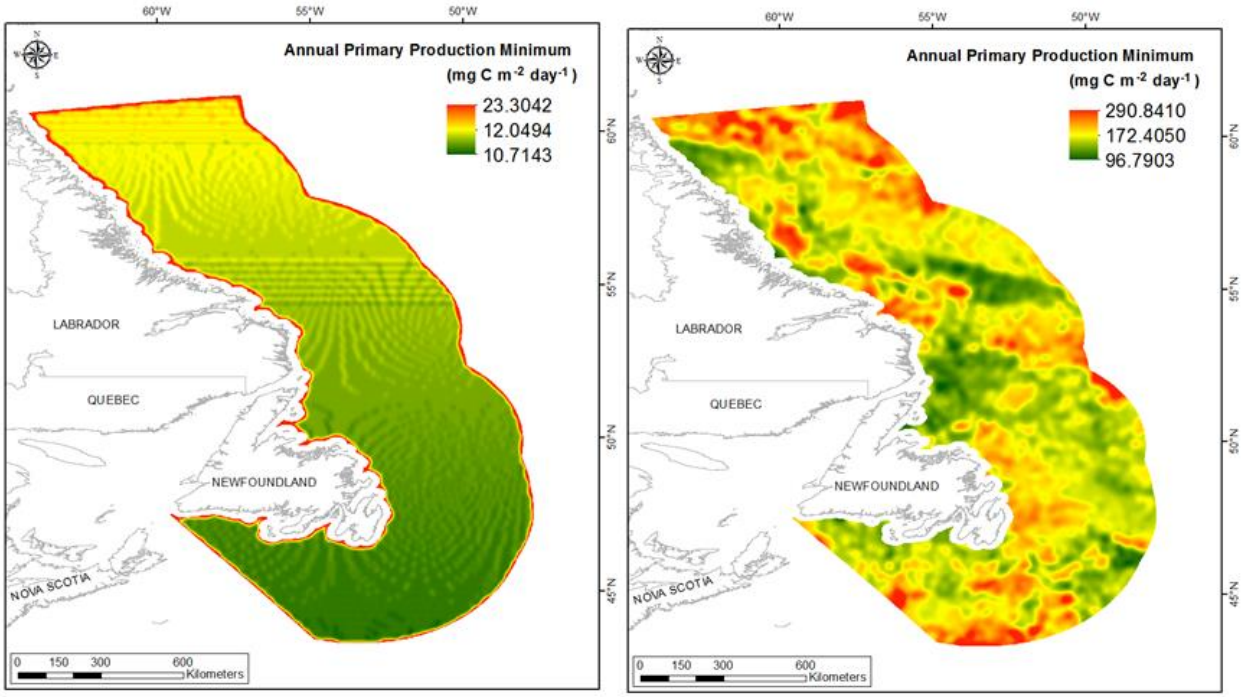

Figure 389. Left panel: Prediction standard error surface of Annual Primary Production Minimum (mg C m^{-2} day^{-1}). Right panel: Interpolated prediction surface of Annual Primary Production Minimum (mg C m^{-2} day^{-1}).

Annual Primary Production Maximum

This variable displayed a bell-shaped distribution with right-skewness (Table 195, Figure 390). The data were higher than predicted by a normal distribution at low and high values; however, the mid-values deviated only slightly from the reference line (Figure 391). The areas of under- and over-prediction showed a weak spatial pattern over the spatial extent with differential bias in the southern half of the spatial extent (Figure 391).

The semivariogram showed moderate autocorrelation present in the data and the model showed a poor fit between measured and predicted values (Figure 392). Although the RMSE and ASE were high (Table 196), all other errors showed that the model was good at prediction. The error map showed medium and low error over most of the study extent but high error around the periphery of the spatial extent (Figure 393). The kriged surface is presented in Figure 393.

Table 195. Distributional properties of Annual Primary Production Maximum (mg C m^{-2} day^{-1}).

Property	Value
Number of Observations	10384
Minimum	352.330
Maximum	2735.300
Mean	1355.900
Median	1318.800
Standard Deviation	292.670
Skewness	0.482
Kurtosis	2.981

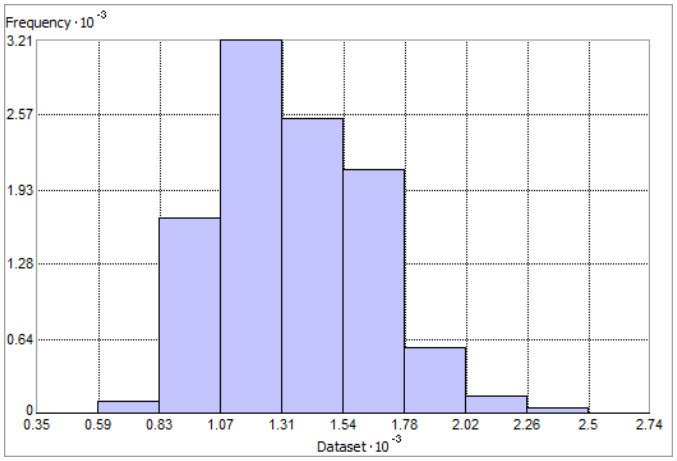

Figure 390. Distribution of Annual Primary Production Maximum (mg C m^{-2} day^{-1}). Histogram was illustrated using 10 bins. X and Y axes are shown at 10^{-3}.

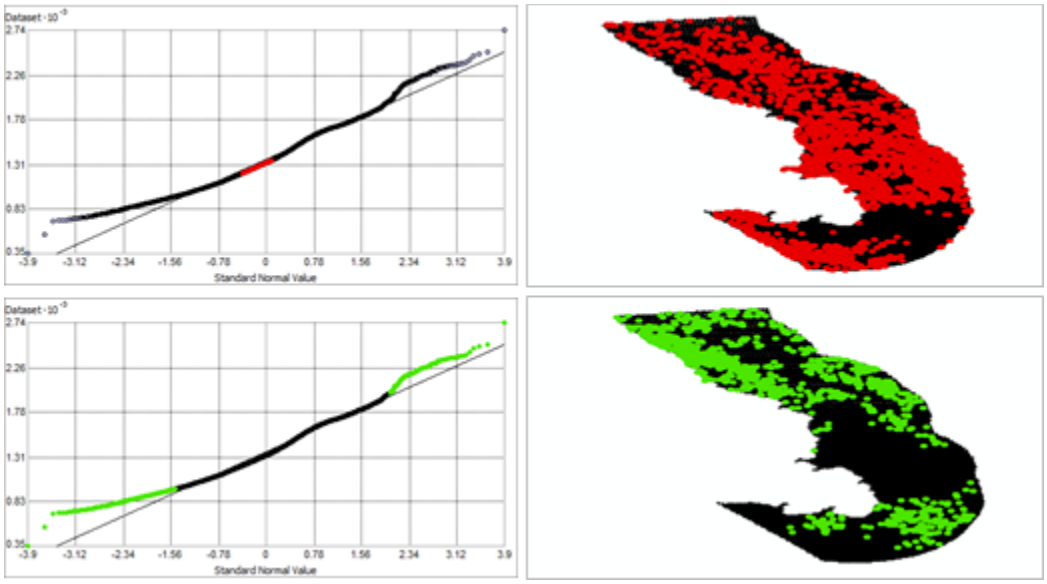

Figure 391. Normal Q-Q plot for data values of Annual Primary Production Maximum (mg C m^{-2} day^{-1}). Points falling under (upper panel) and over (bottom panel) the reference line are mapped.

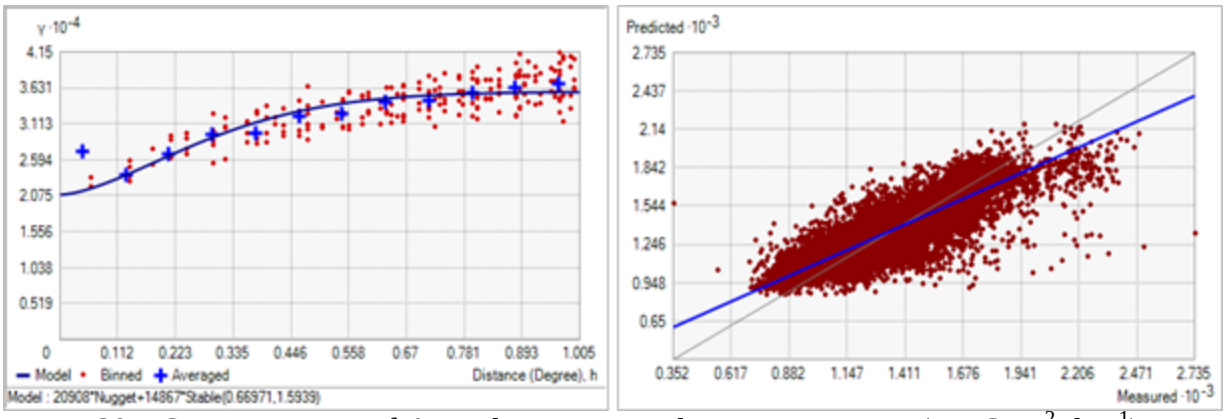

Figure 392. Semivariogram of Annual Primary Production Maximum (mg C m^{-2} day^{-1}). Binned values are shown as red dots; average points are shown as blue crosses; the model fit to the averaged values is shown as a blue line. Lag size: 0.084 degrees; number of lags: 12; Parameter: 1.594; Range: 0.670 degrees; Partial Sill: 14867.360. Right panel: Scatterplot of predicted values versus observed values for the model of Annual Primary Production Maximum (mg C m^{-2} day^{-1}).

Table 196. Results of cross-validation of the kriged model for Annual Primary Production Maximum (mg C m^{-2} day^{-1}).

Prediction error	**Value**
Number of Observations	10384
Overall Mean Error	-0.012
Root Mean Square Prediction Error	159.480
Standardized Mean	-9.394×10^{-5}
Standardized Root Mean Square Prediction Error	1.015
Average Standard Error	156.953

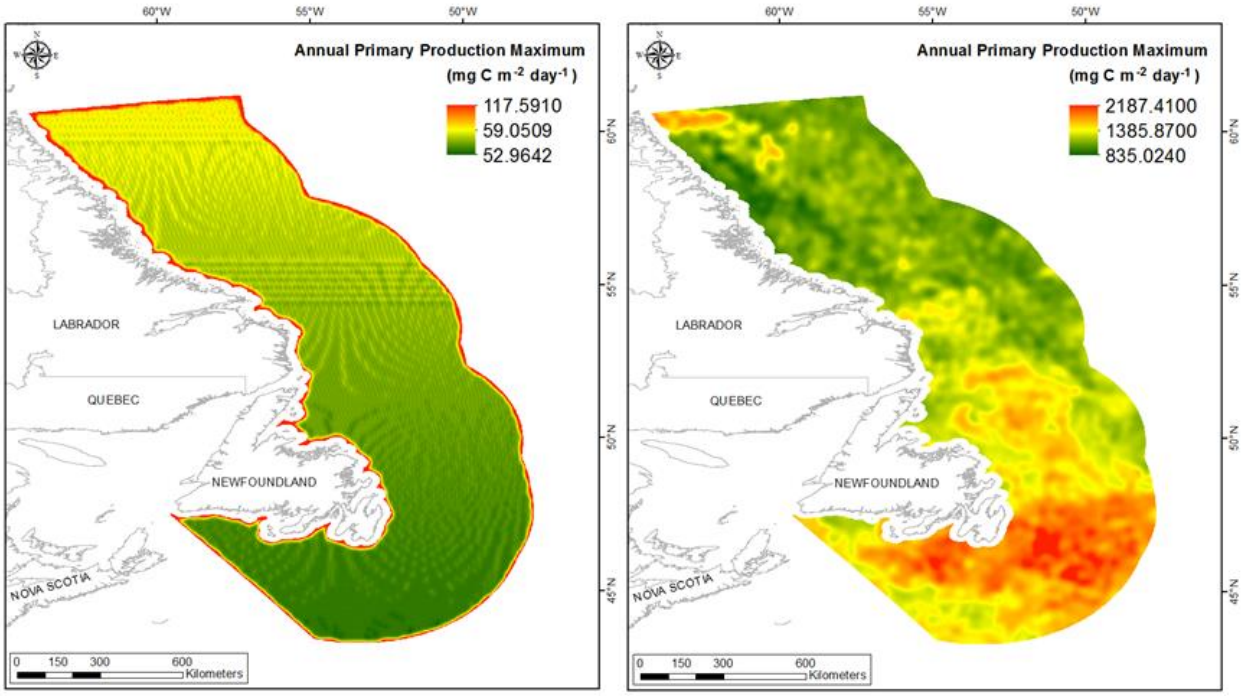

Figure 393. Left panel: Prediction standard error surface of Annual Primary Production Maximum (mg C m^{-2} day^{-1}). Right panel: Interpolated prediction surface of Annual Primary Production Maximum (mg C m^{-2} day^{-1}).

Annual Primary Production Range

This variable displayed a bell-shaped distribution with right skewness (Table 197, Figure 394). The data were higher than predicted by a normal distribution at low and high values; however, the mid-values were well predicted (Figure 395). The areas of over-prediction showed a spatial pattern over the spatial extent (Figure 395).

The semivariogram showed moderate autocorrelation present in the data and the model showed a fair to poor fit between measured and predicted values (Figure 396). Although the RMSE and ASE were high (Table 198), all other errors showed that the model was good at prediction. The error map showed medium and low error over most of the study extent but high error around the periphery of the spatial extent (Figure 397). The kriged surface is presented in Figure 397.

Table 197. Distributional properties of Annual Primary Production Range (mg C m^{-2} day^{-1}).

Property	Value
Number of Observations	10384
Minimum	286.800
Maximum	2564.400
Mean	1183.300
Median	1150.900
Standard Deviation	296.990
Skewness	0.459
Kurtosis	2.952

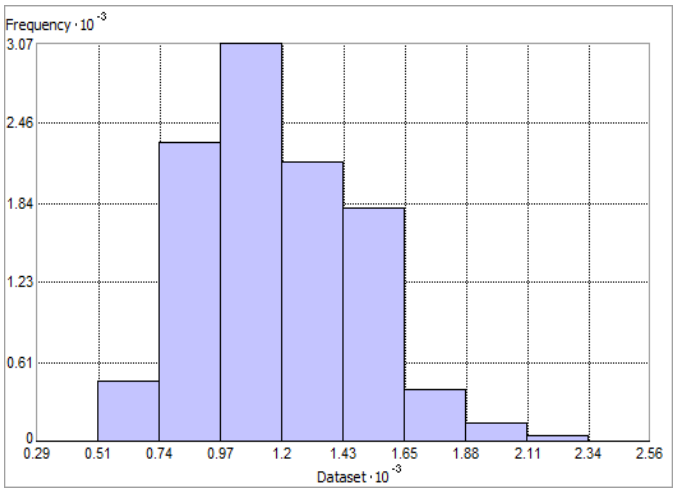

Figure 394. Distribution of Annual Primary Production Range (mg C m^{-2} day^{-1}). Histogram was illustrated using 10 bins. X and Y axes are shown at 10^{-3}.

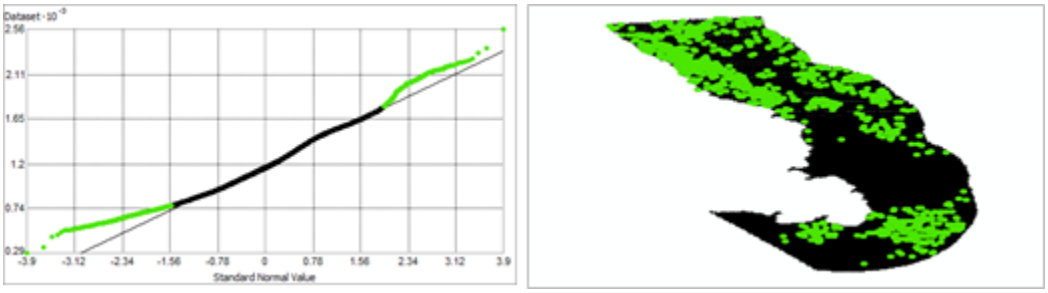

Figure 395. Normal Q-Q plot for data values of Annual Primary Production Range (mg C m^{-2} day^{-1}). Points falling over the reference line are mapped; no points fall under the reference line.

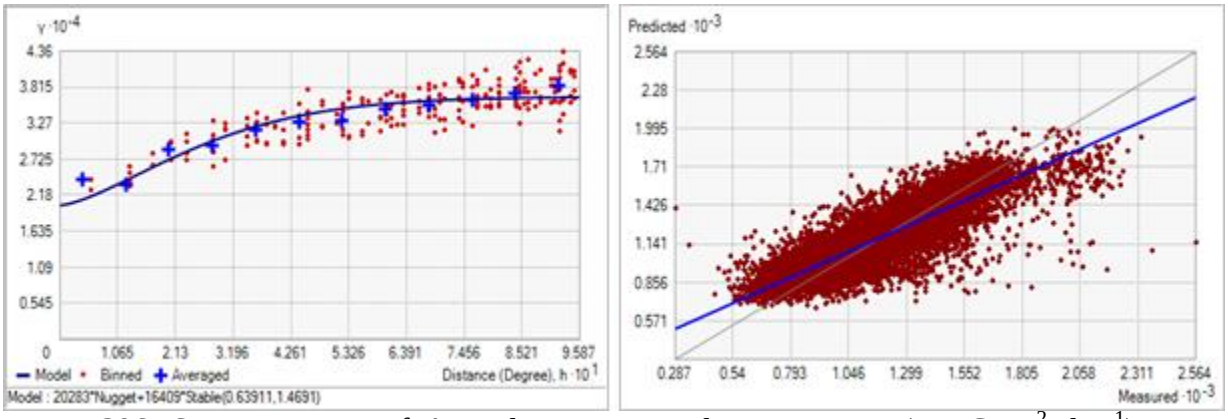

Figure 396. Semivariogram of Annual Primary Production Range (mg C m^{-2} day^{-1}). Binned values are shown as red dots; average points are shown as blue crosses; the model fit to the averaged values is shown as a blue line. Lag size: 0.080 degrees; number of lags: 12; Parameter:

1.469; Range: 0.639 degrees; Partial Sill: 16409.350. Right panel: Scatterplot of predicted values versus observed values for the model of Annual Primary Production Range (mg C m^{-2} day^{-1}).
Table 198. Results of cross-validation of the kriged model for Annual Primary Production Range (mg C m^{-2} day^{-1}).

Prediction error	Value
Number of Observations	10384
Overall Mean Error	5.122×10^{-3}
Root Mean Square Prediction Error	162.084
Standardized Mean	1.464×10^{-5}
Standardized Root Mean Square Prediction Error	1.022
Average Standard Error	158.427

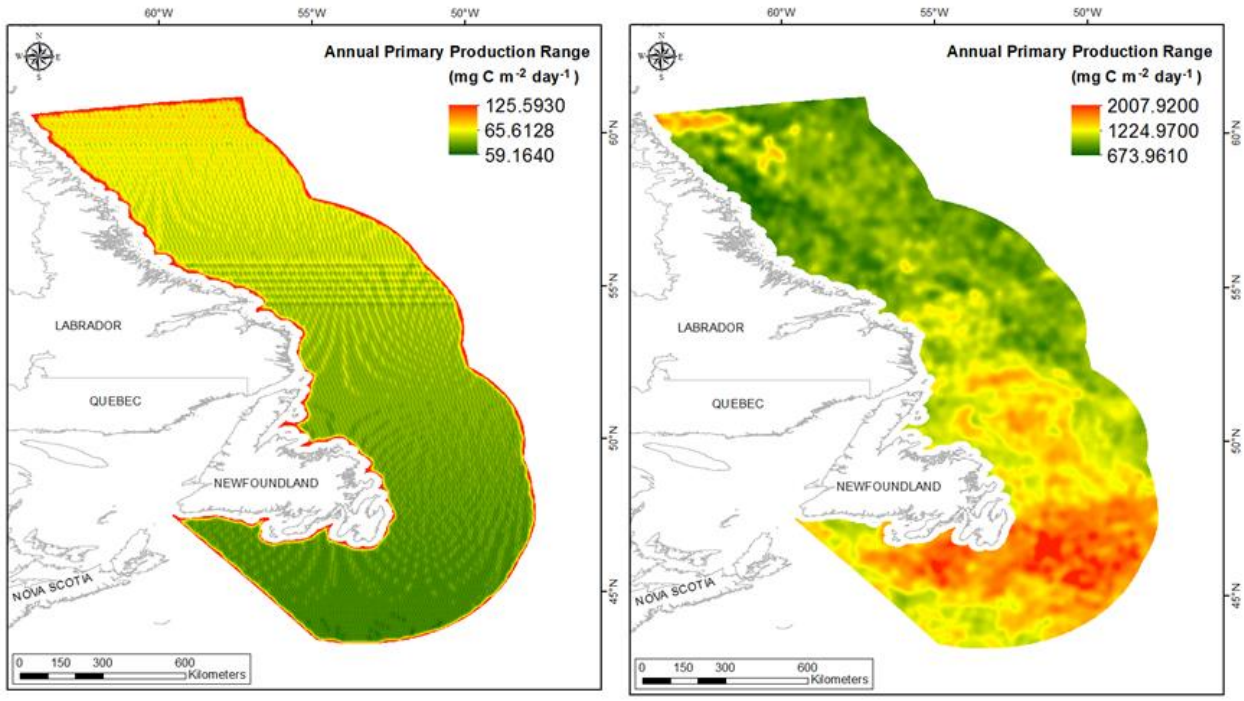

Figure 397. Left panel: Prediction standard error surface of Annual Primary Production Range (mg C m^{-2} day^{-1}). Right panel: Interpolated prediction surface of Annual Primary Production Range (mg C m^{-2} day^{-1}).

Annual Primary Production Average Minimum

This variable displayed a bell-shaped distribution prior to modeling (Table 199, Figure 398). The data were higher than predicted by a normal distribution at low and high values. The lowest point fell under the reference line (Figure 399). The areas of over-prediction showed no spatial pattern over the spatial extent (Figure 399).

The semivariogram showed autocorrelation present in the data and the model showed a poor fit between measured and predicted values (Figure 400). Although the RMSE and ASE were high (Table 200), all other errors showed that the model was good at prediction. The error map showed moderate error over the study extent and high error along the edges (Figure 401). The kriged surface is presented in Figure 401.

Table 199. Distributional properties of Annual Primary Production Average Minimum (mg C m^{-2} day^{-1}).

Property	Value
Number of Observations	10384
Minimum	96.480
Maximum	577.530
Mean	304.960
Median	300.420
Standard Deviation	54.855
Skewness	0.370
Kurtosis	3.040

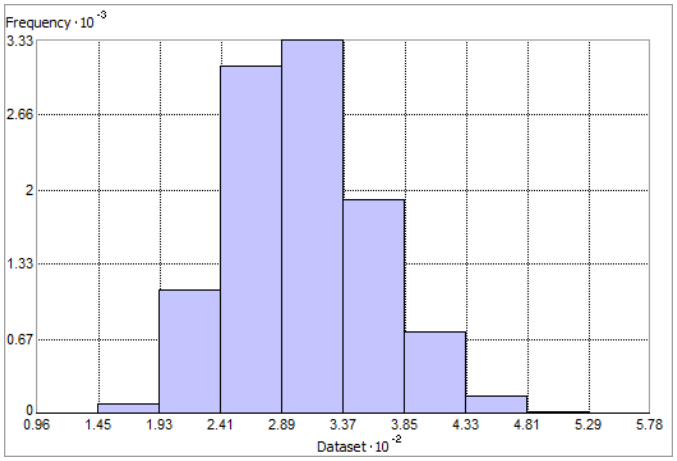

Figure 398. Distribution of Annual Primary Production Average Minimum (mg C m^{-2} day^{-1}). Histogram was illustrated using 10 bins. X axis is shown at 10^{-2}; Y axis is shown at 10^{-3}.

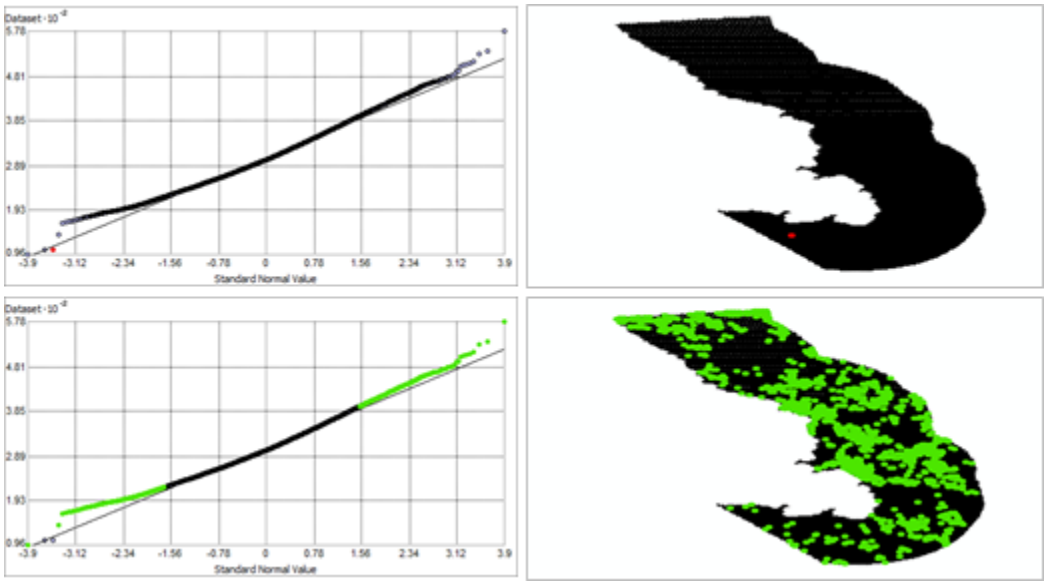

Figure 399. Normal Q-Q plot for data values of Annual Primary Production Average Minimum (mg C m^{-2} day^{-1}). Points falling under (upper panel) and over (bottom panel) the reference line are mapped.

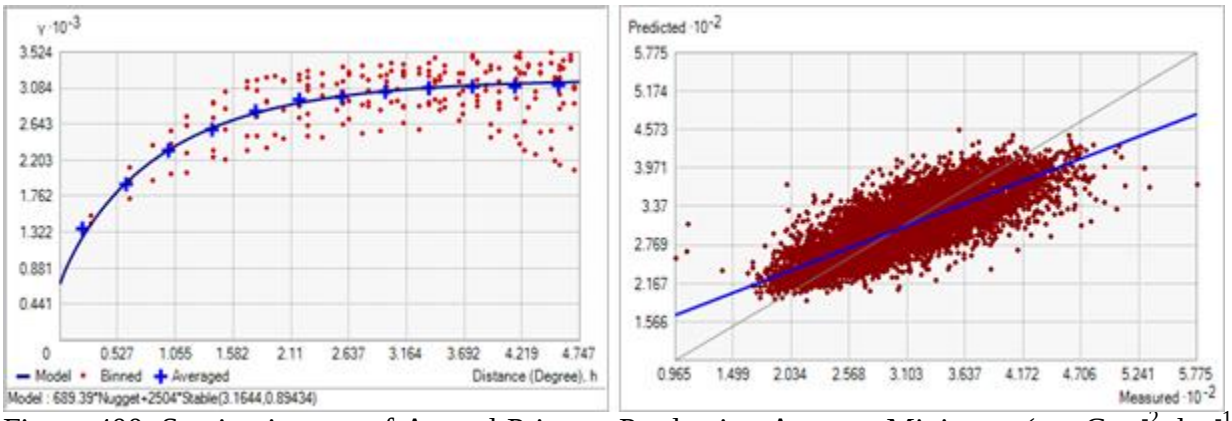

Figure 400. Semivariogram of Annual Primary Production Average Minimum (mg C m^{-2} day^{-1}). Binned values are shown as red dots; average points are shown as blue crosses; the model fit to the averaged values is shown as a blue line. Lag size: 0.396 degrees; number of lags: 12; Parameter: 0.894; Range: 3.164 degrees; Partial Sill: 2503.958. Right panel: Scatterplot of predicted values versus observed values for the model of Annual Primary Production Average Minimum (mg C m^{-2} day^{-1}).

Table 200. Results of cross-validation of the kriged model for Annual Primary Production Average Minimum (mg C m^{-2} day^{-1}).

Prediction error	**Value**
Number of Observations	10384
Overall Mean Error	2.189×10^{-3}
Root Mean Square Prediction Error	33.423
Standardized Mean	-4.899×10^{-5}
Standardized Root Mean Square Prediction Error	1.013
Average Standard Error	32.976

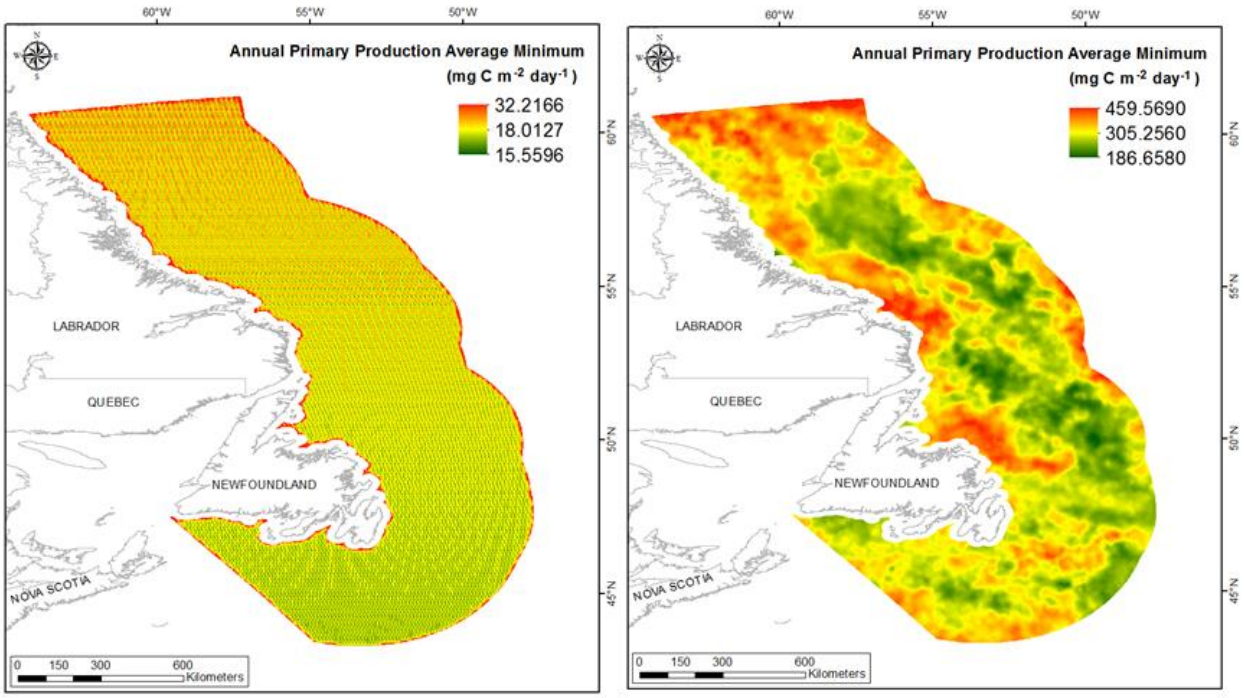

Figure 401. Left panel: Prediction standard error surface of Annual Primary Production Average Minimum (mg C m^{-2} day^{-1}). Right panel: Interpolated prediction surface of Annual Primary Production Average Minimum (mg C m^{-2} day^{-1}).

Annual Primary Production Average Maximum

This variable displayed a bell-shaped distribution prior to modeling (Table 201, Figure 402). The data were higher than predicted by a normal distribution at low values, however the high and mid-values deviated only slightly from the reference line (Figure 403). The lowest values fell under the reference line. The areas of under- and over-prediction showed no strong spatial pattern over the northern portion of the spatial extent, however, the southern portion was biased towards slight under-prediction (Figure 403).

The semivariogram showed moderate autocorrelation present in the data and the model showed a fair fit between measured and predicted values (Figure 404). Although the RMSE and ASE were high (Table 202), all other errors showed that the model was good at prediction. The error map showed medium and low error over most of the study extent but high error around the periphery (Figure 405). The kriged surface is presented in Figure 405.

Table 201. Distributional properties of Annual Primary Production Average Maximum (mg C m^{-2} day^{-1}).

Property	Value
Number of Observations	10384
Minimum	302.020
Maximum	1759.600
Mean	1073.000
Median	1060.300
Standard Deviation	193.400
Skewness	0.271
Kurtosis	2.420

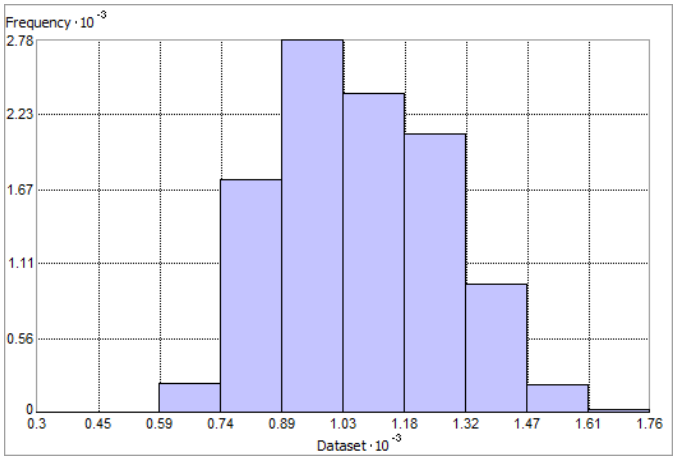

Figure 402. Distribution of Annual Primary Production Average Maximum (mg C m^{-2} day^{-1}). Histogram was illustrated using 10 bins. X and Y axes are shown at 10^{-3}.

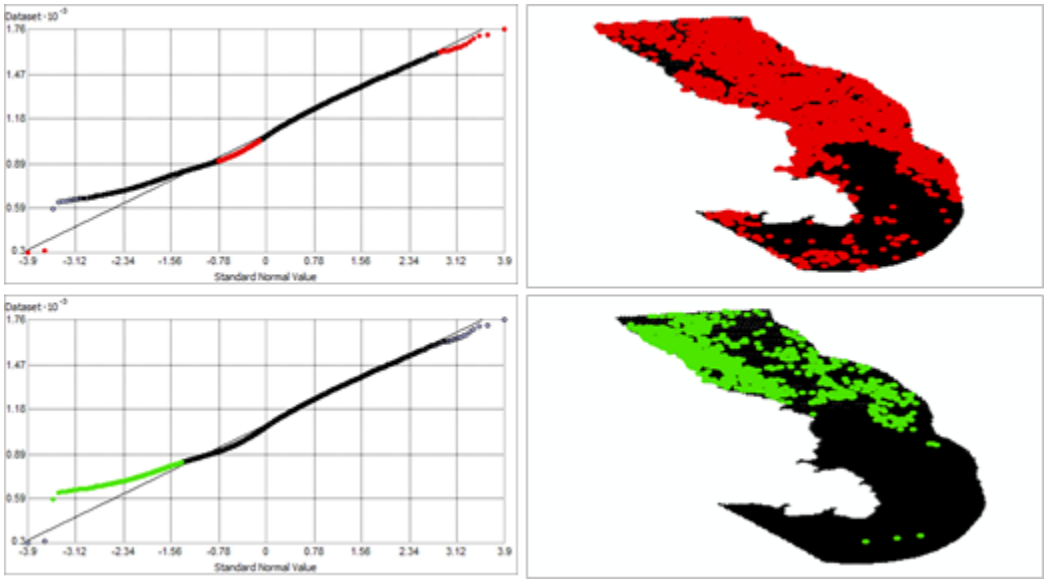

Figure 403. Normal Q-Q plot for data values of Annual Primary Production Average Maximum (mg C m^{-2} day^{-1}). Points falling under (upper panel) and over (bottom panel) the reference line are mapped.

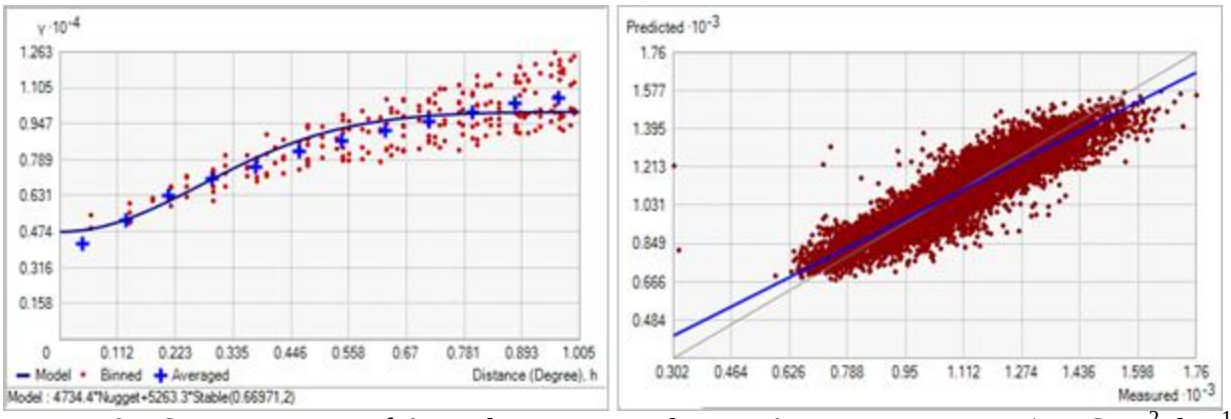

Figure 404. Semivariogram of Annual Primary Production Average Maximum (mg C m^{-2} day^{-1}). Binned values are shown as red dots; average points are shown as blue crosses; the model fit to the averaged values is shown as a blue line. Lag size: 0.084 degrees; number of lags: 12; Parameter: 2; Range: 0.670 degrees; Partial Sill: 5263.322. Right panel: Scatterplot of predicted values versus observed values for the model of Annual Primary Production Average Maximum (mg C m^{-2} day^{-1}).

Table 202. Results of cross-validation of the kriged model for Annual Primary Production Average Maximum (mg C m^{-2} day^{-1}).

Prediction error	**Value**
Number of Observations	10384
Overall Mean Error	-0.034
Root Mean Square Prediction Error	73.503
Standardized Mean	-4.616×10^{-4}
Standardized Root Mean Square Prediction Error	1.006
Average Standard Error	73.049

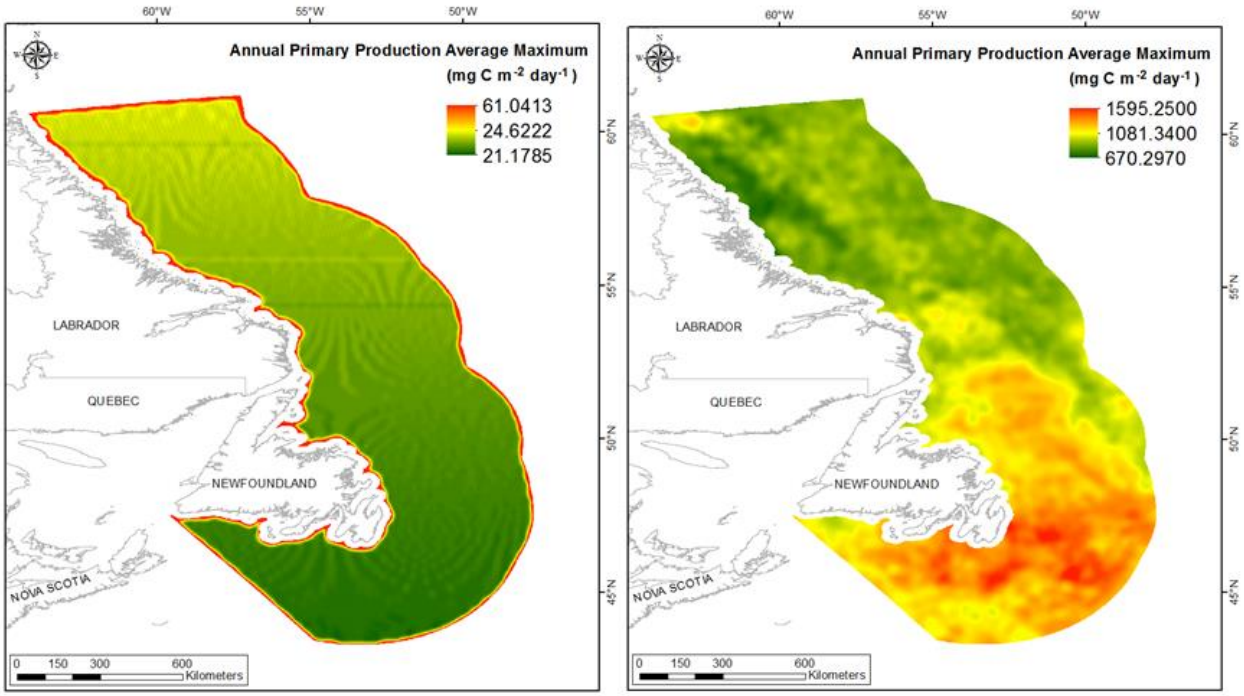

Figure 405. Left panel: Prediction standard error surface of Annual Primary Production Average Maximum (mg C m^{-2} day^{-1}). Right panel: Interpolated prediction surface of Annual Primary Production Average Maximum (mg C m^{-2} day^{-1}).

Annual Primary Production Average Range

This variable displayed a near normal distribution prior to modeling (Table 203, Figure 406). The data were higher than predicted by a normal distribution at low values and lower than predicted at high and mid-values (Figure 407). The areas of under- and over-prediction showed no spatial pattern over the northern portion of the spatial extent with under-prediction appearing in the south (Figure 407).

The semivariogram showed moderate autocorrelation present in the data and the model showed a fair fit between measured and predicted values (Figure 408). Although the RMSE and ASE were high (Table 204), all other errors showed that the model was good at prediction. The error map showed medium and low error over the study extent but high error around the periphery (Figure 409). The kriged surface is presented in Figure 409.

Table 203. Distributional properties of Annual Primary Production Average Range (mg C m^{-2} day^{-1}).

Property	Value
Number of Observations	10384
Minimum	182.730
Maximum	1481.300
Mean	768.080
Median	753.430
Standard Deviation	206.550
Skewness	0.201
Kurtosis	2.347

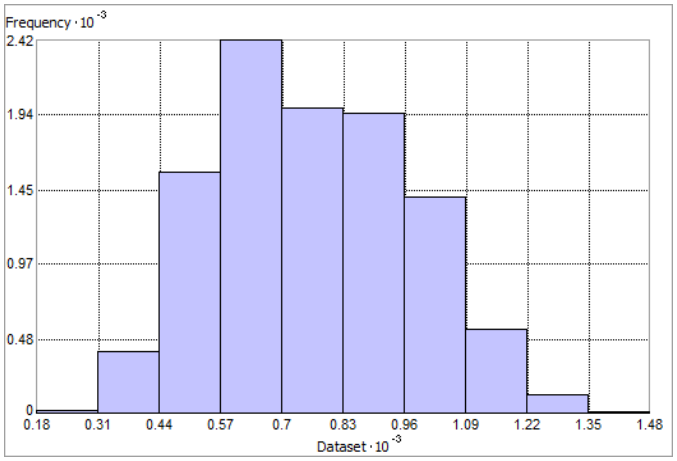

Figure 406. Distribution of Annual Primary Production Average Range (mg C m^{-2} day^{-1}). Histogram was illustrated using 10 bins. X and Y axes are shown at 10^{-3}.

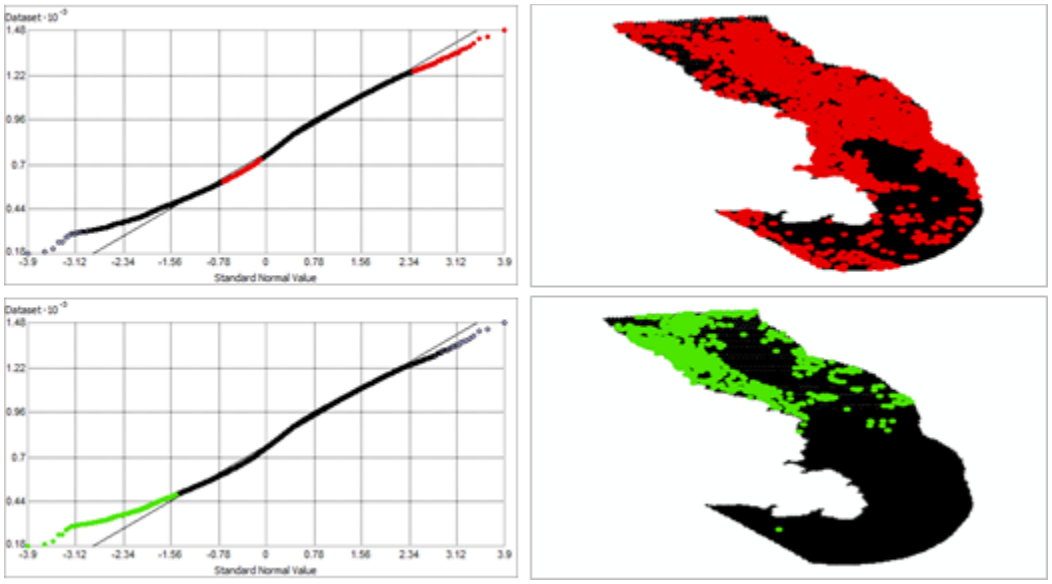

Figure 407. Normal Q-Q plot for data values of Annual Primary Production Average Range (mg C m^{-2} day^{-1}). Points falling under (upper panel) and over (bottom panel) the reference line are mapped.

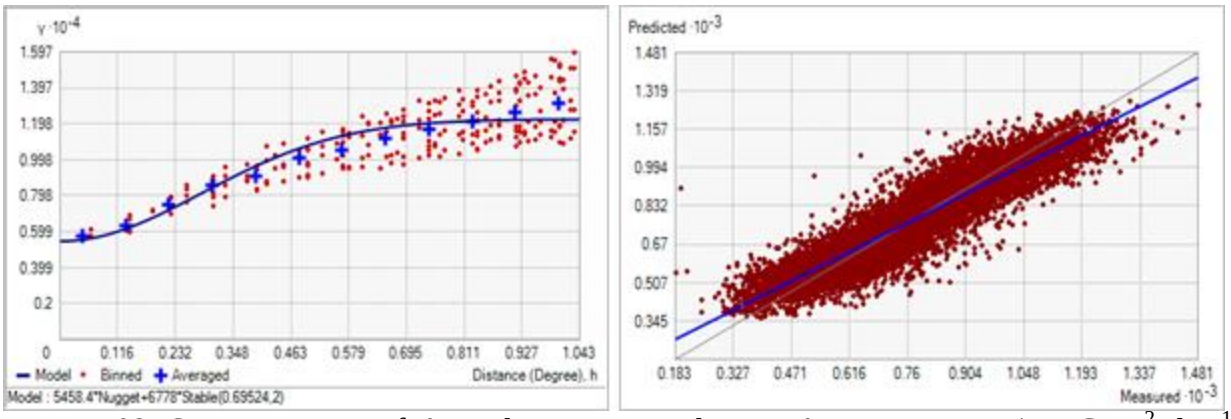

Figure 408. Semivariogram of Annual Primary Production Average Range (mg C m^{-2} day^{-1}). Binned values are shown as red dots; average points are shown as blue crosses; the model fit to the averaged values is shown as a blue line. Lag size: 0.087 degrees; number of lags: 12; Parameter: 2; Range: 0.695 degrees; Partial Sill: 6777.953. Right panel: Scatterplot of predicted values versus observed values for the model of Annual Primary Production Average Range (mg C m^{-2} day^{-1}).

Table 204. Results of cross-validation of the kriged model for Annual Primary Production Average Range (mg C m^{-2} day^{-1}).

Prediction error	**Value**
Number of Observations	10384
Overall Mean Error	-0.045
Root Mean Square Prediction Error	79.963
Standardized Mean	-5.082×10^{-4}
Standardized Root Mean Square Prediction Error	1.020
Average Standard Error	78.412

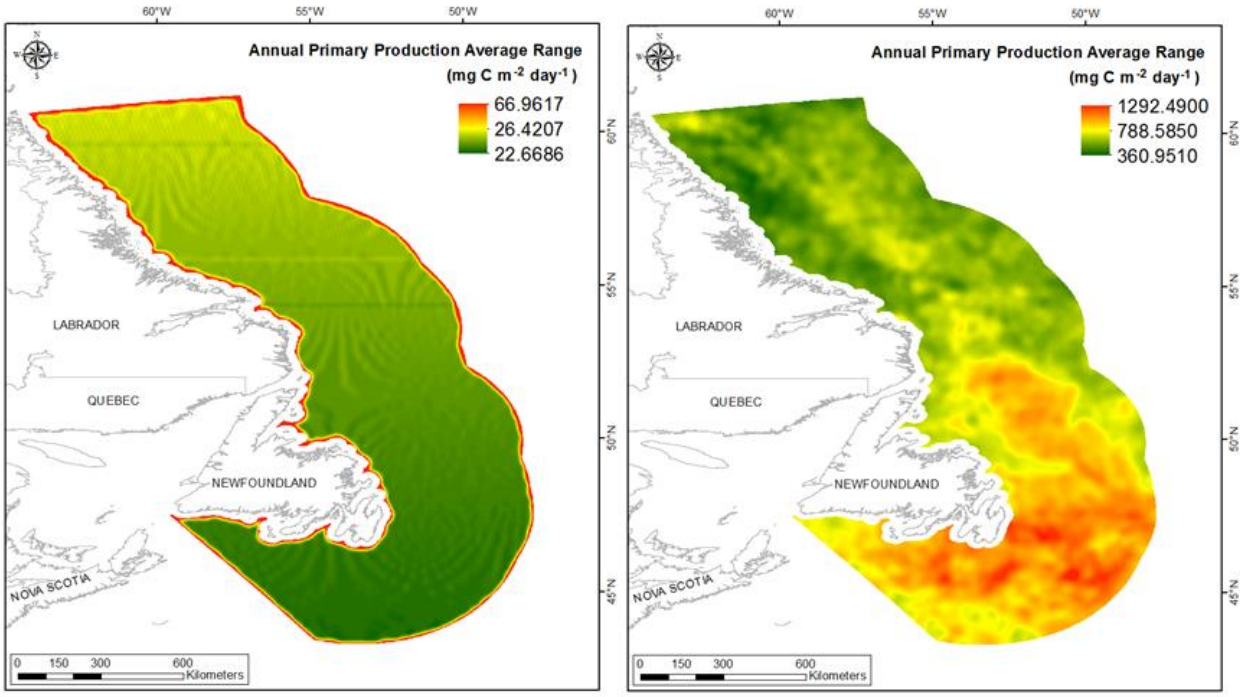

Figure 409. Left panel: Prediction standard error surface of Annual Primary Production Average Range (mg C m^{-2} day^{-1}). Right panel: Interpolated prediction surface of Annual Primary Production Average Range (mg C m^{-2} day^{-1}).

Dissolved Oxygen and Nutrients

Nutrients (e.g. nitrate, phosphate, silicate) are required for the growth of phytoplankton, and therefore directly influence chlorophyll *a* concentration and primary production in surface waters. Generally, as water stratification develops in the spring, nutrients are consumed and drawn down to deeper water by phytoplankton and remain low throughout the rest of the year, while dissolved oxygen decreases (Manasrah et al. 2006). Certain benthic invertebrates also require minerals for their skeletal components (e.g., silicate for sponges).

Dissolved Oxygen

This variable displayed a bell-shaped distribution with left skewness (Table 205, Figure 410). The data were higher than predicted by a normal distribution at low values and lower than predicted at the lowest and the highest values (Figure 411). The areas of under- and over-prediction showed no spatial pattern over the spatial extent (Figure 411).

The semivariogram showed weak autocorrelation present in the data and the model showed poor fit between measured and predicted values (Figure 412). The model showed moderate cross-validation statistics (Table 206). The error map showed a highly discontinuous and patchy

pattern over the study extent with higher error in the north of the study extent (Figure 413). Error was lower at the location of data points. The kriged surface is presented in Figure 413.

Table 205. Distributional properties of Dissolved Oxygen (ml l^{-1}).

Property	Value
Number of Observations	510
Minimum	3.442
Maximum	11.010
Mean	7.845
Median	7.739
Standard Deviation	1.157
Skewness	-0.342
Kurtosis	4.129

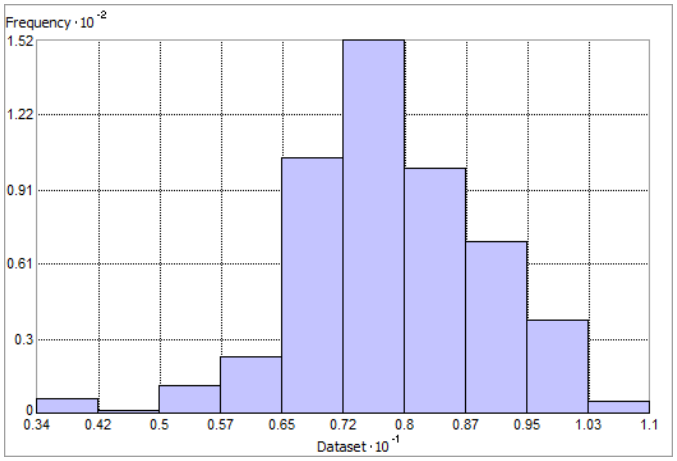

Figure 410. Distribution of Dissolved Oxygen (ml l^{-1}). Histogram was illustrated using 10 bins. X axis is shown at 10^{-1};Y axis is shown at 10^{-2}.

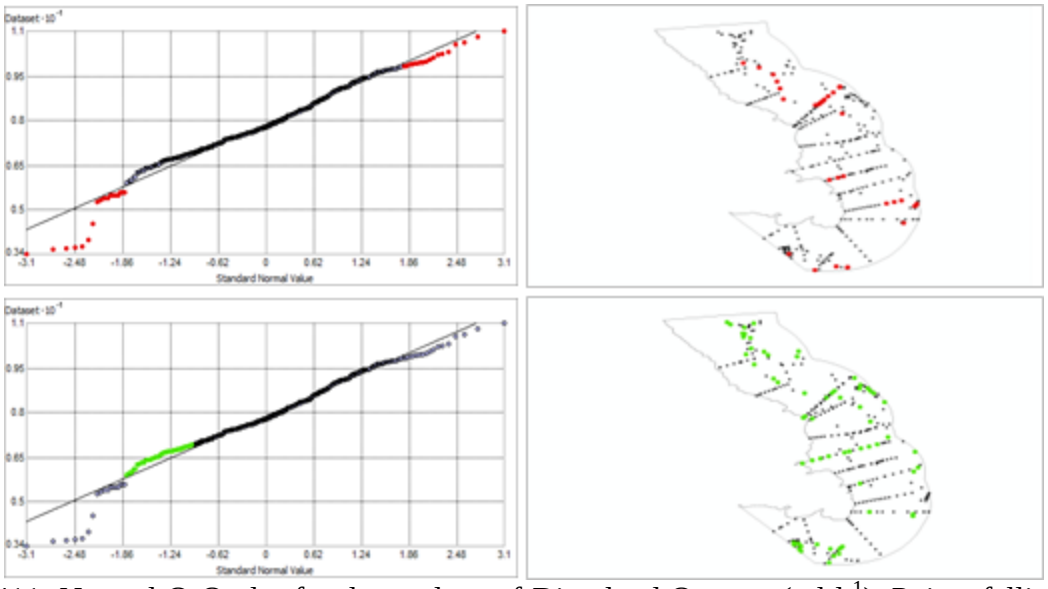

Figure 411. Normal Q-Q plot for data values of Dissolved Oxygen (ml l^{-1}). Points falling under (upper panel) and over (bottom panel) the reference line are mapped.

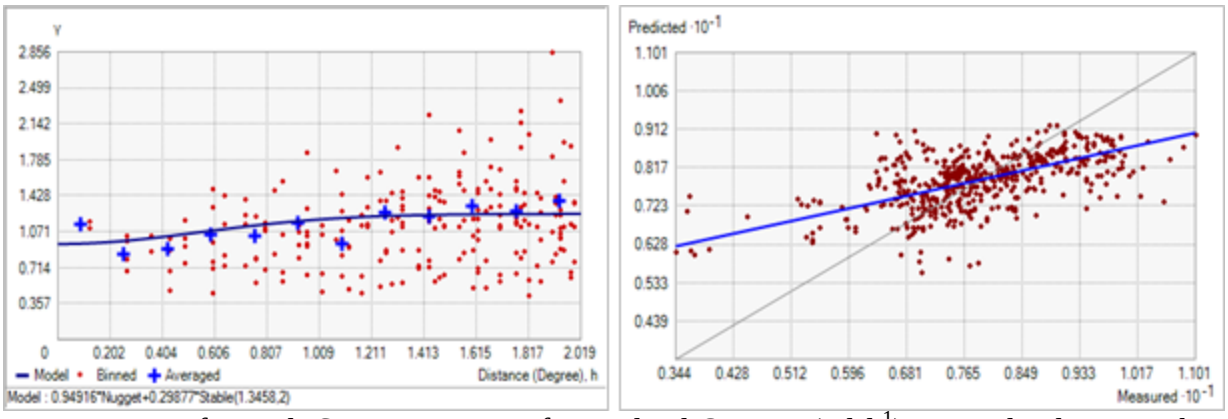

Figure 412. Left panel: Semivariogram of Dissolved Oxygen (ml l^{-1}). Binned values are shown as red dots; average points are shown as blue crosses; the model fit to the averaged values is shown as a blue line. Lag size: 0.168 degrees; number of lags: 12; Parameter: 2; Range: 1.346 degrees; Partial Sill: 0.299. Right panel: Scatterplot of predicted values versus observed values for the variable Dissolved Oxygen (ml l^{-1}).

Table 206. Results of cross-validation of the kriged model for Dissolved Oxygen (ml l^{-1}).

Prediction error	**Value**
Number of Observations	510
Overall Mean Error	3.752×10^{-3}
Root Mean Square Prediction Error	0.950
Standardized Mean	2.878×10^{-3}
Standardized Root Mean Square Prediction Error	0.913
Average Standard Error	1.043

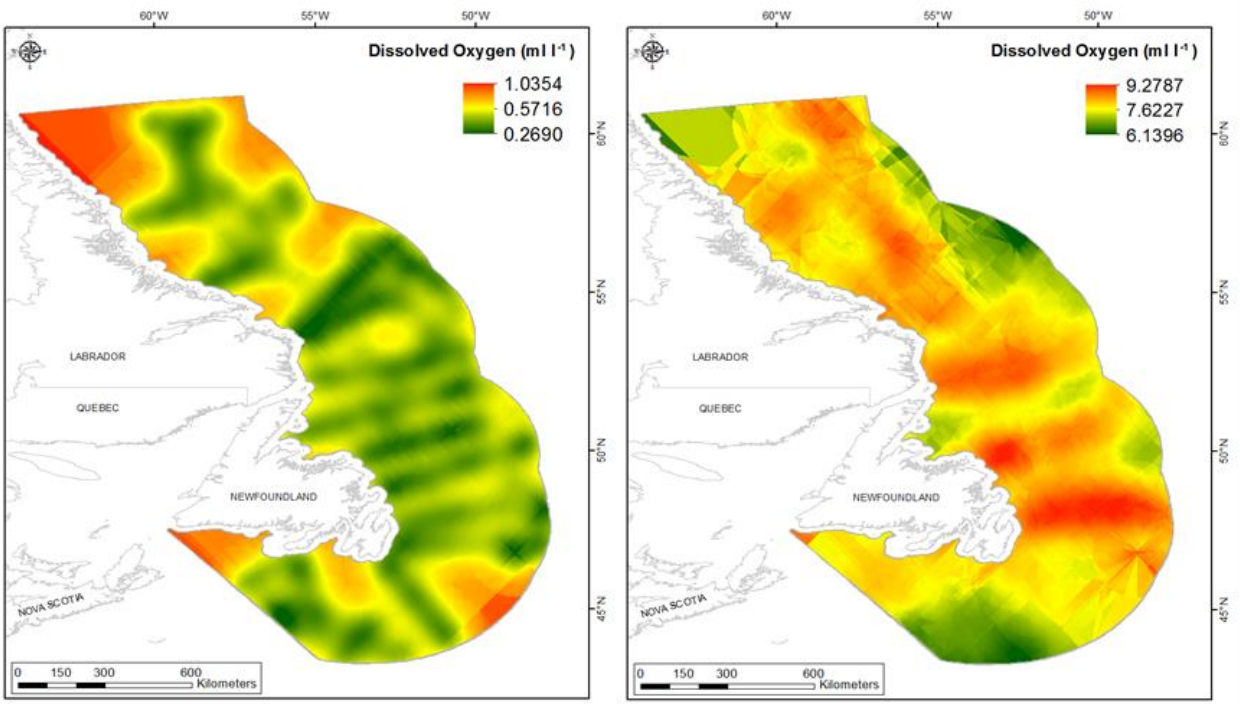

Figure 413. Left panel: Prediction standard error surface of Dissolved Oxygen (ml l^{-1}). Right panel: Interpolated prediction surface of Dissolved Oxygen (ml l^{-1}).

Phosphate

This variable displayed a right-skewness distribution with outlying data in the upper range and kurtosis (Table 207, Figure 414). The data fit a normal distribution with deviation mainly in high and low values (Figure 415). The areas of under- and over-prediction showed no spatial pattern over the spatial extent (Figure 415).

The semivariogram showed little autocorrelation present in the data and the model showed poor fit between measured and predicted values (Figure 416). The model showed good cross-validation statistics (Table 208) indicating that the model was good at prediction. The error map showed a highly discontinuous and patchy pattern over the study extent with higher in the north of the study extent (Figure 417). Error was lower at the location of data points. The kriged surface is presented in Figure 417.

Table 207. Distributional properties of Phosphate (µmol l^{-1}).

Property	Value
Number of Observations	257
Minimum	0.015
Maximum	1.600
Mean	0.308
Median	0.260
Standard Deviation	0.200
Skewness	1.858
Kurtosis	10.441

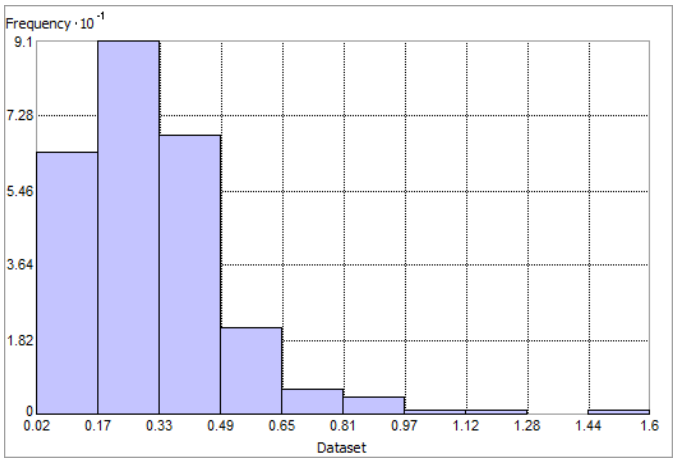

Figure 414. Distribution of Phosphate (µmol l^{-1}). Histogram was illustrated using 10 bins. Y axis is shown at 10^{-1}.

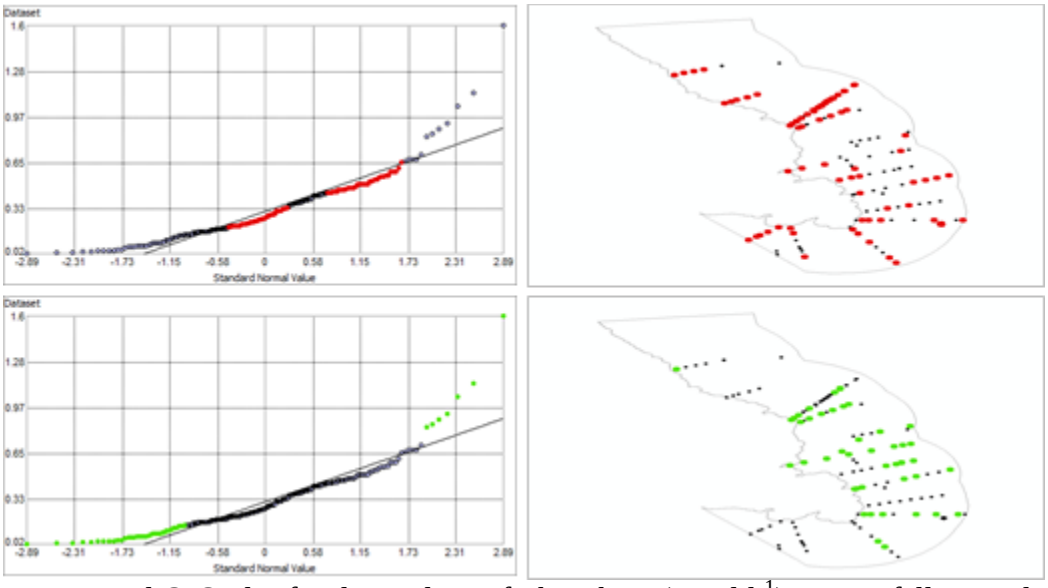

Figure 415. Normal Q-Q plot for data values of Phosphate (µmol l^{-1}). Points falling under (upper panel) and over (bottom panel) the reference line are mapped.

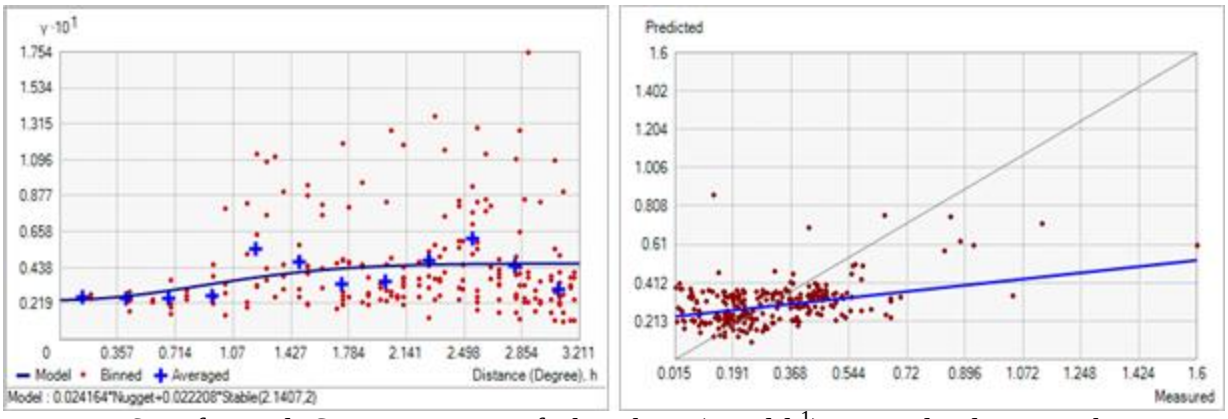

Figure 416. Left panel: Semivariogram of Phosphate (µmol l^{-1}). Binned values are shown as red dots; average points are shown as blue crosses; the model fit to the averaged values is shown as a blue line. Lag size: 0.268 degrees; number of lags: 12; Parameter: 2; Range: 2.141 degrees; Partial Sill: 0.022. Right panel: Scatterplot of predicted values versus observed values for the variable Phosphate (µmol l^{-1}).

Table 208. Results of cross-validation of the kriged model for Phosphate (µmol l^{-1}).

Prediction error	**Value**
Number of Observations	257
Overall Mean Error	-1.593×10^{-3}
Root Mean Square Prediction Error	0.174
Standardized Mean	-9.855×10^{-3}
Standardized Root Mean Square Prediction Error	1.041
Average Standard Error	0.170

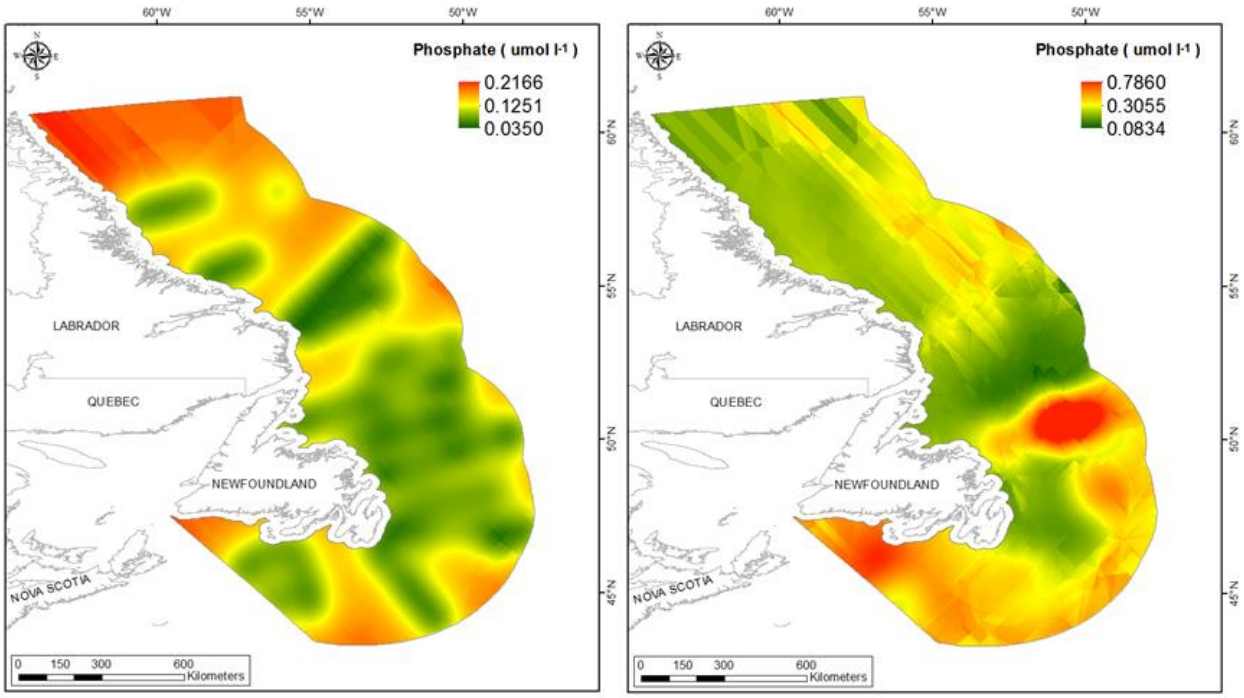

Figure 417. Left panel: Prediction standard error surface of Phosphate (µmol l^{-1}). Right panel: Interpolated prediction surface of Phosphate (µmol l^{-1}).

Silicate

This variable displayed a right-skewed distribution with outlying data in the upper range and kurtosis (Table 209, Figure 418). The data were higher than predicted by a normal distribution at low and high values and lower at mid-range values (Figure 419). The areas of under- and over-prediction showed no spatial pattern over the spatial extent (Figure 419).

The semivariogram showed little autocorrelation present in the data and the model showed poor fit between measured and predicted values (Figure 420). The model showed good cross-validation statistics (Table 210) indicating that the model was good at prediction. The error map showed a highly discontinuous and patchy pattern over the study extent with higher error in the north of the study area (Figure 421). Error was low at the location of data points. The kriged surface is presented in Figure 421.

Table 209. Distributional properties of Silicate (µmol l^{-1}).

Property	Value
Number of Observations	244
Minimum	1.538 x 10^{-3}
Maximum	11.590
Mean	1.865
Median	1.175
Standard Deviation	1.768
Skewness	1.674
Kurtosis	7.133

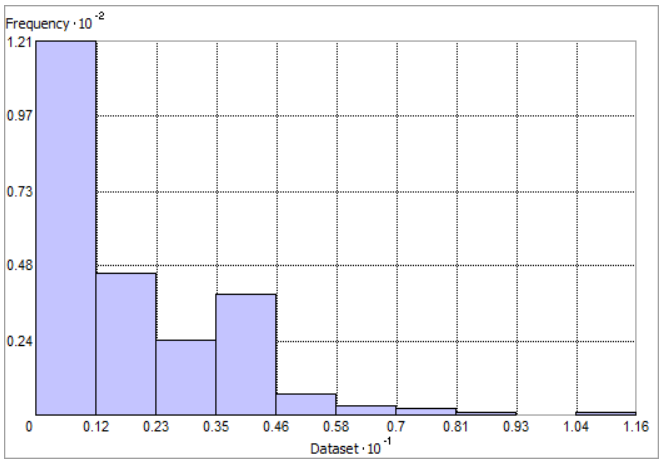

Figure 418. Distribution of Silicate (µmol l^{-1}). Histogram was illustrated using 10 bins. X axis is shown at 10^{-1}. Y axis is shown at 10^{-2}.

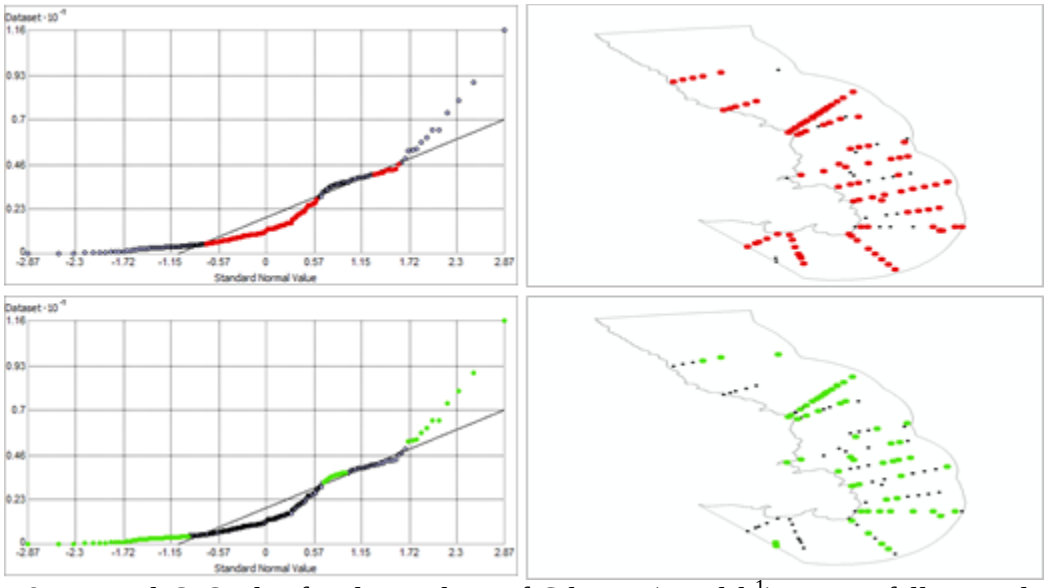

Figure 419. Normal Q-Q plot for data values of Silicate (µmol l^{-1}). Points falling under (upper panel) and over (bottom panel) the reference line are mapped.

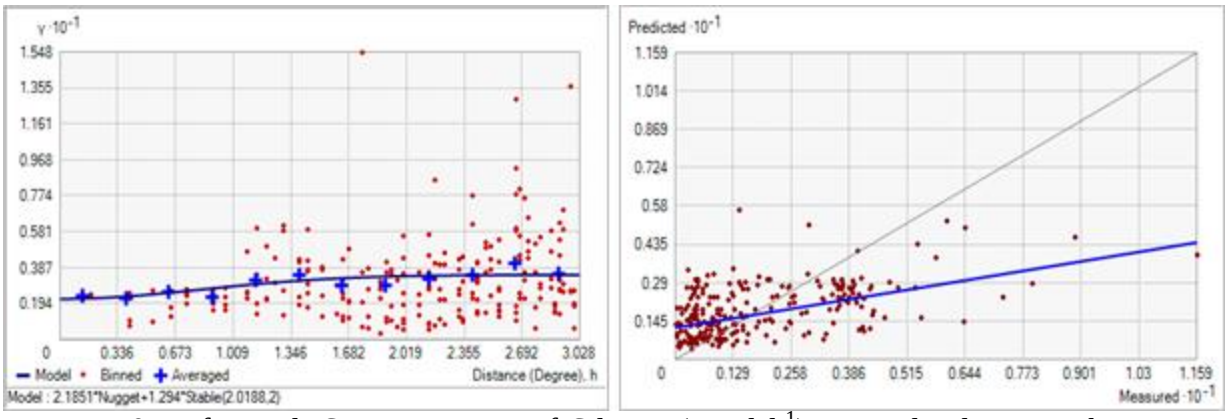

Figure 420. Left panel: Semivariogram of Silicate (µmol l^{-1}). Binned values are shown as red dots; average points are shown as blue crosses; the model fit to the averaged values is shown as a blue line. Lag size: 0.252 degrees; number of lags: 12; Parameter: 2; Range: 2.019 degrees; Partial Sill: 1.294. Right panel: Scatterplot of predicted values versus observed values for the variable Silicate (µmol l^{-1}).

Table 210. Results of cross-validation of the kriged model for Silicate (µmol l^{-1}).

Prediction error	**Value**
Number of Observations	244
Overall Mean Error	-0.14
Root Mean Square Prediction Error	1.522
Standardized Mean	-8.618×10^{-3}
Standardized Root Mean Square Prediction Error	0.959
Average Standard Error	1.602

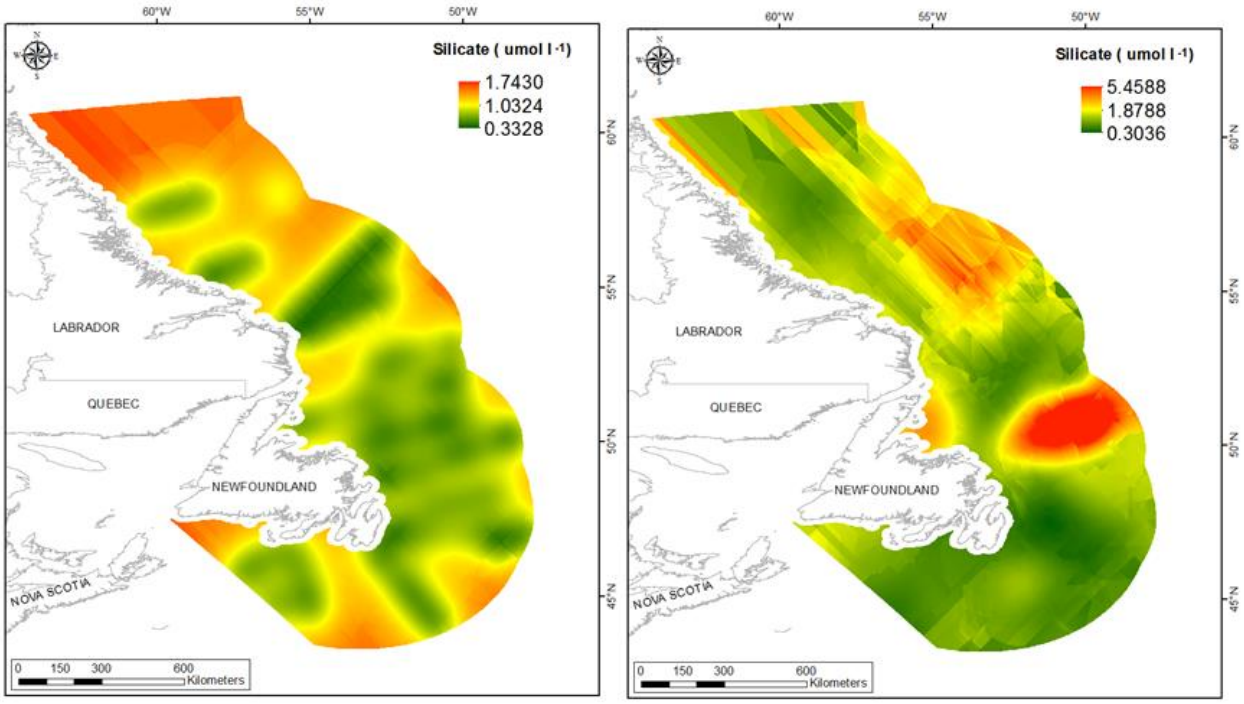

Figure 421. Left panel: Prediction standard error surface of Silicate (µmol l^{-1}). Right panel: Interpolated prediction surface of Silicate (µmol l^{-1}).

ACKNOWLEDGMENTS

Funding for this technical report was received from a Strategic Program for Ecosystem-Based Research and Advice (SPERA) project to E. Kenchington. A. Power (DFO-NWAFC) provided critical partial funding for J.G. We thank G. White (DFO-MAR) for providing the primary production data. We also thank Corinna Favarro (DFO-NL) and Javier Murillo-Perez (DFO-MAR) for reviewing the document.

REFERENCES

Beazley, L.I., Kenchington, E.L., Murillo, F.J., Sacau, M. 2013. Deep-sea sponge grounds enhance diversity and abundance of epibenthic megafauna in the Northwest Atlantic. ICES J. Mar. Sci. 70: 1471-1490.

Beazley, L., Kenchington, E., Murillo, J., Lirette, C., Guijarro, J., McMillan, A., and Knudby, A. 2016a. Species Distribution Modelling of Corals and Sponges in the Maritimes Region for

Use in the Identification of Sensitive Benthic Areas. Can. Tech. Rep. Fish. Aquat. Sci. 3172: vi + 189 p.

Beazley, L., Murillo, F.J., Kenchington, E., Guijarro, J., Lirette, C., Siferd, T., Treble, M., Baker, E., Bouchard Marmen, M., Tompkins MacDonald, G. 2016b. Species Distribution Modelling of Corals and Sponges in the Eastern Arctic for Use in the Identification of Significant Benthic Areas. Can. Tech. Rep. Fish. Aquat. Sci. 3175: vii + 210 p.

Beazley, L., Lirette, C., Sabaniel, J., Wang, Z., Knudby, A., and Kenchington, E. 2016c. Characteristics of Environmental Data Layers for Use in Species Distribution Modelling in the Gulf of St. Lawrence. Can. Tech. Rep. Fish. Aquat. Sci. 3154: viii + 357 p.

Bender, M., Grande, K., Johnson, K. 1987. A comparison of four methods for determining planktonic community production. Limnol. Oceanogr. 32: 1085-1098.

Boyer, T.P., Antonov, J.I., Baranova, O.K., and 12 others. 2013, World Ocean Database 2013. Sydney Levitus, Ed.; Alexey Mishonov, Technical Ed.; NOAA Atlas NESDIS 72, 209 pp.

Breiman, L. 2001. Random forests. Machine Learning 45: 5-32.

Carney, R.S. 2005. Zonation of deep-sea biota on continental margins. Oceanogr. Mar. Biol. Annu. Rev. 43: 211-279.

Carstensen, J., Conley, D.J., Lophaven, S., Danielsson, A., Rahm, L., and Toompuu, A. 2002. Statistical Analysis and Modelling of Phytoplankton Dynamics: Exploitation of Data in the Nordic and Baltic Monitoring Programs, Nordic Council of Ministers.

Cheng, R.T., Ling, C-H., and Gartner, J.W. 1999. Estimates of bottom roughness length and bottom shear stress in South San Francisco Bay, California. J. Geophys. Res. 104: 7715-7728.

de Boyer Montégut, C., Madec, G., Fischer, A.S., Lazar, A., and Iudicone, D. 2004. Mixed layer depth over the global ocean: An examination of profile data and a profile-based climatology. J Geophys Res 109, C12003, doi:10.1029/2004JC002378.

Deutsch, C.V. 1996. Correcting for negative weights in ordinary kriging. Comput. Geosci. 22: 765-773.

ESRI. 2011. ArcGIS Desktop: Release 10. Environmental Systems Research Institute, Redlands, CA.

Feldman, G.C., and McClain, C.R. 2012. Ocean Color Web, SeaWiFS Reprocessing 2010.0, NASA Goddard Space Flight Centre. Eds. Kuring, N. and Bailey, S.W. June, 2012. http://oceancolor.gsfc.nasa.gov/

Goovaerts, P. 1997. Geostatistics for Natural Resources Evaluation. Oxford University Press. 483 p.

Goovaerts, P. 2000. Geostatistical approaches for incorporating elevation into the spatial interpolation of rainfall. J. Hydrol. 228: 113-129.

Guijarro, J., Beazley, L., Lirette, C., Kenchington, E., Wareham, V., Gilkinson, K., Koen-Alonso, M. and F.J. Murillo. 2016a. Species Distribution Modelling of Corals and Sponges from Research Vessel Survey Data in the Newfoundland and Labrador Region for use in

the Identification of Significant Benthic Areas. Can. Tech. Rep. Fish. Aquat. Sci. 3171: vi + 126 p.

Guijarro, J., Kenchington, E., Murillo, F.J., Beazley, L., Lirette, C., Wareham, V., Koen-Alonso, M. 2016b. Species Distribution Modelling of Crinoids, Bryozoans and Ascidians in the Newfoundland and Labrador Region. Can. Tech. Rep. Fish. Aquat. Sci. 3181: v + 60 p.

Gunstra, M., and Van Auken, O.W. 2007. Using GIS to display complex soil salinity patterns in an inland salt marsh (Chapter 19). *In* Developments in Environmental Sciences 5. Concepts and Applications in Environmental Geochemistry. pp. 407-431.

Johnston, K., Ver Hoef, J.M., Krivoruchko, K., and Lucas, N. 2001. Using ArcGIS Geostatistical Analyst. ArcGIS User manual, ESRI. California, Redlands. 300 pp.

Knudby, A., Kenchington, E., Murillo, F.J. 2013. Modeling the distribution of Geodia sponges and sponge grounds in the northwest Atlantic Ocean. PLoS ONE 8(12): e82306. doi:10.1371/journal.pone.0082306.

Kravchenko, A., and Bullock, D.G. 1999. A comparative study of interpolation methods for mapping soil properties. Agron. J. 91: 393-400.

Krivoruchko, K. 2011. Spatial Statistical Data Analysis for GIS Users. ESRI Press, Redlands, CA. 928 p.

Levin, L.A., Etter, R. J., Rex, M.A., Gooday, A.J., Smith, C. R., Pineda, J., Stuart, C. T., et al. 2001. Environmental influences on regional deep-sea species diversity. Annu. Rev. Ecol. Syst. 32: 51-93.

Li, J. and Heap, A.D. 2008. A Review of Spatial Interpolation Methods for Environmental Scientists. Geoscience Australia, Record 2008/23, 137 p.

Lutz, M.J., Caldeira, K., Dunbar, R.B., Behrenfeld, M.J. 2007. Seasonal rhythms of net primary production and particulate organic carbon flux to depth describe the efficiency of biological pump in the global ocean. J. Geophys. Res-Oceans 112: C10011.

Ly, S., Charles, C., and Degré, A. 2011. Geostatistical interpolation of daily rainfall at catchment scale: the use of several variogram models in the Ourthe and Ambleve catchments, Belgium. Hydrol. Earth Syst. Sci. 15: 2259-2274.

MacDonald, I. R., Bluhm, B. A., Iken, K., Gavaev, S., and Strong, S. 2010. Benthic macrofauna and megafauna assemblages in the Arctic Deep-Sea Canada Basin. Deep Sea Res. II 57: 136-152.

Manasrah, R., Raheed, M., and Badran, M.I. 2006. Relationships between water temperature, nutrients and dissolved oxygen in the northern Gulf of Aqaba, Red Sea. Oceanologia 48: 237-253.

Mercier, A., Hamel, J-F. 2011. Contrasting reproductive strategies in three deep- sea octocorals from eastern Canada: *Primnoa resedaeformis*, *Keratoisis ornata*, and *Anthomastus grandiflorus*. Coral Reefs 30: 337-350.

Murillo, F.J., Kenchington, E., Beazley, L., Lirette, C., Knudby, A., Guijarro, J., Benoît, H., Bourdage, H. and Sainte-Marie, B. 2016. Distribution Modelling of Sea Pens, Sponges, Stalked Tunicates and Soft Corals from Research Vessel Survey Data in the Gulf of St.

Lawrence for Use in the Identification of Sensitive Benthic Areas. Can. Tech. Rep. Fish. Aquat. Sci. 3170: vi + 132 p.

Papiol, V., Cartes, J. E., Fanelli, E., and Maynou, F. 2012. Influence of environmental variables on the spatio-temporal dynamics of the bentho-pelagic assemblages in the middle slope of the Balearic Basin (NW Mediterranean). Deep Sea Res. I 61: 84-99.

Platt, T., Sathyendranath, S., Forget, M-H., White III, G.N., Caverhill, C., Bouman, H., Devred, E., Son, S. 2008. Operational estimation of primary production at large geographical scales. Remote Sens. Environ. 112: 3437-3448.

Polovina, J.J., Mitchum, G.T., and Evans, G.T. 1995. Decadal and basin-scale variation in mixed layer depth and the impact on biological production in the Central and North Pacific, 1960-88. Deep-Sea Res. 42: 1701-1716.

Robinson, T.P., and Metternicht, G. 2006. Testing the performance of spatial techniques for mapping soil properties. Comput. Electron. Agric. 50: 97-108.

Shepard, D. 1968. A two-dimensional interpolation function for irregularly-spaced data. *In* Proceedings of the 1968 23rd ACM national conference. Edited by R.B. Blue and A.M. Rosenberg. ACM., pp. 517-524.

Soltwedel, T., Jaeckisch, N., Ritter, N., Hasemann, C., Bergmann, M., and Klages, M. 2009. Bathymetric patterns of megafaunal assemblages from the arctic deep-sea observatory HAUSGARTEN. Deep Sea Res. I 56: 1856-1872.

Spetland, F., Rapp, H.T., Hoffmann, F., and Tendal, O.S. 2007. Sexual reproduction of *Geodia barretti* Bowerbank 1858 (Porifera, Astrophorida) in two Scandinavian fjords. *In* Porifera Research: Biodiversity, Innovation and Sustainability. Edited by M.R. Custódio G. Lôbo-Hajdu, E. Hajdu, and G. Muricy. Rio de Janeiro, Brazil: Museu. Nacional. pp. 613-620.

Sun, Z., Hamel, J.-F., Edinger, E., and Mercier, A. 2010a.Reproductive biology of the deep-sea octocoral *Drifa glomerata* in the Northwest Atlantic. Mar. Biol. 157: 863-873.

Sun, Z., Hamel, J.-F., and Mercier, A. 2010b. Planulation periodicity, settlement preferences and growth of two deep-sea octocorals from the Northwest Atlantic. Mar. Ecol. Prog. Ser. 410: 71-87.

Sun, Z., Hamel, J.-F., and Mercier, A. 2011. Planulation, larval biology, and early growth of the deep-sea soft corals *Gersemia fruticosa* and *Duva florida* (Octocorallia: Alcyonacea). Invert. Biol. 130: 91-99.

Vance, R.R. 1973. On reproductive strategies in marine benthic invertebrates. Amer. Nat. 107: 339-352.

Yamamoto, J.K. 2007. On unbiased backtransform of lognormal kriging estimates. Comput. Geosci. 11: 219-234.

APPENDIX I - Summary of Variables with Negative Values in the Interpolated Prediction Surface Resulting from Ordinary Kriging

Appendix 1 shows a map of each of the seven variables with negative values resulting in the prediction surfaces after spatial interpolation using ordinary kriging. The location of the negative values is highlighted in blue. The data distribution prior to modeling and the numbers of cells with negative values for each variable is presented in Table A1.

Table A1. Summary of environmental variables with negative prediction values resulting from ordinary kriging.

Variable	Negative values in input	Data distribution	Total number of cells	Cells with negative values	Range of negative values
Bottom Salinity Average Range	No	Right-skewed	533592	20	-9.78×10^{-3} to -2.03×10^{-4}
Bottom Current Minimum	No	Right-skewed	533592	5886	-5.55×10^{-3} to -5.00×10^{-8}
Surface Current Minimum	No	Right-skewed	533592	353	-3.26×10^{-3} to -5.00×10^{-6}
Surface Current Average Minimum	No	Right-skewed	533592	65	-2.99×10^{-3} to -3.90×10^{-5}
Maximum Summer Mixed Layer Depth	No	Right-skewed	533592	235	-51.36 to -0.13
Bottom Shear Minimum	No	Right-skewed; outliers	533592	4396	-3.22×10^{-3} to -3.00×10^{-8}
Bottom Shear Average Minimum	No	Right-skewed; outliers	533592	153	-1.66×10^{-3} to -2.00×10^{-6}

Bottom Salinity Average Range

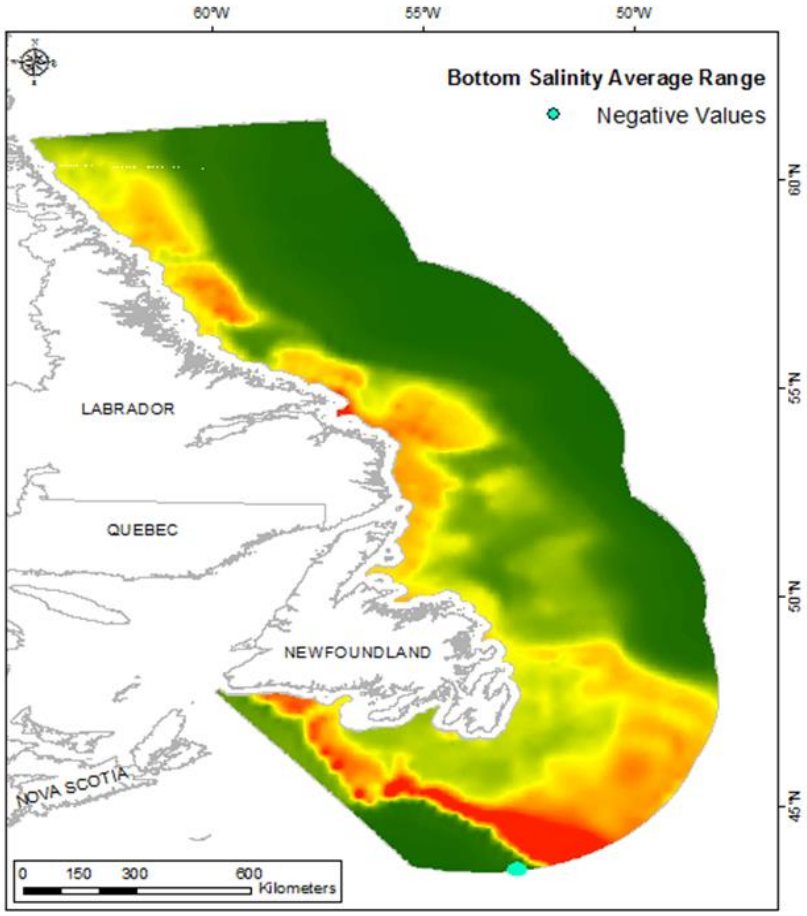

Figure A1. Negative values generated in the interpolated prediction surface of Bottom Salinity Average Range.

Bottom Current Minimum

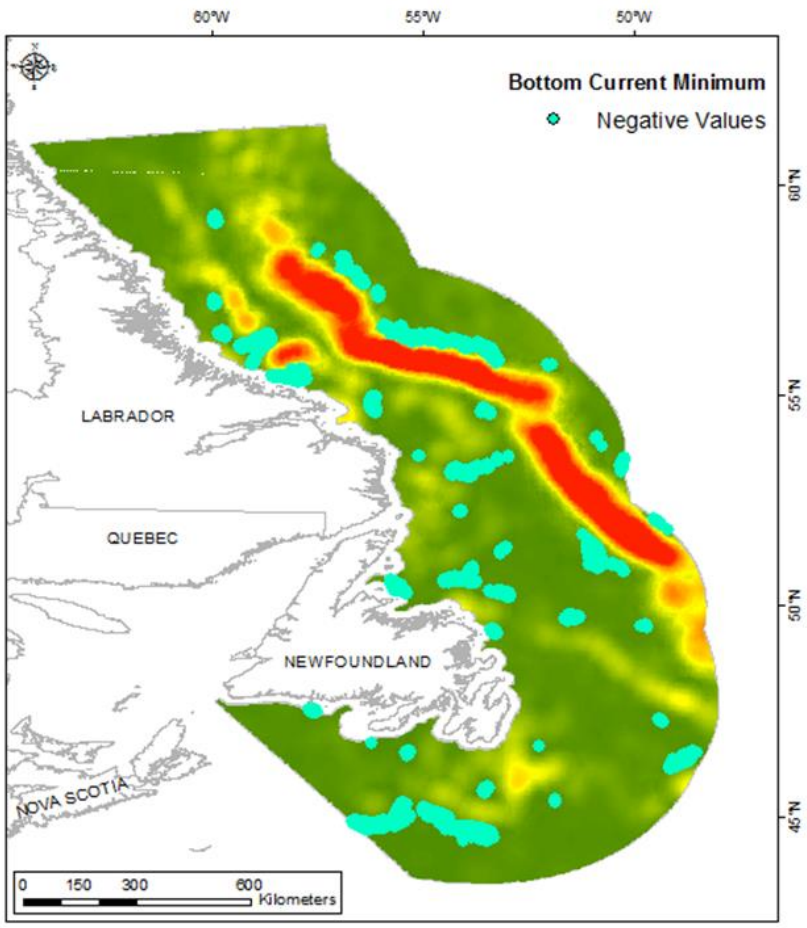

Figure A2. Negative values generated in the interpolated prediction surface of Bottom Current Minimum.

Surface Current Minimum

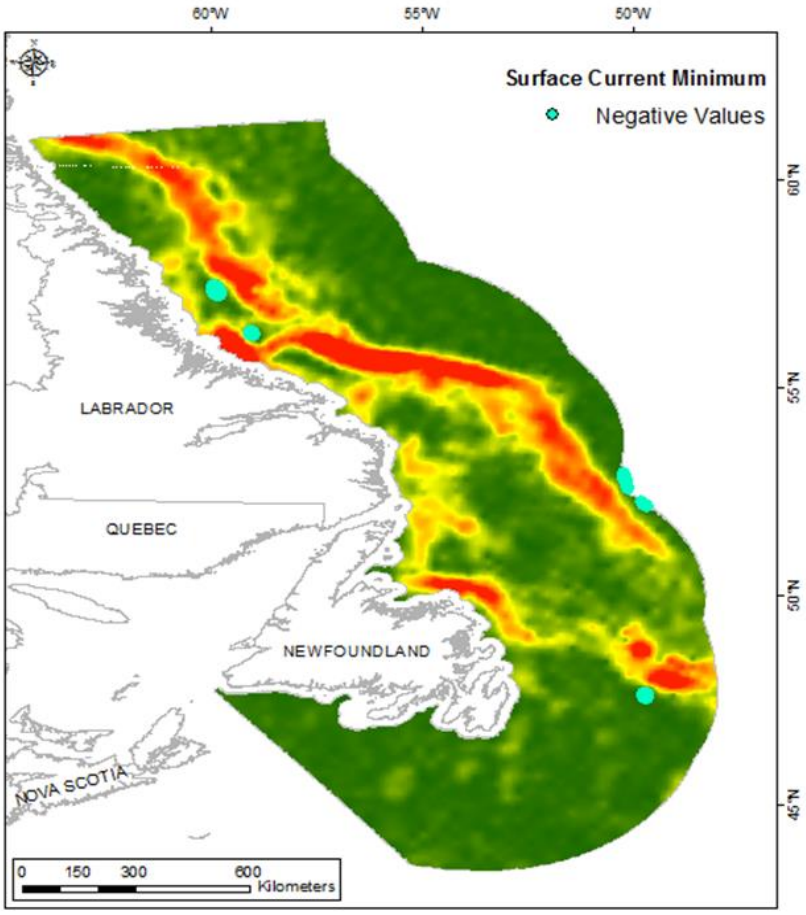

Figure A3. Negative values generated in the interpolated prediction surface of Surface Current Minimum.

Surface Current Average Minimum

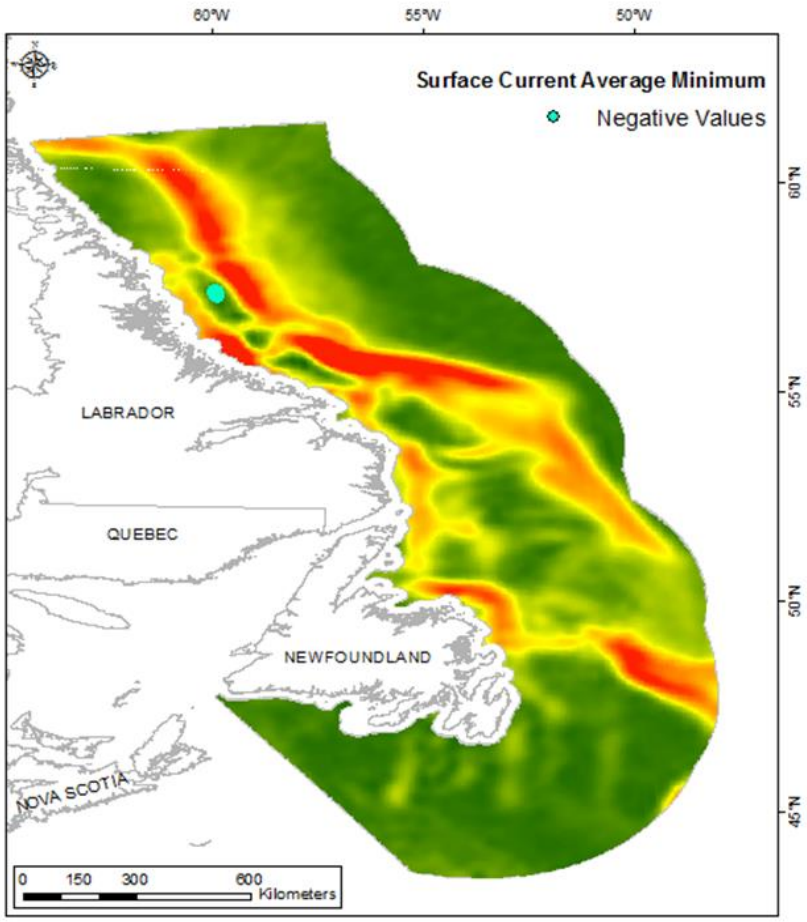

Figure A4. Negative values generated in the interpolated prediction surface of Surface Current Average Minimum in the Newfoundland and Labrador Region.

Maximum Summer Mixed Layer Depth

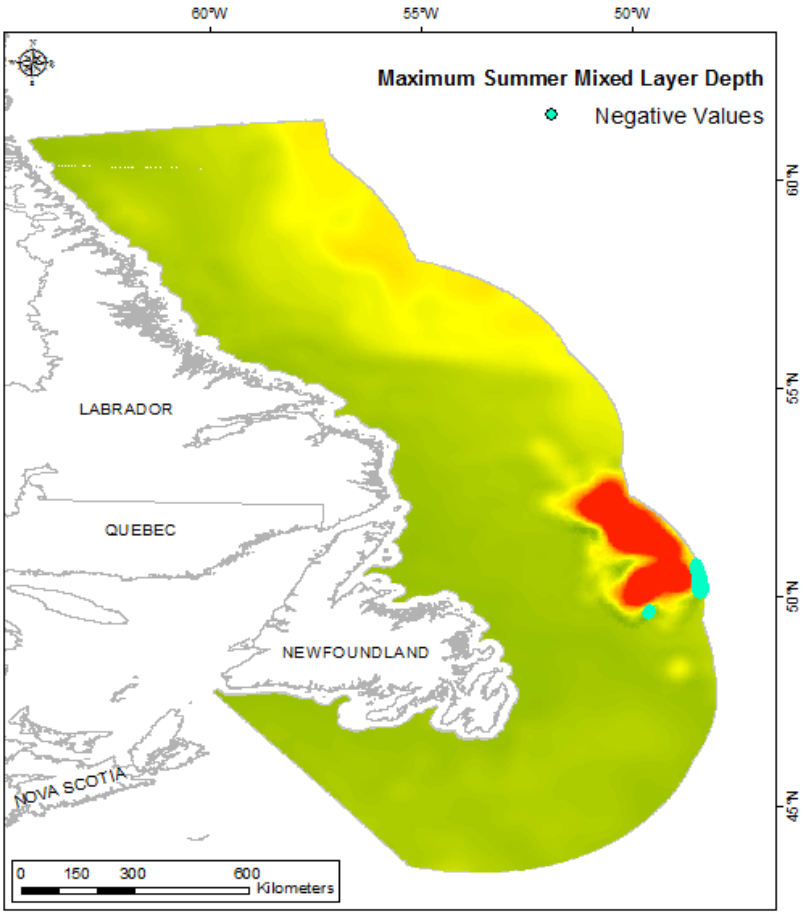

Figure A5. Negative values generated in the interpolated prediction surface of Maximum Summer Mixed Layer Depth.

Bottom Shear Minimum

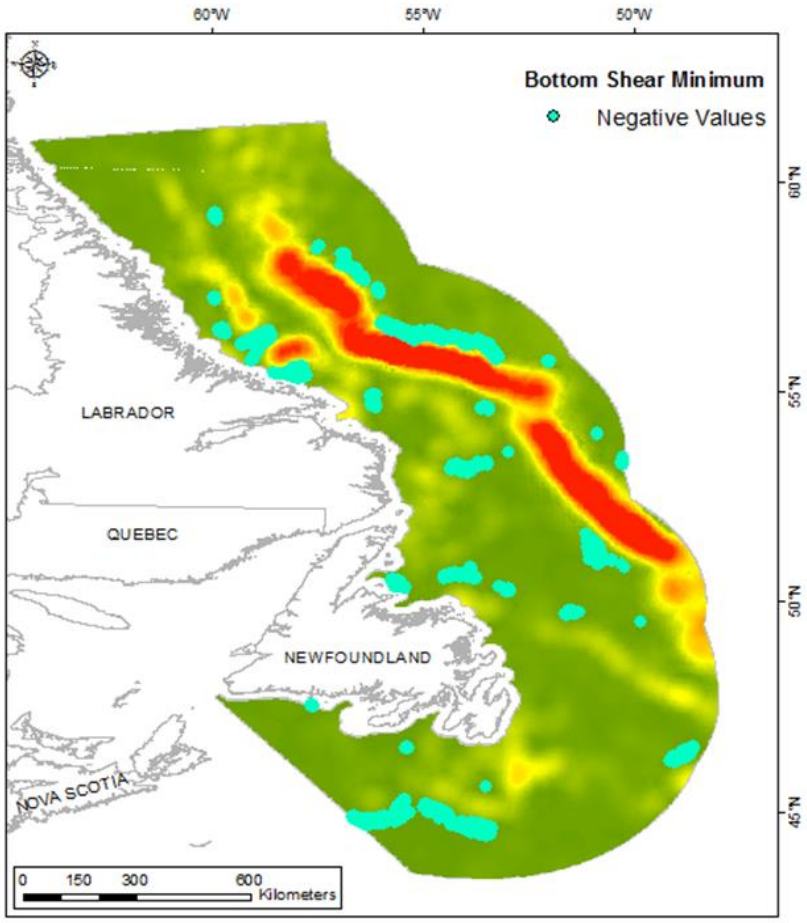

Figure A6. Negative values generated in the interpolated prediction surface of Bottom Shear Minimum.

Bottom Shear Average Minimum

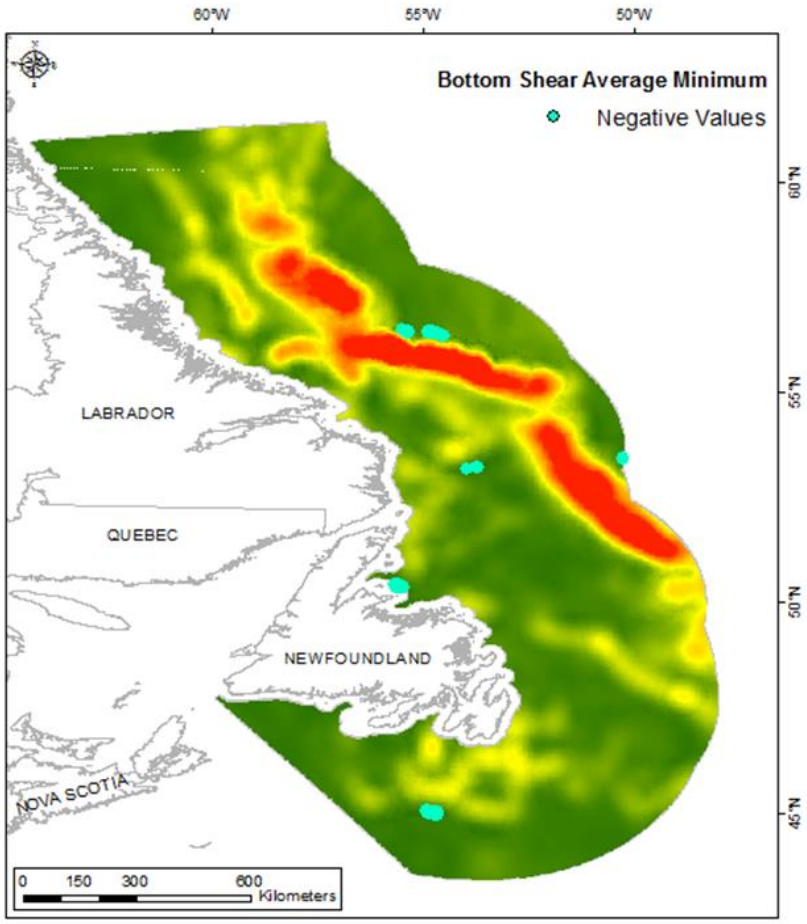

Figure A7. Negative values generated in the interpolated prediction surface of Bottom Shear Average Minimum.